MAGYAR ÁLLAMI
EÖTVÖS LORÁND
GEOFIZIKAI INTÉZET

EÖTVÖS LORÁND
GEOPHYSICAL INSTITUTE
OF HUNGARY

GEOFIZIKAI KÖZLEMÉNYEK

GEOPHYSICAL TRANSACTIONS

ВЕНГЕРСКИЙ
ГЕОФИЗИЧЕСКИЙ
ИНСТИТУТ
ИМ Л. ЭТВЕША

ГЕОФИЗИЧЕСКИЙ
БЮЛЛЕТЕНЬ

CONTENTS

Foreword	*P. G. Teleki, O. Ádám, É. Kilényi*	7
Seismic stratigraphy of the Pannonian Basin in southeastern Hungary	*R. E. Mattick, J. Rumpler, R. L. Phillips*	13
Processes and depositional environments within Neogene deltaic–lacustrine sediments, Pannonian Basin, Southeast Hungary	*I. Bérczi, R. L. Phillips*	55
Magnetostratigraphy of Neogene strata penetrated in two deep core holes in the Pannonian Basin: Preliminary results	*D. P. Elston, G. Hámor, Á. Jámbor, M. Lantos, A. Rónai*	75
Contribution to the determination of the Plio–Pleistocene boundary in sediments of the Pannonian Basin	*A. E. Grosz, A. Rónai, R. Lopez*	89

VOL. 31. NO. 1–3. DEC. 1985. (ISSN 0016—7177)

BUDAPEST

Contrasting types of nearshore sands and gravels from semi-protected Miocene coasts, northern Hungary	*H. E. Clifton, M. Bohn-Havas, P. Müller*	101
Lithologic characteristics and paleogeographic significance of resedimented conglomerate of late Cretaceous age in northern Hungary	*H. E. Clifton, K. Brezsnyánszky, J. Haas*	131
Economic heavy minerals of the Danube river floodplain sediments and fluviolacustrine deposits of northwestern and central Hungary	*A. E. Grosz, F. Síkhegyi, U. P. Fügedi*	157
Details of a Pleistocene coastal succession, Golden Gate National Recreation Area, California	*G. Császár, H. E. Clifton, R. E. Hunter*	169
Geochemical analyses of 12 Hungarian coal samples	*L. G. Somos, P. Zubovic, F. O. Simon*	191
Estimation of kerogene-type by time–temperature pyrolysis method	*I. Fisch, I. Koncz*	205
Structural rotations from paleomagnetic directions of some Permo-Triassic red beds, Hungary	*E. Márton, D. P. Elston*	217
Seismic modeling in a complex tectonic environment	*J. J. Miller, M. W. Lee, É. Kilényi, I. Petrovics, L. Braun, G. Korvin*	231
High resolution interval velocities	*I. Késmárky*	257
Measurement and processing of short-offset vertical seismic profile data	*M. W. Lee, J. J. Miller, G. Göncz*	269
Transient electromagnetic soundings – Development of interpretation methods and application to bauxite exploration	*K. Kakas, F. C. Frischknecht, J. Újszászi, W. L. Anderson, E. Prácser*	295
Comparison of interpretation methods for time-domain spectral induced polarization data	*L. Verő, B. D. Smith, W. L. Anderson, J. Csörgei*	311

Application of the Geological Retrieval and Synopsis (GRASP) program at the Eötvös Loránd Geophysical Institute of Hungary	*R. W. Bowen, F. Csercsik, L. Zilahi-Sebess*	331

TARTALOM

A Pannon medence szeizmikus sztratigráfiai vizsgálata DK-Magyarországon	*R. E. Mattick Rumpler J. R. L. Phillips*	53
A Pannon medence neogén tavi delta üledékeiben megnyilvánuló üledékképződési folyamatok és üledékfelhalmozási környezetek	*Bérczi I. R. L. Phillips*	71
A Pannon medence neogén üledékeinek magnetosztratigráfiai vizsgálata két mélyfúrásban: Előzetes eredmények	*D. P. Elston, Hámor G., Jámbor Á., Lantos M., Rónai A.*	88
Közlemény a pliocén–pleisztocén határmegállapításról az Alföld üledékeiben	*A. Grosz, Rónai A., R. Lopez*	98
Eltérő típusú homok- és kavicsüledékek az Észak-magyarországi miocénből	*H. E. Clifton, Bohnné Havas M., Müller P.*	128
Az Észak-magyarországi átülepített felsőkréta konglomerátum kőzettani jellegei és ősföldrajzi jelentősége	*H. E. Clifton, Brezsnyánszky K., Haas J.*	154
A Duna ártéri képződményeinek valamint ÉNY- és Közép-Magyarország folyami–tavi üledékeinek hasznosítható nehézásványai	*A. E. Grosz, Sikhegyi F., Fügedi U. P.*	167
Part menti pleisztocén rétegsor a Golden Gate üdülő körzetből	*Császár G., H. E. Clifton, R. E. Hunter*	189
12 magyarországi szénminta geokémiai analízise	*Somos L., P. Zubovic, F. O. Simon*	201
Kerogén típusának becslése idő–hőmérséklet pirolízis módszerrel	*Fisch I., Koncz I.*	215
Magyarországi permo-triász vörös üledékek paleomágneses vizsgálata	*Mártonné Szalay E., D. P. Elston*	230

Szeizmikus modellezés bonyolult tektonikai viszonyok között	*J. J. Miller, M. W. Lee, Kilényi É., Petrovics I., Braun L., Korvin G.*	255
Nagyfelbontású sebességfüggvény-becslés	*Késmárky I.*	268
Lyukközeli VSP mérések és feldolgozásuk	*M. W. Lee, J. J. Miller, Göncz G.*	293
A tranziens elektromágneses szondázások kiértékelési módszereinek fejlesztése és a szondázások alkalmazása a bauxitkutatásban	*Kakas K., F. C. Frischknecht, Újszászi J., W. L. Anderson, Prácser E.*	309
Időtartománybeli spektrális gerjesztett polarizációs adatok értelmezési módszereinek összehasonlítása	*Verő L., B. D. Smith, W. L. Anderson, Csörgei J.*	330
A GRASP adatbázis kezelő programrendszer alkalmazása az ELGI-ben	*R. W. Bowen, Csercsik F., Zilahi-Sebess L.*	335

СОДЕРЖАНИЕ

Сейсмостратиграфическое исследование Паннонского бассейна в ЮВ части Венгрии	*Р. Э. Метик Я. Румплер Р. Л. Филипс*	54
Условия и механизм накопления осадков неогеновых озерно-дельтовых образований Паннонского бассейна	*И. Берци Р. Л. Филипс*	71
Предварительные результаты магнитостратиграфических исследований в двух глубоких скважинах в Паннонском бассейне	*Д. П. Элстон Г. Хамор А. Ямбор М. Лантош А. Ронаи*	88
Сообщение об определении плио-плейстоценовой границы в осадочных породах Большой Венгерской Низменности	*Э. Э. Грос А. Ронаи Р. Лопез*	99

Отличающиеся типы песчаных и галечных осадков из миоценовых образований северной Венгрии	*Г. Э. Клифтон* *М. Бон-Хаваш* *П. Мюллер*	129
Литологические характеристики и палеогеографическое значение переотложенных верхнемеловых конгломератов в северной Венгрии	*Г. Э. Клифтон* *М. Бон-Хаваш* *П. Мюллер*	154
Тяжелые минералы в пойменных образованиях р. Дуная и во озерно-речных отложениях северо-восточной и центральной Венгрии	*Э. Э. Грос* *Ф. Шикхеди* *У. П. Фюгеди*	167
Прибрежный разрез плейстоцена в калифорнийском курортном районе Голден Гейт	*Г. Часар* *Г. Э. Клифтон* *Р. Э. Хантер*	189
Геохимический анализ 12-и венгерских угольных проб	*Л. Г. Шомош* *П. Зубович* *Ф. О. Саймон*	201
Оценка типа керогена методом «время-температурного пиролиза»	*И. Фиш* *И. Конц*	216
Палеомагнитное исследование пермо-триасовых красных отложений в Венгрии	*Э. Мартон* *Д. П. Элстон*	230
Сейсмическое моделирование при сложных тектонических условиях	*Дж. Дж. Миллер* *М. В. Ли* *Э. Килени* *И. Петрович* *Л. Браун* *Г. Корвин*	255
Оценка уравнения скорости с высокой разрешающей способностью	*И. Кешмарки*	268
Техника измерений и способы обработки данных ВСП при минимальном расстоянии между пунктом взрыва и скважиной	*М. В. Ли* *Дж. Дж. Миллер* *Г. Гёнц*	293
Развитие способов интерпретации данных электромагнитных зондирований по методу переходных процессов и применение зондирований для разведки бокситов	*К. Какаш* *Ф. Ц. Фришкнехт* *Й. Уйсаси* *В. Л. Андерсон* *Э. Прачер*	310

Сравнение методов интерпретации данных спектральной вызванной поляризации во временной области	*Л. Верё* *Б. Д. Смис* *В. Л. Андерсон* *Й. Чёргеи*	330
Примененые системны программ управления базой данных в Венгерском Геофизическом Институте им. Л. Этвеша	*Р. В. Боен* *Ф. Черчик* *Л. Зилахи-Шебеш*	335

FOREWORD

In 1978, four scientists from the United States Geological Survey (USGS) visited Budapest at the invitation of the Hungarian Central Office of Geology (Központi Földtani Hivatal). The purpose of this exploratory visit was to examine possibilities in exchanging scientists and implementing cooperative research in geosciences under the 1977 United States–Hungary Agreement on Cooperation in Culture, Education, Science and Technology. The USGS delegation visited several institutes, including the Eötvös Loránd Geophysical Institute, the Hungarian Geological Survey, the Oil and Gas Trust and institutes of the Academy of Sciences. The review of programs conducted in Hungarian geoscience institutes indicated that several areas of scientific research were of mutual interest, and that reciprocally, programs of the USGS needed to be made familiar to Hungarian scientists. Accordingly, in April 1979, a delegation from Hungary visited facilities of the USGS in Virginia, Colorado, California, Arizona, and field experiments in Wyoming. A list of possible cooperative subjects, with various degrees of commonality to scientists from both coutries emerged after these visits and from the ensuing discussions. This included seismology, geoelectrical techniques, paleomagnetics, energy resources assessment, and engineering geology. Negotiations led to an agreement on cooperative scientific research for a two-year duration, and in subsequent years that agreement was renewed twice thereafter.

The joint scientific efforts between the Central Office of Geology and the U. S. Geological Survey developed along several lines. A significant effort was made in geophysics, particularly in developing instrumented field methods and numerical algorithms to test for the presence of mineralized zones and ore bodies. Electromagnetic and induced polarization methods were used to probe for bauxite and sulfide deposits. Geophysical modeling, in complex geological terrain, and graphical display methods were developed or exchanged for mutual benefit – an underlying principle of the entire cooperative program. An equally significant effort was expended in understanding the Neogene history of the Pannonian basin, with several holes drilled and cored for oriented samples for deciphering the remanent magnetic record, and 800 km of seismic reflection profiles were analyzed jointly to understand the stratigraphic framework and the evolution of the basin. Concurrently, paleoenvironmental reconstruction was used to study potential reservoir rocks and possible migration paths, as well as to understand depositional facies, sediment sources, and the role that tectonic events played in the structural development of the basin. Geochemical studies of kerogen were to decipher maturation processes for hydrocarbons, and the signal characteristics of seismic reflection data were probed to detect gaseous horizons. Experts were exchanged to understand how data bases were used to manage geological, geochemical, and geophysical data and how best to display these data. Concepts and studies began to merge and supplemented by other investigations in mineral resources (heavy minerals), and in magnetotellurics, and plans were made for intercomparative studies in tectonics.

This compendium of papers presents the progress and some of the results and sucesses of the projects undertaken jointly by the Hungarian earth science institutions and the U. S. Geological Survey, during the first five years of cooperative work. The articles in this volume represent the scientific results presented at a joint conference, held in Budapest, October 1–3, 1984. Notably, not all the subjects envisioned or tried initially as joint efforts endured the test of time and these are not reported in this volume. Those scientific investigations, however, that persevered, established in the process a common foundation of understanding and a spirited desire to search for answers. These attributes were certainly characteristic of not only individual studies, but the cooperative program on the whole.

Significant results include a substantially new analysis of the sources and directions of sedimentation that filled the Pannonian Basin. The deltaic facies analyzed by seismic stratigraphic methods (Mattick, Rumpler and Phillips) and core hole data (Bérczi and Phillips) in southeastern Hungary, were found to represent two distinct stages of deltaic sedimentation in a trough that contains 6000 m of lacustrine and fluvial sedimentary rocks of Neogene and Quaternary age. The older deltaic system was deposited in water of 800–900 m and the younger system was deposited in water depths of 300–400 m. Both deltaic systems contain potential reservoir rocks for petroleum; in the older deltas coarse-grained rocks are stored in delta-slope channels, in the younger deltas coarse-grained rocks are stored chiefly in delta-front sheet sands. The conditions that matured organic matter into petroleum were examined at a few locations by Fisch and Koncz using the method of pyrolysis on rock samples.

Paleoenviroments of late Cretaceous and early to mid-Miocene age are reported on in two papers, respectively, by Clifton, Brezsnyánszky and Haas, and Clifton, Bohn-Havas and Müller. Both emphasize reconstruction of paleogeographic settings, using models of sedimentation, including sources, pathways and sinks for the detritus. Senonian conglomerates of the Bükk Mountains are shown to have been emplaced by westward moving gravity flows, and their source was subsequently moved tectonically to the north. Miocene sands and gravels lend themselves to differentiating inner shelf, nearshore, foreshore, and backshore segments of a paleo-shoreline, where the rate of sedimentation kept pace with a rising sea-level.

A particularly vexing problem has been the definition of the Pannonian stage. What were thought to be paleontological and palynologic timeline indicators have recently been found to be but markers of locally varying paleoenvironments. Hence, magnetostratigraphic studies were initiated by the Hungarian Geological Survey (Elston, Hámor, Jámbor, Lantos and Rónai) as another means to distinguish the time-stratigraphic units composing the Neogene. Preliminary results indicate that the boundary bvetween the Lower and Upper Pannonian can be dated at 8.8 million years, but further studies are needed for completing the reference polarity zonations for the Pannonian (s. l.) and Pleistocene in Hungary. Determination of the Pilo–Pleistocene boundary was also the subject of a study by Grosz, Rónai and Lopez, in this case using heavy

minerals as possible indicators of climatic shifts. The authors believe denser sampling will prove this to be a useful method. A separate study by Márton and Elston also used remanent magnetization to find that the Balaton Highlands rotated 50° counter-clockwise with respect to the Mecsek Mountains, since the magnetization of the studied red beds, a step toward deciphering the tectonic events of that area.

Another major thrust of the cooperative investigations focused on geophysical methods applied to mineral resources. Several investigations, including field work and theoretical modeling, sought improvements in techniques for detecting ore deposits. Among these, Verő, Smith et al. report on the first common basis for interpretation of time-domain and frequency-domain, spectral, induced polarization methods using generalized inversion and the Cole-Cole model. Results on applying time-domain electromagnetic (EM) methods to bauxite deposits and karst terrain (Kakas, Frischknecht et al.) also includes theory for simplified interpretation of time-domain EM soundings. Using seismic profiles from the U. S. Atlantic Continental margin, Késmárky probed possibilities of detecting hydrates based on interval velocities. While this study was based on conventional seismic reflection profiling, Lee, Miller, and Göncz tested theories about vertical seismic profiling with data from field experiments, and their report contains innovations in both the field techniques and in the analysis of the data. Geophysical data lend themselves to modeling – the above metioned papers all incorporate such – but a specific attampt, by Müller, Lee, Kilényi, Petrovics, Braun and Korvin dealt with specific and difficult problems of a tectonically much deformed terrane, that contains coal beds.

Further, other studies in coal and also in heavy minerals are reported. Based on a reconnaissance study, Grosz, Sikhegyi and Fügedi conclude that the amount of particulate gold found in Danube River sediments bears closer and more widespread examination, and that heavy-mineral suites could be used productively to delineate sources and sinks of sedimentation in the Pannonian Basin. The number of samples that could be collected for this study was not adequate to quantify results further; this also was the case for trace element analysis of coal samples by Somos, Zubovic an Simon. This latter investigation showed, however, that Hungarian Jurassic coal is high in trace elements, while Eocene and Miocene coals are high in organic sulfur. Both studies presage significant results if pursued further.

Many of these joint efforts benefitted from gradual understanding of one another's data bases, how such were used to manage and display data. The substance of this is reported by Bowen, Csercsik and Zilahi-Sebess.

These papers signify a progressive shift in emphasis that evolved during the course of five years of joint Hungarian–American research. What began as a collection of independent trials, gradually formed a program of investigation supporting one another, sharing concepts, data and results. Still a beginning, the aims and aspirations matured in October 1984, at the joint conference, to a concerted drive by all to decipher the geological framework, evolution, processes and resources of the Pannonian Basin comprehensively.

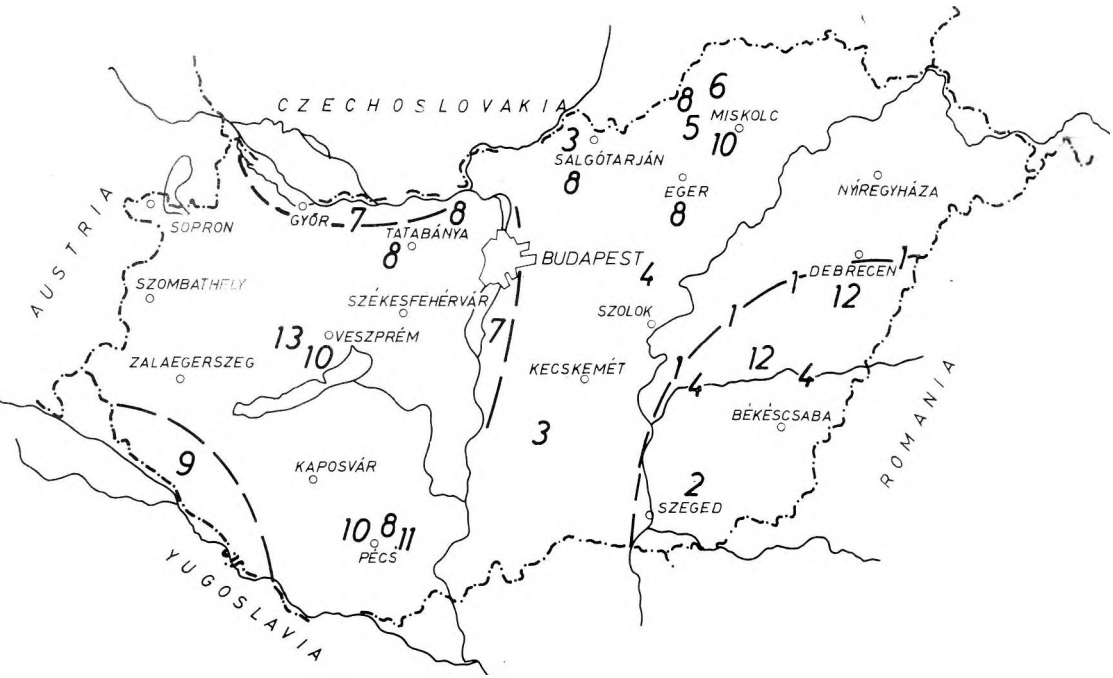

Location map showing USGS—KFH joint field investigation
1 — Seismic stratigraphy, 2 — Sedimentology/depositional environment,
3 — Magnetostratigraphy, 4 — Chronostratigraphy, 5 — Paleoenvironment,
6 — Lithology/Paleogeography, 7 — Heavy minerals, 8 — Coal geochemistry,
9 — Oil geochemistry, 10 — Paleomagnetics, 11 — Seismic modeling,
12 — Vertical seismic profiling, 13 — Transient electromagnetic soundings

A USGS—KFH tudományos–műszaki együttműködési szerződés keretében végzett kutatási témák helyszínei
1 — Szeizmikus sztratigráfia, 2 — Üledékföldtan/üledékfelhalmozódási környezetek,
3 — Magnetosztratigráfia, 4 — Kronosztratigráfia, 5 — Paleokörnyezet,
6 — Kőzettan/ősföldrajz, 7 — Nehézásványok, 8 — Szén-geokémia, 9 — Olaj-geokémia,
10 — Paleomágnesség, 11 — Szeizmikus modellezés, 12 — Vertikális szeizmikus szelvényezés,
13 — Tranziens elektromágneses szondázás

План расположения районов совместных исследований в рамках научно–технического сотрудничества между Геологической службой С. Ш. А. и Центральным геологическим управлением ВНР
1 — Сейсмостратиграфия, 2 — Седиментология/среды осадкообразования,
3 — Магнитостратиграфия, 4 — Хроностратиграфия, 5 — Палеосреда,
6 — Литология/палеогеография, 7 — Тяжелые минералы, 8 — Геохимия угля,
9 — Геохимия нефти, 10 — Палеомагнетизм, 11 — Сейсмическое моделирование,
12 — Вертикальное сейсмическое профилирование, 13 — Электромагнитное зондирование методом переходных процессов

Why the Pannonian Basin? Is it because it covers a large part of Hungary, capturing most of the current geoscientific investigations? Undoubtendly, that is part of the answer, but a small part only. There is a certain fascination that the basin elicits, by virtue of the geologic simplicity of young rock units in some areas and the geologic complexity of surrounding areas and older rock units. The Pannonian Basin is young, it has subsided and infilled at a relatively fast rate, and in the basinal areas, where the sedimentary rocks are relatively undisturbed, sedimentary processes can be studied. The basinal areas overlie a thin crust permeated by high geothermal heat flow that helped generate valuable energy and mineral resources. In surrounding areas and in the older rocks underlying the Pannonian Basin, relatively recent orogenies and volcanism associated with pull-apart tectonics, thrust faulting, and mountain building processes that formed the Alps and Carpathian Mountains are displayed. Many of these attributes have been summarized recently in a special issue of Earth Evolution Sciences (1981). The Pannonian Basin is a virtual laboratory to which geologic processes, seldom as active or found in such abundance, can be modeled.

The papers in this volume reflect but a few probings not only into the subsurface of a geologically unique area but also into ways scientific cooperation can transcend geographic boundaries. We hope, therefore, that these contributions will further scientific interest and knowledge in both Hungary and the United States, and that exchanges of people and ideas will continue in the high-spirited form of prior years.

Reston, Virginia, U.S.A. and
Budapest, Hungary
June, 1985

Paul G. Teleki (USGS)
Oszkár Ádám (KFH)
Éva Kilényi (ELGI)

GEOPHYSICAL TRANSACTIONS 1985
Vol. 31. No. 1–3. pp. 13–54

SEISMIC STRATIGRAPHY OF THE PANNONIAN BASIN IN SOUTHEASTERN HUNGARY

Robert E. MATTICK*, János RUMPLER** and
R. Lawrence PHILLIPS***

Seismic stratigraphic analyses and studies of core samples from three wells indicate that infilling of the Pannonian Basin of Hungary resulted primarily from deltaic sedimentation from the northwest, north, and northeast. Infilling of the basin involved a single cycle of sedimentation which probably began in Sarmatian or earliest Pannonian time when water depths in the basin were > 1,000 meters. The subsequent history of the basin, during Pannonian and Quaternary time, reflects continuously shoaling waters. This shoaling resulted from sediment influx rates that were generally higher than basin subsidence rates.

In general, two stages of delta construction can be recognized. In an early stage of construction, turbidite-fronted deep-water deltas were built in water depths as deep as 800–900 meters. During this early constructional stage, subsidence rates and associated sediment influx rates were high, and upbuilding and southward progradation of large deltaic sediment wedges filled subbasins near the source areas, overwhelmed local basement highs, and spilled sediments into subbasins in the southern part of Hungary. During a later stage of construction, prograding shallow-water deltas were built in water depths of 200–400 meters, and topographically low areas in the southern part of Hungary were filled by sediments discharged from river systems that advanced about 100 km southward across strata deposited during the initial stages of construction.

Seismic evidence indicates that in some areas of the Pannonian Basin, the sedimentary rocks representing the two stages of delta construction are separated by a depositional unit which possibly represents a destructive phase. This unit may have been deposited during a short-lived transgressive phase or, perhaps, it was deposited following a period of accelerated lake shoaling.

The youngest and final stage of deposition is represented by delta plain facies; depositional environments varied from shallow lake, fluvial, and marsh to terrestrial soils. This unit is inferred to represent more widespread lake conditions coupled with continued shoaling and eventual disappearance of the Pannonian lake. During this period of sediment deposition, basin subsidence rates and associated sediment influx rates were probably lower, and the sediment influx rate is inferred to have kept pace generally with the basin's subsidence rate.

Keywords: seismic stratigraphy, Pannonian Basin, deltas, depositional environments

1. Introduction

The Pannonian Basin lies within a large intramontane basin that comprises parts of five countries and is completely encircled by mountain belts of the Carpathian mountain system and the Dinaric Alps *(Fig. 1)*. The general geo-

* U.S. Geological Survey, 914 National Center, Reston, Virginia 22 092
** Geophysical Exploration Company (GKV), POB 213, Budapest, H–1391
*** U.S. Geological Survey, 345 Middlefield Road, MS 999, Menlo Park, California 94 025
Manuscript received: 23 May, 1985

graphic name for the region inside the mountain arc is the Carpathian basin or the intra-Carpathian region [LERNER 1981]. The intramontane region, however, is not topographically uniform, and emergent ranges divide it into several subbasins, the largest of which is the Pannonian Basin. That part of the Pannonian Basin which lies within Hungary generally is subdivided on the basis of topography into the Great Hungarian Plain, the Danube–Rába Lowland and the SW Transdanubian Basin *(Fig. 2)*.

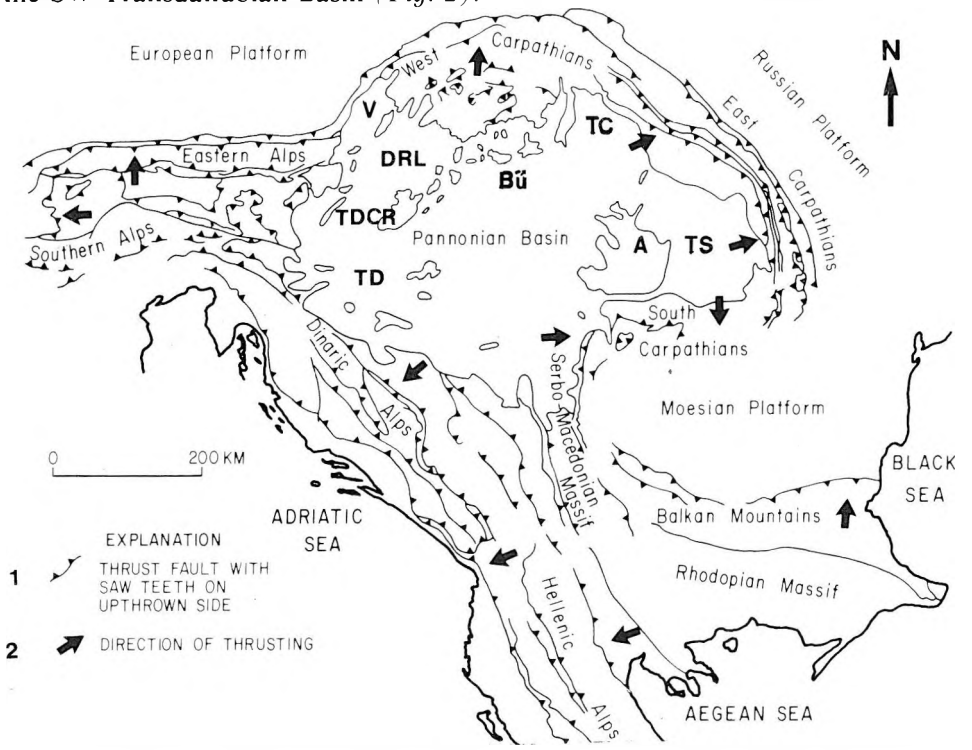

Fig. 1. Location of the Pannonian Basin within the intra-Carpathian region. The Carpathian Basin comprises the Pannonian, Vienna (V), the SW Transdanubian (TD), Transcarpathian (TC) and Transylvanian (TS) basins, the Danube–Rába Lowland (DRL) the Transdanubian Central Range (TDCR), Bükk (Bü) and Apuseni Mountains (A). [Figure modified from BURCHFIEL and ROYDEN 1982, Fig. 1]

1. ábra. A Pannon medence helyzete a Kárpáti-térségben. A Pannóniai, a Bécsi (V), a DNy-Dunántúli- (TD), a K-Kárpáti (TC), és az Erdélyi (TS) részmedence alkotja a teljes, Kárpáti íven belüli medencét. TDCR = Dunántúli középhegység, Bü = Bükk hegység, A = Erdélyi középhegység. [BURCHFIEL–ROYDEN 1982, 1. ábra után módosítással]
1 — feltolódás, fűrészfog a felemelt oldalon; 2 — a kompresszió iránya

Рис 1. Положение Паннонского бассейна в Карпатском регионе. Внутри-карпатский бассейн включает в себя Паннонский, Венский (V), Западно-задунайский (TD), Закарпатский (TC), и Трансильванский (TS) частные впадины, Низменности рр. Дунай–Раба (DRL). TDCR = Задунайское среднегорье, Bü = горы Бюкк, A = Апусенские горы. (По BURCHFIEL–ROYDEN 1982, Рис 1. с модификацией)
1 — надвиг, пилообразное обозначение на приподнятой стороне;
2 — направление сжимающей нагрузки

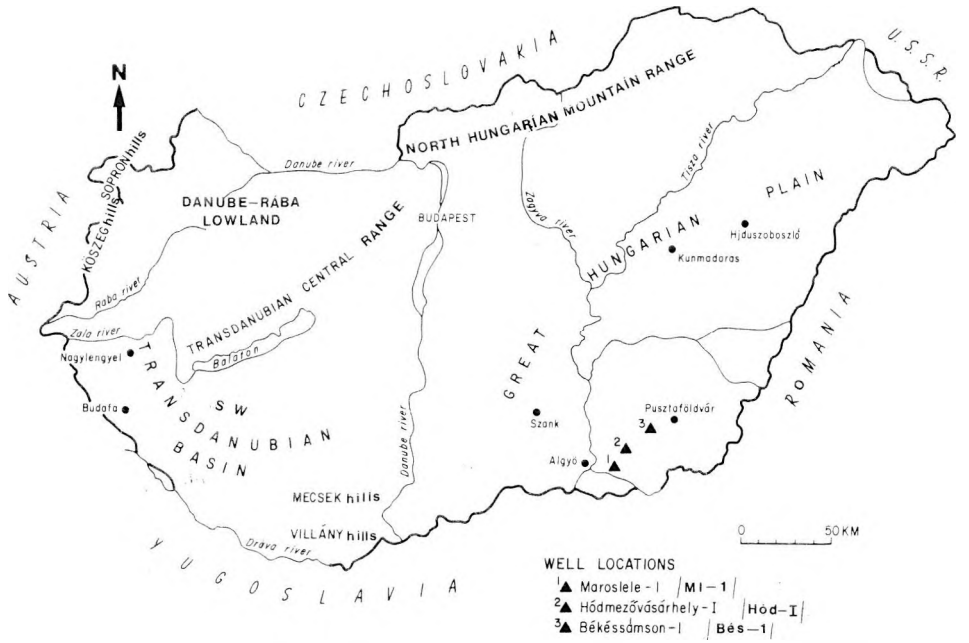

Fig. 2. Geographical place names. [Figure modified from DANK and KÓKAI 1969]

2. ábra. Földrajzi helynevek. [DANK és KÓKAI 1969 után módosítással]

Рис. 2. Географические названия местностей [по DANK–KÓKAI 1969, с модификацией]

In this paper, the principles of seismic stratigraphy [VAIL et al. 1977] are applied in an attempt to reconstruct on a regional basis the post-Mesozoic depositional history of the Pannonian Basin in Hungary. Unconformities are used to bound groups of reflections into seismic sequences that can be correlated over wide areas. The seismic sequences, in turn, are correlated with depositional sequences which can be ordered in a relative time-stratigraphic sense. The unconformities are picked from the seismic records on the basis of discordances between reflectors (or strata) at sequence boundaries. The types of discordance that occur at sequence boundaries are shown in *Figure 3*.

Because the main interest of the authors was the Neogene–Quaternary stratigraphy, older seismic sequences are mapped as basement rocks (basement consists chiefly of Paleozoic and Mesozoic rock units). Well data, however, has shown that, in places, the Paleozoic and Mesozoic rocks are overlain by a thin cover of pre-Pannonian Miocene and Paleogene sedimentary rocks that may have been involved in the tectonic deformation of the basement or deposited during a marine transgression as a thin disconformable or unconformable sheet over the basement surface. In some cases, this thin unit is indistinguishable on seismic records from the underlying Paleozoic and Mesozoic units, and, therefore, the basement complex as mapped on seismic records may include

pre-Pannonian Miocene and Paleogene sedimentary rock units as well as older Paleozoic and Mesozoic rock units.

The seismic profiles analyzed in this study are located in the southeastern part of the Great Hungarian Plain area *(Fig. 4)*. *Table I* references the profile numbers used in this report to the seismic profile numbering system used by the Geophysical Exploration Co. of the National Oil and Gas Trust of Hungary (OKGT). The depth to the basement surface (pre-Cenozoic rocks) is shown in *Figure 5* [KILÉNYI–RUMPLER 1985].

In figures and in the text, abbreviations are used in place of well names. In *Table II*, well abbreviations are listed along with corresponding well names.

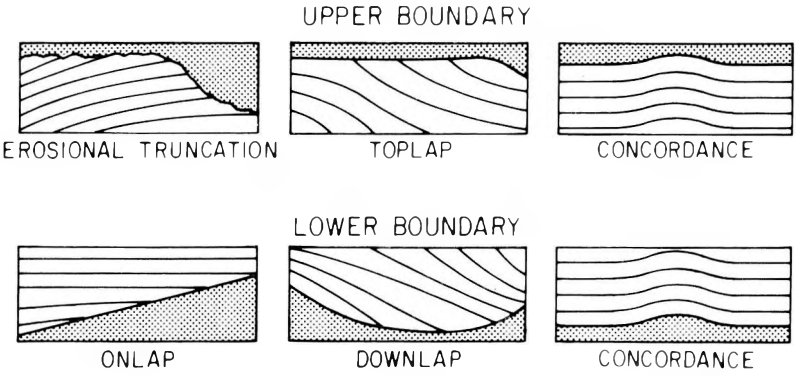

Fig. 3. Possible types of discordant relations found at the upper and lower boundaries (unconformities and disconformities) of seismic or depositional sequences. [Figure modified from VAIL et al. 1977]

3. ábra. A szeizmikus, vagy üledékes rétegösszletek alsó és felső határain lehetséges diszkordancia-összefüggések. [Átvéve: VAIL et al. 1977]

Рис. 3. Возможные связи несогласия на нижнем и верхнем разделах сейсмических или осадочных серий (эрозионные и угловые несогласия) [по VAIL et al. 1977]

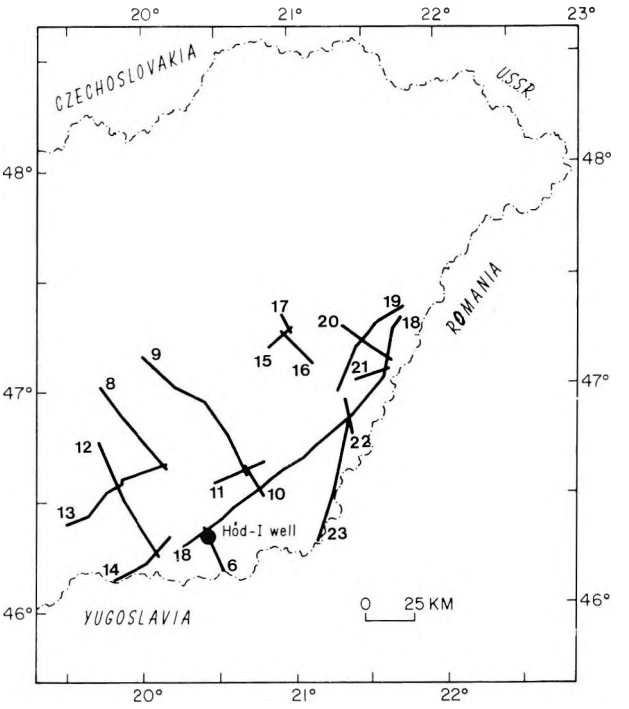

Fig. 4. Location of seismic profiles interpreted in this study. Table I references the profile numbers used on this map to the seismic profile numbering system used by the National Oil and Gas Trust of Hungary. Profile numbers shown here correspond to figure numbers in which seismic records are displayed. Dash-dot symbols show outline of Hungary within studied area

4. ábra. Jelen tanulmányban értelmezett szeizmikus szelvények helyszínrajza. Az I. táblázat tartalmazza az ábraszámozás és az OKGT GKV szelvényszámozása közötti kapcsolatot. Az ábra szelvényszámozása egyezik az egyes szelvények ábra számaival

Рис. 4. Схема расположения сейсмических профилей, интерпретированных в настоящей работе. Таблица I показывает соотношение нумерации рисунков и нумерации разрезов, на Предприятии Геофизического Исследования ГТНГП. Нумерация профилей на рисунке совпадает с номерами рисунков отдельных профилей

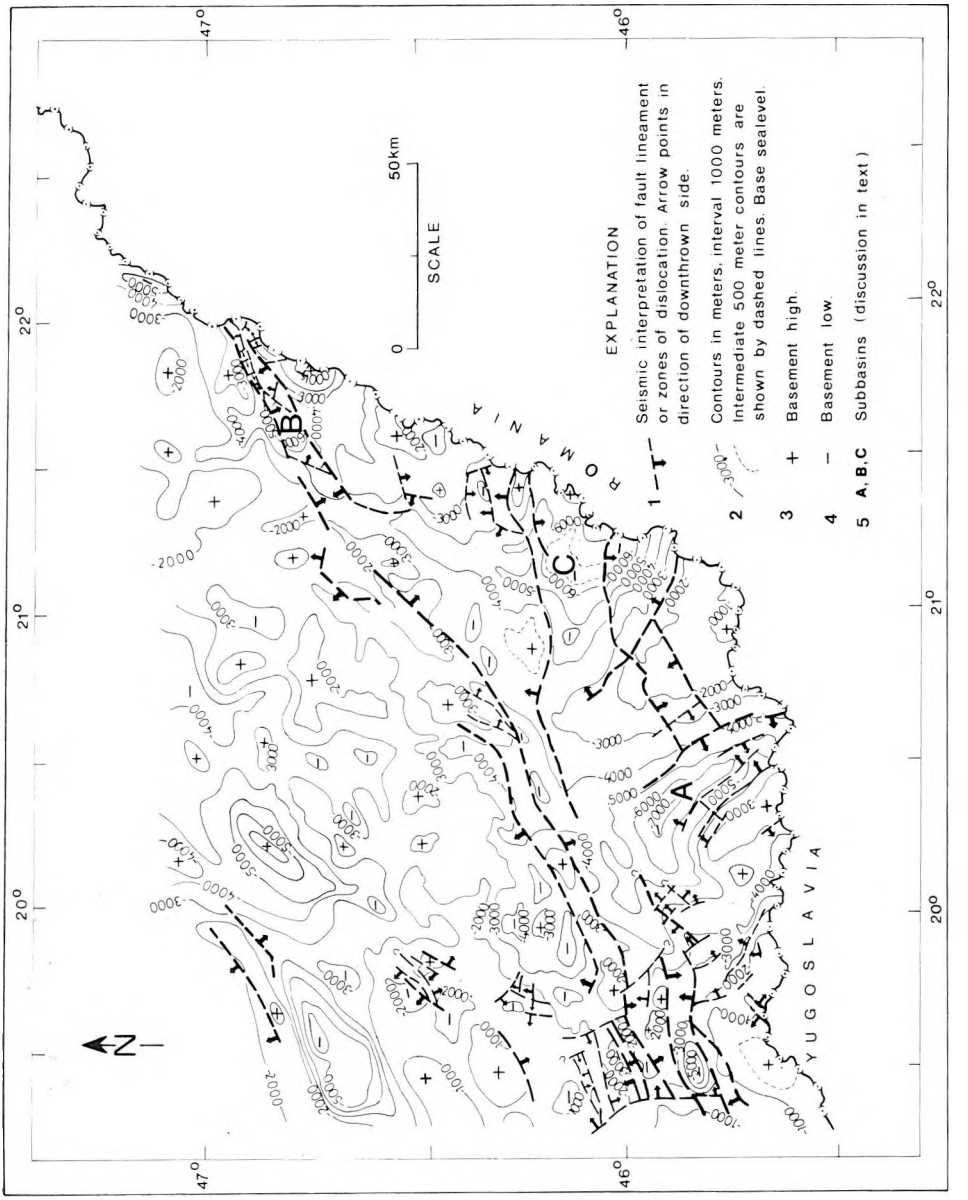

Fig. 5. Structure map of pre-Cenozoic rocks in Southeastern Hungary. Sedimentation patterns within the three subbasins (Makó–Hódmezővásárhely trough (A), Derecske basin (B), and Békés basin (C)) are discussed in text. [Figure modified from KILÉNYI and RUMPLER 1985]

2. Seismic stratigraphy at Hód–I well

The seismic stratigraphy in the vicinity of the Hód–I well is illustrated best on seismic profile 6 *(Fig. 6)*. The seismic profile can be divided into five seismic sequences based on the geometric relationship of reflections to sequence boundaries and on the internal configuration of reflections within sequences. The typical reflection pattern of each sequence (marked by two-way travel times) is shown in *Figure 7*, and, from top to bottom, they are described below.

Sequence V (0.0–1.74 sec; 0–2,003 m): Within this sequence, reflectors are concordant to the bottom sequence boundary. Individual reflectors vary from parallel to wavy. Although reflections are strong (high amplitude), few, if any, can be traced for any distance without interruption.

Correlation with core data [BÉRCZI–PHILLIPS this volume, PHILLIPS–BÉRCZI 1985] indicates that seismic sequence *V* represents delta plain facies; depositional environments varied from shallow lake, fluvial, and marsh to possible terrestrial soils. At the Hód–I well site, the bottom boundary of sequence *V* is placed at 2,003 m, about 514 m higher than the base of delta plain facies as determined from core analyses. This difference in unit boundaries is a good example of the differences that result from seismic sequence analysis in contrast to lithologic analysis. Although delta plain facies lie above and below the bottom boundary of sequence *V*, it will be shown later that the bottom boundary of sequence *V* represents an unconformity, probably related to more widespread lake conditions and shoaling of the Pannonian lake.

Sequence IV (1.74–2.44 sec; 2,003–3,250 m): In general, the internal reflectors form an irregular sigmoid pattern. The relation between reflections and sequence boundaries is one of toplap at the upper boundary and downlap at the lower boundary.

5. *ábra.* A kainozoós képződmények medencealjzatának térképe DK-Magyarországon. 1 – szeizmikus mérésekkel meghatározott törés-, ill. diszlokációs zónák (a nyíl a levetés irányát mutatja); 2 – mélységi szintvonalak, értékköz 1000 m (szaggatott vonal 500 m) tengerszint alatt; 3 – alaphegység magaslat; 4 – alaphegységi mélyzóna; 5 – A, B, C részmedencék (magyarázat a szövegben) [KILÉNYI és RUMPLER 1985 után módosítással]

Рис. 5. Карта рельефа фундамента каинозойских формаций на ЮВ части Венгрии. 1 — зоны разпомов и дислокаций, определенные сейсмическими измерениями (стрелками показывается направление сбрасывания); 2 — изолинии глубин с интервалом в 1000 м (пунктир показывает 500 м) ниже уровня моря; 3 — поднятия фундамента; 4 — прогибы фундамента; 5 — A, B, C частичные впадны обсуждаются в тексте [по KILÉNYI–RUMPLER 1985, с модификацией]

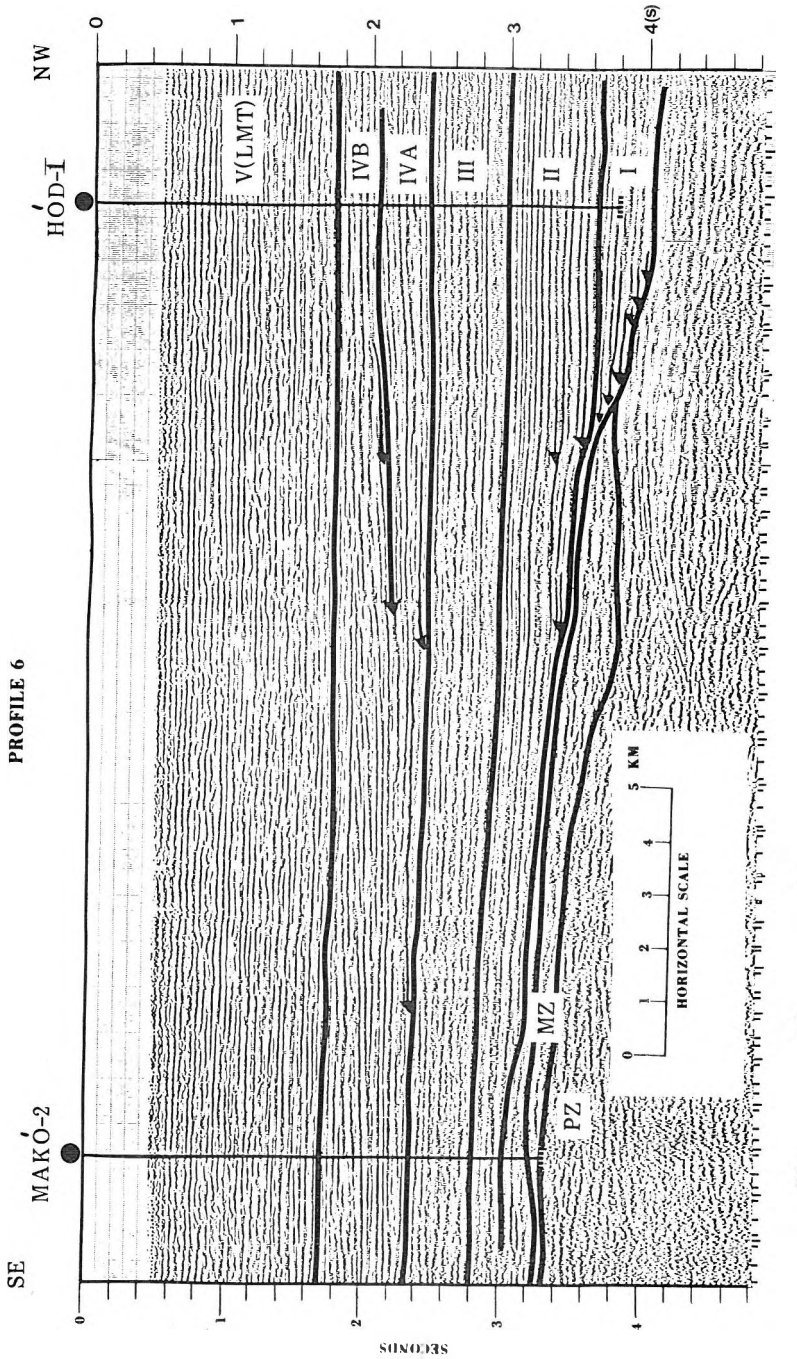
PROFILE 6
SE
MAKÓ-2
HÓD-I
NW
SECONDS
0
1
2
3
4
4(s)
V(LMT)
IVB
IVA
III
II
I
MZ
PZ
HORIZONTAL SCALE
0
1
2
3
4
5 KM

Sequence *IV* can be subdivided into subsequences *IVA* and *IVB* at the Hód–I well site. The subdivision is placed at 2.06 sec (2,517 m). Reflectors above 2.06 sec lie relatively flat, whereas those below 2.06 sec show a definite pattern of progradation to the southeast.

At the Hód–I well, subsequence *IVB* is inferred to represent delta plain facies; to the southeast, where the reflectors of subsequence *IVB* exhibit a strong progradational pattern with a dip of about 4.5 degrees, the facies probably grade to delta front and prodelta. The base of seismic subsequence *IVB* is placed at a depth of 2,517 m, in agreement with the base of delta plain facies as determined from lithologic analysis [BÉRCZI–PHILLIPS this volume, PHILLIPS–BÉRCZI 1985].

Subsequence *IVA* is inferred to represent delta front facies at the Hód–I well site. Southeast of the Hód–I well, where the reflection pattern in subsequence *IVA* suggests lesser dips, the facies probably grade to prodelta.

In general, seismic sequence *IV* represents prodelta, delta front, and delta plain facies. It will be shown, on seismic records from other parts of the basin, that sequence *IV* is part of a supersequence that represents a system of stacked deltas built during a late depositional stage. The term "late depositional stage" is used to distinguish this supersequence from an earlier and more widespread supersequence that represents delta construction during a period when the lake was deeper.

Sequence III (2.44–3.00 sec; 3,250–4,285 m): The boundary between sequences *IV* and *III* is placed immediately below the basalmost reflectors that exhibit the progradational pattern characteristic of sequence *IV*. Reflections in this sequence are concordant to the upper and lower sequence boundaries. The sequence is characterized internally by weak, highly discontinuous, wavy reflections.

Fig. 6. Interpreted seismic reflection profile 6 recorded near the Hód–I well site showing division of the sedimentary rock section into five seismic sequences. Roman numerals identify seismic sequences. Sequence *V* is also referred to as *LMT* in other sections of this report. Location is shown in figure 4. *PZ* and *MZ* are Paleozoic and Mesozoic rocks, respectively, of the basement complex. Note that vertical scale is in time; depths to the tops of seismic sequences are given in text. These depths were determined from a velocity survey conducted at the Hód–I well site

6. ábra. A Hód–I mélyfúrás mellett regisztrált 6 sz. szeizmikus szelvény értelmezett változata, melyen 5 szeizmikus rétegösszlet látható. A római számok a szeizmikus rétegösszleteket jelölik. Az *V.* rétegsort a cikkben *LMT*-ként is nevezzük. A szelvény helye a 4 sz. ábrán látható. A *PZ* paleozoós, az *MZ* mezozoos korú medencealjzati képződményeket jelöl. A szelvény vertikális léptéke idő (s), az egyes szekvenciák mélységét a Hód–I mélyfúrás szeizmikus sebességadatai alapján a szöveges részben adjuk meg

Рис. 6. Вариант интерпретации сейсмического профиля № 6, зарегистрованного близ скважином Hód–I, на котором выделены 5 сейсмических серий. Римскими цифрами обозначены сейсмические серии. Серия *V* в некоторых разделах статьи носит также название *LMT*. Положение профиля показан на рис. 4. Буквами *PZ* обозначены палеозойские формации фундамента бассейна, а буквами *MZ* – мезозойские. Вертикальный масштаб разреза отражает время (s), глубина залегания отдельных серий дана на основании сейсмических скоростей скважины Hód–I в текст

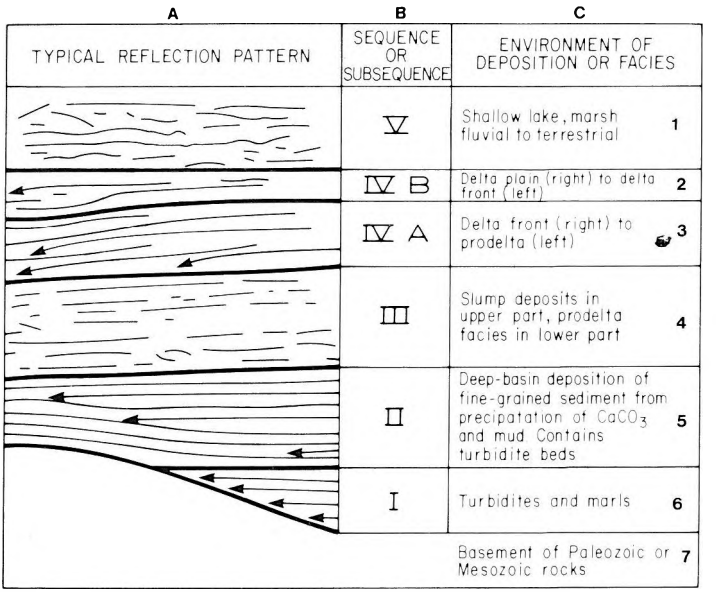

Fig. 7. Typical seismic reflection patterns of five seismic sequences at the Hód–I well site and their inferred environments of deposition or facies. The heavy lines are sequence boundaries, and the arrows show the relationship of internal reflectors to sequence boundaries (*V*, concordant; *IV*, downlap at basal boundary; *III*, concordant; *II*, concordant and onlap, *I*, onlap of basal boundary)

7. ábra. A Hód–I mélyfúrásnál lévő 5 szeizmikus rétegösszlet jellemző reflexió-konfigurációi, és a hozzájuk tartozó üledékképződési környezet és fácies. A vastag vonalak rétegösszlet-határt, a nyilak a belső reflexióknak a rétegösszlet-határokhoz való viszonyát mutatják. A: reflexiós konfigurációk, B: rétegösszletek, ill. al-rétegösszletek, C: üledékképződési környezet, vagy fácies: 1– sekély tavi, mocsári, folyami–szárazföldi; 2 – delta síksági (jobboldalt) – delta front (baloldalt); 3 – deltafront (jobboldalt) – delta előtér (baloldalt); 4 – a felső részen üledék rogyások, az alsó részen delta előtér fácies; 5 – finom szemcsés $CaCO_3$ és iszap lerakódás – mélyvízi fácies, turbidit rétegekkel; 6 – turbiditek és márgák; 7 – paleozoos vagy mezozoos aljzat

Рис. 7. Характерные конфигурации отражений для 5 сейсмических серий близ скважином Hód–I и соответствующие им среды осадкообразования и фации. Жирными линиями показаны разделы между сериями, стрелками – отношение внутренних отражений к разделам серий. A: конфигурации отраженных волн. B: серии и подсерии, C: среды осадкообразования или фаций: 1 — мелководно-озерные, болотные, аллювиально-континентальные; 2 — дельтовых равнин (справа) – дельтовых фронтов (слева); 3 — дельтовых фронтов (справа) – дельтовых форландов (слева); 4 — в верхней части – проседания осадков, в нижней части – фации дельтовых форландов; 5 — тонкозернистые известковистые и илистые отложения – глубоководные фации с прослоями турбидитов; 6 — турбидиты и мергели; 7 — палеозойский или мезозойский фундамент

The absence of strong, continuous reflections, which usually represent alternating beds with different reflection coefficients, together with the preponderance of sandstone in the cores from the Hód–I well indicate that this sequence may represent a relatively massive sandstone unit. However, the absence of strong continuous reflections also may be caused by extensively slumped strata, and evidence of slumping was present in some of the cores [BÉRCZI–PHILLIPS this volume, PHILLIPS–BÉRCZI 1985]. The vertical position of sequence *III* in the stratigraphic column, between a delta (sequence *IV*) and a deep-basin facies (sequence *II*), suggests that the sands could have been deposited in front of an advancing sand-prone delta or deltas.

At the Hód–I well site, seismic sequence *III* lies at depths of between 3,250 and 4,285 m. Based on core analyses [BÉRCZI–PHILLIPS this volume, PHILLIPS–BÉRCZI 1985], therefore, sequence III is equivalent to the lithologic unit inferred to represent prodelta facies. These authors divide the prodelta facies into subfacies *B* (slumped strata) and subfacies *A* (parallel-bedded strata). Such a division cannot be made from the seismic data, and it would appear that the lithologic data make a finer distinction in comparison to the seismic data. As will be shown later, however, seismic evidence from other parts of the Pannonian Basin suggests that updip from the Hód–I well site, at least part of seismic sequence *III* represents distal deposits associated with an early system of deep-water deltas and that deep-water delta construction may have been followed by a short-lived destructive phase. The lower part of seismic sequence *III*, therefore, apparently represents prodelta facies of the older, deep-water delta system, and the upper part of sequence *III* (slumped strata) may represent sands deposited in front of an advancing sand-prone delta system or, perhaps, it represents deposition during a destructive phase.

Sequence II (3.00–3.69 sec; 4,285–5,576 m): Reflections within this sequence are strong and, in general, can be traced across the entire record section or until they terminate to the southeast in an onlap configuration against underlying reflections or reflections that represent the basement surface. Onlapping reflectors alternate with concordant reflectors. The concordant reflectors are parallel with the basal sequence boundary and have the appearance of being draped over the basement surface southeast at the Hód–I well.

The alternation of concordant and onlapping reflectors suggests that layers of deep-basin marl alternate with turbidite deposits. Sediments precipitated from the water column tend to drape over basement highs. The sediments associated with turbidite deposits, however, would have been carried through canyons into the deeper parts of the basin near the water–sediment interface and, therefore, would be expected to show an onlap relation to underlying horizons.

Although core analyses [BÉRCZI–PHILLIPS this volume, PHILLIPS–BÉRCZI 1985] indicate that seismic sequence *II* correlates with deep basin facies at the Hód–I well site, the sequence can be traced seismically updip (northward) where it grades to prodelta, delta front, and delta plain facies. In other sections of this paper, it is shown that sequence *II* represents a deep-water, lateral equivalent

(in time) of a supersequence of stacked deep-water deltas built during an early depositional stage.

Sequence I (3.69–4.05 sec; 5,576–6,150 m): The pattern of reflections within this sequence is similar to that noted for sequence *II*, except that most reflections appear to terminate against the basal boundary (basement surface) in an onlap configuration. At the Hód–I site, correlation with core data [BÉRCZI–PHILLIPS this volume, PHILLIPS–BÉRCZI 1985] and the seismic character (onlap pattern) indicate that sequence *I* represents, for the most part, periodic influxes of coarse-grained sediments into a deep basin where the precipitation of $CaCO_3$ and the deposition of mud from suspension occurred. As will be shown later, some of coarse-grained sediments were transported by turbidite flovs from source areas far to the northwest. In addition, coarse-grained sediments probably were derived from erosion of local basement highs, especially the conglomerate layer penetrated in the Hód–I well at a depth of 5450 m [BÉRCZI–PHILLIPS 1985].

In the next sections of this paper, the authors attempt to trace, on seismic records, the subsurface extent of sequences *I–V* (or their equivalents). Because seismic stratigraphic techniques are employed, the tentative correlations that result are in a time-stratigraphic, rather than a rock-stratigraphic sense. Seismic sequences, by definition, can contain multiple depositional facies and, therefore, multiple lithologies.

For purposes of discussion, the seismic profiles are divided into three groups by area: southwestern, northern, and eastern. Each group contains seismic profiles with common points of intersection. Within each area, therefore, correlation of seismic sequences from profile to profile is relatively good. However, correlation of seismic sequences from area to area is more tentative because the areas are separated by gaps in seismic coverage. In light of this, we tried to develop a labeling system for the numerous seismic sequences and supersequences that would readily suggest to the reader which sequences are, possibly, time-equivalent. In general, we have mapped two supersequences which represent deltaic construction; one represents an early stage, and the other represents a later stage. These two stages are differentiated by the use of uppercase versus lowercase latters; for example, in the southwestern area, D_1–D_6 mark sequences of the early supersequence, and d_1–d_3 mark sequences of the late stage. In the eastern area, B_1–B_8 and b_1–b_4 mark sequences of the early and late stages, respectively. Roman numerals are used for sequences identified at the Hód–I well site (Fig. 6). The use of different symbols or letters in each of the areas implies that correlations between the different areas are tentative. The relation between the various sequences and supersequences is generalized in a summary figure that follows discussions of the three areas.

3. Seismic data

3.1 Southwestern Area

The discussion of seismic data begins with the southwestern area. This area lies directly north of the Hód–1 well, and sedimentation at the well site was chiefly from a northerly direction. It should be possible, therefore, to correlate seismic sequences mapped in the southwestern area with sequences mapped at the Hód–1 well site. The southwestern part of the studied area is in the vicinity of seismic profiles 6, 8–14 and the southwestern part of profile 18 (note that profile numbers are same as figure numbers; therefore, only profile numbers will be given in subsequent text). This area is dominated by a roughly triangular shaped basin that is bounded by basement highs to the northwest, southwest, and northeast (Fig. 5). Based on analysis of seismic records, maximum depths to basement are estimated to be over 7,000 m near the center of the basin (Fig. 5). Numerous lesser basement highs and lows occur throughout the main basin; evidence from seismic-reflection surveys indicates that these are primarily fault-controlled horst and graben structures.

In general, basement topography was established by fault systems activated during middle and late Miocene time. Throughout the history of filling, however, the basin apparently continued to subside along a major fault zone related to a hinge line mapped on the northwestern ends of seismic profiles 8, 9, 12. This hinge line was a controlling factor for much of the sedimentation that infilled the basin from the northwest.

Profile 8 extends furthest to the northwest and is located directly northwest from the Hód–1 well. Four major seismic sequences can be mapped within the sedimentary section along the central and southeastern part of the profile. The sequence boundaries are difficult to trace northwest of the major fault zone at the hinge line. The basalmost sequence is labeled D_4. At the southeast end of the profile, reflectors within D_4 onlap the horizon that represents the basement surface. Sequence D_5, which unconformably overlies D_4 in a downlap relation, exhibits a strong oblique to sigmoid progradation pattern at its upper boundary near the center of the record section. Internal reflectors dip at an angle of about 8 degrees. Further up in the section, sequence D_5 is onlapped by seismic sequence D_6, which, in turn, is onlapped by the uppermost sequence *LMT* (delta plain facies in which depositional environments vary from shallow *l*ake, fluvial and *m*arsh to possible *t*errestrial soils).

The oblique to sigmoid progradation pattern of sequence D_5 is interpreted as indicating deltaic sedimentation. The undaform reflectors (topset beds) are interpreted as representing delta plain facies; the fondaform reflectors (bottomset beds) and the clinoform reflectors (inclined beds) are interpreted as representing prodelta and delta front facies, respectively. The apparent direction of sedimentation was to the southeast, with sediments derived from the northwest. The clinoform reflectors dip at an angle of about 8 degrees. The vertical

distance from undaform to fondaform reflectors indicates that the water depths were about 800 m at the time of deposition.

Because this seismic profile is located directly updip from the Hód–I well, a general correlation between these seismic sequences and some of those mapped on profile 6 can be inferred. The upper part of sequence *LMT* probably correlates to sequence *V*: the seismic character of high-amplitude, intermittent reflectors is similar. The lower part of sequence *LMT* most likely represents the updip continuation of sequence *IV* and consists, therefore, of delta plain facies that represent depositional environments which varied from shallow lake, fluvial, and marsh to terrestrial soils. The gentle divergence of *LMT* reflectors (that is, thickening of beds in a basinward direction) seen on profile 8 (in contrast to the parallel bedding seen on profile 6) probably reflects the fact that the central part of the basin was subsiding as a unit and at a faster rate than the surrounding basin margins.

Sequence D_6 is correlated tentatively with sequence *III*, at least with its upper part that contains slumped strata with a high sandstone content. The absence of coherent reflections in D_6 suggests that the sequence has a high sandstone content or that it may represent slumped strata. On profile 8 sequence D_6 appears to have been deposited at the base of a slope formed by sequence D_5 and older deltaic units. Basal reflectors of D_6 are observed to onlap sequence D_5. In contrast, the basal reflectors of sequences D_5 and D_4 (as well as basal reflectors in older sequences mapped on nearby profiles) terminate against bottom sequence boundaries in a downlap pattern. As will be discussed later in more detail, the onlap pattern of D_6 is inferred to represent a destructive phase. This unit may have been deposited during a short-lived transgressive phase or, perhaps, it was deposited following a period of accelerated lake shoaling. In the latter case, a drop in lake level would have exposed sediments deposited on a steep slope, and remobilization of these sediments could have caused slumping and a widespread distribution of sands towards the center of the basin. At the southeast end of profile 8, sequence D_6 thickens where the unit overwhelmed the basement high at the Felgyő–I well.

On *profile 9* the deltaic character of sequence D_5 and underlying units is more pronounced. Although the correlation between sequence D_4 on seismic profile 8 and D_4(?) on profile 9 must be considered tentative because of the scarcity of seismic data, the units appear to have similar seismic characteristics and to occupy the same stratigraphic position relative to the onlapping D_6 sequence. This would suggest that they are nearly equivalent in age and probably represent the same delta or deltaic system. Comparison of the two profiles indicates, however, that D_5(?) (mapped on profile 9) may be equivalent (in terms of time and source) only to the upper part of D_5 (mapped on profile 8).

On seismic profile 9, at least four depositionally related seismic sequences older than sequence D_5 can be mapped. These are labeled, from youngest to oldest: D_4(?), D_3, D_2, and D_1. Basal reflectors in each of the units terminate against the underlying sequence boundary in a downlap pattern suggestive of

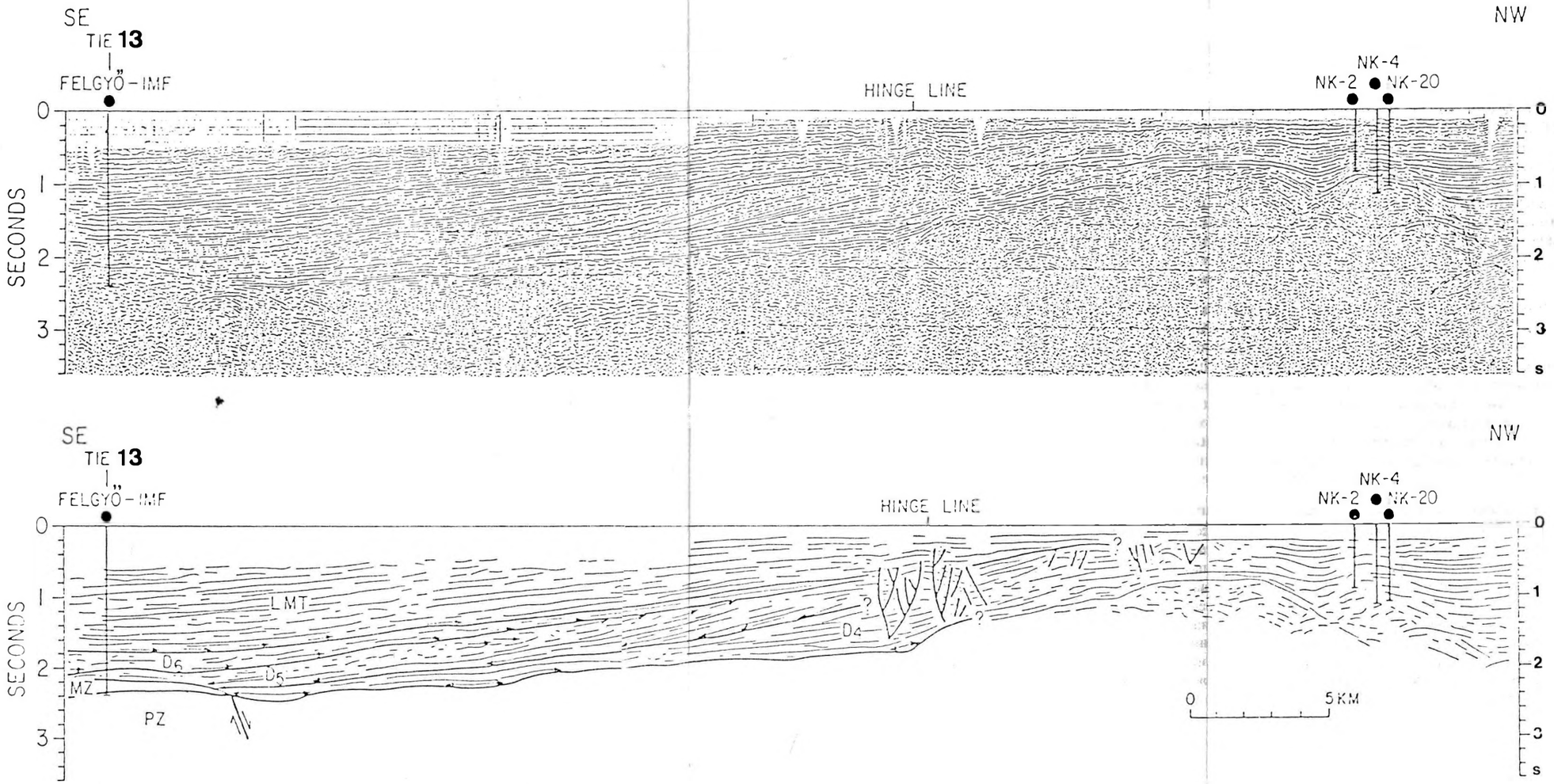
SE
TIE 13
FELGYÖ-IMF
HINGE LINE
NK-4
NK-2
NK-20
NW
SECONDS
0
1
2
3
s
LMT
D6
D5
D4
MZ
PZ
0
5KM

Fig. 8. Seismic profile No. 8. Heavy lines indicate sequence boundaires. D_6, D_5 D_4, and *LMT* designate seismic sequences discussed in text. Question marks at sequence boundaries indicate furthest extent to which boundary could be mapped. Arrows show relation of internal reflections to sequence boundaries. Well names corresponding to abbreviations used in figure are given in Table II. *MZ* and *PZ* represent Mesozoic and Paleozoic rocks, respectively. Question mark following a seqence designation indicates that the sequence equivalency is based on stratigraphic position or other inference, rather than a cross check from intersecting seismic profiles. The term TIE 13 indicates that seismic profile 13 intersects at point shown. Location of profile is shown in figure 4. Major subsidence is inferred to have occurred basinward of the hinge line

8. ábra. 8. sz. szeizmikus szelvény. A rétegösszlet-határokat vastag vonalak jelölik. D_6, D_5, D_4 és *LMT* a szövegben részletezett szeizmikus rétegösszleteket jelölik. A rétegösszlet-határoknál lévő kérdőjelek jelölik a legtávolabbi pontot, ameddig az ill. határ követhető. A nyilak a rétegösszleteken belüli reflexiók kapcsolatát mutatják a határokkal. A fúrások neveit, ill. ezek rövidítéseit a II. táblázat tartalmazza.*MZ*, ill. *PZ* a mezozoos, ill. paleozoos képződményeket jelöl. A rétegösszlet-végződésekhez kapcsolt kérdőjelek pedig arra utalnak, hogy a szekvencia-azonosítás inkább a rétegtani helyzetre és egyéb kapcsolatokra alapozott, kevésbé a keresztező szelvényeken végzett azonosításra. A TIE 13 megjelölés mutatja a szelvénykereszteződés helyét. A szelvények helyzete a 4. ábrán látható. A fő medencesüllyedés a lehajlási tengelytől (hinge line) DK-re történt

Рис. 8. Сейсмический профиль 8. Разделы серий проведены жирными линиями. D_6, D_5, D_4 и *LMT* обозначают рассмотренные в тексте сейсмические серии. Вопросительными знаками у границ толщ обозначаются наиболее удаленные точки, до которых данная граница может быть послежена. Стрелками показаны связи отражений в пределах отдельных серий с разделами. Наименования скважин или их сокращения даны в таблице II. *MZ* и *PZ* обозначают мезозойские и палеозойские формации соответственно. Вопросительные знаки у границ серии указывают на то, что отождествление серии основано скорей на стратиграфическом положении или иных соотношениях, и в меньшей степени на совпадении по пересекающимся профилям. Обозначением TIE 13 показано место пересечения профилей. Размещение профилей приведено на рис. 4. Основное прогибание в пределах бассейна имело место к ЮВ от линии перегриба (hinge line)

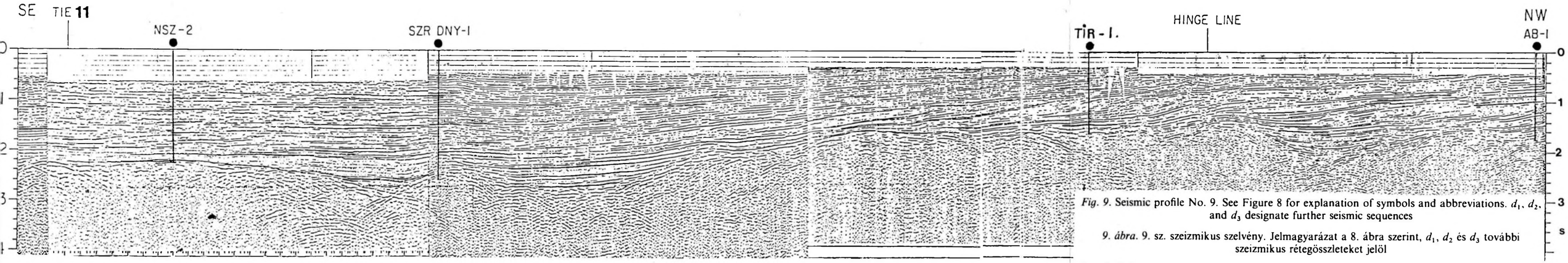

Fig. 9. Seismic profile No. 9. See Figure 8 for explanation of symbols and abbreviations. d_1, d_2, and d_3 designate further seismic sequences

9. ábra. 9. sz. szeizmikus szelvény. Jelmagyarázat a 8. ábra szerint, d_1, d_2 és d_3 további szeizmikus rétegösszleteket jelöl

Рис. 9. Сейсмический профиль 9. Условные обозначения по рис. 8. d_1, d_2, и d_3 обозначают дальнейшие сейсмические серии

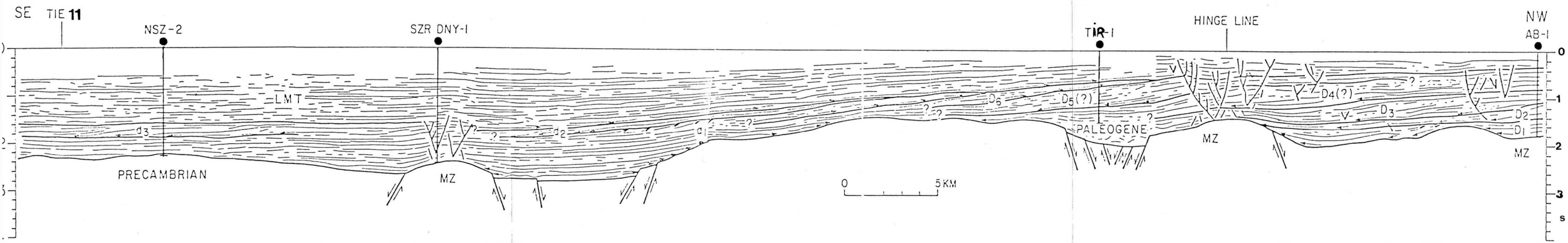

deltaic sedimentation. These units, together with D_5, are interpreted as representing a stacked deltaic system that prograded from the northwest and filled the subsiding basin to a short distance southeast of the hinge line. Sequences D_1–D_5 (supersequence) are inferred to be equivalent to sequence *II* and the lower part of sequence *III* mapped on *profile 10* near the Hód–I site. In proximal settings, this supersequence would be represented by deltas; whereas, in distal settings, this unit would be represented by turbidites (sequence *II*) or prodelta facies (basal part of sequence *III*). The thick turbidite deposits, represented by seismic sequence *I* at the Hód–I well site, may be age equivalent to the basal part of supersequence D_1–D_5 or they could represent still older turbidite-fronted deltas located north of profile 9.

Three seismic sequences overlying sequence D_6 on profile 9 are labeled, from oldest to youngest, d_1, d_2, and d_3. Whereas the reflectors of sequence d_1 are configured in an oblique progradational pattern, the reflectors of sequences d_2 and d_3 show a sigmoid progradational pattern. The sigmoid progradational sequences d_2 and d_3 are more likely to represent sediments deposited in a low-energy environment [SANGREE–WIDMIER 1978]. The considerable upbuilding of the undaform deposits, commonly interpreted as a reflection of rising sea or lake level, probably reflects a high rate of basin subsidence as compared to the sediment influx rate. The clinoform beds dip at an angle of about 5 degrees and the vertical distance between the undaform (topset) and fondaform (bottomset) beds indicates deposition in water depths of 200 m. As compared to sequence d_1, fine-grained clastic sediments probably dominate in sequences d_2 and d_3 because of deposition in a low-energy environment and may represent delta interlobe areas as reported by BERG [1982].

Sequences d_1, d_2, and d_3, as well as sequence *IV* mapped at the Hód–I well site, are believed to be part of a supersequence of shallow water, stacked deltas that prograded southeastward. This equivalency (between the deltas on profile 9 and those mapped, as sequence *IV*, on seismic profile 6) is more in a sense of time and stratigraphic position rather than of deltas. The geographic distance (35 km), however, between profiles 9 and 6 does not preclude the possibility of equivalent deltas or delta systems. Stratigraphically, the two units occupy the same position in the sedimentary rock column, represent sedimentation from the northwest, and were deposited in water depths of 200–300 m.

Sequence *LMT* is readily distinguishable on profile 9 by its characteristic reflection pattern of high-amplitude, intermittent refectors and by the strong onlap pattern at its base. The onlap pattern associated with this sequence is interpreted as indicating more widespread lake conditions. The more widespread lake conditions during deposition of *LMT*, however, must have been coupled with progressive shoaling and eventual disapperance of the Pannonian lake. This conclusion is based on core analyses which indicate that sequence *LMT* represents depositional environments that mark shallower water conditions in comparison to the depositional environments represented by underlying sedimentary rock units. The same characteristics can be observed in SW–NE direction on *profile 11*.

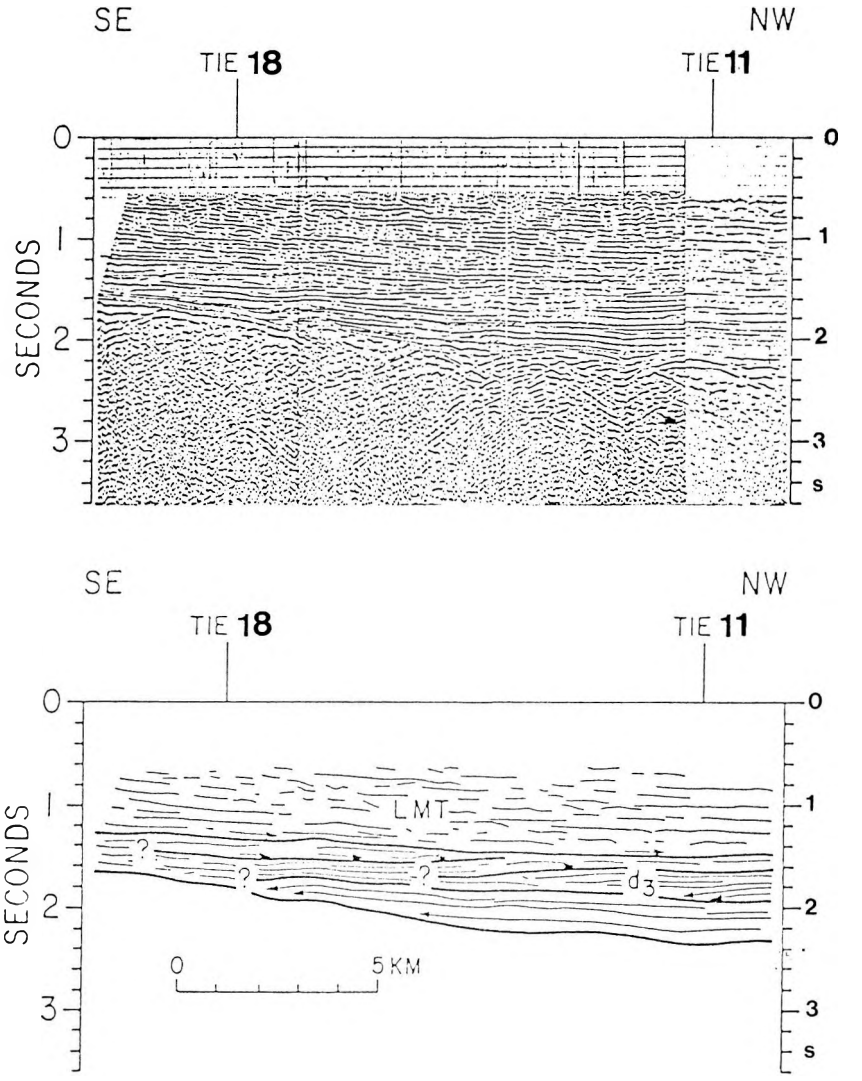

Fig. 10. Seismic profile No. 10. See Figures 8 and 9 for explanation of symbols and abbreviations

10. ábra. 10. sz. szeizmikus szelvény. Jelmagyarázat a 8. és 9. ábra szerint

Рис. 10. Сейсмический профиль 10. Условные обозначения см. на рис. 8 и 9

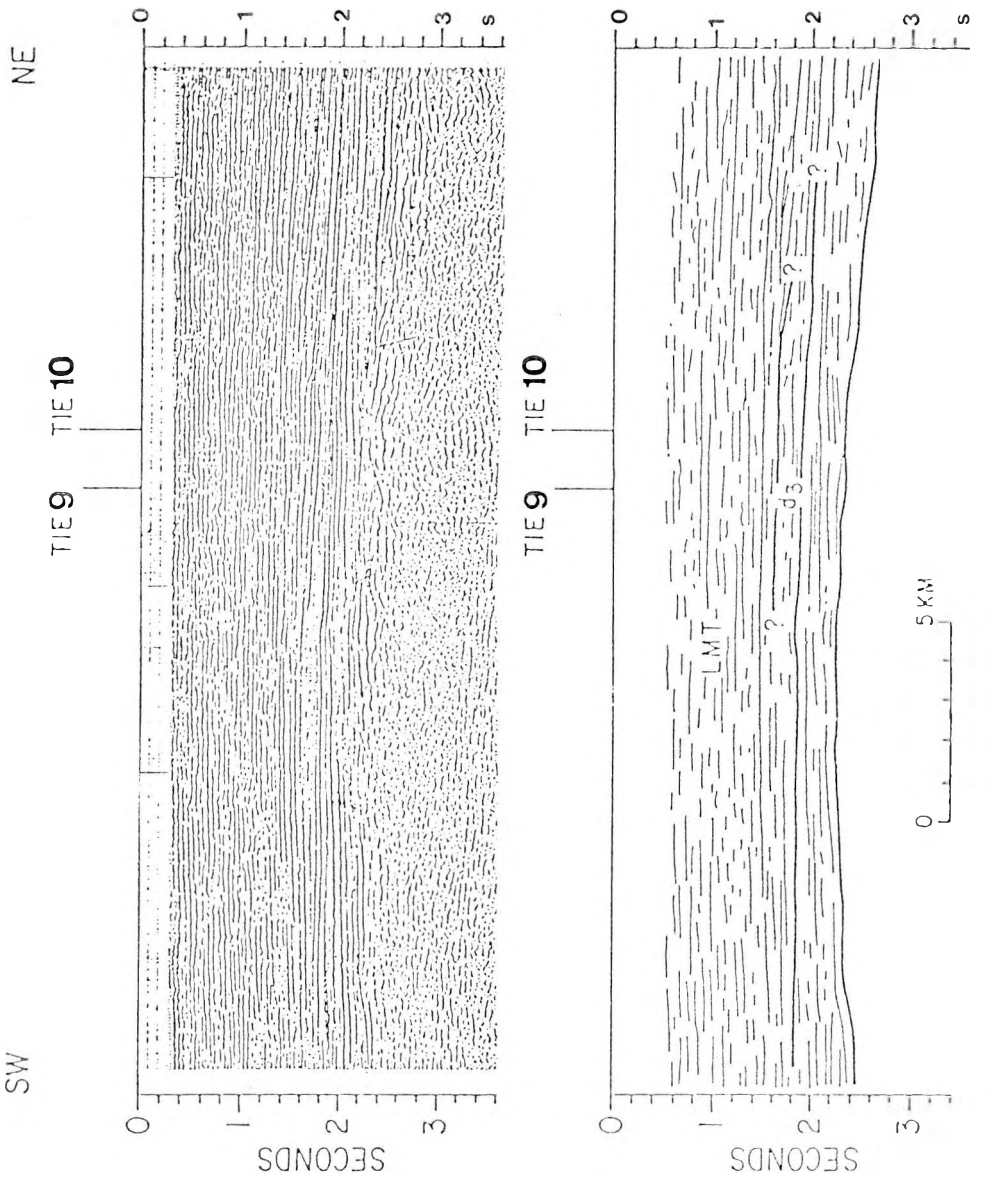

Fig. 11. Seismic profile No. 11. See Figures 8 and 9 for explanation of symbols and abbreviations

11. ábra. 11. sz. szeizmikus szelvény. Jelmagyarázat a 8. és 9. ábra szerint

Рис. 11. Сейсмический профиль 11. Условные обозначения см. на рис. 8 и 9

Most of the seismic units discussed thus far also can be recognized in similar stratigraphic positions on seismic *profile 12*. Seismic sequence D_5, which was mapped on profile 8 can be traced southwest along seismic *profile 13* to seismic profile 12, where the unit again is seen to represent deltaic sedimentation from the northwest that built upward over a large basement high. Sequence D_5 is overlain by D_6 which in turn is overlain by units d_1(?) and d_2(?), which are presumed to be equivalent to sequences d_1 and d_2 mapped on seismic profile 9.

The lateral continuity of units d_1 and d_2 can be seen on seismic *profile 14* which intersects profile 12. On profile 14 these units are combined into unit d_1d_2(?), and the combined unit can be traced a short distance southwest towards the basement high which bounds the basin to the west.

3.2 Northern Area

In the northern part of the study area, three short seismic profiles, 15–17, are available for analysis. The locations are shown in Figure 4. On these profiles, three seismic sequences can be mapped. The basal sequence that directly overlies the basement surface is inferred to represent turbidite deposits that grade upward to sandstone or sandy turbidites. This unit is believed to be related to progradational deltaic sedimentation from the north.

In the overlying sequence, progradation is towards the southwest on *profile 15* and towards the southeast on *profiles 16* and *17*. The general direction of sedimentation, therefore, was probably from a northerly direction. The difference in elevation between the undaform and fondaform beds suggests deposition in water depths of 200–300 m.

Fig. 12. Seismic profile No. 12. See Figures 8 and 9 for explanation of symbols and abbreviations

12. ábra. 12. sz. szeizmikus szelvény. Jelmagyarázat a 8. és 9. ábra szerint

Рис. 12. Сейсмический профиль 12. Условные обозначения см. на рис. 8 и 9

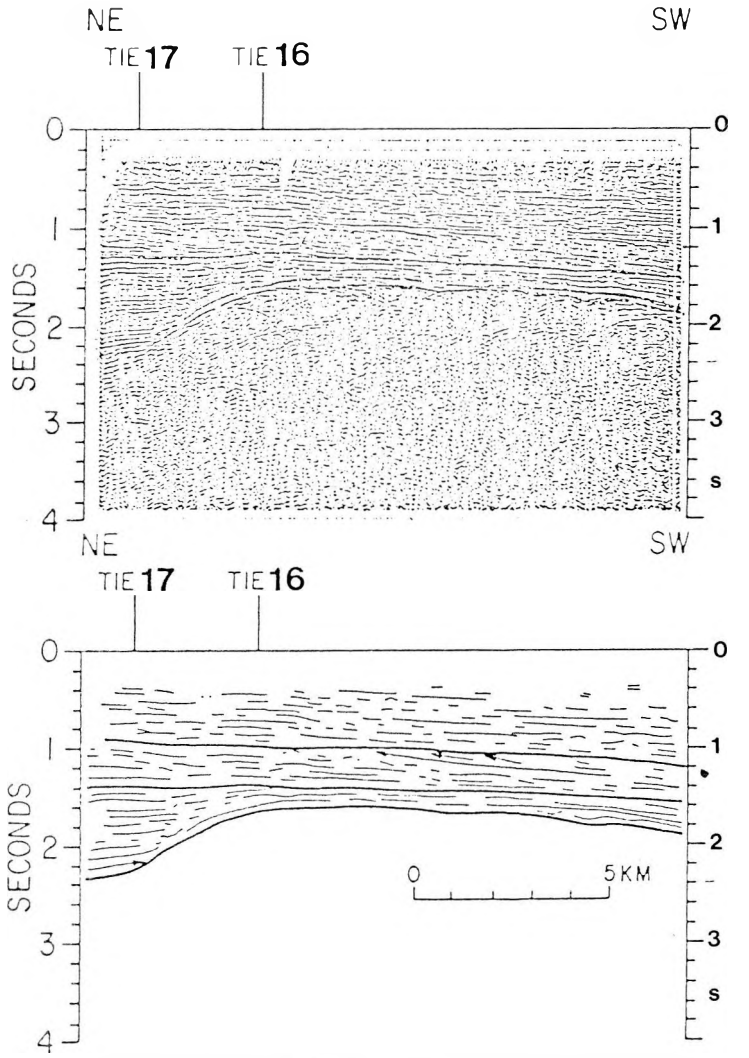

Fig. 15. Seismic profile No. 15. See Figures 8 and 9 for explanation of symbols and abbreviations

15. ábra. 15. sz. szeizmikus szelvény. Jelmagyarázat a 8. és 9. ábra szerint

Рис. 15. Сейсмический профиль 15. Условные обозначения см. на рис. 8 и 9

The uppermost sequence is presumed to be equivalent to sequence *LMT* and, therefore, represents delta plain facies; depositional environments varied from shallow lake, fluvial, and marsh to terrestrial soils.

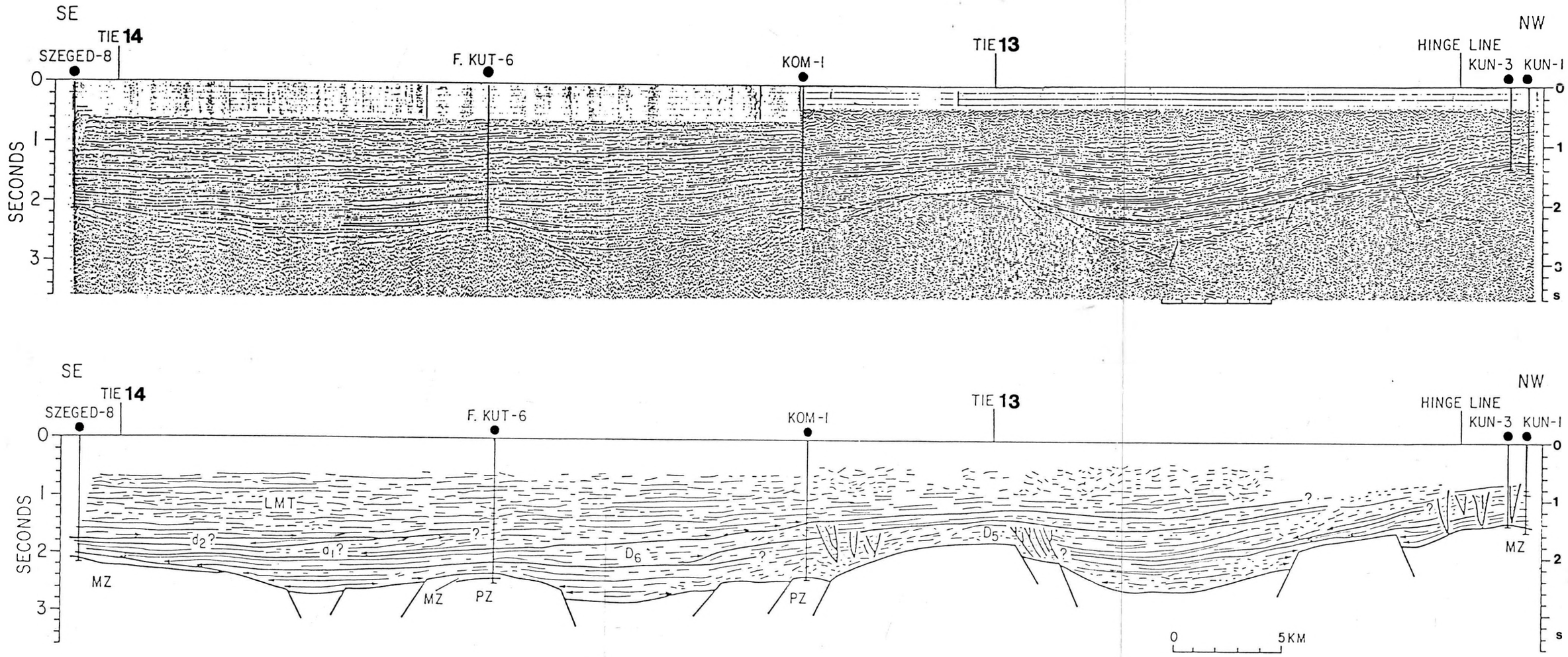
SE
NW
TIE 14
TIE 13
SZEGED-8
F. KUT-6
KOM-1
HINGE LINE
KUN-3
KUN-1
SECONDS
0
1
2
3
s
LMT
d_2?
a_1?
?
D_6
D_5
MZ
PZ
0
5KM

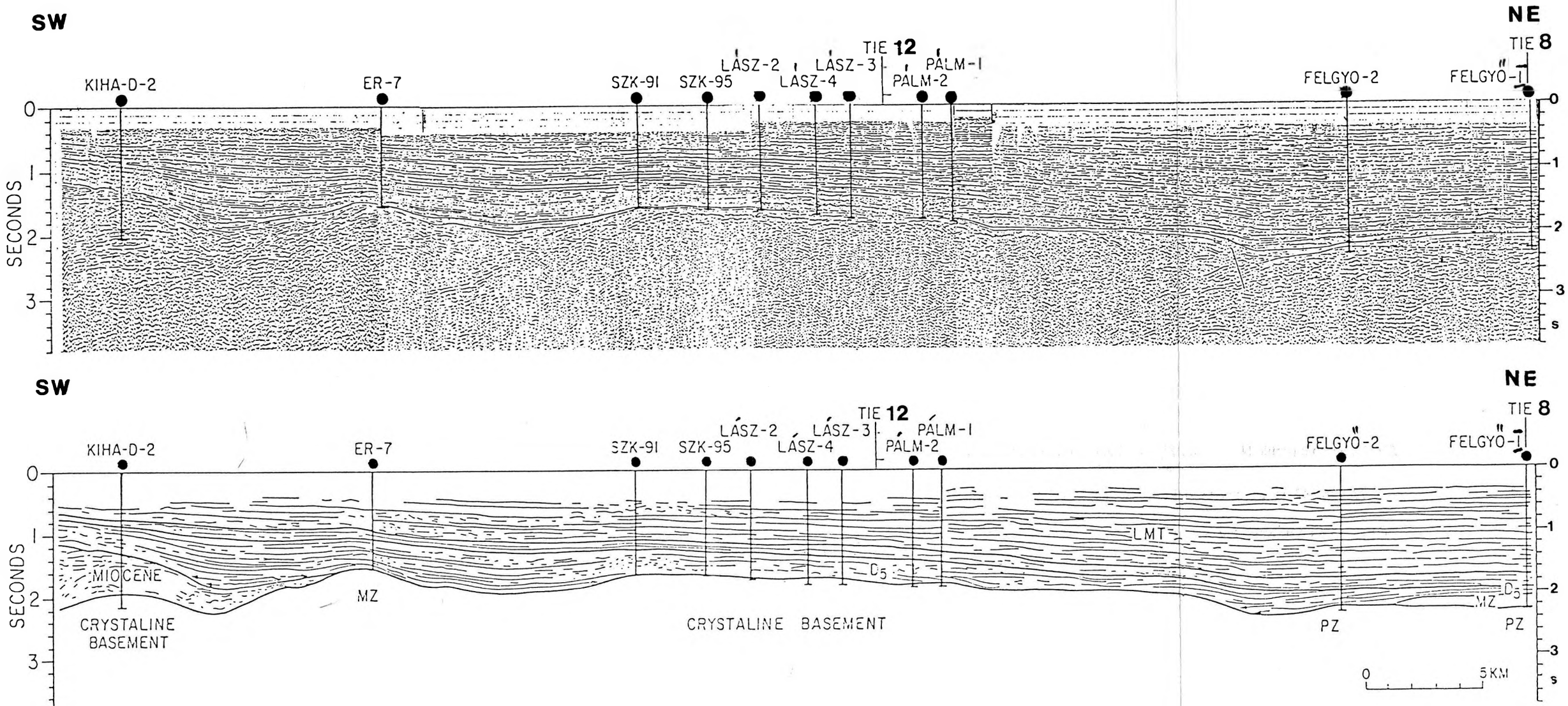
SW
NE
TIE 12
TIE 8
KIHA-D-2
ER-7
SZK-91
SZK-95
LÁSZ-2
LÁSZ-3
LÁSZ-4
PÁLM-1
PÁLM-2
FELGYÓ-2
FELGYÓ-1
SECONDS
0
1
2
3
s
SW
NE
TIE 12
TIE 8
KIHA-D-2
ER-7
SZK-91
SZK-95
LÁSZ-2
LÁSZ-3
LÁSZ-4
PÁLM-1
PÁLM-2
FELGYÓ-2
FELGYÓ-1
SECONDS
MIOCENE
MZ
LMT
D5
CRYSTALINE BASEMENT
CRYSTALINE BASEMENT
PZ
PZ
0
5KM

Fig. 13. Seismic profile No. 13. See Figures 8 and 9 for explanation of symbols and abbreviations

13. ábra. 13. sz. szeizmikus szelvény. Jelmagyarázat a 8. és 9. ábra szerint

Рис. 13. Сейсмический профиль 13. Условные обозначения см. на рис. 8 и 9

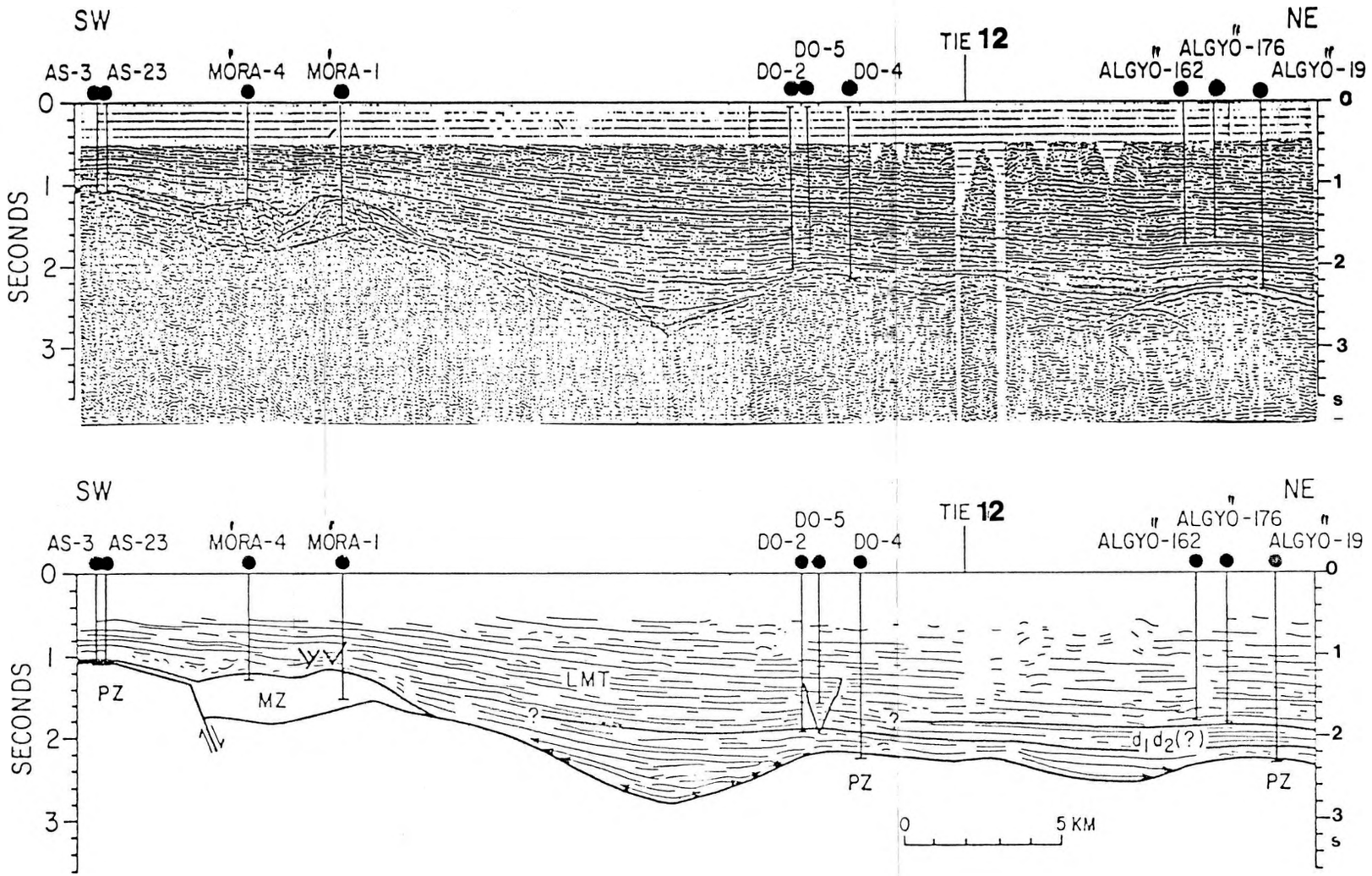
SW
NE
AS-3
AS-23
MORA-4
MORA-1
DO-2
DO-5
DO-4
TIE 12
ALGYO-162
ALGYO-176
ALGYO-19
SECONDS
0
1
2
3
s
PZ
MZ
LMT
?
$d_1 d_2$(?)
0
5 KM

Fig. 14. Seismic profile No. 14. See Figures 8 and 9 for explanation of symbols and abbreviations

14. ábra. 14. sz. szeizmikus szelvény. Jelmagyarázat a 8. és 9. ábra szerint

Рис. 14. Сейсмический профиль 14. Условные обозначения см. на рис. 8 и 9

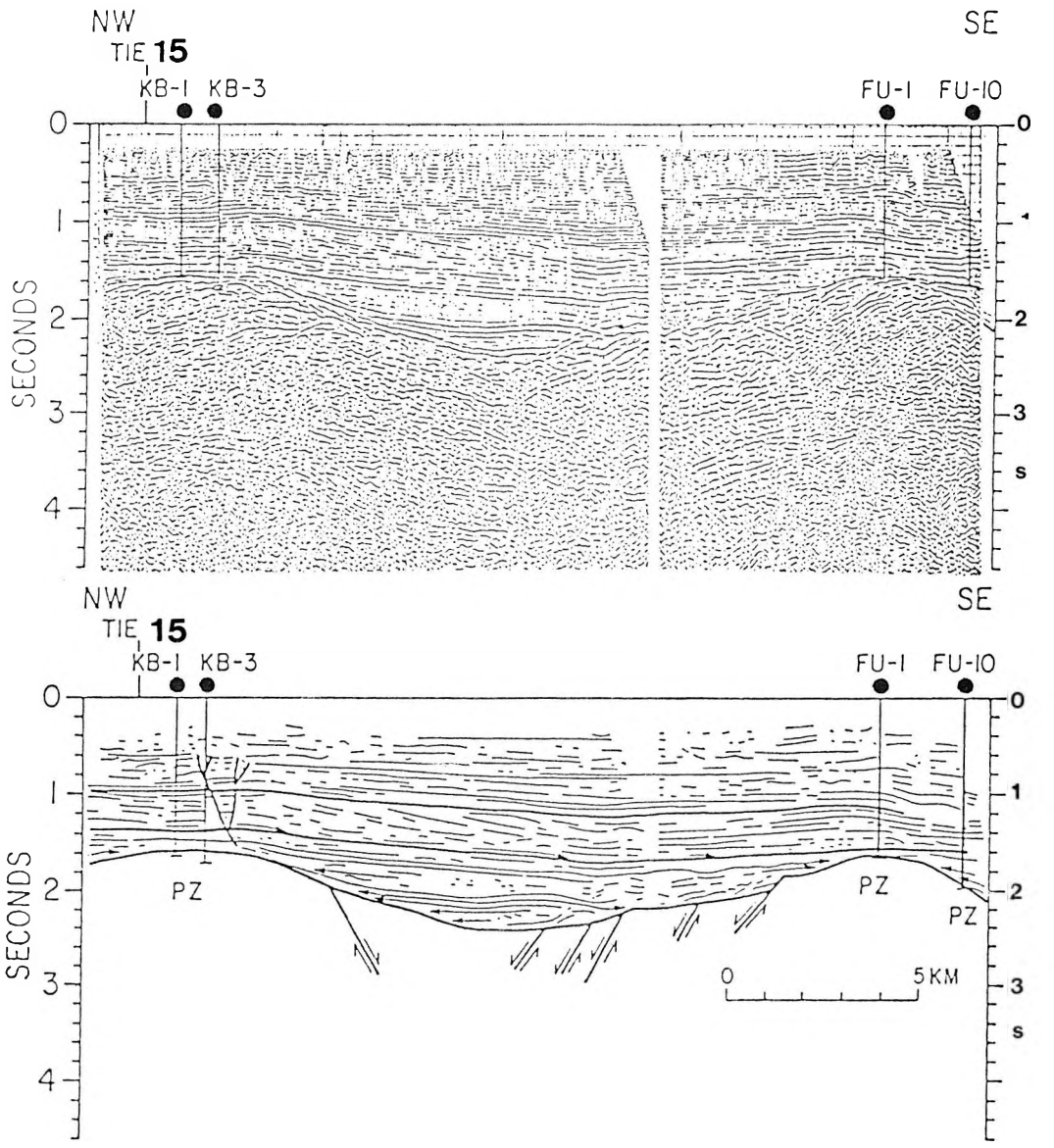

Fig. 16. Seismic profile No. 16. See Figures 8 and 9 for explanation of symbols and abbreviations

16. ábra. 16. sz. szeizmikus szelvény. Jelmagyarázat a 8. és 9. ábra szerint

Рис. 16. Сейсмический профиль 16. Условные обозначения см. на рис. 8 и 9

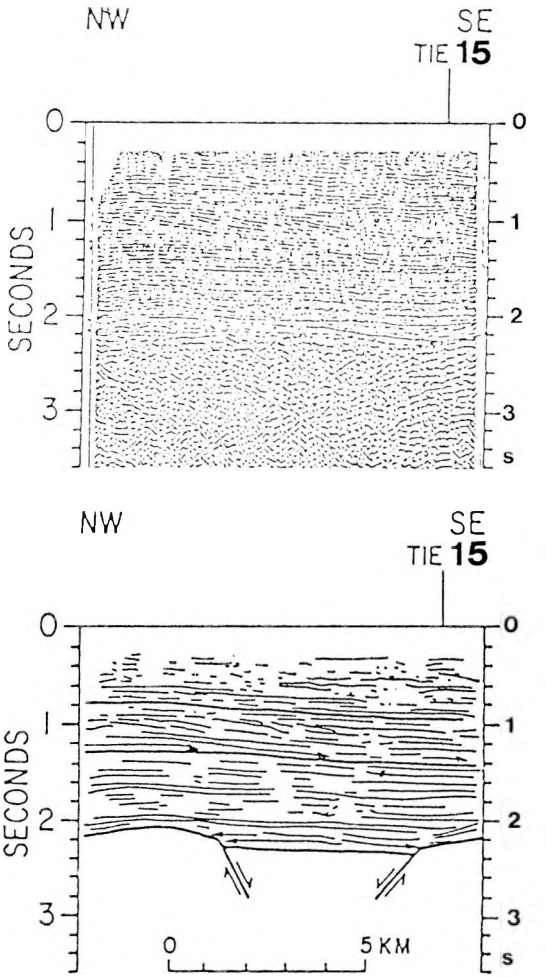

Fig. 17. Seismic profile No. 17. See Figures 8 and 9 for explanation of symbols and abbreviations

17. ábra. 17. sz. szeizmikus szelvény. Jelmagyarázat a 8. és 9. ábra szerint

Рис. 17. Сейсмический профиль 17. Условные обозначения см. на рис. 8 и 9

3.3 Eastern Area

Seismic profiles recorded in the eastern part of the studied area (Figs. 18–23) indicate that the sediments deposited in this area were derived from the north–northeast, transported by a large fluvial system or systems, and deposited as a series of large southwest prograding deltas that built upward a distance of several thousand meters. The seismic sequences, inferred to represent the oldest deltaic units, were mapped at the northeast end of seismic-reflection *profile 18* where four sigmoid progradational seismic sequences (labeled from lowest to highest, B_1–B_4,) are distinguishable. All four of the sequences are seen to pinch out against the northeast flank of a basement high centered near the K–9 well.

The character of the sequences above B_4 (B_5–B_8) are best exhibited on *profile 19*. The continuity of the seismic sequences between profiles 18 and 19 can be seen on *profile 20* which intersects profiles 18 and 19. Sequences B_5–B_8 are interpreted as representing a younger series of southwest-prograding deltas built over the basement high, against which the older system of stacked deltas (B_1–B_4) pinch out. The seismic units are inferred to represent deposition in water depths of about 800–900 m based on the vertical distance between the fondaform and undaform zones where measured on good, continuous reflectors.

Between the base of unit B_1 and the horizon inferred to be the top of the basement rocks (Fig. 18), a thick basal-most seismic sequence, which extends vertically from about 2.4 sec to about 3.6 sec, fills a relatively deep basin from a depth of about 5,500 m to about 3,200 m. Near the center of the basin, strong parallel reflectors (labeled *M*, Fig. 18) can be traced over long distances. On the flank and in the deepest part of the basin, however, the pattern of reflections (labeled *T*) is chaotic to wavy to almost reflection free. The strong, continuous reflections probably represent deep-water marls deposited in a low-energy environment; whereas, mass-transport, slump and creep, and related higher energy turbidity processes are thought to be responsible for the transportation and deposition of the sediments represented by the chaotic to wavy reflection pattern. Core data from the *T* sequence in the Derecske Basin indicate that it consists chiefly of tectonic breccia derived from local basement rocks. The age of this complex is probably Badenian which corresponds to the opening (pulling apart) of the Derecske Basin (written communication, F. Horváth, Eötvös University, Budapest, 1985).

At the Bihu–NY–2 well on profile 18, the lower clinoform and fondaform zones of sequence B_8 are seen to merge into a thick, chaotic to mounded seismic facies that directly overlies the inferred basement horizon on the northeast flank of a shallow basin. B_8 would appear to represent slumped deposits. The stratigraphic position of sequence B_8 suggests that it is equivalent (in time) to seismic sequence D_6 mapped in the southwestern area. Both sequences are inferred to contain slump deposits and to represent the culmination of an early period of delta construction in the Pannonian Basin. This unit could be related to a

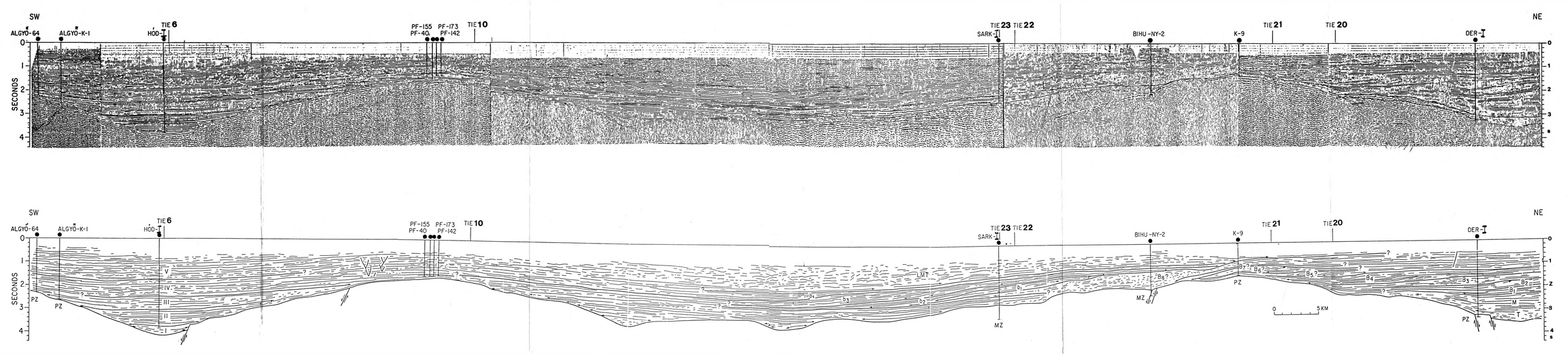
SW
NE
ALGYÖ-64
ALGYÖ-K-I
HÓD-I
TIE 6
PF-155
PF-40
PF-173
PF-142
TIE 10
SARK-I
TIE 23
TIE 22
BIHU-NY-2
K-9
TIE 21
TIE 20
DER-I
SECONDS
0
1
2
3
4
V
IV
III
II
I
PZ
MZ
LMT
D_1
D_2
D_3
D_4
B_1
B_2
B_3
B_4
B_5
B_6
B_7
B_8
M
T
0 5KM

Fig. 18. Seismic profile No. 18. Note that seismic profile 18 extends through both the southwestern and eastern study areas (see text and figure 4 for a discussion of these areas); the designation of seismic sequences on profile 18 therefore, is different from that used on figures 8–14. The seismic sequence designations shown on profile 18 correspond to those used in figures 6 and 19–23

18. ábra. 18. sz. szeizmikus szelvény. Megjegyzendő, hogy a 18. sz. szelvény áthalad a kutatási terület DNy-i és K-i részén is (l. a 4. ábrát és a szöveget), a 18. ábrán lévő rétegösszlet-jelölések ezért eltérnek a 8–14. ábrán jelölt rétegösszletekétől és egyeznek a 6. és 19–23. ábrán láthatókkal

Рис. 18. Сейсмический профиль 18. Необходимо отметить, что профиль 18 пересекает ЮЗ и В части изучаемого района (см. рис. 4 и текст), в связи с чем обозначения серий на рис. 18 отличаются от таковых на рис. 8–14. Обозначения серий на рис. 18, совпадают с обозначениями на рис. 6 и 19–23

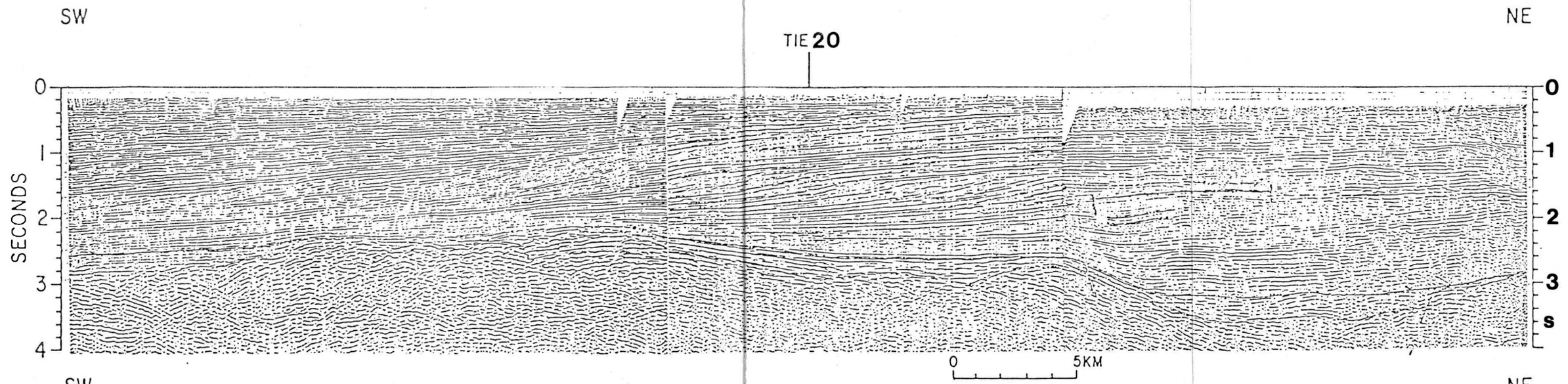
SW
NE
TIE 20
SECONDS
0
1
2
3
4
s
0
5KM

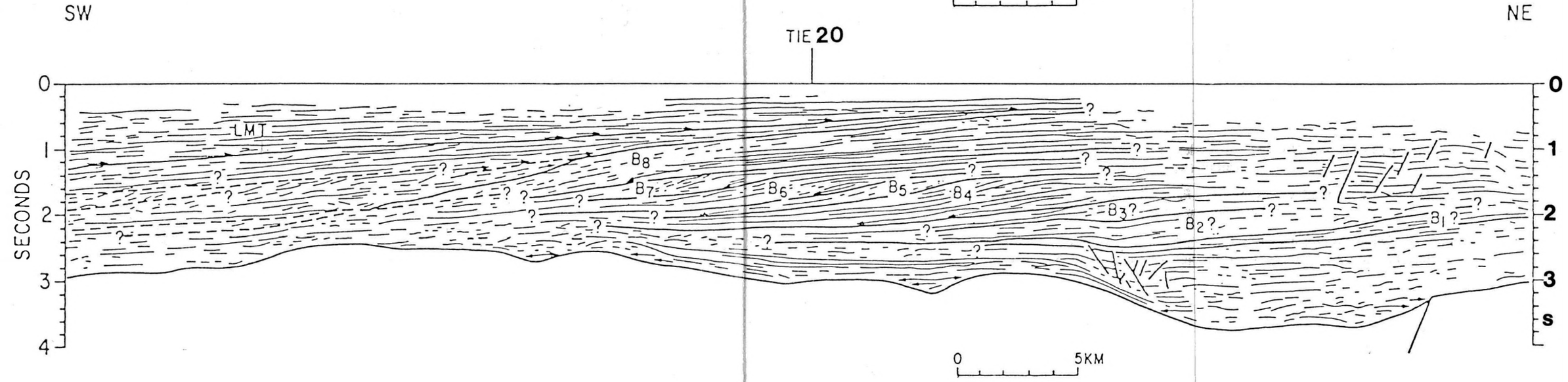
SW
NE
TIE 20
SECONDS
LMT
B8
B7
B6
B5
B4
B3?
B2?
B1?
0
1
2
3
4
s
0
5KM

Fig. 19. Seismic profile No. 19. $B_1 \ldots B_8$ designate seismic sequences. For explanation of other symbols, see previous figures

19. ábra. 19. sz. szeizmikus szelvény. $B_1 \ldots B_8$ további szeizmikus rétegösszleteket jelöl. Az összes többi jelölés az előző ábrákéval azonos

Рис. 19. Сейсмический профиль 19. $B_1 \ldots B_8$ обозначают дальнейшие сейсмические серии. Все остальные условные обозначения совпадают с обозначениями на предыдущих рисунках

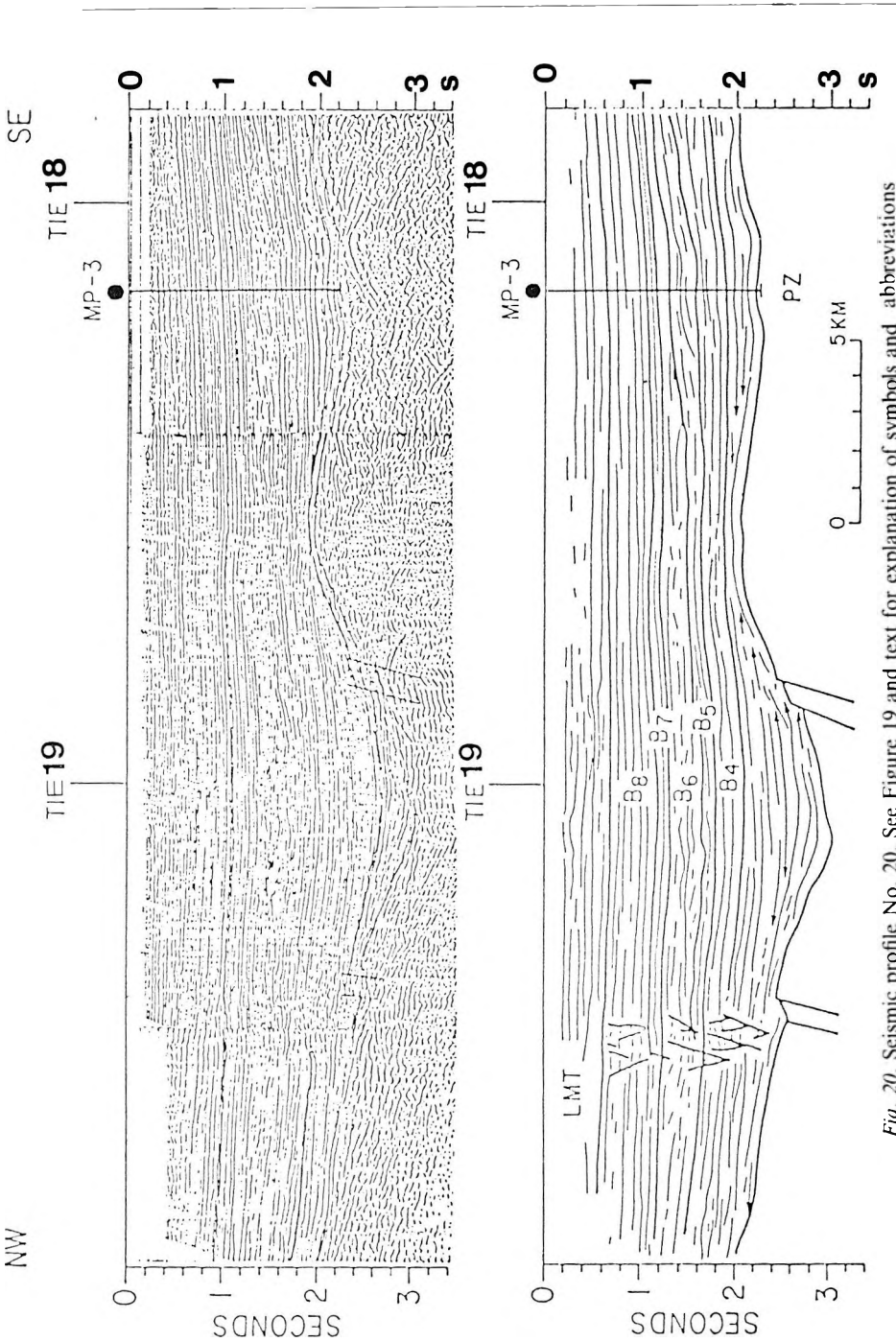

Fig. 20. Seismic profile No. 20. See Figure 19 and text for explanation of symbols and abbreviations

20. ábra. 20. sz. szeizmikus szelvény. Jelmagyarázat a 19. ábra szerint

Рис. 20. Сейсмический профиль 20. Условные обозначения см. на рис.19

shoaling of the lake. A change in lake level would have exposed sediments previously deposited on a steep slope. These exposed sediments could have been remobilized in front of an advancing delta system, and slumping and funneling of sediments through channels allowed sedimentation to bypass the previous slope. Apparently, the deltaic system (B_1–B_8) prograded southwestward, filling much of the basin in the vicinity of the Der–I well. The early deltas pinch out where they encountered a basement high northeast of the K–9 well; later deltas, however, continued to build upward and overwhelmed this basement high.

In some areas, turbidite flows into topographic lows are believed to have occurred prior to or concurrent with delta construction. A possible example is recorded on the southwest end of profile 19 where a series of unconformities are shown by dashed lines. Internal reflections have a chaotic to broken appearance, and noticeable onlap of the lower clinoform beds of the deltaic sequences occurs. Although onlap usually is associated with low-energy depositional environments, the truncation of reflectors and chaotic appearance of reflections indicate deposition in a relatively high energy environment. The sediments represented by the seismic units at the southwest end of profile 19 may be turbidites and may have been derived from a direction roughly perpendicular to the profile (probably from the northwest). The interfingering of the unit boundaries indicates that this would have been concurrent with delta construction to the northeast. It is also possible that the seismic units at the southwest end of profile 19 represent slumped deposits from the large deltas seen at the center of the profile. The numerous angular unconformities, however, suggest erosion by downslope movement or turbidite flows.

Although the major direction of sediment influx during the construction of the stacked delta system B_1–B_8 was from the northeast, minor(?) amounts of sediments also were derived from local basement highs to the east. This conclusion is based on inspection of *profile 21* where seismic sequences, which are tentatively believed to be time correlative to sequences B_5–B_8, are mapped. Here the chaotic seismic character of the internal reflectors suggests downslope movement of sediments from local basement highs by slump and creep and associated gravitational processes.

The youngest deltaic system in this area is represented by seismic sequences b_1–b_4, which are mapped near the center of profile 18 and on *profile 22*. These sequences are similar in seismic character to sequences d_1–d_4 (southwestern area) and suggest deposition in relatively shallow water depths. As indicated by the dip of reflectors in the clinoform zones on both profiles 18 and 22 they appear to represent a continuation of sedimentation derived from the north or northeast following deposition of the sediments represented by unit B_8. Reflectors in the undaform zones of these sequences appear to onlap sequence B_8. This onlap in the undaform zones also appears to have been concurrent with downlap of reflectors in the fondaform zones. The concurrence of onlap and downlap suggests that an abundance of fluvial sediments were supplied while subsidence of the basinal areas continued.

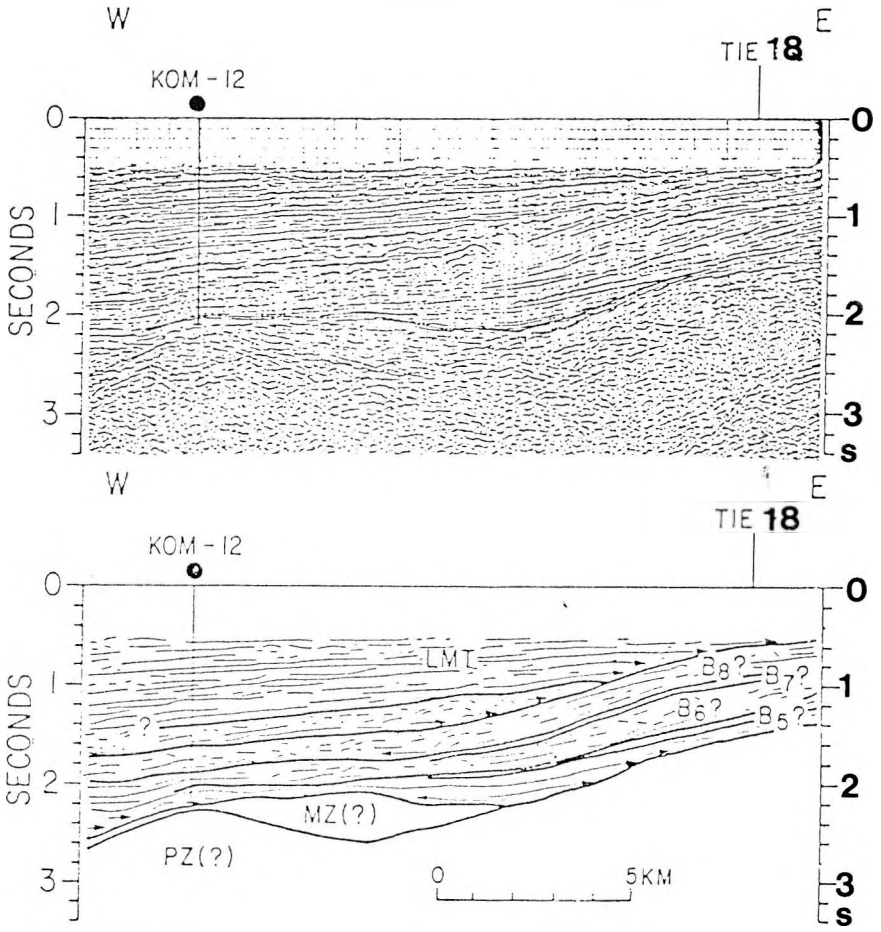

Fig. 21. Seismic profile No. 21. See Figure 19 and text for explanation of symbols and abbreviations

21. ábra. 21. sz. szeizmikus szelvény. Jelmagyarázat a 19. ábra szerint

Рис. 21. Сейсмический профиль 21. Условные обозначения см. на рис. 19

Infilling of basinal areas during deposition of sequences B_1–B_8 is believed to have occurred at a faster rate than basinal subsidence. This is evidenced by the fact that delta system b_1–b_4 was deposited in water depths of 200–400 m compared to water depths of 800–900 m for the deposition of B_1–B_8. Whether this reflects a change in subsidence rates, a change in sediment supply rates, or a combination of both is not known. One might speculate, however, that subsidence rates were greatest during the basin's early history and that they gradually decreased through time as a result of crustal cooling (a generally held concept).

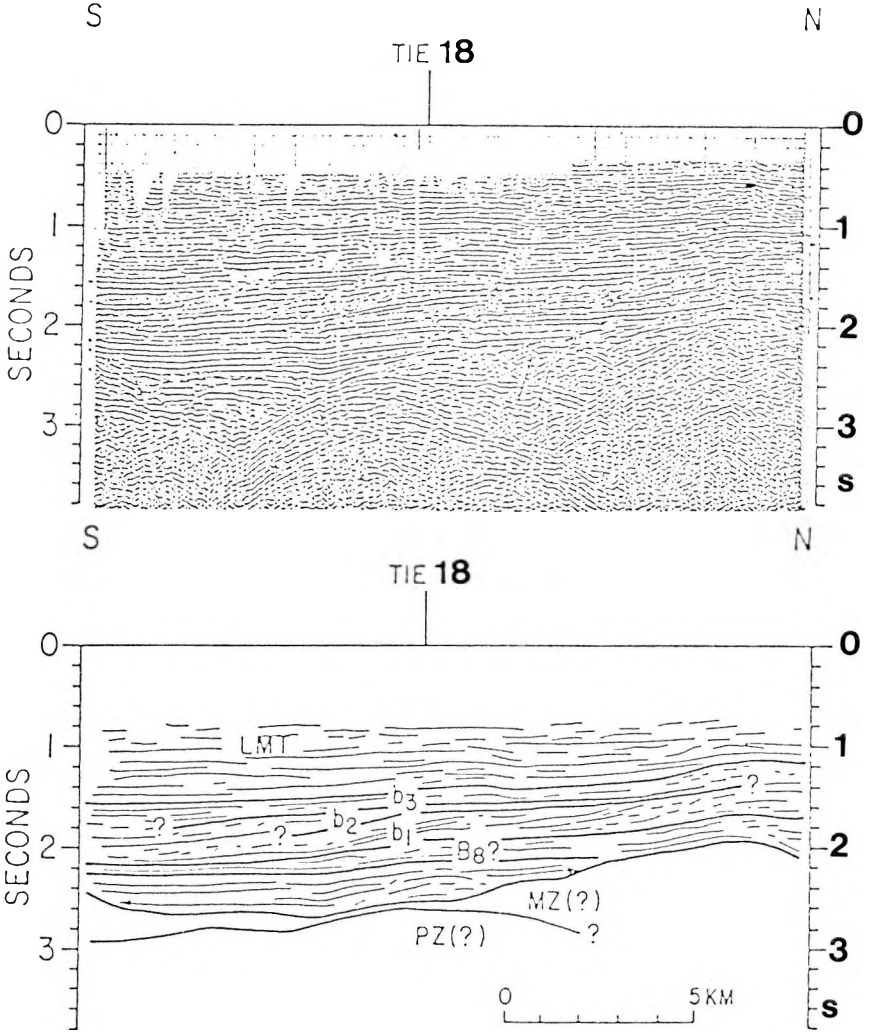

Fig. 22. Seismic profile No. 22. b_1, b_2, b_3 designate further seismic sequences. For explanation of other symbols, see previous figures

22. ábra. 22. sz. szeizmikus szelvény. Jelmagyarázat a 19. ábra szerint. b_1, b_2, b_3 további szeizmikus rétegösszleteket jelöl

Рис. 22. Сейсмический профиль 22. Условные обозначения см. на рис. 19. b_1, b_2, b_3 обозначают дальнейшие сейсмические серии

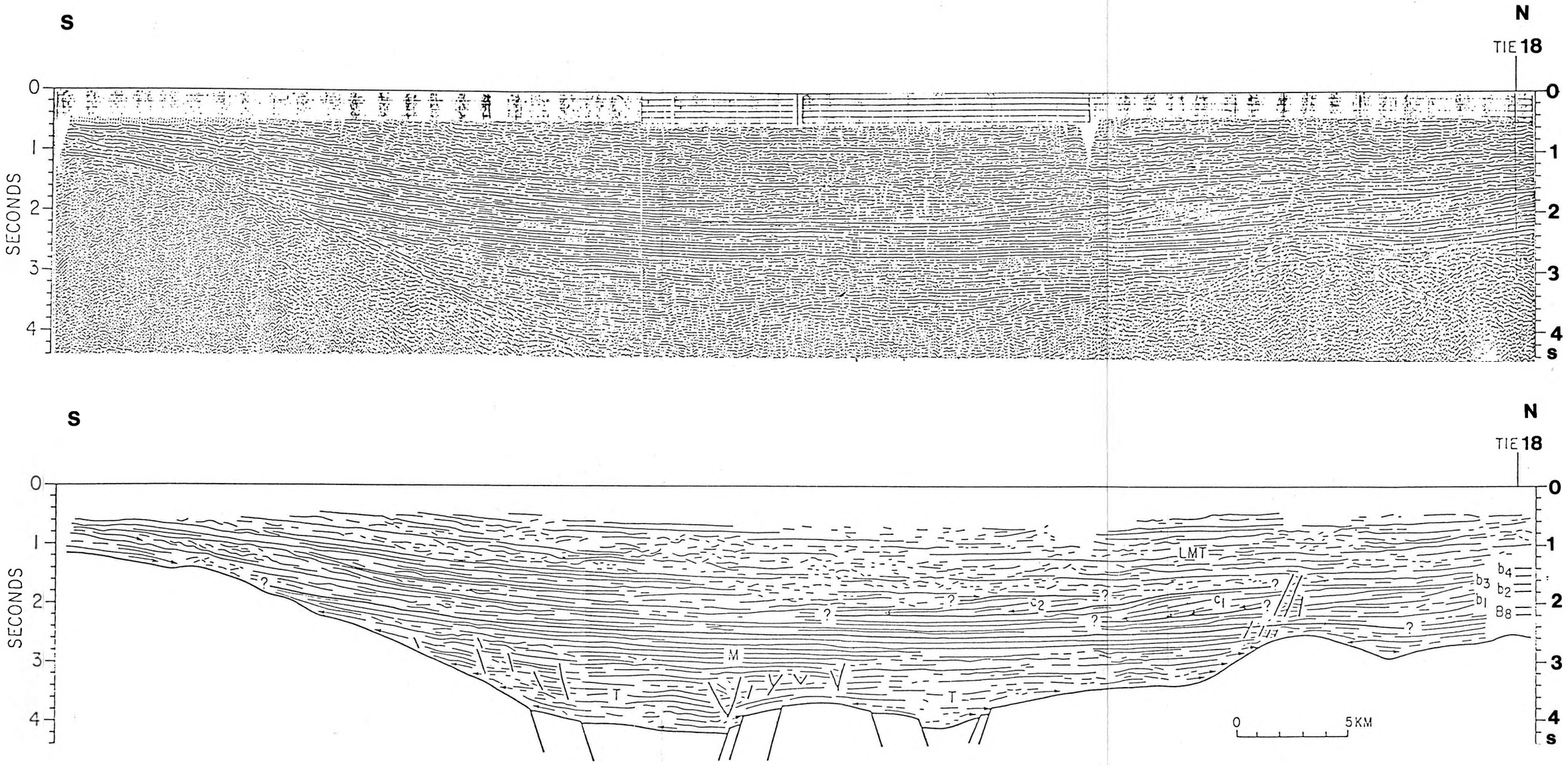
S
N
TIE 18
SECONDS
0
1
2
3
4
s
LMT
M
T
b_4
b_3
b_2
b_1
B8
c_1
c_2
?
0
5KM

Fig. 23. Seismic profile No. 23. c_1, c_2 designate further seismic sequences. For explanation of other symbols, see previous figures

23. ábra. 23. sz. szeizmikus szelvény. Jelmagyarázat a 19. ábra szerint. c_1, c_2 további szeizmikus rétegösszleteket jelöl

Рис. 23. Сейсмический профиль 23. Условные обозначения см. на рис. 19. c_1, c_2 обозначают дальнейшие сейсмические серии

Infilling of basinal areas by lacustrine deltas was widespread during deposition of sequences b_1–b_4 as evidenced by seismic sequences c_1 and c_2, which are mapped on *profile 23*. A comparision of the stratigraphic positions of sequences b_1–b_4 and c_1–c_2 can be made on profile 23 where sequences b_1–b_4 are shown on the far right side at the intersection with profile 18.

Following deposition of sequences b_1–b_4, infilling of topographic lows by shallow lake, fluvial, and marsh deposits and by terrestrial soils continued. This latest history is recorded in the uppermost seismic sequence *LMT* on profiles 18, 19, and 21.

4. Discussion

4.1 General

Figure 24 is a generalized diagram (not to scale) of a composite seismic record that shows the approximate configuration and relationship of seismic sequences mapped in the Pannonian Basin. In the diagram, the inferred source area of the sediments is located to the right, which would correspond to a northwest direction in the case of seismic profiles 8–12 and a northeast direction for profiles 18 and 19. From this diagram, the time relation between the various seismic sequences can be inferred.

The oldest seismic sequence, excluding unit *B* which represents basement rocks, is labeled $(TM)_1$. This unit represents basalmost basin fill and, near the central parts of the deep basins, is inferred to consist chiefly of marls with interbedded turbidites. These rocks probably grade laterally to clastic rocks that were derived from erosion of local basements highs.

Although inferred to be lithologically similar to $(TM)_1$, sequence $(TM)_2$ would appear to span a longer period of time and to contain younger sediments, at least in the upper part of the section, than does $(TM)_1$. This general time relation probably holds true for most of the subbasins in the Great Hungarian Plain area; that is, the basal turbidite–marl sections in subbasins of the Pannonian Basin become progressively younger in the upper part of the section with distance away from the sediment source area. This tendency would appear to be coupled with a thickening of the overall turbidite–marl section in the same general direction, and is related to the progressive infilling of the subsiding basin area by deltaic progradation from source areas to the northwest, north, and northeast. Inspection of Figure 24 indicates that the upper part of $(TM)_2$ represents distal deposits that are age equivalent to deltaic units seen to prograde from the right side of the figure to the left side.

Overlying sequence $(TM)_1$, are a series of seismic sequences characterized by prograding reflections (Fig. 24). These sequences, inferred to represent deltaic sedimentation, can be divided into at least two supersequences, A_1–A_7 and a_1–a_4. The former diagrammatically represents B_1–B_7 (mapped on profiles 18 and 19) and D_1–D_5 (mapped on profile 9); the second represents b_1–b_4 and

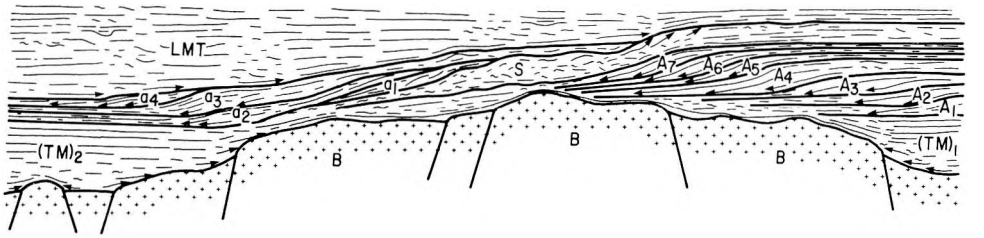

Fig. 24. General configuration of seismic sequences and supersequences in the Pannonian Basin of Hungary. Heavy lines are sequence boundaries. The lowest sequence (*B*), which represents basement rocks (Paleozoic or Mesozoic), is shown by a cross pattern. Lines within each sequence show general seismic character of internal reflectors. Arrows show type of discordance at sequence boundaries. Figure is not to scale and represents a composite of numerous seismic records. Sequences $(TM)_1$ and $(TM)_2$ represent turbidites and marls; A_1–A_7, stacked deltaic system deposited in water depths of 800–900 m; S, slumped strata deposited when delta system prograded across basin margin and probably related to shoaling of lake; a_1–a_4, delta system deposited in water depths of 200–400 m; *LMT*, shallow lake, marsh, and fluvial deposits and terrestrial soils, unit is inferred to have been deposited as the lake continued to shoal and eventually dried up

24. ábra. A Pannon medence szeizmikus rétegösszleteinek és összletcsoportjainak általánosított vázlata. A vastag vonalak rétegösszlet-határokat jelölnek. A legmélyebben lévő (*B*), (paleozoos, vagy mezozoos) alapkőzetet jelöl. Az egyes rétegösszlet-határokon belüli vékony vonalak a belső reflexiók általános képét jelölik, a nyilak pedig diszkordanciákat jelölnek a határoknál. Az ábra nem méretheles, hanem számos szelvény általánosított kompoziciója. $(TM)_1$ és $(TM)_2$ turbidit- és márga-üledékeket jelöl, az A_1–A_7 egymásra rakódott delta rendszer 800–900 m-es vízmélységben rakódott le, az *S*-el jelölt lejtő-előtéri rogyásos rétegösszlet a medenceperemi delta-előrenyomulás erdményeként rakódott le és valószínüleg vízmélység-csökkenéssel kapcsolatos. Az a_1–a_4 jelű delta-üledékek 200–400 m-es vízmélységben keletkeztek, az *LMT* jelü sekélytavi, mocsári, folyóvízi és szárazföldi üledékek akkor képződtek, amikor a tó feltöltődése és kiszáradása folytatódott

Рис. 24. Обобщенная схема сейсмических серий и надсерий Паннонского бассейна. Жирными линиями проведены разделы серий. Самая глубокая серия *(B)* обозначает (палеозойский или мезозойский) фундамент. Тонкими линиями в пределах отдельных серий показана общая картина внутренних отражений. Схема вне масштаба, представляя собой композицию ряда разрезов. $(TM)_1$ и $(TM)_2$ — турбидиты и мергели; A_1–A_7 — нагромождение дельтовых отложений, накорившихся при глубине воды в 800–900 м; *S* — оползшие слои, накопившиеся во время продвижения дельтовой системы сквозь окраину бассейна и, вероятно, связанные с обмелением озера; a_1–a_4 — дельтовая система, накопившаяся при глубине воды в 200–400 м; *LMT* — мелководно-озерные, болотные и речные отложения, а также наземные почвы, предполагается, что толща накопилась в связи с продолжавшимся обмелением озера вплоть до его полного осушения

d_1–d_3 (mapped on the same profiles). The older supersequence (A_1–A_7) is believed to represent an early stage of turbidite-fronted deltas that were constructed in water depths of about 800–900 m. During this period, subsidence rates and corresponding sediment-influx rates must have been exceptionally high because delta construction overwhelmed local basement highs and spilled into adjacent subbasins. The younger supersequence (a_1–a_4) is believed to represent deposition in water depths of 200–400 m during a later stage of basin infilling and is limited areally to distal (relative to the source areas) subbasins or topographic lows.

Although we infer that supersequences B_1–B_7 and D_1–D_5 are approximate time-equivalent units (with a similar inference for supersequences b_1–b_4 and d_1–d_3), the equivalence cannot be firmly established because of the large areal distance between the areas in which the sequences were mapped.

The problem of assigning relative ages to the various deltaic units in the Pannonian Basin relates to assigning a definite time when deltaic construction began. Indirect evidence suggests that delta construction may have begun at least as early as Sarmatian time. In his discussion of a north–south regional profile across Hungary, KŐRÖSSY [1981] notes that, although Sarmatian strata are relatively thick (480 m) in the northeastern part of Hungary, these strata are markedly absent or thin in the Great Hungarian Plain and the Makó–Hódmezővásárhely trough (Hód–I well) areas. The absence of older strata in distal basinal areas would be expected if sedimentation progressed from the source areas to distal basins by deltaic progradation. According to HORVÁTH (written communication, 1985), however, evidence for the absence of Sarmatian strata in the Hód–I well is not convincing. He states that there is good evidence of Badenian strata in the Hód–I well, where the sequence appears continuous, and concludes that Sarmatian strata, although not recognized by fossil evidence, is probably present. Deltaic sedimentation, therefore, may not have started until Pannonian time. The major direction of sedimentation probably was determined by pre-rift or early rift topography at least as early as Badenian time. The course of the major rivers during Pannonian time may have been controlled by Paleogene to early Neogene sedimentary troughs and associated structures. At that time, major north–south delta construction and progradation could have been accelerated when sediment influx from the Carpathian Mountains increased.

According to COLLINSON [1976], a progression from deep-water delta deposits to shallow-water delta deposits is part of the normal evolution of a basinal sequence of sedimentary fill. The author states that turbidite-fronted deep-water deltas are the earliest in any basinal sequence and that they form the main basin fill above deep basinal mudstones. The deep-water deltas are comprised of thick sedimentary sequences that contain a turbidite apron, delta-slope siltstones, and fluviatile-channel sandstones. The younger, shallow-water delta systems generally are comprised of thinner sedimentary sequences, lack turbidite deposits, and are topped by a sheet sandstone attributed to migrating distributaries.

In the Vittorio Veneto region of the Southern Alps, MASSARI [1978] recognized two stages of delta construction during the Tortonian. In this area, early delta development gave rise to a major delta-building event characterized by a high-constructive, turbidite-fronted deep-water delta system. This episode is linked to a single high-bedload fluvial system, probably channelized along a transverse structural depression. After a destructional phase, a second progradational episode took place on the shallow platform created by the early deep-water delta system. The sheet-like geometry and stacked arrangement of the shallow-water delta sequences suggested to MASSARI that this later event can be attributed to lobate-type sub-deltas which were built out into a low energy reservoir by a great number of distributaries with mouth bars dominated by frictional forces.

The shallow-water delta sequences mapped in the Pannonian Basin differ somewhat from the shallow-water delta sequences recognized by MASSARI. In the Southern Alps, the shallow-water progradational episode took place on top of the platform created by earlier deep-water delta construction; whereas, in the Pannonian Basin, shallow-water deltas were constructed basinward of the platform created by the deep-water deltas after southerly advancement of an early fluvial system or systems.

Important differences, from a standpoint of petroleum exploration, may exist between the deep-water delta sequences and the shallow-water delta sequences in the Pannonian Basin. COLLINSON [1976] and MASSARI [1978] emphasize that turbidite-fronted deep-water deltas are characterized by thick sedimentary sequences and the storage of great amounts of coarse-grained sediments in delta slope channels, and of small amounts in distributary mouth bars. Shallow-water deltas, on the other hand, are characterized by the occurrence of delta front sheet-sandstones which are probably related to lobate-type subdeltas. The shallow-water deltas presumably are built in a low energy environment coupled with the existence of a great number of distributaries, and this allows the distributary mouth bar deposits associated with each delta lobe to merge into one another forming major sheet-like bodies [MASSARI 1978]. The dominant mechanism is probably lobe switching which results in a succession of stacked regressive sequences [COLEMAN 1976].

In Figure 24 supersequences A_1–A_7 and a_1–a_4 are separated by sequence *S*. This sequence diagrammatically represents sequence B_8 mapped on profiles 18 and 19 and, possibly, the upper part of sequence *III* (slumped strata) mapped at the Hód–I well site and sequence D_6 mapped on profile 9. On seismic profiles, sequence B_8 appears as a thick massive unit with a chaotic reflection pattern; whereas, sequence D_6, a thinner sequence, is characterized by a strong onlap pattern. Analyses of electric logs from the Bihu–NY–2 well (Fig. 18) indicate that sequence B_8 is composed chiefly of clays and siltstones (personnel communication, István Bérczi, SZKFI). Sequence D_6 has not been penetrated by drilling. Sequences B_8 and D_6 are similar in that they were deposited at the base of a steep slope created by deep-water delta construction and are overlain by sequences which represent a shallow-water prograding episode. The seismic character

(onlap and chaotic reflections) of B_8 and D_6 suggest that they were associated with a destructive depositional phase. Although sequences B_8 and D_6 are inferred to be time-equivalent, this relation is uncertain. In addition, it is also uncertain whether the units represent a local destructive phenonenon or, perhaps, are related to a basinwide destructional phase. In his study of Tortonian strata from the southern Alps, MASSARI [1978] notes that episodes of deep-water and shallow-water delta construction are separated by a destructional phase which he attributes to a short-lived transgressive event. In the Pannonian Basin, however, the location of the destructive phase between deep-water deltas and shallow-water deltas and its possible association with slump deposits suggest that the destructional phase was related to a shoaling of the lake. A drop in lake level, subsequent to the deposition of A_7 (Fig. 24), would have exposed the steep slope associated with constructional sequences A_1–A_7. Sediment input rates to the basin margin were still high, and remobilization of previously deposited sediments in front of an advancing delta front may have caused slumping and sediment bypass of the previous slope.

The youngest cycle of deposition is represented by sequence *LMT* in figure 24. As stated earlier, the unit represents delta plain facies; depositional environments varied from shallow lake, fluvial, and marsh to terrestrial soils. Seismically, sequence *LMT* is marked by basinward divergent reflections and, in marginal areas, by a strong onlap pattern at the base of the sequence.

Analyses of core data [BÉRCZI–PHILLIPS this volume, PHILLIPS–BÉRCZI 1985] indicate that sequence *LMT* represents shallower water environments in comparison to the environments represented by underlying sequences. *LMT*, therefore, is inferred to represent a progressive shoaling, with eventual disappearance, of the Pannonian lake. The strong onlap pattern that occurs at the base of *LMT* is interpreted as evidence of more widespread water conditions (transgression) at the basin margins. This apparent contradiction — shoaling conditions in the central parts of the basin coupled with a transgressive episode at the basin margins — can be explained by considering what is inferred by the term "transgression", as applied to a lacustrine basin, in contrast to the more classical meaning of the term when it is applied to sedimentation cycles that occur in ocean basins. In the classical sense, where applied to ocean basins, the term transgression implies coastal onlap associated with more widespread waters; in conjunction, water depths in marginal areas are increased, and water depths remain relatively unchanged in more central parts of the basin. In the case of a lake, however, more widespread water conditions in marginal areas can be coupled with decreased water depths in the central parts of the basin. The difference results from the fact that oceans contain a relatively infinite volume of water and, therefore, coastal onlap (transgression) and shoaling (regression) usually are not coeval. On the other hand, the volume of water in a lacustrine basin is finite and marginal onlap can be coupled with shoaling conditions in more central parts of the basin.

In general, post-Paleogene infilling of the Pannonian Basin involved a single cycle of sedimentation—that is to say that the history of the basin, during

Pannonian and Quaternary time, reflects continuously shoaling conditions. This shoaling probably resulted from sediment influx rates that were higher than basin subsidence rates. Deltaic sedimentation probably began in Sarmatian or earliest Pannonian time and continued throughout much of the Pannonian (s.l.). Early deltas were constructed in water depths of about 800–900 m, and deep basin marls may have been deposited in water depths > 1000 m. During this early stage of deep-water delta construction, subsidence rates and associated sediment-influx rates were extremely high as evidenced by upbuilding and progradation of large deltaic sediment wedges that filled subbasins near source areas, overwhelmed local basement highs, and spilled sediments into more distal subbasins. During the later stage of shallow-water delta construction, subsidence rates and sediment-input rates apparently slowed; however, sediment-input rates were still higher than the subsidence rates as evidenced by relative outbuilding of individual deltaic wedges. During the final stage of sedimentation, represented by sequence *LMT*, subsidence rates and sediment-input rates were nearly equal as evidenced by the thick section of delta plain sediments penetrated in the Hód–I well.

4.2 Basinal Patterns

Sedimentation patterns within individual subbasins vary depending on the direction of sedimentation and the distance of the subbasin from the source area. The general sedimentation patterns in three subbasins, the Makó–Hódmezővásárhely trough, the Derecske basin, and the Békés basin (Fig. 5), were analyzed.

Makó–Hódmezővásárhely trough (Fig. 25). The oldest sedimentary rocks in this subbasin represent chiefly turbidite deposits containing interbedded deep-basin marls (Fig. 25/A). They correspond to unit *I* penetrated in the Hód–I well where they attain a thickness of about 450 m. The turbidite deposits in this unit represent sediments that were derived from the north–northwest and transported, possibly via subaqueous canyons, to the central and deepest parts of the basin. In the northern part of Hungary, time-equivalent units probably are represented by deltaic progradation .

The next stage of sedimentation (Fig. 25/B) is marked by prograding delta construction. On seismic profile 9, at least four distinct advancing delta fronts can be mapped; the last of these fronts may correlate with a delta front mapped on seismic profile 8. The delta advance, between two basement highs, proceeded toward the central part of the basin from the north–northwest. The age relation between the sediments in this stage and those penetrated in the Hód–I well is not clear. Certainly, age-equivalent turbidite and deep-basin deposits would have reached as far southeast as the central parts of the basin. In the Hód–I well, age-equivalent sedimentary rocks are believed to be represented by unit *II;* but the upper part of unit *I*, as well as the lower part of *III*, also may be equivalent in age.

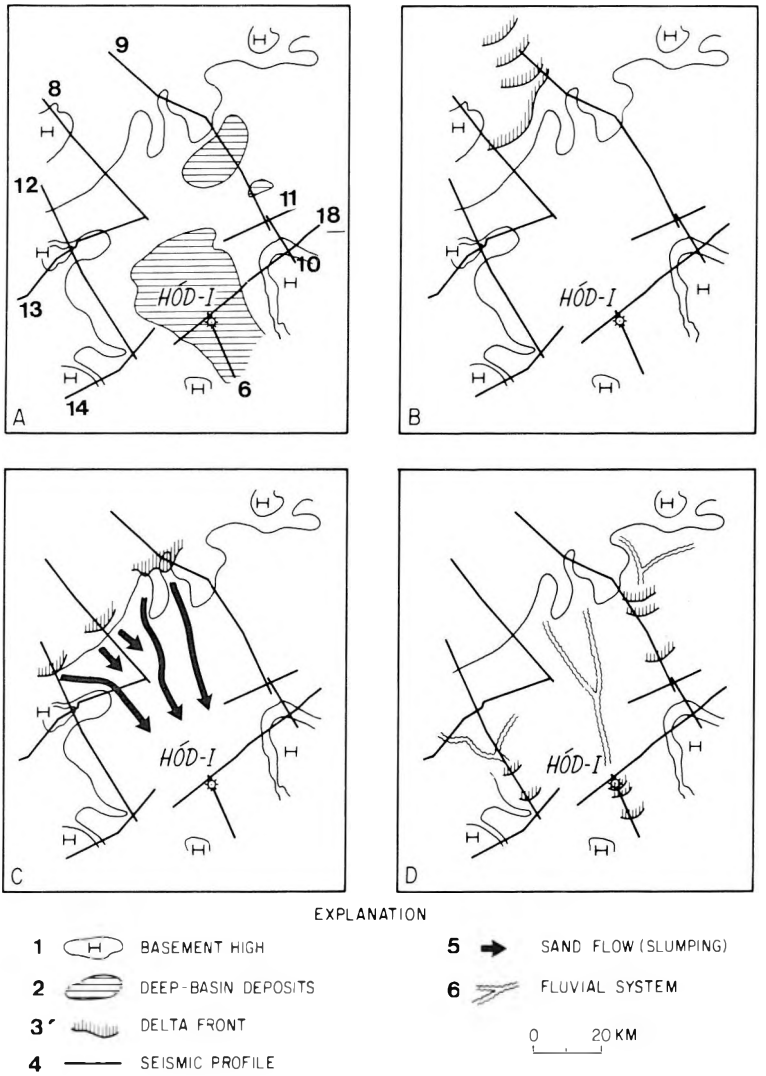

Fig. 25. Four stages of deposition in the Makó–Hódmezővásárhely trough. A) Deposition of early deep-basin turbidites. B) First stage of delta construction. C) Deposition of slump deposits and/or turbidite flow. D) Shallow-water delta construction following shoaling of lake

25. ábra. A Makó–Hódmezővásárhelyi árok négy üledékképződési állapota. A) Korai mély-medencebeli turbiditek lerakódása. B) A delta-képződés első szakasza. C) Üledék rogyások és zagyárak kialakulása. D) sekélyvízi delta-képződés és a beltó feltöltődése
1 – aljzatkiemelkedés; 2 – mélyvízi üledékek; 3 – deltafront; 4 – szeizmikus vonal; 5 – homokfolyam (rogyások); 6 – folyórendszer

Рис. 25. Четыре стадии осадкообразования в грабене Мако–Ходмезёвашархей. А) Отложение турбидитов в раннем глубоководном бассейне. В) Первый этап образования дельты. С) Оползание осадков и становление турбидитных потоков. D) Образование мелководной дельты и заполнение внутреннего озера
1 — возвышение фундамента; 2 — глубоководные отложения; 3 — фронт дельт; 4 — линия профиля сейсморазведки; 5 — песчаные плывуны (оползни); 6 — реки

As the delta wedges advanced further southeastward (Fig. 25/C), the basement high shown in the upper left corner of figure 25/B was owerhelmed, and sediments were deposited near the base of the previous slope by slumping subsequent to a shoaling of the lake. Evidence for this conclusion comes from seismic profile 8. Part of the coarser sediment fraction was transported basinward by turbidite flows or directly downslope by slumping, and some of it reached the central part of the basin in the vicinity of the Hód–I well. The upper part of sequence *III*, penetrated in this well, is inferred to represent sediments involved in this stage of sedimentation. Much of the basin was filled in during this stage.

During the succeeding stage (Fig. 25/D), rivers advanced far to the southeast and discharged as far south as the Hód–I site, which generally had been, until then, the deepest part of the basin. Shallow-water deltas, (mapped on seismic profiles 9, 6, and 12, and penetrated in the Hód–I well) probably related to numerous small rivers, now infilled the basin and the depositional center shifted southward of the Hód–I well site.

The last stage (not shown) was marked by deposits of shallow lake, fluvial, and marsh sediments and terrestrial soils that were deposited as the lake continued to shoal and eventually disappeared. This cycle is represented by sedimentary rocks of unit *V* penetrated in the Hód–I well and of unit *LMT* in other areas.

Derecske basin (Fig. 26). As in discussion of the Makó–Hódmezővásárhely trough, the oldest sedimentary rocks in the Derecske basin are believed to represent a period of turbidite and deep basin marl deposition and the erosion of local basement highs that filled the deepest parts of the basin (Fig. 26/A). The direction of turbidite deposition is not clear but was probably from the northeast as well as the northwest. The earliest deltas (Fig. 26/B) are mapped on seismic profile 18. This system of deep-water (800–900 m) deltas prograded southwestward, where the delta toes are seen to pinch out against a basement high on seismic profile 18. Concurrent with delta progradation, turbidite flows funneled down canyons from a northwest direction.

Subsequently (Fig. 26/C), deep-water (800–900 m) delta construction shifted slightly to the west in the vicinity of seismic profile 19. Southwest progradation continued, and delta upbuilding overwhelmed the basement high shown near the bottom of Figure 26/B. Massive turbidite flows continued to enter the basin from the northwest. Evidence of these flows is seen on seismic profile 19, on which numerous unconformities can be mapped, and strong onlap of the deltas by turbidite sedimentation is evident. During this cycle, minor(?) amounts of sediment entered the basin from the south and east. Seismic evidence from profile 21 suggests that these sediments were not transported any great distance but, rather, were derived from nearby basement highs and transported by slump and creep and downslope mass-transport processes.

Békés basin (Fig. 27). The Békés basin differs from the two subbasins discussed above in that it is located far from sediment source areas which lay to the northwest, north, and northeast. Other subbasins were located between

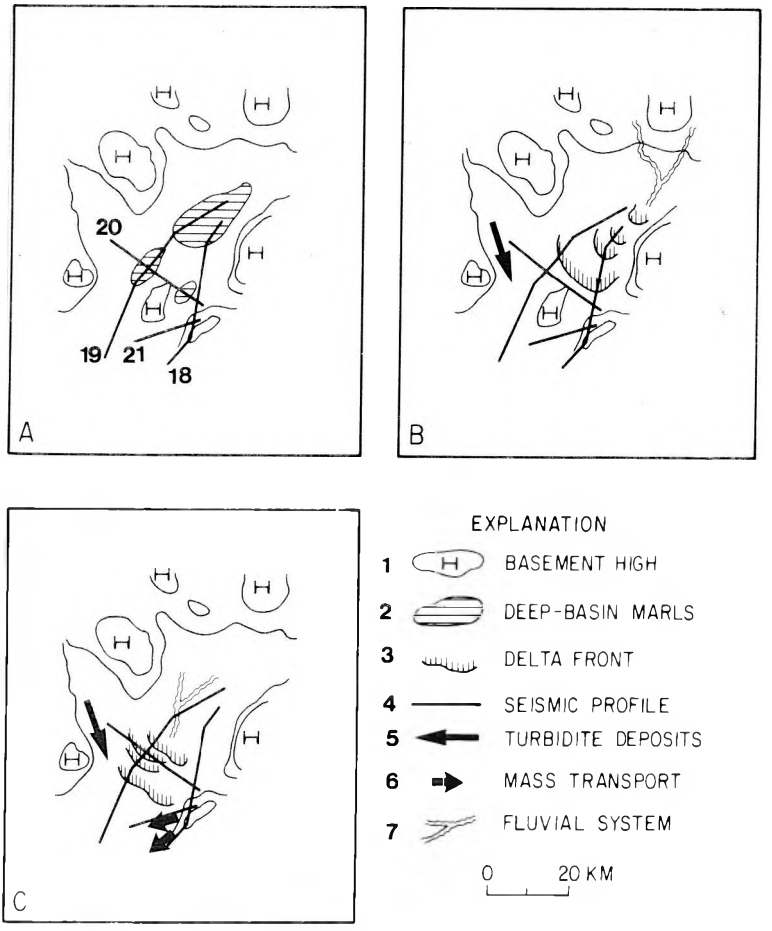

Fig. 26. Three stages of deposition in the Derecske basin. A) Deposition of early deep-basin turbidites. B) First stage of delta construction and turbidite flow down canyon axis. C) Shift of delta construction southwestward

26. ábra. A Derecskei medence feltöltődésének három állapota. A) Korai mély-medencebeli turbiditek lerakódása. B) A delta-képződés első szakasza és zagyárak kanyonok mentén. C) A delta-képződés DNY-i előrenyomulása
1 – aljzat-kiemelkedés; 2 – mélyvízi márgák; 3 – deltafront; 4 – szeizmikus vonal; 5 – turbidit üledékek; 6 – anyagszállítás; 7 – folyórendszer

Рис. 26. Три стадии заполнения бассейна Деречке. А) Отложение турбидитов в раннем глубоководном бассейне. В) Первая стадия формирования дельт и турбидитные потоки вдоль каньонов. С) Продвижение формирования дельты к ЮЗ
1 — возвышение фундамента; 2 — глубоководные мергели; 3 — фронт дельты; 4 — линии профилей сейсморазведки; 5 — турбидиты; 6 — направление сноса осадочного материала; 7 — реки

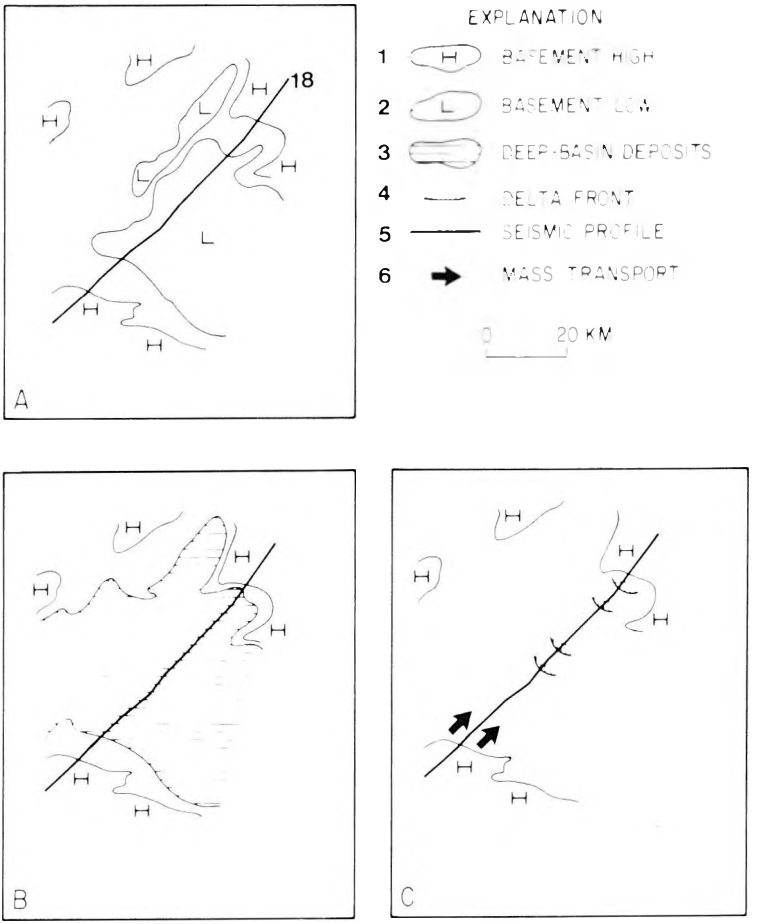

Fig. 27. Two stages of deposition in the Békés basin. A) Location of basement highs and lows at start of deposition. B) Deposition of deep-basin turbidite and marl deposits. C) Stage of shallow-water delta construction following shoaling of lake

27. ábra. A Békési medence feltöltésének két állapota. A) Az üledékképződés kezdetén a medencealjzati magaslatok és mélyedések helyzete. B) A mély-medencebeli turbiditek és márgák lerakodása. C) Sekélyvízi delta-fázis üledékeinek lerakódása és a medence feltöltődése
1 – aljzat-kiemelkedés; 2 – aljzat-bemélyedés; 3 – mélyvízi üledékek; 4 – deltafront; 5 – szeizmikus vonal; 6 – anyagszállítás

Рис. 27. Две стадии заполнения бассейна Бекеш. А) Положение приподнятых и погруженных участков фундамента в начале осадкообразования. В) Отложение турбидитов и мергелей в глубоководном бассейне. С) Отложение осадков мелководной дельтовой фазы и заполнение бассейна
1 — возвышение фундамента; 2 — прогиб в фундаменте; 3 — глубоководные отложения; 4 — фронт дельт; 5 — линии профилей сейсморазведки; 6 — направление сноса осадочного материала

the source areas and the Békés basin. Therefore, it received chiefly finer grained sediments until deltaic sedimentation had prograded across much of the remainder of the Pannonian Basin late in its history. Deep basin deposits in the Békés basin (Fig. 27/B) can be expected to be much thicker and more widespread than in the areas discussed above. Coarse-grained sediments probably are limited to areas in the vicinity of local basement highs where sediment input depended on weathering of local basement rocks and subsequent transport by slump and creep and downslope mass-transport processes (Fig. 27/C). Delta construction (Fig. 27/C) was limited to shallow water deltas (200–400 m), which are probably equivalent in time to the last stages of delta construction in the Makó–Hódmezővásárhely trough.

Table I. Seismic profile numbers used in figure 4 are shown in first column. The second column shows the corresponding seismic profile numbering system used by the National Oil and Gas Trust of Hungary. The first two digits of the last number in column 2 indicate the year in which the seismic record was recorded. The second two digits indicate the fold of the final stacked record section; for example, 7824 indicates that the seismic profile was recorded in 1978 and stacked twenty-four-fold

I. táblázat. A 4. ábrán használt szeizmikus vonalszámozás és a megfelelő OKGT számozás összefüggése. A második oszlop utolsó négy számjegyéből az első kettő a mérés évét, a második kettő a fedésszámot jelöli

Таблица I. Номера сейсмических профилей на рис. 4 приведены в первой колонке. Вторая колонка показывает соответвующую нумерацию сейсмических профилей, применяемую Предприятием Геофизического Исследования ГТНГП. Первые две цифры последнего числа в колонке 2 указывают на год, в котором сейсмограмма была записана. Вторые две цифры показывают кратность окончательной накопленной записи, напр., 7824 показывает, что сейсмический профиль был проработан в 1978 г. и было применено 24-кратное накопление

NUMBER IN THIS REPORT	OKGT NUMBERING SYSTEM
6	A–11–7824
8	VA–11/c–7924
9	A–12/B/C/D, VA–12/E–7824
10	A–12/A–7712
11	OR–24–7824
12	A–10/A–7924, VA–10/B–7824
13	A–19/D/E/F/G/H–7824
14	A–16/x/y–7824
15	FL–7–7606
16	VFL–2–7712
17	FL–20–7512
18	AL–1–7612, A–16, A–16/B/C/D/E/F/G–7624–8024
19	Kö–16–7824, Ka–32–7612,
20	Ka–67–8024, Ka–35/a–7912, Ka–35–7912, Ka–105–8124
21	Ko–44–8024
22	Ko–14–7824
23	A–16/A/L/M/N–7612

Table II. Well names and corresponding abbreviations used in this paper

II. táblázat. A mélyfúrások rövidítése és a megfelelő helységnevek

Таблица II. Буквенные шифры скважин и соответствующие названия населенных пунктов

Abbreviation	Well name
Ab–1	Abony
Algyő–19, 64, 162, 176	Algyő
Algyő–K–1	Algyő–East
Ás–1, 23	Ásotthalom
Bés–1	Békéssámson
Bihu–NY–2	Biharugra
Do–2, 4, 5	Dorozsma
Der–1	Derecske
Er–7	Eresztő
Felgyő–1, 2, 1	Felgyő
F.kút–6	Forráskút
Fu–1, 10	Furta
Hód–1	Hódmezővásárhely
Kb–1, 3	Kaba
K–9	Kőrösszegapáti
Kun–1, 3	Kunszállás
Kom–1, 12	Komádi
Kiha–D–2	Kiskunhalas–South
Lász–2, 3, 4	Jásszentlászló
Makó–2	Makó
Mar–1	Martfű
Móra–1, 4	Mórahalom
Mp–3	Mezőpeterd
Nk–2, 4, 20	Nagykörös
Nsz–2	Nagyszénás
Pálm–1, 2	Pálmonostora
Pf–40, 142, 155, 173	Pusztaföldvár
Sark–1	Sarkadkeresztúr
Szk–91, 95	Szank
Szr DNY–1	Szarvas–Southeast
Tif–1	Tiszaföldvár
Tir–1	Tiszaroff

5. Summary of conclusions

The following conclusions regarding the sedimentary rocks of the Pannonian Basin in Hungary are based on stratigraphic analysis of seismic records and studies of core samples from three wells:

(1) Deltaic sedimentation may have started as early as Sarmatian time and continued throughout much of the Pannonian (s.l.).

(2) Sediment input was chiefly from the northwest, north, and northeast. These directions probably were determined by pre-rift or early rift topography at least as early as Badenian time.

(3) Two distinct stages of delta construction can be recognized: an early, deep-water stage and a later, shallower water stage.

(4) In the early stage of construction, turbidite fronted deltas were built in water depths as deep as 800–900 m. During this stage, subsidence rates and associated sediment-influx rates were high, and upbuilding and southward progradation of large, deltaic sediment wedges filled subbasins near the source areas, overwhelmed local basement highs, and spilled sediments into subbasins in the southern part of Hungary.

(5) During a later stage of construction, deltas were built in water depths of about 200–400 m, and topographically low areas in the southern part of Hungary were infilled by sediments discharged from river systems that had advanced about 100 km southward across strata of the older constructional stage.

(6) Differences, from a standpoint of petroleum exploration, may exist between the two deltaic sequences. Coarse-grained sediments in the deep-water delta system may be limited to large delta slope channels. The shallow-water deltas, in contrast, may be associated with delta front sheet-sands which are related to merging and progradation of distributary mouth bar sands.

(7) In some areas, the sedimentary rocks representing the two stages of delta construction may be separated by a unit that represents a destructional phase. This unit is inferred to be related to a shoaling of the lake or, possibly, a short-lived transgressive event.

(8) The final stage of sedimentation is represented by delta plain facies; depositional environments varied from shallow lake, fluvial, and marsh to terrestrial soils. During this last stage, the lake became more widespread but continued to shoal.

(9) Basal turbidite–marl sections in the deeper parts of the Pannonian Basin become progressively younger in a direction away from the sediment source areas. This tendency is coupled with a thickening of the overall turbidite–marl section in the same general direction.

(10) Distal (in reference to sediment source areas) subbasins received chiefly finer grained sediments until late in their history, when deltaic sedimentation had prograded across much of the remainder of the Pannonian Basin. Older coarse-grained sediments in these basins probably are limited to the vicinity of local basement highs.

(11) The authors have interpreted the Pannonian and Quaternary history of the Pannonian Basin in terms of a continuously shoaling lake due to sediment infilling.

Acknowledgements

The interpretations contained in this report resulted from studies conducted under a cooperative agrement between the U.S. Geological Survey (USGS) and the Central Office of Geology of Hungary. The USGS authors wish to thank the many gracious Hungarian geologists and geophysicists who spent

many hours introducing us to the geology of Hungary. We are especially indebted to I. Bérczi for his detailed explanations of stratigraphy and sedimentary processes, to Á. Jámbor and É. Kilényi for their descriptions of regional geology, and to G. Pogácsás for his review of seismic stratigraphic interpretations in Hungary. Finally, all the authors wish to thank F. Horváth for his critical review (and many helpful additions) of the final manuscript.

REFERENCES

Bérczi I., Phillips R. this volume: Processes and depositional environments of Neogene deltaic–lacustrine sediments, Pannonian Basin, Southeast Hungary.

Berg. O. R. 1982: Seismic detection and evaluation of delta and turbidite sequences: Their application to exploration for the subtle trap. AAPG Bull. **66,** 9, pp. 1271–1288

Burchfiel B. C. and Royden L. 1982: Carpathian foreland fold and thrust belt and its relation to Pannonian and other basins. AAPG Bull **66,** 9, pp. 1179–1195

Coleman J. M. 1976: Deltas: Processes of deposition and models for exploration. Continuing Education Publication Co., Champaign, Illinois, 102 p.

Collinson J. D. 1976: Deltaic evolution during basin fill–Namurian of central Pennine Basin, England. Abstracts with program, 1976 AAPG–SEPM Annual Convention, May 23–26, AAPG Bull. **60,** 4, p. 659

Dank V. E. and Kókai J. 1969: Oil and Gas exploration in Hungary, *in* Hepple P. ed., The exploration for petroleum in Europe and North Africa. London, Institute of Petroleum, pp. 131–145

Kilényi É., Rumpler J. 1985: Pre-Tertiary basement relief map of Hungary. Geophys. Trans. **30,** 4, pp. 425–428

Kőrössy L. 1981: Regional geological profiles in the Pannonian Basin. Earth Evolution Sciences, **1,** 3–4, pp. 223–231

Lerner J. 1981: Satellite image map of the Carpatho–Pannonian region. Earth Evolution Sciences, **1,** 3–4, pp. 180–182

Massari S. F. 1978: High-constructive coarse-textured delta systems, Tortonian, Southern Alps. Evidence of lateral deposits in delta slope channels. Memorie della Societa Geologica Italiana, 18, pp. 93–124

Phillips R. L. and Bérczi I. 1985: Processes and depositional environments of Neogene deltaic-lacustrine sediments, Pannonian Basin, Southeast Hungary: Core investigation summary, U. S. Geological Survey Open File Report 85–360, 66 p.

Sangree J. B. and Widmier J. M. 1978: Seismic stratigraphy and global changes of sea level, Part 9: Seismic interpretation of clastic depositional facies: AAPG Bull. **62,** 5, pp. 752–771

Vail P. R., Mitchum R. M., Jr., Todd R. G., Widmier J. M., Thompson S. III, Sangree J. B., Bubb J. N. and Hatlelid W. G. 1977: Seismic stratigraphy and global changes of sea level, *in* Payton C. E. ed., Seismic stratigraphy – application to hydrocarbon exploration. AAPG Memoir 26, pp. 49–205

A PANNON MEDENCE SZEIZMIKUS SZTRATIGRÁFIAI VIZSGÁLATA DK-MAGYARORSZÁGON

Robert E. MATTICK, RUMPLER János és R. Lawrence PHILLIPS

A szeizmikus sztratigráfiai vizsgálatok, valamint három mélyfúrás magmintáinak részletes analízise arra utalnak, hogy a Pannon medence ÉNY, É és ÉK-i irányból delta-üledékekkel töltődött föl.

A medencefeltöltődés egyetlen szedimentációs ciklusban zajlott le, melynek kezdete a szarmata, vagy a legkorábbi pannon időszakra tehető, amikor a vízmélység 1000 m-nél nagyobb volt. A medence ezt követő fejlődése a pannon és kvarter folyamán a vízmélység fokozatos csökkenését tükrözi. Ezt a csökkenést az üledékbehordás mértékének a medence süllyedést uralkodóan meghaladó mértéke eredményezte.

A delta-feltöltődés két, egymástól jól elkülöníthető fázisra osztható. A delta-képződés korai szakaszában turbidit ciklussal kezdődő mélytengeri delta-üledékek rakódtak le mintegy 800–900 m-es vízmélységben. E korai delta-építési szakaszban a medence-süllyedés, és a kapcsolódó üledékbehordási sebesség nagy volt. A nagy delta üledéksorozat egymásra rakódása és D-i irányú előrenyomulása során feltöltötte a forrásterületekhez közeli részmedencéket, s áthaladva az útjába eső lokális magaslatokon a Magyarország D-i részén lévő részmedencékben rakta le üledékeit. A delta-üledékképződés későbbi szakaszában a fokozatosan előrenyomuló sekélyvízi delta-képződmények mintegy 200–400 m-es vízmélységben keletkeztek. Ezek Magyarország D-i részén lévő mélyterületeken olyan folyami rendszerekből rakódtak le, amelyek a korábbi delta ciklus üledékeit mintegy 100 km-el D-i irányban túlhaladták.

A szeizmikus vizsgálatok arra is utalnak, hogy a Pannon medence bizonyos részein a két delta-képződési ciklust képviselő üledékes kőzeteket olyan üledékképződési egység választja el egymástól, amely valószínűleg egy destruktív fázisnak felel meg. Ez az egység képződhetett rövid idejű transzgressziós ciklus során, vagy esetleg felgyorsult vízmélységcsökkenési ciklus eredményeként.

Az üledékképződés legfiatalabb és egyben befejező ciklusát delta-síkság fáciesű üledékek képviselik, melyben az üledékképződési környezet sekélytavi, folyóvizi, és mocsáritól szárazföldi környezetig változott. Ez az egység egy kiterjedtebb tavi környezetet jelentett, mely a Pannon beltó fokozatos elsekélyesedésével és eltűnésével párosult. Az üledékképződésnek ebben a periódusában a medence süllyedés mértéke és a kapcsolódó üledékbehordási mérték kisebb volt, mint a korábbi szakaszban, és minden bizonnyal egyensúlyban volt egymással.

СЕЙСМОСТРАТИГРАФИЧЕСКОЕ ИССЛЕДОВАНИЕ ПАННОНСКОГО БАССЕЙНА В ЮВ ЧАСТИ ВЕНГРИИ

Роберт Э. МЕТИК, Янош РУМПЛЕР и Р. Лоренс ФИЛИПС

Сейсмостратиграфические исследования, а также детальный анализ кернов из трех глубоких скважин привели к заключению о заполнении Паннонского бассейна материалом, привносившимся с С3, С и СВ.

Бассейн заполнился в результате одного цикла осадконакопления, начавшемся в сарматском веке, но в любом случае не ранее паннонского века, при глубине воды, превышавшей 1000 м. Последующий ход истории развития бассейна в течение паннонского века и четвертичного периода отражает постепенное уменьшение глубины воды. Это уменьшение было вызвано тем, что скорости осадконакопления в целом превышали скорости погружения бассейна.

В общих чертах, в формированиии дельты можно наметить две стадии. В более раннюю из них глубоководные дельты с турбидитами на фронте формировались при глубинах воды в 800–900 м. Во время этой ранней стадии формирования скорости опускания и соответственно скорости поступления осадков были высокими, так что надстраивающиеся и продвигающиеся к югу крупные клинья дельтовых осадков заполнили частные впадины вблизи от источников сноса, переваливались через локальные поднятия фундамента и достигали частные впадины на юге Венгрии. Во время поздней стадии продвигающиеся мелководные дельты формировались при глубине воды в 200–400 м, и пониженные области на юге Венгрии заполнялись осадками, привносившимися реками, продвигавшимися примерно на 100 км к югу через отложения ранней стадии.

Данные сейсморазведки свидетельствуют о том, что в некоторых районах Паннонского бассейна осадки двух стадий формирования дельты разделены осадочной пачкой, возможно, отражающей размыв. Эта пачка, возможно, возникла в течение кратковременной трансгрессии или, может быть, вслед за периодом ускоренного обмеления озера.

Наиболее молодая и заключительная стадия представлена отложениями дельтовых равнин; обстановки осадконакопления варьировали от мелководно-озерных, через речных и болотных до наземных. Предполагается, что соответсвующая толща отражает большее распространение озерных обстановок в совокупности с продолжающимся обмелением и с соответственным исчезновением Паннонского озера. В эту стадию осадконакопления скорости опускания бассейна и сопутствующие скорости поступления осадков были, вероятно, ниже, и предполагается, что осадконакопление в целом компенсировало опускания.

GEOPHYSICAL TRANSACTIONS 1985
Vol. 31. No. 1–3. pp. 55–74

PROCESSES AND DEPOSITIONAL ENVIRONMENTS WITHIN NEOGENE DELTAIC – LACUSTRINE SEDIMENTS, PANNONIAN BASIN, SOUTHEAST HUNGARY

István BÉRCZI* and R. Lawrence PHILLIPS**

Core samples from 3 wells drilled in Neogene strata (3190, 5842, and 2886 m deep) within the Makó–Hódmezővásárhely trough in southeast Hungary define the depositional environments and the sedimentologic history of basin fill. Five major facies are indentified within fluvial–deltaic–lacustrine sediments and include in ascending order: 1) a *basal* facies of turbidite deposited sandstone and conglomerate with interbedded marl; 2) a *deep basin* facies of laminated to massive calcareous to silty marl; 3) a *prodelta* facies containing a lower unit of parallel-bedded sandstone interbedded with marl overlain by a sequence of deformed strata (slumped deposits); 4) a *delta front–delta slope* facies of inclined (5 to 20° dip) and deformed beds of sandstone and marl; and 5) a *delta plain* facies of horizontal beds of sandstone, siltstone, lignite and marl. Two stages of basin fill are recognized, an initial deep lacustrine basin stage where deposition of sand and gravel by turbidity currents along with marl smoothed the irregular topography followed by fluvial–deltaic advancement into the basin from the northwest.

This report presents the results of geologic investigations and a summary of data studied within the Pannonian Basin in Hungary during 1981. The purpose of this study is to interpret and define the depositional environments and sedimentological history recorded within cores obtained from Neogene strata underlying the southern part of the Great Hungarian Plain.

The area of investigation is in southeastern Hungary, northeast of the city of Szeged within the Makó–Hódmezővásárhely trough, located directly east of the Algyő structural high and oil field. The Makó–Hódmezővásárhely trough is a NNW–SSE trending depression containing over 6 km of Neogene and Quaternary sediments [KŐRÖSSY 1981]. Cores from three wells drilled on both flanks and within the center of the trough are the basis of determining the geology, facies and depositional history of the basin fill. The three wells and depths drilled from the west to the east flank of the basin are; 1) Maroslele–1 (Ml), 3190 m; 2) Hódmezővásárhely–I (Hód–I), 5842 m; and 3) Békéssámson–1 (Bés–1), 2886 m.

The basement rocks underlying the Neogene sediments consist mainly of Paleozoic metamorphic rocks and locally Triassic dolomite [BÉRCZI–KÓKAI 1976, MAGYAR–RÉVÉSZ 1976, KŐRÖSSY 1981]. The Neogene sediments filling the basin represent lacustrine marls, turbidites, and deltaic to fluvial marls and clastics. A geophysical profile of the Makó–Hódmezővásáhely trough, including the Hód–I well section, shows at least 3 distinctive seismic units one of which contains inclined southeast prograding strata [VARGA–POGÁCSÁS 1981]. The age determinations are based on reported data included within the well logs and from published well data.

Keywords: depositional environment, deltas, lacustrine sediments, Pannonian Basin

* Hungarian Hydrocarbon Institute, POB 32, Százhalombatta, H–2443, Hungary
** U. S. Geological Survey, 345 Middlefield Road, MS 999 Menlo Park, California 94025
Manuscript received: 13. january, 1985

1. Introduction

The Makó–Hódmezővásárhely trough contains more than 6 km of lacustrine–fluvial sedimentary rocks ranging in age from Neogene to Quaternary. The deepest borehole in Hungary (Hód–1) terminated in Badenian sediments in this trough at a depth of 5842 m b.s.l. *(Fig. 1)*. This preliminary study of the basin-fill facies is based on a detailed investigation of cores from three boreholes that yield a cross-section essentially normal to the depositional trend across the trough: Maroslele–1; Hódmezővásárhely–1; and Békéssámson–1 (Fig. 1).

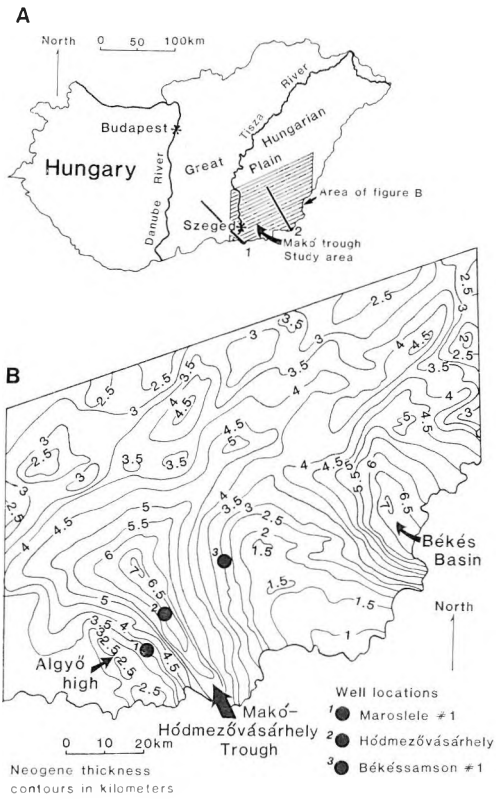

Fig. 1. A) Map of Hungary with location of study area. The two lines, 1 and 2, represent the regional sedimentological profiles of Figures 13 and 14
B) Isopachs of Neogene and younger sediments overlying Paleozoic basement within and adjacent to the Makó–Hódmezővásárhely trough

1. ábra. A) Magyarország térképe a kutatási terület felüntetésével. A két vonal a 13. és 14. ábra regionális üledékföldtani szelvényét jelöli
B) A paleozoos aljzaton települő neogén és fiatalabb üledékek vastagságtérképe (a neogén üledékek vastagsága km-ben van megadva) a Makó–hódmezővásárhelyi árokban

Рис. 1. А) Карта Венгрии с участком исследований. Две линии обозначают региональные стратиграфические разрезы рис. №№ 13 и 14
В) Карта изолиний мощности неогеновых и четвертичных отложеный, залегающих на палеозойском фундаменте в Мако–Ходмезёвашархейском грабене (мощности даны в км)

Analysis of lithologic trends determined from grain size distributions and well log data enabled us to distinguish five main depositional facies that clearly represent a shoaling upwards sequence in a basin that at times contained steep prograding slopes. These five facies have been tentatively identified in ascending order as: 1) a basal facies; 2) a deep basin facies; 3) a prodelta facies; 4) a delta front–delta slope facies; and 5) a delta plain facies. Stratigraphically speaking, these five facies give all the Neogene evolutionary history of the trough from the Middle Badenian (= 15 Ma BP) up to the recent *(Fig. 2)*.

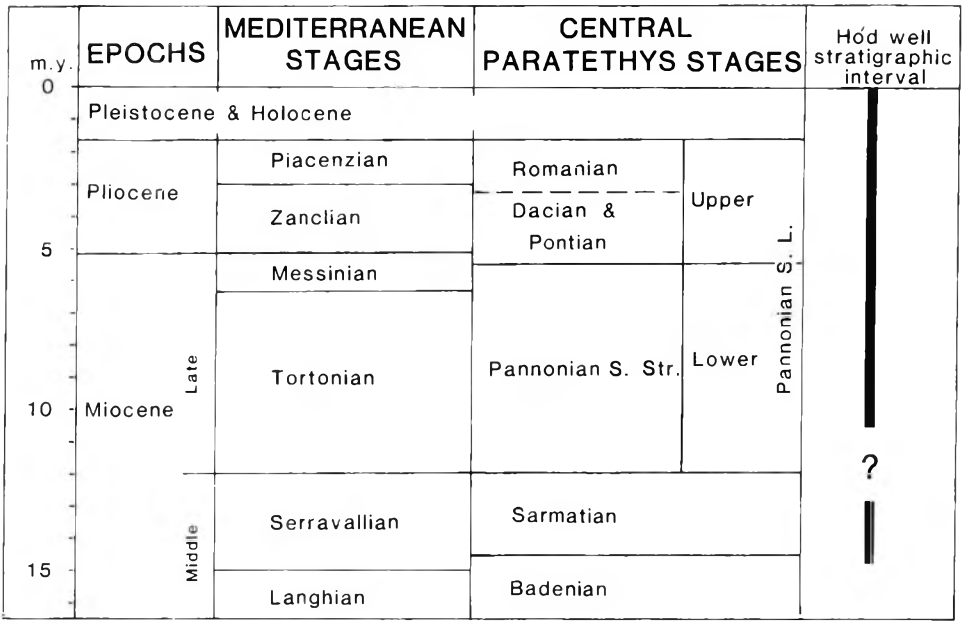

Fig. 2. Age relationships of the Pannonian Basin strata and stratigraphic intervals reported for the Hód–I well

2. ábra. A Pannon-medence rétegeinek korbesorolása és a Hód–I mélyfúrás rétegtani besorolása

Рис. 2. Геологический возраст отдельных свит Паннонского бассейна и стратиграфическое положение отдельных слоев скважины Hód-I

On the basis of evaluation of well-log response analysis, stratification features, and grain size distributions, these five facies could be identified in two adjacent regional profiles (Fig. 1). Within the upper facies (prodelta, delta front – delta slope, and delta plain) several major depositional environments (distributary channel, distributary mouth bar, point bar, and turbidity cones) can also be identified mostly by analyzing the electric well-log response forms.

2. Facies analysis

The basal facies

The basal facies is composed of sandy–marly conglomerate interbedded with marl and is found only in the deepest part of the trench. Borehole Hód–I penetrated 392 m into this unit but failed to reach the pre-Neogene basement or the stratigraphic base of the sequence. The age of the upper part of this unit is about Middle Badenian *(Fig. 3)*.

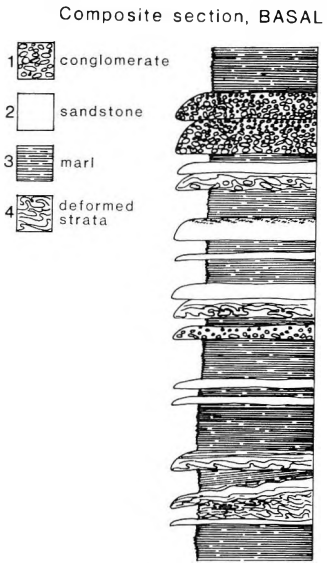

Fig. 3. Composite section of the depositional elements of the basal facies. Turbidites, some conglomeratic, interbedded with marl form the dominate bedding structures

3. ábra. Az alapkonglomerátum üledékképződési egységeinek tipusszelvénye. Az uralkodó rétegzettséget turbidit (némelyike konglomerátumos) és márga váltakozása építi fel 1 — konglomerátum; 2 — homokkő; 3 — márga; 4 — deformált rétegek

Рис. 3. Типичный разрез литостратиграфических единиц базального конгломерата. Преобладающий тип слоистости характеризуется чередованием турбидитов (некоторые из них содержат конгломераты) и мергелей
1 — конгломераты; 2 — песчаники; 3 — мергели; 4 — деформированные слои

Within this facies the interbedded sandstone and marl beds may dip to about 7 to 11 degrees due to penecontemporaneous slumping and deformation of the strata. The sandstone beds are graded (Ta, Tb, and Tc parts of the Bouma sequence), are frequently distorted, and contain marl rip-up clasts. In the non-graded sandstone layers, thin amalgamated beds with small-scale cross-strata or parallel to wavy laminations with marl interbeds are common (Fig. 3). The turbidites most likely flowed along the axis of the basin or may have been locally derived from the flanks of the trough. The periodic occurrence of interbedded marl and sandstone beds dipping at angles of up to 11 degrees suggest either: 1) an irregular lake bottom containing local relief; 2) the strata are filling into previously cut turbidite "channels"; or, 3) deposition of coarse-grained turbidites over muds may have initiated slumping of the sediments if the lake bed contained low angle slopes.

This unit can be clearly distinguished from the adjacent shallow-water basal conglomerates that occur around the margins of the basins. The latter has an obvious psefitic, grain-supported nature with undisturbed bedding and, in contrast to the conglomerates in the deep axial part of the trough, shows rather poor evidence for any significant mass transport (Fig. 3).

The deep basin facies

The deep basin facies overlaps the basal facies in the axial part of the trench. This 1165 m thick series consists of calcareous and argillaceous silty marls of laminated and to a lesser extent massive appearance. No bioturbation

can be observed within the strata *(Fig. 4)*. Seemingly, the sediments were deposited below the oxygen minimum zone. This unit is of Middle to Late Badenian to Pannonian (s. str.) age.

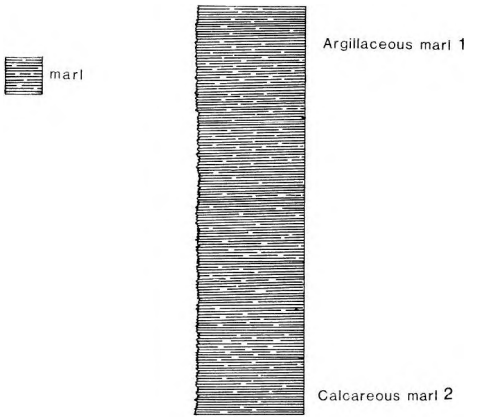

Fig. 4. Composite section of the depositional elements of the deep basin facies. Laminated to massive, calcareous to clay marl forms the depositional elements of this facies

4. ábra. A mélyvízi fácies üledékképződési egységeinek típusszelvénye. A márgák a vékonyan rétegzettől a rétegzetlenig, és a mészmárgától az agyagmárgáig valamennyi változatot felölelik
1 — agyagmárga; 2 — mészmárga

Рис. 4. Типичный разрез литостратиграфических единиц глубоководной фации. Среди мергелей присутствуют все разновидности от тонкослоистых до неслоистостых и от известковистых до глинистых
1 — глинистые мергели; 2 — известковистые мергели

The prodelta facies

The 1035 m thick prodelta facies can be divided into two parts: the upper part (B subfacies; 350 m thick) contains abundant sand and is considered to be a product both of a lacustrine fan system (proximal turbidites) as well as containing sedimentary structures indicating abundant slumping of the strata. Graded beds (Ta, Tab, and Tabc of Bouma sequence) characterize much of the section. The sandstone beds can be amalgamated and may contain dish structures, load casts, flame structures, and marl rip-up clasts. Inclined strata (4 to 25 degree dip) resulted from deformation as well as slumping of strata originally deposited on the delta front – delta slope. Abundant soft sediment deformation features as penecontemporaneous faulting, disrupted bedding or completely overturned beds characterize the deformed strata *(Fig. 5)*.

The lower part of the prodelta facies (horizontal bedded, proximal to distal turbidites, A subfacies; 685 m thick) are characterized by a gradual decrease in the sand bed thickness, in sand to marl ratio and in grain size downward, as well as by the predominance of Tab units of the Bouma sequence. The sandstone beds change from amalgamated strata to solitary small-scale cross-strata interbedded with marl toward the base of this facies *(Fig. 6)*. Horizontal parallel bedding dominates within this subfacies in contrast to the inclined deformed strata in the overlying subfacies. No bioturbation has been observed within strata of this facies.

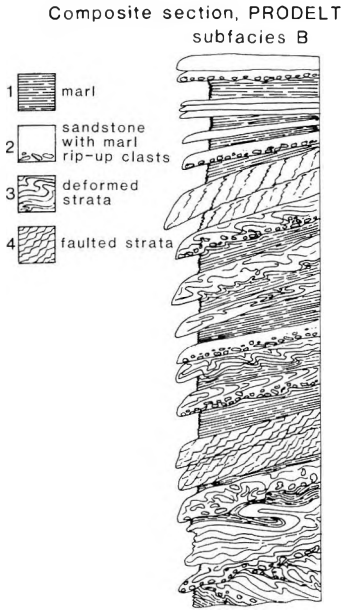

Fig. 5. Composite section of subfacies *B* of the prodelta facies. Slumped and deformed strata interbedded with marl represent deposition from repeated debris flows derived from the delta front slope

5. ábra. A delta előtér *B* alfáciesének típusszelvénye. Az üledékrogyásos és deformált rétegek váltakozása márgával a delta front (lejtőről származó) ismételt törmelékfolyások üledék lerakódásait képviseli
1 — márga; 2 — homokkő–márga feltépett saját anyagú törmelékkel; 3 — deformált rétegek; 4 — elvetett rétegek

Рис. 5. Типичный разрез субфации *B* преддельтовой фации. Чередование оползневых деформированных отложений и мергелей является следствием осаждения в результате многократно повторяющихся обломочных потоков (подводных оползней)
1 — мергели; 2 — песчаники – мергели с переотложенными обломками собственного состава: 3 — деформированные слои; 4 — отложения, нарушенные конседиментационными сбросами

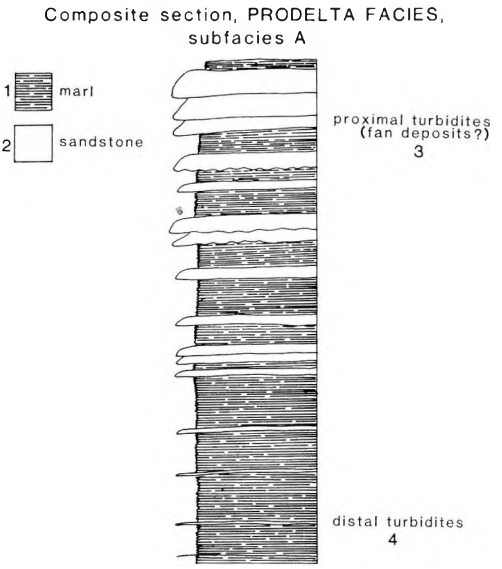

Fig. 6. Composite section of subfacies *A* of the prodelta facies. Sandstone, interbedded with marl, exhibits an increasing bed thickness toward the top of the sequence

6. ábra. A delta előtér *A* alfáciesének típusszelvénye. A homokkő–márga váltakozás felfelé haladva egyre növekvő rétegvastagságokat mutat
1 — márga; 2 — homokkő; 3 — közeli turbiditek (törmelékkúpok); 4 — távoli turbiditek

Рис. 6. Типичный разрез субфации *A* преддельтовой фации. При чередовании песчаников и мергелей мощности отдельных циклов в направлении снизу вверх постепенно увеличиваются
1 — мергели; 2 — песчаники, 3 — близкие турбидиты (конусы выноса); 4 — дальние турбидиты

The delta front – delta slope facies

The delta front – delta slope facies (733 m thick) consists of sandstone and marl both occurring as inclined or in some examples as horizontal parallel beds. The most characteristic feature of this facies is inclined strata dipping up to 20 degrees (most common dip is 5 to 7 degrees). Abundant soft sedimentary deformation (synsedimentary faulting, slumps, and rotation of beds) resulted in the steeply dipping strata. Similar values of dip can also be measured in giant foresets (delta front) in regional profiles. The sandstone beds contain load casts, flame structures and marl rip-up clasts showing well-defined graded bedding, with a predominance of Ta, Tab, and Tabc units of the Bouma sequence *(Fig. 7)*. Bioturbation is now abundant, in the upper 2/3 of the facies. The delta front slope is the most readily distinguished facies of regional extent dominating the sedimentary development of the Neogene strata underlying the Great Hungarian Plain.

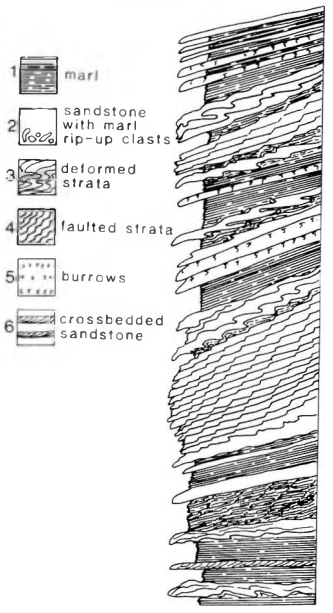

Fig. 7.

7. ábra. Composite section of the depositional elements of the delta front facies. Deformed strata with abundant penecontemporaneous faulting and laminated marls interbedded with sandstone form the common structures of this facies

Fig. 7. A delta front üledékképződési egységeinek típusszelvénye. Deformált rétegek—az üledékképződéssel közel egyidejű vetőkkel—és vékonyan rétegzett márgák, homokkő betelepülésekkel, a jellegzetes felépítés
1 — márga; 2 — homokkő–márga feltépett saját anyagú törmelékkel; 3 — deformált rétegek; 4 — elvetett rétegek; 5 — féregnyomok; 6 — keresztrétegzett homokkő

Рис. 7. Типичный разрез литостратиграфических единиц фронта дельты. Деформированные слои со сбросами близкими по времени образования к осадконакоплению и тонкослоистые мергели с подчиненным количеством песчаников
1 — мергели; 2 — песчаники–мергели с переотложенными обломками собственного состава; 3 — деформированные слои; 4 — слои, нарушенные конседиментационными сбросами; 5 — ходы червей; 6 — косослоистые песчаники

The delta plain facies

The delta plain facies is composed of alternating layers of horizontally bedded sandstone, siltstone and marl. The sandstone and siltstone layers are graded and repeated. Occurrences of small-scale cross-strata as well as bioturbation is also frequent *(Fig. 8)*. Oxidized mudstone intercalations are frequent indicating that this region was sometimes dry land. The increasing importance of terrestrial conditions is also indicated by the common occurrence of lignite beds. The depositional environments vary from shallow lake, fluvial marsh to terrestrial (subaerial). The few deformed stata probably represent sediments slumping into distributary channels.

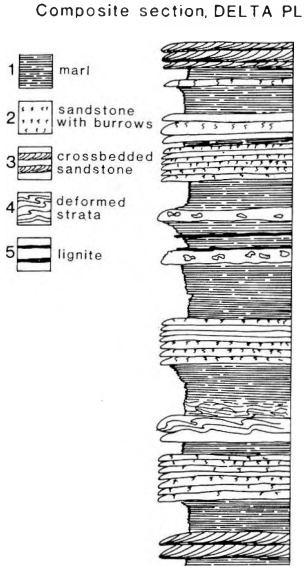

Fig. 8. Composite section of the depositional elements of the delta plain facies. Parallel bedded bioturbated sandstone interbedded with marl forms the major depositional sequences

8. ábra. A delta síkság üledékképződési egységeinek típusszelvénye. Párhuzamosan rétegzett, életnyomos homokkő váltakozása márgával építi fel a rétegsort
1 — márga; 2 — életnyomos homokkő; 3 — keresztrétegzett homokkő; 4 — deformált rétegek; 5 — lignit

Рис. 8. Типичный разрез литостратиграфических единиц дельтовой равнины. Разрез сложен чередующимися песчаниками, содержащими ископаемые остатки, и мергелями. Слоистость параллельная
1 — мергели; 2 — песчаники с ископаемыми остатками: 3 — песчаники с косой слоистостью; 4 — деформированные слои; 5 — лигниты

3. Discussion

Comprehensive lithological, sedimentological profiles as well as a two and/or three dimensional view of the facies distribution are given in *Figures 9–12*. We propose that a highly constructional, fluvial-dominated delta system, which prograded from the northwest toward the southeast, resulted in the filling of the Makó–Hódmezővásárhely trough. Progradation from the northwest is also indicated by the mineralogical composition of the sandstones most of which are lithoarenites containing rock fragments and heavy minerals of metamorphic origin derived from northern and western sources. No volcanic detritus derived from the north and east could be detected within the sediments of the Makó–Hódmezővásárhely trough. The vertical distribution of the facies in relation to

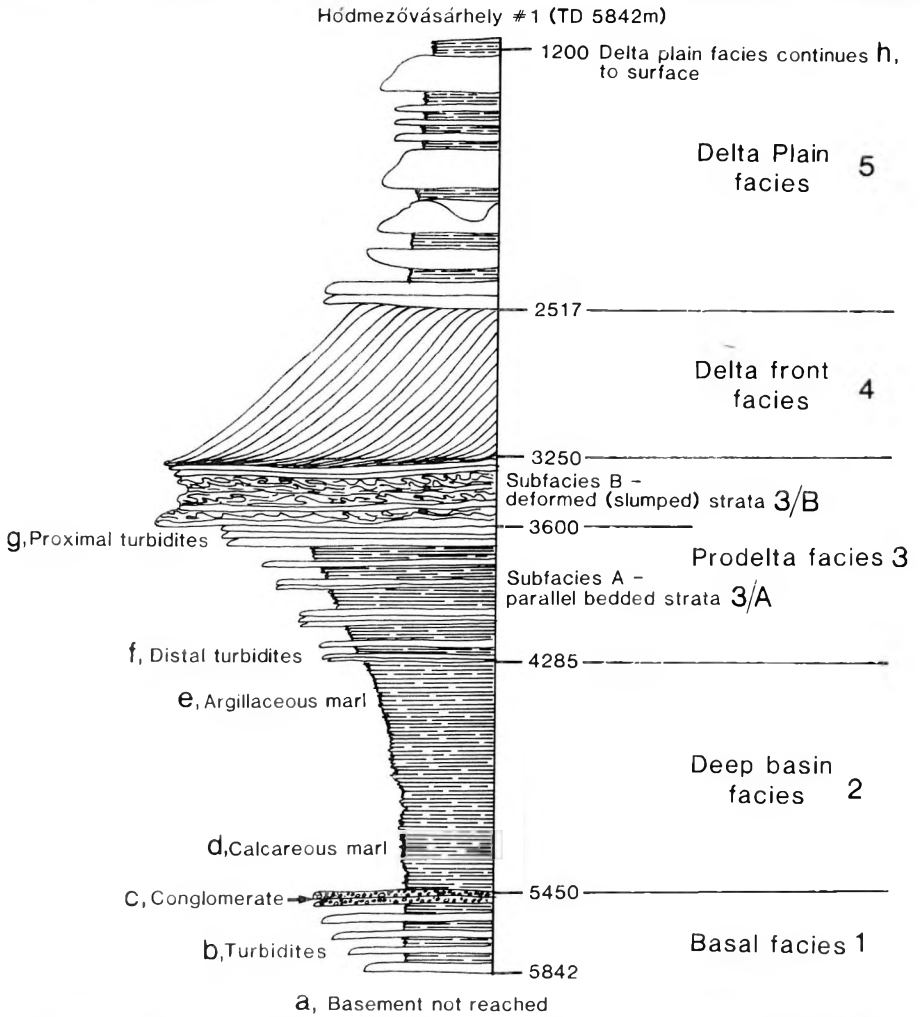

Fig. 9. Stratigraphic section and facies recorded in part of the Hódmezővásárhely–I well. The depths are recorded in meters

9. ábra. Rétegtani szelvény és fácies beosztás a Hód–I mélyfúrásban (mélység m-ben)
1 — alapkonglomerátum: a – az aljzatot nem érték el, b – turbiditek, c – konglomerátum; 2 — mélyvízi fácies: d – mészmárga, e – agyagmárga; 3 — delta előtér; 3/*A* alfácies, párhuzamos rétegzettséggel (f – távoli turbiditek, g – közeli turbiditek); 3/*B* alfácies, deformált (üledékrogyásos) rétegekkel; 4 — delta front; 5 — delta síkság: h – folytatódik a felszínig

Рис. 9. Стратиграфическая колонка и фациальное подразделение отложений скважины Hód–I (глубины в метрах)
1 — базальный конгломерат: a — фундамент не вскрыт; b — турбидиты; c — конгломераты; 2 — глубоководная фация: d — известковистые мергели; e — глинистые мергели; 3 — преддельтовая фация; 3/*A* — субфация с параллельной слоистостью; f — дальние турбидиты; 3/*B* — субфация с деформированными (оползневыми) слоями; 4 — фронт дельты; 5 — дельтовая равнина; h — продолжается до нынешней поверхности

the paleorelief (Figures 9–10) refers to a two-step infillment process. The first step produced a smoothing of the rugged paleorelief, followed by a delta progradation, which itself was a three-step progradational process (see below).

The Neogene evolution of the trench as well as the adjacent areas crossed by the regional geological profiles *(Figs. 13–14)* can be tentatively summarized as follows: at the beginning of Badenian time, the rapidly subsiding areas quickly reached the stage of deep basin (pelitic) sedimentation. Failure (slumping) of sediments on the steep slopes of the trench resulted in the transport and reworking of coarse-grained sediments as turbidites. Thus the matrix of the basal facies is mud deposited from suspension as well as chemically precipitated $CaCO_3$, to which there were periodic influxes of coarse-grained sediments. The turbidites may have flowed either along the axis of the trench or down its flanks. Periodic occurrences of steeply dipping marl and sandstone interbeds suggest an irregular bottom topography with slumping strata and/or infill of previously formed turbidite channels. (We use "turbidite" to mean predominantly sediment gravity flow deposits.)

The deep basin facies is also composed of sediments derived from settling of mud and chemically precipitated $CaCO_3$ (Figs. 11–12). Fossils with $CaCO_3$ shells are rare (possibly transported?), thus biogenic effects of $CaCO_3$ precipitation can be certainly excluded. The bedding shows no biogenetic disturbances of any kind. This is the end of the first phase of the infilling process.

The proximal part of overlying prodelta facies is dominated by periodic influxes of sand by turbidity flows that exhibit decreasing energy toward the distal regions of the trough (Figs. 11–12). The amalgamated sandstone beds (these represent the top of the prodelta series) may overlie or interfinger with slumped deposits of fan deposits surrounding the deep lake channel systems.

The steeply dipping and laterally extensive beds of the delta front – delta slope facies (Figs. 11–12) were deposited mainly by gravity flows along with grain flows of varying intensity, as well as by slumping of previously deposited sediments. Suspended sediments and chemically precipitated $CaCO_3$ were also deposited along with the coarse-grained clastics. The vertical distance between topset and bottomset strata indicated that a maximum of about 700 m water depth may have existed during deposition of this sequence in the deepest part of the depression. The inclined delta front strata form the most readily identifiable unit on seismic reflection profiles throughout this region. The seismic profiles show a general southeast dip resulting from delta progradation from the northwest, but in the central part of the Great Hungarian Plain a southwest dip can be observed [Pogácsás–Völgyi 1982, and Mattick et al. this volume] suggesting that multiple fluvial–deltaic systems advanced into the basin.

Finally the shallow lake, fluvial and especially the marsh and terrestrial (oxidized) sediments in the delta plain facies (Figs. 11–12) indicate the final stages of sedimentation in the Makó–Hódmezővásárhely trough.

These 5 principal facies can also be distinguished laterally within the Neogene Pannonian Basin sediments. The two regional sedimentological profiles (Figs. 13–14), based on regional seismic profiles, show a clearly defin-

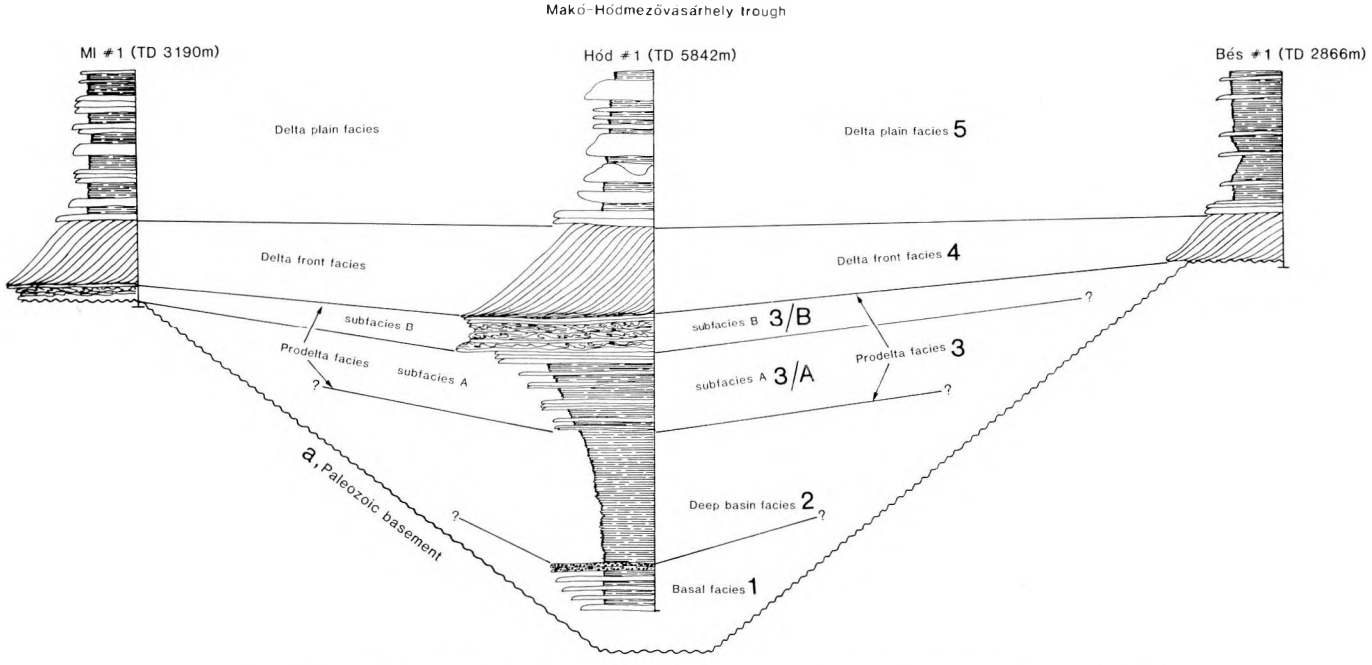

Fig. 10. Lateral facies relationships within the three wells drilled within and on the flanks of the Makó–Hódmezővásárhely trough

10. ábra. A Makó–Hódmezővásárhelyi árokban, ill. szárnyain fúrt három mélyfúrás közötti fácies-kapcsolatok
1 — alapkonglomerátum; a — paleozoos aljzat; 2 — mélyvízi fácies; 3 — delta előtér fácies: *A* alfácies, *B* alfácies; 4 — delta front; 5 — delta síkság

Рис. 10. Фациальные взаимоотношения трех скважин, пробуренных в Мако–Ходмезёвашархейском грабене и на его флангах
1 — базальный конгломерат; а — палеозойский фундамент; 2 — глубоководная фация; 3 — преддельтовая фация: субфация *A*, субфация *B*; 4 — фронт дельты; 5 — дельтовая равнина

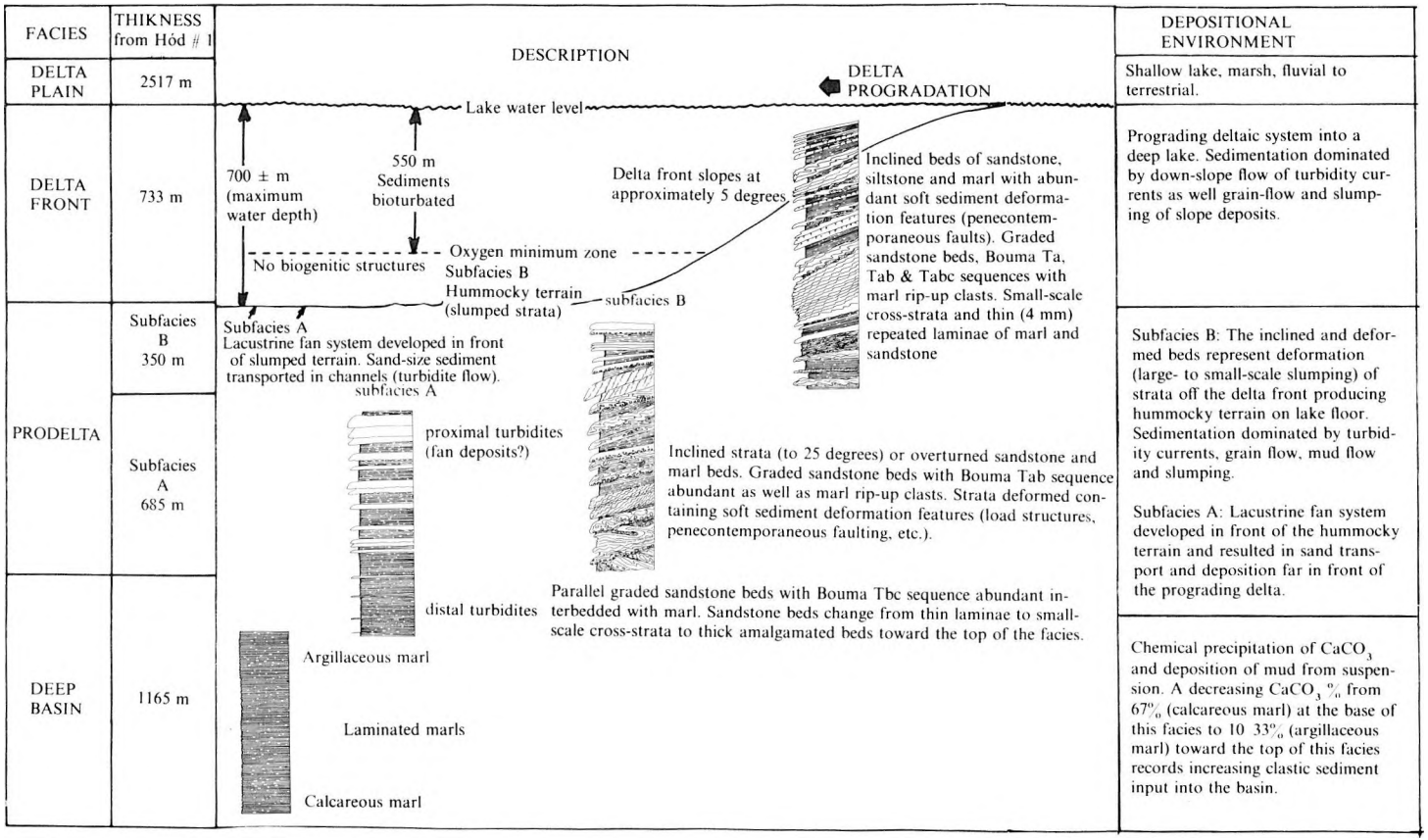

Fig. 11. Processes and depositional environments of a prograding delta within the Pannonian lacustrine system

able three-step progradation form with an upward fining sequence of silt–shale alternation. The lowermost siltstone bodies are reworked deposits consisting of slumps, grain-flows and mud flows. These 3 phases of progradation can be tentatively identified in both profiles. Cluster and factor analysis of the major geometrical parameters (total thickness of the Pannonian s.l.; the distance of the top and bottom of each lithostratigraphic (facies) units as well as the distance of the Neogene basement from the surface) show close relationship between the delta slope and proximal as well as distal turbidite bodies corroborating the genetic connections defined by the classical sedimentological methods. The regional extension of this facies model throughout the Pannonian Basin should be one of the future tasks for sedimentologists joining this project.

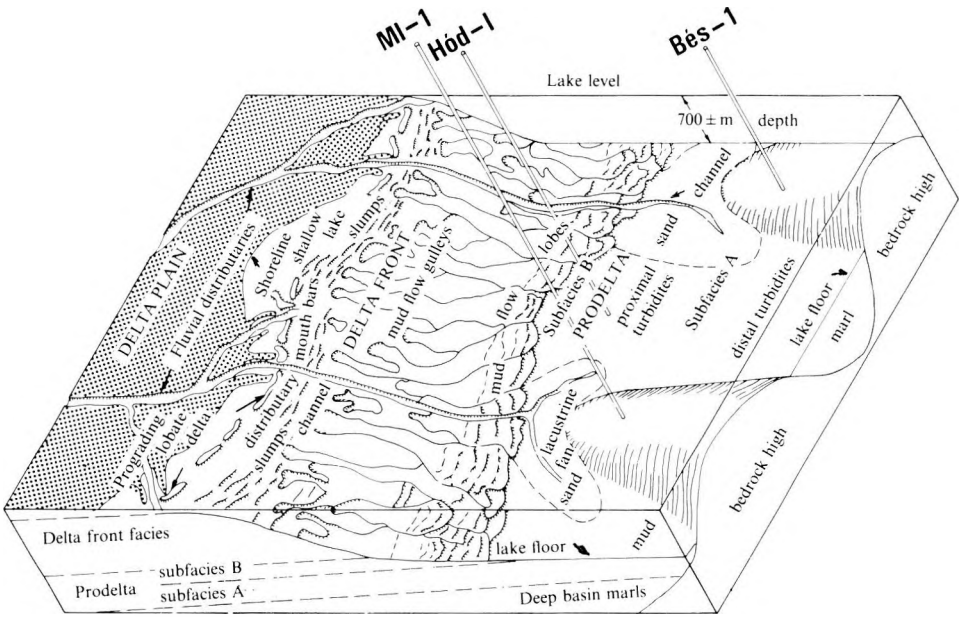

Fig. 12. Major depositional processes within a fluvial-dominated delta system. A prograding lobate delta system probably contained a channel system connecting the fluvial distributaries to the prodelta lacustrine fan. Progradation of the fluvial delta results in the vertical assemblage of facies and sedimentary sequences observed within the cores from the Makó–Hódmezővásárhely trough

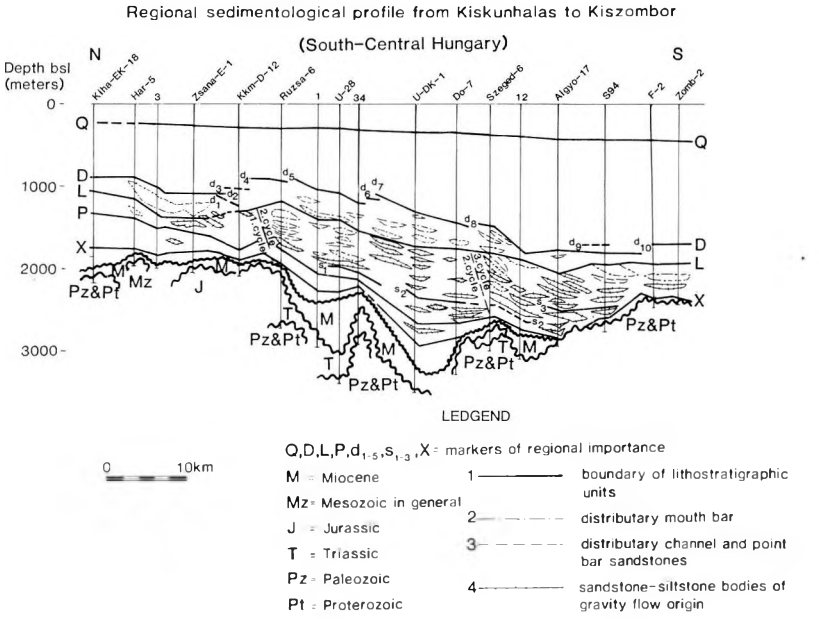

Fig. 13. Sedimentological profile of the south-central Pannonian Basin showing major sand bodies within Neogene deltaic–lacustrine facies (see Figure 1/A, line 1, for profile location). The boreholes from which the profile was constructed are listed at the top of the section

13. ábra. Regionális üledékföldtani szelvény Kiskunhalas és Kiszombor között, a neogén tavi–delta fácies főbb homok testeivel (helyszínét lásd az 1/A ábrán)
Q, D, L, P, d_{1-5}, s_{1-3}, X — regionális markerek; 1 — kőzetrétegtani egységek határa; 2 — folyóágak torkolati zátonyai; 3 — folyóágak medre és mederbeli zátonyhomokkő; 4 — gravitációs folyás eredetü homokkő–aleurolit testek

Рис. 13. Региональный литостратиграфический разрез по профилю Кишкунхалаш–Кишзомбор с главными телами песчаного состава неогеновой озерно–дельтовой фации (место расположения см. на риц. 1/A)
Q, D, L, P, d_{1-5}, s_{1-3}, X — региональные маркирующие горизонты; 1 — границы литостратиграфических единиц; 2 — устьевые банки отдельных рукавов; 3 — отдельные рукава и накапливающиеся в них песчаники русловых банок; 4 — песчаники и алевролиты, образовавшиеся в результате гравитационного течения

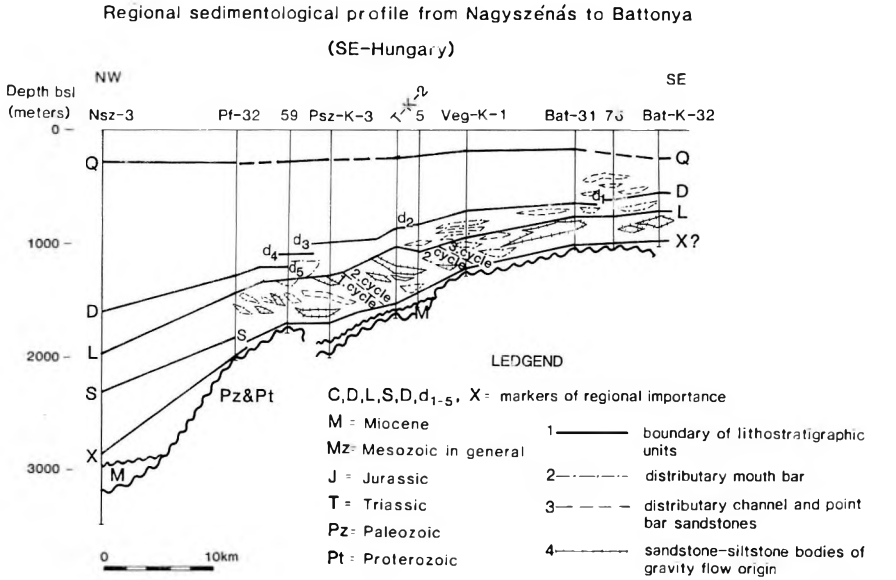

Fig. 14. Sedimentological profile of the southeast Pannonian Basin showing major sand bodies within Neogene deltaic–lacustrine facies (see Figure 1/A, line 2, for profile location). The boreholes from which the profile was constructed are listed at the top of the section

14. ábra. Regionális üledékföldtani szelvény Nagyszénás és Battonya között a neogén tavi–delta fácies főbb homok testeivel (helyszínét lásd 1/A ábrán)
C, D, L, S, D, d_{1-5}, X – regionális markerek; 1 — kőzetrétegtani egységek határa; 2 — folyóágak torkolati zátonyai; 3 — folyóágak medre és mederbeli zátonyhomokkő; 4 — gravitációs folyás eredetű homokkő–aleurolit testek

Рис. 14. Региональный литостратиграфический разрез по профилю Надьсенаш–Баттоня с главным телами песчаного состава неогеновой озерно-речной фации (место расположения см. на рис. 1/A)
C, D, L, S, D, d_{1-5}, X — региональные маркирующие горизонты; 1 — границы литостратиграфических единиц; 2 — устьевые отмели рукавов рек; 3 — отделеные рукава и накапливающиеся в них песчаники русловых банок; 4 — песчаники и алевролоты, образовавшиеся в результате гравитационного течения

4. Conclusions

(1) The most complete Neogene sequences can be fo nd in the central (Hungarian) part of the Pannonian Basin.
(2) Gravity-flow sediment transport maintained an important role throughout the whole period of Neogene sedimentation.
(3) There is a three-stage progradational delta system in Late Miocene–Pliocene of the southern part of the Great Hungarian Plain, overlying a basal mud-supported conglomerate and deep lake marl sequence of Middle Badenian to Sarmatian age. This pre-deltaic phase produced a smoothing of the rugged paleorelief.
(4) The key formation is the delta (basin?) slope facies which is easily correlatable over the area studied. Its recent (i.e. post-diagenetic) thickness (= 700 m) refer to a lake sedimentation system with considerable areal extension.
(5) Distributary channel, point bar, distributary mouth bar sandstone units, and gravity flow transported sandstone–siltstone bodies can be recognized in the well logs from the petroleum exploratory wells. The identification of the fluvial bar system is very important in deciphering the Neogene evolutional history of the area studied.
(6) The comprehensive analysis of the sedimentological control of the evolutional history will improve the regional lithostratigraphic correlation.
(7) Trends of future investigations are:
- sedimentological analysis of additional profiles,
- regional correlation and contouring of the different facies units,
- localization of regional pinchout zones.

REFERENCES

Bérczi I., Kókai J. 1976: Hydrogeological features of some deep-basins in SE-Hungary as revealed by hydrocarbon exploration. Annales Instituti Geologici Publici Hungarici, **59,** 1–4, pp. 69–93

Kőrössy L. 1981: Regional geological profiles in the Pannonian Basin. Earth Evolution Sciences, **1,** 3–4, pp. 223–231

Magyar L., Révész I. 1976: Data on the classification of Pannonian sediments of the Algyő area. Acta Mineralogica–Petrographica, **22,** 2, pp. 267–283

Mattick R. E., Rumpler J. and Phillips R. L. this volume: Seismic stratigraphy of the Pannonian Basin in Hungary

Pogácsás Gy., Völgyi L. 1982: Correlation of east-Hungarian Pannonian sedimentary facies on the basis of CH-prospecting seismic and well log sections. Proc. 27th Geophys. Symp. Bratislava, **A(I),** pp. 322–336

Varga I., Pogácsás Gy. 1981: Reflection seismic investigations in the Hungarian part of the Pannonian Basin. Earth Evolution Sciences, **1,** 3–4, pp. 232–239

A PANNON MEDENCE NEOGÉN TAVI DELTA ÜLEDÉKEIBEN MEGNYILVÁNULÓ ÜLEDÉKKÉPZŐDÉSI FOLYAMATOK ÉS ÜLEDÉKFELHALMOZÁSI KÖRNYEZETEK

BÉRCZI István és R. Lawrence PHILLIPS

A Makó–Hódmezővásárhelyi árokban (DK-Magyarország) mélyített, a neogént feltáró mélyfúrások (mélységük 3190, 5842, ill. 2886 m) magmintái alapján meghatározható a medencét kitöltő üledéksor változó üledékképződési környezete és üledékföldtani fejlődéstörténete. Öt fontosabb fácies különíthető el, a tavi-delta–folyóvízi sorozatban alulról felfelé haladva: 1) *„alapkonglomerátum"*, agyagos mátrixú konglomerátum, homokkő, turbidit; 2) *mélyvízi fácies*, finoman rétegzett vagy rétegzetlen aleurolitos vagy tiszta mészmárga; 3) *delta-előtér fácies*, amelynek alsó része márga betelepüléseket tartalmazó vízszintesen, párhuzamosan rétegzett homokkőből (távoli turbiditek?), felső része zavart rétegzettségű, üledékrogyásokat is tartalmazó közeli turbiditekből áll; 4) *delta-front, delta-lejtő fácies*, látványosan dőlő (5–20°), deformált homokkő, aleurolitos homokkő és márga rétegekkel; 5) *delta síkság fácies*, a legváltozatosabb litológiájú egység, homokkő, aleurolitos homokkő, lignit és márga rétegekből, meder kitöltés, mederközi síkság, övzátony, torkolati zátony üledékfelhalmozódási egységekből épül fel. A feltöltődés két fázisa ismerhető fel: egy kezdeti mélyvízi, amikor is a lerakódó homok, kavics, márga a szabálytalan topográfiát elsimította, majd erre települt az északnyugatról előrenyomuló folyóvízi–delta sorozat.

УСЛОВИЯ И МЕХАНИЗМ НАКОПЛЕНИЯ ОСАДКОВ НЕОГЕНОВЫХ ОЗЕРНО-ДЕЛЬТОВЫХ ОБРАЗОВАНИЙ ПАННОНСКОГО БАССЕЙНА

Иштван БЕРЦИ и Р. Лоренс ФИЛИПС

На основе исследования керна буровых скважин в Мако–Ходмезёвашархейском грабене (с глубинами 3190 м, 5842 м и 2886 м), появилась возможность реконструкции условий накопления осадков, заполняющих бассейн неогеновых образований и отличающихся высокой изменчивостью, а также истории геологического развития. Снизу вверх по направлению разреза озерно–дельтовых–речных отложений можно выделить 5 следующих главных фациальных типов: 1) *«базальный конгломерат»* – конгломерат, основную массу которого составляют глины, песчаники, турбидиты; 2) *глубоководная фация* – известковые мергели, алевролитовые или чистые, тонкослоистые или без слоистости; 3) *придельтовая фация* – нижняя часть ее разреза представлена горизонтальными параллельными слоями песчаников с прослойками мегрелей (дальние турбидиты), а в верхней части залегают близкие турбидиты с дисгармоничной слоистостью, имеющие местами следы оползневых явлений; 4) *фации фронта и склона дельты* – содержит наклонно залегающие (5–20°) деформированные песчаники с прослойками алевритовых песчаников и мергелей; 5. *фация дельтовой равнины* – характеризуется наибольшей литологической изменчивостью и состоит из слоев различного состава: песчаники, алевролитовые песчаники, лигниты и мергели.

В генетическом смысле это – отложения долин, междолинных равнин, а также поясовых и устьевых банок. Можно выделить две фазы заполнения: начальную глубоководную фазу, в процессе которой осаждающиеся пески, галечники и мергели выравнивали все неровности рельефа, и позднюю, в процессе которой речная дельтовая серия, надвигающаяся с северо-востока, накладывалась на вышеуказанные отложения.

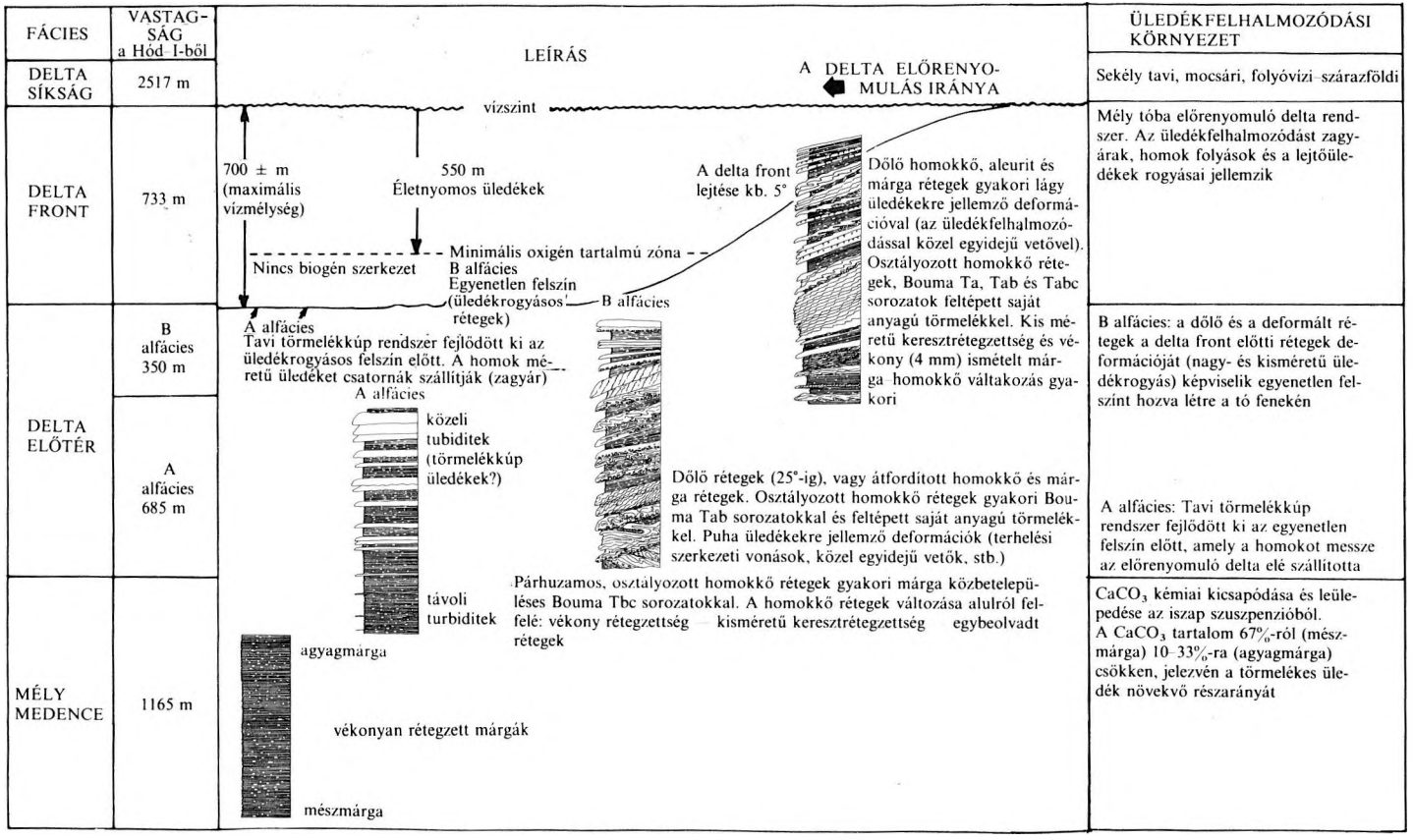

11. ábra. Üledékképződési folyamatok és üledékfelhalmozódási környezetek a pannóniai tórendszer előrenyomuló deltájában

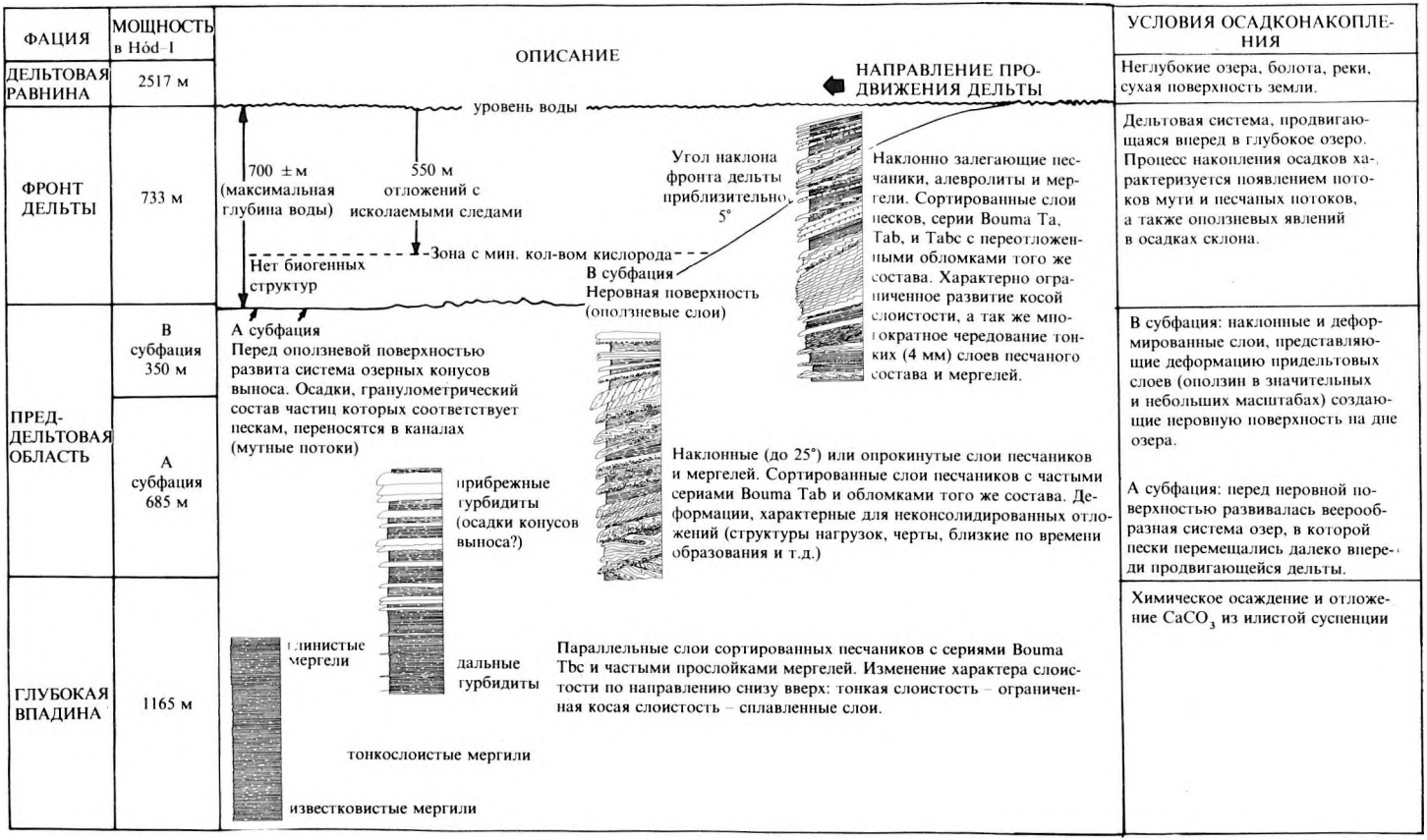

Рис. 11. Процессы и условия осадконакопления в продвигающейся дельте паннонской озерной системы

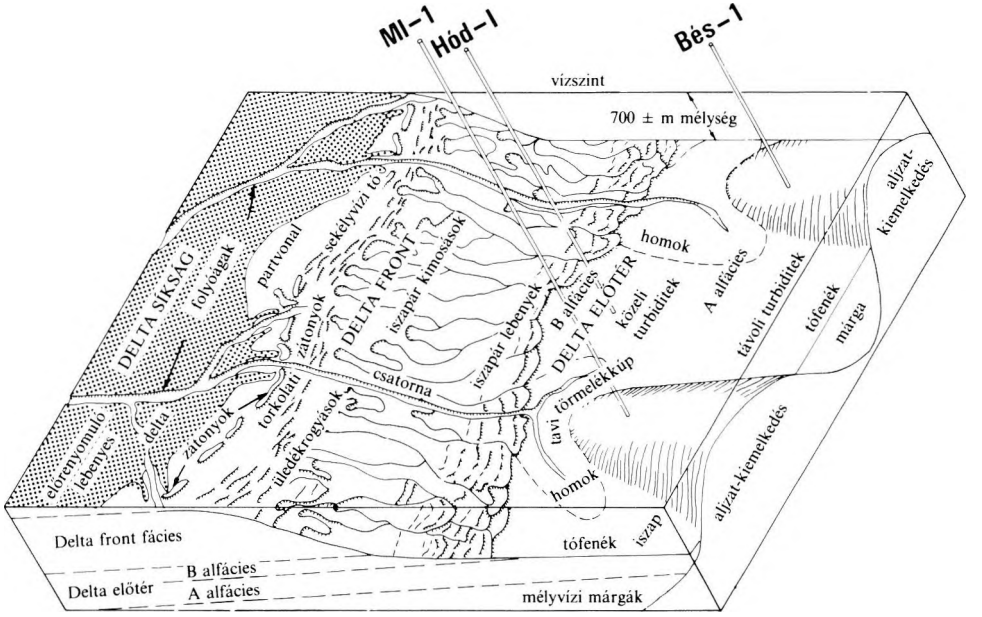

12. ábra. Fő üledékképződési folyamatok egy folyami deltarendszerben. Az előrenyomuló lebenyes deltarendszer valószínűleg tartalmazott egy csatornarendszert, amely összekötötte a folyóágakat az előtér tavi törmelékkúpjával. A folyóvízi delta előrenyomulása a fáciesek és üledéksorok vertikális egymásutániságát eredményezi, amely megfigyelhető a Makó–Hódmezővásárhelyi árok fúrásainak magmintáin

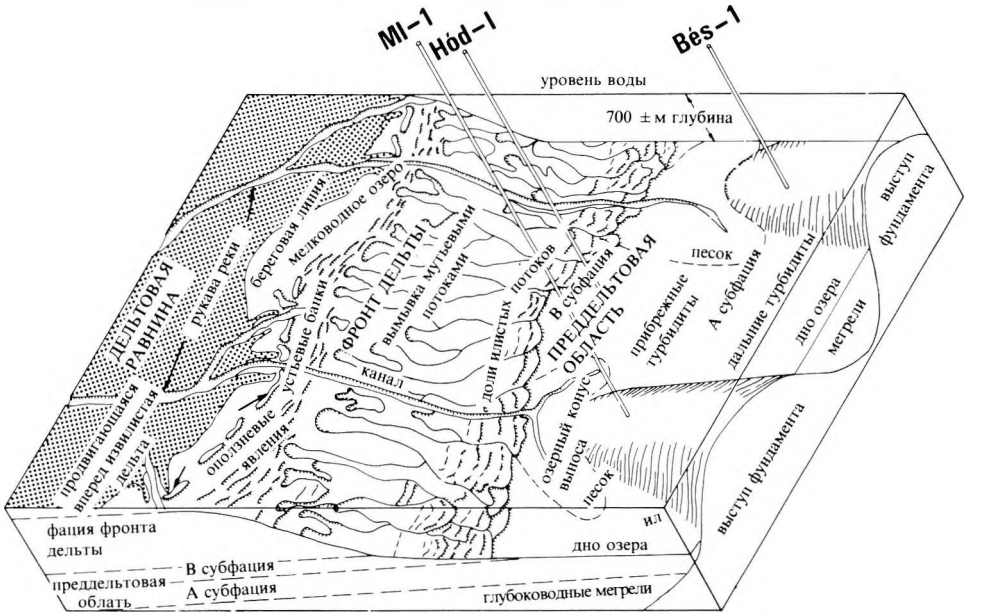

Рис. 12. Главные процессы накопления осадков в системе речной дельты. В продвигающейся извилистой системе дельты, по всей вероятности, существовала и система каналов, соединяющая рукава реки с озернотипным конусом выноса придельтовой области. В результате продвижения дельты в кернах скважин Мако–Ходмезёвашархейского грабена хорошо наблюдается вертикальная смена одних фаций и свит последующими

GEOPHYSICAL TRANSACTIONS 1985
Vol. 31. No. 1—3. pp. 75–88.

MAGNETOSTRATIGRAPHY OF NEOGENE STRATA PENETRATED IN TWO DEEP CORE HOLES IN THE PANNONIAN BASIN: PRELIMINARY RESULTS

Donald P. ELSTON*, Géza HÁMOR**, Áron JÁMBOR**,
Miklós LANTOS** and András RÓNAI**

Neogene strata cored in two 1200 m-deep holes drilled in the central and northern parts of the Pannonian Basin (Kaskantyú–2 and Sámsonháza–16a, respectively) were sampled on < 1 m intervals for development of polarity records that might be correlated with the generally accepted polarity time scale. The Kaskantyú–2 drill hole penetrated strata of Pleistocene and Pliocene age in its upper part, and a nearly complete, Late Miocene section in its lower part. Strata of Pliocene and Late Miocene age are assigned to the Pannonian (s.l.) stage. The strata were found to be stably magnetized, which allowed development of a polarity zonation that is provisionally correlated with the polarity time scale for the interval from perhaps as much as 12 to about 2 million years (Ma) ago. The polarity zonation from the Kaskantyú–2 core hole has allowed a rate of about 120 m/Ma to be estimated for the accumulation of sediments in the south-central Pannonian Basin during late Miocene and Pliocene time. The zonation in the upper part of the Kaskantyú–2 borehole correlates generally with a polarity zonation assigned to the Early Pleistocene and Pliocene reported from core holes previously drilled near Dévaványa and Vésztő in the east-central basin.

The Sámsonháza–16a core hole in the northern part of the basin penetrated pre-Pannonian Neogene strata. The magnetization, weak and unstable for a large part of the section, precluded development of a polarity zonation that could be correlated in its own right with the polarity time scale. The few intervals of stable magnetization thus could only be tentatively related to the polarity time scale by employing nannoplankton age assignments for the section, supplemented by K/Ar dates extrapolated to the section. Although the resulting correlations are uncertain, they nonetheless suggest that much of the pre-Pannonian complex in the Sámsonháza–16a section accumulated during relatively short intervals of time.

Keywords: stratigraphy, magnetostratigraphy, chronostratigraphy, Neogene, Paratethys, Pannonian Basin

1. Introduction

We present here preliminary results of a study of the polarity records from two deep holes cored in the south-central and northern Pannonian Basin of Hungary. One hole, Kaskantyú–2, was drilled in strata of south-central Hungary assigned to the Lower and Upper Pannonian stage (s.l.), which includes strata of late Miocene and Pliocene age. The second hole, Sámsonháza–16a, was drilled in pre-Pannonian Neogene strata of north-central Hungary. The holes were cored to depths of about 1200 m. More than 2500 samples oriented with respect to the up-direction of the cores were collected and analysed at the Paleomagnetics Laboratory at Flagstaff, Arizona.

* U.S. Geological Survey, 2255 North Gemini Drive, Flagstaff, AZ 86001
** Hungarian Geological Survey, POB 106, Budapest, H–1442
Manuscript received (revised form): 26 July, 1985

One objective of this study was to provide time-lines, by developing correlations with the polarity time scale, so that Neogene sections of the Pannonian Basin can be better placed in the geologic time scale. This would lead to an improved understanding of correlations, facies relations, sedimentologic and structural history, and evolution of the basin during Neogene time. For Hungary, this also should lead to an improved understanding of hydrocarbon evolution and accumulation in the Pannonian Basin, particularly when paleomagnetically „dated" Pannonian horizons are extrapolated to the deep parts of the basin by means of other geophysical methods. For this scientific field, a high resolution polarity record potentially obtainable from strata of the Pannonian Basin holds promise for allowing an improved polarity zonation to be developed for the interval 5–12 Ma ago, which would more than double the current terrestrially derived polarity zonation that is relatable to the oceanic polarity record.

The magnetostratigraphic studies reported here have been carried out through a bilateral cooperative agreement between the U.S. Geological Survey (U.S.A.) and the Central Office of Geology (Hungary) for the analysis of the two boreholes. Results are preliminary because work on the Kaskantyu–2 drill cores has not yet been completed.

2. Geologic setting

Stratigraphic and paleontologic studies have shown that the Paratethys was not connected with the open ocean during the Neogene [Laskarev 1924]. The planctonic foraminifera studies [Cicha–Seneš 1968, Steininger–Seneš 1971] have shown that the molluscan- and planctonic foraminifera-based correlations of the late 19*th* century contained facies-related temporal errors of about 6 to 7 Ma. In view of the foregoing, direct paleontologic correlations of Miocene and Pliocene strata of the Pannonian stage (s.l.) with the oceanic record have not been possible, and correlations thus have to be derived from chronostratigraphic methods.

The stratigraphic sequence in the Pannonian Basin, at places, contains intercalated volcanic deposits. These have locally allowed the age of the strata gto be assessed by K/Ar determinations [Hámor et al. 1979, and Balogh et al. 1982]. Additionally, detailed magnetostratigraphic records have been developed from two thick sections cored in the Great Hungarian Plain [Cooke et al. 1979] of the east-central basin. This paleomagnetic work made it possible to identify the boundary between the Pleistocene and Pliocene in the basin-filling sequence, and also to infer an approximate position for the lower boundary of strata of Pliocene age. However, temporal relationships for underlying strata in the Pannonian Basin with respect to the polarity time scale (particularly for strata assigned to the middle and lower parts of the Pannonian stage, s.l.) required additional magnetostratigraphic study. To achieve this, two deep holes (cored to their full depts, ~ 1200 m) were drilled to intersect an anticipated complete, composite Neogene section, and these sections were subjected to multidisciplinary studies, including magnetostratigraphic analysis.

3. Stratigraphy of the boreholes

The locations of two holes whose cores were analysed for this study are shown in *Figure 1.* Kaskantyú–2 is located in the middle part of the Danube–Tisza interfluve, whereas Sámsonháza–16a is located in the central part of the North Hungarian Highland Range. Although hiatuses exist, much of the Neogene sequence of the Pannonian Basin is penetrated in these two holes. Partially correlative strata penetrated by the Dévaványa and Vésztő drill holes [COOKE et al. 1979] are located in the east central part of the Pannonian Basin, east of the Tisza River (Figure 1).

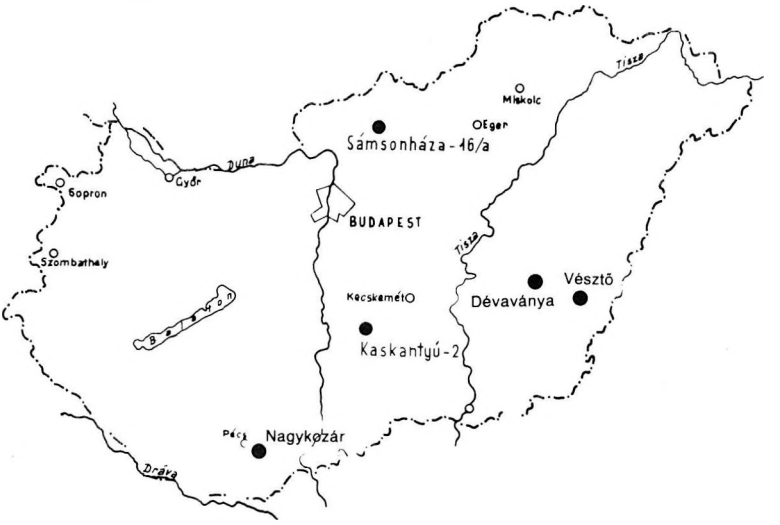

Fig. 1. Location map showing the boreholes studied

1. ábra. A tanulmányozott fúrások helye

Рис. 1. Схема расположения изучаемых скважин

The base of the sequence penetrated in the Kaskantyú–2 borehole *(Figure 2)* begins with deposits of a Late Badenian (Middle Miocene) transgression. Deposition was followed by apparently uninterrupted accumulation that continued to the top of the Sarmatian (early Late Miocene). The basal part of the overlying Pannonian sequence is missing, because strata belonging to the *Pleurozonaria ultima* zone, and to the lower half of the *Spiniferites bentori* zone, are absent. Above this, pelitic-sandy strata were deposited without interruption to the top of the Pannonian (s.l.) stage. Basal deposits of late Pliocene age (early Pleistocene according to the Hungarian classification of time stratigraphic units) overlie the Pannonian strata, which in turn are followed by a minor(?) hiatus and the deposition of younger Pleistocene deposits. Most of the Pleistocene section was not sampled because it was unsuitable for paleomagnetic study

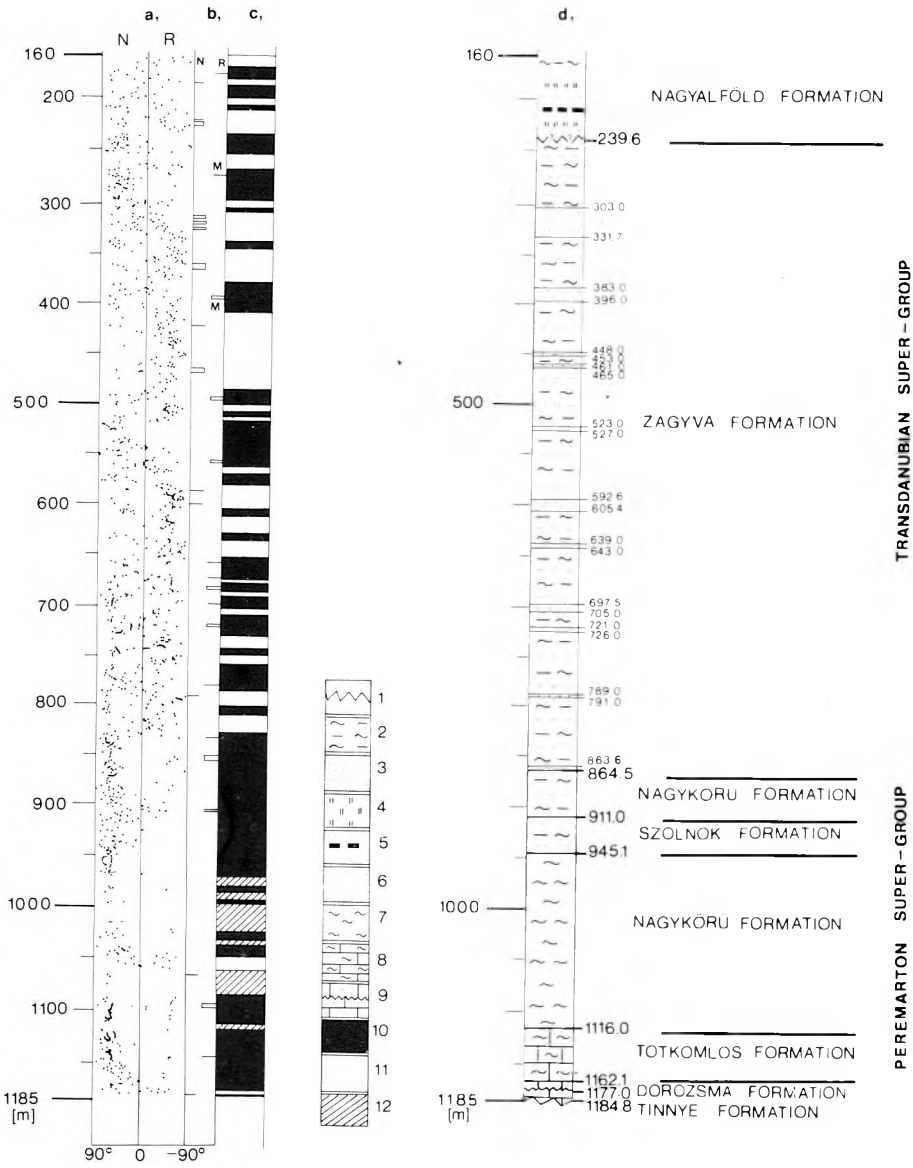

Fig. 2. Lithostratigraphy and magnetostratigraphy of borehole Kaskantyú–2
Columns: a) inclination; b) short reversals (M means mixed polarity); c) magnetostratigraphic zonation; d) lithology. 1 — unconformity; 2 — clayey marl; 3 — sand; 4 — variegated clay; 5 — huminite-bearing clay; 6 — silt; 7 — marl; 8 — calcareous marl; 9 — coarse clastic ooidal limestone with conglomerate; 10 — normal magnetization; 11 — reverse magnetization; 12 — no data

The Kaskantyú–2 borehole sequence has been analysed for *Dinoflagellata* planktonic microfossils by SÜTŐ-SZENTAI [written communication, 1983], for molluscs by KORPÁS-HÓDI [written communication, 1983], and for ostracods by KORECZ [written communication, 1983]. Additionally, a relatively fresh sample of rhyolite tuff from the Nagykozár–2 drill hole has been analysed to obtain a K/Ar date from biotite [BALOGH et al. 1983, written communication]. This date, 11.6 ± 0.5 Ma, comes from strata closely overlying the lower boundary of Lower Pannonian strata, therefore providing an approximate age for this boundary. Various ages have been reported for strata at different levels of the Pannonian stage (s.l.). The boundary between the Lower and Upper Pannonian based on molluscan fauna is considered to lie at about 7 Ma [KORPÁS-HÓDI 1983]. This age, however, differs considerably from the approximately 5 Ma value inferred from K/Ar dates obtained from Pannonian basalts [BALOGH et al. 1982], which lie near the boundary between strata assigned to the Lower and Upper Pannonian. Alternatively, a boundary drawn between the Lower and Upper Pannonian stages in the Kaskantyú–2 drill core lies at about 8.8 Ma on the basis of paleomagnetic correlations. Lastly, a boundary drawn between *Spiniferites bentori* and *Spiniferites validus* has been proposed as a stage boundary within the Pannonian s.l. [JÁMBOR–KORPÁS-HÓDI–SZÉLES–SÜTŐ-SZENTAI 1985]. This boundary corresponds with a stratigraphic position low in the Kaskantyú–2 section [SÜTŐ-SZENTAI 1983]. It is at a level that appears to be older than 11 Ma old on the basis of preliminary correlation of the Kaskantyu–2 section with the polarity time scale.

The Sámsonháza–16a drill hole *(Figure 3)* bottomed in strata assigned to the Egerian (Late Oligocene and Early Miocene) stage. The Egerian strata are unconformably overlain by Ottnangian (late Early Miocene) strata, strata that in turn may be turncated by an unconformity. Above this, strata assigned to the Karpathian (late Early Miocene) stage consist of coarse to fine clastics grading upwards to siltstone and marl. These are overlain by tuffaceous strata locally containing andesite flows, all of which are assigned to the Badenian stage (Middle Miocene).

2. ábra. A Kaskantyú–2 mélyfúrás lito- és magnetosztratigráfiája
Oszlopok: a) inklináció; b) rövid átfordulások (M = kevert polaritás); c) magnetosztratigráfiai zonáció; d) litológiai rétegsor. 1 — diszkordancia; 2 — agyagmárga; 3 — homokkő; 4 — tarkaagyag; 5 — huminites agyag; 6 — iszap; 7 — márga; 8 — mészmárga; 9 — durvaszemű ooidos mészkő konglomerátummal; 10 — normál mágnesezettség; 11 — fordított mágnesezettség; 12 — nincs adat

Рис. 2. Лито- и магнитостратиграфия скважины Кашкантю–2
Столбцы: a) наклонение; b) кратковременные перевороты (M = смешанная полярность); c) разделение магнитостратиграфических зон; d) литологический колонка. 1 — несогласие; 2 — глинистые мергели; 3 — песчаники; 4 — пестроцветные глины; 5 — глины со содержанием органического вещества; 6 — или; 7 — мергели; 8 — известковые мергели; 9 — обломочные ооидовые известняки с конгломератамы; 10 — нормальная намагниченность; 11 — обратная намагниченность; 12 — нет данных

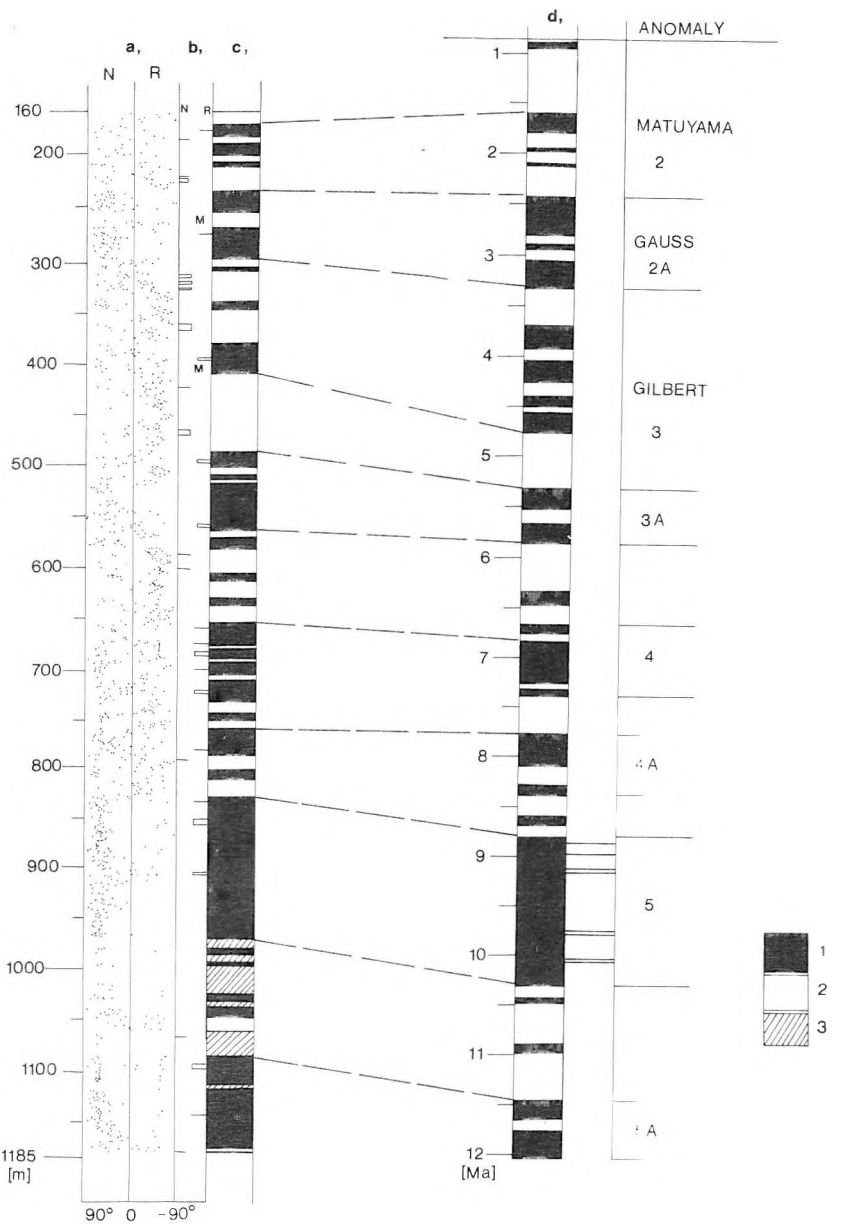

Fig. 3. Preliminary correlation of the polarity zonation of the Kaskantyú–2 core hole with the polarity time scale of LOWRIE and ALVAREZ [1981]
Columns: a) inclination; b) short reversals (M means mixed polarity); c) magnetostratigraphic zonation; d) polarity time scale. 1 — normal magnetization; 2 — reverse magnetization; 3 — no data

4. Paleomagnetic analysis

The Kaskantyú–2 and Sámsonháza–16a drill holes were cored in full, employing a 5.9 m long core barrel. The cores were sampled at approximately 0.5 m intervals at the drill site. Initially, no samples of unconsolidated sediments or very hard rock were collected, giving rise to a few rather large gaps in paleomagnetic records (a maximum of 20 m length). Subsequently, approximately 200 second-stage samples were collected from the major unsampled intervals in the Kaskantyú–2 section, and from across the section to check on the validity of several intervals of one- and two-sample "reversals". Analysis of the second stage samples has not yet been completed.

Approximately 2600 first stage samples were processed in the paleomagnetics laboratory at Flagstaff, Arizona. Following measurement of the natural remanent magnetization (NRM), a series of pilot samples were subjected to stepwise alternating field demagnetization analysis for identification of the ranges of stability in representative materials. In view of the behavior observed during demagnetization analysis, the remaining Kaskantyú–2 samples were partially demagnetized in 50 oersted (oe) (= 5 mT or milliTesla) fields, and the samples from Sámsonháza–16a were partially demagnetized in 75 oe (7.5 mT) fields.

Samples that were considered to be reliable for development of a polarity zonation exhibited inclinations $>20°$, and intensities $>2\times10^{-7}$ emu/cm^3 (or $\sim 2\times10^{-4}$ A/m). Samples having lower reliability, but for which only one of the conditions was met, were also considered to be potientially useful and employed in the evaluation. Finally, samples exhibiting very low intensities and/or inclinations near 0° were not used for the determination of polarity. Moreover, reversals controlled by a single sample also were not used for development of a polarity zonation. Such "reversals" were provisionally considered to have arisen from the inadvertent inversion of individual samples.

Kaskantyú–2: Of the two coreholes, Kaskantyú–2 yielded much the better material for paleomagnetic analysis. Intensities are moderate, 10^{-5} to 10^{-6} emu/cm^3 (10^{-2} to 10^{-3} A/m). From demagnetization results (not presented here), the entire sequence was seen to have a rather stable remanent magnetization. Problems with interpretation arose from a rather large number of stratigraphically narrow, apparent polarity reversals, and from a few intervals not

3. ábra. A Kaskantyú–2 mélyfúrás előzetes korrelációja a LOWRIE és ALVAREZ [1981] féle polaritás–idő skálával

Oszlopok: a) inklináció; b) rövid átfordulások; c) magnetosztratigráfiai zonáció; d) polaritás–idő skála. 1 — normál mágnesezettség; 2 — fordított mágnesezettség; 3 — nincs adat

Рис. 3. Предварительная корреляция скважины Кашкантю–2 с международной шкалой время–полярность

Столбцы: a) наклонение; b) коротки перевороты; c) магнитостратиграфические зоны; d) зависимость полярности от времени. 1 — нормальная намагниченность; 2 — обратная намагниченность; 3 — нет данных

sampled near the base of the cored section (Figures 2 and 3). Second-stage sampling was undertaken with the object of resolving several of the uncertainties.

A preliminary correlation of the Kaskantyú–2 polarity zonation with the polarity time scale of LOWRIE and ALVAREZ [1981] is proposed in Figure 3. The correlation is based mainly on pattern matching of the principal intervals of normal and reverse polarity, and secondarily on the number and relative thickness of the narrower polarity intervals. Magnetic anomaly 5 plays an important role in the interpretation. Note that the proposed correlation of the top of anomaly 5, at ~ 8.8 Ma, lies close to or coincides with the lithologic boundary between strata assigned to the Lower and Upper Pannonian stage. However, the unavailabity of samples from some of the underlying strata has precluded a more certain identification of the position of the base of anomaly 5, or a less ambiguous correlation with the polarity time scale for strata that are inferred to be ~ 10 Ma and older in age.

The correlation with the polarity time scale shown in Figure 3 contains information on the rate of accumulation of sediments in the Danube–Tisza interfluve area of south-central Hungary during the late Miocene and Pliocene. The accumulation rate for the interval from about 860 to 240 m depth, extending from near the top of anomaly 5 to the inferred top of the Gauss normal polarity epoch, was virtually constant at about 120 m/Ma *(Fig. 4)*. This rate of accumulation is about two-thirds of that, calculated from the Dévaványa and Vésztő core holes [COOKE et al. 1979 and RÓNAI 1981].

Sámsonháza–16a: In the pre-Pannonian strata cored in Sámsonháza–16a, the strategy of employing a potential polarity zonation differed markedly from the strategy used for the Pannonian and post-Pannonian drill core records obtained from the more central parts of the Pannonian Basin. In the latter, correlations with the polarity time scale were developed by assuming that deposition was more or less continuous across the intervals studied, an assumption based on stratigraphic records, now supported by paleomagnetic records. In contrast, the polarity record obtained from Sámsonháza–16a was compromised by severe geologic as well as paleomagnetic complications.

Many samples from borehole Sámsonháza–16a are characterized by low to very low intensities, which for many samples scarcely exceeded the noise level of the cryogenic magnetometer (see *Figure 5*). Additionally, a persistent viscous component was observed for these intervals, suggesting an unstable magnetization. Lastly, there are many gaps in the magnetostratigraphic coverage. The foregoing deficiencies, alone, precluded correlation of the contained polarity record with the polarity time scale.

In spite of the above, parts of the magnetic record have been provisionally related to the polarity time scale by employing the nannoplankton record, supported by K/Ar ages extrapolated to the section (Figure 5). These temporal data strongly suggest that the section penetrated in the Sámsonháza drill hole accumulated irregularly through time, and at markedly different rates of accumulation. Nannoplanktonic results [NAGYMAROSY 1983] indicate that the inter-

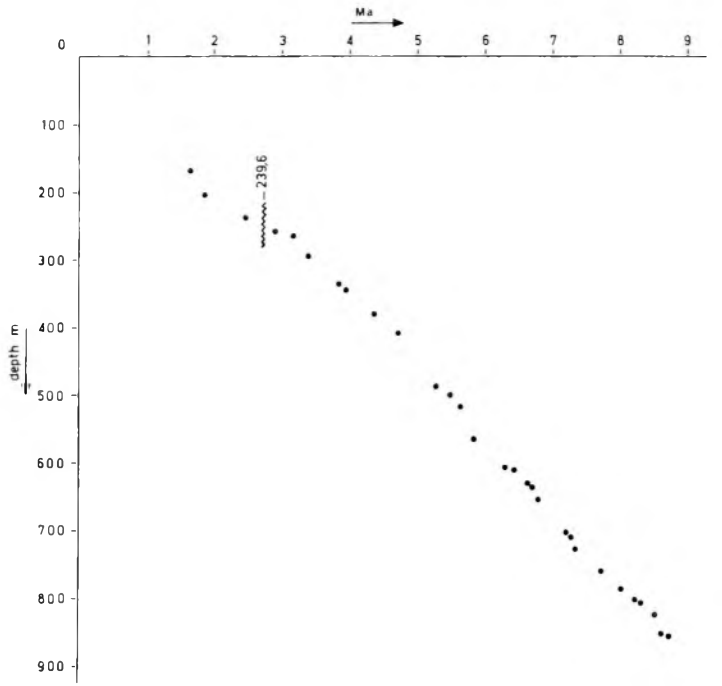

Fig. 4. Accumulation rate of sediments during the Late Miocene and Pliocene from proposed correlation of the polarity zonation of the Kaskantyú–2 core hole with the polarity time scale

4. ábra. Üledékfelhalmozódási sebesség a felsőmiocénben és a pliocénben, a Kaskantyú–2 mélyfúrás polaritászónái és a nemzetközi polaritás–idő skála korrelációjából

Рис. 4. Скорость осадконакопления в верхнем миоцене и в плиоцене, рассчитанная на основе корелляции зон полярности глубокой скважины Кашкантю–2 с международной шкалой время–полярность

val from 211 m to 712 m can be assigned to nannoplankton zone 4 (NN4), which from the compilation of HAQ [1983] has an assigned age range of about 17.0 to 18.4 Ma. This age range includes a substantial part of an interval of apparent normal polarity, and questionable normal polarity, in the Sámsonháza–16a core (Figure 5). Nannoplankton zone 5, from the upper part of the interval of questionable normal polarity, has an assigned age range of about 15 to 17 Ma. Above this, from a stably magnetized interval, an extrapolated K/Ar age appears to require a correlation of this and the underlying strata with anomaly 5C, which has an assigned age range of 16.2 to 17 Ma. Thus, strata extending from a depth of less than 100 m to more than 800 m would seem to have accumulated during an interval of time considerably less than 2 Ma. It is a stratigraphic interval that corresponds to the development of "schlieren" in the region during early Miocene time [NOSZKY sen. 1912, CSEPREGHY-MEZNERICS 1951, HÁMOR– JÁMBOR 1969]. About 200 m beneath this, an interval of stable

normal polarity corresponds with nannoplankton zone 2 (NN2), for wich an age range of 19.6 to 23.0 Ma has been assigned [HAQ 1983, NAGYMAROSY 1981]. This basal normal polarity interval, consequently cannot be correlated with the polarity time scale.

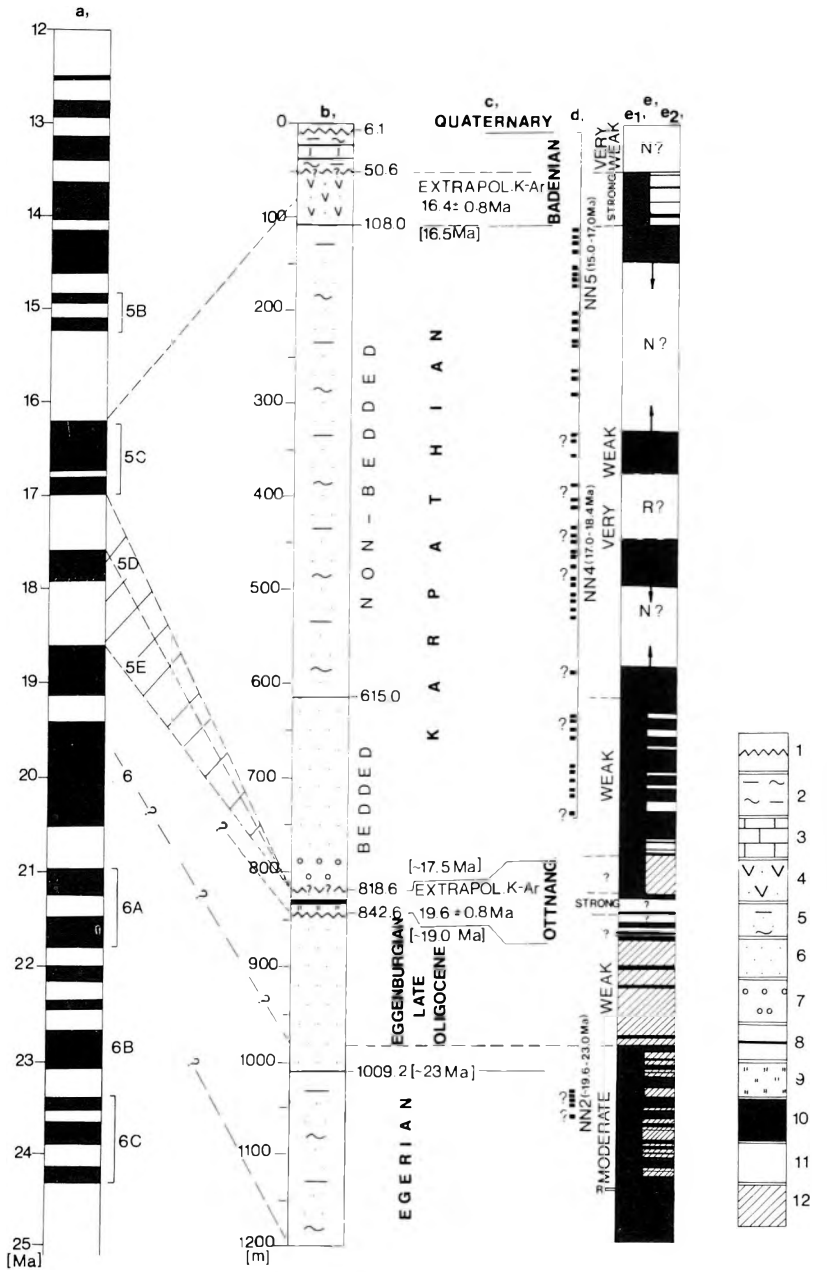

5. Summary

Evidence summarized in the preceeding sections leads to the following general conclusions.

(1) The Kaskantyú–2 drill hole appears to have penetrated a section of strata of early Pleistocene, Pliocene, and Miocene age that spans polarity anomaly intervals 2 through possibly 5A, extending from about 1.7 to perhaps as much as 12 Ma. Within this, the section assigned to the Pannonian stage (s.l.) extends from approximately the Late Miocene, at perhaps 11.5 Ma, across Late Miocene and Pliocene time, with an upper boundary that appears to coincide with the boundary between the Matuyama and Gauss polarity epochs. Consequently, the Pannonian stage (s.l.) includes the Tortonian, Messinian, and Zanclean stages of Mediterranean stratigraphy.

Fig. 5. Lithostratigraphy and apparent polarity zonation from the Sámsonháza–16a core hole, and a possible correlation with the polarity time scale employing nannoplankton age assignments and K/Ar ages extrapolated to the section

Columns: a) polarity time scale after LOWRIE and ALVAREZ [1981], b) lithology; c) chronostratigraphic units; d) nannoplankton zones; e) magnetostratigraphic zonation: e_1) interpretation, with classification (contradictions and uncertainty indicated); e_2) measurement. 1 — unconformity; 2 — clayey marl; 3 — limestone; 4 — andesite pyroclastics; 5 — argillaceous–calcareous–sandy aleurolite; 6 — sandstone; 7 — gravel; 8 — lignite; 9 — variegated clay; 10 — normal magnetization; 11 — reverse magnetization; 12 — no data

5. ábra. A Sámsonháza–16a mélyfúrás litosztratigráfiai és magnetosztratigráfiai beosztása, valamint ennek egy lehetséges korrelációja a nemzetközi polaritás–idő skálával, felhasználva nannoplankton- és extrapolált K/Ar kormeghatározási adatokat

Oszlopok: a) polaritás–idő skála LOWRIE és ALVAREZ [1981] után; b) litológiai rétegsor; c) kronosztratigráfiai egységek; d) nannoplankton zónák; e) magnetosztratigráfiai zonáció: e_1) értelmezés osztályozással (ellentmondások és bizonytalanságok feltüntetésével), e_2) mérési adatok. 1 — diszkordancia; 2 — agyagmárga 3 — mészkő 4 — andezit piroklasztit 5 — agyagos–meszes–homokos aleurolit; 6 — homokkő; 7 — kavics; 8 — lignit; 9 — tarkaagyag; 10 — normál mágnesezettség; 11 — fordított mágnesezettség; 12 — nincs adat

Рис. 5. Литостратиграфическое и магнитостратиграфическое расчленение глубокой скважины Шамшонхаза–16а, и одна из возможных корелляций с международной шкалой время–полярность, используя данные определения возраста по наннофлоре и экстраполированные данные определения возраста K/Ar методом

Столбцы: а) зависимость полярности от времени по LOWRIE и ALVAREZ [1981]; b) литопогическая колонка; c) хроностратиграфические единицы; d) наннопланктоновые зоны; e)магнитостратиграфические зоны: e_1) интерпретация с классификацией (с указанием противоречий и ненадежностей); e_2) измеренные данные. 1 — несогласие; 2 — глинистые мергели; 3 — известняки; 4 — андезитовые туфы; 5 — глинисто–известково–песчаные алевриты; 6 — песчаники; 7 — щебень; 8 — лигнит; 9 — пестроцветные глины; 10 — нормальная намагниченность; 11 — обратная намагниченность; 12 — нет данных

A boundary between the Lower and Upper pannonian, drawn at the contact between the Nagykörü and overlying Zagyva Formations in the Kaskantyú–2 drill hole (at about 864 m; Figure 2) lies at the approximate level of the top of anomaly 5 at 8.8 Ma. This boundary differs markedly from an age approximately 5 Ma reported for Pannonian basalt occurring near a boundary that separates [illegible]ssigned to the Lower and Upper Pannonian [Balogh et al. 1982]. From paleomagnetic correlations, the Miocene–Pliocene boundary in the Kaskantyú–2 section lies within the Zagyva Formation, at a depth of about 450 m. An estimatd provisional age for the base of the Pannonian in the Kaskantyú–2 section of about 11.5 Ma, accords with a K/Ar age on biotite extrapolated from the Nagykozár–2 borehole. Lastly, Pannonian sediments, correlated with the polarity time scale for the interval from about 9 to 2 Ma, accumulated at a rather uniform rate of about 120 m/Ma.

(2) The Pliocene and Pleistocene polarity zonation from the Kaskantyú–2 core hole generally correlates with earlier results from the Dévaványa and Vésztő core holes drilled in the Great Hungarian Plain [Cooke et al. 1979]. The lowermost Pleistocene (late Pliocene of usage elsewhere) sequence [Nagyalföld Formation = Vésztő Formation in Cooke et al. 1979] has an age of 1.5 to 2.4 Ma from paleomagnetic correlations. The "Pleistocene" age for the Nagyalföld Formation has been confirmed by ostracode results [Korecz 1983].

(3) Paleomagnetic study of samples from the Sámsonháza–16a core hole have served only to help refine geologic interpretations related to the time required to accumulate the strata, interpreted primarily from nannoplankton zonations and extrapolated K/Ar ages. A large part of the section in the Sámsonháza drill hole, associated with "schlieren" assigned to the Karpathian stage, appears to have accumulated in less than a two million year span of time, correlated principally with magnetic anomaly 5C.

These efforts to date have led to promising although as yet incomplete results. A continuing effort is needed toward development of a reference polarity zonation for the Pannonian (s.l.) and Pleistocene sections of the Pannonian Basin. It is a zonation that has yet to be demonstrated by a reproducibility derived from the analysis of a third cored section. A 1.9 km-thick section cored at Tiszapalkonya in the northeastern part of the Basin is expected to provide the needed control.

Application of a reference polarity zonation for the Pannonian (s.l.) to the seismic stratigraphy in relatively shallow parts of the basin would provide time-lines that could be extrapolated into deep parts of the basin. This would allow the Neogene stratigraphy to be evaluated at depth, which should lead to an improved understanding of facies relations and the evolution of structure at depth. Polarity time-lines may never be developed for the deep parts of the basin because depths of burial greater than a few kilometers could very likely have caused remagnetization of the strata.

REFERENCES

BALOGH K., JÁMBOR Á., PARTÉNYI Z., RAVASZ-BARANYAI L., SOLTI G. 1982: K/Ar dating of basaltic rocks in Transdanubia, Hungary (in Hungarian with English abstract) Föld. Int. Évi Jelentése az 1980. évről. (Annual Report of the Hung. Geol. Inst.) pp. 243–260

BALOGH K., ÁRVA-SÓS E., PÉCSKAI Z. 1983: K/Ar dating of Neogene volcanic rocks (in Hungarian) Manuscript, MÁFI Database

CICHA I., SENEŠ J. 1968: Sur la position du Miocène de la Paratethys centrale dans le cadre du Tertiaire de l'Europe. Geol. Sbornik (Geol. Carpatica) **19,** 1, Bratislava

COOKE H. B. S., HALL J. M., RÓNAI A. 1979: Paleomagnetic sedimentary and climatic records from boreholes of Dévaványa and Vésztő, Hungary. Acta Geol. **22,** 1–4, pp. 89–109

CSEPREGHY-MEZNERICS I. 1951: The fauna of "schlieren" and sandstone of Salgótarján (in Hungarian with Russian abstract) Földtani Közlöny (Bull. of the Hung. Geol. Soc.). **81,** 3–4, pp. 303–319

HÁMOR G., JÁMBOR Á. 1969: La Miocène moyenne en Hongrie. In: Materiaux des Séances Plénaires et Sections de la Conférences de Neogène en Hongrie. pp. 25–48, MÁFI. Budapest

HÁMOR G., RAVASZ-BARANYAI L., BALOGH K. 1979: K/Ar dating of Miocene pyroclastic rocks in Hungary. Ann. Geol. des Pays Hell. pp. 491–500

HAQ B. U. 1983: Jurassic to recent nannofossil biochronology: an update. In: Nannofossil biostratigraphy (ed. Haq B. U.) Benchmark papers in geology. **78** pp. 368–387 Hutchinson Ross Publishing Co., Stroudsburg, Pa. USA

JÁMBOR Á., KORPÁS-HÓDI M., SZÉLES M., SÜTŐ-SZENTAI M. 1985: Zentrales Mittleres Donaubecken: Bohrung Lajoskomárom Lk-1, S-Balaton. In: Chronostratigraphie und Neostratotypen Bd. VII. Miozän der Zentralen Paratethys, M_6 Pannonien. pp. 204–241

KORECZ A. 1983: The ostracode fauna of the Pannonian (s.l.) of borehole Kaskantyú–2 (in Hungarian). Manuscript, MÁFI Database

KORPÁS-HÓDI M. 1983: The mollusc fauna of the Pannonian (s.l.) of borehole Kaskantyú–2 (in Hungarian). Manuscript MÁFI Database

LASKAREV N. V. 1924: Sur les equivalents du Sarmatien superieur en Serbie. Zbornik Cvijić, Beograd

LOWRIE W., ALVAREZ W. 1981: One hundred million years of geomagnetic polarity history. Geology, **9.** pp. 392–397

NAGYMAROSY A. 1981: Chrono- and biostratigraphy of the Pannonian Basin: A rewiew based mainly on data from Hungary. Earth Evolution Sciences, **1,** 3–4, pp. 183–194

NAGYMAROSY A. 1983: Nannoplankton examination of formations penetrated by borehole Sámsonháza–16a (in Hungarian). Manuscript, MÁFI Database

NOSZKY J. sen. 1912: Geological conditions of the Salgótarján coal district (in Hungarian). A Koch A. memorial edition pp. 67–70, Budapest

RÓNAI A. 1981: Magnetostratigraphy of Pliocene–Quaternary Sediments in the Great Hungarian Plain. Earth Evolution Sciences, **1,** 3–4, pp. 265–267

STEININGER F., SENEŠ J. 1971: Einleitung. In: Chronostratigraphie und Neostratotypen Bd. II. M_1 Eggenburgien [illegible] 20

SÜTŐ-SZENTAI M. 1983: The organic microplankton flora of borehole Kaskantyú–2 (in Hungarian). Manuscript, MÁFI Database

A PANNON MEDENCE NEOGÉN ÜLEDÉKEINEK MAGNETOSZTRATIGRÁFIAI VIZSGÁLATA KÉT MÉLYFÚRÁSBAN: ELŐZETES EREDMÉNYEK

Donald P. ELSTON, HÁMOR Géza, JÁMBOR Áron, LANTOS Miklós és RÓNAI András

A Pannon medence középső és északi részén két ~1200 m-ig folyamatos magmintavétellel mélyített mélyfúrásban (Kaskantyú–2 és Sámsonháza–16a) 1 m-nél sűrűbben vettek mintát, hogy a polaritás változásokat korrelálják az általában elfogadott nemzetközi polaritás–idő skálával. A Kaskantyú–2 mélyfúrás felső része pleisztocén és pliocén rétegeket, alsó része majdnem a teljes felsőmiocént harántolta. A pliocén és felsőmiocén rétegeket a Pannon emeletbe (s. l.) sorolják.

A rétegek stabil mágnesezettséget mutattak, így lehetséges volt egy magnetosztratigráfiai beosztás felállítása, amelyet korreláltak a nemzetközi polaritás–idő skála 12–2 millió éves szakaszával, noha ez a korreláció nem tekinthető véglegesnek. Ebből kb. 120 m/millió év üledékfelhalmozódási sebesség volt becsülhető a Pannon medence középső–déli részére a felsőmiocén és a pliocén idejére. A Kaskantyú–2 mélyfúrás felső szakaszának magnetosztratigráfiai beosztása általában korrelálható az alsópleisztocénre és a pliocénre elfogadott, két korábbi mélyfúrásban (Dévaványa és Vésztő), a Pannon medence középső–keleti részére megállapított beosztással.

A Sámsonháza–16a mélyfúrás, a medence északi részén, pannon előtti neogén rétegeket is harántolt. A mágnesezettség a szelvény nagy részén gyenge és labilis, így önmagában nem korrelálható a nemzetközi polaritás–idő skálával. Egyes, stabil mágnesezettségű intervallumok csak a nannoplankton kormeghatározás segítségével kapcsolhatók — kísérleti jelleggel — a polaritás–idő skálához, felhasználva a rendelkezésre álló K/Ar kormeghatározási adatokat a fúrásra extrapolálva. Bár az eredményként kapott korreláció bizonytalan, azt sugallja, hogy a pannon előtti üledékek relative rövid idő-intervallumokban halmozódtak fel.

ПРЕДВАРИТЕЛЬНЫЕ РЕЗУЛЬТАТЫ МАГНИТОСТРАТИГРАФИЧЕСКИХ ИССЛЕДОВАНИЙ НЕОГЕНОВЫХ ОТЛОЖЕНИЙ В ДВУХ ГЛУБОКИХ СКВАЖИНАХ В ПАННОНСКОМ БАССЕЙНЕ

Доналд П. ЭЛСТОН, Геза ХАМОР, Арон ЯМБОР, Миклош ЛАНТОШ и Андраш РОНАИ

В двух скажинах глубиной приблизительно 1200 м, пробуренных при непрерывном отборе керна в средней и северной частях Паннонского бассейна, отбор пров для палеомагнитных измерений проводился при интервале меньше 1 м, чтобы изменения полярност скореллировать с международной шкалой времени полярности. Верхняя часть скважины Кашкантю–2 пересекла плейстоценовые и плиоценовые отложения, а ее нижняя часть почти полностью пересекла верхнемиоценовые слои. Плиоценовые и верхнемиоценовые слои приурочены к Паннонскому ярусу (s. l.). Поскольку установлено, что намагниченность слоев стабильная, удалось провести магнитостратиграфическое расчленение, впоследствии скореллированное с интервалом от 12 до 2 миллионов лет международной шкалы время–полярность. Однаку эту корелляцию нельзя считать окончательной. В средней и южной частях Паннонского бассейна скорость осадконакопления в верхнем миоцене и в плиоцене по оценкам составляет около 120 м/миллион лет. Магнитостратиграфически верхнюю часть разреза скважины Кашкантю–2 можно в основном скореллировать со схемой, принятой для средней и восточной частей Паннонского бассейна на основе двух ранее пробуренных глубоких скважинах (Девааня и Вестё).

Глубокая скважина Шамшонхаза–16а, пробуренная в северной части бассейна, пересекла и неогеновые отложение древнее паннонских. Намагниченность в большей части разреза слабая и нестабильная следовательно, нет бозможности для корелляции с международной шкалой время–полярность. Некоторые интервалы, в которых намагниченность стабильная, могут быть в опытном порядке связаны с шкалой времени полярности, используя при этом данные определения возраста по паннофлоре и данные определения возраста K/Ar методом, экстраполированные на скважину. Хотя корелляция, полученная в результате проведенных работ, не является надежной, все же можно предполагать, что накопление отложений древнее паннонских происходило в сравнительно короткие интервалы времени.

GEOPHYSICAL TRANSACTIONS 1985
Vol. 31. No. 1–3. pp. 89–99

CONTRIBUTION TO THE DETERMINATION OF THE PLIO–PLEISTOCENE BOUNDARY IN SEDIMENTS OF THE PANNONIAN BASIN

Andrew E. GROSZ* András RÓNAI** and Ricardo LOPEZ*

Results of a preliminary test to establish the usefulness of studies of heavy-mineral assemblages in resolving the Plio–Pleistocene boundary in sediments of the Pannonian Basin indicate that heavy minerals in samples from the Dévaványa and Vésztő boreholes have been subjected to at least two episodes of weathering. At approximately 440 m in the Dévaványa, and at approximately 500 m in the Vésztő cores, garnet is significantly less abundant and more deeply weathered than elsewhere in the examined sections. These intervals of depleted and weathered garnet are roughly coincident with the Plio–Pleistocene boundary as determined by other methods. Another episode indicated by the presence of mineral grains cemented by authigenic pyrite at approximately 605 m in the Dévaványa core can be correlated with an analogous interval at approximately 650 m in the Vésztő core. The results also indicate that detailed heavy-mineral studies, in conjunction with other methods, may be useful in deciphering the geologic and depositional history of the Neogene/Quaternary sediments in the Pannonian Basin.

Keywords: heavy minerals, weathered garnet, authigenic pyrite, Plio–Pleistocene boundary, Pannonian Basin

1. Introduction

Intervals of geologic time are separated from one another on the basis of significant changes observed in the development of life on earth, that is, in the faunal and floral history. This classic method of biostratigraphy, however, fails to discriminate between the Neogene and Quaternary systems in the Pannonian Basin [RÓNAI 1983].

Recent studies and investigations indicate that paleomagnetic polarity reversals are useful for setting up the Quaternary stratigraphic sequences and for tracing the boundary between the Neogene and the Quaternary [RÓNAI 1983]. Currently, there are two viewpoints about where to set the Neogene/Quaternary boundary. One recommends the Matuyama–Gauss paleomagnetic boundary (2.4 Ma) as the start of the Quaternary; the other chooses the Olduvai event (1.8 Ma) [RÓNAI 1983]. Both are close to the onset of colder and more humid climate on the globe.

In Hungary, the boundary favored by local workers is associated with the Matuyama–Gauss paleomagnetic polarity reversal, making the length of the

* U.S. Geological Survey, National Center, Reston, VA 22 092
** Hungarian Geological Survey, POB 106, Budapest, H–1442
Manuscript received: 12 February, 1985

Quaternary 2.4 million years [RÓNAI 1983]. The rationale for this is as follows: during the last 5–10 million years the Carpathian Basin was epeirogenetically uplifted resulting in the regression of the Pannonian Lake. The Miocene–Pliocene lake occupied the entire Carpathian Basin; more than 5000 m of lacustrine sediments were deposited. When the lake level dropped and the lake bottom became exposed, a period of fluvial sedimentation started. Correlative changes in the floral and faunal assemblages took place. The disappearance of the Pannonian Lake is roughly coincident with the Matuyama–Gauss polarity reversal *(Fig. 1)*.

About the same time the climate changed drastically. While the desiccation of the Pannonian Lake was taking place, the climate was hot and dry. The dried lake bottom was controlled by a desert climate; the sediments are devoid of signs of flora or fauna. The hot temperatures are thought to have diminished subsequently, but the climate remained warm. Of greater significance was the change in humidity. The annual precipitation had been increasing rapidly, and the region became thickly vegetated. The abundance of vegetation climaxed during the Olduvai paleomagnetic event. Subsequent fluctuations in both temperature and precipitation took place, however, vegetative cover never climaxed as before. The desert climate is indicated by the total sterility of the sediments deposited during the time of desiccation. Rich molluscan and ostracode finds, along with rich pollen assemblages are characteristic of the sediments deposited before and after the desert period. The profound changes in the geomorphology, tectonism, and climate are the reasons why the date of the disappearance of the Pannonian Lake is placed at the end of the Pliocene, and the date of the start of fluvial sedimentation is placed at the onset of the Quaternary, roughly at the Matuyama–Gauss boundary *(Fig. 2)*.

In most boreholes of the Pannonian Basin the fluvial sedimentation can be discerned by the cyclical change in granulometry. Pliocene sedimentation is characterized by rapid and sharp transition from sandy to clayey sediments. In the fluvial sediments the granulometry changes gradationally from gravel or sand to clay, and again gradationally, to sand or gravel (a sediment cycle). These cycles are recurrent on a regional basis; in the Pannonian Basin, 9–10 smaller cycles, or 4–5 larger cycles in the Quaternary sediment sequences can be defined where they are complete. This cyclic sedimentation in the Quaternary can be ascribed to changes in the quantity and coarseness of sediments available to fluvial transport caused by either the step-like subsidence of the basin bottom resulting in a shifting channel system, or by the changing humidity of the climate, or by combinations thereof *(Fig. 3)*.

The members of the INQUA Subcommission on the Plio–Pleistocene Boundary and of Geological Correlation Project 41 (Pliocene/Pleistocene boundary) are formulating a resolution regarding the (revised) definition of the Plio–Pleistocene boundary in the Vrica section of Calabria, Southern Italy, to be submitted to the IUGS International Committee on Stratigraphy [BERGGREN et al. 1984]. This resolution will propose locating the Plio–Pleistocene boundary stratotype 3–6 m above the top of the Olduvai normal polarity event, resulting

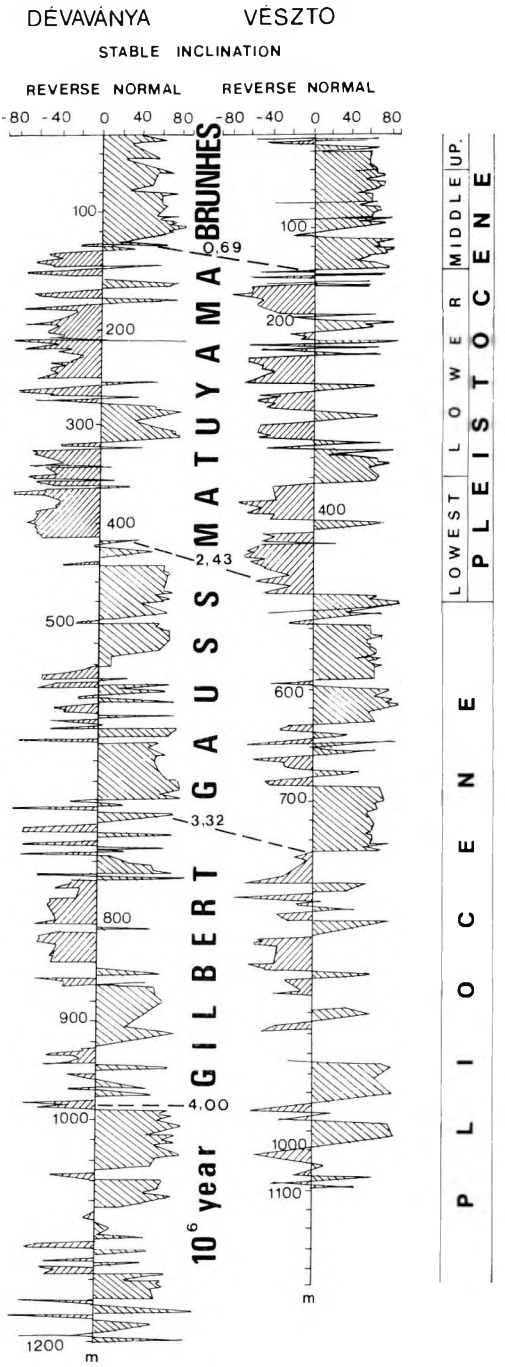

Fig. 1. Paleomagnetic measurements on the core-samples of the Dévaványa and Vésztő boreholes [after COOKE–HALL–RÓNAI 1979]

1. ábra. A dévaványai és vésztői fúrás magmintáinak paleomágneses vizsgálata [COOKE–HALL–RÓNAI 1979]

Рис. 1. Палеомагнитные измерения, проведенные на пробах из девавaньской и вестёйской скважин [COOKE–HALL–RÓNAI 1979]

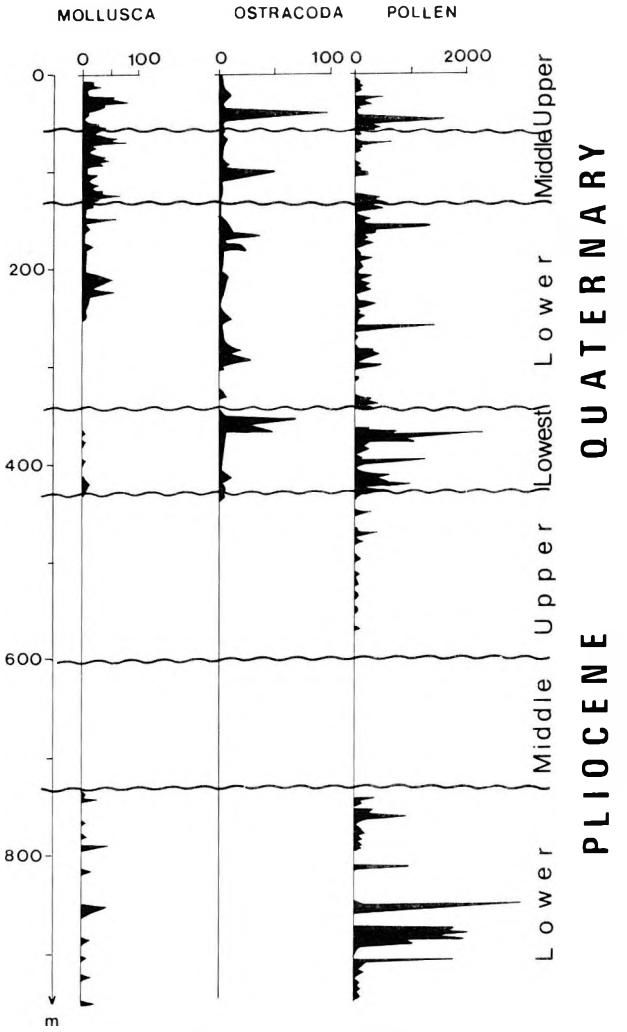

Fig. 2. Number and distribution of paleontologic finds from the borehole of Jászladány (Hungary)

2. ábra. Paleontológiai leletek száma a jászladányi fúrásban

Рис. 2. Количество палеонтологических ископаемых остатков ясладаньской скважины (Венгрия)

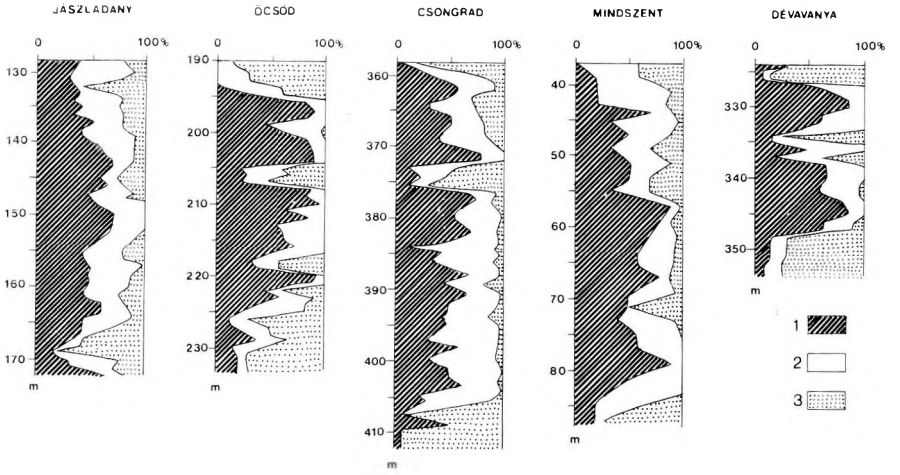

Fig. 3. Examples of fluvial sedimentary cycles
1 — clay and silt (0.0–0.02 mm); 2 — sand flour (0.02–0.06 mm); 3 — sand (0.06–2.0 mm)

3. ábra. Példák folyami üledékképződési ciklusokra
1 — agyag és iszap; 2 — homokliszt; 2 — homok

Рис. 3. Образцы для структуры зерен речных циклов осадконакопления
1 — глина и шлам; 2 — песчаная мука; 3 — песок

in continuity with some previous studies which placed the boundary at the top of the Olduvai event, at approximately 1.6 Ma [HAQ et al. 1977, BERGGREN et al. 1980].

The present study on the heavy minerals from selected intervals within the two boreholes (Dévaványa and Vésztő) was conducted to test the extent to which mineralogic data support the positioning of the Plio–Pleistocene boundary based on previous paleomagnetic, palynologic, paleontologic, and granulometric data [RÓNAI 1983]. Samples were chosen to straddle the indicated boundary zone suggested by the above mentioned criteria. This approach is based on our knowledge that certain heavy-mineral species such as garnet, amphibole group minerals, epidote, and others are susceptible to leaching and eventual dissolution during periods of weathering associated with humid climates [ISPHORDING–RICCIO 1969, COE 1979, FRIIS 1974, CAZEAU 1974, and others] *(Fig. 4)*.

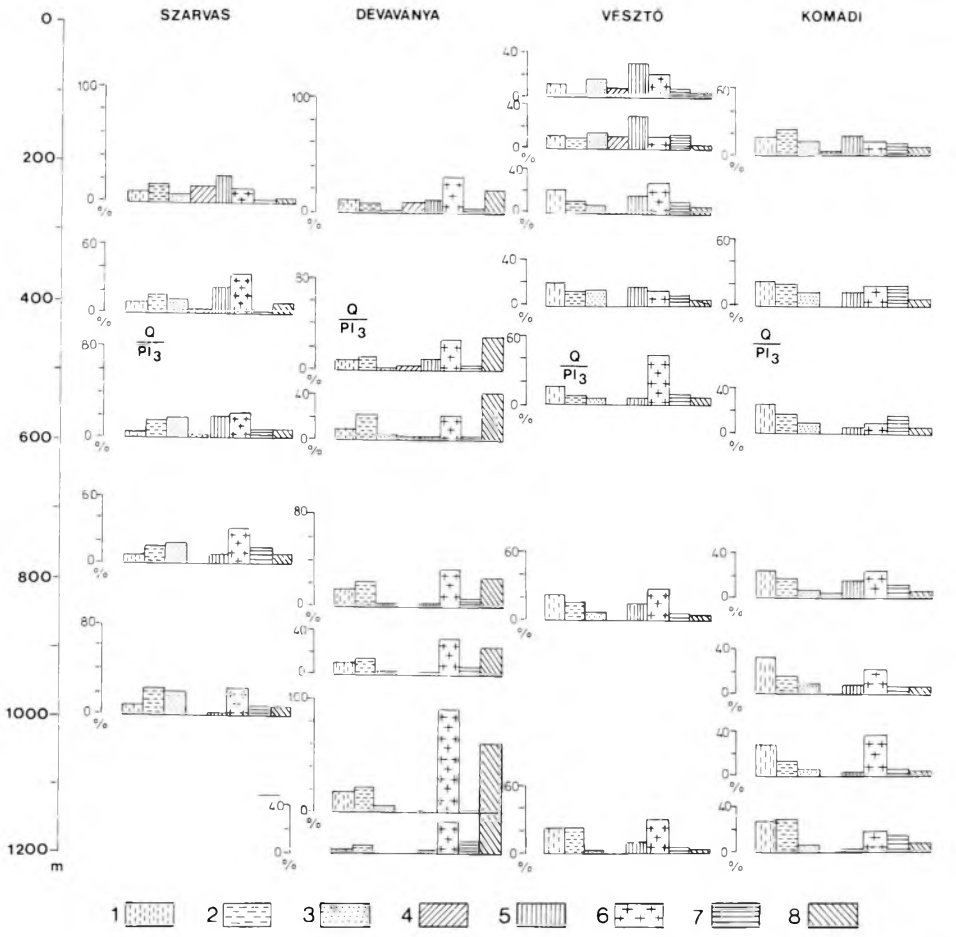

Fig. 4. Heavy mineral composition of the borehole cores in the Körös-Basin (analysed by I. Elek 1980)
1 — magnetite, ilmenite; 2 — garnet; 3 — epidote; 4 — pyroxene; 5 — amphibole; 6 — clorite, biotite; 7 — epigene; 8 — metamorphics (tourmaline, disthene, zirkon)

4. ábra. A Körös-medence fúrási magmintáinak nehézásványösszetétele (Elek I. analízise, 1980)
1 — magnetit, ilmenit; 2 — gránát; 3 — epidotit; 4 — piroxén; 5 — amfibol; 6 — klorit, biotit; 7 — epigén; 8 — metamorf ásványok (turmalin, disztén, cirkon)

Рис. 4. Тяжеломинеральный состав песчаных осадков в скважинах бассейна Кёрёш
1 — магнетит, ильменит; 2 — гранат; 3 — эпидотит; 4 — пироксен; 5 — амфобол; 6 — хлорит, биотит; 7 — эпиген; 8 — метаморфические ископаемые (турмалин, дистен, циркон)

2. Laboratory procedures

Laboratory procedures were directed specifically toward a reconnaissance study of the presence or absence of weathered minerals in the heavy-mineral assemblage that are thought to be indicative of periods of low sedimentation rates or of extensive periods of subaerial weathering associated with humid climates. No attempt was made to detail exhaustively the full heavy-mineral assemblage; major mineral species accounting for approximately 90% of the mineral assemblage were documented in the form of broad mineral groups (that is, garnet, sheet silicates, tourmaline, pyroboles, and so on).

Approximately 500–1400 grams of sample representing a thickness of 1.00 to 4.70 m of sand-size material was chip-and-channel sampled (where unconsolidated) from six intervals in each of the Vésztö and Dévaványa cores at the Szolnok repository. In the laboratory, each of the 12 samples was initially sieved in dry condition with a U.S. Standard 18 mesh screen (1.00 mm). The 18 mesh (< 1.00 mm) fraction was hand washed and processed for its clay content by decantation. The sand-sized material was then processed for its heavy-mineral content by use of bromoform (SG > 2.85) and methylene iodide (SG > 3.25) to yield two dense fractions: > 3.25, and > 2.85 to < 3.25. Density separation was followed by removal of the strongly paramagnetic minerals by use of a hand-held magnet. The balance of the heavy minerals in each sample was processed into three magnetic subfractions on a Frantz Isodynamic Magnetic Separator* set at 15 degrees forward and 20 degrees side slopes (0.0–0.5, 0.5–1.0, and > 1.0 ampere fractions). In this manner the heavy-mineral assemblage of each sample was fractionated into groups of three to five mineral species each, principally to facilitate the mineral identification process. The mineral species in each magnetic fraction were examined by use of petrographic and binocular microscopes; the percentage of individual mineral species was visually estimated and summed across density and magnetic fractions. The relatively small quantities coupled with the very fine grained nature of the heavy minerals made the identification process difficult, and as a consequence the number of unidentified opaque mineral species is relatively high. Density was not compensated for in the tabulation shown on *Table I*. The identification of some minerals was done by X-ray diffraction techniques (Beth D. Martin, USGS, Reston). As the > 1.00 mm and decanted fractions were not examined for their heavy-mineral content, and as sheet-silicate minerals wash out readily by decantation, thus skewing the results in the direction of higher density minerals such as zircon and rutile, the analytical data may not be fully representative of the total assemblage.

* Use of trade names does not constitute endorsement by the U.S. Geological Survey

3. Results and conclusions

The six samples from the Vésztő borehole, representing medium to very fine grained sand units between 430.9 and 688.0 m depth, average about 1.5% (SG > 2.85) and 0.72% (SG > 3.25) heavy minerals. The six samples from the Dévaványa borehole, also representing sand-sized sediments from 437.5 to 653.8 m depth average about 1.4% (SG > 2.85) and 0.7% (SG > 3.25) heavy minerals. The sieve and heavy-mineral analyses are given on Table I.

Visual examination of the mineralogic data of the two sets of samples suggests correlation based on the presence of depleted and deeply weathered garnet in samples *D1, D2* and *V2*. This correlatable mineralogic horizon is just below the Matuyama/Gauss paleomagnetic boundary.

Another significant correlation between the two sets of samples is the presence of mineral grains cemented by authigenic pyrite in samples *V5* and *D4*. As these samples are likely to be lacustrine, the sulfide cement may signify a change in water chemistry, or it may signify that the base of the deeply weathered section is the top of the lacustrine deposits; strong *in-situ* weathering indicates humid fluvial conditions. The relative abundance of pyrobole group minerals (particularly brown amphibole) in samples *D5, D6, V5,* and *V6* coupled with the presence of sulfides higher up in the section suggests possible subdivision of the Pliocene section.

General mineralogic trends include the relative abundance of magnetite, ilmenite, leucoxene, epidote group, and iron oxides in the Vésztő samples and relatively more garnet group minerals in the Dévaványa samples. These differences strongly suggest different source areas for the sediments. To what extent these qualitative and quantitative differences reflect source area, depositional environment, weathering history, or combinations thereof cannot be resolved until detailed regional heavy-mineral data are available for correlation with paleomagnetic, paleontologic, granulometric, and other data.

Other, more subtle, mineralogic differences are suggested by the data on table I; however, the reconnaissance nature of the mineralogic determinations precludes definitive correlations. Detailed mineralogic determinations of the members of the garnet, pyrobole, aluminosilicate, and sheet silicate groups of minerals would probably yield additional, and perhaps definitive, correlation data.

Not all sand units were examined; only the material that was visibly coarser than average was sampled for this study, so that even though the results of this study suggest that of the two obviously weathered correlative horizons the lowermost is more significant geologically, the spacing of the samples from the cores limits the accuracy of correlation. Examination of the heavy-mineral assemblages in continuous samples from the intervals straddling the questioned boundary line would likely clarify this problem. Additionally, inasmuch as the

Sample No.[1]	Depth interval in meters	Wt.% > 18 mesh[2]	Wt.% Sand	Wt.% Clay[3]	Wt.% SG > 2.85	Wt.% SG > 3.25	Percent of SG > 2.85: MAGNETITE	ILMENITE	RUTILE	LEUCOXENE	EPIDOTE[4]	ZIRCON	TOURMALINE	GARNET	ALUMINOSILICATES[5]	SHEET SILICATES[6]	STAUROLITE	PYROBOLES[7]	IRON OXIDES	SULFIDES	OTHERS[8]
V1	430.9–433.4	0.1	74.3	25.6	1.2	0.6	1.5	8	4	3	0.5	3	4.5	22	5	17	4	2	6	N	10
V2	498.2–500.2	1.1	82.0	16.9	1.4	0.2	2.0	6	2	0.5	1	0.5	5	9.5	1.5	32	2	4	23	N	8
V3	503.5–506.5	0.0	74.3	25.7	1.4	1.0	10.0	13	3	3	2.5	2	4	24	2	11	4.5	1	9	N	7
V4	603.5–606.9	0.1	82.4	17.5	1.0	0.5	5.0	8	2	2	1	2	1.5	13	2.5	20	6	2	14	N	13
V5	650.8–652.8	2.2	79.5	18.3	1.2	0.5	5.0	11	3	2	1	2	3	19	1	22.5	2	14	0.5	5	6
V6	686.1–688.0	0.4	89.8	9.8	2.5	1.5	3.0	8	4	4	0.5	2	2.5	15	3.5	25	2	20	1	N	8
D1	437.5–441.9	0.0	82.4	17.6	1.4	0.5	2.0	6	1.5	1	P	1	2	9	3	51	6	4	6	N	7
D2	494.0–498.7	0.2	78.1	21.7	2.0	0.4	1.0	2	1.5	1	0.5	1	3	9	2	57	7	4	1	N	10
D3	566.2–567.6	0.5	76.4	23.1	2.8	2.2	1.0	3	7	P	P	5	4	30	4.5	24	10	P	N	N	11.5
D4	604.0–606.8	0.1	81.1	18.9	0.8	0.4	2.0	6	2.5	2	P	2	5	26	2	41	3	3	P	3	2.5
D5	646.0–647.0	0.2	87.8	12.0	0.6	0.3	0.5	3	2.5	P	1	2.5	1	23	2	29	9	11	1	N	14.5
D6	649.7–653.8	0.1	86.4	13.5	0.9	0.4	0.5	3	1.5	2	0.5	0.5	7	20	4	37	7	8	5	N	4

1) Samples designated "V" are from the Vésztő borehole
Samples designated "D" are from the Dévaványa borehole
2) > 1.00 mm; mostly clayballs
3) Determined by difference in weight after decantation
4) Include piedmontite?, clinozoisite, pumpellyite, zoisite
5) Includes kyanite, sillimanite, andalusite?
6) Includes micas, chlorite, chloritoid
7) Includes augite?, amphibole, tremolite, actinolite, glaucophane, hypersthene, enstatite?, diopside
8) Includes a variety of minerals: quartz, feldspar, clayballs, unidentified opaques, polyminerallic grains, schist fragments, apatite, sphene, anatase and others
N None detected
P < 0.5%

Table 1. Sieve and heavy-mineral analyses of selected sandy units within the Vésztő and Dévaványa boreholes

1. táblázat. Szemeseméret és nehézásvány vizsgálat a vésztői és a dévaványai fúrás egyes homok rétegeiben

Таблица 1. Анализ зернистости и тяжелых минералов в отделных песчаных слоях скважин Вестё и Девавапья

sulfide-bearing horizon suggests the possible subdivision of the Pliocene stratigraphic sequence, heavy-mineral work in that portion of the stratigraphic column is recommended. Similarly, an examination of the heavy-mineral assemblages in sediments straddling the Olduvai event is also recommended.

REFERENCES

Berggren W. A., Burckle L. H., Cita M. B., Cooke H. B. S., Funnell B. M., Gartner S., Hays J. D., Kennett J. P., Opdyke N. D., Pastouret L., Shackleton N. J., Takayanagi Y. 1980: Towards a Quaternary time scale. Quaternary Research, **13.** pp. 277–302

Berggren W. A., Kent D. V., Van Couvering J. A. 1984: Neogene geochronology and chronostratigraphy. *Pre-print*, Woods Hole Oceanographic Institution, Woods Hole, MA, 02543, 92 p.

Cazeau C. J. 1974: Heavy minerals of Quaternary sands in South Carolina. *In* Post-Miocene stratigraphy central and southern Atlantic Coastal Plain, R. Q. Oaks, Jr. and J. R. Dubar eds., Utah State University Press, pp. 174–178

Coe C. J. 1979: Geology of the Plio-Pleistocene sediments in Escambia and Santa Rosa Counties, Florida. Unpublished M. S. thesis, Florida State University, 115 p.

Cook H. B. S., Hall J. M., Rónai A. 1979: Paleomagnetic, sedimentary and climatic records from boreholes of Dévaványa and Vésztő. Acta Geologica Hungarica, **22,** 1–4 pp. 89–109

Friis H. 1974: Weathered heavy-mineral associations from the young Tertiary deposits of Jutland, Denmark. Sedimentary Geology, **12,** 3, pp. 199–213

Haq B. U., Berggren W. A., Van Couvering J. A. 1977: Corrected age of the Pliocene/Pleistocene boundary, Nature, **269,** 5628 pp. 483–488

Isphording W. C., Riccio J. 1969: Petrology and identification of the Citronelle Formation in Alabama [abs.]. Geological Society of America Abstracts with Programs, **4,** 2, pp. 82–83

Rónai A. 1983: Geological history of the Körös basin during the Quaternary (in Hungarian with English abstract). Földtani Közlöny (Bull. of the Hung. Geol. Soc.), **113,** 1, pp. 1–25

KÖZLEMÉNY A PLIOCÉN–PLEISZTOCÉN HATÁRMEGÁLLAPÍTÁSRÓL AZ ALFÖLD ÜLEDÉKEIBEN

Andrew E. GROSZ, RÓNAI András és Ricardo LOPEZ

A Pannon medencében kísérleteket végeztünk abból a célból, hogy fel lehet-e használni nehéz ásványtani vizsgálatokat sztratigráfiai célokra, pl. a neogén–kvarter határ megállapítására. A laza üledékekből nyert fúrásmintákban ugyanis a fauna és flóra maradványok hiánya a sztratigráfiai határok kimutatását nehézzé teszi.

A dévaványai és a vésztői fúrásból vett mintákban az ásványszemek részletes vizsgálata legalább két ízben mutatott ki erős mállást és viseltességet. 440 m körül a dévaványai és 500 m körül a vésztői fúrásban a gránátszemek aránya jelentősen kevesebb mint más mélységszakaszokban és viseltesebbek. E mélységek nagyjából megegyeznek az egyéb adatok alapján várható plio–pleisztocén határ helyével. Egy másik megfigyelhető esemény az ásványszemek autochton pirittel való cementáltsága a dévaványai fúrásban 605 m mélység táján, amit korrelálni lehet a vésztői fúrás hasonló szakaszával 650 m mélységben. Az eredmények igazolják, hogy a részletes nehéz-ásványtani vizsgálatok egyéb vizsgálatokkal karöltve hasznosak lehetnek az üledékképződés fejlődésének elemzésében és sztratigráfiai (N/Q) megítélésében.

СООБЩЕНИЕ ОБ ОПРЕДЕЛЕНИИ ПЛИО–ПЛЕЙСТОЦЕНОВОЙ ГРАНИЦЫ В ОСАДОЧНЫХ ПОРОДАХ БОЛЬШОЙ ВЕНГЕРСКОЙ НИЗМЕННОСТИ

Эндру Э. ГРОС, Андраш РОНАИ и Рикардо ЛОПЕЗ

В Большом Венгерском Бассейне были проведены исследования с той целью, можно ли использовать тяжелые минералогические анализы в стратиграфических целях, например, для определения границы между неогеновыми и четвертичными отложениями.

Отсутствие остатков фауны и флоры в рыхлых осадках проб, полученных из кернового материала скважин, представляет собою трудность для выявления стратиграфических границ.

Детальное исследование минеральных зерен, взятых из проб девавaньской и вестёйской скважин, по крайней мере в двух случаях показало сильную эродированность и разрушение. На глубине около 440 м в девавaньской скважине и 500 м в вестёйской скважине соотношение гранатовых зерен значительно меньшее, чем на других отрезках разреза, и зерна более подвергнуты разрушению. Эти глубины примерно совпадают с ожидаемым положением лио–плейстоценовой границы на основании других данных. Другое наблюдаемое явление представляет собою цементированность минеральных зерен с автигенным пиритом в девавaньской скажине в районе глубины 605 м, что можно коррелировать со схожим отрезком на глубине 650 м вестёйской скажины. Результаты показывают, что детальные минералогические анализы вместе с другими анализами могут быть полезны при анализе процесса осадкообразования и стратиграфических определениях (N/Q).

GEOPHYSICAL TRANSACTIONS 1985
Vol. 31. No. 1–3. pp. 101–129

CONTRASTING TYPES OF NEARSHORE SANDS AND GRAVELS FROM SEMI-PROTECTED MIOCENE COASTS, NORTHERN HUNGARY

H. Edward CLIFTON*, Margit BOHN-HAVAS** and Pál MÜLLER**

Dissimilar types of nearshore clastic deposits occur in the Miocene sediment of northern Hungary. One of these is exposed in a small sand pit east of the village of Csokvaomány; it is part of the Salgótarján Formation of Ottnangian (early Miocene) age. The deposit is characterized by a 6.5-m-thick vertical sequence that appears to include inner shelf, nearshore, foreshore and backshore facies in upward-shallowing progression. The sequence is readily interpreted as the result of a shoreline prograding into an arm of the Miocene sea. The other deposit is exposed in a gravel pit east of the village of Nekézseny; it is part of the Egyházasgerge Formation of Karpathian (early or middle Miocene) age. This deposit consists of 21 m of calcareous and dolomitic sandy gravel deposited on a Paleozoic carbonate rock platform (or locally on a layer of fine siliciclastic sand just above this platform). The Paleozoic rock surface is intensively bored by *Lithophaga*. Fragments of bivalve shells, *Lithophaga*-bored pebbles, and large burrows in the gravel attest to deposition in a marine environment. The oscillatory velocities required to move the larger pebbles and paleogeographic constraints suggest deposition in water no more than several meters deep. Systematic vertical variation within the gravel is limited mostly to an upward fining of the siliciclastic component (fine sand near the base, silty very fine sand and clay near the top). The deposit is inferred to have occurred at the foot of a topographically high area (possibly an island) underlain by carbonate rock. Deposition of calcareous and dolomitic detritus was rapid enough to maintain a relatively constant water depth during the interval of sea level rise. The simultaneous retreat of an initially-adjacent siliciclastic shoreline to the north caused a fining of the siliciclastic component. Gravel deposition ceased upon inundation of the carbonate rock high, and accumulation of fine-grained sediment of the Garáb Formation completed Karpathian deposition.

Keywords: Miocene, marine shoreline deposits, progradation, molluscs, Northern Hungary

1. Introduction

The character of clastic shoreline deposits depends on the interplay of many factors, including the texture of available sediment, the physical dynamics of the environment, the biota, and the balance between sedimentation rate and relative change of sea level. This paper describes two different deposits that formed along Miocene shorelines in northern Hungary and analyzes their contrasting charasteristics in terms of causal factors.

During the lower and middle Miocene (Eggenburgian, Ottnangian, Karpathian and Badenian stages) narrow, shallow arms of the sea extended episodically across Hungary [CSÁSZÁR et al. 1982]. Gravel, sand, mud, volcanic ash and

* U. S. Geological Survey, 345 Middlefield Road, Menlo Park, California 94 025
** Hungarian Geological Survey, POB 106, Budapest, H–1442
Manuscript received: 12 February, 1985

lignite accumulated in the shallow seaways or in the coastal swamps that locally bordered them. The distribution, stratigraphy, and lithologic character of these deposits have been established through the combined study of outcrops and boreholes developed through the Ottnangian brown coal research program of the Hungarian Geological Survey [SCHRÉTER 1929, 1945, and 1954, BALOGH 1964, RADÓCZ 1975, BOHN-HAVAS 1978].

Most of these deposits remain unconsolidated and are well-exposed only in artificial cuts. The exposures described here are in sand/gravel pits and are subject to change as the pits are expanded or abandoned.

2. Paleogeographic Setting

The deposits lie on the north flank of the Bükk Mountains; the pits in which they are exposed lie a short distance east of the villages of Csokvaomány and Nekézseny, respectively *(Fig. 1)*. They formed within the Egercsehi–Ózd Basin (the western part of the Borsod Basin). The boundaries of the basin are the

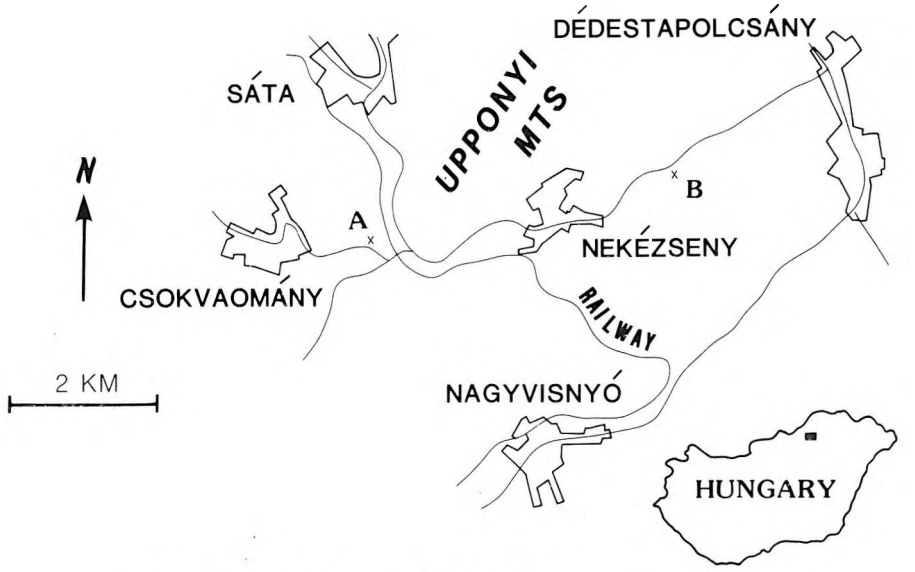

Fig. 1. Location of Miocene shoreline deposits described in this paper.
A — Ottnangian progradational sequence east of Csokvaomány; *B* — Karpathian calcareous gravel east of Nekézseny

1. ábra. A leírt miocén part menti üledékek helye.
A — ottnangi progradáló rétegsor Csokvaománytól keletre; *B* — kárpáti mészanyagú kavics Nekézsenytől keletre

Рис. 1. Размещение миоценовых прибрежных осадков, рассматриваемых в этой статье
А — Оттнангская проградационная толща восточнее с. Чокваомань; В — Известковистый галечник карпатского возраста восточнее с. Некежень

lower Paleozoic blocks of the Szendrő Mountains to the northeast, the Paleozoic–Mesozoic unit of the Bükk Mountains to the southeast, and the Pétervására Platform to the west. The northeast–southwest trending Egercsehi–Ózd trough apparently formed during the Savian orogenic phase (late Oligocene to early Miocene). The Miocene deposits in the trough are of Eggenburgian–Ottnangian (22–19 Ma) and Karpathian-lower Badenian (19-15 Ma) age [HÁMOR 1980, 1984].

The Eggenburgian and Ottnangian deposits represent two complete geologic cycles. During the Eggenburgian stage, the sea transgressed over northern Hungary from a north–northwest direction as a consequence of the Savian orogenic movements. Its transgression over the western part of the Borsod area filled the Egercsehi–Ózd Basin. A second Ottnangian sedimentary cycle *(Fig. 2)* more or less duplicated the earlier transgression [HÁMOR–HALMAI 1975]. The Savian orogeny produced grabens that partly filled with rhyolitic tuffs erupted from marginal fractures (Gyulakeszi Rhyolite Tuff Formation, *Figure 3*).

Overlying the rhyolitic tuff in many places in the Egercsehi–Ózd Basin are sand, silt and clay of Ottnangian age: the Salgótarján Browncoal Formation (Fig. 3). This unit, which contains seams of lignite, formed during a slow transgression that was interrupted by minor oscillations of the sea. The faunal assemblages of the unit change progressively from brackish-water in the lower part to marine in the upper part. The lignites apparently formed under a humid climate in coastal swamps bordering the marginal sea.

During the Karpathian and Badenian stages another pair of sedimentary cycles ensued a different paleogeographic setting. As a result of the Styrian orogenic phase, a direct connection was established with the Mediterranean. Marine transgressions progressed from southwest to northeast through the Hungarian Basin to the Carpathians. The Karpathian transgression reached the area discussed here *(Fig. 4)* through the Budapest–Cserhát–Egercsehi–Ózd sedimentary trough [HÁMOR–HALMAI 1975, HÁMOR 1983]. Littoral sand and gravel (Egyházasgerge Formation) and open marine marl and mud (Garáb Schlier Formation) accumulated during the Karpathian cycle (Fig. 2). Both units bear a marine macrofauna.

3. The Csokvaomány deposit

The older of the two deposits considered here is exposed in a small sand pit north of the highway about 1.5 km east of the village of Csokvaomány (Fig. 1). The width of the present wall of the pit is on the order of 10 m across, and about 10–12 m of section are exposed. Two depositional successions are present, separated by an erosional surface. The lower succession consists primarily of crossbedded and burrowed pebbly sand, in which a few oyster shells are scattered. The upper succession is mostly fine sand containing mud interbeds and numerous shell and shell fragments. The fauna *(Table I)* indicates that these deposits belong to the Ottnangian Salgótarján Browncoal Formation (Fig. 2).

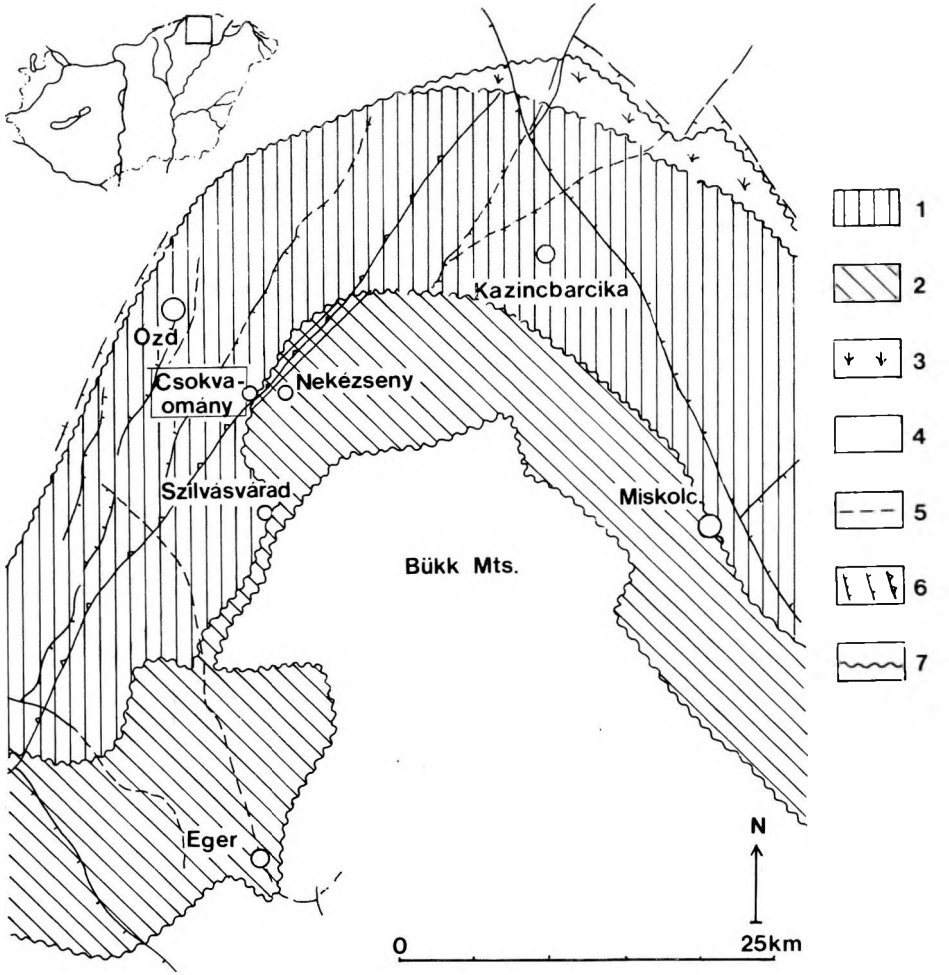

Fig. 2. Sketch map of paleogeography in northern Hungary during Ottnangian time
1 — paralic coal swamp; 2 — freshwater variegated clay; 3 — freshwater coal swamp; 4 — landmass; 5 — facies boundaries; 6 — structural elements; 7 — boundary of sedimentary basin

2. ábra. Északmagyarország ottnangi ősföldrajzának vázlata.
1 — paralikus kőszénmocsár; 2 — édesvízi tarkaagyag; 3 — édesvízi kőszénmocsár; 4 — szárazföld; 5 — fácies határ; 6 — szerkezeti elemek; 7 — az üledékes medence határa

Рис. 2. Картосхема палеогеографии территории Северной Венгрии в оттнангийское время
1 — болото образования паралических углей; 2 — пресноводные пестрые глины; 3 — пресноводное болото образования углей; 4 — суша; 5 — фациальная граница; 6 — структурные элементы; 7 — граница осадонного бассейна

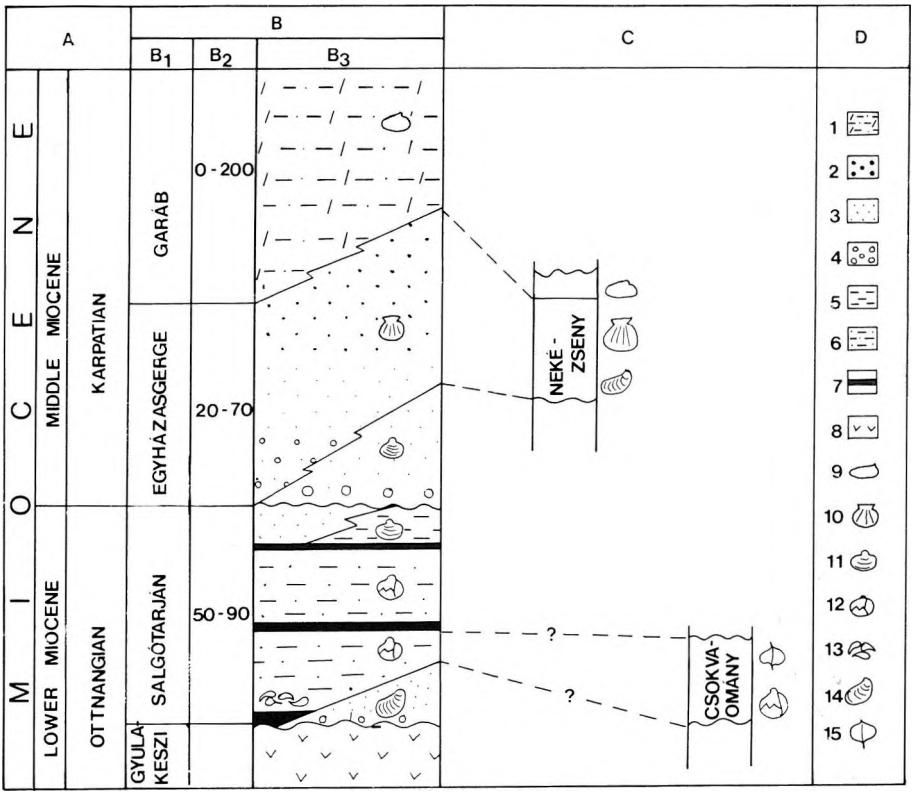

Fig. 3. Miocene (Ottnangian and Karpathian) units of the Egercsehi – Ózd Basin
A — Chronostratigraphy; B — Litostratigraphy; B_1 — Formation; B_2 — Average thickness; B_3 — Rock sequence; C — Location; D — Key to symbols.
1 — clayey silt; 2 — sandstone; 3 — sand; 4 — pebbles; 5 — clay; 6 — silt; 7 — browncoal seam; 8 — rhyolite tuff; 9 — *Macoma–Nucula* ass.; 10 — *Chlamys;* 11 — *Corbula–Anadara;* 12 – *Cardium–Pirenella–Theodoxus;* 13 — *Congeria;* 14 — *Crassostrea;* 15 — *Megatrola* fragments

3. ábra. Az egercsehi–ózdi medence miocén (ottnangi és kárpáti) egységei.
A — Kronosztratigráfia; B — Litosztatigráfia; B_1 — Formáció; B_2 — Átlagos vastagság; B_3 — Rétegsor; C — Lelőhely; D — Jelmagyarázat
1 — agyagos aleurit; 2 — homokkő; 3 — homok; 4 — kavics; 5 — agyag; 6 — aleurit; 7 — szén; 8 — riolittufa; 9 — *Macoma–Nucula* asszociáció; 10 — *Chlamys*; 11 — *Corbula–Anadara* asszociáció; 12 — *Cardium–Pirenella–Theodoxus* asszociáció; 13 — *Congeria*; 14 — *Crassostrea*; 15 — növénymaradvány

Рис. 3. Миоценовые (оттнангий и карпатий) единицы Эгерчехи–Оздского бассейна
A — Хроностратиграфия; B — Литостратиграфия; B_1 — Формация; B_2 — Средняя мощность; B_3 — Разрез; C — Месторождение; D — Условные обозначения
1 — глинистые алевриты; 2 — песчанник; 3 — пески; 4 — гальки; 5 — глины; 6 — алевриты; 7 — уголь; 8 — липаритовые туфы; 9 — ассоциация *Macoma–Anadara;* 10 — *Chlamys;* 11 — ассоциация *Corbula–Anadara;* 12 — ассоциация *Cardium–Pirenella–Theodoxus;* 13 — *Congeria;* 14 — *Crassostrea;* 15 — растительные остатки;

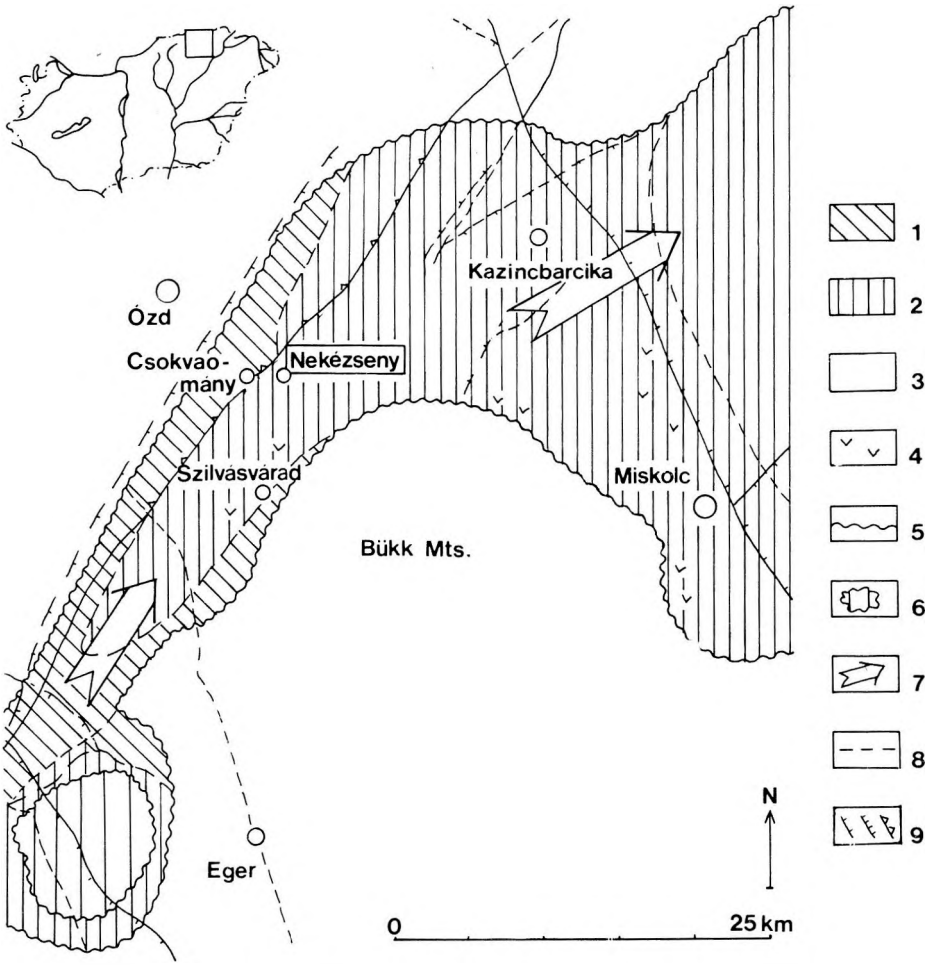

Fig. 4. Sketch map of paleogeography in northern Hungary during Karpathian time
Depositional facies: 1 — littoral, 2 — sublittoral, shallow open water. 3 — landmass; 4 — rhyolite tuff; 5 — coast-line during maximal transgression; 6 — sedimentary basin during regression; 7 — direction of transgression; 8 — facies boundaries; 9 — structural elements

4. ábra. Északmagyarország kárpáti ősföldrajzának vázlata.
Fácies: 1 — partszegélyi, 2 — sekély szublitorális tengeri. 3 — szárazföld; 4 — riolit tufa; 5 — partvonal maximális elöntés idején; 6 — üledékgyűjtő; 7 — transzgresszió iránya; 8 — fácieshatár; 9 — szerkezeti elemek

Рис. 4. Картосхема палеогеографии территории Северной Венгрии в карпатийское время
Фации: 1 — прибрежная, 2 — мелководного сублиторального моря, 3 — континентальная; 4 — риолитовые туфы; 5 — береговая линия во время максимального прилива; 6 — осадконакопители; 7 — направление трансгрессии; 8 — фациальная граница; 9 — структурые элементы

Table I. Fossil assemblage in the Ottnangian deposit exposed east of Csokvaomány
I. táblázat. Ottnangi bentos faunaegyüttesek (Csokvaomány)
Таблица I. Комплекс ископаемых остатков отложений оттнангийского яруса в обнажении к востоку от Чокваоманя

Fossils: Mollusca
Bivalvia: *Musculus* sp.
Congeria sp.
Ostrea sp. (juv.)
Cardium sociale Krauss
Cardium sp.
Pitaria cf. *islandicoides* Lam.
Gastropoda: *Theodoxus pictus* Fer.
Hydrobia sp.
Pirenella sp.
Annelida
?Polychaeta
Arthropoda
Ostracoda
Megaflora fragments

The shoreline deposits described here occur in the underlying succession, which composes the lower 6.5 m of the exposure. This section displays a distinctive vertical sequence *(Fig. 5)*. The lowermost exposed strata consist of interlaminated mud and fine sand, the top of which is interrupted by layers of structureless coarse pebbly sand. The mud layers become progressively thinner, fewer and more discontinuous upward; they are absent in the section higher than about 2.5 m above the base. About 2 m above the base the sand and gravel change from predominantly structureless to mostly crossbedded. The section becomes progressively more pebbly up-section, culminating in a crossbedded gravel bed about 5 m above the base. Above this bed, the sediment become progressively finer and passes from planar-parallel laminated sand into structureless muddy sand that contains fossil root structures. This is capped by a thin (2–4 cm) lignite bed that is locally overlain by as much as 20 cm of mud that contains numerous gastropod shells. An erosional surface *(Fig. 6)* locally covered by a thin conglomerate (and scattered large clasts of silicified wood) terminates the lower succession.

The vertical sequence closely resembles those that form in response to a prograding shoreline [HARMS et al. 1982]. In such a sequence, successively higher parts of the section represent progressively shallower parts of the nearshore environment. A key horizon in this sequence lies at the upward transition fromcrossbedded gravel to planar-bedded pebbly sand (the 0 m reference in Figure 5), which marks the presumed position of sea level. The lowermost strata in the sequence represent conditions of low energy under which mud and fine sand accumulated. Deposition in this quiet-water regime was interrupted episodically by the introduction of coarser sand in response to infrequent storms. If sea level is assumed to have remained more or less constant during the progradation, these conditions existed at depths as shallow as 4–5 m. The presence of pebbles greater than 1 cm in diameter in the storm deposits suggests

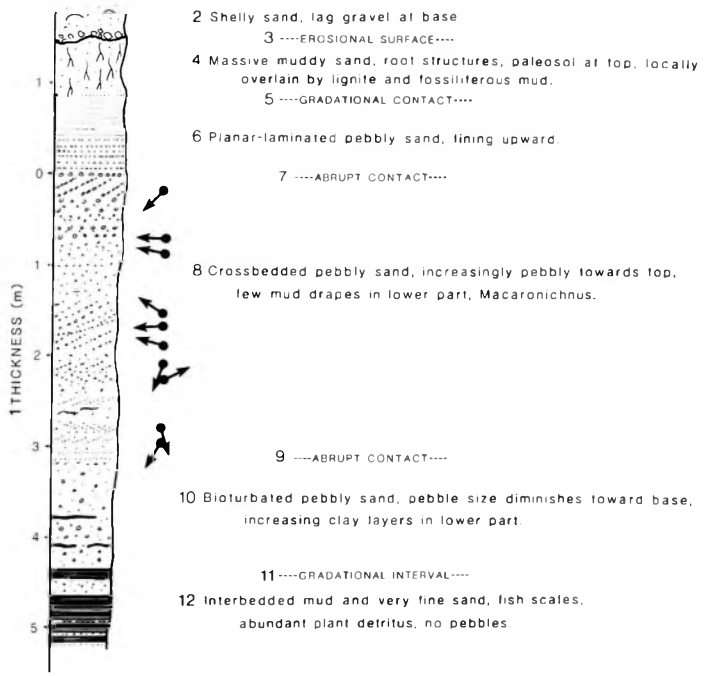

Fig. 5. Stratigraphic column of the lower sedimentary sequence exposed in the sand pit east of Csokvaomány. Arrows indicate crossbedding dip directions

5. ábra. A Csokvaománytól keletre lévő homokgödörben feltárt alsó üledékösszlet rétegoszlopa. A nyilak a keresztrétegződés dőlési irányait jelzik.

1 — vastagság; 2 — kagylóhéjas homok, maradékkavics a bázison; 3 — eróziós felszín; 4 — rétegzetlen iszapos homok, gyökérnyomok, őstalaj felül, részben lignittel és kövületes iszappal fedve; 5 — fokozatos átmenet; 6 — síkrétegzett kavicsos homok, felfelé finomodik; 7 — éles határ; 8 — keresztrétegzett kavicsos homok, felfelé egyre kavicsosabb, kevés iszaplepény alul, *Macaronichnus*; 9 — éles határ; 10 — bioturbált kavicsos homok, a kavicsok mérete lefelé csökken, egyre növekvő agyagrétegek az alsó részen; 11 — fokozatos átmenet; 12 — iszap- és nagyon finom homokrétegek váltakozása, halpikkelyek, sok növényi maradvány, nincs kavics

Рис. 5. Стратиграфическая колонка нижней осадочной толщи, обнажающейся в карьере песка восточнее с. Чокваомань. Стрелы показывают направления падения косой слоистости

1 — мощность; 2 — песок с облоками ракишек, в основе остатки гальки; 3 — поврхность эрозии; 4 — неслоистые пески, следы корней, в верхней части древние почвы, частично покрытые лигнитами и окаменелым удом; 5 — постепенный переход; 6 — галечниковые пески, имеющие горизонтальную слоистость, в верхних частях более мелкий; 7 — резкая граница; 8 — галечниковые пески, имеющие поперечную слоистость, в верхних частях все более галечниковые, внизу мало илистых лепешкообразных включений, *Macaronichnus*; 9 — резкая граница; 10 — биотурбированные галечниковые пески, размер галек уменьшается по направлению вниз, в нижней части все больше глиннистых слоев; 11 — постепенный переход; 12 — чередование слоев ила и очень мелкозернистых песков, рыбная чешуя, много растительных детритов, отсутствие галек

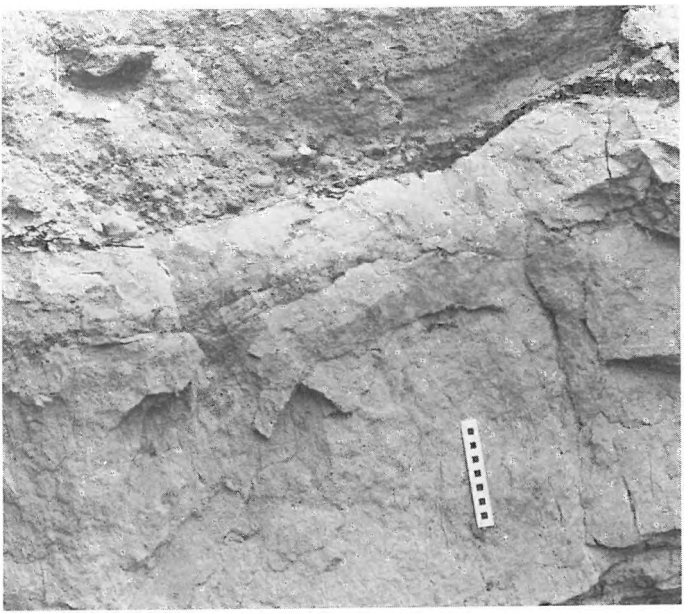

Fig. 6. Top of the lower sedimentary sequence in sand pit east of Csokvaomány. Light-colored interval is a probable paleosol. Dark-colored lignitic layer caps the light interval on right side of photograph. On left side of photograph, gravel conglomerate and pebbly, shell-bearing sand of the overlying sequence lie on the presumed paleosol. Dark near-vertical structures near centimeter scale are carbonized root structures

6. ábra. A Csokvaománytól keletre lévő homokgödör alsó üledékösszletének felső része. A világos szinű réteg valószínűleg őstalaj. Sötét lignites réteg fedi a világos szintet a kép jobb oldalán. A fénykép bal oldalán a feltételezett őstalajon kavicskonglomerátum és kavicsos kagylóhéjas homok települ. Ezek a felsőbb üledékösszlet részei. A sötét, közel függőleges szerkezetek a centiméter-skála közelében meszesedett gyökérnyomok

Рис. 6. Верхи нижней осадочной толщи в карьере песка восточнее с. Чокваомань. Светлый интервал представляет собой вероятный палеосол. Темноцветный слой лигнита покрывает в виде шапки светлоцветный интервал на правой стороне фотографии. На левой стороне, предположенная ископаемая почва (палеосол) перекрывается галечниковыми конгломератами и песками с гальками и раковинами, относящимися к стратиграфически вышележащей толще. Темные, приблизительно вертикальные структуры недалеко от сантиметрового масштаба представляют собой обугленные корневые структуры

that maximum orbital velocities exceeded 1 m/s [KOMAR–MILLER 1975]. Such velocities are produced at this depth by waves 1.3 to 2 m high [CLIFTON, in press]. The accumulation of fine mud suggests that the non-storm waves were no more than several tens of cm high and with periods in the range of 3 to 4 s [CLIFTON, in press].

With continued sedimentation the shoreline advanced seaward, the water shallowed, and the storm effects became increasingly common. At depths greater than about 3 m (again assuming no significant change in sea level) only

the largest storms could stir the bottom, and the storm-generated currents were so infrequent that infaunal activity could mix the resulting deposits *(Fig. 7)*. A few outlines of dissolved bivalve shells confirm the presence of a molluscan fauna. Tubular burrows 1 to 1.5 cm (Fig. 7) in diameter suggest that the infaunal assemblage included burrowing decapods similar to present day *Callianassa* [WEIMER–HOYT 1964]. The preservation of a few discontinuous layers of clay up to 3 cm thick may reflect an infaunal aversion to burrowing through such very fine-grained sediment (Fig. 7).

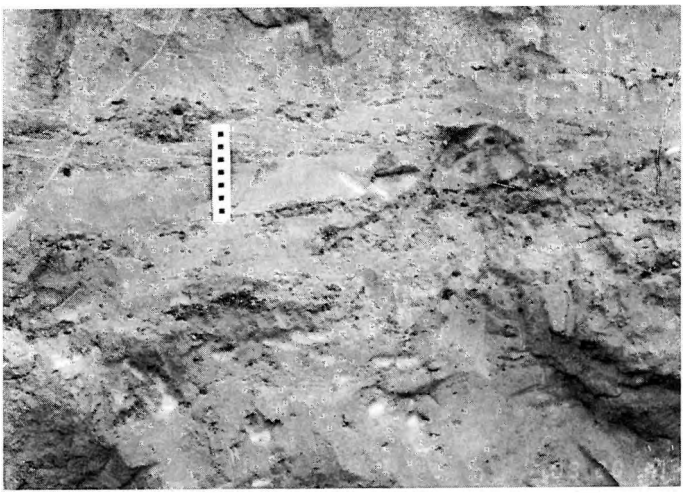

Fig. 7. Lower part of the lower sequence at sand pit east of Csokvaomány. Base of scale at contact between predominantly stratified sand (above) and predominantly bioturbated sand (below). Note large clay-lined, sand-filled burrow about 30 cm to lower right of scale

7. ábra. Az alsó összlet alsó része a Csokvaománytól keletre lévő homokgödörben. A centiméter-skála alja jelzi a határt az elsősorban rétegzett homok (fent) és az elsősorban bioturbált homok közt (lent). Figyeljük meg a skálától jobbra, lent mintegy 30 cm-re lévő homokkal tele, agyaggal tapasztott ásásnyomot

Рис. 7. Нижняя часть нижней толщи в карьере песка восточнее с. Чокваомань. Основание шкалы на контакте между преимущественно слоистыми песками (вверху) и преимущественно биотурбационными песками (внизу). См. крупный ход черви, заполненный песком и глинистым натеком на расстоянии примерно 30 см от нижнего правого конца масштаба

The section from 0–3 m on Figure 5 consists mostly of crossbedded pebbly sand *(Fig. 8)*. Most of the foresets dip in a generally westward, or offshore, direction (Fig. 2). Such an orientation suggests a dominance of rip currents. The cross-strata show no evidence of the "bundles" [ALLEN–HOMEWOOD 1984] that are produced by alternating tidal currents. The rip currents were probably generated during storms, and the bottom was stirred often enough to suppress the effects of bioturbation. Clusters of small sinuous, light-colored tubular burrows *(Macaronichnus)* occur within some of the crossbedded units. Such

structures are produced today by errant polychaetes several tens of centimeters below the seafloor [CLIFTON–THOMPSON 1978], where they have a relatively high potential for preservation. A few lenticular clay drapes or flasers in the lower part of the crossbedded section represent the accumulation of suspended fine material on a rippled surface, perhaps in the aftermath of a storm.

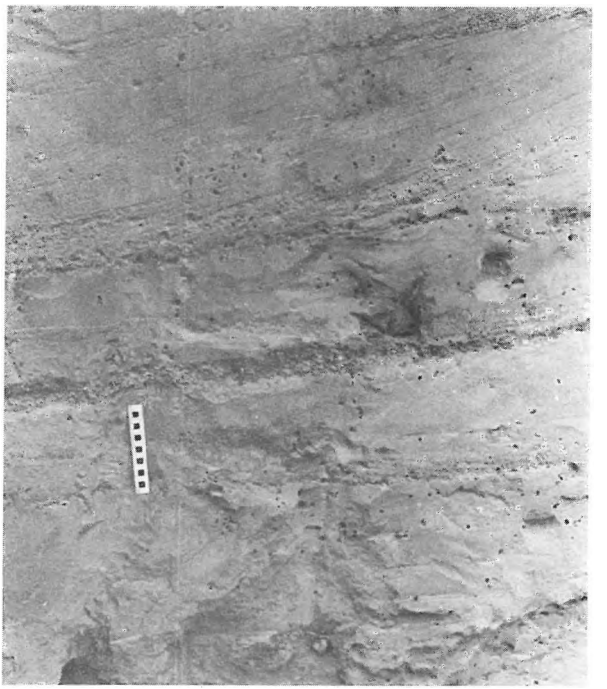

Fig. 8. Crossbedded pebbly sand and gravel layers, middle part of lower sequence in sand pit east of Csokvaomány. Base of centimeter scale marks transition to bioturbated sediment. Dark spots are modern-day insect borings

8. ábra. A Csokvaománytól keletre lévő homokgödör alsó üledéksszletének középső részén fekvő keresztrétegzett kavicsos homok- és kavicsrétegek. A centiméter-skála alja jelzi a bioturbált üledékbe való átmenetet. A sötét pettyek mai rovarok likai

Рис. 8. Косослоистые галечниковые пески и галечники, средняя часть нижней толщи в карьере песка восточнее с. Чокваомань. Основание сантиметрового масштаба представляет собой переход в осадок, нарушенный биотурбацией. Темные пятна являются современными дырками, пробуренными насекомыми

A pronounced change from crossbedding to planar-parallel lamination marks the top of the crossbedded section. Planar-laminated strata *(Fig. 9)* compose about 80 cm of the section that shows a general upward fining. At the top, the laminated section grades into a muddy, structureless sand that contains fossil root structures (Fig. 6). The planar-laminated section is interpreted as a beach foreshore deposit. Inverse size grading within some of the laminations

Fig. 9. Planar-laminated sand and gravel, upper part of lower sequence in sand pit east of Csokvaomány. Centimeter scale

9. ábra. Síkrétegzett homok és kavics. A Csokvaománytól keletre lévő homokgödör alsó összletének felső része. Centiméter-skála

Рис. 9. Плоскослойчатые пески и гальки, образующие верхи нижней толщи в карьере песка восточнее с. Чокваомань. Сантиметровый масштаб

(Fig. 10) supports this interpretation; inverse size grading is a common feature of modern foreshores, where it is produced by wave backwash [CLIFTON 1969]. The interface between beach foreshore deposits and the underlying nearshore sediment in a prograding sequence typically is marked by crossbedding that is inclined to seaward [CLIFTON et al. 1971]. Foresets in gravel immediately beneath the planar-laminated strata dip toward 230° (offshore) (Fig. 5). Such an orientation is consistent with the inferred paleogeographic setting for this deposit (Fig. 2).

The strata that overlie the foreshore facies are more enigmatic. The fossil root structures (which can be distinguished from decayed modern roots by their carbonization, limonitic encrustation, and infilling by sand) imply subaerial exposure. It is not clear whether this exposure is part of the progradation (e.g., as a backshore facies) or is related to subsequent tectonic (or eustatic) events.

A single discarticulated bivalve shell *(Pitaria)* in the muddy sand just above the foreshore facies suggests nearly normal marine salinity, but it is not clear whether the shell was deposited in a muddy embayment or was washed onto a subaerial platform behind the beach by a storm. The muddy sand is quite coarse and contains a few small scattered pebbles that could occur in either

environment. At its top, the muddy sand is stained orange beneath a thin (6–10 cm) layer that is bleached white, a probable paleosol. Above this paleosol lies a thin (2–4 cm) lignite that is overlain by a discontinuous fissile mud bed that locally attains a thickness of 20 cm. This mud contains small gastropod shells (*Theodoxus*) and fragments of other mollusk shells, as well as ostracod casts. Also present are specimens of the foraminifera *Ammonia* sp., which by its sole occurrence indicates a brackish-water environment (P. Quinterno, 1984, personal communication). The mud probably represents deposition in a shallow marginal embayment. An erosional interval terminates the lower succession. Faunal remains in the lower succession are insufficient to specify the salinity. The trace fossils present could be produced by organisms that occur in a wide range of salinities. The inferred presence of meter-high storm waves is consistent with the basinal dimensions shown in Figure 2 [CLIFTON, in press].

The deposits in the upper succession, above the erosional surface, appear to have been deposited in an estuarine setting, as suggested by a fauna that indicates a brackish-water environment. The presence of *Congeria* indicates salinities in the range of 0.5 to 3.0 parts per thousand and the association of *Cardium*, *Theodoxus*, and *Pirenella* suggests salinities in the range of 3.0 to 16.5 parts per thousand.

Fig. 10. Inverse textural grading in planar-laminated sand shown in Figure 9. Note sharp upper contacts to coarser laminae in section above centimeter scale

10. ábra. Inverz gradáltság a 9. ábrán bemutatott síkrétegzett homokban. Figyeljük meg a durvább laminák felé a hirtelen átmenetet, a centiméter-skála fölött

Рис. 10. Противоположная градация гранулометрического состава осадков и плоскослойчатых песках, показанных на *рис.* 9. См. резкий верхний контакт с более грубозернистыми пластинками в разрезе над сантиметровым масштабом

4. The Nekézseny deposit

The other nearshore sand and gravel deposit described here is exposed in a gravel pit about 200 m south of the highway, 2 km east of the village of Nekézseny (Fig. 1). The total length of the exposure in the pit approaches 100 m, and a total of about 28 m of section exists in the walls of the pit *(Fig. 11)*. The primary exposure *(Fig. 12)* is on a face that trends approximately north–south. The strata dip slightly to the east. A cut on the north side of the highway opposite the pit exposes sand that may be stratigraphically equivalent to that in the lower part of the quarry.

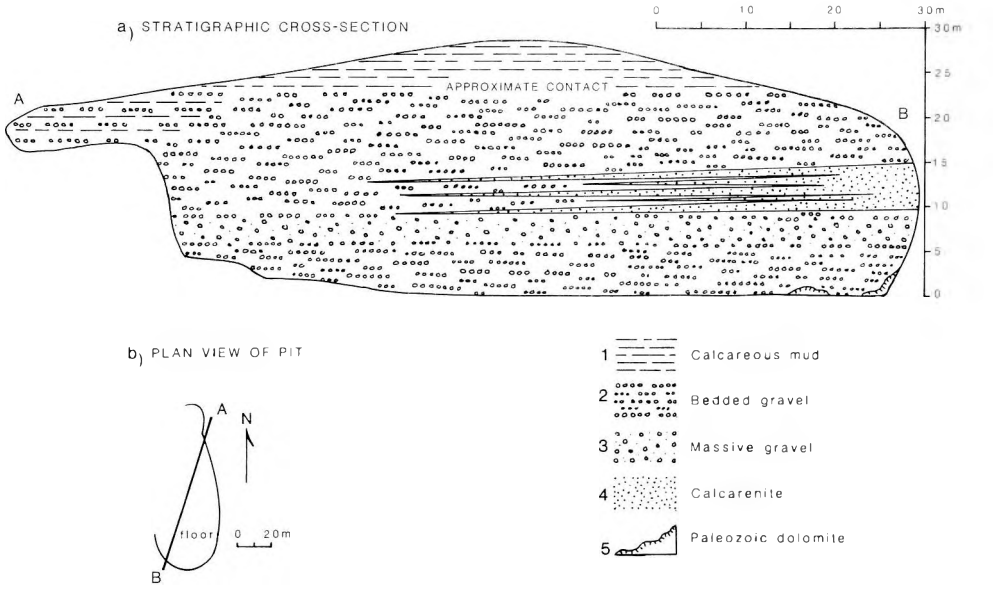

Fig. 11. Generalized sketch of section exposed in the gravel pit east of Nekézseny

11. ábra. A Nekézsenytől keletre lévő kavicsbánya által feltárt szelvény általános vázlata.
a) Rétegtani keresztmetszet; b) A bánya alaprajza
1 — meszes iszap; 2 — rétegzett kavics; 3 — rétegzetlen kavics; 4 — mészhomok;
5 — paleozoos dolomit

Рис. 11. Обобщенная схема разреза галечникового карьера восточнее с. Некежень
а) Стратиграфический разрез; b) Смена шахты
1 — известковый ил; 2 — слоистые гальки; 3 — неслоистые гальки; 4 — известковые пески; 5 — палеозойские доломиты

The lower 21 m of section in the pit is predominantly gravel. The fauna in this section *(Table II)* indicate that it is part of the Egyházasgerge Formation (Fig. 2). The top of the section in the pit consists mostly of layered mud, and is part of the Garáb Formation (Fig. 2).

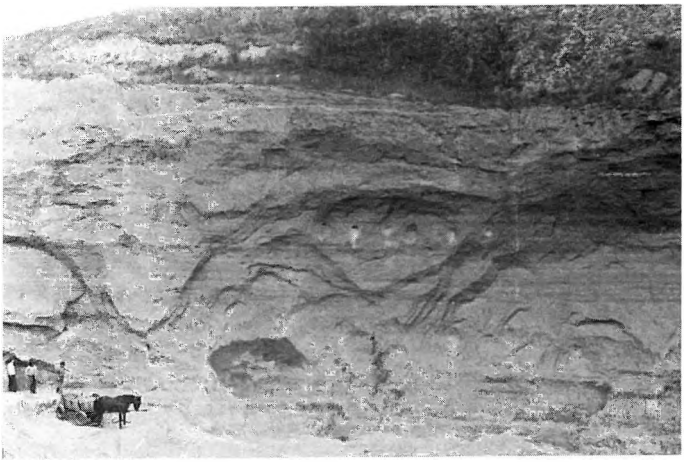

Fig. 12. Wall of gravel pit exposed east of Nekézseny

12. ábra. A Nekézsenytől keletre lévő kavicsbánya fala

Рис. 12. Стена галечникового карьера восточнее с. Некежень

Table II. Fossil assemblage in the Karpathian deposit exposed east of Nekézseny

II. táblázat. Kárpáti bentos faunaegyüttesek (Nekézseny)

Таблица II. Комплекс ископаемых остатков отложений карпатского яруса в обнажении к востоку от Некежения

Fossils: Porifera
Cliona sp
Mollusca
Bivalvia: *Lithophaga lithophaga* L.
Chlamys multistriata Poli
Chlamys opercularis hevesensis Schréter
Spondilus crassicosta Lam.
Anomia ephippium L.
Ostrea sp.
Gastrochaena sp.
?*Jouanettia* sp.
Arthropoda
Ostracoda
Cirripedia: *Balanus concavus* Bronn
Tentaculata
Bryozoa

The floor of the pit locally consists of a Paleozoic (Permian) carbonate rock. The borings of rock-boring clams *(Lithophaga)* cover the surface of this carbonate rock and confirm its exposure to a marine environment during the Miocene *(Fig. 13)*. The bedrock surface drops to the north more steeply than do the overlying strata. In the northwest part of the pit, the topographically lower parts of this surface are directly overlain by fine-grained micaceous

quartzose sand, which in turn is abruptly overlain by carbonate-pebble conglomerate. The bedrock locally projects into this conglomerate on the northwest side of the pit, and is directly overlain by it on the southwest side. The *Lithophaga* borings in both cases are filled with quartz sand, suggesting that the bedrock was bored, covered by fine terrigeneous sand, then locally exhumed and subsequently covered by calcareous gravel. Barnacles on the parts of the surface that project into the gravel probably were extant during gravel deposition, which probably therefore occurred at intertidal or greater depths. In the southwest part of the pit a pavement of carbonate cobbles and boulders covers the lower parts of the surface *(Fig. 14)*. These clasts show less evidence of *Lithophaga* borings than does the surface itself.

Most of the sediment exposed in the pit consists of carbonate rock clasts that range in size from coarse sand to cobbles more than 10 cm across *(Fig. 15)*. The pebbles and cobbles range from subangular to well-rounded, whereas the sand-size material is predominantly subangular. The clasts lithologically resemble the Paleozoic carbonate rock at the base of the deposit, and siliciclastic components are conspicuously absent from the coarse sand and gravel. Pebbles displaying well-defined *Lithophaga* borings *(Fig. 16)* can be found throughout the section. In addition, as many as 5% of the pebbles show concave surfaces that may be scars of *Lithophaga* borings.

Fine-grained micaceous quartzose sand occurs as matrix material and as a few thin beds in the lower part of the gravel. This sand lithologically resembles that which underlies the gravel on the northern side of the quarry. Very fine silty,

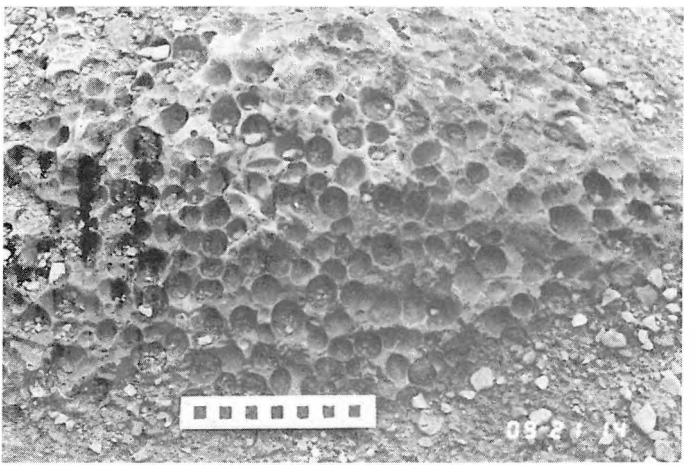

Fig. 13. Lithophaga borings on Paleozoic carbonate rock surface exposed in the lower part of the gravel pit east of Nekézseny

13. ábra. A Nekézsenytől keletre lévő kavicsbánya alján feltárt paleozoos karbonátkőzetben lévő *Lithophaga*-fúrások

Рис. 13. Дырки, пробуренные каменоточцами *(Litophaga)* в палеозойской карбонатной породе, вскрытой в нижней части галечникового карьера восточнее с. Чокваомань

Fig. 14. Accumulation (near centimeter scale) of cobbles and boulders at the base of the conglomerate east of Nekézseny. Paleozoic carbonate rock surface ic exposed at base of wall to left of scale

14. ábra. Görgetegek és tömbök felhalmozódása (a centiméter-skála közelében) a Nekézsenytől keletre lévő konglomerátum alján. A paleozoos karbonátkőzet felszíne a fal alján van feltárva, a skálától balra

Рис. 14. Накопление (вблизи сантиметрового масштаба) галек и валунов в основании конгломератов восточнее с. Некежень. Поверхность палеозойской карбонатной породы обнажается в основании стены карьера налево от масштаба

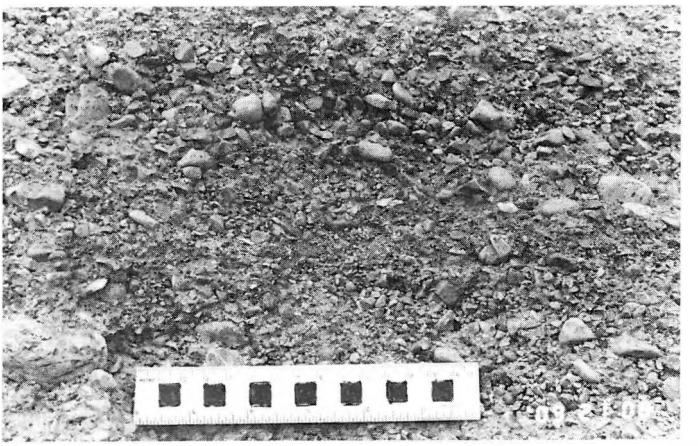

Fig. 15. Calcareous and dolomitic gravel in lowermost 5 m of section, pit east of Nekézseny. Note angularity of many clasts and suggestion of right-dipping imbrication

15. ábra. Mészkő- és dolomitkavics a szelvény legalsó öt méterén, a Nekézsenytől keletre lévő bányában. Figyeljük meg, hogy a törmelék jelentős része szögletes s jobbra dőlő imbrikációt sejtet

Рис. 15. Известковистые и доломитовые галечники в самых нижних 5 м разреза в карьере восточнее с. Некежень. См. угловатость большого количества обломков и предполагаемое правое падение чешуйчатости

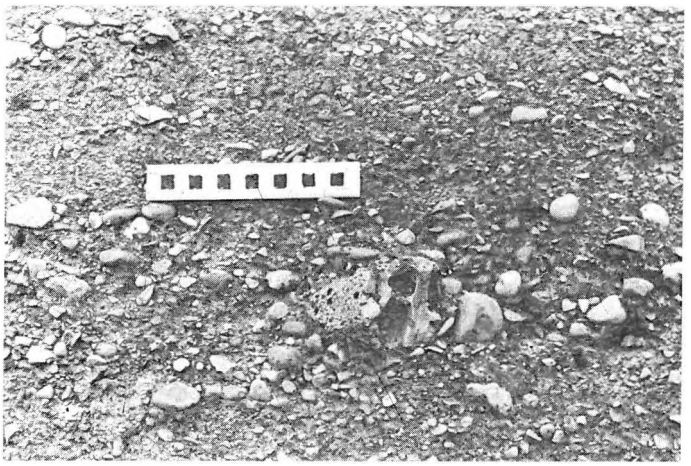

Fig. 16. Calcareous and dolomitic gravel, upper part of pit east of Nekézseny. Note variability of clast roundness and large *Lithophaga*-bored pebbles

16. ábra. Mészkő- és dolomitkavics a Nekézsenytől keletre lévő bánya felső részén. Figyeljük meg a törmelék gömbölyítettségének változó voltát és a nagy, *Lithophaga* által fúrt kavicsokat

Рис. 16. Известковистые и доломитовые галечники в верхней части карьера восточнее с Некежень. См. изменчивость окатанности обломков и крупные гальки, пробуренные каменоточцами (*Litophaga*)

micaceous, predominantly carbonate sand and mud occurs in lenticular layers up to 4 cm thick and as matrix in the upper part of the gravel, particularly on the northern side of the pit. The muddy layers typically are unburrowed and show no evidence of desiccation cracks. Some rest atop laterally continuous layers of relatively coarse pebbles *(Fig. 17)*. Some of the thicker muddy layers show a well-defined textural grading into clay at their tops. This muddy sediment resembles the fine-grained material in the overlying Garáb Formation.

Shell fragments are common in the gravel. Nearly all are abraded, and most lie with concave sides up. Articulated *in-situ* bivalves were not seen. One fragment of *Siderastrea* coral was found in the upper part of the gravel.

The conglomerate generally displays distinct stratification *(Fig. 18)*. Most of the beds can be traced laterally for only a few meters. The sediment lacks the degree of sorting of sand and gravel into discrete laterally continuous beds that typifies some wave-worked gravel [Clifton 1973]. Lenticular calcarenite beds 10–20 cm thick exist, particularly in the middle part of the gravel section. Some of these beds show internal parallel-lamination or high-angle foreset bedding. Low-angle cross-stratification is evident in much of the conglomerate *(Fig. 19)*. The cross-strata dip at angles of 10° or less in units a few tens of cm thick.

A striking feature of the gravel is a textural grading within many of the gravel beds. Such beds typically are a few cm thick; they are composed of fine limestone gravel at the base that grades upward into calcarenite at the top *(Fig.*

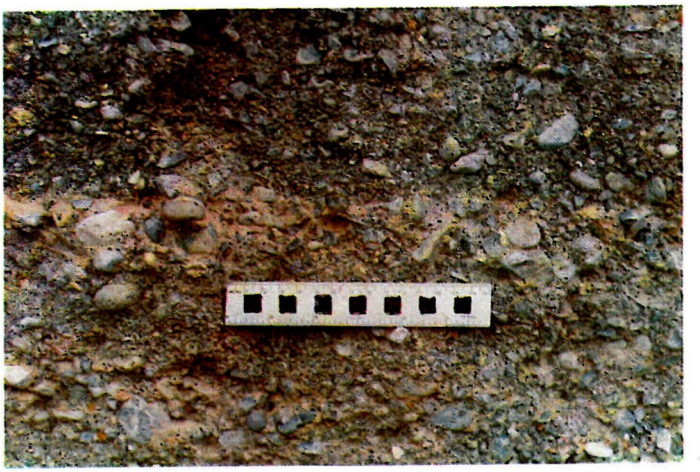

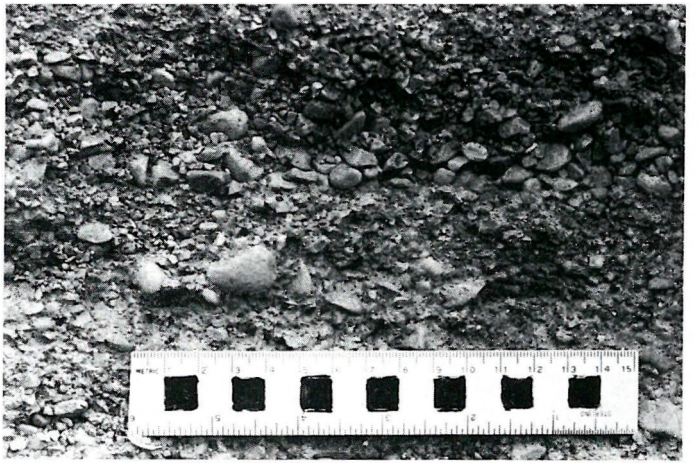

Fig. 17. Muddy (very fine silty sand) layer in gravel; upper part, north end of pit east of Nekézseny. Note layer of somewhat coarser pebbles immediately beneath fine layer

17. ábra. Iszapos (nagyon finom aleuritos homok) réteg a kavicsban, a Nekézsenytől keletre lévő bánya északi végének tetején. Figyeljük meg azt a valamivel durvább kavicsokból álló réteget, amely közvetlenül a finom réteg alatt van

Рис. 17. Илистый (весьма тонкозернистые алевритистые пески) слой в галечниках в верхней части северного конца карьера восточнее с. Некежень. См. слой несколько более грубозернистых галечников непосредственно под тонкозернистым слоем

Fig. 20. A) Graded layer in calcareous and dolomitic gravel, pit east of Nekézseny. Note absence of matrix in gravel at base of layer (cm scale).
B) Low-angle foresets composed of graded layers. Yellow colour due to quartzose sand matrix (cm scale)

20. ábra. A) Gradált réteg a mészkő- és dolomitkavicsban, kavicsbánya Nekézsenytől keletre. Figyeljük meg, hogy a réteg alján nincs mátrix a kavicsban
B) Gyengén dőlő, osztályozott rétegekből álló nyúlványok. A sárga szint a kvarcos homok mátrix okozza (cm skála)

Рис. 20. А) Проявление сортированности гранулометрического состава в известковистых и доломитовых галечниках в карьере восточнее с. Некежень. См. отсутствие цемента в галечниках в основании слоя (сантиметровый масштаб)
В) Выходы слоев с небольшим углом наклона и в сортированных осадках. Желтый цвет обусловлен цементом, сложенным кварцевыми песками (сантиметровый масштаб)

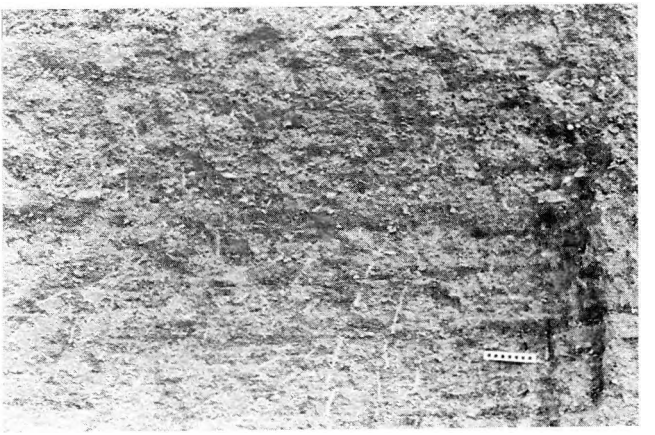

Fig. 18. Stratification in gravel, pit east of Nekézseny. Centimeter scale

18. ábra. Rétegződés a kavicsban. Kavicsbánya Nekézsenytől keletre. Centiméter-skála

Рис. 18. Слойчатость в галечниках в карьере восточнее с. Некежень. Сантиметровый масштаб

Fig. 19. Low-angle cross-stratification in lowermost 5 m of section, pit east of Nekézseny

19. ábra. Kishajlású keresztrétegzettség a szelvény alsó öt méterén. Kavicsbánya Nekézsenytől keletre

Рис. 19. Косая слоистость с небольшим углом наклона в низах самых нижних 5 м разреза карьера восточнее с. Некежень

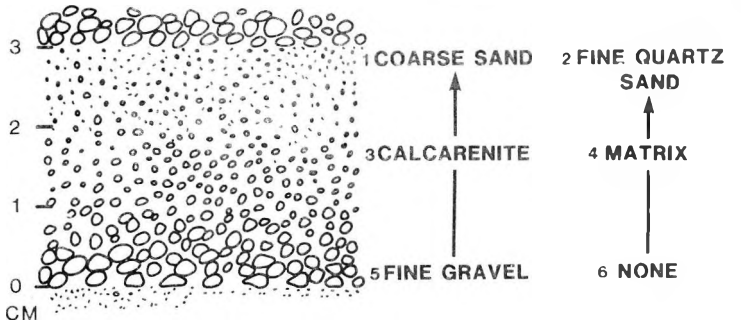

Fig. 21. General character of graded cycles in lowermost 5 m of gravel, pit east of Nekézseny

21. ábra. A gradált ciklusok általános jellege a kavics alsó öt méterén, a Nekézsenytől keletre lévő kavicsbányában.
1 — durva homok; 2 — finom kvarchomok; 3 — mészhomok; 4 — mátrix; 5 — apró kavics; 6 — hiány

Рис. 21. Общий вид циклов отсортированности осадков в самых нижних 5 м галечников в карьере восточнее с. Некежень
1 — грубые пески; 2 — мелкозернистые кварцевые пески; 3 — известковые пески; 4 — матрица; 5 — мелкие гальки; 6 — отсутствие

20). In the lower part of the pit, the fine-grained quartzose sand commonly forms a matrix to the coarse calcarenite at the top of a graded bed *(Fig. 21)*. The fine gravel in the lower part of such beds is matrix-free. The graded beds form depositional cycles in much of the gravel and compose many of the low-angle foresets in the unit.

Biogenic structures are present in the gravel in the form of clay-lined tubes *(Fig. 22)*. Most of these are 1–2 cm in diameter. The largest have a central, gravel-filled core 3 cm across enclosed by a 1-cm-thick rim of clay-matrixed gravel. The tubes are somewhat sinuous, and most are subvertical. Branches were not observed but may exist. One enlarged "turn-around chamber" occurs at a right-angle turn in a burrow. The burrows resemble in many ways those produced today by decapods such as *Callianassa*.

Directional features within the gravel are remarkably diverse. The low-angle foresets in the gravel dip primarily toward the southeast, whereas the high-angle foresets dip mostly toward a sector that ranges from northeast to northwest. Measurement of the long axes of 50 pebbles in the lower part of the unit showed a well-defined south–southeast, north–northwest trend. A similar orientation was visually evident on a bedding surface exposure high in the pit. Many of the pebbles in the conglomerate show a clear imbrication *(Fig. 23)*. The direction of imbrication is variable. In the lower part of the quarry the predominant inclination direction seems to be toward the south, whereas in the upper part it seems to be predominantly toward the north.

Lateral trends in clast size are evident within the gravel. Measurement of the long axes of the 25 largest pebbles within a m^2 surface of the same beds 30 m apart showed a clear decline in size (5.8 cm to 3.7 cm) in a northeasterly

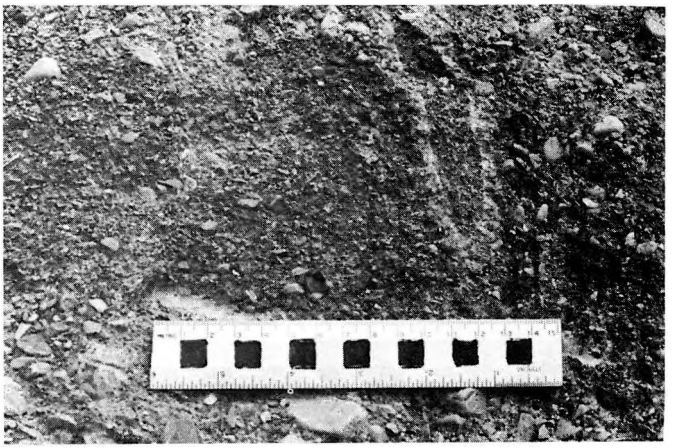

Fig. 22. Clay-lined burrow in gravel, pit east of Nekézseny. Note filling by carbonate sand. Cm scale

22. ábra. Agyaggal tapasztott ásásnyomok a kavicsban, a Nekézsenytől keletre lévő bányában. Figyeljük meg a karbonáthomokos kitöltést. Cm skála

Рис. 22. Дырка, пробуренная организмами в галечниках, изнутри покрытая пленкой глины в карьере восточнее с. Некежень. См. заполнение карбонатным песком. См масштаб

Fig. 23. Well-defined pebble imbrication (dipping to the right). Lower 5 m of gravel, pit east of Nekézseny. Note graded units

23. ábra. Határozott kavics-imbrikáció (dőlés jobbra). A kavics alsó öt métere, kavicsbánya Nekézsenytől keletre. Figyeljük meg a gradált egységeket

Рис. 23. Выраженная чешуйчатость галек (с наклоном направо). Нижние 5 м галечников в карьере восточнее с. Некежень. См. отсортированные единицы

direction. A similar decrease probably exists in the upper part of the gravel, although it is impossible to trace the same set of beds from the southern part of the exposure to the northern part. In the upper part of the quarry, pebbles commonly exceed 5 cm at the southern end of the exposure, whereas 60 m to the north, pebbles larger than 5 cm are uncommon in the same general part of the section. Local concentrations of coarse pebbles, however, do exist in the northern part of the quarry.

Unlike the Miocene deposit exposed east of Csokvaomány, the gravel in the pit east of Nekézseny does not display a vertical sequence that can be readily

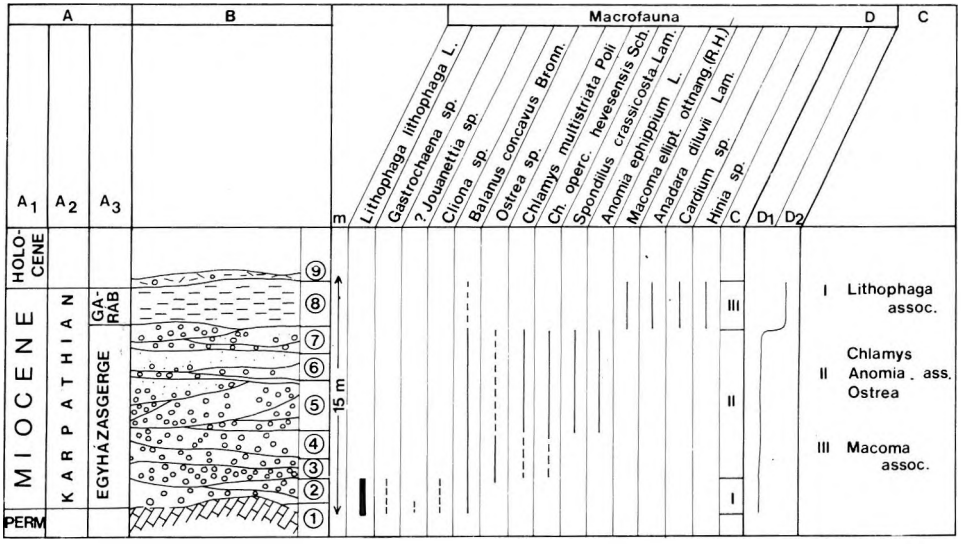

Fig. 24. Stratigraphic variation in macrofauna, gravel pit east of Nekézseny.
A — Cronostratigraphy: A_1 — age, A_2 — stage, A_3 — formation; B — Lithofacies; C — Assemblages; D — Environment: D_1 — eulitoral, D_2 — sublitoral; 1 — limestone; 2 — gravel with limestone blocks; 3 — sandy coarse gravels; 4 — gravelly sand; 5 — sand including coarse gravels; 6 — gravelly sand; 7 — sandy coarse gravels; 8 — silty clay; 9 — Holocene detritus

24. ábra. Rétegtani változás a makrofaunában, kavicsbánya Nekézsenytől keletre.
A — Kronosztratigráfia: A_1 — kor, A_2 — emelet, A_3 — formáció; *B* — Litofácies; *C* — Faunaegyüttesek; *D* — Környezet: D_1 — eulitorális, D_2 — szublitorális; 1 — mészkő; 2 — mészkőtömbös kavics; 3 — homokos durva kavics; 4 — kavicsos homok; 5 — durva kavicsos homok; 6 — kavicsos homok; 7 — homokos durva kavics; 8 — közetlisztes agyag; 9 — fiatal törmelék

Рис. 24. Стратиграфическое изменение в макрофауне в галечниковом карьере восточнее с. Некежень
A — Хроностратиграфия: A_1 — возраст, A_2 — ярус, A_3 — формация; B — Литофациальные; C — Фаунистические сообщества; D — Среда; D_1 — эвлиторальная; D_2 — сублиторальная; 1 — известняки; 2 — гальки с известняковыми блоками; 3 — песчаные грубые гальки; 4 — галечные пески; 5 — грубогалечные пески; 6 — галечные пески; 7 — песчаные грубые гальки; 8 — алевритовые глины; 9 — молодые обломки

interpreted in terms of changes in depositional environment. The uppermost gravel in the pit closely resembles that exposed 21 m stratigraphically below at the base of the pit. Environmentally significant vertical variation in the section may be limited to subtle differences in matrix composition, changes that are associated with lateral variations, and the transition to the finer-grained Garáb Formation near the top of the pit. Stratigraphic variation in the macrofauna assemblage *(Fig. 24)* may also be significant.

The basal 5 m of gravel exposed in the pit (Fig. 13) is typically well-bedded. Burrows are rare and southeast-dipping low-angle foresets in units 0.2–0.6 m thick are particularly well displayed on the southwestern part of the pit wall. The lower part of this section contains much very fine quartzose sand as matrix and thin beds, particularly near the base. The aforementioned measured decrease in pebble size toward the northeast occurs in this part of the section.

The section from 5 to 8 m above the base shows very little internal structure. Local brown patches of iron oxidation on the order of 5–10 cm across are common. On fresh exposure, many of these can clearly be seen in association with tubular burrows like those described in a preceding paragraph. It is probable that the structureless aspect of this part of the section results from intense bioturbation. A few very rare lenses of crossbedded calcarenite in the otherwise structureless sandy gravel suggest that the gravel was probably originally layered much like that immediately above and below. The middle part of the structureless section contains a laterally persistent layer of scattered coarse (5–8 cm) rounded carbonate rock clasts.

The section from 8–13 m above the base of the gravel contains beds and lenses of calcarenite. This sand is composed mostly of subangular carbonate fragments between 0.5 and 1.0 cm in diameter. Shell fragments are a common component, and quartzose sand, abundant in the lower part of the gravel, is almost non-existent. The lateral distribution of the calcarenite differs within the pit. On the nearly inaccessible southwestern wall, sand dominates the section, but it largely lenses out within a few tens of meters to the northeast. Calcarenite beds are generally absent in equivalent section at the northern part of the pit. In the central part of the quarry, burrows are particularly evident in this part of the section.

The uppermost 7–8 m of gravel resembles that in the lowermost 5 m. Quartzose sand in this upper section is less abundant and finer than that near the base of the gravel. Discrete layers of very fine-grained silty sand and mud are common in the northern part of the pit but absent in southern exposures where similar fine sediment is present only as matrix. As in the lower 5 m of section, decimeters-thick units of foresets defined by graded gravel layers dip gently toward the southeast.

The contact of the gravel with the overlying Garáb Formation lies within a 3.5–4 m interval that is covered by overburden. Above this interval, about 3 m of the Garáb Formation is exposed at the top of the pit. This unit consists of micaceous silty mud that contains isolated one-pebble-thick layers of limestone granules and pebbles less than 1 cm across and shell fragments. Shell fragments

are also abundantly scattered within the muddy section (the *Macoma* association, Fig. 24).

The deposits in the gravel pit are not so readily explained as those in the sand pit east of Nekézseny. Many lines of evidence suggest deposition in very shallow water, but the specific depth range and the origin of the observed features in the deposit are rather speculative.

The macrofauna occur in three distinct associations. The lowermost association (Fig. 24) is characterized by many bivalve specimens, particularly *Lithophaga*. The association is confined to the proximity of the Permian carbonate rock surface, which is so densely covered by borings as to limit the available space for other rock-clinging forms (such as oysters or barnales). Most of the borings are those of *Lithophaga; Cliona* traces exist but are relatively rare. The association is autochthonous and lacks exotic elements. All species could have lived together along a rocky limestone or dolomite shoreline.

The main body of the calcareous gravel contains an allochthonous macrofaunal association (Fig. 24) that is characterized by the genera *Chlamys, Anomia* and *Ostrea*. The shells occur predominantly as worn fragments, commonly riddled by boring organisms (such as *Cliona* and *Balanus*). This and the relatively high density of the shells indicate post-mortem transportation. The general ecologic coherence of the assemblage suggests that the fauna coexisted in a shallow wave-swept sandy environment and accumulated near their living site.

The third *(Macoma)* macrofaunal association occurs in the Garáb Formation (Fig. 24). It is characterized by a relatively low fossil density, a small percentage of shell fragments, and many single and a few paired bivalve shells. The assemblage is para-autochthonous; most of the species could have co-existed in a silty or clayey substrate of a shallow sea.

The physical processes that controlled deposition of the gravel and sand are not unequivocally clear. The angularity of the clasts implies a rather limited abrasional history (particularly upon consideration of the softness of carbonate rock relative to siliceous clasts). The variability of imbrication direction within the gravel suggests paleocurrents from diverse directions.

The water depth was probably no more than a few meters. The high degree of lateral variability of the sediment in the quarry suggests rapid facies change of the type commonly found in very shallow water. The abundance of large pebbles throughout the gravel likewise suggests shallow depths. Threshold curves indicate a requirement for wave-generated oscillatory currents of at least 2 m/s to move a quartz sphere 5 cm in diameter [KOMAR–MILLER 1975]. Many of the limestone and dolomite clasts in the gravel are probably equivalent hydraulically to such a quartz sphere, and currents of 2 m/s accordingly would seem fairly common. Airy wave theory provides a basis for estimating the combinations of wave height, wave period, and water depth that will produce this velocity [CLIFTON–DINGLER 1984]. *Figure 25* shows these combinations under the assumption that the only current present is due to passing waves. At a water depth of 10 m oscillatory currents equivalent to 2 m/s would require waves on the order of 4–5 m high—an unlikely amplitude given the paleogeo-

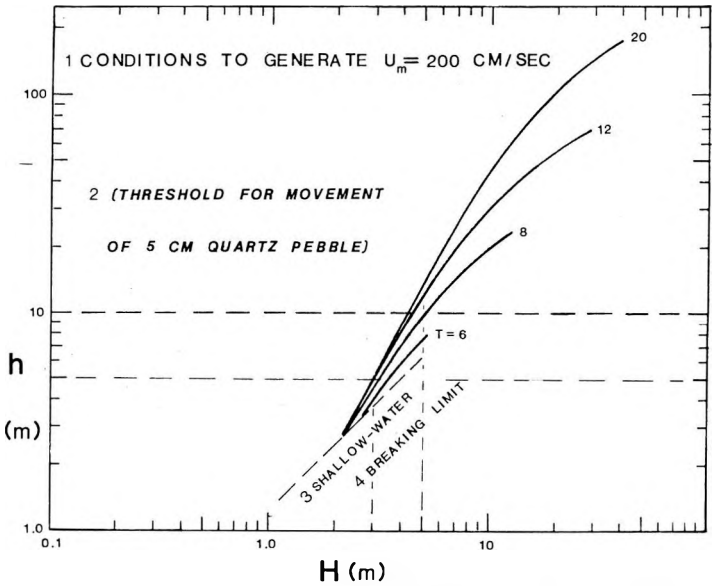

Fig. 25. Combinations of wave height, wave period and water depth required to initiate movement of a quartz pebble 5 cm in diameter

25. ábra. Az öt centiméter átmérőjű kvarckavics megmozdításához szükséges kombinációja a hullámmagasságnak, hullámperiódusnak és vízmélységnek
1 — U_m = 200 cm/s áramlást létrehozó körülmények; 2 — (5 cm-es kvarckavics megmozdításának küszöbértéke); 3 — sekélyvíz; 4 — hullámtörés határa

Рис. 25. Сочетание высоты волн, их периодичности и глубины водоема, необходимое для перемещения кварцевой гальки диаметром 5 см
1 — условия, создающие приток U_m = 200 см/сек; 2 — (граничное значение, необходимое для сдвижения кварцевой гальки размером 5 см); 3 — мелководье; 4 — граница разлома волн

graphic setting (Fig. 4). At a water depth of 5 m somewhat more reasonable waves (on the order of 3 m high) would be required.

Many of the specific features in the gravel are difficult to explain. The graded low-angle foresets that occur in much of the gravel are a good example. It is not clear whether these layers result from a specific event such as a storm or flood (if the gravel represents the seaward part of a small fan-delta), or from the lateral migration of large ripples. Wave ripples in gravelly sediment near rocky shorelines where the sand supply is limited or in bays where waves are small are known to have finer material concentrated on their crests [INMAN 1957]. If such ripples migrated laterally during active sedimentation, the resultant climbing-ripple structure might resemble the graded foresets.

The inconsistency of directional features is also difficult to interpret. High-angle foresets in the calcarenite dip in a generally northerly direction, whereas low-angle foresets in the gravel dip predominantly toward the southeast. Grain size variations are inconsistent (a northerly fining in the lower and upper parts

of the gravel, a northerly coarsening in the central part of the section containing the calcarenite), as are pebble orientation patterns (northwest–southeast long axis trend and variable imbrication direction). Such directional variability suggests that different processes influenced this sediment. The directional data, the lithologic homogeneity of the clasts, as well as the abundance of shell fragments and *Lithophaga*-bored clasts throughout the deposit, suggest that the deposit is not a fan-delta composed of fluvial detritus. Similarly it does not appear to be a simple beach–nearshore deposit as typified by the Csokvaomány example.

Perhaps the most reasonable interpretation is that the gravel accumulated at the foot of a rocky sea cliff of substantial relief under conditions of slowly rising sea level. The lack of pronounced vertical change in the 20 m of gravel suggests that sediment accumulated on the sea floor at about the same rate as sea level rose. Possibly the volume of carbonate rock detritus was augmented by a fluvial fan-delta contribution. The regional paleogeography (Fig. 4) suggests that the sea cliff was on the north side of a small island (perhaps a karstic feature) composed of Permian carbonate rock.

Under this interpretation, the initial gravel deposition occurred in the general proximity of a shoreline to the north. Quartzose sand associated with this shoreline is intermixed with the lowermost part of the gravel. As sea level rose and the shoreline retreated to the north, the amount of available siliciclastic sand near the island diminished. Subsequently, finer-grained siliciclastic sediment formed the matrix of the gravel, and, in quieter water away from the island shore, accumulated in discrete beds. When sea level inundated the island, gravel deposition ceased, and the fine-grained sediment of the Garáb Formation began to accumulate on the sea floor.

Such an interpretation is consistent with some of the directional features. It would explain the northerly decrease in pebble size. The clean carbonate sand that lenses out to the north in the central part of the section can be explained as a beach or near-beach deposit that, like some modern beaches, changed from sand to gravel a short distance offshore. The north-dipping high-angle foresets in this sand accordingly could be either "toe-of-beach" or rip current structures.

The origin of southeasterly dip of the low-angle foresets in the gravel remains enigmatic. Such a direction intuitively seems improbable in this paleogeographic setting for upslope (northeast) climbing wave ripples. Conceivably the foresets might reflect deposition on the flank of a localized accumulation of gravel such as a small fan-delta. The grading in the foresets could be due to discrete depositional events (such as a storm or flood), or to the climbing of wave-formed ripples across a southeast-facing, gently-stepped surface.

5. Conclusions

The paleoenvironmental setting of the nearshore deposits described here is generally similar—both accumulated near the shoreline of a narrow Miocene seaway. The lithologic character of the two deposits, however, differs markedly.

Their difference is probably due more to contrasts in the rate of sea level change relative to sedimentation rate and in the textural composition of the available sediment than to differences in the physical environment.

One deposit, part of the Salgótarján Formation, appears to be a prograding shoreline deposit. A variety of depositional environments—inner shelf, nearshore, foreshore, and backshore—are compressed into a shallowing-upward sequence less than 7 m thick. Storm deposits are recognizable in the lower part of the section. The sedimentary structures and directional features are nicely consistent with the reconstructed paleogeography. Development of the progradational sequence terminated with a renewed transgression of the sea.

The second deposit, part of the Egyházasgerge Formation, is not so readily interpreted, despite being very well exposed over a laterally and vertically extensive gravel pit face. The succession here appears to have accumulated during an episode of marine transgression in which the rate of gravel deposition seems to have been more or less equivalent to the rate of sea level rise. The gravel is apparently derived from a Paleozoic carbonate rock upland immediately to the south, possibly even from shoreline erosion of an island formed in part by karstic processes.

Many of the features in the gravelly deposit can be explained in terms of a marine transgression in which an initially adjacent siliciclastic shoreline retreated to the north. As a consequence of this shift, the siliciclastic sediment at the Nekézseny gravel pit became progressively finer with time. Concurrently, calcareous and dolomitic sand and gravel accumulated adjacent to the upland until it was inundated and deposition of silt and clay then prevailed at this site.

REFERENCES

Allen P. A., Homewood P. 1984: Evolution and mechanics of a Miocene tidal sand wave. Sedimentology, **31,** 1., pp. 63–81

Balogh K. 1964: Geologischen Bildungen des Bükk-Gebirges. MÁFI Évkönyv (Annales Inst Geol. Publ. Hung.), **48,** 2, 719 p. Budapest

Bohn-Havas M. 1978: Biostratigraphical and paleoecological evaluation of Miocene macrofauna on the lignite-exploration area of Mikófalva (in Hungarian). Report. 60 p. MÁFI Database, Budapest

Clifton H. E. 1969: Beach lamination–nature and origin. Marine Geology, **7,** 6, pp. 553–559

Clifton H. E. 1973: Pebble segregation and bed lenticularity in wave-worked versus alluvial gravel. Sedimentology **20,** 1, pp. 173–187

Clifton H. E. in press: Interpretation of paleoenergy levels from sediment deposited on ancient wave-dominated shelves. Can. Soc. Petroleum Geologists Memoir

Clifton H. E., Dingler J. H. 1984: Wave-formed structures and paleoenvironmental reconstruction. Marine Geology, **60,** 1–4, pp. 165–198

Clifton H. E., Hunter R. E., Phillips R. L. 1971: Depositional structures and processes in the high-energy nonbarred nearshore. J. Sedimentary Petrology, **41,** 3, pp. 651–670

Clifton H. E., Thompson J. K. 1978: *Macaronichnus segregatis* – a feeding structure of shallow marine polychaetes. J. Sedimentary Petrology, **48,** 4, pp. 1293–1302

Császár G., Haas J., Halmai J., Hámor G., Korpás L. 1982: The role of middle and late Alpine tectonic phases in the geological evolution of Hungary (in Hungarian). MÁFI Évi Jel. az 1980. évről (Annual Report of the Hung. Geol. Inst.), pp. 509–516

HÁMOR G. 1980: The age of Neogene tectonic phases in the Paratethys realm. 26^{e} Congrés Géol. Internat. (Res.), Paris, 1, p. 384

HÁMOR G. 1983: The quantitative methods of palaeogeographical reconstruction. MÁFI Special Papers 2, 70 p. Budapest

HÁMOR G. 1984: Paleogeographic reconstruction of Neogene plate movements in the Paratethyan realm. Acta Geol. Hung. **27**, 1–2, pp. 5–21

HÁMOR G., HALMAI J. 1975: Palaeogeographical map of the Miocene of northern Hungary (in Hungarian). MÁFI Database, Budapest

HARMS J. C., SOUTHARD J. B., WALKER R. G. 1982: Structures and sequences in clastic rocks. S.E.P.M. Short Course No. 9, Soc. Econ. Paleontologists Mineralogists, Tulsa, Okla., 249 p.

INMAN D. L. 1957: Wave-generated ripples in nearshore sands. Tech. Memo. Beachs Eros. Bd. U.S., No. 100

KOMAR P. D., MILLER M. C. 1975: Sediment threshold under oscillatory waves. Proc., 14th Conf. on Coastal Engr., pp. 756–775

RADÓCZ GY. 1975: Explanations for the 200,000 scale geological map series of Hungary (in Hungarian). 257 p. MÁFI, Budapest

SCHRÉTER Z. 1929: Mining-geological description of the lignite deposits of counties Borsod and Heves (in Hungarian). MÁFI, 394 p. Budapest

SCHRÉTER Z. 1945: Geologische Aufnahmen im Gebiete von Uppony ferner im Gebiete von Putnok (in Hungarian, with German abstract). MÁFI Évi Jelentés az 1941–42. évről (Annual Report of the Hung. Geol. Inst.), pp. 161–237, Budapest

SCHRÉTER Z. 1954: Relevé géologique dans les environs de Szilvásvárad (in Hungarian, with French abstract). MÁFI Évi Jelentés az 1952. évről (Annual Report of the Hung. Geol. Inst.), 135 p. Budapest

WEIMER R. J., HOYT J. H. 1964: Burrows of *Callianassa major* SAY, geologic indicators of littoral and shallow neritic environments. J. Paleontology, **38**, 4, pp. 761–767

ELTÉRŐ TÍPUSÚ HOMOK- ÉS KAVICSÜLEDÉKEK AZ ÉSZAK-MAGYARORSZÁGI MIOCÉNBŐL

H. Edward CLIFTON, BOHNNÉ HAVAS Margit és MÜLLER Pál

A vizsgált üledéksorok az Egercsehi–Ózdi árokban keletkeztek. Itt az eggenburgi–ottnangi üledékek két teljes ciklust képviselnek, melyek közé a Gyulakeszi Riolittufa Formáció települ. E fölött a felső ciklushoz tartozó Salgótarjáni Barnakőszén Formáció homokos, aleuritos és agyagos, lignit-tartalmú üledékei települnek. E formációba tartozó üledéksort tár fel a Csokvaománytól K-re lévő kis homokgödör. A szelvény alsó része progradáló parti üledéknek tekinthető, iszap-homokrétegek felfelé fokozatosan keresztrétegzett kavicsba mennek át, melyet laminált homok, gyökérnyomos iszap, vékony lignitzsinór és csigás iszap takar, s a sor eróziós felszínnel zárul. A kavics és a laminált homokréteg határa az egykori tengerszintet jelzi. A sor egyes tagjai a progradáció során egyre sekélyebbé váló környezet sávjában ülepedhettek le. A fauna a Salgótarjáni Barnakőszén Formációra utal, de nem ad felvilágosítást a sótartalomra. Csupán az eróziós felszín felett települő, lagúna-eredetű üledékekben találhatók 0,5–3,0 illetve 3,0–16,5‰-os sótartalomra jellemző alakok vagy együttesek.

A kárpáti–badeni korszakban is két üledékciklust figyelhetünk meg. Az alsó, kárpáti korú ciklusba tartozik az Egyházasgergei Formáció. Ennek része a Nekézsenytől keletre, egy kavicsbányában feltárt kavicsösszlet. A fekü paleozoos karbonát-felszínt Lithophaga-kagylók tömegei fúrták meg. Erre 21 m mészkő- és dolomitanyagú kavics települ, részben közvetlenül, részben kvarchomok közbetelepüléssel. A fauna tengeri üledéket jelez. A nagyobb kavicsokat mozgató oszcilláló vízmozgást legfeljebb néhány méter mély vízben képzelhetjük el, az adott ősföldrajzi helyzetben. A szemnagyságban mutatkozó rendszeres változás arra szoritkozik, hogy a sziliklasztkomponens felfelé finomodik (lent finom homok, feljebb aleuritos igen finom homok, majd agyag). Feltesszük, hogy az üledék egy kiemelt terület (talán egy sziget) lábánál rakódott le, a transzgresszióval lépést tartó üledékképződéssel. Így a helyi eredetű mészkő–dolomit-törmelék nagyjából azonos

vízmélységet jelez a szelvényben. Az eredetileg szomszédos sziliklasztos partvidék visszahúzódása az ilyen komponens finomodásában mutatkozik meg. A karbonátos sziklasziget teljes elöntése után a kavicsképződés és ülepedés megszűnt, s a Garábi Slir Formáció finomszemű üledékei zárták a kárpáti korú üledékképződést.

ОТЛИЧАЮЩИЕСЯ ТИПЫ ПЕСЧАНЫХ И ГАЛЕЧНЫХ ОСАДКОВ ИЗ МИОЦЕНОВЫХ ОБРАЗОВАНИЙ СЕВЕРНОЙ ВЕНГРИИ

Г. Эдвард КЛИФТОН, Маргит БОН-ХАВАШ и Пал МЮЛЛЕР

Исследованные осадочные породы происходят из канав Эгерчехи и Озда. Здесь осадки эггенбурга–оттнанга представляют собою два полных цикла, среди которых залегают образования Дьюлакеси Риолитово–Туфовой Формации. Над ними лежат относящиеся к верхнему циклу песчаные, алевритовые и глинистые осадки, а также содержащие лигнит, Шалготарянской Буроугольной формации. Разрез осадочных образований, относящихся к этой формации, вскрыт в небольшой песчаной яме, находящейся на восток от Чокваомань. Нижнюю часть разреза можно рассматривать как перемещавшиеся береговые осадки, илисто–песчаные слои вверх по разрезу постепенно переходят в поперечно слоистые гальки, которые покрыты ламинированным песком, илом со следами корней, тонкими шнурами лигнита и ракушечным илом, разрез заканчивается поверхностью эрозии. Граница галек и слоя ламинированного песка обозначает прежний уровень моря. Отдельные члены разреза во время продвижения отлагались в полосе все более мелкого окружения. Фауна указывает на Шалготарянскую Буроугольную формацию, но не дает объяснения относительного содержания солей. Только в осадочных образованиях лагунового происхождения, находящихся над поверхностью эрозии, можно встретить особи и комплексы, характерные для 0,5–3,0 и 3,0–16,5‰-ного солесодержания.

В карпатско–баденском периоде времени также наблюдаются два цикла осадконакопления. Нижний, карпатского возраста, и представлен Эдьхазашгергейской Формацией. Часть этой формации представлена толщей галек, вскрытой в большом галечниковом карьере на восток от Некежень. Лежащая в подошве поверхность палеозойских карбонатов пробурена массами представителей раковин Lithophaga. На них налегают в мощности 21 м известняковые и доломитовые гальки частично непосредственно, частично с включениями кварцевого песка. Фауна указывает на осадки морского происхождения. Колеблющееся движение вод, передвигавших более большие гальки, мы можем представить для вод в несколько метров глубиной в бывшем палеогеографическом положении. Систематическое изменение, наблюдаемое в размере зерен, показывает, что силикластические компоненты в направлении вверх становятся мельче (внизу мелкий песок, выше алевритовый очень мелкий песок, затем глина). Предполагаем, что осадки отложились у подножья одного приподнятого участка (может быть острова) во время осадкообразования, проходившего вместе с трансгрессией. Таким образом, известняково–доломитовые обломки местного происхождения в разрезе большей частью указывают на идентичные глубины воды. Отступление первоначально соседней силикластовой береговой территории проявляется в таком измельчении компонентов. После полного погружения в воды карбонатового скалистого острова прекратилось образование галек и накопление осадков, и процесс осадкообразования карпатского возраста завершили тонкозернистые осадки Гарабской Шлировой Формации.

GEOPHYSICAL TRANSACTIONS 1985
Vol. 31. No. 1–3. pp. 131–155

LITHOLOGIC CHARACTERISTICS AND PALEOGEOGRAPHIC SIGNIFICANCE OF RESEDIMENTED CONGLOMERATE OF LATE CRETACEOUS AGE IN NORTHERN HUNGARY

H. Edward CLIFTON*, Károly BREZSNYÁNSZKY** and János HAAS***

Late Cretaceous (Senonian) conglomerate is exposed in northern Hungary at the boundary between the Bükk and Uppony Mountains litho-tectonic units. It rests depositionally on rocks of the Uppony unit. The conglomerate is locally well-exposed in artificial cuts. A railroad cut on the southwestern side of the village of Nekézseny and a road cut east of the village of Csokvaomány form the basis for this paper. Several lines of evidence (particularly graded sandstone beds) indicate that the Nekézseny section is structurally overturned. The conglomerate occurs in flow units that are in some places fairly obscure. Many of the thicker units follow a textural pattern of being inversely graded at the base, ungraded in their central portion and normally graded at the top. A clast-supported framework in which pebbles are aligned with short axes normal to bedding is common to most of the units. The most reliable long-axis orientation and imbrication data (from the less structurally disturbed Csokvaomány exposure) suggest paleotransport to the northeast. The textural character of the conglomerate and its fabric suggest that most of it was emplaced by flows that were intermediate between cohesive debris flows and high-density turbidity currents. The absence of clasts from the Bükk Mountains litho-tectonic unit suggests that the structural convergence of the Bükk and Uppony units occurred after deposition of the conglomerate (or that the Bükk Mountains unit was not exposed during deposition). Many of the clasts are derived from the Aggtelek–Rudabánya Mountains litho–tectonic unit, which presently is exposed well to the northeast of the area of Late Cretaceous conglomerate occurrence. The paleotransport direction suggests that either source rock in this unit extends well to the south in the subsurface or that the source was subsequently transported tectonically to the north along the Darnó tectonic line.

Keywords: resedimentation, conglomerates, Upper Cretaceous, paleogeography, Hungary

1. Introduction

Conglomerate of Late Cretaceous Senonian (Campanian) age crops out in northern Hungary in a narrow belt between the Bükk and the Uppony Mountains *(Figs. 1* and *2)*. Although the conglomerate is of limited extent (the outcrop belt between the villages of Dédestapolcsány and Csokvaomány is but 8 km long), it is a key unit for interpreting late Mesozoic paleogeography and tectonics. Called the Nekézseny Conglomerate Formation by BREZSNYÁNSZKY and HAAS [1984], it is the only Cretaceous unit known to exist in northern Hungary. Accordingly, it provides critical information on post-Jurassic–pre-

* U. S. Geological Survey, 345 Middlefield Road, Menlo Park, California 94 025
** Central Office of Geology (KFH), POB 22, Budapest, H–1251
*** Hungarian Geological Survey, POB 106, Budapest, H–1442
Manuscript received: 12 February, 1985

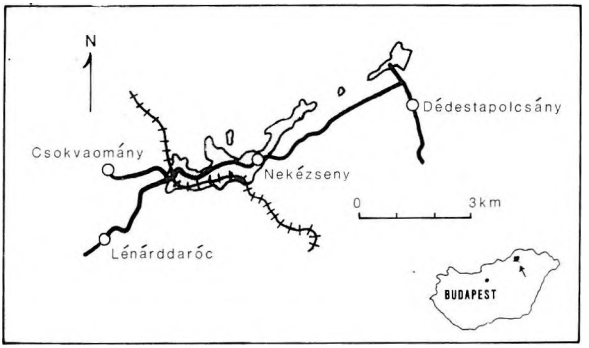

Fig. 1. Location of the Late Cretaceous conglomerate (shaded area) in northern Hungary

1. ábra. A felsőkréta Nekézsenyi Konglomerátum elterjedése (árnyalt terület) Észak-Magyarországon

Рис. 1. Распространение верхнемеловых конгломератов в Северной Венгрии

Fig. 2. Generalized lithologic map of tectonic units in the vicinity of the Late Cretaceous conglomerate in northern Hungary (symbols on left side of explanatory column indicate areas of exposure, symbols on right side indicate subsurface occurrence)
1 — Late Cretaceous conglomerate; 2 — Bükk unit, Jurassic meta-siltstone and diabase; 3 — Bükk unit, Triassic shallow- and deep-marine sedimentary and volcanic rocks, in part slightly metamorphosed; 4 — Bükk unit, Carboniferous to Permian shallow-marine formations; 5 — Uppony unit, various lithologies, Devonian to Carboniferous rocks, slightly to moderately metamorphosed; 6 — Bükk unit, various lithologies; 7 — Aggtelek–Rudabánya unit, Triassic shallow- and deep-marine formations, in part slightly metamorphosed

2. ábra. A felsőkréta Nekézsenyi Konglomerátum környezetében található szerkezeti egységek egyszerűsített földtani térképe (a jelkulcs bal oldalán feltüntetett jelek a kibúvásokat, a jobb oldali jelek a felszín alatti elterjedést jelölik)
1 — Felsőkréta Nekézsenyi Konglomerátum; 2 — Bükki egység, jura pala és diabáz; 3 — Bükki egység, triász sekély- és mélytengeri üledékes és magmás képződmények, részben gyengén metamorfizálódva; 4 — Bükki egység, karbon–perm sekélytengeri képződmények; 5 — Upponyi egység, különböző kifejlődésű devon–karbon képződmények, gyengén, ill. közepes mértékben metamorfizálódva; 6 — Bükki egység, tagolás nélkül; 7 — Aggtelek–Rudabányai egység, triász sekély- és mélytengeri képződmények, részben gyengén metamorfizálódva

Рис. 2. Схематическая геологическая карта тектонических единиц в районе развития верхнемеловых конгломератов в Северной Венгрии (знаки на левой стороне колонки легенды обозначают выходы на дневную поверхность верхнемеловых конгломератов, знаки на правой стороне обозначают их распространение на глубине)
1 — верхнемеловые конгломераты; 2 — Бюккская единица, юрские алевролитовые сланцы и диабазы; 3 — Бюккская единица, триасовые мелководные и глубоководные осадочные отложения и магматические образования, частично слегка метаморфизованные; 4 — Бюккская единица, каменноугольно–пермские, мелководные, морские отложения; 5 — Уппоньская единица, разнообразные по литологическому составу, девонско-каменноугольные отложения, слабо- или умеренно метаморфизованные; 6 — Бюккская единица, без расчленения; 7 — Аггтелек–Рудабаненская единица, триасовые мелководные или глубоководные, морские отложения, частично слабометаморфизованные

Senonian geologic history and post-Senonian deformational processes [BREZSNYÁNSZKY–HAAS 1984].

The conglomerate lies at the boundary between two litho-tectonic units in an area of complicated and poorly understood structure. On the north side, the Uppony Mountains are underlain by Devonian and Carboniferous basaltic volcanic rocks and carbonate and siliciclastic metasediments (Fig. 2). The conglomerate rests depositionally on slightly metamorphosed Paleozoic rocks of this complex. South of the conglomerate lie mostly Late Paleozoic and Early Mesozoic mainly slightly metamorphosed and partly unmetamorphosed platform and deep-water carbonate rocks of the Bükk Mountains. The rocks appear to be thrust over the conglomerate on its southern margin. Further north, across

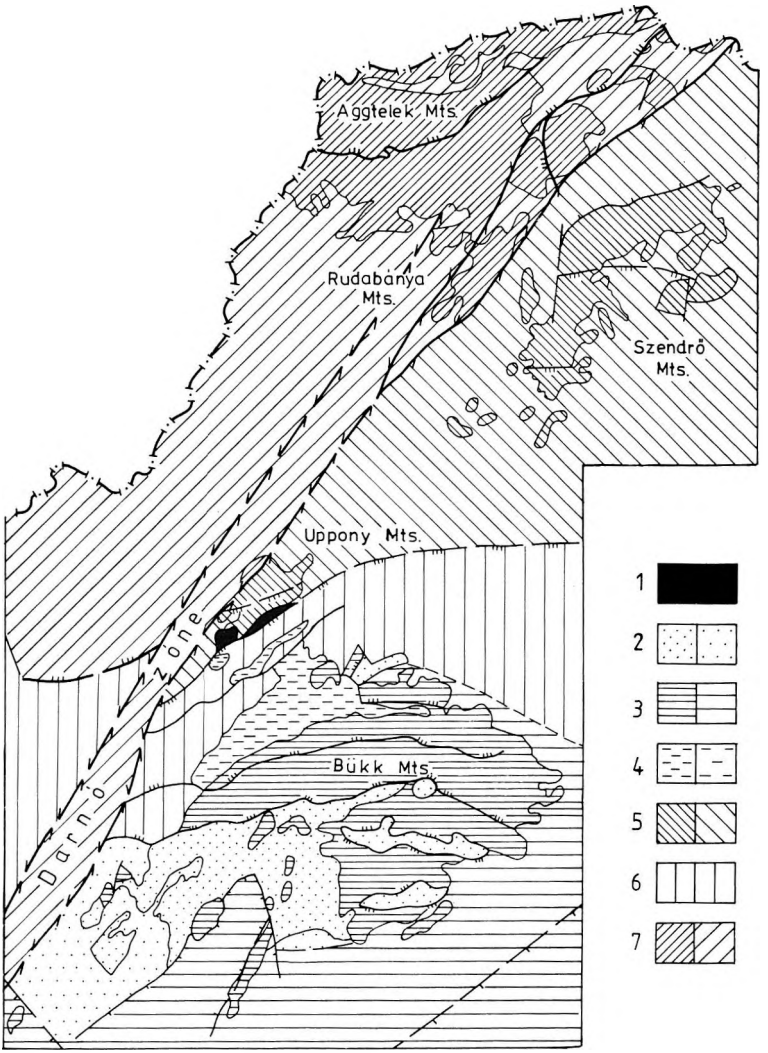

a major fault zone (Darnó Zone), lies another litho-tectonic unit, that of the Aggtelek and Rudabánya Mountains (Fig. 2). This unit consists of overthrust sheets or nappes of slightly metamorphosed basic igneous rocks and sedimentary deposits of Triassic and Jurassic age, capped by unmetamorphosed carbonate rocks of Triassic age.

Natural exposure of the conglomerate is generally poor; it is best seen in a few artificial cuts. Because of the limited exposure and the substantial structural complexity of the area, the thickness of the unit is presently unknown. The conglomerate is composed of rounded to subrounded pebbles and cobbles of diverse composition. Although most of the conglomerate appears to be clast-supported, intervals of pebbly mudstone are present. Typically the thickness of the conglomerate beds is measured in meters, in contrast to the associated beds and lenses of sandstone that generally are only several tens of centimeters thick. Near its basal contact with underlying Paleozoic rocks, the conglomerate is reddish and the associated sands are faintly cross-bedded. Elsewhere in the section, however, the predominance of textural grading indicates that most of the conglomerate was emplaced by sediment gravity flows [BREZSNYÁNSZKY–HAAS 1984]. In its easternmost exposure near Dédestapolcsány, the conglomerate is interbedded with rudist-bearing masses of carbonate rock that presumably slumped from adjacent shallow-water reefs.

After its initial description and age assignment [BÖCKH 1867] this deposit has, until recently, been little studied. Earlier interpretations were that the conglomerate formed in a shallow marine environment [SCHRÉTER 1945] during a transgression following the Austrian orogenic phase [PANTÓ 1954]. BALOGH [1964] suggested that it formed in a depression that developed between the Bükk and Uppony Mountains by Cretaceous tectonism. Recent palynological studies have refined the chronostratigraphic framework of the unit [SIEGL–FARKAS 1984]. BREZSNYÁNSZKY and HAAS [1984] provide a general description of the lithology of the conglomerate, its structural character, and its significance relative to the interpretation of the geology of the region. The present paper focuses on the sedimentologic aspects of the unit, particularly as they apply to depositional processes and the paleogeographic setting for this deposit.

2. Methods

This report is based on the detailed examination of the two best exposures of the conglomerate. The best of these is a railroad cut on the southwestern side of the village of Nekézseny (Fig. 1) that serves as the stratotype section [BREZSNYÁNSZKY–HAAS 1984]. The other occurs in a road cut about 1 km east of the village of Csokvaomány (Fig. 1). In each exposure the section was measured and flow units were delineated to the best extent possible.

The identification of flow (or sedimentation) units can be an uncertain process. The boundaries in this study were placed primarily at abrupt changes in texture. Contacts between most of the units exposed in the two sections

seemed fairly obvious. Careful examination of some apparent units, however, suggested that they were composite. The process is further complicated by large masses of pebbles within some flows that seem to result from remobilization of previously deposited material. Subunit designations are assigned to multiple flow units in a conglomerate or pebbly mudstone that could not be clearly traced laterally.

Each unit or subunit was examined visually to determine the character of textural grading, the orientation of the clasts relative to bedding, the general proportions of clasts and matrix, and the composition and orientation of exceptionally large clasts. The visually-perceived character of textural grading was checked by actually measuring the pebbles in selected units (12 at Nekézseny and 3 at Csokvaomány). The degree of induration of the conglomerate makes difficult the removal of pebbles from many beds, and accordingly only the apparent long axis was recorded. The size of the largest 11 pebbles in a 20-cm-thick interval a meter wide was recorded in the field, and the apparent long axis was averaged for the smallest 10 of these. Elimination of the largest pebble in each sample reduced the undue influence of an isolated anomalously large clast. The general consistency of the results suggests that the technique is adequate for defining textural grading, even though the measured grain size differs somewhat from the actual size.

The long-axis orientation of the clasts was also measured within some beds. At the Csokvaomány exposure the long axis of 20 distinctly rod-like pebbles (long axis > twice the short and intermediate axes) within the bedding plane was measured at three levels within three different units. This approach was not attempted at Nekézseny because the considerable structural complexity at this exposure makes it difficult to reconstruct the original horizontal position.

In addition, the junior authors examined in detail the shape, size, orientation and lithology of 100 pebbles in a 1-m^2 area in one locality at the Csokvaomány exposure and four localities in the Nekézseny cuts. Long axis orientation, *a*, *b*, and *c* axis length, and roundness (using an empirical scale of 0–4) were measured in the field. Field and thin-section analyses were used to assign the clasts among five general lithologic groups following the procedures of BREZSNYÁNSZKY and HAAS [1984].

3. Results – The Nekézseny Exposure

A railroad cut provides an impressive north–south exposure *(Fig. 3)* of the Late Cretaceous conglomerate on the southwestern side of the village of Nekézseny, within 200 m of the train stop. The length of the exposure is more than 100 m and the maximum height of the wall is almost 20 m. The conglomerate is exposed on both sides of the cut; the eastern side is a single vertical wall, whereas the western side is cut into a series of narrow stepped terraces at approximately 5 m intervals. Both walls are inaccessible beyond the ground level.

The rock is much fractured [BREZSNYÁNSZKY–HAAS 1984, Fig. 2]. Although many of the fractures seem not to displace the strata, offset of one to several meters is common. Many of these faults follow or partly follow the margins of sandstone beds. The fault that intersects the base of the west wall at 67 m is of

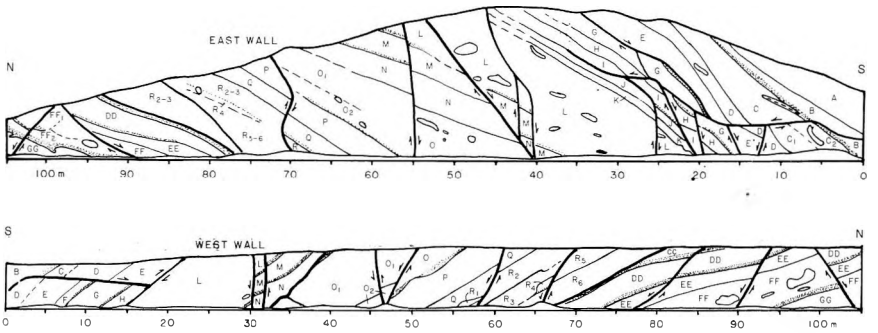

Fig. 3. Conglomeratic units as exposed in the walls of the Nekézseny railroad cut

3. ábra. A nekézsenyi vasúti bevágásban feltárt konglomerátum rétegsor

Рис. 3. Разрез конгломератов, вскрытый в откосе железной дороги у с. Некежень

Fig. 4. Graded sandstone bed, top of unit *FF*, west wall of the Nekézseny railroad cut at about the 100 m point of Fig. 3. Pencil points downward toward top of bed (assuming section is overturned). Note sharp contact with presumably overlying coarse conglomerate

4. ábra. Osztályozott rétegzettséget mutató (gradált) homokkő réteg, az *FF* egység tetején, a nekézsenyi vasúti bevágás nyugati falának kb. 100 m-nél lévő szakaszán (3. ábra). A lefelé mutató ceruza a réteg teteje felé mutat (feltételezve, hogy a szelvény átbuktatott). Figyelmet érdemel az éles határ az eredetileg feltehetően fedő helyzetű durva konglomerátum felé

Рис. 4. Горизонт песчаника отсортированной слоистости, верхи единицы *FF*, западный откос железной дороги около отметки 100 м (Рис. 3). Карандаш направлен острым концом вниз в сторону верхов пласта (допустив, что разрез опрокинут). Бросается в глаза резкий контакт с вышележащими грубообломочными конгломератами

unknown direction and amount of displacement and breaks the continuity of the measured section.

Several lines of evidence indicate that the section is overturned, as suggested by BREZSNYÁNSZKY and HAAS [1984]. The typical direction of textural fining in these exposures is downward. Inverse grading is a well-known feature of many resedimented conglomerates [WALKER 1975], but it is virtually unknown to occur repeatedly in sand beds tens of centimeters thick. Such beds in the Nekézseny conglomerate consistently become finer in a downward direction *(Fig. 4)*, strongly suggesting that the beds are overturned. Sandstone injections into the base of overlying conglomerate *(Fig. 5)*, scour at the base of the conglomerate beds, and the fine structure of rippled beds in the sandstone support the concept of an overturned section. The stratigraphic section shown in *Figure 6* is therefore constructed on the assumption that the beds are overturned.

The lowermost (southern) part of the section is particularly difficult to correlate between the two walls of the cut. This difficulty appears to derive both from disruption by faulting and from the lateral variability of the units. The identification of units on the western cut between 0 and 15 m (Figs. 3 and 6) must therefore be considered tentative.

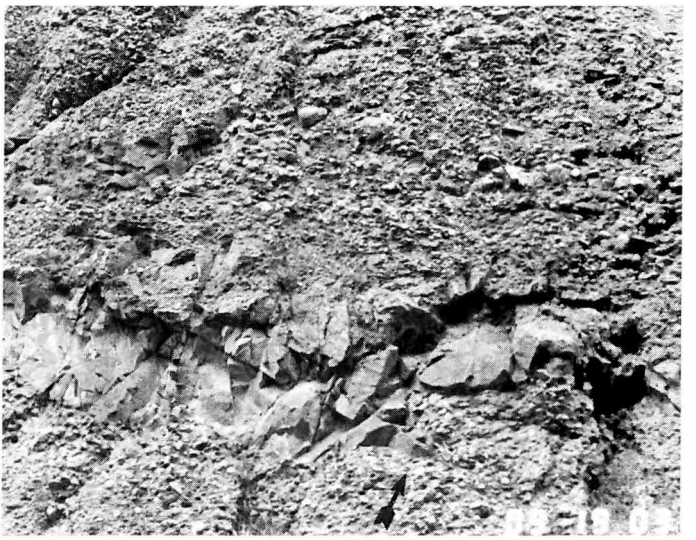

Fig. 5. Sandstone injection into base of unit *GG*, east wall of the Nekézseny railroad cut at about the 99 m point of Fig. 3. Overturned section. Note normal grading in conglomerate beds

5. ábra. Homokkő injektálódás a *GG* egység bázisába, a nekézsenyi bevágás K-i falában a 99 m-nél lévő szakaszon (3. ábra). A szelvény átbuktatott. Figyelmet érdemel a konglomerátum rétegek normál osztályozott rétegződése

Рис. 5. Инъекция песчаника в основание единицы *GG*, восточный откос железной дороги у с. Некежень около отметки 99 м (Рис. 3). Опрокинутый разрез. См. нормальную градацию в слоях конгломерата

The lowermost unit *(A)* is identified only on the eastern wall, where it is inaccessibly exposed. This unit may be a composite of several flows; in the absence of definitive criteria, it is here treated as a single unit. *Unit A* contains some very coarse conglomerate in its lower part (the base is not clearly exposed) and the top appears to be graded. *Unit B* is the lowermost flow that can be fully delineated. It contains a large (8 m) lense of very coarse conglomerate and grades up into a prominent sandstone bed, which in turn locally grades into a mudstone bed.

Unit C is the first truly accessible unit at the south end of the eastern wall. It is a complicated unit containing large mudstone rip-ups in its lower part. Just above the large mudstone clast nearest the track level *(Fig. 7)* is a concentration on fine pebbles that may be overlain by a second unit (C_2). This distinction is not clear above a sub-horizontal fault (Fig. 7) and the concentration may represent a remobilized mass of fine pebbles rather than the result of textural grading. The variation in clast size to the base of the large mudstone clast is shown in *Figure 8*.

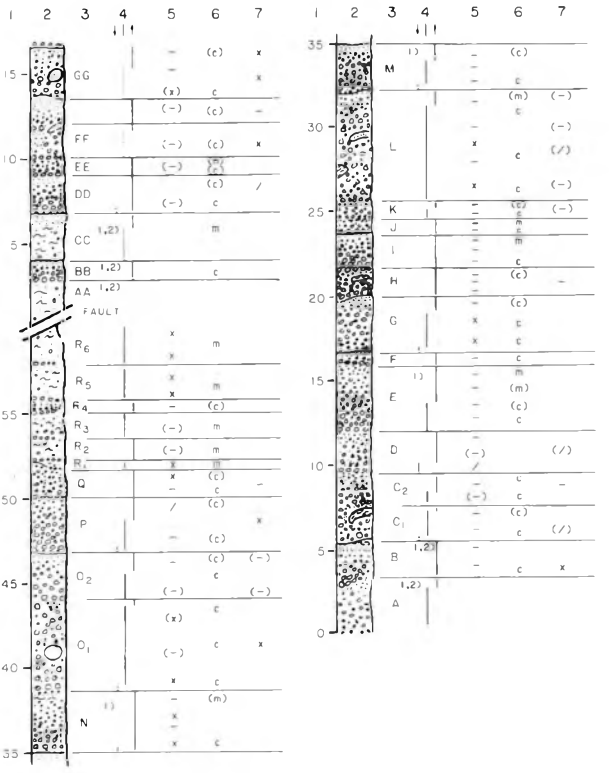

Unit D is broken by faults where it is accessible. Measurement of clast size variation in the lower 1.8 m of this unit shows it to be an inversely- to normally-graded conglomerate (Fig. 8).

Unit E is also broken by faults. The complete unit is exposed at an accessible level only on the west wall of the cut. The variation of clast size within the lower 3 m on the eastern cut is shown in Figure 8.

Unit F is a thin (1 m) unit that is completely present only on the western wall. The unit grades upward from coarse conglomerate into sandstone. On the eastern wall the conglomerate is missing, either because it represents a local channel or is cut out by faults; only the sandstone can be seen.

Unit G overlies the sandstone of unit *F* and grades upward into sandstone. The complete succession can be seen only on the western wall. On the eastern wall of the cut, the unit is disrupted by faults. The clast size variation in unit *G* is shown in Figure 8.

Units H and *I* are prominently graded conglomerate units that are well displayed on the upper part of the eastern wall. Unit *I* grades upward into a sandstone bed. The clast size variation in unit *H* is shown in Figure 8.

Units J and *K* are seen only on the eastern wall. Both are graded. The base of *J* is marked by injections from the underlying sandstone. A thin mudstone

Fig. 6. Stratigraphic section and lithologic features, Nekézseny railroad cut
1 — thickness (m); 2 — lithologic column; 3 — unit designation [1) thickness estimated, 2) inaccessible]; 4 — direction of textural grading (direction of arrow indicates direction of coarsening, line without arrow indicates ungraded section); 5 — general orientation of clasts (— = parallel to stratification, / = imbricate clasts, *x* = random orientation, parentheses indicate probable orientation); 6 — nature of clast support [*c* = clast supported, *(c)* = probably clast supported, m = matrix supported, *(m)* = probably matrix supported]; 7 — presence of anomalously large clasts (orientation as indicated in column 5)

6. ábra. A nekézsenyi bevágás rétegtani szelvénye és litológiai jellegei
1 — vastagság (m); 2 — rétegoszlop; 3 — az egység megjelölése [1) a vastagság becsült, 2) hozzáférhetetlen]; 4 — a szöveti osztályozottság iránya (a nyíl a durvulás irányába mutat, a nyíl nélküli vonal nem osztályozott szakaszt jelöl); 5 — a törmelékszemcsék általános irányítottsága (— = a rétegzéssel párhuzamos, / = imbrikáció, *x* = véletlenszerű orientáció, a kerek zárójel a valószínű orientációt jelzi); 6 — a törmelékszemcsék viszonyának jellege [*c* = szemcsevázú, *(c)*: valószínűleg szemcsevázú, *m* = matrix alapú, *(m)* = valószínűleg matrix alapú]; 7 — az anomálisan nagy méretű szemcsék megjelenésének helye (az irányítottság jelölése az 5. oszlopéhoz hasonlóan)

Рис. 6. Стратиграфическая колонка и литологические особенности. Откос дороги у с. Некежень
1 — мощность (м); 2 — литологическая колонка; 3 — наименование единицы [1) подсчитанная мощность, 2) недоступный]; 4 — направление градацией по текстуре (направление стрелы показывает направление увеличения размера зерен, линия без стрелы обозначает отрезок без градацией); 5 — общая ориентация обломков, (— = параллельно напластованию, / = обломки, расположенные внахлёстку, *x* = беспорядочная ориентация, скобки показывают вероятность ориентации); 6 — характер соотношения обломков [*c* = скелет сложен обломками, *(c)* = скелет, по-видимому, сложен обломками, *m* = скелет представлена цементом, *(m)* = скелет, по-видимому, представлена цементом]; 7 — присутствуют аномально крупные обломки (ориентацию см. у колонки 5)

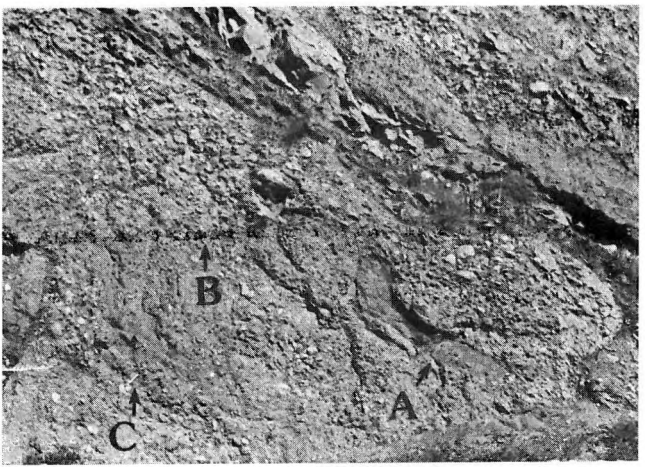

Fig. 7. Anomalously large mudstone clast (*A*) in unit *C*, east wall of the Nekézseny railroad cut (4–14 m, Fig. 3). Note apparent contact (coarse over fine conglomerate; C_2 over C_1) stratigraphically just above the large clast. Contact is not discernible higher on the face in section above subhorizontal fault (*B*). Large rip-up of mudstone at base of unit *C* above the fault. 15 cm scale (*C*) in lower part of unit *D* (below fault)

7. ábra. Anomálisan nagyméretű iszapalapú intraklaszt (*A*) a *C* egységben, a nekézsenyi bevágás K-i falában (4–14 m, 3. ábra). Figyelmet érdemel, hogy a határ (durva a finom konglomerátum fölött; C_2 a C_1 fölött) éppen a nagyméretű intraklaszt fölött (rétegtani értelemben) húzódik. A réteghatár a közel horizontálisan húzódó törési sík (*B*) fölött már nem követhető. Említést érdemel egy nagyméretű felszakadt iszapalapú intraklaszt a *C* egység bázisán a törési sík fölött. A 15 cm-es méretarányjelző rúd (*C*) a *D* egység alsó részén látható (a törési sík alatt)

Рис. 7. Аномально крупный обломок аргиллита (*A*) в единице *C*, восточный откос железной дороги у с. Некежень (4–14 м, Рис. 3). См. кажущийся контакт (грубообломочные конгломераты над тонкозернистыми; C_2 над C_1) стратиграфически чуть-чуть над крупным обломком. Контакт не прослеживается выше по разрезу над субгоризонтальным разломом (*B*). В основании единицы *C*, над плоскостью разлома наблюдается большой разрыв в аргиллитах. Масштабная рейка 15 цм (*C*) в нижней части единицы *D* (под плоскостью разлома)

bed that occurs locally at the top of *J* may be the source for mudstone clasts within overlying unit *K*.

Unit L consists of about 6 m of conglomerate that grades into sandstone at its top. The unit contains a number of large (> 1 m) blocks of sandstone and mudstone and local concentrations of relatively small pebbles that may have been remobilized from pre-existing deposits. Faint grading in the unit suggests that it may be a composite of 3 separate flows, each about 2 m thick. The plot of clast size variation (Fig. 8), however, shows clearly only the grading at the top of the unit.

Neither *unit M* nor *N* is completely accessible, and the thicknesses indicated in Figure 6 are estimated rather than measured. Both units are graded, unit *M* passing into sandstone at its top and unit *N* into a fine pebbly mudstone.

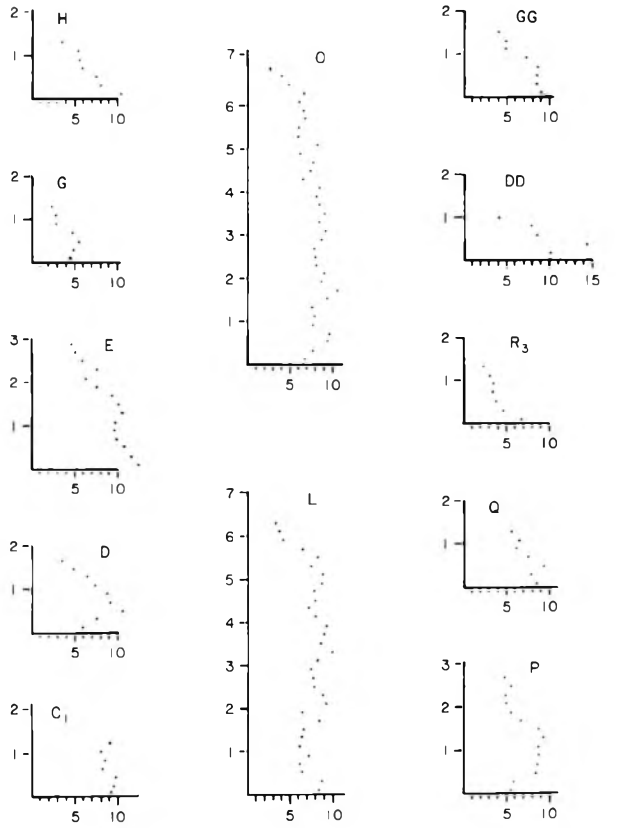

Fig. 8. Vertical variation in average maximum clast size in selected units, Nekézseny railroad cut. Vertical axis is distance (m) above base of unit; horizontal axis is average apparent long axis dimension (cm) of 10/11 clasts as measured in section 20 cm high and 1 m wide.

8. ábra. A maximális szemcseméretek átlagának vertikális változása a nekézsenyi bevágás egyes kiválasztott egységeiben. A függőleges tengelyen az egység bázisától való távolságot (m), a vízszintes tengelyen a hossztengelyek látszólagos átlagos méretét (cm) tüntettük fel 20 cm magas, 1 m széles szakaszon mért 10/11 szemcse alapján

Рис. 8. Изменение по вертикали средних значений максимальных размеров зерен в избранных единицах, откос железной дороги у с. Некежень. Вертикальная ось — это расстояние (м) от основания единицы; горизонтальная ось — это средний, кажущийся размер по продольной оси (см) 10/11 обломков, измеренный в разрезе с высотой 20 цм и шириной 1 м

Unit O resembles unit *L* in its thickness and in the presence of large clasts. On the western wall and the upper part of the eastern wall, this unit appears to consist of two separate graded conglomerates, O_1 and O_2. The upper of these (O_2) grades upward into a sandstone bed. The distinction between the two units is not evident on the plot of clast size variation (Fig. 8).

Units P and *Q* are both prominently graded, although *P* shows inverse

grading at its base (Fig. 8). Unit *Q* grades upwards into sandstone on the lower part of the eastern wall.

Unit R is a complex interval dominated by mudstone. As many as 6 separate subunits may exist within this interval, but because of the general lack of lithologic contrast, lateral variability, and possibility of substantial relief on the depositional surface, they cannot be clearly delineated. A lenticular subunit (R_1) seems to fill local irregularities in the top of unit *Q*. Otherwise the basal subunit (R_2) is an ungraded disorganized pebbly mudstone about 2 m thick that may contain masses or clasts 50 cm across of remobilized conglomerate. Subunit R_3 also is a pebbly mudstone, but one in which the clasts are aligned and texturally graded (Fig. 8). Subunit R_4 is a thin (0.8 m) and obviously graded conglomerate within the pebbly mudstone. Subunits R_5 and R_6, like subunits R_2 and R_3, can be separated only on the western wall, where a layer of coarse clasts defines the base of R_6. Unit *R* is separated from the strata to the north by a fault of unknown direction of movement or displacement. It is possible that the mudstone interval on the south side of the fault correlates in part with mudstone units inaccessibly exposed on the western wall north of the fault, but in the absence of well-defined correlation the units north of the fault are shown as a separate sequence (Figs. 3 and 6).

Units AA, BB, and *CC* are visible above the first step on the west wall but could not be inspected at close range. *AA* and *CC* appear to be disorganized pebbly mudstones whereas unit *BB* is a graded conglomerate. Both units *BB* and *CC* grade upward into prominent sandstone beds.

Units DD and *EE* are graded conglomerates. Unit *DD* grades upward into a sandstone bed; the variation in clast size in this bed is shown in Figure 8.

Unit FF is a complicated unit that seems to represent large-scale remobilization of a subunit (FF_1) by a subsequent flow (subunit FF_2). Isolated masses of graded conglomerate 1–2 m across exist on both walls *(Fig. 9)*. On the eastern face (the only place where the subunits can be delineated) the remobilized subunit (FF_1) grades upward into sandstone and mudstone. At its top, the upper subunit grades into a prominent sandstone bed.

Unit GG is the northernmost unit that can be clearly defined. The conglomerate scours into the underlying sandstone on the western wall, and large injections of sandstone into the base of this conglomerate are visible on the eastern wall. The variation in clast size in this unit is shown in Figure 8.

The conglomerate beds in the Nekézseny railroad cut show a fairly consistent pattern of grading (Fig. 6). Many of the beds are inversely graded at their base. Visually, this inverse grading is particularly evident in the basal 5–10 cm of the conglomerate, although the clast measurements (Fig. 8) show that it commonly extends through the lowermost 40 cm. Normal grading characterizes the upper part of nearly every bed. The thinner (< 2 m) beds typically seem to be either normally or inverse-to-normally graded, whereas thicker beds generally have an ungraded portion between their inversely graded base and normally graded top.

Most of the conglomerate is clast-supported (Fig. 6). Clasts are dispersed

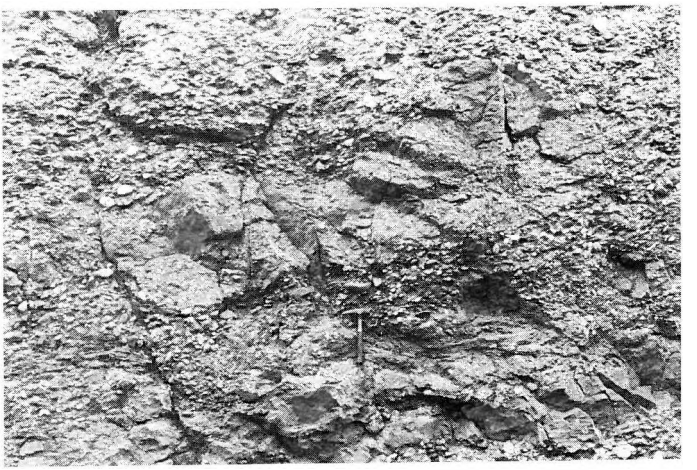

Fig. 9. Large mass of remobilized conglomerate above hammer, unit *FF*, west wall of Nekézseny railroad cut (95–100 m, Fig. 3)

9. ábra. Nagyméretű átmozgatott konglomerátum blokk a kalapács felett. *FF* egység, a nekézsenyi bevágás Ny-i fala (95–100 m, 3. ábra)

Рис. 9. Крупная переотложенная глыба конгломерата над молотком, единица *FF*, западный откос железной дороги у с. Некежень (95–100 м, Рис. 3)

within the matrix only in the pebbly mudstone interval (unit *R*) or near the tops of the conglomerate beds. Most of the beds show a vague- to well-defined clast alignment parallel to bedding (Fig. 6), and imbrication is suggested in a number of beds. Anomalously large mudstone or sandstone clasts are common in the conglomerate. The smaller of these (tens of cm across) are restricted to the ungraded portions of the beds. These anomalous clasts seem typically to be imbricated or aligned parallel to bedding.

Because of the structural complexity at this outcrop, directional features are of questionable significance. In general, the pattern of imbrication suggests a northerly component of transport when the beds are rotated around the strike to their presumed original horizontal position. The orientation, however, of 100 pebbles at four different localities in these exposures suggests paleotransport to the southeast *(Fig. 10)*.

Figure 11 summarizes the relative abundance, roundness and relative size of the five main clast types. The dominant clast type is carbonate rock. The composition of the carbonate clasts differs, but none show evidence of metamorphism. Many of the carbonate clasts contain microfossils; the ages of such clasts range from Lower Triassic to Upper Jurassic. Quartzite (including metamorphosed quartzitic sandstone and siliceous shales) and sandstone clasts are also abundant. Most of the sandstone clasts show evidence of low-grade metamorphism. Radiolarian chert and calcareous phyllite clasts of the green schist facies are important minor constituents of the conglomerate.

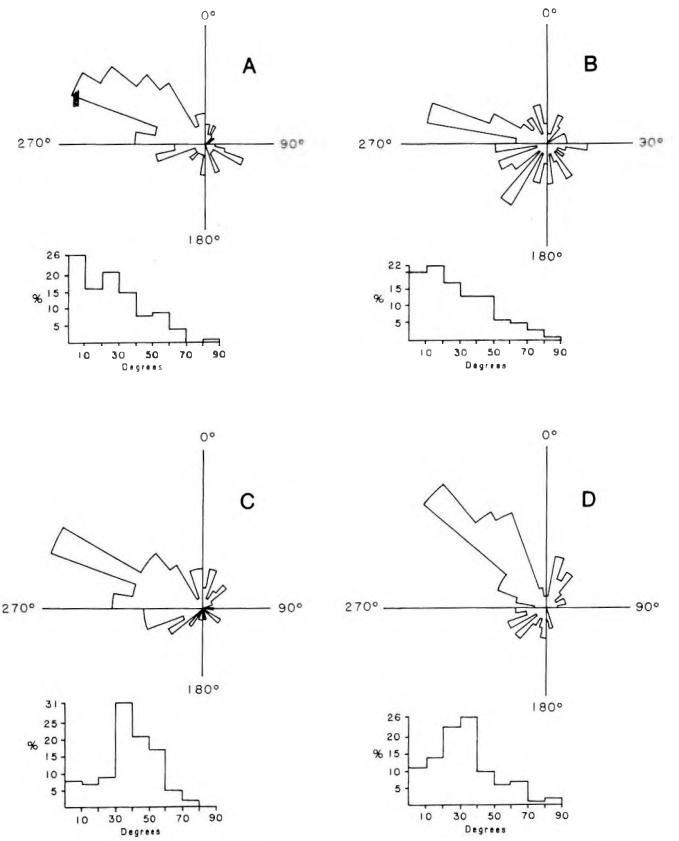

Fig. 10. Orientation (inclination direction) of long axes of 100 pebbles relative to the plane bedding from 4 different 1 m^2 plots, Nekézseny railroad cut. Diagrams *A*, *B*, *C* and *D* represent different localities

10. ábra. A kavics hossztengelyek irányítottsága a rétegződési síkhoz viszonyítva (inklináció) 100 szemcsén, 4 különböző, egyenként 1 m^2 felületen végzett mérések alapján. Nekézsenyi vasúti bevágás

Рис. 10. Ориентация (направление наклона) продольных осей 100 обломков относительно плоскости напластования по четырем участкам с площадью в 1 $м^2$, железнодорожный откос у с. Некежень. Диаграммы *A*, *B*, *C* и *D* показывают разные места

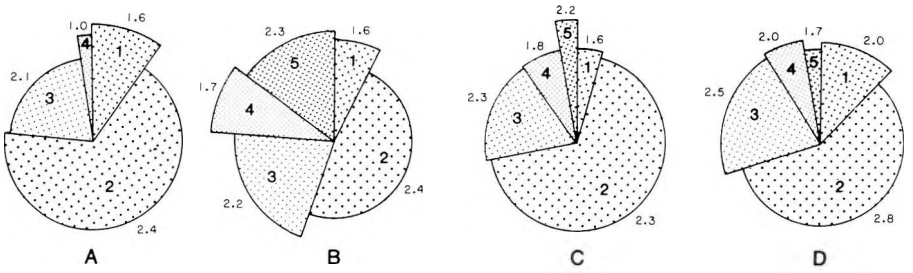

Fig. 11. Relative abundance of 5 main clast types at the 4 localities of Fig. 10 (pie diagram: 1 — quartzite; 2 — carbonate rock; 3 — sandstone; 4 — chert; 5 — calcareous phyllite). Length of pie segment indicates clast size (1/2 average long axis length) of each lithologic group. Numbers at margin of diagram indicate roundness on scale of 0 (angular) to 4 (well-rounded)

11. ábra. Az 5 fő szemcsetípus relatív gyakorisága a 10. ábrán feltüntetett 4 mérési helyen (kördiagram: 1 — kvarcit; 2 — karbonátos kőzet; 3 — homokkő; 4 — tűzkő; 5 — mészfillit). Az egyes kőzettípusokat jelző szegmensek hossza a szemcseméretet jelzi (a hossztengely méretének 1/2-e). A diagram szélénél feltüntetett számok a kerekítettséget jelzik a 0 (szögletes), 4 (jól kerekített) skálán

Рис. 11. Относительная частота встречаемости 5 главных типов обломков по 4 участкам, показанным на Рис. 10 (пай-диаграмма: 1 — кварциты, 2 — карбонатная порода, 3 — песчаники, 4 — кремний, 5 — известковистые филлиты). Длина сегмента диаграммы обозначает размер обломков (половина средней длины продольной оси) для каждой литологической группы. Цифры на краю диаграммы обозначают окатанность по шкале от 0 (угловатые обломки) до 4 (хорошо окатанные)

4. Results – The Csokvaomány Exposure

The second exposure is a cut on the north side of the road between Nekézseny and Csokvaomány, about 100 m east of the intersection with the road to Lénárddaróc. The exposure is about 50 m long and up to 8 m high. The beds strike north–south and dip 35° to the west; grading in sandstone interbeds indicates that they are right-side-up. A normal fault near the center of the cut repeats the section *(Fig. 12)*. Otherwise the beds are little disrupted structurally.

A total of about 16 m of section was measured at this exposure *(Fig. 13)*. A few beds at either end of the cut were excluded from the section due to poor exposure (east end) or inaccessibility (west end).

The lowermost well-exposed unit *(A)* is a conglomerate that sharply overlies a pebbly mudstone. The conglomerate grades upward into a sandstone bed that locally is cut out by the overlying conglomerate *(B)*. A layer of fine pebbles about 80 cm above the base suggests that unit *B* may be a composite unit, although this is not reflected in the size variation of the larger clasts *(Fig. 14)*. *Unit B* grades into a sandstone bed at its top that is overlain by another thinner conglomerate unit *(C)*.

Unit D almost certainly represents a composite of several flows. About 1.3 m above the base of the unit, a discontinuous layer of fine pebbles indicates the boundary between subunits D_1 and D_2. This layer lies beneath a large

(10 × 60 cm) mudstone clast. About 2.3 m above the base another layer of fine (1–5 cm) pebbles underlies an interval about 0.5 m thick that contains numerous mudstone clasts. This subunit (D_3) grades at its top into a fine, granular conglomerate, which locally shows excellent imbrication. The top subunit (D_4) is a coarse-graded sandy conglomerate. The contact between D_3 and D_4 has a relief of several tens of centimeters. The granular conglomerate at the top may be in part a remobilized mass; it laterally terminates abruptly against a coarser conglomerate that seems to link subunits D_4 and D_3 *(Fig. 15)*.

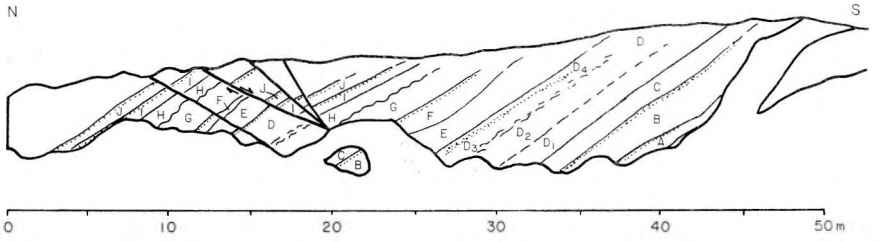

Fig. 12. Conglomeratic units as exposed in the road cut east of Csokvaomány

12. ábra. A csokvaományi útbevágásban feltárt konglomerátum rétegsor

Рис. 12. Разрез конгломератов, вскрытый в откосе дороги к востоку от с. Чокваомань

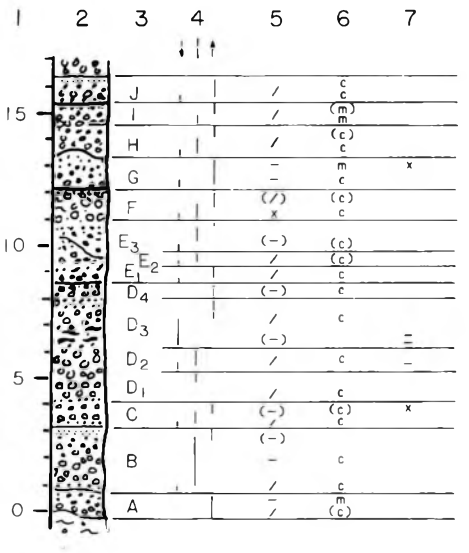

Fig. 13. Stratigraphic section and lithologic features, Csokvaomány road cut. Legend as indicated for Figure 6

13. ábra. Rétegoszlop és litológiai jellegek, csokvaományi útbevágás. A jelkulcs a 6. ábráéval azonos

Рис. 13. Стратиграфическая колонка и литологические особенности в откосе дороги у с. Чокваомань. Легенду см. у Рис. 6

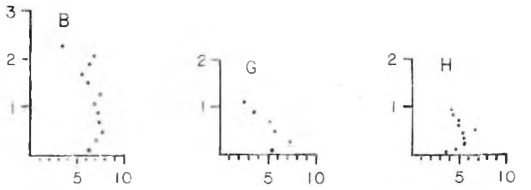

Fig. 14. Vertical variation in average maximum clast size in selected units, Csokvaomány road cut. Axes as indicated for Figure 8.

14. ábra. A maximális szemcseméretek átlagának vertikális változása a csokvaományi bevágásban. Az ábrázolásmód a 8. ábráéval azonos

Рис. 14. Изменение по вертикали средних значений максимальных размеров зерен в избранных единицах в откосе дороги у с. Чокваомань. Оси соответствуют осям, изображенным на Рис. 8

Fig. 15. Abrupt lateral termination of granular conglomerate just left of cm scale, top of unit D_3, Csokvaomány road cut at about 27 m (Fig. 12). Bedding is nearly flat in this view

15. ábra. Konglomerátum lencse hirtelen laterális elvégződése a cm skálától balra. D_3 egység teteje, csokvaományi útbevágás 27. méterénél (12. ábra).
A rétegződés majdnem vízszintes ebből a nézőpontból

Рис. 15. Внезапное окончание в боковом направлении линзы конгломератов налево от сантиметровой шкалы в верхах единицы D_3 в откосе дороги у с. Чокваомань, около отметки 27 м (Рис. 12). Слоистость в данном случае является почти горизонтальной

Unit E also appears to be a composite of small flow units. The bottom 80 cm consists of conglomerate that grades into fine (0.5–2 cm) pebbles at its top. It is overlain by a coarser conglomerate (E_2, 10–50 cm thick) that in turn is overlain in irregular contact by a lenticular bedded conglomerate (E_3). Subunit E_3 has the appearance of a channel fill, but it also may be a remobilized gravel. The near-vertical orientation of clasts adjacent to the contact in the underlying subunit *(Fig. 16)* suggests deformation rather than a simple scour-fill.

The overlying *Unit F* is highly variable. On the eastern side of the fault, this unit consists of about a meter of very coarse conglomerate containing subspherical clasts up to 20 cm in diameter. This conglomerate grades upward into about 30 cm of muddy, somewhat indurated, pebbly sandstone. On the western side of the fault, the lower part of this interval is occupied by a lenticular pebbly mudstone that grades upwards into a similar muddy pebbly sandstone.

Unit G is a graded conglomerate with a muddy matrix *(Fig. 17)*. In the upper part, the clasts are dispersed in the matrix. The contact with the overlying

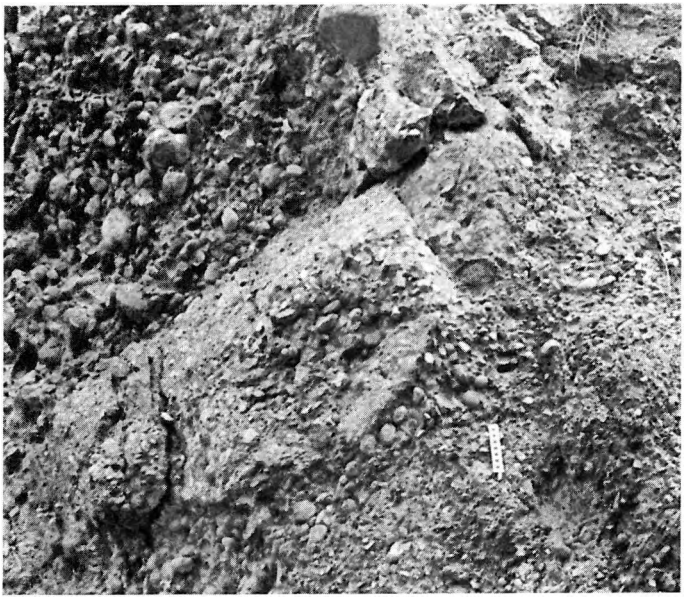

Fig. 16. Possible channel near top of unit *E*, Csokvaomány road cut at about 25 m (Fig. 12). Note near-vertical orientation of pebbles below base of "channel" (above cm scale)

16. ábra. Valószínű csatorna az *E* egység tetejének közelében. Csokvaományi útbevágás, kb. 25 m-nél (12. ábra). Figyelmet érdemel a „csatorna" bázisa alatti kavicsok közel vertikális irányítottsága (a cm-skála felett)

Рис. 16. Вероятное русло палеотранспорта вблизи верхов единицы *E* в откосе дороги у с. Чокваомань, около отметки 25 м (Рис. 12). См. субвертикальную ориентацию обломков ниже основания »русла« (над сантиметровой шкалой)

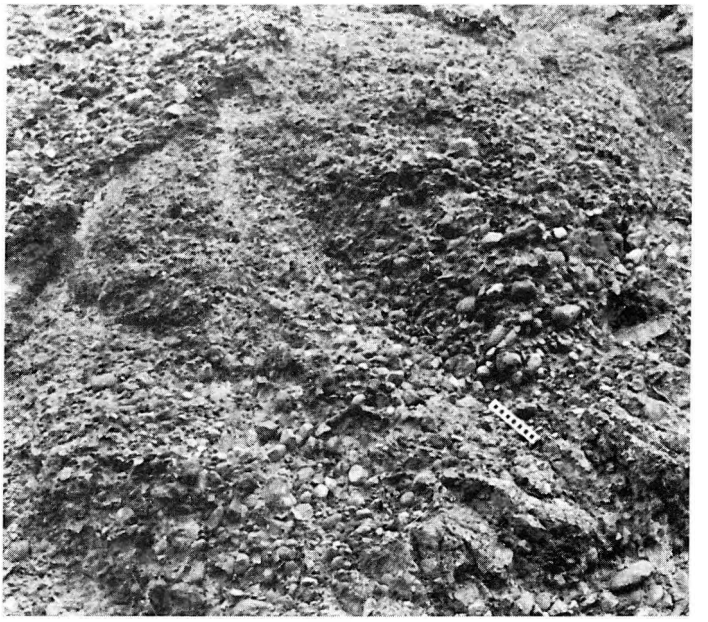

Fig. 17. Graded conglomerate, unit *G*, Csokvaomány road cut at about 10 m (Fig. 12). Centimeter scale

17. ábra. Osztályozott rétegződést mutató konglomerátum, *G* egység, csokvaományi útbevágás, kb. a 10 m-nél (12. ábra)

Рис. 17. Конгломераты с отсортированными обломками в единице *G* в откосе дороги у с. Чокваомань, около отметки 10 м (Рис. 12). Сантиметровая шкала

Unit H is irregular. The size variation of clasts in these two units is shown in Figure 14. *Units I* and *J* cap the section. Both are graded conglomerates that grade upward into sandstone.

The character of the conglomerate in the Csokvaomány cut generally resembles that in the railroad cut at Nekézseny. The flow units in the road cut seem to be somewhat thinner and imbrication more common, but the significance of this difference is uncertain.

The long-axis orientation of the clasts was measured in units *B*, *G*, and *H* (20 distinctly elongate pebbles from the top, middle and bottom of each unit) and in unit *D* (100 clasts). A summary of these measurements (*Figs. 18* and *19*) shows a consistent, well-defined long axis alignment in a northeast–southwest direction. No significant variation in clast orientation was noted in the measurements taken from different parts of the same bed. Imbricated pebbles at this exposure consistently indicate transport toward the northeast.

The clast composition at this exposure (Fig. 19) generally resembles that at the Nekézseny cut (Fig. 11). The data suggest that the clasts in the Csokvaomány exposure are slightly more rounded than those at Nekézseny; the significance of this difference is uncertain.

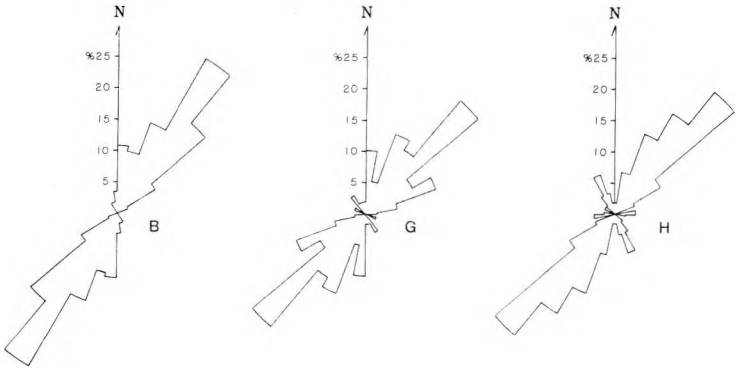

Fig. 18. Orientation of apparent pebble long axes in units *B*, *G* and *H*, Csokvaomány road cut. Pebbles were included only if the apparent long axis exceeded by twice the length of the apparent intermediate axis. Each rose diagram includes 20 pebbles at the basal part of the unit, 20 from the middle, and 20 from the top part

18. ábra. Látszólagos kavics hossztengely-irányítottság a *B*, *G*, *H* egységben, csokvaományi útbevágás. Csak azokat a szemcséket vettük figyelembe, melyeknél a látszólagos hossztengely hossza meghaladta a látszólagos kereszttengely méretének kétszeresét. Minden rózsadiagram 20 kavicsot ábrázol az egység bázisáról, 20-at a közepéről és 20-at a tetejéről

Рис. 18. Кажущаяся ориентация продольных осей галек в единицах *B*, *G* и *H* в откосе дороги у с. Чокваомань. Гальки учтены только в случае, если кажущаяся продольная ось вдвое превышала длину кажущейся поперечной оси. В каждой диаграмме-позетке содержится по 20 галек из базальной части единицы, 20 — из середины и 20 — из верхов

5. Processes of emplacement

The processes whereby these conglomerates were transported and deposited can be partly inferred from their texture and fabric. LOWE [1982] summarizes the mechanisms capable of moving coarse sediment by sediment gravity flow into deep water and suggests the character of the resulting deposits. Relevant mechanisms include cohesive flows in which the larger clasts are supported by the strength or cohesiveness of a sediment–water matrix, grain flows in which the clasts are dispersed by their intergranular collisions, and high density turbidity currents in which the clasts are borne by the combined turbulence of the flow and the relatively high density of the sediment–water fluid.

Each of these mechanisms should be considered an "end-member" that produces a distinctive kind of deposit [MIDDLETON–HAMPTON 1976]. The products of cohesive flows are generally considered to be ungraded and without a preferred clast orientation. Those of grain flows are thought to be inversely graded with a flow-parallel clast orientation and an imbrication that dips "up-stream." Deposits from turbidity currents are normally graded with a clast orientation like that produced by grain flow [see WALKER 1975].

The Late Cretaceous deposits described here show evidence of all three transport mechanisms. The ungraded portions of the sedimentary units (par-

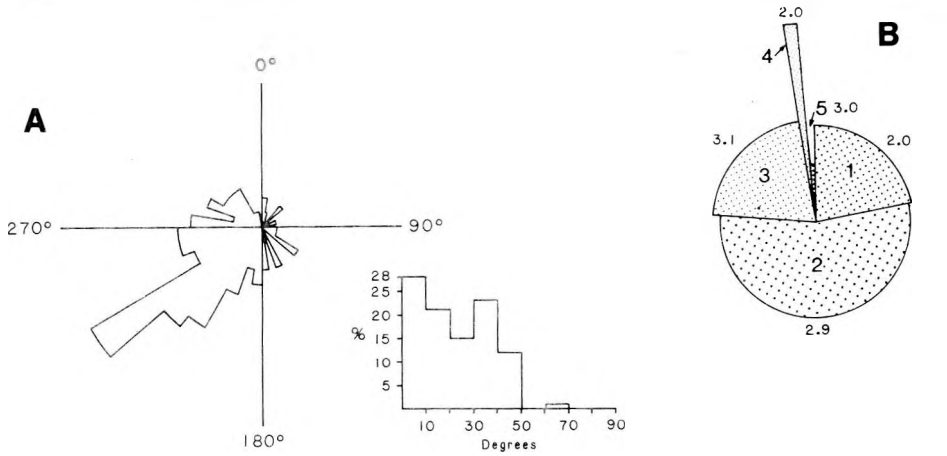

Fig. 19. A) Orientation (inclination direction) of 100 pebbles relative to plane of bedding in 1 m² plot, unit *D*, Csokvaomány road cut
B) Relative abundance of 5 major clast types, their roundness and relative size. Explanation of figure is the same as for Figure 11

19. ábra. A) A kavicsok irányítottsága a rétegzési síkhoz viszonyítva 100 kavics 1 m²-es felületén való mérése alapján, *D* egység, csokvaományi útbevágás.
B) Az 5 fő kavicstípus relatív gyakorisága, kerekítettségük és relatív méretük. Az ábramagyarázat azonos a 11. ábráéval

Рис. 19. А) Ориентация (направление наклона) 100 галек по отношению к плоскости напластования по участку с площадью 1 м² в единице *D* в откосе дороги у с. Чокваомань
В) Относительная частота встречаемости 5 главных типов обломков, их окатанность и относительные размеры. Легенда та же самая, что и для Рис. 11

ticularly where they are thick and contain anomalously large clasts, as with units *L* and *O* in the Nekézseny exposure) are attributable to cohesive flow. The clast-supported character of these conglomerates suggests that the associated sediment–water fluid may have functioned more as a lubricant than as an actual supporting mechanism for the clasts [LOWE 1982]. The inverse grading at the base of many of the units probably results from grain flow that developed at the base of the flows, perhaps in the initial phase of deposition. The normally graded parts of the conglomerate probably result from deposition from high-density turbidity currents. The common occurrence of normal grading in the upper parts of the conglomerate units suggests that these either developed at the top of the overall flow or were generated in the final phase of deposition.

It is probable that many of the units represent processes intermediate between the "end-members" of cohesive flow and turbidity currents. The sub-horizontal orientation of the clasts in many of the ungraded parts of the conglomerate is more well-defined than is typical for cohesive debris flows. Some of the matrix-supported conglomerates, which might be interpreted as the result of cohesive flow, are well-graded (e.g. unit R_3 at Nekézseny). As intermediate types of deposits they may bear on the interpretation of the evolution of coarse sediment gravity flows [see LOWE 1982].

6. Paleogeographic implications

The composition of the pebbles and the presumed paleotransport directions bear on the interpretation of Late Cretaceous paleogeography in northern Hungary and subsequent tectonism in this area. The clasts appear to be predominantly derived from sources that presently are exposed to the north and northeast of the present exposures of the conglomerate [BREZSNYÁNSZKY–HAAS 1984]. The limestone pebbles consist to a large degree of Triassic rock types that presently exist in the Aggtelek and Rudabánya Mountains. The Jurassic shallow-water limestone that occurs as pebbles is known to exist only in the Slovakian part of the Aggtelek Mountains further north. The quartzite, siliceous schist, sandstone and calcareous phyllite clasts resemble lithologies that exist in the Uppony Mountains. The Mesozoic rock types of the Bükk Mountains are notably absent in the conglomerate.

The paleotransport direction to the northeast at the Csokvaomány exposure and to the southeast at the structurally complicated Nekézseny cut suggest that the source areas at the time of deposition lay to the west, perhaps even to the southwest. It is possible that the transport directions at these two exposures do not reflect regional paleoslope, but they are quite consistent within each exposure. If regionally significant, the transport directions imply either that the Aggtelek–Rudabánya litho-tectonic unit extends well to the southwest in the subsurface or that it has been displaced to the northeast by post-Senonian movement along the Darnó Zone of Neogene faulting (Fig. 2).

The conglomerate lies depositionally on rocks of the Uppony litho-tectonic unit and the composition of the pebbles indicates a contribution of clasts from this unit. The absence of metamorphosed rock types of the Bükk Mountains tectonic unit among the clasts in the conglomerate suggests that either the structural convergence of the Bükk and Uppony units occurred in post-Senonian time, or the Bükk Mountains unit was not exposed during deposition of the conglomerate.

7. Conclusions

a) The Late Cretaceous conglomerate in northern Hungary consists primarily of gravel that was emplaced by sediment gravity flows.

b) At its best exposure, the railroad cut at Nekézseny, the conglomerate is tectonically overturned. Many small normal faults occur. A large fault of unknown displacement presently precludes development of a continuous stratigraphic section at this exposure.

c) Many of the flow units in the conglomerate show a consistent pattern of vertical sequence. A thin layer of inversely-graded pebbles at the base passes upward into a central ungraded portion that in turn passes upward into normally graded gravel and sand at the top.

d) Most of the conglomerate is clast-supported and the pebbles lie predomi-

nantly with long axes parallel to bedding or inclined (imbricated) in an upflow direction. A few pebbly mudstones composed of matrix-supported conglomerate occur.

e) Some of the flows that emplaced the gravel had sufficient competence to bear giant clasts (up to 2 m across) of mudstone and sandstone and to remobilize similarly sized masses of previously deposited gravel. Many flows appear to have been intermediate between the end-members of the cohesive flow and high-density turbidity current.

f) Possible source for the clasts in the conglomerate are presently exposed in the Aggtelek and Rudabánya Mountains to the northeast and in the Uppony Mountains immediately to the north. Paleotransport indicators in the conglomerate suggest paleotransport from the west.

g) The absence of clasts from the Bükk Mountains tectonic unit in the conglomerate, which lies depositionally on rocks of the Uppony tectonic unit, suggests that either the rocks of the Bükk unit were not exposed or these two units converged structurally to their present position in post-Senonian time.

REFERENCES

BALOGH K. 1964: Die geologischen Bildungen des Bükk-Gebirges. Annales Inst. Geol. Publ. Hung. **48,** 2, pp. 555–705

BÖCKH J. 1867: Die geologischen Verhältnisse des Bükk-Gebirges und der angrenzenden Vorberge. Jahrbuch der K.K.Geol. Reichsanstalt, **17.** pp. 225–242

BREZSNYÁNSZKY K., HAAS J. 1984: The Nekézseny Conglomerate Formation of Senonian age: a sedimentological and tectonic study of the stratotype section (in Hungarian with English abstract). Földtani Közlöny (Bull. of the Hung. Geol. Soc.), **114,** 1, pp. 81–100

LOWE D. R. 1982: Sediment gravity flows: II. Depositional models with special reference to the deposits of high-density turbidity currents. Sed. Petrology, **52,** 1, pp. 279–298

MIDDLETON G. V., HAMPTON M. A. 1976: Subaqueous sediment transport and deposition by sediment gravity flows. In Stanley, D. J. and Swift, D. J. P. eds., Marine Sediment Transport and Environmental Management, John Wiley and Sons, New York, pp. 197–218

PANTÓ G. 1954: Le levé des gîtes métalliques dans la montagne de Uppony (in Hungarian with French abstract). MÁFI Évi Jelentése az 1952. évről (Annual Report of the Hung. Geol. Inst.), pp. 91–110

SCHRÉTER Z. 1945: Geologische Aufnahmen im Gebiete von Uppony, Dédes und Nekézseny, Ferner im Gebiete von Putnok. MÁFI Évi Jelentése az 1941–1942. évekről (Annual Report of the Hung. Geol. Inst.), pp. 197–237

SIEGL-FARKAS Á. 1984: Palynostratigraphy of the Upper Cretaceous in the Uppony Mts (in Hungarian with English abstract). MÁFI Évi Jelentése az 1982. évről (Annual Report of the Hung. Geol. Inst.), pp. 101–117

WALKER R. G. 1975: Generalized facies models for resedimented conglomerates of turbidite association. Geol. Soc. America Bull. **86,** 6, pp. 737–784

AZ ÉSZAK-MAGYARORSZÁGI ÁTÜLEPÍTETT FELSŐKRÉTA KONGLOMERÁTUM KŐZETTANI JELLEGEI ÉS ŐSFÖLDRAJZI JELENTŐSÉGE

H. Edward CLIFTON, BREZSNYÁNSZKY Károly és HAAS János

A szerzők részletes szedimentológiai vizsgálatokat végeztek a felsőkréta Nekézsenyi Konglomerátum Formáció nekézsenyi és csokvaományi alapszelvényén. A vizsgálat alapján levont főbb következtetések a következők:

a) A konglomerátumok elsősorban gravitációs üledékfolyással átülepített törmelékszemcsékből állnak.

b) A nekézsenyi vasúti bevágás alapszelvényében a szedimentológiai jellegek a rétegsor átbuktatottságát támasztják alá (6. ábra). A csokvaományi szelvény viszont nincs átbuktatott helyzetben (13. ábra).

c) A konglomerátum üledékfolyási egységein belül jellemző vertikális tagoltságot lehetett megfigyelni. Az egységek bázisán vékony, fordított osztályozott rétegződést (gradációt)mutató réteg észlelhető, amely az egység középső részén rétegződésmentes szakaszba megy át, végül az egység felső részében normális osztályozott rétegződés jelentkezik finomkavicsba, majd homokba átmenő szemcsemérettel.

d) A konglomerátum leggyakrabban szemcsevázú és a kavicsok hossztengelye többnyire a rétegdőléssel párhuzamos, vagy azzal szöget zár be, vagyis imbrikációt mutat.

e) Az üledékfolyások némelyike 2 métert elérő nagyságú kőzetblokkok szállítására is alkalmas volt. A nagy blokkok egy része intraformációsnak tekinthető, amennyiben a korábban lerakódott kavicsrétegek anyagából áll. Az üledékfolyási egységek sokszor átmenetet képeznek a kohéziós folyás és a nagy sűrűségű zagyár áramlás által létrehozott üledéktípusok között.

f) A konglomerátum kavicsainak feltételezhető lehordási területe olyan kőzetekből állt, amelyek jelenleg az Aggtelek–Rudabányai-hegységben és az Upponyi-hegységben ismertek. A konglomerátumban mért szállítási irányok Ny-ról történő szállítást jeleznek.

g) A bükki metamorf mezozoos kőzetek hiánya az Upponyi aljzatra települő konglomerátumban arra utal, hogy a Bükki egység kőzetei vagy nem voltak a felszínen a szenonban, vagy a Bükki és az Upponyi egység egymáshoz viszonyított helyzete a szenon után lényegesen megváltozott.

ЛИТОЛОГИЧЕСКИЕ ХАРАКТЕРИСТИКИ И ПАЛЕОГЕОГРАФИЧЕСКОЕ ЗНАЧЕНИЕ ПЕРЕОТЛОЖЕННЫХ ВЕРХНЕМЕЛОВЫХ КОНГЛОМЕРАТОВ В СЕВЕРНОЙ ВЕНГРИИ

Г. Эдвард КЛИФТОН, Кароль БРЕЖНЯНСКИ и Янош ХААС

Верхнемеловые (сенонские) конгломераты обнажаются в Северной Венгрии на границе между литотектоническими единицами гор Бюкк и Уппонь. Они налегают на породы Уппоньской единицы. В некоторых местах конгломераты хорошо обнажены в откосах дорог и других искусственных обнажениях. В основе настоящей работы легло изучение откоса железной дороги в юговосточной части села Некежень и откоса дороги к северу от села Чокваомань. Ряд данных (в особенности фактический материал песчаников отсортированной слоистости) свидетельствуст о том, что разрез Некежень представляет собой опрокинутую структуру. Конгломераты принадлежат к различным единицам по режиму течения и переноса осадков, причем местами это все проявляется совсем мутно. Многие из мощных единиц обнаруживают тестурные черты, свидетельствующие об обратной отсортированности осадков в основании единицы, их неотсортированности в центральной части единицы и нормальной отсортированности в её верхах. Большинству рассматриваемых единиц присуща такая упорядоченность кластического материала, при которой гальки выстроены линиями, так, что краткие оси галек направлены перпендикулярно плоскости напластования. Судя по наиболее надежной ориентации продольных осей и по данным расположения обломков внахлёстку (из структурно менее нарушенного разреза Чокваомань) палеотранспорт был направлен на северо-восток. Текстурный характер конгломератов и их структурные особен-

ности свидетельствуют о том, что большинство конгломератов было переотложено потоками, промежуточными по характеру между когезивными обломочными потоками и весьма густыми мутьевыми потоками. Присутствие обломков в литотектонической единице гор Бюкк указывает на то, что сближение (конвергенция) структур Бюккской и Уппоньской единиц имело место после отложения конгломератов (или что Бюккская единица не была обнаженной во время отложения осадков). Большое количество обломков происходило из лито-тектонической единицы Аггтелек-Рудабаня, которая в настоящее время широко обнажена к северо-востоку от площади развития верхнемеловых конгломератов. Направление палеотранспорта указывает на то, что на глубине любая исходная порода в данной единице распространяется далеко на юг и источник пирания обломочного материала был тектонически перенесен на север вдоль тектонической линии Дарно.

GEOPHYSICAL TRANSACTIONS 1985
Vol. 31. No. 1–3. pp. 157–167

ECONOMIC HEAVY MINERALS OF THE DANUBE RIVER FLOODPLAIN SEDIMENTS AND FLUVIOLACUSTRINE DEPOSITS OF NORTHWESTERN AND CENTRAL HUNGARY

Andrew E. GROSZ*, Ferenc SIKHEGYI** and Ubul P. FÜGEDI**

A cooperative pilot project designed to assess the feasibility for heavy-mineral-resource identification in fluvial terrace deposits of the Danube River and in fluviolacustrine deposits of Neogene and Quaternary ages in northwestern and central Hungary resulted in the discovery of gold in southern Danube River sediments and indicated that garnet also occurs in significant quantities. In addition, smaller concentrations of titanium minerals and zircon, have been found, but whether these minerals have significant vertical and lateral distributions, is yet to be investigated.

Mineralogic analyses of panned heavy-mineral concentrates obtained from 26 fluvial sediment samples of Holocene age from northwestern Hungary (Kisalföld) gave an average heavy-mineral content of 0.7% of which about half consists of garnet, titanium minerals, and zircon. Gold was found in six of the eight samples taken; one additional sample contained native silver. Fluvial sediments on and south of Szentendre Island contain concentrations of heavy-minerals comparable to those found in the northwestern samples; however, gold is significantly more abundant and occurs in coarser grains than that in the northwestern samples.

Mineralogic analyses of the heavy-mineral assemblages of fluviolacustrine sediments of Neogene to Quaternary age, as well as of eolian sediments of northwestern and central Hungary showed that on the average the heavy-mineral fraction is less than 0.5% in these sediments of which only about 35% is garnet, titanium minerals, and zircon combined. Two of 11 samples analyzed contain gold.

A test of the spectral gamma-ray radiation signatures of various deposit types suggests measurable differences between sediments enriched in heavy-minerals relative to those that contain trace quantities; however, additional data for the quantification of the differences are needed.

Keywords: heavy-minerals, placers, gold, garnet, zircon, titanium minerals, gamma-ray spectrometry

1. Introduction

Areally and volumetrically extensive deposits of sand and gravel, particularly those associated with the Danube River, in the Pannonian Basin of Hungary are potential sources of economically valuable detrital heavy-minerals such as garnet (used as an abrasive), aluminosilicate minerals (refractory applications), zircon (ore of zirconium and hafnium, abrasive and refractory), rutile (ore of titanium), gold, and others.

This preliminary report is based on a limited amount of data that was assembled under auspices of a pilot project conducted jointly by the U.S. Geological Survey and the Hungarian Geological Survey in August 1983. The

* U.S. Geological Survey, National Center, Reston, VA 22092
** Hungarian Geological Survey, POB 106, Budapest, H–1442
Manuscript received: 16 April, 1985

aim of the project was to assess the feasibility of identifying heavy-mineral (henceforth HM) resources of economic value in fluvial terrace deposits of the Danube River and in fluviolacustrine deposits of Neogene and Quaternary ages.

2. Previous work

Historical accounts relate that gold-bearing placers in the region have been mined as early as the time of the Late Roman Empire, that is, at the end of the 4th century A.D. Economically valuable accumulations of detrital gold at several localities in the western portion of the Carpathian Basin have been known since the beginning of this millenium. Gold bullion with the marks of Roman mints found in the region document this; trace element and silver content of the bullion indicate placer origins from the western Carpathian Basin [PANTÓ 1935].

The "golden age" of placer mining in the region is considered to have occurred in the last century. The most famous placer gold mining localities in northwestern Hungary are Ásvány, Halászi, Aranyosszíget, and Ács along the Danube River, however a number of localities occur on the Mura, Dráva, Maros, and Aranyos Rivers, where gold, thought to have originated in the Alps and the Carpathians, has been mined. The end of the "golden age" came with the onset of flood control engineering projects that interrupted the deposition of surficial pay gravels. Nonetheless, small quantities of detrital gold continued to be recovered by one-man operations in recent times.

The first systematic investigation of the economic potential of the auriferous sediments in the northwestern portion of Hungary was conducted between 1932 and 1935 [PANTÓ 1935]. The objectives of the investigation were to appraise the economic worth of previously known occurrences and to establish the vertical and horizontal extents of gold-bearing gravels. Sampling procedures included shallow-depth augering by hand, and surface grab-sampling. Screening, sluicing, and hand-panning were used to concentrate the gold particles which are traditional techniques used in northwestern Hungary. PANTÓ [1935] states these methods, employed also in his studies, recovered 97 to 98% of the gold present in a sample. He further states that the recovered gold flakes were extremely fine-grained and thin (averaging 100,000 flakes/gram); the largest flake recovered weighed slightly less than 0.4 milligrams. The purity of the gold was measured to be about 950. In light of the results of our reconnaissance study, and recovery rates from similarly fine-grained deposits elsewhere in the world [MACDONALD 1983], we feel that a claim of 97 to 98% recovery is unreasonably high, perhaps by as much as 35%. In this context it must be noted that in his study Pantó examined only gravels. Not surprisingly, therefore, Pantó concluded that gold accumulations in fluvial sediments of northwestern Hungary had no practical importance for industrial exploitation. It should also be noted here that, with the exception of pyrite which was analyzed for gold and silver, and a few suspect grains associated

with the platinum-group, the heavy-mineral assemblage was not evaluated for byproduct, or coproduct potential.

More recently, a reconnaissance study of the heavy-mineral content of sediments of the Danube–Rába Lowland (Kisalföld) was conducted by the Mecsek Ore Mining Enterprise (MÉV) in 1960. In that study 29 shallow auger borings collected at 0.5 to 3.0 km intervals yielded 133 discrete samples. Analyses of the samples yielded an average of 0.5 to 1.0 kg/m^3 heavy-minerals, however in the vicinity of Ács values as high as 12.5 kg/m^3 were found, but very little mineralogic work was done on minerals other than gold and magnetite. The report by MÉV [CSALAGOVITS 1962] stressed, however, that the data were not sufficiently reliable, because of concentrating techniques used. The report mentions that garnet was present in the heavy-mineral assemblage.

A number of other reports of investigations related to geologic or stratigraphic problems in Hungary include general information on heavy-minerals in sediments, but the authors did not encounter any that referred specifically to the the economic potential of the heavy-minerals either from the qualitative or from the quantitative standpoint.

3. Field methods used in this investigation

Recent alluvial fills and terraces as well as fluviolacustrine deposits of Pliocene(?) age were sampled along the length of the Danube River in Hungary, to determine the heavy-mineral (HM) assemblages, by means of laboratory petrologic analyses and by measuring their spectral emmisivity with a 4-channel gamma-ray spectrometer.

Sediment samples were collected by a variety of techniques, selected mostly to suit the types of exposures available for sampling. The principal type was the channel sample collected along river bluffs, and along walls of sand and gravel borrow pits. Other types of techniques used were trenching, power augering and grab sampling. At most locations samples weighing 1 to 8 kilograms in bulk were collected per meter of exposure, although at a few localities (specifically in very coarse grained deposits) as much as 15 kilograms of sediments were collected per meter of exposure. Large samples were needed because many of the deposits contained large fractions of coarse sand and gravel; lesser quantities would have yielded quantities of HM concentrates too small for deriving acceptable statistical values on such high-value, low-concentration minerals as rutile, zircon, and gold. Locations where samples were collected are shown on *Figures 1* and *2*, and megascopic descriptions of the samples are given on *Table I*.

Field processing of the samples consisted of weighing the bulk sample, followed by dry-screening with a sieve of approximately 2 mm aperture. The gravel fraction (>2 mm) was discarded, and the sand fraction (<2 mm) was weighed after a period of air drying. Subsequently the sand fraction was processed for its heavy-mineral content by use of bowl-shaped enameled wash basins and a gold pan. The washing and concentrating procedures were aimed at removing

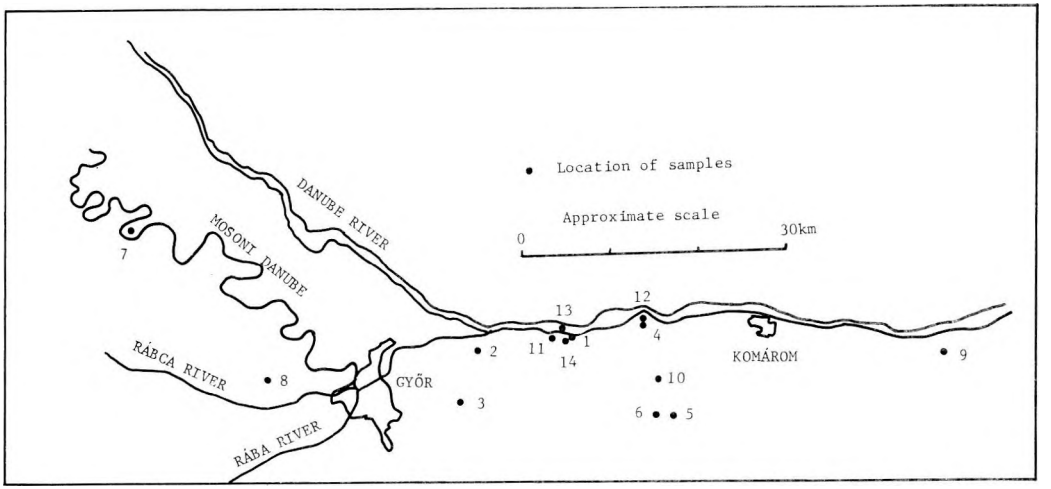

Fig. 1. Map showing locations of samples collected in northwestern Hungary (Danube–Rába Lowland)

1. ábra. A Kisalföldön vett minták helyszínrajza

Рис. 1. Точки отбора проб в северо-западной Венгрии

the clay content by decantation and by elutriation. These procedures produced initially a 60 to 90% heavy-mineral concentrate.

Inasmuch as these techniques are difficult to implement uniformly by a field party of several members, significant variations in the quantitative and possibly qualitative aspects of the HM assemblages obtained should be expected. For one, it is well known that frequency estimations based on minerals separated by both panning and heavy liquids methods are not comparable. When panning is used, minerals such as staurolite, garnet, tourmaline, micas, and chlorite are lost, and minerals such as zircon are proportionately concentrated. In addition, because many of the samples were not thoroughly dry after screening, the reported weight percentages of heavy-minerals are expected to be lower than had the samples been completely dry, as they are a percentage of dry minerals in a wet sample.

Field investigations also included spectral gamma-ray radiation measurements at a few sampling localities of Holocene age and on a number of deposits of Pliocene(?) age. These measurements were made to test the gamma-ray radiation emmisivity of the various sediment types as a possible guide to delineating HM-enriched deposits.

Exploration for heavy-mineral deposits using gamma-ray radiometry is based on the presumption that radioactive heavy minerals (monazite, zircon, sphene) are concentrated with the non-radioactive heavy minerals (ilmenite, rutile, leucoxene, and others). Previous studies on the applicability of spectral

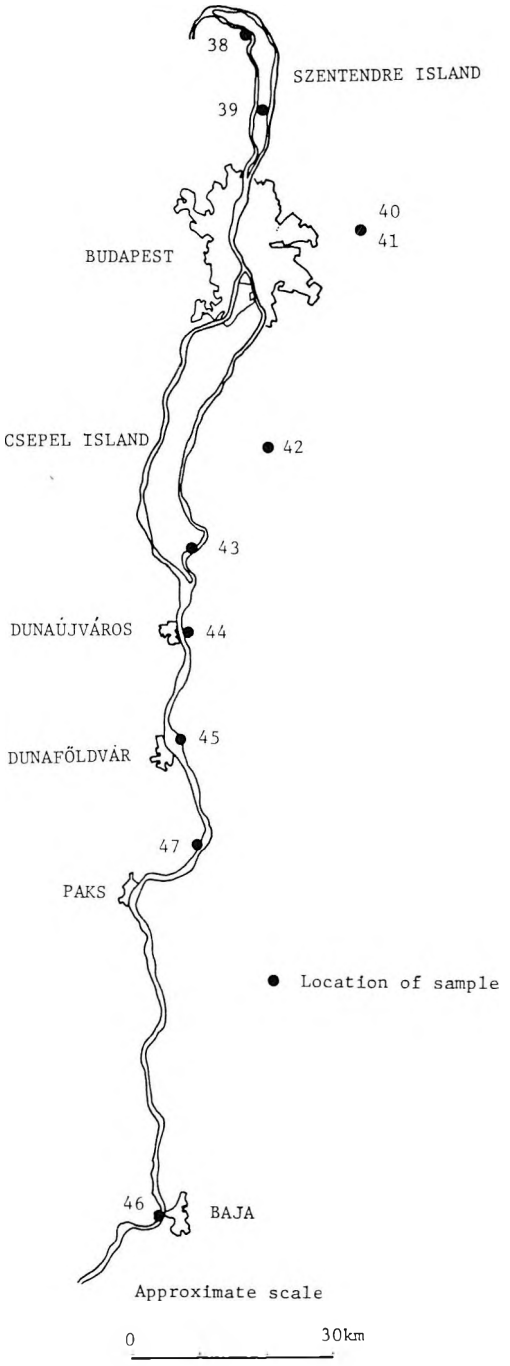

Fig. 2. Map showing locations of samples collected in central Hungary

2. ábra. A Duna mentén vett minták helyszínrajza

Рис. 2. Точки отбора проб в центральной Венгрии

gamma-ray radiometric data to the exploration for HM deposits have shown that such deposits have characteristic radioelemental spectra (dominated by thorium) where radioactive mineral species are present in the heavy-mineral assemblage that is exposed at, or within several centimeters of the surface [ROBSON–SAMPATH 1977, FORCE et al. 1982, MAHDAVI 1964, GROSZ 1983]. The radioactive elements are present either in the crystal lattices or occur as inclusions in the chemically and physically stable minerals, or both, and therefore secular equilibrium of the radioactive daughter products with the parent element can be assumed. Where an anomaly is not caused by radioelements in resistate heavy minerals, the assumption of equilibrium may not be valid. Clay rich sediments contain potassium–40 in minerals such as muscovite, biotite, and illite, and may contain uranium-series nuclides adsorbed on clay minerals; hence areas where clay is common should be anomalous in radioactivity with respect to sandy terranes.

At each locality a four channel spectral gamma-ray scintillometer containing a large volume (1900 cubic centimeters) NaI detector was used to measure both the total field intensity as well as the components of the gamma-ray radiation field. To achieve constant geometry at each locality the detector unit of the instrument was suspended about 0.75 meter above the surface from a tripod. After temperature equilibration and standardization against a barium–133 gamma-ray source, the count rate was measured at the following gamma-ray energies: (1) 2.62 MeV (million electron volts) from thallium–208 in the thorium–232 series; (2) 1.76 MeV from bismuth–214 in the uranium–238 series; and (3) 1.46 MeV from potassium–40. The counting time at each locality did not exceed 8 minutes. Field data were reduced to radioelement concentrations using the method given by STROMSWOLD and KOSANKE [1978]. Results of these measurements are shown in *Tables II* and *III*.

4. Laboratory procedures

Laboratory procedures were directed at qualifying and quantifying those HM species that would account for about 90% percent of each assemblage. No attempt was made either to investigate in detail or to document the full HM assemblages, because the aim of this study was to establish the relative abundances of broad mineral groups (garnet, sheet silicates, tourmaline, pyroboles, etc.) and the general distribution of economically valuable mineral species in the HM assemblages.

The 47 initial mineral concentrates (60–90% HM) prepared in the field were air dried and subsequently subjected to a bromoform-based density separation. This step was followed by removing the ferromagnetic and strongly paramagnetic minerals using a hand-held magnet. The balance of the HM in each sample was further processed into 3 magnetic subfractions on a Frantz Isodynamic Magnetic separator* set at 15 forward and 20 degrees side slopes (0,0–0.5,

* Use of trade names does not constitute endorsement by the USGS

0.5–1.0, and >1.0 Ampere fractions). In this manner, the HM assemblage of each sample was fractionated into groups of 2 to 6 mineral species in each, principally to facilitate the mineral identification process. The mineral species in each magnetic subfraction were identified and quantified by use of petrographic and binocular microscopes; the estimated percentage of mineral species was summed across magnetic fractions. Density was not compensated for in the tabulation given on Table II. The identification of a few of the minerals was done by X-ray diffraction techniques (Beth D. Martin and Joan Fitzpatrick, USGS, Reston).

Because the gravel (>2.00 mm) and the clay fractions were not examined for their HM content, the data shown in Table II may not be fully representative of the total assemblage; very fine-grained mineral species such as zircon, rutile, and gold, for example, as well as sheet silicate minerals that tend to wash out easily are likely underrepresented.

5. Results

Results of this initial investigation indicate that a wide range of HM contents and a wide range of mineral species, including gold, are present in sediments deposited and reworked by the Danube River. Sediments of fluviolacustrine and windblown origins also have a wide range of HM species, however quantities are smaller than in fluvial deposits.

Fluvial terrace deposits of the Danube River sampled in northwestern Hungary average about 0.7%. HM in a range of 0.02 to 3.95% on a bulk sample basis. The HM content of the sand fraction (<2.00 mm) is about double that of the bulk samples averaging about 1.5% in a range of 0.05 to 11.83%. About 50% of the HM assemblage in fluvial deposits of the northwest consist of garnet, ilmenite, rutile, and zircon combined. Of the 26 samples 6 contained gold, and one sample contained native silver.

Fluviolacustrine (Pliocene?) deposits sampled in northwestern Hungary average less than 0.5% HM of which less than 45% are garnet, ilmenite, rutile, and zircon combined. One sample of 7 contained visible gold.

Deposits of windblown sand sampled in nortwestern Hungary average about 1.0% HM of which about 60% consist of garnet, ilmenite, rutile, and zircon combined. None of the 3 samples contained visible gold.

Deposits of Pliocene(?) age sampled in central Hungary east of the Danube River floodplain contain the lowest concentrations of HM averaging 0.04% of which 34% consist of garnet, ilmenite, rutile, and zircon combined. One of the two samples contained a small flake of gold.

Deposits of the Danube River on and south of Szentendre Island have quantities of HM comparable to those found in the northwest, however, garnet, ilmenite, rutile, and zircon combined account for slightly more than 60% of the assemblages. Gold was visible in 6 of 8 samples.

In regard to the grain-size distribution of the more abundant HM species of economic interest, sieve analyses of the garnet-rich fractions (0.0 to 0.5 Ampere magnetic subfraction) of samples 31 and 43 indicate that the bulk of the garnet is between 0.25 and 0.125 mm (fine sand). In sample 31 about 20% of the garnet is between 0.35 and 0.25 mm (medium sand), whereas in sample 43 only about 6% fall into this size class. In sample 43 about 11% of the garnet is between 0.125 and 0.044 mm (fine sand to coarse silt); only about 4% in sample 31 fall into this category. Less than 2% of the garnet in both samples are coarser than 0.044 mm (medium sand) and less than 0.044 mm (coarse to very fine silt). These variations in the grain-size distribution of the garnet group are thought to reflect on the comminution of the minerals due to transport; the relative abundance of the coarser grained garnets in sediments on and south of Szentendre Island are indicative of a source of garnet probably from the region of the Danube River bend.

Zircon and rutile in both sets of samples are finer grained than 0.125 mm; the <0.044 mm fraction of the samples is composed almost entirely of rutile, zircon, and gold. However, gold occurring south of Budapest is generally coarser than 0.044 mm at its coarsest. Ilmenite in both samples is between 0.25 and 0.044 mm (fine sand to coarse silt).

A relatively important qualitative and quantitative change in the HM assemblage occurs starting with sample 38 on Szentendre Island. At this locality, and to the south, garnet, tourmaline, staurolite, and pyrobole group minerals are coarser grained than those found in samples from Northwest Hungary, and magnetite and ilmenite are significantly more abundant. This relative coarseness of grain size suggests a nearby source area, probably the Pilis–Börzsöny–Central Slovakian mountain range at, and north of the bend in the Danube River.

A comparison of the spectral gamma-ray radiation characteristics of the two principal sediment types investigated is given on Table III. The data are suggestive of measurable differences in both total count and spectral radiometric signatures of the deposit types, however the existing data are so far inadequate to characterize the HM-enriched sediments. Additional measurements are expected to resolve this limitation.

6. Conclusions

Fluvial terrace deposits of the Danube River, fluvio-lacustrine deposits of Pliocene(?) age, and deposits of windblown sand have a wide range of HM contents and a large variety of mineral species.

Results of this reconnaissance study indicate a significant potential for garnet and gold, and a smaller potential for titanium minerals and zircon, although the sizes and numbers of samples preclude an accurate definition of resource potential. Detailed mineralogic analyses coupled with chemical analyses would likely show additional minerals and elements of economic interest.

In addition to documenting the discovery of detrital gold in sediments of

the Danube River on and south of Szentendre Island, this investigation underscores the importance of collecting large-volume samples for assessment of low-frequency/high value mineral (i.e. gold) resources.

Acknowledgments

The authors wish to extend their gratitude to the following individuals for their assistance in preparing this report: Lívia Ravasz, Frigyes Franyó, István Marsi, and Miklós Kaiser of the Hungarian Geological Survey and Beth D. Martin, and Joan Fitzpatrick of the U.S. Geological Survey.

REFERENCES

CSALAGOVITS I. 1962: Report on placer deposit investigation of the Danube, Lajta and Rába rivers drift areas (in Hungarian). MÉV Report, 106, Pécs, Hungary

FORCE E. R., GROSZ A. E., LOFERSKI P. J., MAYBIN A. H. 1982: Aeroradioactivity maps in heavy-mineral exploration—Charleston, South Carolina area. U.S. Geological Survey Professional Paper 1218, 19 p.

GROSZ A. E. 1983: Application of total-count aeroradiometric maps to the exploration for heavy-mineral deposits in the Coastal Plain of Virginia, with a section on field spectrometer data reduction by K. L. Kosanke. U.S. Geological Survey Professional Paper 1263, 20 p.

MACDONALD E. H. 1983: Alluvial mining. Chapman and Hall, London, New York, 508 p.

MAHDAVI A. 1964: The thorium, uranium, and potassium contents of Atlantic and Gulf Coast beach sands. *In* Adams J.A.S., and Lowder W.M., eds., The natural radiation environment. University of Chicago Press, Chicago, pp. 87–114

PANTÓ D. 1935: Die Frage der Goldwäscherei an der Donau (in Hungarian with German abstract). Földtani Közlöny (Bull. of the Hung. Geol. Soc.), **65,** 1–3, pp. 182–274

ROBSON D. F., SAMPATH N. 1977: Geophysical response of heavy-mineral sand deposits at Jerusalem Creek, New South Wales. BMR (Australia Bureau of Mineral Resources) Journal of Australian Geology and Geophysics, **2,** 2, pp. 149–154

STROMSWOLD D. C., KOSANKE K. L. 1978: Calibration and error analysis for spectral radiation detectors. Institute of Electrical and Electronics Engineers Transactions on Nuclear Science, **NS-25,** 1, pp. 782–786

SAMPLE LOCALITY NO.	SAMPLE NO.	SAMPLE TYPE[1]	SAMPLE INTERVAL IN CM	DESCRIPTION
1	2	C	100	gray poorly sorted sandy gravel
1	3	C	30	gray sandy gravel
1	4	C	40	orange oxidized gravelly sand
1	5	C	30	gray gravelly micaceous sand
2	6	C	150	beige medium to fine sand (windblown)
2	7	C	650	gray–beige sandy gravel
2	8	C	50	gray gravelly medium to fine sand
2	9	G	30	gray and orange sandy gravel (from creoturbed pocket)
2	24	G	N/A[2]	gray gravelly sand (from bottom of creoturbed pocket)
3	10	C	100	buff gray very fine sand (windblown)
3	11	C	250	gray–beige sandy gravel
3	12	C	800	orange medium to fine sand, low angle crossbedded
3	13	C	350	orange medium to fine sand, low angle crossbedded
3	14	C	900	orange medium to fine sand, low angle crossbedded
4	15	C	100	buff gray very fine sand (windblown)
4	16	C	150	gray medium to fine sand, low angle crossbedded
4	17	C	500	gray sandy gravel
5	18	C	150	gray medium to fine sand
5	19	C	550	gray sandy gravel
6	20	C	600	beige–orange medium to fine slightly gravelly sand, high angle crossbedded
7	21	C	400	gray sandy gravel
8	22	C	250	tan–beige medium to fine sand, low angle crossbedded
9	23	C	350	tan–orange medium to fine sand low angle crossbedded
10	25	A	250	orange very fine sand
10	26	A	150	gray–tan gravelly sand
11	27	A	50	dark gray medium to fine sand
11	28	A	60	dark gray gravel with medium to coarse sand
11	29	A	100	tan gray sandy gravel
11	30	A	100	light tan gray–tan sandy gravel
11	31	A	100	light tan gray–tan sandy gravel
12	32	A	50	light yellow–orange sandy gravel
12	33	A	150	light yellow–orange sandy gravel
12	34	A	100	gray sandy and pebbly gravel
12	35	A	200	gray sandy and pebbly gravel
13	36	G	N/A	light gray–tan modern Danube River sandy gravel
14	37	C	100	tan–beige medium to very fine sand
15	38	G	N/A	gray modern Danube River floodplain sandy gravel
16	39	C	250	tan–orange sandy gravel
17	40	C	150	orange oxidized sandy gravel
17	41	C	300	orange oxidized medium to very fine sand
18	42	G	N/A	gray–beige sandy gravel
19	43	G	N/A	gray–beige sandy gravel
20	44	G	N/A	gray–beige sandy gravel
21	45	G	N/A	gray medium to fine sand (natural concentrate)
22	46	G	N/A	dark gray medium to very fine sand (natural concentrate)
23	47	G	N/A	light gray–beige sandy gravel (dredged Danube thalweg sample)

1) C denotes channel, G denotes grab, A denotes auger samples
2) not applicable

Table I. Description of samples collected for heavy-mineral analyses

I. táblázat. A nehéz-ásvány elemzésre vett minták leírása

Таблица I. Основные характеристики шлиховых проб

Sample No.	Gravel[1]	Weight percent Sand[2]	Weight percent SG >2.85 in I.W.[3]	<2 mm	PERCENT OF SG >2.85: MAGNETITE	ILMENITE	RUTILE	EPIDOTE[4]	ZIRCON	TOURMALINE	GARNET	ALUMINO SILICATES[5]	DOLOMITE[6]	STAUROLITE	PYROBOLES[7]	SHEET SILICATES[8]	OTHERS[9]	GOLD[13]	SPECTRAL GAMMA-RAY MEASUREMENTS: % K	eU ppm	eTh ppm
2	53	47	0.02	0.05	10)	2	3	8	3	4	43	9	10	7	3	5	3	1	1.76 ± .04	3.34 ± 0.28	10.17 ± 0.38
3	59	41	0.33	0.82	11)	3	3	15	3	1	35	17	2	4	7	4	6				
4	15	85	0.71	0.83	11)	2	3	7	4	3	30	17	P	3	17	10	4				
5	27	73	2.23	3.04	10)	P	4	3	4	P	10	5	54	2	1	12	5				
6	0	100	2.30	2.30	11)	4	3	6	3	P	50	15	P	6	3	3	7		0.96 ± 0.03	2.40 ± 0.19	6.98 ± 0.27
7	71	29	0.19	0.66	11)	P	3	8	2	1	49	12	P	6	8	6	5		1.15 ± 0.03	1.69 ± 0.16	4.30 ± 0.23
8	19	81	0.29	0.36	10)	2	P	12	P	3	25	14	12	10	12	5	5				
9	62	38	0.20	0.53	10)	4	1	6	1	2	58	13	P	3	2	2	8				
24	73	27	0.36	1.35	10)	7	3	13	3	3	30	8	3	5	9	8	8	1			
10	0	100	0.11	0.11	10)	4	2	2	2	1	57	19	P	5	2	P	6		1.72 ± 0.04	5.84 ± 0.33	9.89 ± 0.39
11	63	37	0.09	0.26	11)	3	2	15	2	4	40	7	10	6	5	2	4				
12	0	100	0.14	0.14	11)	5	3	13	3	1	32	20	2	4	7	3	7				
13	0	100	0.58	0.58	11)	2	4	10	5	3	22	23	1	2	6	5	7				
14	0	100	0.27	0.27	11)	3	2	14	1	2	33	18	6	2	7	8	4				
15	0	100	0.81	0.81	11)	6	3	13	3	P	44	7	8	4	5	1	6				
16	0	100	0.97	0.97	1)	10	5	13	5	2	24	10	11	6	6	2	5		1.30 ± 0.04	4.30 ± 0.29	11.77 ± 0.37
17	62	38	0.13	0.36	11)	8	2	8	2	2	61	3	2	2	1	2	7		1.12 ± 0.03	2.79 ± 0.21	7.54 ± 0.29
18	0	100	1.32	1.32	11)	6	3	14	3	2	48	7	4	5	2	P	6				
19	81	19	0.09	0.47	11)	4	4	14	2	2	47	4	3	7	3	5	5	1			
20	6	84	0.07	0.07	10)	2	2	20	2	2	33	6	7	4	3	12	7				
21	60	40	0.16	0.42	11)	2	2	7	2	2	67	5	2	3	P	4	4		1.03 ± 0.02	1.33 ± 0.13	3.34 ± 0.18
22	0	100	0.31	0.31	11)	3	3	9	2	1	38	7	25	2	3	1	6		1.55 ± 0.04	2.96 ± 0.24	7.14 ± 0.32
23	0	100	0.71	0.71	1)	8	4	16	2	3	44	3	4	4	7	1	3	1	1.61 ± 0.04	3.79 ± 0.28	10.16 ± 0.37
25	0	100	0.31	0.31	10)	5	3	13	2	3	31	7	6	5	6	12	7				
26	34	66	0.51	0.78	10)	6	4	11	3	6	34	6	4	3	5	13	5				
27	79	21	1.02	4.87	11)	4	3	6	P	5	50	6	7	4	3	5	7				
28	54	46	0.80	1.81	11)	5	2	9	1	5	31	7	20	2	1	7	10				
29	31	69	2.53	3.66	11)	3	2	8	P	3	23	4	31	5	4	11	6				
30	52	48	0.75	1.57	11)	4	2	10	2	3	34	9	5	4	4	15	8				
31	67	33	3.95	11.83	11)	7	1	6	1	2	58	4	3	2	1	6	9	18			
32	54	46	0.64	1.39	10)	3	3	9	1	1	31	8	26	2	2	7	7				
33	60	40	0.24	0.60	10)	6	2	10	1	1	48	4	10	4	4	5	5	1			
34	52	48	0.71	1.50	11)	3	4	11	4	2	46	6	4	4	7	5	4	2			
35	58	42	0.16	0.39	10)	4	3	7	2	2	45	8	12	2	2	2	8				
36	0	100	1.01	1.01	11)	5	2	P	2	3	67	2	3	3	3	3	7	10			
37	0	100	0.09	0.09	10)	4	2	7	2	3	25	6	34	4	2	1	10				
38	45	55	0.10[12]	0.18[12]	7)	4	P	6	P	12	5	5	2	4	9	P	6	14	2.04 ± 0.05	4.53 ± 0.33	11.83 ± 0.43
39	60	40	0.10[12]	0.25[12]	4)	2	2	7	2	9	52	4	1	3	11	T	4		1.75 ± 0.04	2.99 ± 0.25	8.19 ± 0.35
40	77	33	0.02[12]	0.06[12]	11)	25	7	19	4	7	5	12	3	14	P	T	4		1.52 ± 0.04	1.94 ± 0.22	7.99 ± 0.32
41	0	100	3.75[12]	3.75[12]	1)	16	6	34	3	6	2	13	2	7	2	T	6	15			
42	?	100	0.38[12]	0.38[12]	2)	5	8	10	3	3	43	10	4	5	4	P	9	1	1.17 ± 0.03	2.05 ± 0.17	4.12 ± 0.23
43	65	35	0.16[12]	0.46[12]	1)	8	2	8	2	2	64	4	P	5	3	P	4	30	1.30 ± 0.03	2.20 ± 0.19	5.38 ± 0.25
44	65	35	0.05[12]	0.16[12]	4)	3	1	12	P	10	43	4	7	5	7	P	6		1.41 ± 0.03	2.76 ± 0.21	5.91 ± 0.24
45	0	100	0.55[12]	0.55[12]	2)	3	3	9	3	6	50	5	3	5	11	1	8	13	1.57 ± 0.04	3.52 ± 0.26	8.71 ± 0.34
46	0	100	1.74[12]	1.74[12]	1)	4	4	7	4	6	64	6	P	3	4	P	10	16	1.58 ± 0.04	3.63 ± 0.27	9.61 ± 0.36
47	60	40	0.11[12]	0.28[12]	3)	2	1	7	1	5	58	3	4	8	7	P	7	1			

1) >2.00 mm fraction
2) <2.00 mm fraction, includes clay
3) initial weight
4) includes clinozoisite, pumpellyite, zoisite
5) includes kyanite, sillimanite, andalusite
6) includes calcite
7) includes amphibole, tremolite, actinolite, glaucophane, hypersthene, augite, diopside
8) includes chlorite, biotite, muscovite, and chloritoid
9) may include a variety of minerals including quartz, sulfides, clayballs, corundum?, unidentified opaques, xenotime?, limonite, polymineralic grains, schist fragments, apatite, leucoxene, phosphatic shell fragments, sphene, monazite, anatase, and others
10) <0.05%
11) 0.05÷0.5%
12) estimate based on 2 kg/liter density of bulk sample
13) number of identified flakes, beads, or grains

Table II. Screen and heavy-mineral analyses of samples from northwestern and central Hungary

II. táblázat. ÉNy- és Közép-magyarországi minták kavics- és homoktartalma, valamint nehéz-ásvány elemzési eredményei

Таблица II. Относительное содержание галки и песка в пробах; минеральный состав тяжелой фракции

Sediment type	No. of locations	Total count counts/second	%K	eU ppm	eTh ppm	eTh/eU	eU/%K	eTh/%K
Danube River deposits	11	197	1.33 ± .03	2.54 ± .20	6.38 ± .28	2.5	1.9	4.8
Pliocene(?) deposits	9	261	1.60 ± .04	3.72 ± .27	9.92 ± .36	2.7	2.3	6.2

Table III. Comparison of spectral gamma-ray radiation signatures of Danube River and Pliocene(?) sediments

III. táblázat. Dunai üledékek és pliocén képződmények spektrális gamma-sugárzási jellegének összehasonlítása

Таблица III. Сравнительные характеристики спектра гамма-излучения террасовых отложений и плиоценовых образований

A DUNA ÁRTÉRI KÉPZŐDMÉNYEINEK VALAMINT ÉNY- ÉS KÖZÉP-MAGYARORSZÁG FOLYAMI–TAVI ÜLEDÉKEINEK HASZNOSÍTHATÓ NEHÉZÁSVÁNYAI

Andrew E. GROSZ, SIKHEGYI Ferenc és FÜGEDI P. Ubul

A nehézásvány-források kimutatására a Duna terasz üledékekben, valamint ÉNY- és Közép-Magyarország folyami–tavi üledékeiben közös, amerikai–magyar program indult. A kutatás arany kimutatásához vezetett a Dunának Budapesttől délre eső szakaszán, továbbá gránát kiugró mennyiségét is jelezte. Ezen kívül kisebb mértékű titán-ásvány és cirkon feldúsulások is jelentkeznek, de eloszlásuk nem kellőképp ismert.

ÉNY-Magyarország (Kisalföld) 26 db, holocén korú, folyóvízi mintájának ásványtani analízise 0,7%-os átlagos nehézásvány-koncentrációt adott, melynek mintegy felét gránát, Ti-ásványok és cirkon teszi ki. A nyolc, aranyra szedett mintából hatban találtunk aranyat, további egy minta termés ezüstöt tartalmazott. A Szentendrei-szigeten és tőle délre, a folyóvízi üledékek az ÉNY-Magyarországon található nehézásvány-koncentrációkhoz hasonló értékeket adnak: ugyanakkor az arany lényegesen gyakoribb és durvább szemű, mint a Kisalföldről származó mintákban.

A neogén és kvarter folyami–tavi üledékek valamint ÉNY- és Közép-Magyarország szélfútta üledékeinek nehézásvány együtteseit elemezve látható, hogy ezen üledékek nehézásvány frakciója nem éri el a 0,5%-os átlagot s a gránát, Ti-ásványok és a cirkon részaránya csupán 35%-os. Tizenegy vizsgált mintából kettő tartalmazott aranyat. A különböző üledéktípusok spektrális gammasugárzási jellegeinek mérése azt sugallja, hogy a nehézásványokban viszonylag gazdagabb üledékek a kisebb tartalmúakhoz képest mérhető különbségeket mutatnak, ugyanakkor kiegészítő adatok szükségesek e különbségek számszerű jellemzésére.

ТЯЖЁЛЫЕ МИНЕРАЛЫ В ПОЙМЕННЫХ ОБРАЗОВАНИЯХ Р. ДУНАЯ И ВО ОЗЕРНО-РЕЧНЫХ ОТЛОЖЕНИЯХ СЕВЕРО-ВОСТОЧНОЙ И ЦЕНТРАЛЬНОЙ ВЕНГРИИ

Эндру Э. ГРОС, Ференц ШИКХЕДИ и Убуль П. ФЮГЕДИ

В рамках венгерско–американского сотрудничества был составлен рабочий проект с целью установления возможностей выявления источников тяжелых минералов в составе террасовых отложений р. Дуная, а также в неогеновых и четвертичных озерно-речных образованиях северо-западной и центральной Венгрии. В результате работы было выявлено одно непромышлжнное накопление золота в пойменных отложениях Дуная к югу от Будапешта, которое сопровожалось повышенным содержанием граната в составе тяжёлой фракции. Кроме того, были уставлены и небольшие скопления титановых минералов и циркона, но пока не ясно, имеют ли они значительное распростнение по вертикали и латерали.

В 26 пробах, отобранных из четвертичных речных отложений СЗ Венгрии, среднее содержание тяжёлой фракции – 0,7 вес. %, примерно 50% от которого состовляют гранат, циркон и минералы титана. Из 8 проб, взятых с целью выявления накоплений золота, его наличие установлено в 6. Кроме того, в одной пробе отмечено и самородное серебро.

Концентрации тяжелых минералов в пробах, отобранных с о-ва Сентендре и ниже по повышается в них, и сами зернышки становятся более крупными, чем в пробах с территории Низменности рр. Дунай–Раба.

Рассматривая неогеновые и четвертичные, озеро-речные, а также, золические отложения СЗ и центральной Венгрии видно, что в данных образованиях среднее содержание тяжёлой фракции 0,5 вес. % и относительное содержание граната, циркона и минералов титана — только 35%. Из 11 проб присутствие золота замечалось всего в двух. В результате изучения природы гамма-излучения образований разных типов можно предполагать, что показатели гамма-излучения осадочных образований с бо́льшими содержаниями тяжёлой фракции действительно больше, чем в других отложениях, однако для установления количественных закономерностей необходимы дальнейшие исследования.

GEOPHYSICAL TRANSACTIONS 1985
Vol. 31. No. 1–3. pp. 169–189

DETAILS OF A PLEISTOCENE COASTAL SUCCESSION, GOLDEN GATE NATIONAL RECREATION AREA, CALIFORNIA

Géza CSÁSZÁR*, H. Edward CLIFTON** and Ralph E. HUNTER**

The Merced Formation of the San Francisco Peninsula is a thick succession of shelf and coastal deposits of Pliocene and Pleistocene age. In sea cliff exposures south of San Francisco in the Golden Gate National Recreation Area, the Merced occurs in two extensive north-dipping sections separated by a 2-km-long landslide under which the strata strike approximately parallel to the beach. This paper describes, in detail, the lowermost part of the northern segment and documents its stratigraphic equivalence with the uppermost part of the southern segment. The strata in the examined section of the Merced include two distinctive marker beds, a 400,000 year-old ash bed and the "Upper Gastropod Bed" of ASHLEY [1895].

A variety of depositional environments are represented: tidal channels and flats, fluvial channels, backshore flats, ponds and eolian dunes. The general pattern of deposition is: coastal embayment → eolian dune → embayment → fluvial → embayment → backshore → open marine nearshore. The succession records more of the sediment deposited during marine transgression than is generally found in other parts of the Merced and in associated beds.

Keywords: depositional environment, stratigraphy, Merced Formation, San Francisco, California

1. Introduction

The sea cliffs that extend about 6 km southward from the Fort Funston area of Golden Gate National Recreation Area, at the southwest corner of the city of San Francisco, expose about 1,700 m of Pliocene and Pleistocene sediments. The strata at the northern and southern ends of this succession dip to the north. About 200 m of the upper (northern) part of the section have been measured in detail [HUNTER–CLIFTON 1982], as has about 720 m of the lower (southern) part of the section [HUNTER at al. 1984, CLIFTON–STAGG in preparation].

The two measured sections are separated by a 2-km-long interval that is disrupted by a large landslide. Exposures of strata above, below and within the landslide indicate that they strike nearly parallel to the beach, and certain key beds (especially a prominent ash bed) can be traced between the two stratigraphically intact segments. The critical strata (about 70 m of section below the ash bed) for establishing correlation between these segments present a special problem. They are exposed in an almost intact section just north of the landslide, and in a broken section within the landslide on the beach just north of the former (prior to the 1982 movement of the landslide) parking area at Thornton

* Hungarian Geological Survey, POB 106, Budapest, H–1442
** U. S. Geological Survey, 345 Middlefield Road, Menlo Park, California 94025
Manuscript received: 25 April, 1985

Beach State Park. The lower part of this section is intact but very poorly exposed on the upper part of the sea cliff south of Thornton Beach.

This report presents the results of a detailed study of this critical part of the section just north of the large landslide. We compare the strata here to those strata exposed to the south and demonstrate a basis for stratigraphic continuity between the two intact sections. We also interpret the depositional environments in which these strata formed and relate them to changes in shoreline position with time.

Micropaleontological analyses and X-ray diffraction analyses were conducted with the aim of improving the resolution of the facies and environmental interpretation. We are thankful to P. Quinterno (USGS) for the micropaleontological analyses and to L. Farkas (MÁFI) for the X-ray diffraction analyses.

2. Background

Setting

The Pliocene and Pleistocene succession we address lies in a structural trough that strikes obliquely NW-SE across the San Francisco Peninsula *(Fig. 1)*. On its southern side this succession is cut by the San Andreas fault. The exposures described in this report are located on the western margin of the San Francisco Peninsula near Lake Merced, for which the unit was named. The shoreline here consists mainly of sea cliffs as high as 60 m, composed of relatively unconsolidated sediment. Because the strata are tilted to the north, a complete section can be followed at the base of the cliff. The exposure varies. Small landslides commonly bury the section for short (100–200 m) distances, and a large landslide obscures the succession for 2 km south of Fort Funston, the location of the section described here. The exposure is further modified by the seasonal movement of sand off and onto the beach. Typically, the best exposure occurs in winter when much of the sand is removed by storms. The observations presented here were made during January and February 1983, a period of unusually intense storms along the California coast. This had a positive effect, in that we could examine parts of the section that are generally unexposed, moreover, the rocks at the base of the cliffs were particularly clean owing to the storm activity.

Previous work

The unit in which our section occurs was first described by LAWSON [1893] under the name "Merced series". On the basis of fossils, LAWSON determined that the age of the unit was Pliocene. ASHLEY [1895] continued the examination and named a distinctive fossiliferous bed in the formation the "Upper Gastropod Bed." GLEN [1959] made a comprehensive evaluation of the fauna of the Merced and divided the formation into an upper and a lower member, the contact being placed at the base of the "Upper Gastropod Bed". From the composition of the fauna he suggested that most of the type Merced Formation

formed in a shallow sheltered basin. He also inferred from lignite and diatomite in the upper member that some of the deposition occurred in a fresh-water lake or pond. GLEN further interpreted the upper member of the Merced Formation to have formed in the Early Pleistocene and the lower member in the Late Pliocene.

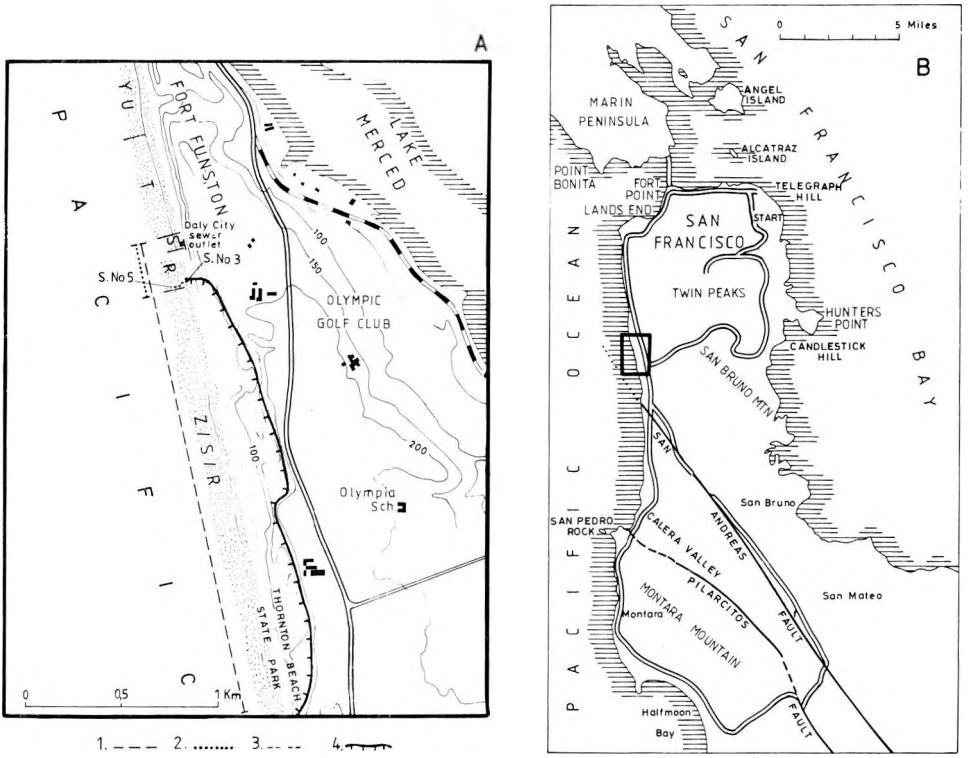

Fig. 1. Index map of Fort Funston area, San Francisco Peninsula.
A) Detailed map of the area between Fort Funston and Thornton Beach
1 — studied seacliff stretch; 2 — seacliff studied in detail; 3 — major sections reviewed in the paper; 4 — landslide
B) San Francisco Peninsula with location of the area enlarged

1. ábra. Helyszínrajz a San Francisco félszigeti Fort Funston környékéről
A) Részlettérkép Fort Funston és Thornton Beach között
1 — a vizsgált partszakasz; 2 — részletesen tanulmányozott szakasz; 3 — a dolgozatban tárgyalt fontosabb szelvények 4 — földcsuszamlás
B) San Francisco félsziget a kinagyított terület kontúrjával

Рис. 1. Абрис местности Форт Фанстон (п-ов Сан Франциско)
А) Детальная карта района Форт Фанстон — Торнтон Бич
1 — исследованный участок берега; 2 — детально изученный фрагмент участка; 3 — важнейшие разрезы, обсуждаемые в статье; 4 — оползни
В) Полуостров Сан Франциско с контуром увеличенного участка

HALL [1965/a, 1965/b, 1966] made a sedimentologic analysis of the Merced and concluded from the mineralogy that a major change in provenance is indicated about 75 m below the "Upper Gastropod Bed". He used this change to define the boundary between the upper and the lower members. HALL also noted that the "Upper Gastropod Bed" is actually composed of two separate shelly layers. His paper presents an excellent cross-sectional sketch of the strata in the sea cliffs.

ADDICOTT [1969] examined the paleogeographic implications of the mollusks of the area and concluded that the type Merced embayment was a narrow coastal feature that did not extend as far south as the present southern part of San Francisco Bay. He noted a tendency for the Late Pliocene deposits in the San Francisco–Monterey Bay area to develop in embayments that opened to the northwest.

Another frequently noted distinctive bed in the Merced is a volcanic ash [SARNA-WOJCICKI 1976], typically 20 to 40 cm thick, which lies stratigraphically about 40 m above the "Upper Gastropod Bed". MEYER et al. [1980] assign an age of 400,000 years to this ash based on radiometric dating.

HUNTER and CLIFTON [1982] present a detailed description and facies analysis of the stratigraphic sequence above the ash bed. They show that the depositional record is characterized by a series of alternating transgressions and regressions. Their methods guided our present analysis.

Fig. 2. Stratigraphic column of the Merced Formation studied at Fort Funston.
1 — tuff; 2 — gravel; conglomerate or pebbly sand; 3 — scattered pebbles in sand; 4 — bedded or laminated sand or sandstone; 5 — crossbedded sand; 6 — convolute or lenticular bedding; 7 — structureless or poorely bedded sand; 8 — clayey and/or silty sand and sandstone; 9 — siltstone; 10 — sandy or silty mudstone; 11 — structureless mudstone; 12 — mudstone intercalation; 13 — laminated mudstone; 14 — beds rich in organic material; 15 — plant remains; 16 — roots; 17 — small-scale bioturbation; 18 — large-scale bioturbation; 19 — extra large bioturbation; 20 — insect burrows; 21 — Bivalve beds; 22 — scattered Bivalves; 23 — scoured surface

2. ábra. A Merced Formáció rétegoszlopa Fort Funstonnál
1 — tufa; 2 — kavics, konglomerátum vagy kavicsos homok; 3 — kavics hintéses homok; 4 — rétegzett vagy laminált homok és homokkő; 5 — keresztrétegzett homok; 6 — zavart (convolute) vagy lencsés rétegzés; 7 — szerkezet nélküli vagy gyengén rétegzett homok; 8 — agyagos és/vagy kőzetlisztes homok és homokkő; 9 — aleurolit; 10 — homokos vagy kőzetlisztes agyagkő; 11 — rétegzetlen agyagkő; 12 — agyagkő betelepülés; 13 — leveles agyagkő; 14 — szerves anyagban gazdag rétegek; 15 — növénymaradványok; 16 — gyökérnyomok; 17 — kis méretű bioturbáció; 18 — nagy méretű bioturbáció; 19 — extra nagy méretű bioturbáció; 20 — rovar járat; 21 — kagyló tartalmú réteg; 22 — szórványos megjelenésű kagyló; 23 — kimosott felszín

Рис. 2. Разрез формации Мерсед при местности Форт Фанстон
1 — туфы; 2 — галечники, конгломераты или галечные пески; 3 — пески с россыпями гальки; 4 — слоистые или ламинированиные пески и песчаники; 5 — песчаники с косой слоистостью; 6 — конволютная или линзовая слоистость; 7 — пески неструктурные или слабо слоистые; 8 — глинистые и/или алевритовые пески и песчаники; 9 — алевриты; 10 — песчаные или алевритовые глины; 11 — глины без слоистости; 12 — прослойка глин; 13 — листоватые глины; 14 — слои, богатые органическим веществам; 15 — остатки растений; 16 — следы корней; 17 — мелкая биотурбация; 18 — крупная биотурбация; 19 — уникальная биотурбация; 20 — ходы насекомых; 21 — слой с остатками раковин; 22 — редко встречающиеся раковины; 23 — размытая поверхность

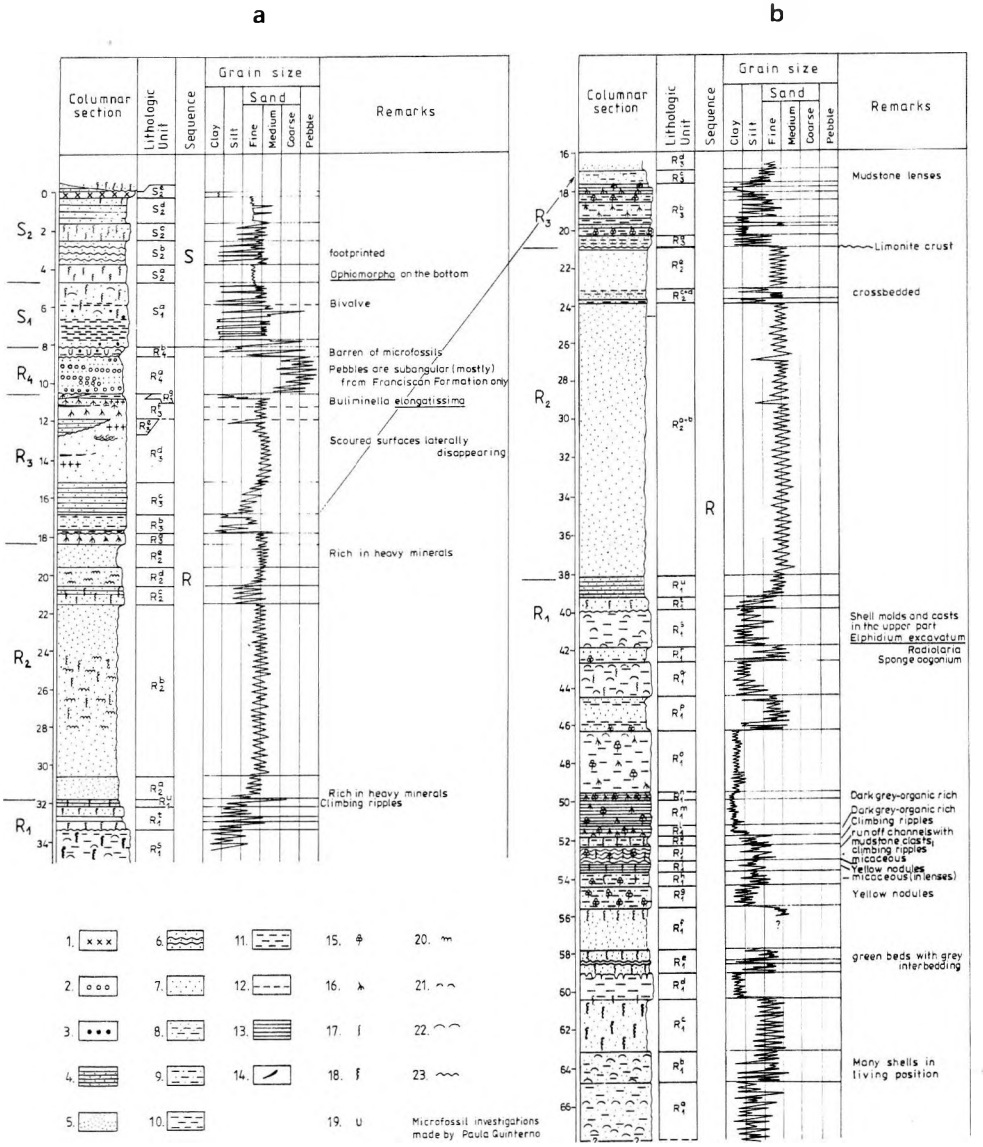
a
b
Columnar section
Lithologic Unit
Sequence
Grain size
Clay
Silt
Sand
Fine
Medium
Coarse
Pebble
Remarks
S
R
footprinted
Ophiomorpha on the bottom
Bivalve
Barren of microfossils
Pebbles are subangular (mostly) from Franciscan Formation only
Buliminella elongatissima
Scoured surfaces laterally disappearing
Rich in heavy minerals
Rich in heavy minerals
Climbing ripples
Mudstone lenses
Limonite crust
crossbedded
Shell molds and casts in the upper part
Elphidium excavatum
Radiolaria
Sponge oogonium
Dark grey-organic rich
Dark grey-organic rich
Climbing ripples
run off channels with mudstone clasts, climbing ripples
micaceous
Yellow nodules
micaceous (in lenses)
Yellow nodules
green beds with grey interbedding
Many shells in living position
Microfossil investigations made by Paula Quinterno

As a consequence of the present study, HUNTER et al. [1984] extended the detailed analysis for an additional 200 m below the base of the section described here. They considered the transgressive–regressive cycles that characterize the Merced in the context of eustatic sea-level oscillations, tectonic events and fluctuation in sedimentation rate. The estimated sedimentation rate for the 470 m of the section described by them is about 55 cm/1000 years.

The section considered in detail here extends stratigraphically down-section from the ash bed to strata that lie about 14 m below the "Upper Gastropod Bed". Geographically, the exposures extend north from the large landslide between Fort Funston and Thornton Beach to a position just north of the Daly City sewer outfalls. These exposures are within the Fort Funston area of Golden Gate National Recreation Area. The strata contained in this section are exposed to the south as well—within the landslide block—just north of Thornton Beach and in an undisrupted section high on the sea cliffs just south of the landslide. The section within the landslide block is occasionally very well exposed by winter storms, but the stratigraphic continuity is broken by numerous fractures. South of the landslide the section is again continuous but exposures of the beds considered in this report are very poor.

Field methods

A complete continuous section was not available because at various intervals small slides and small-scale faulting covered the exposure. Accordingly, overlapping sections were measured at different but nearby locations and correlated on the basis of lithology *(Fig. 2)*. The section shown in Figure 2/a includes the upper part of the succession, which was measured in continuous exposure southward from the Daly City sewer outfalls. The other section (2/b) represents the combination of several closely spaced sections to the south immediately below the viewing platform and hang-glider port at Fort Funston and includes the lower part of the succession. The overlapping parts of the two sections are separated laterally by a distance of some 40 m.

3. Stratigraphic composition

The 68 m thick section analyzed in this paper consists of a variety of sediment types: mud, silt, sand, gravel and volcanic ash. The degree of induration is variable—some beds are well-indurated, whereas others are almost totally unconsolidated. In this report we employ both rock terminology (siltstone, mudstone, conglomerate, etc.) and unconsolidated sediment terms (sand) depending on our qualitative evaluation of the degree of induration.

The sedimentary deposits within the section differ greatly in texture, sedimentary structures (including biogenic structures) and fossils. These variations record changes in depositional environment that serve as the basis for subdivision of the stratigraphic elements within the section.

We divide the section into two primary sequences, following the approach

of HUNTER and CLIFTON [1982] and HUNTER et al. [1984]. These sequences are designated *R* and *S* (Fig. 2/a and b) in order to remain consistent with the terminology of HUNTER et al. [1984]. Each sequence represents a major cycle of transgression and regression.

These are further subdivided following the approach of HUNTER and CLIFTON [1982] and HUNTER et al. [1984] into subsequences (R_1, R_2, R_3, R_4, S_1 and S_2) of generally uniform depositional environment. In this report we further subdivide these subsequences into units (R_1^a, R_1^b, etc.) that represent distinct environmental elements. The complete subdivision is shown in Fig. 2.

Sequence R

Sequence *R* comprises about 60 m of the section presented here. In the section at Fort Funston, the base of this sequence is not exposed. The base is exposed only in the upper part of the sea cliffs south of Thornton Beach. HUNTER et al. [1984] indicated a total thickness of 63 m for sequence *R* and divided the sequence here into 4 subsequences which are described below.

The exposed part of basal subsequence at Fort Funston (R_1) is about 30 m thick (*Figs. 3* and *4*). It consists predominantly of silt or mudstone with numerous intercalations of fine- or medium-grained sandstone. Fossils are common and trace fossils and root structures are locally abundant. The upper part of the subsequence crops out in the sea cliff, but its lower part is exposed only on the beach where it is well-exposed only in winter when much of the beach sand is stripped away.

Distinct textural trends exist within the subsequence. The basal units (R_1^a, R_1^b, R_1^c) are quite sandy. The lowermost two units (R_1^a and R_1^b) contain numerous bivalves, many in growth position *(Fig. 5)*. The concentration of shells is missing from the equivalent part of the section to the south at Thornton Beach. Unit R_1^c lacks fossils but is intensively bioturbated. It is overlain by a generally structureless but locally laminated mudstone, R_1^d, that has a scoured surface at its top *(Fig. 6)*.

Unit R_1^d is sharply overlain by a structureless sandstone of green to gray color (R_1^e) which contains large fragments of carbonized wood. Mudstone intercalations are common in the lower part. This unit is overlain by about 10 m of predominantly fine-grained sediment (units R_1^f–R_1^o) in which plant remains are common *(Fig. 7)*. Small channels are present in unit R_1^j *(Fig. 8)* and ripples occur in R_1^j and R_1^k *(Fig. 9)*. Units $R_1^{h\,k}$ show numerous burrows 3—5 mm in diameter, and root structures are evident in the top 5 m of these strata (in units $R_1^{l\,o}$, *Fig. 10)*. Fine lamination, defined by alternating light and dark layers, characterizes units $R_1^{l\,n}$ *(Fig. 11)*. Units R_1^n and R_1^l are dark due to the high content of carbonaceous material. Yellow-brown nodules occur in units R_1^q and R_1^i (Fig. 7). The top of unit R_1^o is a scoured surface marked by large (6–10 mm) borings.

The upper part of subsequence R_1 (units $R_1^{p\,u}$) is rather poorly exposed in the lowermost part of the sea cliffs at Fort Funston, where it is broken by

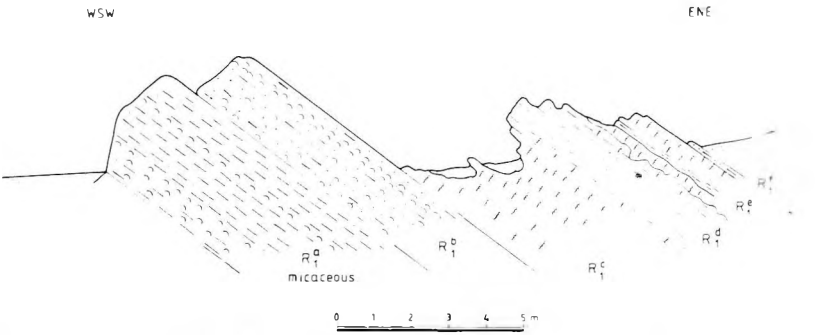

Fig. 3. Lowermost beds (units R_1^a to R_1^f) exposed on the beach at the south end of Fort Funston (section No. 5). For legend, see Fig. 2

3. ábra. Fort Funston D-i elvégződésénél (5. sz. szelvény) a parton feltárt legalsó rétegek (R_1^a–R_1^f egységek). Jelkulcs a 2. ábránál

Рис. 3. Самые нижние слои (R_1^a–R_1^f), обнаженные на пляже в южной части местности Форт Фанстон. Условные обозначения см. на рис. 2

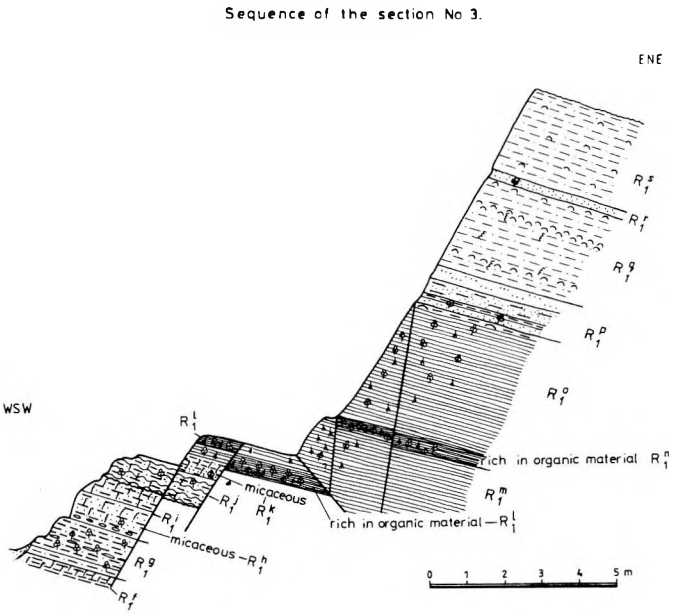

Fig. 4. Intertidal and supratidal mudstone beds (units R_1^{q-o}) of section No. 3 at the hang-glider stairway at Fort Funston. Embayment deposit. For legend, see Fig. 2

4. ábra. Árapály övi és e fölötti agyagkő rétegek (R_1^{q-o}) a 3. sz. szelvényben a Fort Funstonnál lévő sárkányrepülő-lépcsőnél. Öböl üledék. Jelkulcs a 2. ábránál

Рис. 4. Слои интратидальных и супратидальных глин (R_1^{q-o}) в разрезе №3 у лестницы дракона в местности Форт Фаунстон. Отложения залива. Условные обозначения см. на рис. 2

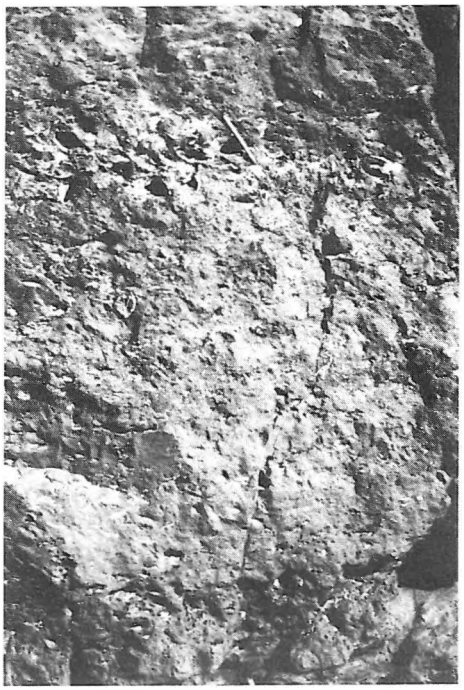

Fig. 5. Bivalve-bearing mudstone (R_1^a) with some shells in living position (channel lag)

5. ábra. Kagyló tartalmú agyagkő (R_1^a) benne néhány élő helyzetben megőrződött teknővel (csatorna-láb üledék)

Рис. 5. Глины (R_1^a), содержащие раковины, и несколько раковин, сохраненных в живом положении (отложения подножья канала)

Fig. 7. Silty mudstone beds of intertidal zone with yellow nodule horizons (R_1^{g-h}). Embayment deposit

7. ábra. Kőzetlisztes agyagkő az árapályzónából növénymaradvánnyal és sárga gumó-szinttel (R_1^{g-h}). Öböl üledék

Рис. 7. Алевритовые глины из приливно-отливной зоны с остатками растений и прослойкой желтых конкреций (R_1^{g-h}). Отложения залива

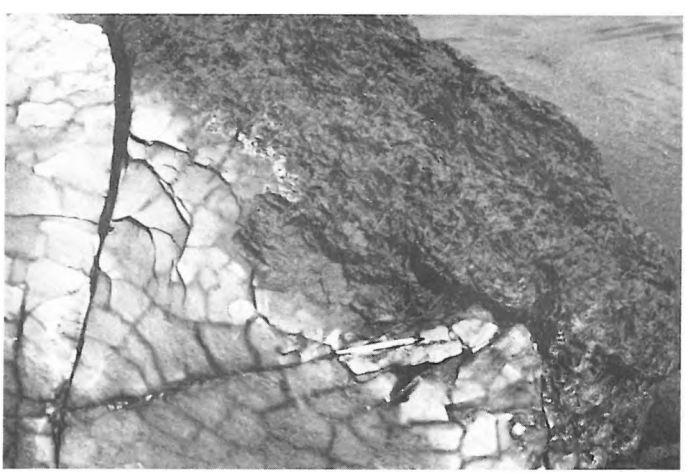

Fig. 6. Contact between embayment cycles. Scoured surface between structureless mudstone (R_1^d unit) and highly burrowed sandstone (R_1^e unit)

6. ábra. Öböl üledékciklusok közötti érintkezés. Kimosási felszín a szerkezet nélküli agyagkő (R_1^d) és az erősen féregnyomos homokkő (R_1^e) között

Рис. 6. Контакт между отдельными циклами осадконакопления залива. Поверхность размыва между неструктурными глинами (R_1^d) и сильно биотурбированными песчаниками (R_1^e)

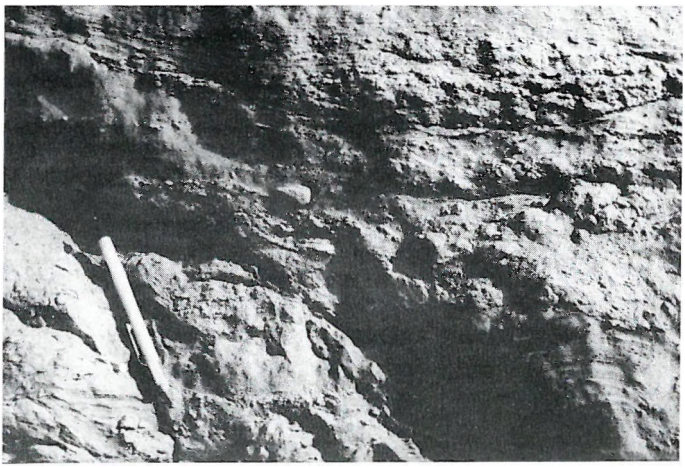

Fig. 8. Run-off channels filled with mudstone clasts (R_1^j) of intertidal zone. Embayment deposit

8. ábra. Iszaptörmelékkel kitöltött elvesztő csatornák (R_1^j) az árapály zónában. Öböl üledék

Рис. 8. Каналы поглощения, заполненные илом (R_1^j) в приливно-отливной зоне. Отложения залива

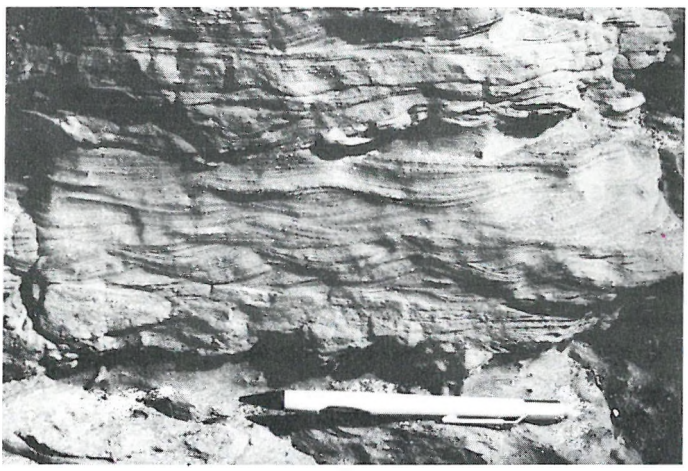

Fig. 9. Current ripples in siltstone (R_1^j). Embayment deposit

9. ábra. Áramlási hullámfodrok aleurolitban (R_1^j). Öböl üledék

Рис. 9. Волноприбойные знаки течения в алевролите. Отложения залива

Fig. 10. Wavy and horizontal lamination in mudstone with root structures (R_1^n) deposited in supratidal salt marsh

10. ábra. Hullámos és vízszintes laminációs árapályöv fölötti sós mocsárban képződött agyagkőben, gyökérnyomokkal (R_1^n)

Рис. 10. Волнистая и горизонтальная ламинация в глинах, образованных в соленом болоте при супратидальных условиях, со следами корней (R_1^n)

numerous small faults and is fairly intensively weathered. This part of the section becomes progressively sandier upward and contains two well-defined concentrations of shells (R_1^q and R_1^s). Similar concentrations occur in the equivalent part of the section to the south at Thornton Beach–the "Upper Gastropod Bed" of ASHLEY [1895]. Because of weathering and solution, intact shells are found only in the lower part of the upper concentration at Fort Funston, although numerous casts and molds attest to the original distribution of the mollusks *(Fig. 12)*.

At Thornton Beach, the lower shell concentration is overlain by gently-inclined, large-scale cross strata in which numerous burrows are evident and which contain shells in their lowermost part. Similar structures are not visible at Fort Funston, perhaps due to the poor quality of exposure at this part of the section. The first of the sandy intervals (R_1^p) above the muddy middle part of R_1 contains plant fragments near its base. Marine microfossils *(Elphidium excavatum*, radiolarians and possible remains of sponges) occur in unit R_1^s (Paula Quinterno, 1983, personal communication).

The uppermost units of subsequence R_1 (R_1^t and R_1^u) are compositionally transitional into the overlying sandy beds of subsequence R_2 (Fig. 12). Both units consist of fine-grained, non-micaceous sand, rich in heavy minerals (which may be responsible for the greenish cast to the sand). The lower unit, R_1^t, is intensely bioturbated and contains somewhat more fine-grained sediment than does the overlying unit. Units R_1^u and R_2^a contain a combination of planar lamination and ripple lamination. These occur in alternating sets in which the base of the planar-laminated sand is sharp and typically marked by a concentration of heavy minerals that diminishes upward within the planar laminations. These units differ slightly, and perhaps significantly, between the two measured section at Fort Funston (Fig. 2). They tend to be muddier and more thoroughly bioturbated in the northern section, and the planar-laminated intervals are thinner and less frequent than in the southern section 40 m away.

Subsequence R_2 consists mostly of fine- to medium-grained, well-sorted, non-micaceous sand in which large scale (> 1 m) crossbeds are common. The subsequence is 14 m thick in the northern section and 17 m thick in the southern section. The basal unit of R_2 at the northern section (R_1^a) contains abundant heavy minerals, resembling somewhat the underlying sand (R_1^u) *(Figs. 12, 13* and *14)*. This distinction could not be found in the southern section. The middle 4 m of unit R_2^b is somewhat mottled, probably by burrowing organisms; this feature could not be found in the more poorly exposed southern section.

The upper part of R_2 contains two somewhat muddy intervals (R_2^c and R_2^d); in the northern section, the lower of these, R_2^c, contains small burrows. In the southern section these units are manifested only as clay intercalations within the sand *(Fig. 15)*. The top units of subsequence R_2 (R_2^d and R_2^e) contain abundant opaque heavy minerals that, in unit R_2^e, defined fine laminations.

Subsequence R_3, about 8 m thick, is lithologically more variable than the underlying subsequence. The lower part of R_3 (units R_3^{a-d}) was identified in both

Fig. 11. Laminated tidal mudstone (R_1^m). Embayment deposit

11. ábra. Árapályövi laminált agyagkő (R_1^m) öböl üledékből

Рис. 11. Ламинированные глины, образованные в зоне прилива. Отложения залива

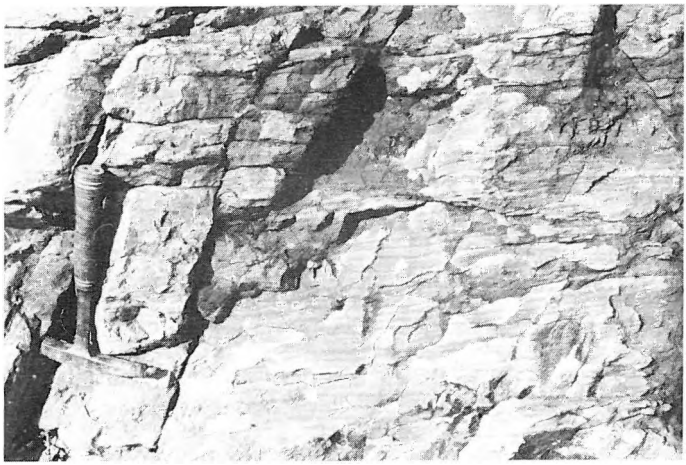

Fig. 13. Low-angle scours in heavy-mineral-bearing cyclic sand. Synsedimentary small-scale faults (lower part) and convolute structure (upper part). Eolian to backshore

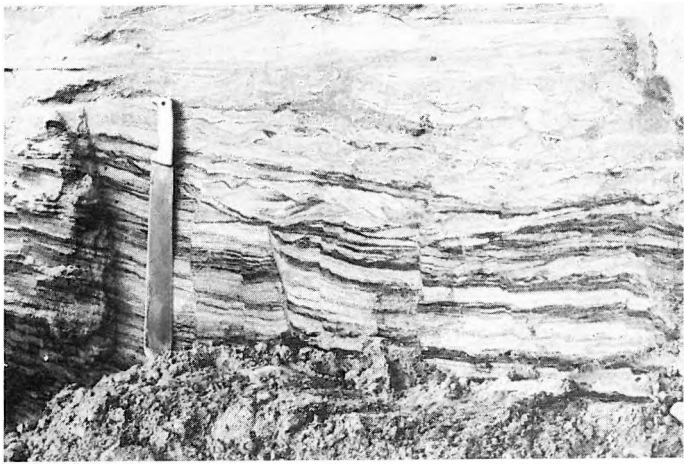

13. ábra. Kis dőlésszögű kimosási felület a nehézásvány tartalmú ciklikus felépítésű homokban, kis méretű, üledékképződéssel egyidejű vetőkkel (alsó rész) és zavart szerkezettel (felső rész). Eolikustól a partszegélyiig

Рис. 13. Пологая поверхность размыва в песчаниках с большим содержанием тяжелой фракации, с небольшими сбросами синседиментационного характера (нижняя часть) и конволютной структурой (верхняя часть). Отложения от эолого до прибрежного

Fig. 14. Cyclic heavy mineral concentrarion of probable storm origin (R_2^a). Climbing-ripples (lower unit) and wave ripples (upper part) between major heavy mineral beds

14. ábra. Ciklikus felépítésű, valószínűleg vihar eredetű nehézásvány koncentráció (R_2^a). Fölfelé vándorló (alsó egység) és hullámzás eredetű hullámfodrok (felső rész) a főbb nehézásvány tartalmú rétegek között

Рис. 14. Скопление тяжелых минералов, возникшее, вероятно, в результате бури, с циклическим строением (R_2^a). Волноприбойные знаки, мигрирующие вверх (нижняя часть) или возникшие в результате воздействия волн (верхняя часть), наблюдающиеся среди основных толщ

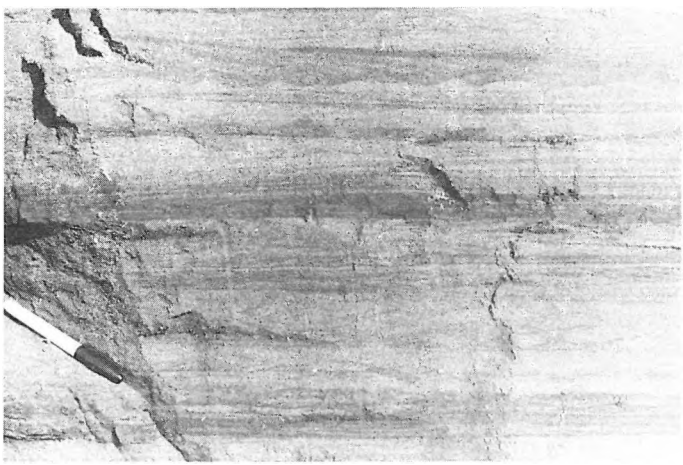

the northern and southern sections; the upper part was examined only in the northern section.

The lower two units (R_3^a and R_3^b) differ somewhat between the two sections. In the southern section these units are primarily mudstone with some sand intercalations; root structures and plant remains are more abundant, and much of the sediment is well-bedded (flat lamination defined by alternating layers of mud and fine sand). In the northern section these units are thinner, more sandy, and display fewer sedimentary structures.

The thickest unit, R_3^d, in the subsequence consists primarily of medium-grained, non-micaceous sandstone. Stratification for the most part is obscure at best, although heavy mineral lamination occurs in the upper part of the unit. Small yellow-brown nodules locally concentrated in the unit consist mostly of equal amounts of montmorillonite (34%) and quartz (34%), and lesser amounts of plagioclase (18%) and potassium feldspar (László Farkas, 1983, personal communication). Two small paleo-channels, up to a meter deep, are visible in the central part of the unit. The smaller is 1.5 m wide, whereas the larger one can be traced for more than 10 m before the exposure is lost. Both channels are best defined where they are deepest and lose their definition laterally as the contact rises within the unit. Both channels are filled with sand that, near its base, has strata that appear to be deformed and broken by soft-sediment deformation.

Near the top of subsequence R_3, vertical cylindrical structures of slightly different color (gray-brown) and induration are abundant, and may represent some type of root structure. The subsequence is capped by a thin gray silty clay (R_3^q) that is truncated to the north along an overlying erosional surface *(Fig. 16)*. Although this clay superficially resembles an ash bed, X-ray diffraction analysis shows that it is a sediment mineralogically similar to the other sample analyzed (László Farkas, 1983, personal communication). Unit R_3^q appears to be a marine or brackish-water deposit; a sample contained one specimen of the microfossil *Buliminella elongatissima* (Paula Quinterno, 1983, personal communication).

Subsequence R_4, 2.5 m thick, grades from pebbly sandstone (R_4^a) into a pebbly sandy mudstone (R_4^b). Unit R_4^a is mostly a light brown medium- to coarse-grained sandstone (Fig. 16) that contains abundant subangular to subrounded pebbles up to 10 cm in diameter. The sand is non-micaceous and contains no evident concentrations of heavy minerals. The pebbles, mostly a mixture of chert and sandstone clasts, appear to be derived entirely from local Franciscan Formation sources. The abundance of the gravel is laterally variable. At one place it composes nearly the entire unit *(Fig. 17)*, whereas 50 m to the south it occurs only in scattered lenses 15–20 cm thick (Fig. 16). The base of the unit is an erosional surface of up to 30 cm of relief. Where sand lies at the base, the contact is not easily discernible.

The upper unit, R_4^b *(Figs. 16, 18, 19* and *20)*, is greatly disrupted by large borings (10 cm or more in cross-dimension and as much as 40 cm deep) that are

Fig. 12. "Upper Gastropod Bed" of Ashley [1895] (mudstone at the bottom — R_1^s), migrating tidal channel fill (middle part — R_1^t), and sand of eolian to backshore (at the top — R_2^a)

12. ábra. Ashley [1895] féle „Felső gastropoda réteg" (a kép alján agyagkő — R_1^s), migráló árapály-csatorna kitöltés (középső rész — R_1^t) és az eolikustól a partszegélyig (backshore) terjedő homok (felső rész – R_2^a)

Рис. 12. «Верхний гастроподовый слой» [Ashley 1895] (внизу — аргиллит R_1^s), отложения, заполняющие мигрирующий приливно-отливный канал (средняя часть — R_1^t), и пески с характером, меняющимся от эолового до прибрежного (верхняя часть — R_2^a)

Fig. 15. Wavy mud laminae in well-sorted fine-grained sand deposited in a lacustrine environment

15. ábra. Hullámos iszap réteg a jól osztályozott, finom szemcsejű tavi homokban

Рис. 15. Прослойки волнистых илов в хорошо сортированных тонкозернистых озерных песках

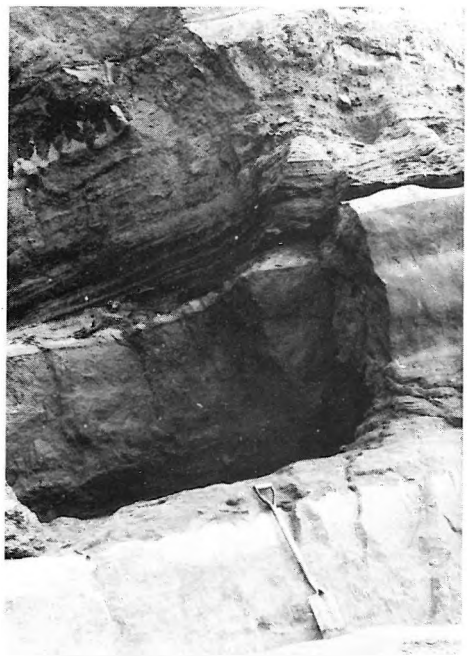

Fig. 16. Paleosol with uneven scour (lower half — R_3^f), flat to lenticular bedding, fluvial sand and gravel with small-scale crossbedding (R_4^a) and large-scale burrows at the top (R_4^b)

16. ábra. Egyenetlen kimosási felületű őstalaj (a kép alsó felén — R_3^f), lapos és lencsés rétegzésű folyóvízi homok és kavics, kis méretű keresztrétegzéssel (R_4^a) és a tetején nagy méretű féregnyomokkal (R_4^b)

Рис. 16. Ископаемый грунт с неровной поверхностью размыва (внизу – R_3^f), речные пески и гальки с пологой и линзовой, а также, в незначительной мере, и косой слоистостью (R_4^a),вверху с большой биотурбацией (R_4^b)

Fig. 17. Two cycles of graded fluvial gravel (R_4^a) located 30 m from the site in Fig. 16

17. ábra. Két, osztályozott rétegződést mutató folyóvízi kavics ciklus (R_4^a) a 16. ábrán jelölt ponttól 30 m-nyire

Рис. 17. Два цикла образования речных галек с градацией (R_4^a) находится в 30 метрах от точки на рис. 16

Fig. 18. Borings by large clams in pebbly sand (R_4^b). The upper boundary between the R_4^b unit and the micaceous sand of the new transgression is completely disrupted by clams

18. ábra. Nagy testű fúrókagylók által létrehozott járatok a kavicsos homokban (R_4^b). Az R_4^b és új transzgresszió csillámos homokja közötti határt a kagylók teljesen elroncsolták

Рис. 18. Биотурбации возникшие в результате жизне деятельности больших моллюсков, в галечных песках (R_4^b). Контакт между R_4^b и слюдяными песками новой трансгрессии был уничтожен полностью

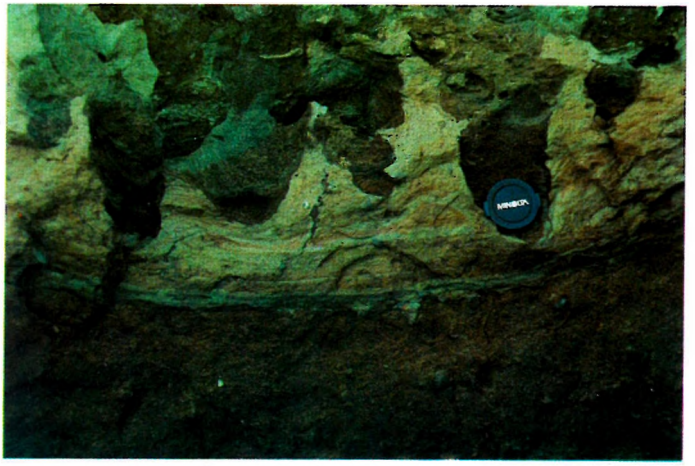

Fig. 19. A detail of the previous picture showing the secondary discoloring of pebbly sand

19. ábra. Az előző kép részlete, amely a kavicsos homok másodlagos elszíneződését jelzi

Рис. 19. Фрагмент предыдущей картины, на котором наблюдается вторичная окраска галечных песков

Fig. 20. General view of subsequences R_4 and S_1 (sandstone with mudstone intercalations)

20. ábra. Az R_4 és az S_1 tagozat áttekintő képe (homokkő, agyagkő betelepüléssel)

Рис. 20. Обзорный вид подгруппы слоев R_4 и S_1 (с прослойками песчаников и глин)

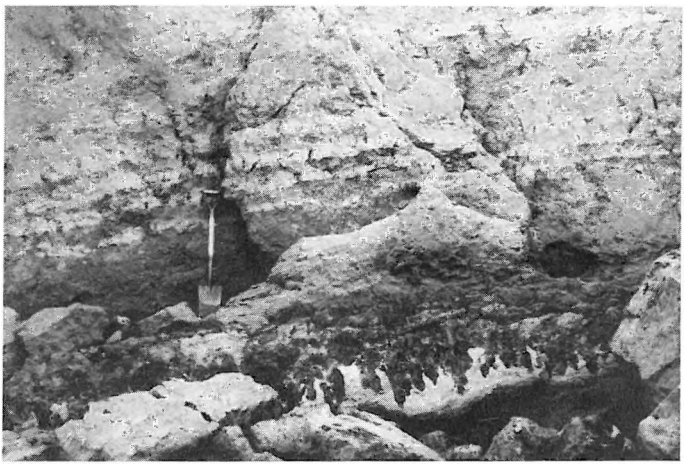

Fig. 22. Load structures of vertebrate footprints in intertidal embayment sand (S_3^b bed)

22. ábra. Gerinces lábnyomának terhelési szerkezete öbölbeli árapályövi homokban (S_3^b réteg)

Рис. 22. Приливно-отливные пески залива со структурами нагрузки от следов позвоночных (слой S_3^b)

Fig. 23. Footprints on bedding surface of an intertidal embayment sand bed. Bilobate structures are interpreted to be hoofprints of split-hoofed ungulates

23. ábra. Lábnyomok az öbölbeli árapályövi homokréteg felszínén. A ceruza hasított körmű patás lábnyomára mutat

Рис. 23. Следы животных на поверхности слоя песков приливно-отливного генезиса. Карандаш показывает на след парнокопытного животного

filled by sand from the overlying unit (S_1^a). Although the upper contact of R_4^b is much obscured by this biogenic mixing, the two types of sediment can be distinguished, primarily by their mica content. The sand in unit R_4^b is nonmicaceous, whereas the overlying sandstone contains abundant mica. The top of unit R_4^b locally is marked by a limonitic stain (Fig. 18). A few of the borings conform to the shape of large bivalves at their base, and the molds of smaller (4 cm) clams are present in the mixed sediment. No microfossils could be found in the mudstone of unit R_4^b (Paula Quinterno, 1983, personal communication).

Sequence S

The upper sequence in our section, sequence *S*, is only 8 m thick. It consists of two subsequences present everywhere plus a third one locally present at the top. The lower subsequence, S_1, is slightly more than 3 m thick *(Figs. 20* and *24)* and consists primarily of structureless, medium- to fine-grained sandstone. A few small scattered pebbles of Franciscan lithology occur at the base and in the middle of the unit (S_1^a). In the lower part of the unit a series of four mudstone layers, 4–15 cm thick, are intercalated with the sandstone *(Fig. 21)*. Numerous circular tubes, that may resemble *Ophiomorpha* and *Thalassanoides*, mostly 1–2 cm in diameter and filled with sand, are visible within the mud layers and indicate the highly bioturbated nature of the unit. Bivalve molds and *Ophiomorpha*-like trace fossils occur near the top of the unit.

The overlying subsequence, S_2, consists mostly of fine- to medium-grained micaceous sandstone *(Fig. 24)* that locally is silty. In general, it is well-bedded, although biogenic structures are abundant.

One unit, S_2^b, is marked by much deformational structure *(Fig. 22)*. The origin of the deformation is evident on a bedding plane surface which is presently exposed on the beach. There, on fresh exposure, the footprints of numerous mammals [Van der Lingen – Andrews 1969], including split-hoofed ungulates and canids, can be seen *(Fig. 23)*. This surface, unfortunately, almost certainly will be lost by erosion within a few years.

The upper part of subsequence S_2, especially units S_2^b and S_2^c, is marked by numerous vertical tubes, 3–6 mm in diameter. Unit S_2^d contains sand with abundant heavy minerals; parallel lamination and climbing ripple structures typical of eolian processes are also present in this unit [Hunter et al. 1984].

Near the top of subsequence S_2 is a distinctive white ash bed, up to 40 cm thick *(Figs. 24, 25* and *26)*, that has been the subject of much study [Meyer et al. 1980, Sarna-Wojcicki et al. in press]. The relative purity of the ash implies an air-fall accumulation. At its top the ash is locally reworked, and climbing adhesion-ripple structures (Fig. 25) composed of ash are present [Hunter et al. 1984].

The part of subsequence S_2 above the ash bed consists of sand up to 2 m thick. The lower part of this sand contains reworked volcanic ash and structures formed by wind ripples. A subtle erosional surface exists a few tens of centimeters above the ash bed. U-shaped tubular burrows extend into the sediment

below this erosion surface, and, where the surface approaches the ash bed, the burrows extend into the ash (Fig. 26). Such burrows, which are filled with sand from the overlying bed, are particularly striking in their contrast to the surrounding ash. In outcrops high on the bluff, subsequence S_2 is overlain by subsequence S_3, a lens of indistinctly stratified mud or mudstone as thick as 0.5 m. Subsequence S_3 is missing at beach level.

A pronounced erosional surface overlain by gravel *(Fig. 27)* caps sequence *S*. Above this surface lies pebbly sandstone assigned to sequence *T* by HUNTER and CLIFTON [1982] and HUNTER et al. [1984].

4. Environmental interpretation

The depositional environments represented within this section *(Fig. 28)* are mostly those of embayments and nonmarine settings. Open marine facies (foreshore, nearshore and shelf) that occur in abundance elsewhere in the Merced [HUNTER et al. 1984] are absent.

Subsequence R_1 consists mostly of the deposits of coastal embayments. The lower part of the unit consists of two fining-upward successions, R_1^{a-d} and R_1^{e-o}. The base of both successions is marked by lag deposits (shells in $R_1^{a,b}$ and wood fragments in R_1^e). Both successions are interpreted to have resulted from the lateral migration of ancient tidal channels and closely resemble those inferred from the study of modern tidal embayments [CLIFTON–PHILLIPS 1980]. The structureless or laminated mudstone (R_1^d), and the units with small channels and climbing ripples ($R_1^{j,k}$) are interpreted as intertidal flats. The rooted laminated mud (R_1^{l-n}) closely resembles that produced on modern supratidal flats above the influence of normal astronomical tides [CLIFTON–PHILLIPS 1980].

The upper part of subsequence R_1 cannot be so clearly interpreted where we measured this section. To the south, however, this part of the section (which contains the "Upper Gastropod Bed") is also clearly composed of shallowing-upward tidal channel-flat sequences. Unit R_1^i is characterized by gently inclined cross-strata and much burrowing, suggesting that it also represents the fill of a migrating tidal channel. The uppermost unit of subsequence $R_1(R_1^u)$ and the lowermost unit of subsequence $R_2(R_2^a)$ are particularly puzzling. Alternations of planar-laminated and ripple-laminated sandstone, in which the basal part of the planar-laminated sand is marked by concentration of heavy minerals, suggest that this unit possibly represents the overwash of storms into a lagoonal tide flat. The lateral variability of these two units suggests the postulated storm overwash was of rather local extent.

Subsequence R_2 is interpreted to be mostly of eolian origin. The large-scale crossbedding suggests migrating sand dunes. The clay-rich intercalations in the vicinity of units R_2^c and R_2^d may represent interdune ponds. The burrowing associated with these units (which may to a large extent be due to insects) suggest that the water table stood fairly high at this time.

Fig. 21. Alternating bioturbated sand and mudstone beds (lower part of S_1^a). *Ophiomorpha*-type burrows, among others

21. ábra. Életnyomos homok és agyag rétegek váltakozása (az S_1^a alsó része), többek között *Ophiomorpha* típusú járatokkal

Рис. 21. Чередование слоев биотурбированных песков (нижняя часть S_1^a) с различными биотурбациями (например, *Ophiomorpha*)

Fig. 24. General view of bioturbated embayment sandstone with mudstone intercalations (lower half of the picture — subsequence S_1) and well-bedded intertidal and supratidal sand (subsequence S_2) capped with white volcanic ash bed (S_2^v)

24. ábra. Az agyagkő betelepüléses életnyomos öbölbéli homokkő (a kép alsó fele — S_1 tagozat) és a jól rétegzett, fehér vulkáni hamu réteggel (S_2^v tagozat) záruló árapályövi és efölötti homok (S_2) áttekintő képe

Рис. 24. Обзорный вид биотурбированных заливных песчаников с прослойкой глин (нижняя часть картины — подгруппа слоев S_1) и интра- и супратидальной серии песков подгруппа слоев (S_2), содержащихся в белом вулканическом пепле с хорошей слоистостью (S_2^v).

Fig. 25. White ash bed of air-fall accumulation — S_2^v and reworked ash laminae. Climbing adhesion ripples in the first lamina directly above the main ash body. The upper third of the ash bed is mixed with other sediments

25. ábra. A levegőből hullott fehér vulkáni hamu réteg — S_2^v és áthalmozott hamu laminák. A vándorló adhéziós hullámfodrok közvetlenül a fő hamu réteg fölötti első laminán láthatók. A hamu réteg felső harmada egyéb üledékekkel keveredett

Рис. 25. Белые вулканические пеплы, выпавшие из воздуха — S_2^v, и переотложенные ламины пепла. Мигрирующие адгезионные волноприбойные знаки видны на первой ламине непосредственно над основным слоем пепла. Верхняя треть слоя пепла перемешана с другими осадками

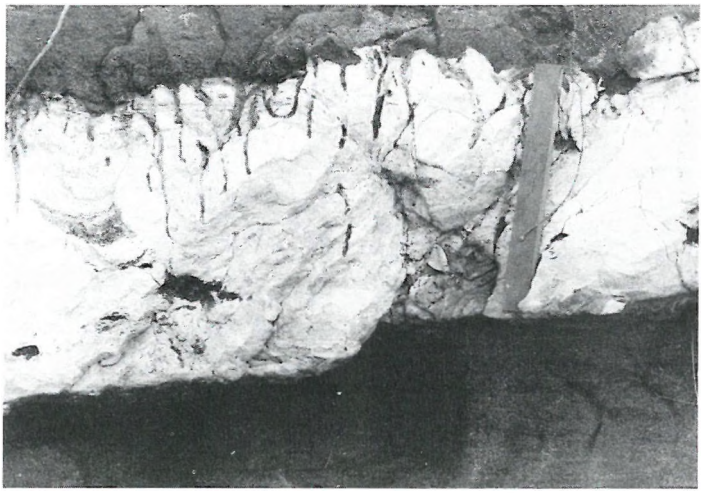

Fig. 26. Vertical borings (or burrows) and a U-tube in ash bed (S_2^e) filled by sand from the overlying bed

26. ábra. Vertikális fúrási nyomok és egy U-cső a vulkáni hamurétegben (S_2^e), amelyet a fedőből származó homok tölt ki

Рис. 26. Следы вертикальной биотурбации и одна U-образная трубка, заполненная песками кровли в слое вулканических пеплов (S_2^e)

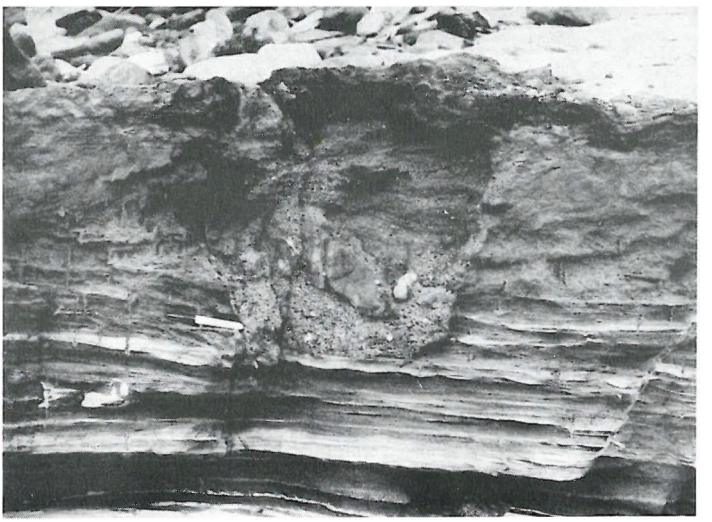

Fig. 27. Erosional surface above the ash bed capped by pebbly sand of a new transgression

27. ábra. Eróziós felszín egy új transzgesszió kavicsos homokrétegével záruló hamuréteg fölött

Рис. 27. Эрозионная поверхность над слоем пепла, заключенная в галечных песках новой трансгрессии

Subsequence R_3 seems to have been deposited mostly under nonmarine conditions. Paleosols are present and root structures occur at the base (R_3^a) and in the upper part (in units R_3^{g-f}). Thin channel-fills (unit R_3^e) above erosional surfaces suggest subaqueous deposition for part of the subsequence. The thin fine-grained layer at the top of subsequence R_3 (unit R_3^g) contains at least one specimen of a foraminiferal species that suggests a renewed incursion of the sea.

Subsequence R_4 appears to be a fluvial deposit derived from the local Franciscan Formation. The fine material of unit R_4^b may be part of a fining-upward continuation of the underlying bed, but its iron content somewhat reduced, possibly as a consequence of the subsequent transgression.

Sequence S records a new transgression of the sea. Subsequence S_1 is interpreted to be an embayment (probably tidal channel to tidal flat) deposit that developed atop the fluvial deposits of subsequence R_4. Bivalves living in the mud at the base of this embayment contributed to a mixing of sediment of the two subsequences at their interface

The filling of the embayment represented by S_1 resulted in the development of intertidal or supratidal flats on which Pleistocene mammals left their footprints. Shortly thereafter an ashfall occurred, probably over a subaerial depositional surface. Not long after the deposition of the ash a new major transgression of the sea began. The first effects of this incursion may be recorded by the return to wet conditions, indicated by the "U-shaped" burrows in the uppermost part of subsequence S_2, and by the deposition of fresh-water or estuarine mud of subsequence S_3. The full onset of the transgression is recorded by the erosional surface that terminates sequence S.

5. Correlative beds in area south of Fort Funston

Sequences R and S can be traced for 2 km along the coast south of the Fort Funston area *(Fig. 29)*. Their extent, which is more than twice as long as any other part of the Merced Formation, results from the two sequences being exposed in a wide structural terrace, where the beds are nearly horizontal. The underlying and overlying beds, in contrast, are exposed in oblique sections across monoclines, where the beds dip relatively steeply, or in relatively narrow structural terraces. Because sequences R and S can be traced so far, lateral facies changes are better known in these two sequences than in the rest of the Merced Formation.

Outcrops of sequences R and S are found both in the head scarp of the large landslide that occurs in the structural terrace and in the sea cliffs that have been cut in the landslide mass. Unfortunately, the head scarp and the sea cliffs are only 0.2 km apart, not far enough to furnish much information on facies changes in a direction perpendicular to the shoreline. Although certain changes in thickness and character of the subdivisions of sequences R and S can be noted along the 2-km-long stretch of outcrops, the beds are more notable for their

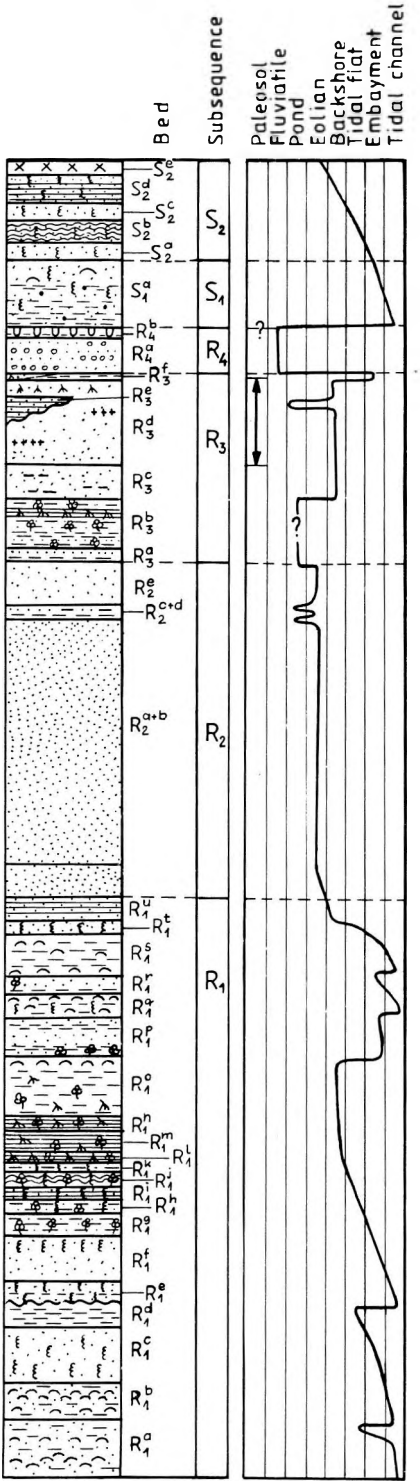

Fig. 28. Environmental interpretation of the Fort Funston section

28. ábra. A Fort Funston-i szelvény környezeti értelmezése

Рис. 28. Интерпретация окрестности разреза местности Форт Фанстон

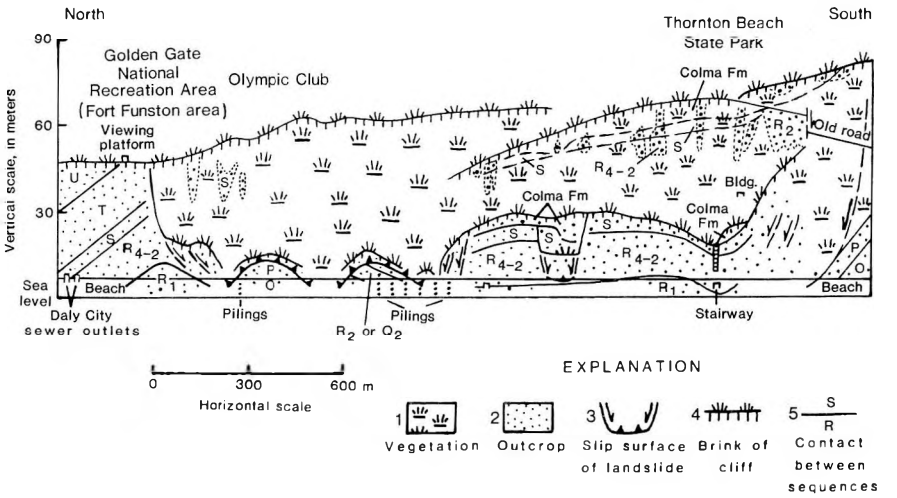

Fig. 29. Profile of coastal cliffs between Thornton Beach State Park and Fort Funston area of Golden Gate National Recreation Area. Profile is viewed looking eastward

29. ábra. A Golden Gate üdülőkörzetbeli Thornton Beach Állami Park és Fort Funston közötti parmenti szelvény, Ny-felől (az óceán felől) nézve

1 – növényzet; 2 – kibúvás; 3– csúszási felület; 4 – lejtőperem; 5 – rétegcsoportok közötti határ

Рис. 29. Разрез между местностью Форт Фанстон и Государственным Парком Торнтон Бич (курортный район Голдэн Гейт) с запада (со стороны океана)

1 — вегетация; 2 — обнажения; 3 — поверхность скольжения; 4 — край склона; 5 — ганица между группами слоев

relative uniformity than for their variations *(Fig. 30)*. The most notable lateral change is a local thickening of muddy embayment deposits, here assigned to subsequence S_1, in the northwest corner of the Olympic Club, a country club just south of Fort Funston. Subsequence S_1, which is 3.4–6.7 m thick in outcrops to the north and south, is 13–15 m thick in the Olympic Club outcrop. In this outcrop subsequence S_1 erosionally overlies crossbedded eolian sand of subsequence R_2 and gradationally underlies poorly exposed sand of subsequence S_2; no outcrop of the volcanic ash bed in subsequence S_2 was found here. It is not clear whether the unusually great thickness of subsequence S_1 in the Olympic Club outcrop is due to (i) a facies change from the sand of subsequence S_2 into mud; (ii) a facies change from the gravel, sand, and paleosols of subsequences R_4 and R_3 into mud; or (iii) the cutting of a channel into sequence R, followed by the deposition of a muddy channel fill.

Another noteworthy lateral change in the 2-km-long stretch of coast is significant variation in the thickness of subsequence R_4, the alluvial sand, gravel, and mud at the top of sequence R. This unit is locally absent but, where present, may attain a thickness of 6 m. It tends to be thicker adjacent to the Olympic Club. This, together with the fact that a marine or brackish-water

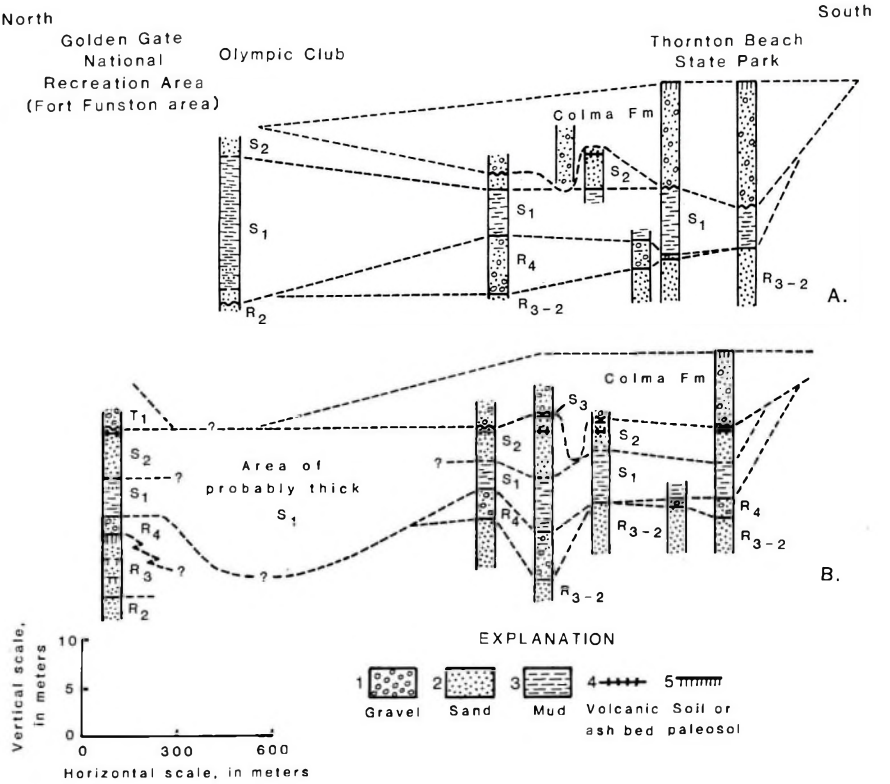

Fig. 30. Stratigraphic cross sections of part of the Merced Formation (upper part of sequence *R* and sequence *S*) and Colma Formation between Thornton Beach State Park and Fort Funston area of Golden Gate National Recreation Area. A) Cross section along head scarp of landslide, B) Cross section along sea cliffs

30. ábra. A Merced Formáció egy (az *R* és az *S* rétegcsoport felső) részének és a Colma Formáció rétegtani szelvénye a Golden Gate üdülő körzetbeli Thornton Beach Állami Park és Fort Funston között. A) Szelvény a földcsuszamlás peremén, B) Szelvény a meredek partvonal alsó részén

1 – kavics; 2 – homok; 3 – iszap; 4 – vulkáni hamu réteg; 5 – talaj, vagy őstalaj

Рис. 30. Стратиграфическая сводка части Формации Мерсед (группы слоев *R* и *S* — верхняя часть) и формации Колма по обнажениям от Государственного Парка Торнтон Бич до местности Форт Фанстон. А) Разрез по краю оползня, В) Разрез по низу крутого берега

1 — гапьки; 2 — пески; 3 — илы; 4 — вулканические иеилы; 5 — грунты или палеогрунтю

microfossil was found in a thin mud bed (unit R_3^q) at the base of subsequence R_4 at Fort Funston, suggests that the unit may be an estuary-bordering alluvial-apron deposit that intertongues with the thick embayment mud (subsequence S_1) in the Olympic Club outcrop. Even if there is no intertonguing between subsequences R_4 and S_1, both units may thicken toward the same paleovalley.

Still another noteworthy change is the variation in the thickness of the volcanic ash bed in subsequence S_2. Although locally absent, the air-fall part of the ash bed can be as thick as 0.3 m. The air-fall ash is locally overlain by reworked ash and interbedded sand as thick as 2 m. Sedimentary structures indicate that in places the reworked ash was deposited on dry to moist eolian sand flats; where the reworked ash is thickest, however, the environment was subaqueous, probably a shallow lake, marine embayment, or stream.

The Merced Formation in the 2-km-long structural terrace is overlain by the Colma Formation, which in this area consists mostly of backshore sand and pebbly sand, with a thin interval of beach sand and gravel locally at its base. The youngest unit beneath the Colma is subsequence S_3, a thin mud that occurs at Fort Funston and at a few places between Fort Funston and Thornton Beach. Locally the erosion surface at the base of the Colma cuts as much as 7 m deep into the top of subsequence S_1. In its coastal outcrops the Colma pinches out toward both the north end and the south end of the structural terrace.

6. Conclusions

The depositional history of the section we describe differs from that of the progradational sequences present in most of the Merced Formation [HUNTER et al. 1984]. In those largely progradational sequences, transgressive intervals are represented primarily by erosional surfaces overlain by a thin lag deposit of gravel. The section presented here records transgressive intervals in much greater detail. The lower part of the section (subsequence R_1) records a transgression that appears to have occurred in a series of steps, each marked by a shallowing-upward sequence of a migrating tidal channel or filling embayment. Apparent steps may result in part from the effects of migrating channels during continuous, relatively uniform transgression.

Subsequences R_2, R_3 and R_4 were mostly deposited under eolian or other nonmarine conditions, probably during a regression of the sea. A short-lived minor transgression is suggested by the microfossil in unit R_3^q, and subsequence R_4 may have formed during the initial stage of the transgression that led to the deposition of sequence S.

A new and more pronounced transgression is recorded by the embayment (tidal channel-flat) facies in subsequence S_1. An ensuing stable shoreline or possibly limited regression is indicated by the nonmarine deposits (S_2^{b-e}) that overlie this deposit. The beginnings of a new transgression are suggested by the presence of U-shaped burrows in sand above the ash bed, near the top of sequence S, and by the mud (subsequence S_3) that locally caps the sequence.

A subsequent significant transgression eroded the upper part of sequence S and deposited nearshore sand and gravel of sequence T on the erosional surface [HUNTER et al. 1984].

It cannot presently be established whether the fluctuations in sea level were caused by eustatic changes, tectonic effects, or some combination of the two processes.

REFERENCES

ADDICOTT W. O. 1969: Late Pliocene mollusks from San Francisco Peninsula, California and their paleogeographic significance. Proceedings of the California Academy of Sciences, Fourth series, **37**, 3, pp. 57–93

ASHLEY G. H. 1895: The Neocene (sic) of the Santa Cruz Mountains. I-Stratigraphy. Proceedings of the California Academy of Sciences, Second series, 5, pp. 273–367 (reprinted in Stanford Univ. Publs. Geol. Paleontol., no 1.)

CLIFTON H. E. 1982: Estuarine deposits. In SCHOLLE P. A., SPEARING D. eds.: Sandstone depositional environments. Am. Assoc. Petroleum Geologist Mem. 31, pp. 179–189

CLIFTON H. E., STAGG J. in preparation: Lithofacies in the Merced Formation in sea cliff exposures north of Wood Gulch. U. S. Geological Survey Open-file Report

GLEN W. 1959: Pliocene and lower Pleistocene of the western part of the San Francisco Peninsula. University of California. Publications in Geological Sciences, 36, pp. 147–198

HALL N. T. 1965/a: Petrology of the type Merced Group, San Francisco Peninsula, California. Unpublished M. A. thesis, University of California, Berkeley, 126 p.

HALL N. T. 1965/b: Late Cenozoic stratigraphy between Mussel Rock and Fleishhacker Zoo, San Francisco Peninsula. In Guidebook for field conference I., northern Great Basin and California., 7th INQUA Congress. pp. 151–158

HALL N. T. 1966: Fleishhacker Zoo to Mussel Rock (Merced Formation)—A Plio–Pleistocene nature walk. California Div. Mines and Geology Mineral Information Service, **19**, 11, pp. 522–525

HUNTER R. E., CLIFTON H. E. 1982: Description of beds exposed at Fort Funstone, Golden Gate National Recreation Area, nortwestern San Francisco Peninsula, California. U. S. Geological Survey Open-file Report, No 82–1055

HUNTER R. E., CLIFTON H. E., HALL N. T., CSÁSZÁR G., RICHMOND B. M., CHIN J. L. 1984: Pliocene and Pleistocene coastal and shelf deposits of the Merced Formation and associated beds, northwestern San Francisco Peninsula, California. SEPM Field Tripe Guidebook No. 3. 1984 Midyear Meeting

LAWSON A. C. 1893: The post-Pliocene diastrophism of the coast of southern California. University of California, Department of Geological Sciences, Bull. 1, pp. 115–160

MEYER C. E., WOODWARD M. J., SARNA-WOJCICKI A. M., NAESER C. W. 1980: Zircon fission-track age of 0.45 million years on ash in the type section of the Merced Formation, west-central California. U. S. Geological Survey Open-file Report No. 80–1071, 52 p.

SARNA-WOJCICKI A. M. 1976: Correlation of late Cenozoic tuffs in the central Coast Ranges of California by means of trace- and minor-element chemistry. U. S. Geological Survey. Prof. Paper 972, 30 p.

SARNA-WOJCICKI A. M., MEYER C. E., BOWMAN H. R., HALL N. T., RUSSELL P. C., WOODWARD M. J., SLATE J. L. in press: Correlation of the Rockland ash bed, a 400,000 year-old stratigraphic marker in northern California and western Nevada, and implications for mid-Pleistocene paleogeography of central California. Quat. Geol.

VAN DER LINGEN G. J., ANDREWS P. B. 1969: Hoofprint structures in beach sand. Jour. Sed. Petrology **39**, pp. 350–357

PART MENTI PLEISZTOCÉN RÉTEGSOR A KALIFORNIAI GOLDEN GATE ÜDÜLŐ KÖRZETBŐL

CSÁSZÁR Géza, H. Edward CLIFTON és Ralph E. HUNTER

A szerzők a San Francisco félsziget jellegzetes self és part menti törmelékes pliocén–pleisztocén képződményének, a Merced Formáció felső, pleisztocén rétegsorának főként terepi makroszkópos megfigyeléseiről adnak számot, de felhasználnak néhány mikrofauna és ásványkőzettani vizsgálati eredményt is. San Franciscótól D-re a Csendes-óceán partján a Szent András törés közelében (1. ábra) 10–60 m magas, meredek, pusztuló falban lévő, többnyire csak kisebb-nagyobb lejtőmenti törmelékfolyásokkal takart feltárás-sorban az É-ra dőlő Merced Formációt egy 2 km hosszú, a partvonallal párhuzamos, ma is élő földcsuszamlás tagolja két szakaszra. Jelen munka a térképmellékleten (1. ábra) jelzett partszakasz É-i részének (a földcsuszamlástól É-ra) részletes leírása mellett a D-i partszakasz legfelső részével való rétegtani azonosságát is igazolja. A Merced Formáció a vizsgált szelvényszakaszban két kiemelkedő jelentőségű marker réteget, a 400 000 éves vékony tufaréteget és az ASHLEY [1895] által „felső gastropoda rétegként" leírt, kagyló és néha csigaházakat tömegesen tartalmazó kőzetlisztes agyagkő réteget tartalmaz.

Változatos üledékképződési környezeteket lehetett elkülöníteni, amelyek az alábbiak: árapály csatorna, árapály síkság, fluviális csatorna, háttéri parti síkság, tó, eolikus dűne. Az üledékképződés általánosított, egyszerűsített menete az alábbi: esztuárium jellegű öböl, eolikus homok, öböl, folyóvízi, öböl, háttéri parti síkság, nyílttengeri partközeli. A rétegsorban gyakoribb a tengeri transzgresszió eredményeként képződött üledék, mint amennyi a Merced Formációban vagy a vele társult rétegekben általánosan ismert. Az egyes üledékképződési környezettípusok jellegzetes képviselőit számos fénykép és a kifejlődések változásait néhány részletes szelvényrajz is szemlélteti.

ПРИБРЕЖНЫЙ РАЗРЕЗ ПЛЕЙСТОЦЕНА В КАЛИФОРНИЙСКОМ КУРОРТНОМ РАЙОНЕ ГОЛДЕН ГЕЙТ

Геза ЧАСАР, Г. Эдвард КЛИФТОН и Ралф Э. ХАНТЕР

Авторы отчитываются главным образом о полевых макроскопических наблюдениях характерного шельфа и прибрежных обломочных плиоцен-плейстоценовых образований Мерседской формации верхней части плейстоценового разреза, но используют также результаты анализов некоторых микрофаун и минералопетрографических исследований.

К югу от Сан Франциско на берегу Тихого океана, вблизи разлома Святого Андрея (рис. 1) в серии обнажений, расположенной в крутой эродированной стене высотой в 10–60 м, в большинстве случаев покрытой коллювиально-делювиальными отложениями, Мерседская формация, падающая на север расчленена на два отрезка живущим и в настоящее время оползнем, параллельным линии берега.

Настоящая работа, кроме детального описания северной части, обозначенной на приложенной карте (рис. 1) берегового отрезка (к северу от оползня), доказывает также его стратиграфическую идентичность с самым верхним отрезком южной берега. Мерседская формация в рассматриваемых частях разреза содержит два маркирующих горизонта, имеющих выдающееся значение, тонкий слой туфа, имеющий возраст 400 000 лет и описанный ASHLEY [1895] как «верхний гастроподовый горизонт» слой супесных алевролитов, содержащий большое количество двустворчатых раковин и гастроподов.

Были выделены разнообразные фации осадконакопления: канал отлива, плоскость отлива, флювиальный канал, фоновая береговая равнина, озеро, эоловые дюны. Упрощенный, обобщенный процесс осадкообразования следующий: залив типа эстуарий, эоловые пески, залив, флювиальные, лагунные, фоновая береговая равнина и прибрежный участок открытого моря. В стратиграфическом разрезе наиболее часто встречаются осадки, образовавшиеся в результате морской трансгрессии, чем известные обычно в Мерседской формации или в связанных с ней слоях.

Отдельные характерные представители типов фаций осадконакопления представлены на многих фотографиях, и изменения развитий показаны на нескольких детальных разрезах.

GEOPHYSICAL TRANSACTIONS 1985
Vol. 31. No. 1–3. pp. 191–203

GEOCHEMICAL ANALYSES OF 12 HUNGARIAN COAL SAMPLES

László G. SOMOS*, Peter ZUBOVIC** and Frederick O. SIMON**

Twelve channel samples of coal collected from coal beds in Hungary were analyzed in the U.S. Geological Survey laboratories. The coal beds are Jurassic (Lias) and Tertiary age and are of lignite to bituminous rank. Unusually high sulfur contents and high organic sulfur concentrations characterize the coal from beds that are of Eocene and Miocene age. The coal and coal ash from coal beds of Lias (Jurassic) age are high in many trace elements. These geochemical data suggest a need for additional coal-quality data to resolve environmental concerns when coal from these coal beds are burned in power plants.

Keywords: geochemistry, coal, environment protection, ultimate analysis, proximate analysis

1. Introduction

The geochemistry of Hungarian coal was investigated under a cooperative agreement between the United States Geological Survey (USGS) and the Hungarian Central Office of Geology. The objectives of this study were: the interlaboratory comparisons of analytical data, increasing geochemical knowledge about Hungarian coal beds, and supplementing the USGS coal data base on world coal quality. Initially, twelve channel samples were sent to the USGS for a variety of analyses as shown in *Fig. 1*. Six additional samples were received by the USGS and are currently being analyzed. This paper reports on the analytical data for the chemical components and physical properties of the first 12 coal samples.

2. Description of coal samples

The location and a partial description of the coal samples are given in *Table I*. The coal beds sampled are Jurassic (Lias) and Tertiary in age and are lignite to bituminous rank. The older coal beds (Jurassic) are bituminous rank; the higher rank of these coal beds is caused in part by the thermal effects produced by intrusions of ultrabasic magmas into the underlying strata during Early Cretaceous time and in part by folding and faulting during Cretaceous time.

The coal samples can be grouped into four chronostratigraphic units. Samples H–11 and H–12 (Table I) are from the Mecsek coal basin in the

* Hungarian Geological Survey, POB 106, Budapest, H–1442
** U.S. Geological Survey, 956 National Center, Reston, VA 22092
Manuscript received: 14 March, 1985

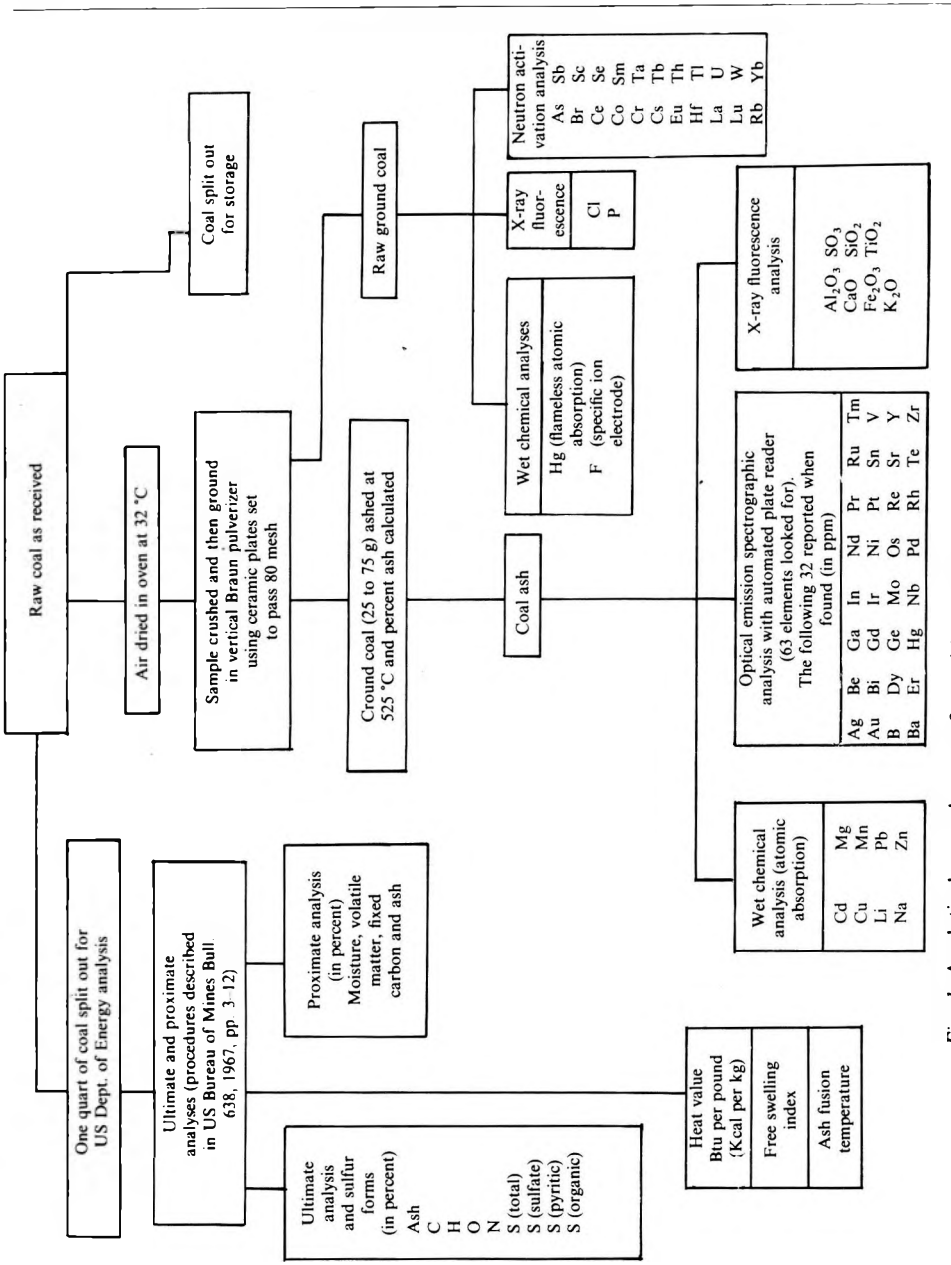

Fig. 1. Analytical procedures performed by USGS on Hungarian coal samples

Hungarian sample No.	USGS sample No.	County	Latitude (N)	Longitude (E)	Coal bed	Age	Rank	Sampled thickness (cm)
H–10	W218560	Komárom	474500	184110	Újebszőny	Eocene	Subbituminous	350.0
H–11	W218561	Baranya	460800	181700	Mecsek	Jurassic	Bituminous	400.0
H–12	W218562	Baranya	460700	181800	Mecsek	Jurassic	Bituminous	800.0
H–13	W218563	Nógrád	480200	195100	Mákvölgy	Miocene	Subbituminous	200.0
H–14	W218564	Heves	475020	200200	Visonta	Pliocene	Lignite	1,000.0
H–15	W218565	Heves	475100	200300	Visonta	Pliocene	Lignite	1,000.0
H–16	W218566	Borsod	481800	202600	Putnok	Miocene	Subbituminous	370.0
H–17	W218567	Komárom	474000	181100	Lencsehegy	Eocene	Subbituminous	400.0
H–18	W218568	Nógrád	480400	195000	Szorospatak	Miocene	Subbituminous	250.0
H–19	W218569	Komárom	474500	184400	Dorog	Eocene	Subbituminous	300.0
H–20	W218570	Komárom	473500	182200	Tatabánya	Eocene	Subbituminous	400.0
H–21	W218571	Fejér	473200	181750	Oroszlány	Eocene	Subbituminous	250.0

Table 1. Descriptions for 12 channel samples of coal from Hungary

1. táblázat. 12 db magyarországi szén résminta leírása

Таблица 1. Описание 12 венгерских бороздовых проб

southern part of the Transdanubian Region. These bituminous coal beds are of Jurassic age and are from the oldest industrial black-coal field in Hungary. The mined coal beds, in underground mines that extend to about 700 meters below the surface, range in thickness from less than 2 meters to 15 meters. The coal from the Mecsek coal basin generally has a high ash content and heating value. The coal beds and enclosing strata were folded and faulted by tectonic activity during Cretaceous time.

The second group samples (H–10, H–17, H–19, H–20 and H–21) are from brown coal (subbituminous) deposits of Eocene age. These deposits are in the central Transdanubian Region of Hungary. The thickness of the mineable coal beds ranges from 2 to 8 meters and the coal is recovered by underground mining techniques. Faulting and erosional features affect the mining/extraction process. The coal beds in this group have ash contents and heating values that range from low to high.

The third group of samples (H–13, H–16 and H–18) are from brown coal deposits of Miocene age. These deposits are located in the north and northeastern part of Hungary and generally consist of 3 to 4 thin coal beds. The coal beds are mined by underground methods and are located 50 to 200 meters below the surface. Coal beds included in this group have low heat values and high ash content.

The fourth group of samples (H–14 and H–15) are from lignite deposits of Pliocene age. These deposits are located in the northern part of the Hungarian lowland region. The coal is recovered by open-pit operation. The thickness of the coal beds ranges from 5 to 50 meters and locally the beds are covered by surficial material as much as 220 meters in thickness. Tectonic effects are not evident in these coal beds. Lignites from these deposits have very low heat values and a very high moisture content. Coal resources in these deposits are believed to be extensive.

3. Discussion of the analytical results

The analytical procedures performed on the coal and coal ash are shown in Fig. 1. Data on individual samples are listed in the tables. Interpretations described in this discussion are tentative because of the small number of samples. *Table II* gives the data on proximate, ultimate, and other analyses which are used to classify coal. Where there are two values given, the numbers on the left are values obtained by Hungarian laboratories for the Hungarian Geological Survey. *Table III* is a comparison of the average values of the data in Table II obtained by USGS laboratories with those obtained by the Hungarian laboratories. In both tables, the largest analytical differences are found in the moisture loss (by air-drying) and organic sulfur determinations. The smallest average percentage differences are found in the total sulfur, ash, moisture- and ash-free heat value, and moisture- and ash-free volatile matter and fixed-carbon determinations. For individual samples, there are large differences for ash and

		Eocene H-10		Lias H-11		Lias H-12		Miocene H-13		Pliocene H-14		Pliocene H-15		Miocene H-16		Eocene H-17		Miocene H-18		Eocene H-19		Eocene H-20		Eocene H-21	
Ash	(R)	34.9	36.1	23.0	15.5	12.2	13.6	15.9	6.6	9.4	16.3	9.4	11.7	20.0	11.4	9.5	26.0	37.0	22.4	5.7	17.8	7.9	5.3	14.5	9.2
	(MF)		40.2		15.9		13.8		8.6		23.0		15.3		15.3		28.7		25.3		19.7		6.0		11.3
	(MAF)																								
Moisture	(R)	13.0	10.3		2.3		1.4	29.8	23.5	51.4	44.5	51.0	49.2		25.6	15.0	9.5	13.3	11.6	15.0	9.7	13.7	12.1	19.5	18.9
	(MF)																								
	(MAF)																								
Organic sulfur	(R)	3.4	2.65		0.95	2.78	1.08		2.42		0.75		0.75		2.58		5.91		0.33	4.7	3.36		2.28		2.97
	(MF)		2.96		0.97		1.10		3.16		1.35		1.48		3.47		6.53		0.37		3.72		2.59		3.66
	(MAF)		4.94		1.16		1.27		3.46		1.91		1.92		4.09		9.16		0.50		4.63		2.76		4.13
Total sulfur	(R)		7.3		2.2	3.14	2.1	3.2	3.2		1.2		0.9	2.0	3.0	7.0	7.3		0.4		8.1		2.5		3.0
	(MF)		8.2		2.2		2.2		4.1		2.2		1.7		4.0		8.0		0.4		9.0		2.9		3.7
	(MAF)		13.7		2.6		2.5		4.5		3.1		2.2		4.7		11.3	0.7	0.6		11.2	4.6	3.1		4.2
Heat value (Kcal/kg)	(R)	3,251	3,330	5,728	6,730	6,768	7,150	3,206	4,720	2,062	2,490	2,010	2,470	3,246	4,110	5,112	4,480	3,198	4,710	5,459	5,040	5,398	6,720	4,377	5,110
	(MF)	3,479	3,710		6,880		7,250		6,170		4,480		4,860		5,530		4,950	3,424	5,330		5,580	5,709	7,130		6,310
	(MAF)	6,671	6,210		8,190		8,410		6,750		6,330		6,310		6,530		6,940	6,888	7,130		6,950	7,280	7,580		7,110
Air-dried loss	(R)	10.5	5.0		1.1		0.5		18.2		37.1		42.5		16.9		5.1		6.5		5.9		5.3		8.9
	(MF)																								
	(MAF)																								
Volatile matter	(R)		27.5		29.3		27.5	27.3	34.7		23.6		22.8		33.0	35.8	36.6	22.9	26.1	37.8	35.0		47.5		40.6
	(MF)	27.8	30.7		29.9		27.9		45.3		42.6		44.9		44.3		40.4		29.6		38.8		54.0		50.0
	(MAF)		51.4	33.0	35.6	31.4	32.4		49.6		60.2		58.3		52.3		56.7		39.6		48.3		57.4		56.4
Fixed carbon	(R)		26.0		53.0		57.5	27.0	35.2		15.6		16.3		30.1	39.7	27.9	26.8	39.9	41.5	37.5		35.2		31.4
	(MF)	24.3	29.1		54.2		58.3		46.0		28.2		32.1		40.4		30.9		45.1		41.5	37.2	40.0		38.7
	(MAF)		48.6		64.4		67.6		50.4		39.8		41.7		47.7		43.3		60.4		51.7		42.6		43.6

Table II. Classification data for 12 Hungarian coal samples (*R*, as received; *MF*, moisture free; *MAF*, moisture and ash free)

II. táblázat. 12 db magyarországi szénminta technológiai jellemzői (*R* = nyerssszén; *MF* = száraz szén; *MAF* = száraz, hamumentes szén)

Таблица II. Технологические характеристики 12 венгерских угольных проб (*R* = сырой уголь, *MF* = обезвоженный уголь, *MAF* = обезвоженно-беззольный уголь)

Determination (content)	HGS	USGS	Difference %
Ash (R)	16.6	16.0	3.7
Moisture (R)	24.6	21.0	17.1
Organic sulfur (R)	3.6	2.4	50.0
Total sulfur (R)	3.8	3.9	2.6
Heat value (R)	4,151	4,718	12.0
(MF)	4,204	5,390	22.0
(MAF)	6,949	6,973	0.3
Air-dried loss	10.5	5.0	110.0
Volatile matter (R)	31.0	33.1	6.3
(MF)	27.8	30.7	9.5
(MAF)	32.2	34.0	5.3
Fixed carbon (R)	33.8	35.1	3.7
(MF)	37.2	40.0	7.0
(MAF)	44.6	47.6	6.3

Table III. Comparison of USGS and Hungarian Geological Survey data for 12 samples of Hungarian coal. Heat value in Kcal/kg, all other data in percent; *R*, as received; *MF*, moisture-free; *MAF*, moisture- and ash-free

III. táblázat. 12 db magyarországi szénmintán a USGS-ben és a MÁFI-ban végzett összehasonlító elemzéseinek eredményei. Fűtőérték Kcal/kg-ban, egyéb adatok százalékos formában; *R* = nyersszén; *MF* = száraz szén; *MAF* = száraz, hamumentes szén

Таблица III. Результаты сравнительных анализов, выполненных в ГСА и ВГИ на 12 венгерских угольных пробах. Теплоотдача в ккал/кг, другие данные в %%; *R* = сырой уголь, *MF* = обезвоженный уголь, *MAF* = обезвоженно-беззольный уголь

total sulfur contents. It is evident from Table II, that a systematic loss of moisture occurred in the coal samples that were shipped to the USGS laboratories. This moisture loss affected other analytical results reported on an "as-received" basis. This effect is evident for heat value and volatile matter (Table III). The differences between data from USGS and Hungarian laboratories are smaller on a moisture- and ash-free basis compared to the "as-received" basis.

An evaluation of these analytical data by chronostratigraphic groups is given in *Table IV*. The results in column 5 ("Composite") are averages of columns 1 through 4. The "Nat. Inv." column gives the average data for ash and heat values of coals enumerated in the Hungarian Annual National Inventory of Coal Reserves. The high ash contents and low heat values in the National Inventory reflect contamination of samples by incorporation of roof and floor rocks during the mining process.

Figure 2 shows the correlation between the heating value and ash + moisture. There are no characteristic differences among the chronostratigraphic groups. By eliminating the moisture, better correlation functions are obtained between ash and heating values as shown in *Figure 3* and the following equations

Pliocene..... Kcal/kg = 77(39–A) (1)

Miocene..... Kcal/kg = 91(54–A) (2)

Eocene ..... Kcal/kg = 63(80–A) (3)
Lias ..... Kcal/kg = 111(76–A) (4)
where A is the percent ash.

Content		Pliocene	Miocene	Eocene	Lias	Composite	Nat. Inv.
Ash	(R)	11.7	18.9	16.7	16.1	16.3	22.9
	(MF)	26.2	20.0	21.2	17.0	19.8	
Moisture	(R)	49.0	20.8	13.7	1.9	20.9	
Organic sulfur	(R)	0.75	1.78	3.61	1.60	2.39	
	(MF)	1.42	2.33	3.89	1.04	2.61	
	(MAF)	1.91	2.68	5.12	1.22	3.33	
Total sulfur	(R)	1.1	2.4	5.9	2.5	3.5	
	(MF)	2.0	2.8	6.4	2.2	4.1	
	(MAF)	2.6	3.3	8.7	2.6	4.9	
Heat value	(R)	2,258	3,865	4,783	6,594	4,435	2,592
	(MF)	4,670	5,113	5,267	7,065	5,386	
	(MAF)	6,320	6,824	6,964	8,300	7,019	
Air-dried loss	(R)	39.8	13.9	6.8	0.8	12.6	
Volatile matter	(R)	23.2	28.8	37.3	28.4	31.8	
	(MF)	43.8	39.7	40.3	28.9	38.9	
	(MAF)	59.3	47.2	54.0	33.1	47.3	
Fixed carbon	(R)	16.0	31.8	34.2	55.3	33.9	
	(MF)	30.2	43.8	34.5	56.3	39.0	
	(MAF)	40.8	52.8	46.0	66.0	50.1	

Table IV. Averages of classification analyses for the different chronostratigraphic groups. Heat value in Kcal/kg, all other values in percent; *R*, as received; *MF*, moisture free; *MAF*, moisture and ash free

IV. táblázat. Különböző korú szenek technológiai elemzésének eredményei. Fűtőérték Kcal/kg-ban, egyéb adatok százalékos formában; *R* = nyersszén; *MF* = száraz szén; *MAF* = száraz, hamumentes szén

Таблица IV. Результаты технологических анализов углей различного возраста. Теплоотдача в ккал/кг, другие данные в %%, *R* = сырой уголь, *MF* = обезвоженный уголь, *MAF* = обезвоженно-беззольный уголь

These functions are important to the evaluation of the level of contamination during mining. One of the principal problems of mining operations is the high contamination rates. According to the National Inventory, planned dilution rates are: Pliocene coal beds, 4%; Miocene coal beds, 6%; Eocene coal beds, 5%; and Lias coal beds, 18%. Real dilution rates can be obtained by using values in Figure 3 and equations 1–4 for real heating values (Lias, 4783 Kcal/kg;

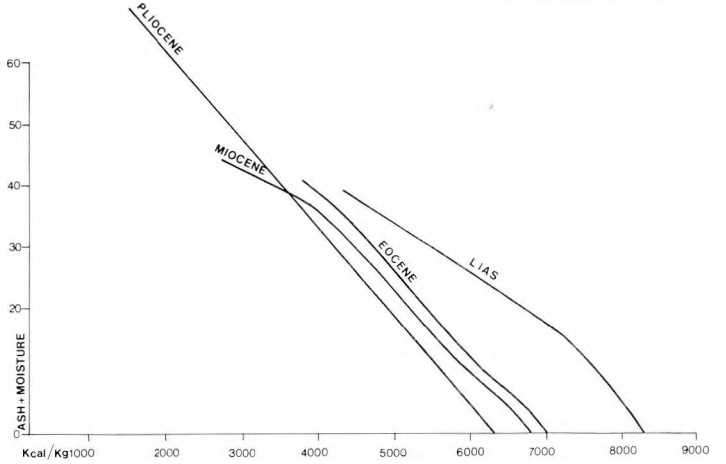

Fig. 2. Ash + moisture—heating value relationship

2. ábra. Hamu + nedvesség — fűtőérték függvény

Рис. 2. Зависимость: зольность + влажность — теплоотдача

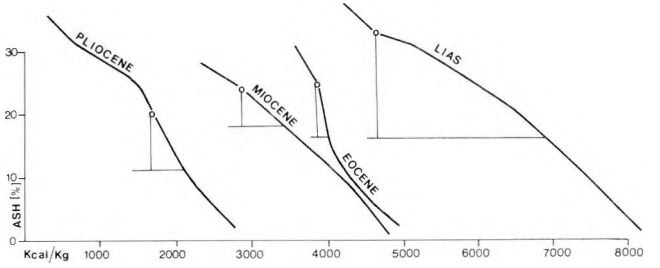

Fig. 3. Ash—heat value relationship

3. ábra. Hamu — fűtőérték függvény

Рис. 3. Зависимость: зольность — теплоотдача

Eocene, 3916 Kcal/kg; Miocene, 2908 Kcal/kg; and Pliocene, 1963 Kcal/kg). Comparison of the real and planned contamination rates for coal beds of Pliocene and Eocene age shows higher dilution rates than expected in the National Inventory:

Age	% Ash*
Pliocene	13.5
Miocene	22.0
Eocene	17.8
Lias	32.9

* Calculated from Equations 1–4.

Figure 4 shows the relation between total sulfur and heat values; these relations are important to making decisions about the environmental consequences of coal mining. The coal beds of Eocene age are very high in sulfur and the data indicate that the sulfur content increases as the heating value rises. Hence measures should be implemented to control sulfur emission when these coals are used in power plants.

Table V shows the major element concentrations in the ash of the different coal groups and averages for each element. Coal beds of Tertiary age are lower in SiO_2, K_2O, TiO_2, and Al_2O_3 and higher in CaO and MgO than coals of Jurassic (Lias) age. These data suggest different environments of deposition for the coal beds during the Jurassic and the Tertiary.

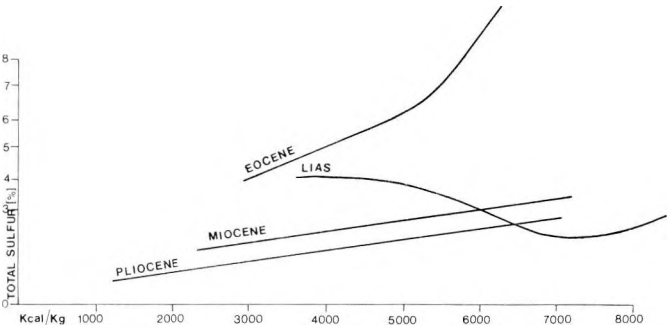

Fig. 4. Total sulfur—heating value relationship

4. ábra. Összes kén — fűtőérték függvény

Рис. 4. Зависимость: общее содержание серы — теплоотдача

	Composite		Pliocene		Miocene		Eocene		Lias	
	Mean	disp%	Mean	disp%	Mean	disp%	Mean	disp%	Mean	disp%
SiO_2	36.7	43.6	43.0	1.0	39.0	47.2	25.2	43.6	55.5	1.0
Al_2O_3	16.4	44.1	17.0	1.0	15.7	10.8	13.1	66.5	25.0	16.0
CaO	11.5	81.3	11.9	18.1	9.3	74.4	16.3	66.9	2.4	80.3
MgO	1.9	56.8	2.8	1.8	2.0	50.8	2.1	47.6	0.4	5.7
Na_2O	1.1	80.9	0.2	7.3	1.9	33.6	1.3	64.3	0.3	4.4
K_2O	1.4	67.2	1.0	2.1	2.0	55.3	0.8	69.2	2.3	4.3
Fe_2O_3	10.1	85.8	6.2	29.0	8.6	78.9	12.8	91.2	9.5	5.8
TiO_2	0.5	56.2	0.4	7.5	0.3	7.4	0.5	58.6	0.9	8.3
P_2O_5	0.1	107.0	0	–	0.1	46.8	0.1	44.6	0.2	75.0
SO_3	13.5	90.8	10.6	13.2	15.3	70.1	18.5	76.0	1.1	36.4

Table V. Averages (in percent) of major elements in the ash. Disp % = (standard deviation × 100)/mean

V. táblázat. Főelemek átlagértékei a hamuban. Disp = (standard szórás × 100)/átlag

Таблица V. Средние значения главных элементов в золе. Disp. = (стандартное рассеяние × 100)/среднее значение

Table VI gives data on average trace element contents in the coal ash by chronostratigraphic group. The coal beds of Jurassic age have higher concentrations of 30 of the 36 elements tested than the Tertiary coal beds. B, Ba, Mn, Rb, Sc, and Sr are lower in the Jurassic coal beds while Be, Ce, Hg, La, Mo, Nb,

	Composite		Pliocene		Miocene		Eocene		Lias	
	Mean	disp%	Mean	disp%	Mean	disp%	Mean	disp%	Mean	disp%
Ag	0.2	56.2	0.1	–	0.1	–	0.2	42.3	0.3	34.5
B	575.0	100.8	91.0	9.2	973.0	20.2	688.0	138.0	180.0	22.2
Ba	738.0	113.0	210.0	9.5	790.0	55.3	992.0	116.5	555.0	51.3
Be	18.4	167.4	11.8	36.2	3.9	37.8	2.6	63.0	860.0	10.5
Cd	0.3	76.6	0.2	16.6	0.1	45.0	0.3	64.6	0.5	67.3
Ce	181.0	135.0	60.0	1.7	84.0	21.8	71.0	68.5	720.0	11.1
Co	15.6	68.3	23.5	48.9	11.4	59.8	9.9	78.4	28.0	3.6
Cr	92.0	54.2	98.0	2.6	45.0	41.6	109.0	56.3	114.0	14.5
Cs	12.6	70.0	7.8	3.8	16.1	79.6	9.1	59.7	21.0	9.5
Cu	56.0	42.8	51.0	23.5	45.0	31.1	50.0	31.3	94.0	28.3
Eu	3.0	70.6	2.0	5.0	1.2	55.6	3.4	64.9	5.7	13.2
Ga	21.0	58.1	18.0	2.9	17.0	29.2	18.0	68.7	40.0	24.1
Ge	10.0	110.0	9.0	50.5	5.0	3.9	6.0	52.6	30.0	53.3
Hg	8.8	159.1	3.3	9.1	2.9	14.9	2.1	43.2	40.0	5.0
La	92.0	139.8	30.0	1.7	37.0	48.9	37.0	56.2	375.0	12.0
Li	65.0	64.3	36.0	8.3	55.0	14.3	72.0	72.9	89.0	46.9
Lu	1.0	108.5	1.3	38.5	0.4	28.8	0.3	47.8	3.3	3.0
Mn	282.0	67.7	545.0	15.6	323.0	40.3	210.0	80.6	140.0	72.0
Mo	20.4	160.2	4.8	37.5	7.3	53.2	11.7	102.8	92.5	8.1
Nb	43.0	172.3	9.0	17.6	12.0	23.6	10.0	22.4	205.0	12.2
Ni	97.0	77.1	118.0	53.2	49.0	65.1	81.0	96.1	190.0	0
Pb	14.1	117.5	5.5	9.1	11.0	70.8	5.2	7.7	49.5	7.1
Rb	128.0	76.2	65.0	3.1	182.0	77.5	129.0	67.5	110.0	9.1
Sc	18.3	54.1	28.0	10.7	11.0	7.8	15.5	72.5	26.5	1.9
Sm	11.6	79.4	5.9	3.4	5.3	41.5	5.3	66.8	42.5	10.5
Sr	1,890	96.8	445	7.9	1,183	33.5	3,020	73.9	1,570	71.9
Ta	0.7	117.3	0.2	41.5	0.2	47.9	0.6	116.0	2.1	7.3
Tb	2.6	85.2	1.9	18.9	2.0	37.6	1.4	50.1	7.3	10.3
Th	26.3	93.6	22.0	0	19.3	27.2	11.8	60.1	77.5	20.0
U	25.0	122.8	5.8	3.4	12.2	80.5	24.3	147.5	65.0	13.8
V	120.9	60.6	130.0	7.6	60.7	45.2	115.8	70.2	215.0	2.3
W	0.9	94.4	0.6	0	0.6	23.6	0.5	41.1	2.8	23.6
Y	58.2	91.8	60.5	25.6	31.0	22.5	28.8	66.4	170.0	5.9
Yb	8.2	100.6	9.7	34.0	3.9	17.9	3.3	48.2	25.5	5.9
Zn	60.1	72.6	79.0	7.6	35.7	57.1	50.0	68.4	103.0	65.0
Zr	346.5	168.9	123.5	21.4	126.7	7.4	66.2	65.9	1,600	25.0

Table VI. Averages (in ppm) of minor and trace elements in ash. Disp% = (standard deviations × 100)/mean

VI. táblázat. Ritka és nyomelemek koncentráció értékei a hamuban. Disp = (standard szórás × 100)/átlag

Таблица VI. Значения концентраций редких элементов и в следах. Disp. = (стандартное рассеяние × 100)/среднее значение

Sm, and Zr are four or more times higher. It should be noted that volatile elements such as Hg are calculated from whole coal data to the ash basis; it is doubtful whether any Hg (or other volatile elements) survives the ashing procedure.

On a whole-coal basis, the individual samples from coal beds of Jurassic age exhibit higher trace element contents, but to a lesser extent than on an ash basis. The high trace element contents in the ash and on a whole-coal basis is additional evidence of a different depositional environment of these coals compared to the others.

4. Conclusions

Data for twelve samples of coal from Hungary show some very unusual concentrations of chemical components. These components range from high organic sulfur content in coal beds of Miocene and Eocene age and the high trace element content in coal beds of Jurassic age. To corroborate these preliminary findings, detailed studies of the depositional environments of the Hungarian coal fields should be undertaken and additional samples should be collected and analyzed in order to relate depositional changes to geochemical differences. Care should be taken to minimize moisture losses in the future collection and shipment of additional coal samples.

12 MAGYARORSZÁGI SZÉNMINTA GEOKÉMIAI ANALÍZISE

SOMOS László, Peter ZUBOVIC és Frederick O. SIMON

A MÁFI — USGS kétoldali együttműködés során 12 db magyarországi szénmintát vizsgáltak meg az USGS központi geokémiai laboratóriumában (Reston). A rendkívül széles körű elemzések során a hagyományos technológiai és minősítési vizsgálatokon túlmenően környezeti szennyezőanyag-tartalom és széles körű nyomelem, illetve ritkafém tartalom meghatározásra is sor került.

A kisszámú mintavételezés eredményének MÁFI — USGS közös módszertani értékelése elsősorban szénminősítési és környezetvédelmi feladatokra ad konkrét megoldási ötleteket. A minták kis száma miatt az eredmények csak kvalitatíve értékelhetők.

ГЕОХИМИЧЕСКИЙ АНАЛИЗ 12-И ВЕНГЕРСКИХ УГОЛЬНЫХ ПРОБ

Ласло Г. ШОМОШ, Петер ЗУБОВИЧ и Фредерик О. САЙМОН

В ходе двустороннего сотрудничества между Венгерским геологическим институтом (ВГИ) и Геологической службой США (ГСА) 12 венгерских образцов углей исследовались в центральной геохимической лаборатории ГСА (Рестон). В течение необычайно широкого круга исследований помимо традиционных технологических и качественных анализов было проведено определение содержания веществ, загрязняющих окружающую среду, и содержания многочисленных редких металлов и в следах.

Совместное (ВГИ—ГСА) методическое оценивание результатов исследования небольшого количества образцов дает идеи для возможного разрешения задач, в первую очередь, в областях качественной оценки углей и защиты окружающей среды. Результаты, вследствие малого количества образцов, могут быть оценены только квалитативно.

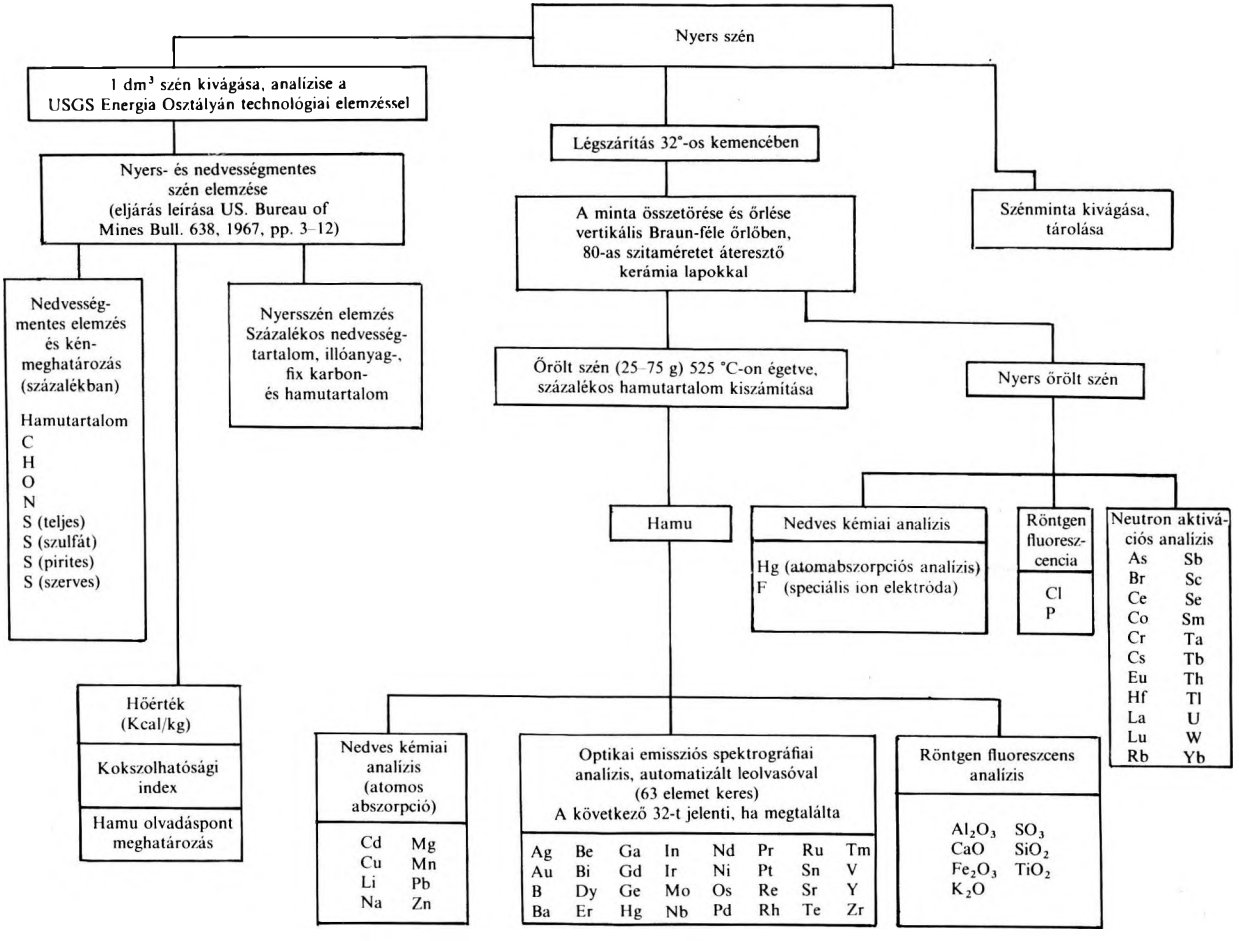

1. ábra. Mintavizsgálati folyamatábra

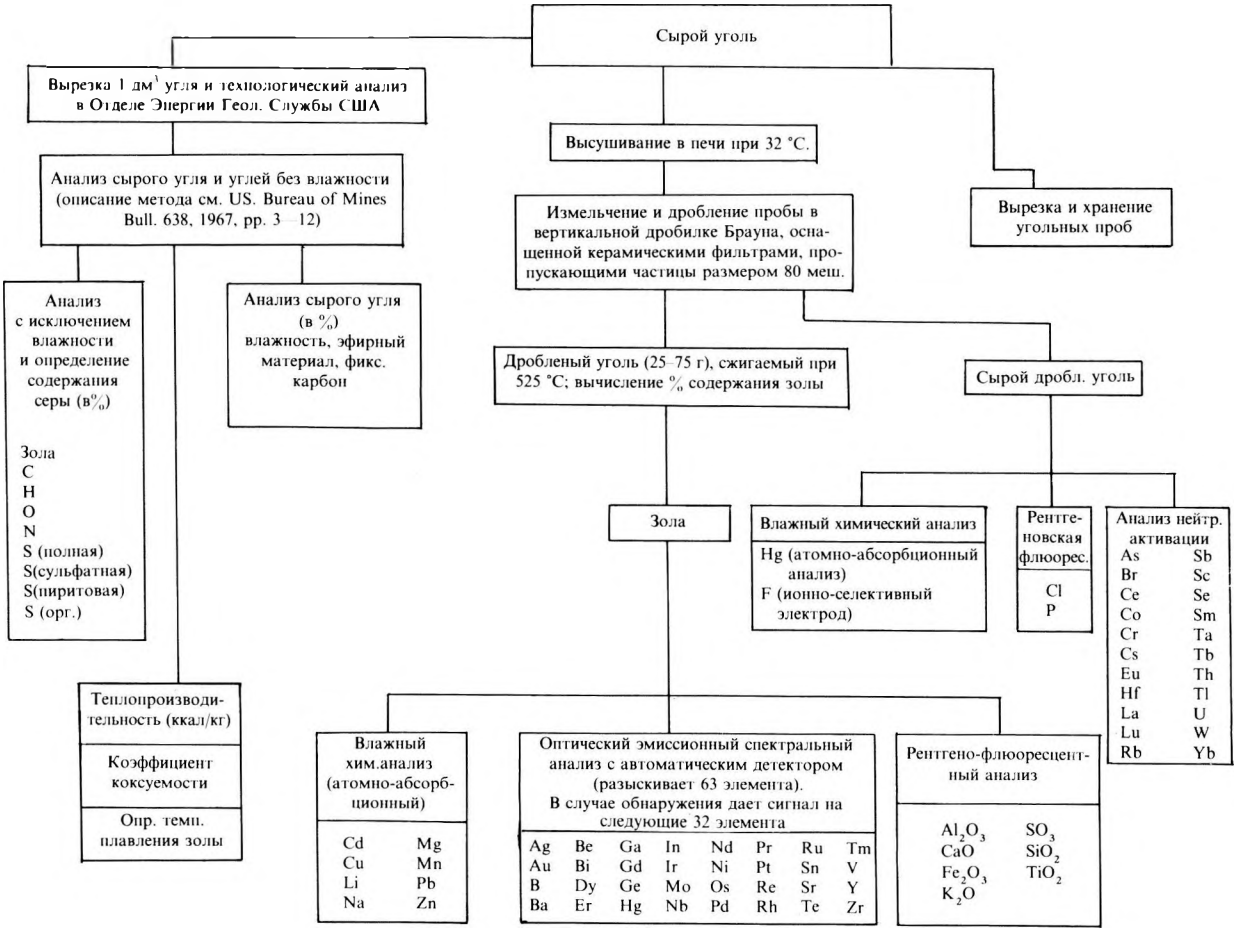

Рис. 1. Непрерывное изображение исследования образцов

GEOPHYSICAL TRANSACTIONS 1985
Vol. 31. No. 1–3. pp. 205–216

ESTIMATION OF KEROGENE-TYPE BY TIME – TEMPERATURE PYROLYSIS METHOD

Iván FISCH* and István KONCZ*

A simple time–temperature pyrolysis method is described, by means of which, or more precisely by gas chromatographic examination of the pyrolysis products, kerogene types (H_2-rich or H_2 depleted) and their marine or terrestrial origin are determined.

The method appears to be successful in adding critical information to the quantitative evaluation of the hydrocarbon resource potential of sediments in SW Hungary.

Keywords: gas chromatography, kerogene type, pyrolysis, hydrocarbon potentials

1. Introduction

Those constituents of the organic matter in sedimentary rocks that are insoluble in common organic solvents are collectively called kerogene. During the last decade several pyrolysis experiments have been conducted for the purpose of estimating or determining the hydrocarbon-productivity of the kerogene and by deduction, the resource potential of certain sedimentary beds and deposits.

Numerous descriptions of pyrolysis methods can be found in the literature, which differ from one another on the basis of the samples examined, the analytical conditions, the measured parameters and components.

As it regards materials, pyrolysis experiments can be performed on organic matters isolated from the inorganic matrix [HARWOOD 1977], or on non-isolated organic matters [GRANSCH–EISMA 1966, ESPITALIÉ et al. 1977]. The pyrolysis can be made using total organic matter [CLAYPOOL–REED 1976] or using only the part of the organic matter, which is insoluble in organic solvents. According to the widely used Rock–Eval method the pyrolysis is performed on the rock sample, that is on the non-isolated total organic matter. In this investigation pyrolysis measurements were made on carbonate-free, extracted, non-isolated organic samples.

As it regards the experimental conditions, pyrolysis methods commonly used differ according to the variation in time, temperature and pressure applied. For instance, the temperature can be increased gradually in step-wise increments [LEVENTHAL 1976], continuously [BARKER 1976] or can be maintained at a constant value. In this study the latter was applied.

* Hungarian Hydrocarbon Institute, POB 32, Százhalombatta, H–2443 Hungary
Manuscript received: 15 March, 1985

As far as the examined parameters and components are concerned, pyrolysis methods commonly applied can differ in that, the pyrolysis products [SOURON et al. 1974, GIRAUD 1970, JONATHAN et al. 1975, DE ROUCHET 1978] or the post-pyrolysis organic residue [GRANSCH–EISMA 1966] or both are examined. In this study, which describes time–temperature pyrolysis experiment, the pyrolysis products were examined, using a glass-ampoule technique.

The glass-ampoule, time–temperature pyrolysis method had been developed in Hungary in 1978–79 for model compounds [FISCH et al. 1980], however, its application to natural core samples was introduced for the first time in the course of this investigation.

Before subjecting them to pyrolysis, the core samples were powdered, acidized to eliminate the carbonates, extracted with chloroform and consequently with a mixture of benzene–acetone–methanol. As a result, the core samples so treated contained organic carbon only in the form of kerogene.

The time–temperature pyrolysis experiments and the gas chromatographic examinations of the produced gaseous and liquid hydrocarbons were conducted at the Organic Geochemical Laboratories of the U.S. Geological Survey, in Reston, Virginia.

2. Location of samples and experiments

The rock samples used in this study were obtained from the Dráva Basin, which is a sub-basin of the greater Pannonian Basin (for its geologic and sedimentologic description, see SZALAY–KONCZ 1981). The Neogene basement consists of Mesozoic and Paleozoic sedimentary rocks with varying subsidence and thermal history. The geothermal gradients in the Dráva Basin, calculated from the present temperature values, measured in deep oil exploration wells, are in the range of 35–55 °C/km. Lower than average geothermal gradients are commonly observed at the middle of the basin, where the Neogene sediments are thick. In contrast, the higher geothermal gradients can be found at the edges of the basin, where the Neogene basement is closer to the surface. In the fringe areas of the basin, characterized by very thick Miocene sediments, signs of oil genesis were found on the basis of the vitrinite-reflectance values and bituminological parameters at a depth interval of 2.5—3.0 km, corresponding to a temperature range of 110–140 °C. The very intensive primary migration of the crude oil can be assigned to a depth interval of 3.0–3.5 km and to a temperature range of 140–180 °C [SZALAY–KONCZ 1981].

Pyrolysis experiments had been performed on sixteen drilled core samples. Two of the core samples were obtained from very young (recent) sediments (Barnegat Bay (BB) and Cedar Creek (CC), Atlantic Coastal Region, USA). All of the other core samples were collected from exploration wells, drilled in the SW part of Hungary. Their location are shown in *Fig. 1.*

Before pyrolysis the two recent core samples were treated with chloroform and the other core samples were acidized with HCl and were then subsequently

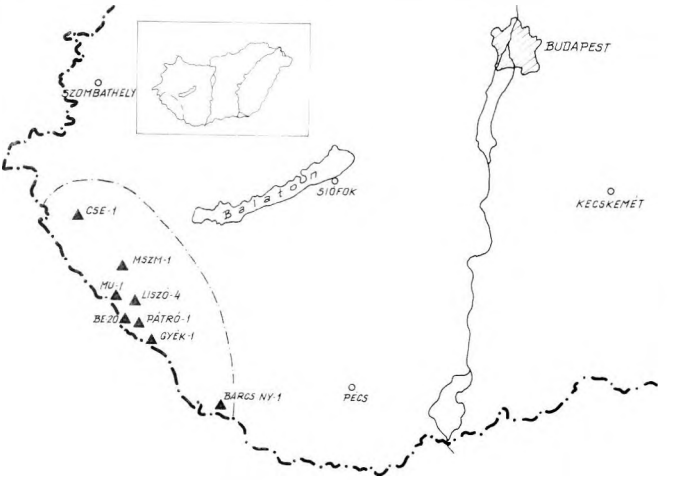

Fig. 1. Location of the samples

1. ábra. A minták területi elhelyezkedése

Рис. 1. Площадное распределение проб пород

subjected to an extraction with chloroform and then with a mixture of benzene–acetone–methanol.

From these prepared core samples 1 g size subsamples were extracted and placed into glass ampoules, which were made of high melting-point glass. After inserting the 1 g subsamples, the ampoules were sealed in flame and the pyrolysis tests were made in laboratory oven at a maximum temperature of 280 °C for a duration of 3 hours. The temperature in the oven was gradually increased to 280 °C during 2 hours, then was maintained at 280 °C during 3 hours followed by cooling during the next 2 hours. Hence the total heating time was about 7 hours. From each initial rock sample two subsamples were pyrolyzed for the determination of the gaseous products and the extractable liquid hydrocarbons.

For determination of the gaseous products the ampoules were placed into 200 ml volume glass jars. The jars were filled with a saturated NaCl solution with the exception of a 15 ml headspace, which was flushed with helium before sealing. After sealing the jars, the ampoules were shattered by vigorous shaking and the released gaseous hydrocarbons were collected into the headspace. Subsequently, gas samples were extracted 1 ml each with a gas syringe through the rubber seal below the sealing cap. In every case, the breaking of the ampoules was successful.

The gaseous or light hydrocarbon products (as high as C_6 carbon number) were separated on Porapak R and HHKel F columns. Quantitative analyses were made on the basis of data obtained using the Porapak R column. The measurements were made on two different gas chromatographs using Porapak R and HHKel F columns.

For determination of the higher carbon number (liquid) hydrocarbon

products, the ampoules were shattered in empty glass jars and the pyrolysed rocks were extracted with chloroform in Soxhlet equipment during a 24 hour period. After extraction, the chloroform was distilled off by rota distillation and the pyrolysis products were dried using a nitrogene evaporator. Before gas chromatographic examinations the extracts were dissolved in 0.5 ml n-hexane and from these solutions 1.8 microliter samples were injected on to *SCOT OV 101* and *FS OV 101* capillary columns.

3. Results and discussion

Results of these tests showed that the organic carbon content of the rock samples ($C_{org.}$) fell in the 0.006–0.021 g/g_{rock} interval with the exception of three carbonate-type rock samples. These carbonate-type samples have characteristically low organic carbon content (0.001–0.002 g/g_{rock}), therefore their bitumoid coefficients, that is the chloroform-soluble bitumoids organic carbon ratios on a g/g basis, are not authentic.

The important geochemical parameters of the rock samples and of the extracted bitumoids are listed in *Table I.* In the tables the following symbols are used:

S_K —chloroform soluble bitumoids g/100 g rock
S_B —benzene–acetone–methanol soluble bitumoids; g bitumoids/100 g rock
C_T —organic carbon in the bitumoid-free and carbonate-free rocks; g C/100 g rock (free)
C_{org} —total organic carbon (bitumoid C + kerogene C); g C/100 g rock
B_K —bitumoid coefficient; g bitumoid carbon/g rock
M —HCl insoluble residue; g residue/100 g rock
R_o —vitrinite reflectance, %
LP —Lower Pannonian
Mioc. —Miocene
U.Cr. —Upper Cretaceous
Tr. —Triassic

Based on the concentration values of the chloroform-soluble bitumoids (S_K), the bitumoid-coefficient and the ratio of the chloroform-soluble/benzene–acetone–methanol soluble bitumoids (S_K/S_B), migrated bitumoids were thought to be present in the Cse–1/3 and Be–20/45 rock samples.

Low bitumoid coefficients, which remained after the primary migration of the chloroform-soluble bitumoids, were observed in the rock samples having relatively high vitrinite-reflectance values, such as those below:

	B_K	R_0 (%)
Cse–1/3	0.035	0.88
Cse–1/12	0.027	1.37
Mu–1/5	0.006	3.01

Well No Core No	Depth (m)	Age	Rock type	S_K (w/w%)	S_B (w/w%)	C_T (w/w%)	$C_{org.}$ (w/w%)	B_K	M (w/w%)	R_0	*Pyrolysis products* $\frac{\sum(C_1 \div C_6)}{C_T}$ g/g	 $\frac{(C_1 + C_2)}{C_{3^+}}$ g/g
Barcs Ny–1/1	3011–3016	LP	clay–marl	0.081	0.013	1.300	0.611	0.166	41.3	0.55	0.578	0.579
Barcs Ny–1/2	3344–3351	Mioc.	clay–marl	0.087	0.016	1.461	0.841	0.083	52.0	0.65	0.388	0.608
Csesztreg												
Cse–1/2	3419–3420	Mioc.	siltstone	0.185	0.016	1.137	0.912	0.162	66.0	0.78	0.338	0.863
Cse–1/3	3579–3580	Mioc.	siltstone clay–marl	0.035	0.017	1.185	0.791	0.035	63.2	0.88	1.027	0.398
Cse–1/8	3799–3802	Mioc.	dolomite	0.059	0.099	2.893	0.108	0.437	1.9	–	0.065	0.029
Cse–1/11	3817–3824	U.Cr.	dolomite	0.030	0.005	2.243	0.174	0.138	6.5	–	0.089	0.017
Cse–1/12	3824–3832	U.Cr.	dolomite lime–marl	0.021	0.007	1.479	0.617	0.027	40.3	1.37	0.507	0.348
Pátró–1/6	1434–1442	LP	limestone siltstone	0.099	0.007	1.176	0.754	0.010	63.0	–	0.195	0.907
Pátró–1/7	1521–1527	LP	clay–marl	0.039	0.028	1.089	0.770	0.041	65.7	0.62	0.920	0.310
Belezna												
Be–20/45	2418–2435	Mioc.	siltstone–marl	0.591	0.041	3.356	2.112	0.224	47.9	0.58	0.184	0.632
Gyékényes												
Gyék–1/6	2913–2921	Mioc.	claystone	0.093	0.023	1.223	1.087	0.068	81.3	0.67	0.371	0.972
Murakeresztúr												
Mu–1/5	3345–3350	Tr.	dolomite– claystone	0.011	0.011	1.579	1.481	0.006	92.6	3.01	0.060	0.970
Liszó–4/7	2315–2318	Mioc.	claystone	0.100	0.030	1.017	0.903	0.089	78.5	–	0.014	0.410
Magyarszentmiklós												
Mszm–1/17	4130–4136	Tr.	claystone– limestone	0.012	0.006	1.215	0.120	0.080	8.7	1.00 (3090) Mioc.	0.208	0.686

Table I. Organic geochemical parameters of the rock samples

I. táblázat. A kőzetminták szerves geokémiai paraméterei

Таблица I. Керогенный пиролиз. Определение легких продуктов углеводорода

On the basis of the stable carbon isotope measurements made from the kerogene of the rock samples, marine organic matter was found in the Cse–1/2 and Cse–1/3 Miocene samples, while terrestrial organic matter was found in the Cse–1/11, Cse–1/12, Barcs Ny–1/1 and Barcs Ny–1/2 samples. The results of the GC-based measurements of the gaseous or light hydrocarbons generated during the pyrolysis are shown in *Table II.*

Maximum gas production was observed from the CC–37 sample (USA). Fifty per cent of the total gas products was methane. In comparison, the proportion of the methane is smaller in the gas mixtures generated from the other core samples. Maximum light hydrocarbon production was found to occur in the clay–marl type rocks. Minimum light hydrocarbon production was noted to occur in dolomitic rocks.

Considering these preliminary results, an exact relationship between the generation of the light (gaseous) hydrocarbons and the geologic age and burial depth of the rock samples can not be ascertained. It seems to be very likely, however, that—in the case of the Mu–1/5 and Mszm–1/17 samples—the minimum light and liquid hydrocarbon production is caused by overmatured kerogenes which have a high alteration degree ($R_0 = 3.01$ and 1.00 in Table I.).

In examining the possible relationships between the bitumoid-coefficients and the kerogene pyrolysis products, it can be stated that prior to the primary migration of the bitumoids, in the core samples of the same drilling, the bitumoid-coefficients and the unit values of the kerogene pyrolysis products show relationship *(Table III.)*.

According to this relationship, higher amounts of hydrocarbon mixtures were formed during the pyrolysis from those kerogenes which had higher bitumoid-coefficients. The maximum liquid hydrocarbon production (generated during the pyrolysis) is shown to contain a very complex hydrocarbon mixture, in which the carbon number range of the components is broad, usually between C_8 and C_{25}.

Similarly, in the generation of the C_1–C_6 hydrocarbons, the maximum liquid hydrocarbon production (yield) appears to be related to the clay–marl type rocks *(Table IV.)*.

As characteristic examples, the pyrograms of the Cse–1/11 and Barcs Ny–1/2 samples are shown in *Figs. 2* and *3*.

The average or medium liquid hydrocarbon production shows a predominance of the n-alkanes in the range of C_9–C_{18}. The pyrograms do not exhibit relationship with the rock types. It can be stated, however, that in the case of the Cse–1/8 and Cse–1/12 samples, the presence of isoprenoid-type hydrocarbons is also indicative of dolomitic type rocks besides the predominance of n-alkanes *(Table V.)*.

Minimum liquid hydrocarbon production can be related to those rock samples in which the kerogenes are obviously overmatured. As a characteristic example, the pyrogram of the Mszm–1/17 sample is shown in *Fig. 4*. Minimum liquid hydrocarbon yields were observed in the two recent samples, BB–25 and CC–37 too, in which the original organic matter content were high. In these

Wells and Core Numbers	Depth (m)	Rock type	$\sum C_1 - C_6$ (ppm/g)	C_1 (ppm/g)	Ethylene (ppm/g)	C_2 (ppm/g)	C_3 (ppm/g)	$\sum C_4$ (ppm/g)	$\sum C_5$ (ppm/g)	$\sum C_6$ (ppm/g)	Benzene (ppm/g)
BB # 25	sed.–water interface	–	4,940.7	1,470.4	365.7	322.9	790.7	977.3	447.3	566.3	0.38
CC # 37	sed.–water interface	–	30,226.6	15,510.5	2,391.6	1,694.5	4,211.8	3,580.5	1,347.9	1,489.7	8.68
Barcs Ny–1/1	3011	clay–marl	7,515.0	1,065.6	1,352.4	337.5	1,232.0	2,542.2	576.6	407.1	3.75
Barcs Ny–1/2	3344	clay–marl	5,670.0	661.9	1,243.3	224.5	1,163.8	1,795.9	291.6	251.5	–
Csesztreg											
Csc–1/2	3419	siltstone	3,843.6	788.4	788.8	203.5	558.3	1,031.4	218.0	254.9	–
Cse–1/3	3580	clay–marl, siltstone	12,173.0	1,377.5	1,619.8	466.1	1,744.3	5,016	1,266.0	676.8	3.29
Cse–1/8	3800	dolomite	1,869.4	42.9	4.9	4.7	140.3	593.8	332.1	750.8	0.45
Cse–1/11	3817	dolomite	1,990.2	26.9	1.6	4.8	220.3	1,249.8	323.5	163.2	0.30
Cse–1/12	3824	dolomite, limestone	7,503.6	911.8	800.5	232.4	485.1	3,098.5	984.3	991.0	22.20
Pátró–1/7	1521	clay–marl	10,018.5	1,290.9	770.8	306.6	1,184.0	4,198.1	1,409.3	859.0	0.15
Pátró–1/6	1434	siltstone	2,292.3	481.0	537.7	73.9	317.1	402.6	75.8	404.1	4.95
Belezna											
Be–20/45	2418	marl with siltstone	6,180.4	1,448.8	512.5	433.3	813.2	2195.1	469.0	308.5	3.00
Gyékényes											
Gyék–1/6	2913	claystone	4,542.6	813.6	1,200.0	224.9	674.9	1,352.5	165.4	111.2	–
Murakeresztúr											
Mu–1/5	3345	dolomite–claystone	952.8	302.2	145.0	22.0	35.4	52.1	55.2	341.0	–
Magyarszentmiklós											
Mszm–1/17	4130	clay–limestone	2,530.3	415.3	553.9	60.3	272.4	433.0	207.9	587.4	–
Liszó–4/7	2315	claystone	141.4	41.1	–	–	9.8	65.8	24.6	–	–

Table II. Kerogen pyrolysis. Determination of the light hydrocarbon products

II. táblázat. Kerogén pirolízis. A könnyű szénhidrogén termékek meghatározása

Таблица II. Параметры образцов пород по органической геохимии

samples the kerogenes are obviously far from the so-called "maturation window", that is their maturation is in a very early stage or, in other words, their alteration degrees are very low. According to the experiments, these recent samples (very young sediments) could produce only methane in any significant quantity.

Well No / Core No	Depth (m)	Vitr. refl. R_0	Bitumoid coeff. B_K	$\frac{\sum(C_1 \div C_6)}{C_T}$	Relative liquid hydrocarbon production
Barcs Ny–1/1	3000	0.55	0.106	0.578	very high
Barcs Ny–1/2	3100	0.65	0.083	0.388	high
Pátró–1/6	1400	–	0.010	0.195	minimum
Pátró–1/7	1500	0.62	0.041	0.920	minimum

Table III. Relationship between the bitumoid coefficients and the unit values of the kerogen pyrolysis products

III. táblázat. Összefüggés a bitumoid koefficiens és a kerogén pirolízis termékek egységértékei között

Таблица III. Зависимость коэффициентов битумоида от единичных значений продуктов юрогенного пиролиза

Well No / Core No	Depth (m)	Age	Rock type	Remarks
Cse–1/3	3580	Lower Miocene	clay–marl, siltstone	Complex mixture Carbon number range: C_9—C_{25}
Cse–1/11	3820	Upper Cretaceous	dolomite	Complex mixture Carbon number range: C_8—C_{28}
Barcs Ny–1/1	3015	Miocene	clay–marl	Complex mixture Carbon number range: C_9—C_{25}
Barcs Ny–1/2	3350	Miocene	clay–marl	Complex mixture Carbon number range: C_8—C_{25}

Table IV. Kerogen pyrolysis. Maximum liquid hydrocarbon production

IV. táblázat. Kerogén pirolízis. Maximális folyékony szénhidrogén termelés

Таблица IV. Керогенный пиролиз. Максимальная добыча жидкого углеводорода

Well No / Core No	Depth (m)	Age	Rock type	Remarks
Cse–1/2	3420	Lower Miocene	siltstone	n-alkane predominance; Range: C_9—C_{18}
Cse–1/8	3800	Miocene	dolomite	n-alkane + isoprenoid predom. Range: C_{10}—C_{28}
Cse–1/12	3830	Upper Cretaceous	lime–marl, limestone, dolomite	n-alkane + isoprenoid predom. Range: C_9—C_{18}
Gyék–1/6	2920	Miocene	claystone	n-alkane predominance Range: C_9—C_{18}
Be–20/45	2430	Miocene	marl with siltstone	n-alkane predominance Range: C_9—C_{24}

Table V. Kerogen pyrolysis. Medium liquid hydrocarbon production

V. táblázat. Kerogén pirolízis. Közepes folyékony szénhidrogén termelés

Таблица V. Керогенный пиролиз. Средняя добыча жидкого углеводорода

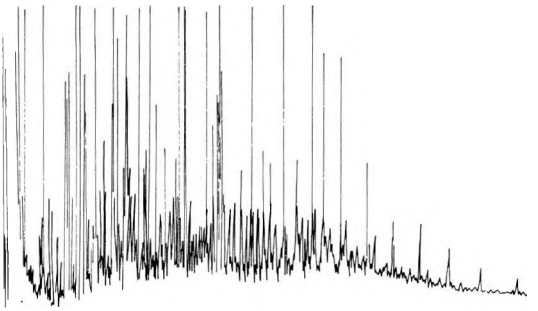

Fig. 2. Pyrogram of the kerogen from the Cse–1/11 core sample

2. ábra. A Cse–1 fúrás 11. sz. magmintájából származó kerogén pirogramja

Рис. 2. Пирограмма керогена керна № 11 скважины Cse–1

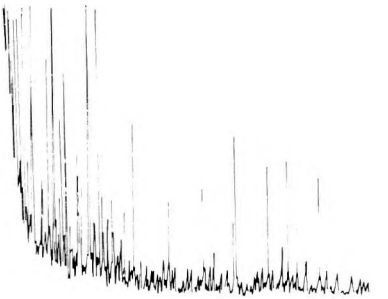

Fig. 3. Pyrogram of the kerogen from the Barcs Ny–1/2 core sample

3. ábra. A Barcs Ny–1 fúrás 2. sz. magmintájából származó kerogén pirogramja

Рис. 3. Пирограмма керогена керна № 2 скважины Barcs Ny–1

The primary purpose of the time–temperature pyrolysis method described herein is to show a means to determine the character of the kerogene-type compounds without specifically isolating them. Hence, concerning the generation of the C_1–C_6 and C_8–C_{25} range hydrocarbons, the following observations can be made:

i) Hydrogen-rich, oil-prone kerogen type compounds can be presumed to exist in the Cse–1/3, Cse–1/11, Barcs Ny–1/1 and Barcs Ny–1/2 rock samples.

ii) Hydrogen-depleted, very poor hydrocarbon-producing kerogen type compounds can be presumed to exist in the Cse–1/2, Cse–1/8 and Pátró–1/6 rock samples.

Based upon these preliminary results, the estimation of the quantity and character of the hydrocarbons that may be generated, that is the potential hydrocarbon-productivity of sediments and rocks, based on the glass-ampoule, time–temperature pyrolysis method, using simple equipment, is promising.

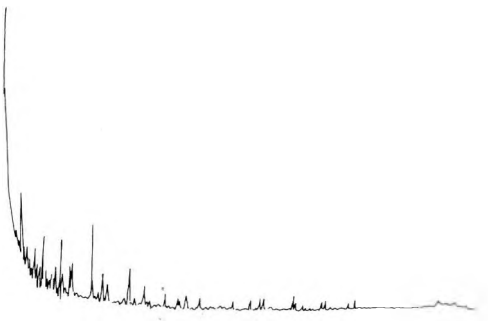

Fig. 4. Pyrogram of the kerogen from the Mszm–1/17 core sample

4. ábra. Az Mszm–1 fúrás 17. sz. magmintájából származó kerogén pirogramja

Рис. 4. Пирограмма керогена керна № 17 скважины Mszm–1

4. Conclusions

The time–temperature pyrolysis method seems to be useful in the estimation of the kerogene type without its specific isolation.

The vertical, log–like examination of the cores of exploratory drillings by the time–temperature pyrolysis method would probably be a successful approach in the quantitative evaluation of the hydrocarbon resource potential of sedimentary deposits.

Acknowledgements

The authors wish to express their thanks to Dr. Robert E. Miller for helpful scientific advice. Special thanks are due to Terry Lerch for the excellent GC measurements. We are also grateful to D. Owings, D. Ligon and W. Walker for technical assistance. The authors wish to express their thanks to Dr. Paul G. Teleki for useful comments concerning this manuscript.

REFERENCES

BARKER C. 1976: Pyrolysis techniques for source-rock evaluation. AAPG Bull. **58,** 11, pp. 2349–2361

CLAYPOOL G. B., REED F. K. 1976: Thermal analysis for source-rock evaluation: Quantitative estimate of organic richness and effects of lithologic variation. AAPG Bull. **60,** 4, pp. 608–626

ESPITALIÉ J., LAPORTE J. L., MADEC M., MARQUIS F., LEPLAT P., PAULET J., BOUTEFEU A. 1977: Méthode rapide des roches méres de leur potentiel pétrolier et de leur degrée d'évolution. Revue de l'Inst. Francais du Pétrole **32,** 1, pp. 23–42

FISCH I., OLÁCSI I., TAKÁCS J., VÖRÖS J. 1980: Pyrolysis and gas chromatographic examination of phytol and isoprenoid hydrocarbons. Pre-calculation of retention indices by computer. Journal of Analytical and Applied Pyrolysis **1,** pp. 275–295

GIRAUD A. 1970: Application of pyrolysis and gas chromatography to geochemical characterization of kerogen in sedimentary rock. AAPG Bull. **54,** 3, pp. 439–455

GRANSCH J. A., EISMA E. 1966: Characterization of the insoluble organic matter of sediments by pyrolysis. Adv. in Org. Geochem., Proc. 3rd Int. Congr., pp. 407–426

HARWOOD R. J. 1977: Oil and gas generation by laboratory pyrolysis of kerogen. AAPG Bull. **61,** 12. pp. 2082–2102

JONATHAN D., L'HOTE G. M., DU ROUCHET J. 1975: Analyse geochimique des hydrocarbures légers par thermovaporisation. Revue de l'Inst. Francais du Pétrole **30,** 1, pp. 65–88

LEVENTHAL J. S. 1976: Stepwise pyrolysis gas chromatography of kerogen in sedimentary rocks. Chemical Geology **18,** 7, pp. 5–20

DE ROUCHET J. 1978: Indices chimiques pour l'evaluation de l'état diagenetique des huiles et des roches sapropéliques. Revue de l'Inst. Francais du Pétrole **33,** 1, pp. 33–45

SOURON C., BOULET R., ESPITALIÉ J. 1974: Étude par spectrométrie de masse de la décomposition thermique sous vide de Kerogénes appartenant a deux lignées évolutives distinctes. Revue de l'Inst. Francais du Pétrole **29,** 5, pp. 661–678

SZALAY Á., KONCZ I. 1981: Genese und Migration der Kohlenwasserstoffe in den Neogen-Depressionen des Pannonischen Beckens Ungarns. Zeitschrift für angewandte Geologie **27,** 6, pp. 226–272

KEROGÉN TÍPUSÁNAK BECSLÉSE IDŐ–HŐMÉRSÉKLET PIROLÍZIS MÓDSZERREL

FISCH Iván és KONCZ István

A szerzők ismertetnek egy egyszerű, ún. idő–hőmérséklet pirolízis módszert, melynek segítségével, pontosabban a keletkezett pirolízis termékek gázkromatográfiás vizsgálatával becsülni lehet a kőzetminták kerogénjének típusát (H_2-ben gazdag, jó olajképző, ill. H_2-ben szegény, gyenge olajképző), ill. annak tengeri vagy szárazföldi eredetét.

A módszer alkalmazhatónak látszik az üledékes kőzetek szénhidrogén potenciáljának becslésére. Más geokémiai módszerekkel kapott információkkal egybevetve növelheti a szénhidrogén-prognózis pontosságát.

ОЦЕНКА ТИПА КЕРОГЕНА МЕТОДОМ «ВРЕМЯ–ТЕМПЕРАТУРНОГО ПИРОЛИЗА»

Иван ФИШ и Иштван КОНЦ

Простым методом «время–температура пиролиза» на основе газо-жидкостной хроматографии продуктов пиролиза можно произвести оценку типа керогена пород (богатых водородом, с хорошей нефтеобразующей способностью, бедных водородом, со слабой нефтеобразующей способностью), а также их морское или терригенное происхождение.

Метод пригоден для оценки потенциала происхождения углеводородов осадочных пород. Сравнивая результаты, полученные этим методом, с информацией, полученной другими геохимическими методами, данный метод может повысить надёжность прогноза углеводородов.

GEOPHYSICAL TRANSACTIONS 1985
Vol. 31. No. 1-3 pp. 217-230

STRUCTURAL ROTATIONS FROM PALEOMAGNETIC DIRECTIONS OF SOME PERMO-TRIASSIC RED BEDS, HUNGARY

Emő MÁRTON* and Donald P. ELSTON**

Oriented samples of Permo-Triassic red beds were collected at five localities in the Balaton Highlands, one locality in the Bükk Mountains, and two localities in the Mecsek Mountains. The objective was to obtain paleomagnetic directions, and poles calculated therefrom, for the evaluation of possible structural rotations for these different tectonic blocks.

Statistically well defined paleomagnetic directions were obtained following stepwise thermal cleaning and the analysis of measured and removed remanence at each step for four localities in the Balaton Highlands (normal polarity) and for two localities in the Mecsek Mountains (reversed polarity).

The directions depart significantly from the present field direction indicating an ancient remanence. However the carriers of the magnetization appear complex and may contain post-folding as well as pre-folding components of magnetization. Nonetheless, tilt-corrected directions that support the results of an earlier paleomagnetic study indicate that Balaton Highlands are rotated about 50° in a counter-clockwise sense with respect to the Mecsek Mountains (Mecsek Mountains Decl. 177.4°, Incl. −5.0°, reversed polarity; Balaton Highlands, Decl. 307.2°, Incl. 11.0°, normal polarity).

Comparison is made with paleomagnetic results from rocks of comparable age in the Mediterranean area.

Keywords: palaeomagnetism, complex magnetization, thermal demagnetization, structural rotation, central Mediterranean

1. Introduction

From the viewpoint of plate tectonics, Hungary belongs to the tectonically complicated Mediterranean region. Paleomagnetic measurements have already shown that even a small area, such as that of Hungary, can be subdivided into terranes that have had different rotational histories arising from Alpine orogenesis [MÁRTON–MÁRTON 1978, 1980].

In view of the lack of fully oriented drill cores, paleomagnetic studies for tectonic analysis have been restricted to the sampling of outcrops. Results of this work have shown that minimum two units lie west of the River Danube

* Eötvös Loránd Geophysical Institute of Hungary, POB 35, Budapest, H–1440
** U.S. Geological Survey, 2255 North Gemini Drive, Flagstaff, AZ 86001
Manuscript received: 24 April, 1985

(Transdanubia), one including the Transdanubian Central Range*, and the other including Southeast Transdanubia comprising the Mecsek Mts. and Villány hills.

East of the Danube River, we have only a very limited knowledge of the subdivision and the history of rotations. Outcrops of rock older than Pannonian age are found in the North Hungarian Mountain Range. The paleomagnetic directions known from that area [MÁRTON 1980/a, MÁRTON 1981, MÁRTON 1983] lead to the conclusion that at least certain parts of the North Hungarian Mountain Range were rotated in a counter-clockwise sense prior to occupying their present position. Thus the North Hungarian Mountain Range could have moved in coordination with the Transdanubian Central Range, but the estimate of the duration and the degree of the coordination cannot yet be made.

The paleomagnetic technique has been most commonly applied for continental-scale tectonic studies. Each continent has a unique apparent polar wandering path (successive determinations of the position of the magnetic poles relative to a continent), which represents its movements relative to the Earth's axis of rotation. Because the paths represent the movements of continents with respect to one another, the past positions of the continents can be reconstructed by matching polar wander curves. This principle can be applied across all levels, because not only the major continents, but even small tectonic units can have unique polar paths. Eventually, we should be able to reconstruct the relative motions of the Mediterranean fragments, although the recognition of the paleomagnetically different units and the construction of their respective polar paths will be a long process. Nevertheless, each new determination contributes to the general solution, and at the same time places new constraints on any plate-tectonic reconstruction model.

Paleomagnetically, the Permian Period is poorly defined in Hungary. We decided to attack the problem of determining paleomagnetic poles from fine-grained clastic red beds by joining forces. The method developed in the United States on collecting suitable samples and isolating the remanence residing in detrital hematite [for example, ELSTON–PURUCKER 1979], was integrated with experience accumulated in Hungary on analyzing complex magnetizations in general [MÁRTON 1980/b, MÁRTON 1984], and unraveling of multi-component remanence of red limestones in particular [MÁRTON et al. 1980].

2. Sampling and laboratory treatment

In 1982, we collected samples at five localities in the Balaton Highlands (part of the Transdanubian Central Range), one locality in the Bükk Mountains (North Hungarian Mountain Range), and two localities in the Mecsek Mountains (Southeast Transdanubia, *Fig. 1*).

* In an attempt to unify geographical names, the editors use "Transdanubian Central Range" in accordance with former usage of Geophysical Transactions. The authors used "Transdanubian Central Mountains", and in some references it appears as "Transdanubian Middle Mountains"

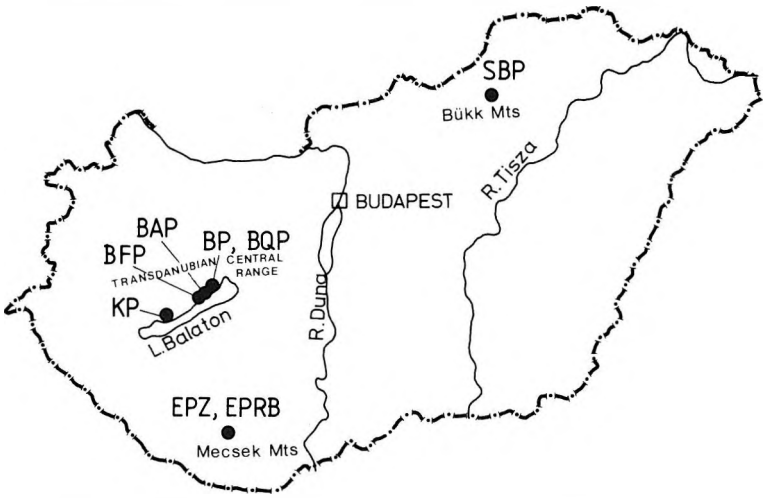

Fig. 1. Sampling localities in Permo-Triassic red beds of Hungary
Balaton Highlands: *BP* — Balatonalmádi, Vadvirág utca; *BQP* — Balatonalmádi, quarry; *BAP* — Balatonarács; *BFP* — Balatonfüred; *KP* — Kővágóörs
Mecsek Mountains: *EPZ* — Egédpuszta; *EPRB* — Boda
Bükk Mountains: *SBP* — Szilvásvárad, Bácsóvölgy

1. ábra. Permo-triász vörös üledékek mintavételi helyei Magyarországon
Balatonfelvidék: *BP* — Balatonalmádi, Vadvirág utca; *BQP* — Balatonalmádi, kőfejtő; *BAP* — Balatonarács; *BFP* — Balatonfüred; *KP* — Kővágóörs
Mecsek hegység: *EPZ* — Egédpuszta; *EPRB* — Boda
Bükk hegység: *SBP* — Szilvásvárad, Bácsóvölgy

Рис. 1. Места взятия образцов пермо-триасовых красноцветных отложений в Венгрии
Прибалатонске горы: *BP* — с. Балатоналмады, улица Вадвираг; *BQP* — с. Балатоналмады, карьер; *BAP* — с. Балатонарач; *BFP* — г. Балатонфюред; *KP* — с. Кёвагоёрш
Мечекские горы: *EPZ* — Эгедпуста; *EPRB* — с. Бода
Горы Бюкк: *SBP* — Силвашварад, дол. Бачо

The remanence and the susceptibility of each sample was measured in the natural state. Pilot samples, selected to represent each of the localities, were partially cleaned by stepwise heating and cooling in a magnetically field-free space. The remanence and the susceptibility were measured after each step.

The pilot studies indicated that the natural remanence cleans readily, i.e., the plot of the vectors trace as lines that project to the origins of orthogonal demagnetization diagrams at an early stage of the demagnetization analysis *(Figs. 2a, 2c, 3a, 3c, 4a, 4c)*. All pilot samples exhibited decreases in susceptibility at moderate temperatures *(Figs. 2b, 2d, 3b, 3d, 4b, 4d)* due to the conversion of maghemite to the stable mineral hematite. In some pilot samples, the susceptibility remained unchanged on further heating *(Figs. 2b, 2d, 3b, 4b)*, whereas in other samples the susceptibility increased abruptly *(Figs. 3d, 4d)* indicating the formation of a new magnetic phase. Increases in susceptibility were accompanied by the onset of spurious magnetizations *(Figs. 3c, 4c)*, i.e., the end

points of the magnetic vectors that formerly plotted as straight line traces (slight deviations from a line being permitted), became erratic.

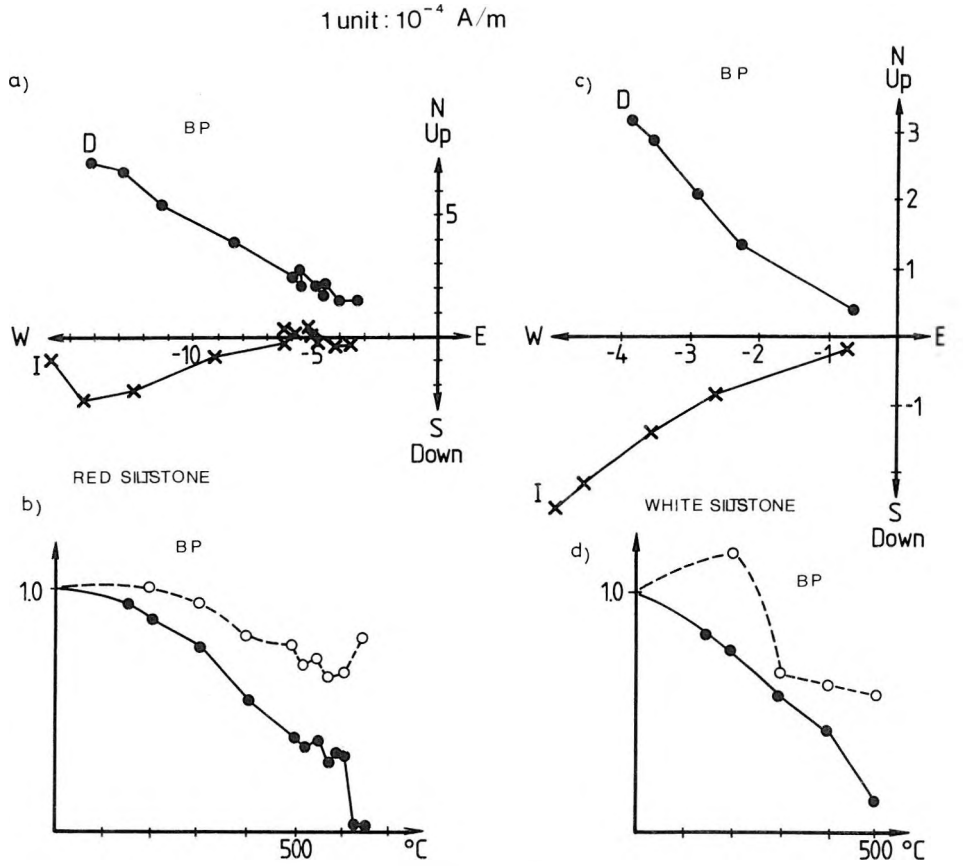

Fig. 2. a) and *c)*. Orthogonal plots of the change in direction and intensity of the natural remanence on stepwise heating: *D*, declination; *I*, inclination
b) and *d)*. Change of the intensity (solid circle) and the susceptibility (open circle) on stepwise heating, both normalized with respect to initial values

2. ábra. a) és *c)*. A természetes remanens mágnesezettség irányának és intenzitásának változása lépcsőzetes hőkezelésre: *D*, deklináció, *I*, inklináció. Ortogonális vetületek
b) és *d)*. A kezdeti értékre normalizált intenzitás (teli körök) és a szuszceptibilitás (üres körök) változása lépcsőzetes hőkezelésre

Рис. 2. a) и *c)*. Изменение направления и интенсивности естественной остаточной намагниченности при ступенчатой термообработке: *D* — склонение, *I* — наклонение. Ортогональные проекции
b) и *d)*. Изменение отнесенных к исходным значениям интенсивности (полные круги) и восприимчивости (пустые круги) при ступенчатой термообработке

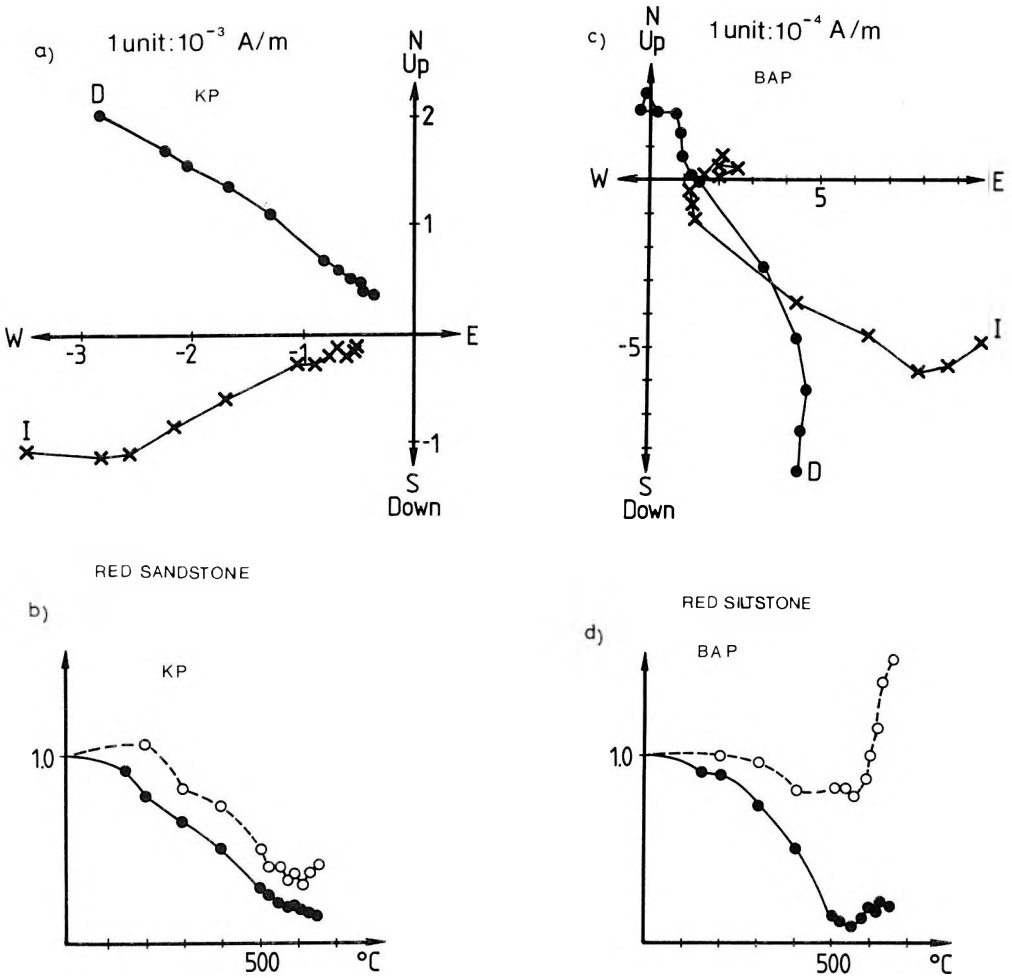

Fig. 3. a) and *c)*. Orthogonal plots of the change in direction and intensity of the natural remanence on stepwise heating: *D*, declination; *I*, inclination
b) and *d)*. Change of the intensity (solid circle) and the susceptibility (open circle) on stepwise heating, both normalized with respect to initial values

3. ábra. a) és *c)*. A természetes remanens mágnesezettség irányának és intenzitásának változása lépcsőzetes hőkezelésre: *D*, deklináció, *I*, inklináció. Ortogonális vetületek
b) és *d)*. A kezdeti értékre normalizált intenzitás (teli körök) és a szuszceptibilitás (üres körök) változása lépcsőzetes hőkezelésre

Рис. 3. а) и *с)*. Изменение направления и интенсивности естественной остаточной намагниченности при ступенчатой термообработке: *D* — склонение, *I* — наклонение. Ортогональные проекции
b) и *d)*. Изменение отнесенных к исходным значениям интенсивности (полные круги) и восприимчивости (пустые круги) при ступенчатой термообработке

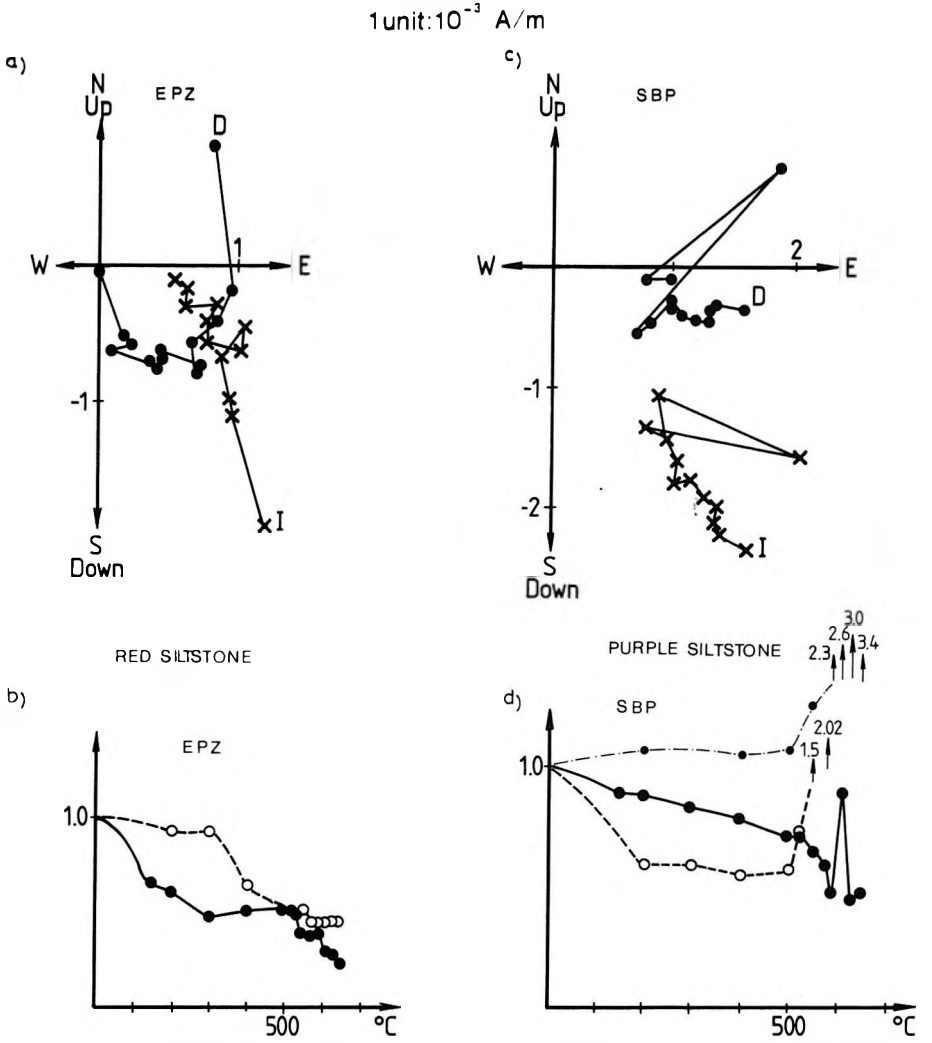

Fig. 4. a) and *c)*. Orthogonal plots of the change in direction and intensity of the natural remanence on stepwise heating: *D*, declination; *I*, inclination
b) and *d)*. Change of the intensity (solid circle) and the susceptibility (open circle) and the degree of susceptibility anisotropy (small dots in Fig. 4d) on stepwise heating, all normalized with respect to initial values

4. ábra. a) és *c)*. A természetes remanens mágnesezettség irányának és intenzitásának változása lépcsőzetes hőkezelésre: *D*, deklináció, *I*, inklináció. Ortogonális vetületek
b) és *d)*. A kezdeti értékre normalizált intenzitás (teli körök) és a szuszceptibilitás (üres körök), valamint a szuszceptibilitás anizotrópia fok (pontok a 4/d ábrán) változása lépcsőzetes hőkezelésre

Рис. 4. a) и *c)*. Изменение направления и интенсивности естественной остаточной намагниченности при ступенчатой термообработке: *D* — склонение, *I* — наклонение. Ортогональные проекции
b) и *d)*. Изменение отнесенных к исходным значениям интенсивности (полные круги) и восприимчивости (пустые круги), а также степени анизотропии восприимчивости (точки на рис. 4/d) при ступенчатой термообработке

Optimum cleaning temperatures for the individual collections were selected based on the behavior of the pilot samples. The following criteria were used:

1) the remanence becomes single-component, with intensities adequate for measurement;
2) magnetization residing in undesirable magnetic minerals, such as maghemite and hydrated iron oxides, is removed;
3)new mineral phases with high susceptibilities are not formed.

All samples were cleaned at the optimum temperatures selected for the individual localities, and commonly at lower and higher temperatures than optimum, as well.

Stable directions: Partial demagnetization of the samples at the optimum temperatures yielded statistically well-defined directions for two sample groups from the Mecsek Mountains (*EPZ* and *EPRB*, Fig. 1) and for one group from the Balaton Highlands *(BP*, Fig. 1 and *Table I)*. These groups are designated as reliable in the traditional sense.

Sites *BQP* from the Balaton Highlands and *SBP* from the Bükk Mountains (Fig. 1) exhibited large scatter at all cleaning temperatures. Thus, they are useless for tectonic evaluation.

The traditional approach of isolating a stable direction failed for three sample groups from the Balaton Highlands. We found, however, that the remanences of sites *BAP* and *BFP* (Fig. 1) are statistically well defined and plot away from the present field direction at lower than optimum temperatures *(Fig. 5)*. We could even improve the statistics of the groups by calculating the locality means from subtracted vectors (removed remanence) instead of the measured ones (Table I). The demagnetization analysis indicates that the "meaningful" signal in these rocks resides in the metastable mineral maghemite rather than in hematite.

Subtracted vectors proved to be extremely useful for locality *KP*. The measured vectors here exhibit a great-circle distribution throughout, i.e., the overprint along the present field direction could not be removed. Examination of the subtracted vectors, however, revealed two components of the composite magnetization: one plotting close to and the other plotting well away from the present field direction *(Fig. 6)*. The locality mean direction, of course, was calculated from the directions that lay well away from the present field (Table I).

Sampling location	Code	N/N_0	$\bar{D}^0$	$\bar{I}^0$	k	α_{95}	$\bar{D}_c^0$	$\bar{I}_c^0$	Cleaning	Remarks
Balaton Highlands										
Balatonalmádi	*BP1*	20/20	323	49	21	7.8	319	9	500 °C	red siltstone + with marl, maghemite decays below 500 °C
Balatonfüred	*BFP1*	9/9	308	29	15	13.8	295	0	400 °C	scatter too large abowe 400 °C,
	BFP1	9/9	301	24	53	7.1	293	−8	subtracted vectors 400–500 °C	maghemite decays below 400 °C
Balatonarács	*BAP1*	29/29	327	55	14	7.3	309	21	NRM subtracted vectors	scatter too large at 525 °C
	BAP1	29/29	322	53	25	5.7	307	18	NRM — 525 °C	no explanation for the scatter
Kővágóörs	*KP1*	8/12	309	47	113	4.9	310	24	subtracted vector 400–500 °C	maghemite decays at 525 °C
Mecsek Mountains										
Egédpuszta	*EPZ1*	11/11	167	−20	35	6.1	185	−10	525 °C	maghemite decays below 525 °C
Boda	*EPRB1*	17/17	188	−31	25	9.8	170	0	500 °C	maghemite decays at 500 °C

N_0 – number of samples collected
N – number of useful samples
$\bar{D}^0$ – mean paleomagnetic declination in the present system of coordinates
$\bar{I}^0$ – mean paleomagnetic inclination in the present system of coordinates
k – Fischer's precision parameter
a_{95} – radius of circle of confidence at 95 % probability level
$\bar{D}_c^0$ – mean paleomagnetic declination after tilt correction
$\bar{I}_c^0$ – mean paleomagnetic inclination after tilt correction

Table I. Summary of paleomagnetic results on Permo-Triassic red beds, Hungary

I. táblázat. A magyarországi permo-triász kőzeteken meghatározott paleomágneses irányok összefoglalása

Таблица I. Сводка палеомагнитных направлений, определенных на пермо-триасовых породах Венгрии

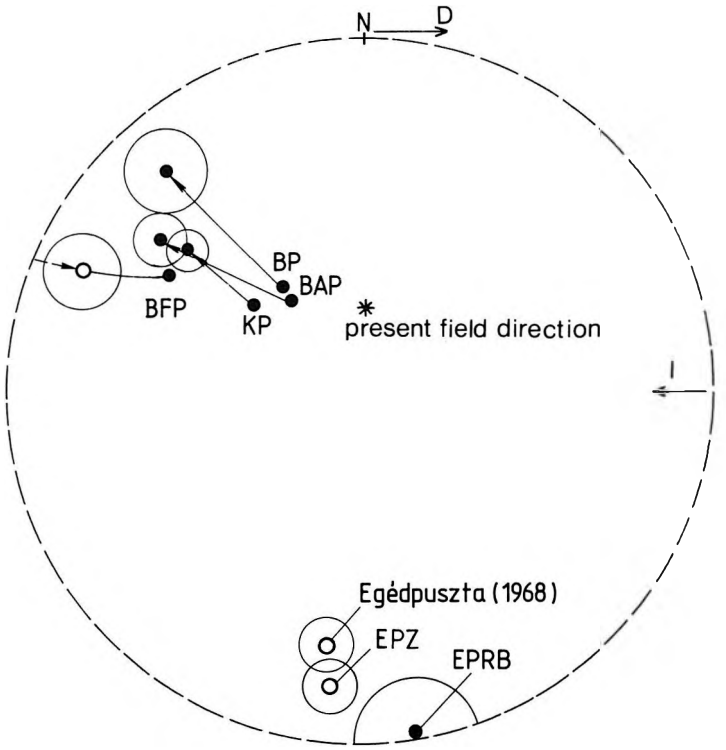

Fig. 5. Stereographic plot showing locality means after tilt correction (enclosed by circles drawn at the 95 percent confidence level). Sites from the Balaton Highlands without confidence circles are directions before correction for tilt. For labels refer to Fig. 1. An earlier result from Egédpuszta (same locality as *EPZ*) is show for comparison. Although the confidence circles are similar, the new result is an improvement, because the *k* value, indicating the degree of divergence of the vectors, is better for *EPZ* than for Egédpuszta, 1968

5. ábra. A mintavételi helyek dőlés-korrigált középirányai α_{95}-tel. A konfidencia körök nélküli középirányok a Balaton-felvidéki mintavételi helyek középirányai tektonikai korrekció előtt. A jelölések magyarázatára lásd 1. ábra. Összehasonlításképpen egy korábbi meghatározás eredményét is ábrázoltuk Egédpusztáról (*EPZ*-vel azonos mintavételi hely). Bár a konfidencia körök hasonlóak, az új eredmény mégis jobb minőségű, mint a régi, mert *k* értéke, amely a vektorok párhuzamosságát jellemzi, jobb *EPZ*-re, mint az Egédpuszta 1968-as meghatározásé

Рис. 5. Средние направления мест взятия образцов после внесения поправки за наклон с α_{95}. Средние направления без кругов доверия представляют собой средние направления мест взятия образцов Прибалатонских горах перед внесением тектонической поправки. Условные обозначения даны на рис. 1. Для сопоставления изображены также результаты прежнего определения с Эгедпуста (место одинаковое с *EPZ*). Хотя круги доверия похожи, новый результат все-таки отличается по качеству по сравнению со старым результатом, потому что значение *к*, которое обозначает параллельность векторов, лучше для *EPZ*, чем определение на Эгедпуста в 1968 г

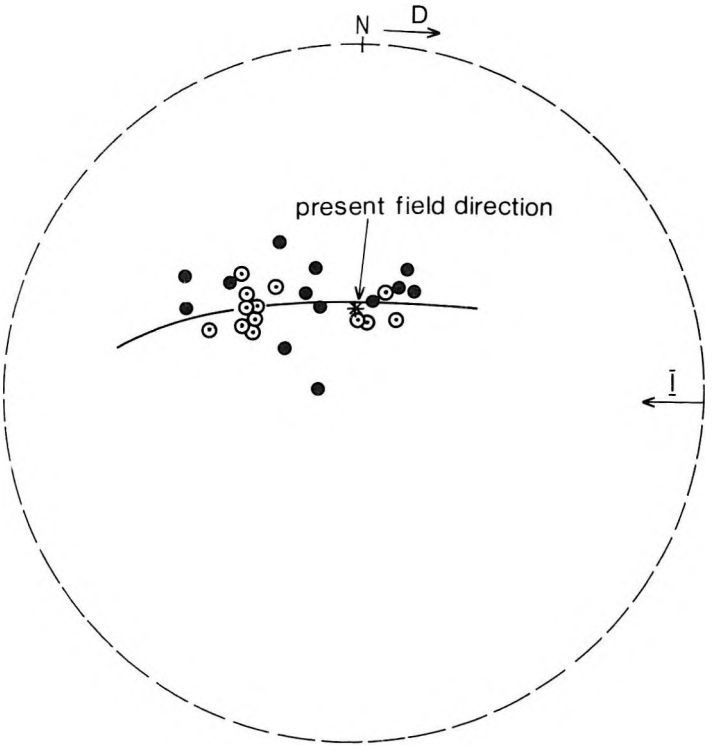

Fig. 6. Balaton Highlands, site *KP*. Stereographic plot showing measured vectors at 500 °C (solid circles) and removed vectors between 500 °C and 400 °C (points encircled)

6. ábra. Balaton-felvidék *KP* jelű mintavételi hely. Az 500 °C-os tisztítási lépésben mért (teli körök) és az 500 és 400 °C között elveszített (bekarikázott pontok) mágnesezettség irányai szögtartó vetületen

Рис. 6. Место взятия образца с обозначением *KP* в Прибалатонских горах. Приведены направления намагниченности, замеренной в шагу очищения в 500 °C (полными кругами) и потеренной между 500 и 400 °C (обведенные кружком точки), на стереографической проекции

3. Discussion

The locality mean directions for the statistically well defined groups are shown in Figure 5. The directions, corrected for local tilt, are plotted with their confidence circles at the 95 per cent probability level. As seen in Figure 5, all directions depart significantly from the present field direction, indicating high stability and an ancient age for the remanence no matter what the carrier of the magnetization is. Moreover, the locality mean directions from the Mecsek Mountains plot in a different part of the sphere than directions from the Balaton

Highlands. This latter observation supports the earlier conslusion of MÁRTON and MÁRTON [1978, 1980] that the Transdanubian Central Range and the Mecsek Mountains have undergone different rotations.

The foregoing conclusions are not influenced by the actual age of the magnetization, which we cannot demonstrate to be older than the tectonic phase responsible for the local tilts.

Unfolding, i.e. correction for local tilts, is one of the most powerful tests for establishing an early age for remanent magnetization. When the scatter in directions significantly increases on unfolding, the characteristic remanence postdates tilting of the strata. In contrast, if the scatter decreases significantly, the remanence is older than the folding. When a magnetization is sufficiently stable to survive a tectonic episode, there is a reasonable chance that the magnetization was acquired early, either during or shortly after accumulation of the strata.

The fold test was not conclusive for the sampled localities because neither a significant decrease nor an increase in scatter was observed on application of tilt corrections. One reason is that the differences in the local positions are small with respect to the uncertainty of the individual mean directions (as expressed in the value of α_{95}, see Table I). Alternatively, some of the localities may exhibit pre-folding remanences, whereas others may exhibit postfolding remanences.

Although a better control on the actual ages of the statistically well defined magnetizations is desirable, results from the present study are not inferior to results obtained from rocks of similar age elsewhere in the Mediterranean area.

Rotations of areas relative to their present positions, and with respect to other tectonic units, are best shown by declinations. The mean declination for the Balaton Highlands points to the western-southwestern connection of the Transdanubian Central Range, whereas the mean declination of the Mecsek Mountains points to an eastern–southeastern connection *(Fig. 7)*, similar to declinations for other than Permian rocks [MÁRTON 1984, 1985].

The actual age of the magnetization is not critical for the analysis of rotations because the declinations, corrected and uncorrected for tilt, are very similar. However, inclinations are more of a problem. The tilt-corrected inclinations fit the overall picture (Fig. 7), i.e., they are low and indicate that, as in other parts of the Mediterranean, the units sampled in Hungary accumulated at a near-equatorial latitude.

However, the inclinations obtained for the Balaton Highlands disagree with inclinations obtained from somewhat younger Hungarian strata to an extent that it appears to contradict their supposedly close geologic ages (late Permian and early Triassic). Moreover, even the highest corrected inclination (*KP1*, Table 1) is much lower than the inclinations obtained from Triassic marine strata (+38°, +41°, +35°, +35°, +33°, oldest Scythian, youngest Carnian) [MÁRTON–MÁRTON 1983]. In order to solve this problem, studies need to be continued in two directions. On the one hand, additional work is needed on red beds that display significantly different tilts. On the other hand, the possibility of the existence of an inclination error in the red beds will have to

be investigated (and eliminated?) and the reason(s) for the existence of markedly different inclinations between the red beds and the somewhat younger gray marls elucidated and resolved.

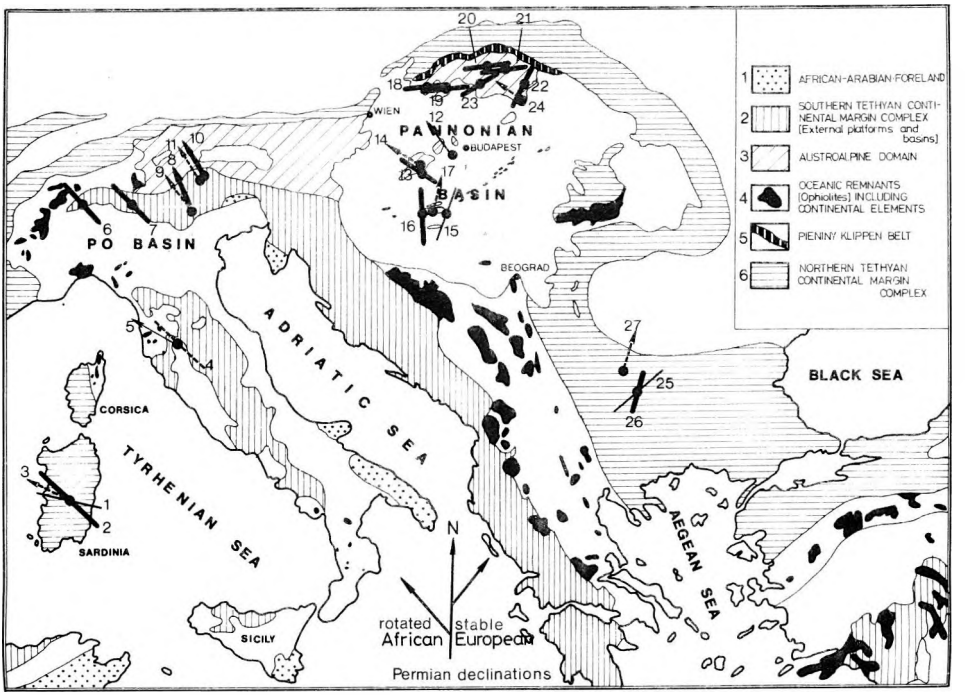

Fig. 7. Declinations measured on Carboniferous, Permian, and Triassic rocks of the Central Mediterranean.

References: 1. EDEL et al. 1981; 2. ZIJDERVELD et al. 1970 a, WESTPHAL et al. 1976; 3. HORNER–LOWRIE 1981; 4. VANDENBERG 1979; 5. VANDENBERG–WONDERS 1976; 6. HEINIGER 1979; 7. HEINIGER 1979; ZIJDERVELD et al. 1970/b, FÖRSTER et al. 1975; 8. ZIJDERVELD et al. 1970/b; 9. MANZONI 1970; 10. MANZONI 1970; 11. MANZONI 1970; 12. MÁRTON 1984; 13. Present paper; 14. MÁRTON–MÁRTON 1983; 15. MÁRTON 1984; 16. Present paper; 17. MÁRTON, unpublished; 18–23. KRS et al. 1982; 24. MÁRTON, unpublished; 25–27. NOZHAROV et al. 1980

7. ábra. A középső Mediterrán területről karbon, perm és triász kőzeteken meghatározott deklinációk irányai

1 — Afrikai–Arábiai előtér; 2 — a Tethis déli kontinentális szegély üledékei; 3 — Ausztro-alpi terület; 4 — óceáni maradványok (ofiolitok), kontinentális elemekkel; 5 — Pieniny szirtöv; 6 — a Tethis északi kontinentális szegély üledékei

Рис. 7. Направления склонения, определенные на породах карбона, перма и триаса со средней части бассейна Средиземного моря

1 — Афро-Арабский форланд; 2 — осадки южно-континентального борта Тетиса; 3 — Австро-альпийская территория; 4 — океанические остатки (офиолиты) с континентальными элементами; 5 — зона Пьенинских утесов; 6 — осадки северо-континентального борта Тетиса

REFERENCES

EDEL J. B., MONTIGNY R., and THUIZAT R. 1981: Late Palaeozoic rotations of Corsica and Sardinia: new evidence from paleomagnetic and K-Ar studies. Tectonophysics, **79**, 3–4, pp. 201–223

ELSTON D. P. and PURUCKER M. F. 1979: Detrital magnetization in red beds of the Moenkopi Formation (Triassic), Gray Mountain, Arizona. Journ. Geophys. Res. **84**, B4, pp. 1653–1665

FÖRSTER H., SOFFEL H., ZINSSER H. 1975: Palaeomagnetism of rocks from the Eastern Alps north and south of the Insubrian line. N. Jb. Geol. Paläont. Abh. **149**, pp. 112–127

HEINIGER C. 1979: Palaeomagnetic and rockmagnetic properties of the Permian volcanics in the western Southern Alps. J. Geophys. **46**, 4, pp. 397–411

HORNER F. and FREEMAN R. 1983: Palaeomagnetic evidence from pelagic limestones for clockwise rotation of the Ionian zone, Western Greece. Tectonophysics, **98**, 1–2, pp. 11–27

HORNER F. and LOWRIE W. 1981: Paleomagnetic evidence from Mesozoic carbonate rocks for the rotation of Sardinia. J. Geophys. **49**, 1, pp. 11–19

KRS M., MUSKA P., PAGAC P. 1982: Review of palaeomagnetic investigations in the West Carpathians of Czechoslovakia. Geologické práce, Bratislava, 78, pp. 39–58

MANZONI M. 1970: Palaeomagnetic data of middle and upper Triassic age from the Dolomites (Eastern Alps, Italy). Tectonophysics, **10**, 4, pp. 411–424

MÁRTON E. 1980/a: Palaeomagnetism of upper Palaeozoic and Triassic sediments from the Bükk Mts, Hungary. Seventh ann. mtg. of the EGS, Budapest. Programme and abstracts, p. 126

MÁRTON E. 1980/b: Multicomponent natural remanent magnetization of migmatites, Mórágy area, Southwest Hungary. Earth Planet. Sci. Lett. **47**, 1, pp. 102–112

MÁRTON E. 1981: Palaeomagnetism of some early Triassic rocks from the Jósvafő-Perkupa area (in Hungarian). Report of ELGI

MÁRTON E. 1984: Palaeomagnetism of the magmatic rocks of the Velence-Mountains, Hungary (in Hungarian with English abstract). Magyar Geofizika, **25**, 2–3, pp. 48–61

MÁRTON E. 1985: Tectonic implications of palaeomagnetic results for the Carpatho-Balkan and adjacent areas, in The geological evolution of the Eastern Mediterranean. Dixon, J. E. and Robertson, A. H. F., eds. Spec. Publ. Geol. Soc. N. 17, pp. 645–654

MÁRTON E. 1984: Palaeomagnetism of Palaeozoic granitoids and connected metamorphic rocks in Hungary. IGCP5 Newsletter, **6**, pp. 65–71

MÁRTON E., MÁRTON P. 1978: On the deviation of Mesozoic palaeopoles of the Middle Mountains of Transdanubia and of the Villány-mountains (in Hungarian with English abstract). Magyar Geofizika, **19**, 4, pp. 129–136

MÁRTON E., MÁRTON P. 1980: Palaeomagnetic indication of differential rotations northwest and southeast of the Zagreb–Zemplen tectonic line in Transdanubia, Hungary. Seventh ann. mtg. of the EGS, Budapest. Programme and abstracts, p. 97

MÁRTON E., MÁRTON P., HELLER F. 1980: Remanent magnetization of a Pliensbachian limestone sequence at Bakonycsernye (Hungary). Earth Planet. Sci. Lett. **48**, 1, pp. 218–226

MÁRTON E., MÁRTON P. 1983: A refined apparent polar wander curve for the Transdanubian Central Mountains and its bearing on the Mediterranean tectonic history. Tectonophysics, **98**, 1–2, pp. 43–57

MÁRTON P. 1983: Palaeomagnetism of Oligocene–Miocene sediments from the North Hungarian Range, Hungary (in Hungarian). Report of the Eötvös University

NOZHAROV P., PETKOV N., YANEV S., KROPACEK V., KRS M., PRUNER P. 1980: A palaeomagnetic and petromagnetic study of upper-Carboniferous, Permian and Triassic sediment, NW Bulgaria. Studia geoph. et geod. **24**, 3, pp. 252–284

VANDENBERG J. 1979: Implications of new palaeomagnetic data from the Verrucano (Tuscany, Siena) for its age and tectonic position. Geologica Ultraiectina, 20, pp. 137–146

VANDENBERG J., WONDERS A. A. H. 1976: Paleomagnetic evidence of large fault displacement around the Po-basin. Tectonophysics, **33**, 3–4, pp. 301–320

WESTPHAL M., ORSINI J., VELLUTINI P. 1976: Le microcontinent Corso–Sarde, sa position initiale: donnees paleomagnetiques et raccords geologiques. Tectonophysics, **30**, 1–2, pp. 141–157

ZIJDERVELD J. D. A., DE JONG K. A., VAN DER VOO R. 1970/a: Rotation of Sardinia: Palaeomagnetic evidence from Permian rocks. Nature, **226**, pp. 933–934

Zijderveld J. D. A., Hazeu G. J. A., Nardin M., Van der Voo R. 1970/b: Shear in the Tethys and the Permian paleomagnetism in the Southern Alps, including new results. Tectonophysics, **10**, 5–6, pp. 639–661

MAGYARORSZÁGI PERMO-TRIÁSZ VÖRÖS ÜLEDÉKEK PALEOMÁGNESES VIZSGÁLATA

MÁRTONNÉ SZALAY Emő és Donald P. ELSTON

Irányított mintákat gyűjtöttünk öt permo-triász vörös homokkő feltárásból a Balaton-felvidéken, egy feltárásból a Bükk hegységből és két feltárásból a Mecsek hegységből. Célunk az volt, hogy paleomágneses irányokat és pólusokat határozzunk meg, amelyek alkalmasak a különböző tektonikai egységek lehetséges rotációinak kiértékelésére.

Statisztikusan jól definiált irányokat sikerült meghatározni a Balaton-felvidék négy, a Mecsek hegység két feltárásából származó kőzetein több lépésben végzett termikus tisztítás és a mért és eltávolított remanencia elemzésének eredményeként.

Az irányok szignifikánsan eltérnek a mai tér irányától és ez a remanencia idős korát bizonyítja. Ennek ellenére a mágnesezettség hordozói komplexek és egyaránt lehetnek gyűrődés előttiek és utániak is. Mégis, a helyi dőléssel korrigált irányok, amelyek a korábbi paleomágneses eredményekkel összhangban vannak, azt mutatják, hogy a Balaton-felvidék kb. 50°-ot fordult el a Mecsek hegységhez képest (Mecsek hegység: deklináció: 177,4°, inklináció: −5,0°, fordított polaritás; Balaton-felvidék: deklináció: 307,2°, inklináció: 11,0°, normál polaritás).

A meghatározott irányokat összehasonlítjuk a Mediterrán területről ismert hasonló korú paleomágneses eredményekkel.

ПАЛЕОМАГНИТНОЕ ИССЛЕДОВАНИЕ ПЕРМО-ТРИАСОВЫХ КРАСНОЦВЕТНЫХ ОТЛОЖЕНИЙ В ВЕНГРИИ

Эмё МАРТОН и Доналд П. ЭЛСТОН

Ориентированные образцы были собраны из пяти обнажений пермо-триасовых красноцветных песчаников в Прибалатонских горах, из одного обнажения в горах Бюкк и двух обнажений в горах Мечек. Наша цель заключалась в определении палеомагнитных направлений и полюсов, которые позволяют оценить возможные вращения различных тектонических единиц.

Удалось определить статистически надежные направления на породах, езятых из четырех обнажений Прибалатонских гор и двух обнажений Мечекских гор, в результате ступенчатой термической чистки и анализа замеренной и удаленной при чистке остаточной намагниченности.

Направления характерно отклоняются от направления настоящего поля, что подтверждает дверность остаточной намагниченности. Несмотря на это, носители намагниченности являются сложными и могут происходить из доскладчатой или послескладчатой эпохи. Все-таки, направления, поправленные за местные наклоны, которые согласуются с прежними палеомагнитными результатами, показывают, что район Прибалатонских гор совершил поворот на ок. 50° по сравнению с Мечекскими горами (горы Мечек: склонение: 177,4°, наклонение: −5,0°, обратная полярность; Прибалатонские горы: склонение: 307,2°, наклонение: 11,0°, нормальная полярность).

Определенные направления были сопоставлены с палеомагнитными разультатамы для пород подобного возраста, которые известны в бассейне Средиземного моря.

GEOPHYSICAL TRANSACTIONS 1985
Vol. 31. No. 1–3. pp. 213–255

SEISMIC MODELING IN A COMPLEX TECTONIC ENVIRONMENT

John J. MILLER*, Myung W. LEE*, Éva KILÉNYI**,
Ilona PETROVICS**, László BRAUN** and Gábor KORVIN**

The only known cokable hard coal occurrence of Hungary is found in the Mecsek Mountains of southern Hungary. ELGI has been trying since 1955 to apply the seismic technique to hard coal prospecting and in 1977 began to use the seismic reflection method.

The complex tectonic style of the area, seismic horizons of short lateral extent cut by near vertical normal faults and some thrust faults, have caused the processing and interpretation of the recorded data to be extremely difficult.

A cooperative effort involving ELGI and USGS scientists began in 1982 involving the use of two-dimensional modeling to create synthetic seismic sections from interpretation of the recorded data integrated with geologic information from boreholes.

The first model showed the initial interpretation to be erroneous and resulted in the reprocessing and re-interpretation of the seismic line. The second model was calculated using ray-trace and wave-equation methods and confirmed some parts of the new interpretation.

This study shows the value in using modeling in an iterative manner to aid the processor and interpreter. In addition, the limitations of both modeling and the CDP method of exploration are pointed out.

Keywords: seismic modeling, coal exploration, reflection seismics, complex tectonism, Mecsek Mts

1. Introduction

The single known cokable hard-coal occurrence in Hungary is found in the Mecsek Mountains, in southern Hungary. The Jurassic (Lias) hard coal has been intensively and continuously mined since the middle of the last century in the Pécs–Komló territory and, as shown by increasing demands, is still of economic significance. A new region, considered to be prospective, is the eastward continuation of the present-day mining area. The first exploratory boreholes were drilled in 1976, and the available data suggest that the coal deposits are comparable in economic significance to those of the Pécs–Komló district. In the Mecsek Mountains, the Eötvös Loránd Geophysical Institute (ELGI) has applied seismic techniques to hard coal prospecting since 1955. It was found that refraction surveys could successfully be used to map the relief and depth of the Middle Triassic carbonate structures, additionally, these techniques provided information about the thickness of the Miocene formation. Nonetheless, all of the information gained from the refraction surveys proved insufficient to resolve

* U. S. Geological Survey, Denver Federal Center, P. O. Box 25045, Denver, Colorado 80225
** Eötvös Loránd Geophysical Institute of Hungary, POB 35, Budapest, H–1440
Manuscript received: 5 March, 1985

the tectonic pattern even in an approximate fashion. Therefore, during the gradual development of seismic reflection methodology, ELGI has repeatedly needed to return to the study-site armed with novel geophysical techniques.

Among the techniques tested, dynamite surveys, first applied in 1977, proved that reflection seismics may be the proper method. But they also revealed serious obstacles to reflection surveying, caused by rough and covered topography, absence of roads, and difficult drilling conditions. Therefore VIBROSEIS® measurements, carried out since 1980, were specially designed for the topography and the roads by making the track of the vibrators curvilinear and deviating from the line of geophones

The main exploration problem is the complex tectonic environment: the seismic horizons are dissected by normal and thrust faulting into blocks of short horizontal extension. This has required, first of all, increasing the lateral resolution of the seismic method.

2. Geological background

The location of the experimental profile is shown in *Figure 1* with the surface geology indicated. Surface geology and drilling data provided the following stratigraphic information: the deepest formation encountered in the South Máza area is dolomite of the Anisian–Ladinian stage of the Middle Triassic, (T_2^{a-l}), known from borehole V–21. This is overlain by a limy marl deposit of the Ladinian stage (T_2^l), followed by alternating fluvial, deltaic, lacustrine and lagoonal layers of Carnian (T_3^k), Norian (T_3^n) and Rhaetian (T_3^r) ages. The last member of the Triassic is a 500–600 m thick sandstone layer of varying grain size and induration which is overlain by the Early Jurassic (Lower Lias) coal-bearing formation (of the Hettangian $J_1^{h_1}$). The coal-bearing formation consists of two rhythmic sedimentary cycles. The lower one reveals fluvial, tidal, marshland, deltaic and even littoral sedimentation cycles; in the upper one, littoral and mud-flat sedimentary cycles repeat one another. The Triassic–Jurassic boundary can only be drawn by means of pollen assemblages. The estimated thickness of the coal-bearing formation is 350–450 m. It is made up of coal seams of varying thickness and quality, of shales, aleurolite, sandstone layers and tuffite. Within the coal measures, one frequently encounters Late Cretaceous diabase instrusions which decrease coal quality.

The overlying sandstone group (of lower Sinemurian substage, $J_1^{s_1}$) was deposited without unconformity. It consists of limy sandstones, aleurolites, marls, and shaly marls; its average thickness is 250 m. The marl group of the cover, belonging to the upper Sinemurian substage ($J_1^{s_2}$), was also created by continuous sedimentation, it mainly consists of marl, subordinately of clayey marl. Its thickness is 150–200 m. It is followed by a group of spotty marl layers

® The use of trade names does not constitute an endorsement by the Eötvös Loránd Geophysical Institute or by the U. S. Geological Survey.

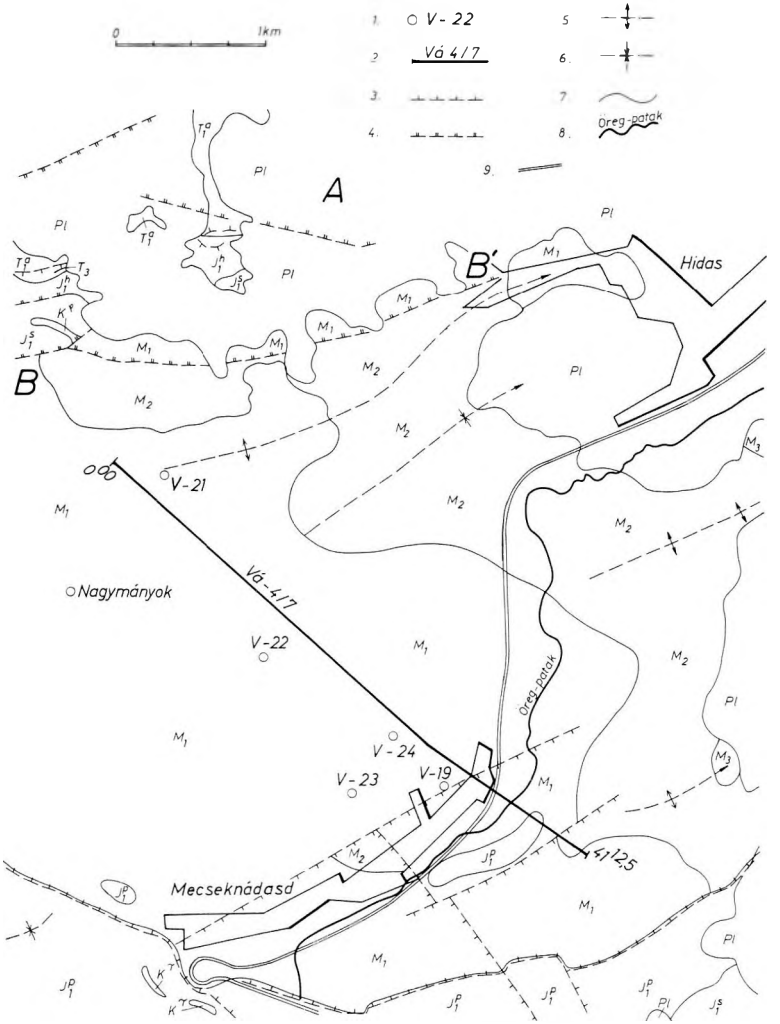

Fig. 1. Geologic map of the study area with locations of the seismic profile and boreholes
1 — borehole; 2 — seismic profile; 3 — fault; 4 — overthrust; 5 — axis of anticline; 6 — axis of syncline; 7 — boundary of geological formations; 8 — brook; 9 — road

1. ábra. A kutatási terület földtani térképe és a kísérleti szeizmikus vonal helyszínrajza
1 — mélyfúrás; 2 — szeizmikus vonal; 3 — vető; 4 — feltolódás; 5 — antiklinális tengelye; 6 — szinklinális tengelye; 7 — képződményhatár; 9 — út

Рис. 1. Геологическая карта района разведки и план экспериментальной сейсмической линии
1 — глубокая скважина, 2 — сейсмическая линия, 3 — сброс, 4 — надвиг, 5 — ось антиклинали, 6 — ось синклинали; 7 — раздел формации; 8 — ручей; 9 — дорога

($J_1^{s_3}$) of a thickness of about 300 m, consisting of marl and limy marl. These sediments ($J_1^{s_1} - J_1^{s_3}$) can be comprehensively termed as a marl formation of sublittoral–neritic facies. On the study site there is no information about the thickness of Middle Lias (J_1^p) sedimentary series or its relation to the overlying unit, in other places the thickness can reach 1000 m. Their material is clayey marl, marl, limy marl, sandy marl, and limy sandstone. Upper Lias and Dogger age layers ($J_1 - J_2$) were only found in two boreholes. Their estimated thickness is 40 m. The Bajocian ($J_2^{b_1}$) is represented by marl and limy marl, its thickness is 70 m. The steeply dipping Malm formations (J_3) consist mainly of different kinds of marls; their penetrated thickness is 120 m.

Younger Mesozoic age is represented by the Lower Cretaceous diabase intrusions found in all boreholes, as well as the 150-m thick formation found in the V–11 hole, consisting of volcanic sedimentary breccia and volcanogenic sandstone successions.

The eroded Mesozoic surface is covered by Miocene (M) lacustrine rocks, followed by fluvial and volcanic rocks. The youngest Pleistocene–Holocene formations (Pl–H) of the site are the loess, the clayey loess, erosional detritus, and Holocene soil uncomformably overlying the Miocene layers or the Mesozoic rocks.

It is far from easy to sum up briefly the tectonic framework of this area, partly because of the intricate tectonic pattern, and partly because of the differing opinions expressed in the literature. In general though:

(a) The folding mechanism of the easily traceable Austrian orogenic phase (mid-Cretaceous epoch) created the folds with NE–SW oriented axes, having broken flanks and transverse faults.

(b) The folded structural elements are joined by SE-dipping overthrusts of NE–SW strike. The displacement along these planes of motion is NW-directed.

(c) In the epoch following folding, with the decreasing compression, SE-ward dipping faults of 300–400 m throw occurred in the Northern Nappe Belt, and parallel with it to the SE. The Northern Nappe Belt (A) and its southeastern edge, the Northern Overthrust Line (BB′), delimit the study area from the north.

(d) Subsequent to (or possibly simultaneously with) the formation of the longitudinal faults, transverse (WNW–ESE directed), SSW-ward dipping faults appeared.

(e) The ENE–WSW and the NE–SW-directed faults are of Tertiary age. The southward dipping large fault of 800–1200 m amplitude, parallel with the Óbánya Valley, represents the southern boundary of the site.

(f) The structural forms of the Mesozoic formations have affected the denudation following elevation, the beginning of Neogene sedimentation, and the initial phase of the development of the new structures as well. Consequently, folded structures of ENE–WSW strikes are rather frequent.

(g) Within the Neogene basin, longitudinal and transverse faults can be traced—some of them indicating the reactivation of earlier faults—with approximate displacements of 30–100 m. How far to the east the area extends, has

not been clarified to date. In some parts of the area, the hard coal group had been denuded as far down as the uplifted Triassic formations.

3. The model

A common technique used in the interpretation of complex structures is to make a geologic model from interpretation of available borehole and seismic data, calculate the two-dimensional (2-D) seismic response of this model, and compare the results to the original seismic data. A good match between the model response and the original data gives confidence in the geologic interpretation. A poor match necessitates reinterpretation of the available data. A theoretical discussion of seismic modeling is given in the AIMS® (Advanced Interpretive Modeling System) Users Reference Manual, published by Geoquest International, Inc. [1983], together with an extensive bibliography. A case history on the use of ray-trace modeling for a refined delineation of a complex salt dome structure is given in MAY and COVEY [1983]. The first attempt to use AIMS modeling package, to calculate two-dimensional seismic models from borehole data in the area of interest, was made in May 1982. Unfortunately, the seismic data for the area were not processed adequately for this purpose at that time.

A renewed attempt was made in November 1982, based on a copy of the seismic section processed with the routine package *(Fig. 2)*, a geologic model interpreted from the borehole data along the line, and a preliminary interpretation of the seismic line defined in terms of two-way seismic travel time. These data were used in model calculations in 1983.

The results generated by the first model proved that the original standard processing of the line (performed using the SDS–3 program package [TIMÁR 1984] on the RYAD–35 computer) had not yet achieved the definition of an acceptable model, as shown by the poor match beetwen the input model and the synthetic results. In the next, refined processing cycle, a more definitive, high-resolution, noise-free time section was sought, by means of true amplitude preservation, proper deconvolution, and thorough editing of the field records (records with too large lateral offsets were left out). The correlation of seismic horizons was further enhanced by automatic static corrections and coherency filtering.

The following were the main deviations from the standard scheme of processing:

(a) use of floating point results after demultiplexing (previously: fixed point),

(b) true amplitude recovery (instead of the previously applied digital Automatic Gain Control), and

(c) a special Vibroseis deconvolution (VIBRODECON) on the original field seismograms (previously: spike deconvolution) followed by a post-stack zero-phase deconvolution. The resulting time section is shown in *Figure 3*.

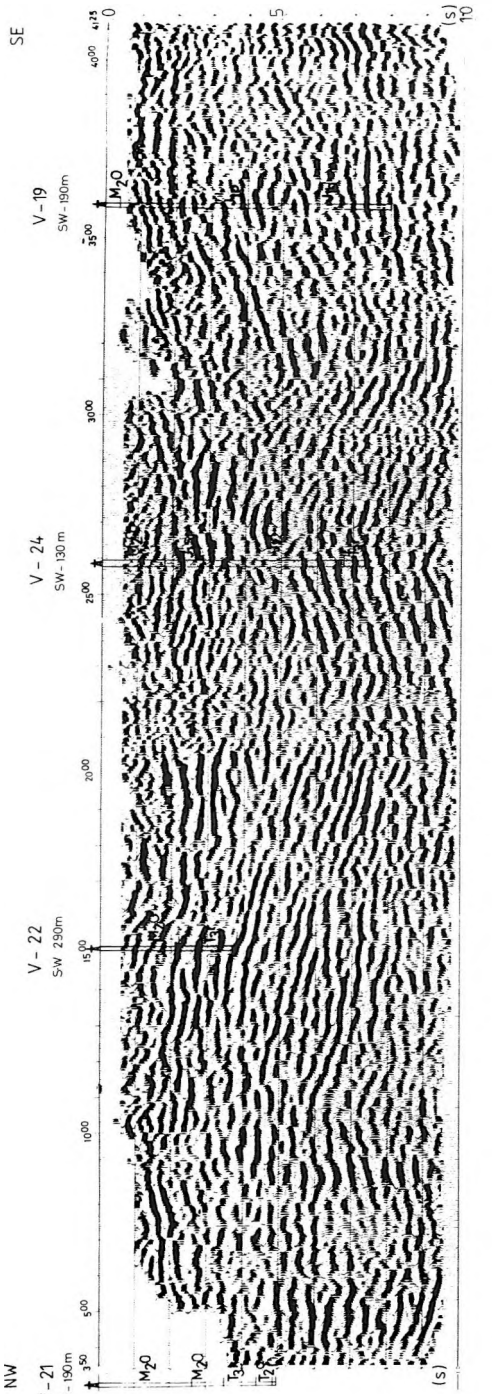

Fig. 2. Routinely processed time section

2. ábra. Időszelvény rutin feldolgozással

Рис. 2. Временной разрез, полученный в результате обработки в производственном порядке

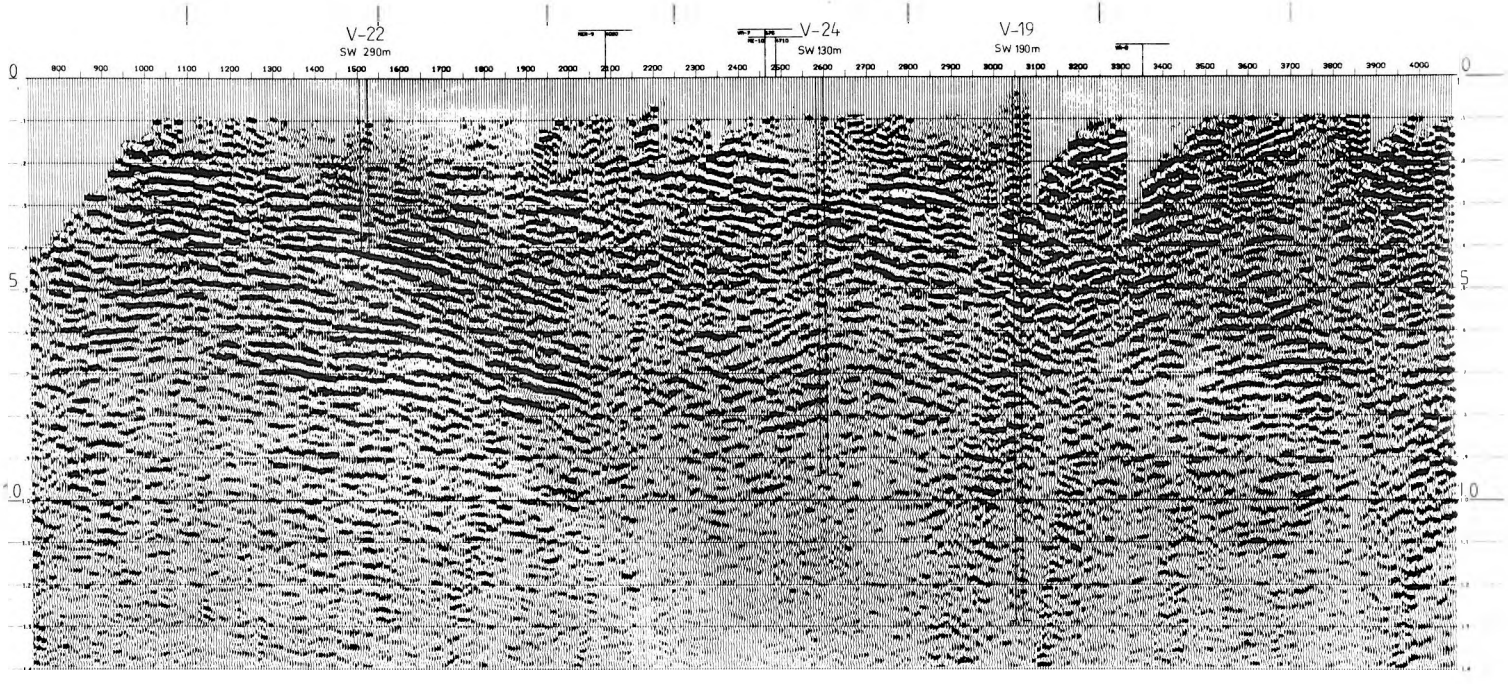

Fig. 3. Time section after refined processing

3. ábra. Időszelvény finomított feldolgozással

Рис. 3. Временной разрез, полученный в результате более тонкой обработки

Wave equation migration was applied next (*Fig. 4*). The main difficulty in processing was proper determination of the velocity functions to be used for migration. As indicated by the low signal-to-noise ratio, steeply dipping fault planes, and the short lateral extent of the layers seen in Figure 4, made delineation of clearly identifiable reflectors, necessary for a proper velocity analysis, difficult to achieve. The velocities used in the second modeling effort were approximated in successive steps: the velocity functions applied for the computation of the rough stack were checked again by means of a velocity scan after automatic static corrections, and the derived velocities were used to obtain the final time section. These velocity functions were plotted, corrected according to the available well-log and geologic data, and the variation of the velocities along the profile was constructed. The $v(x, t)$ function formed the basis of the depth transformation after migration. During the geologic interpretation, the velocities of the given layers were determined on the basis of a joint interpretation of the computed interval velocities and the acoustic logs; care was taken that only negligible deviations would occur between the velocities accepted in the model and the RMS velocities obtained from seismic velocity determinations.

For the better enhancement of the tectonic planes, pie-slice filtering was applied (7 channels, 20–40 Hz frequency bandwidth, 1000 m/s boundary velocity). The pie-slice filtered time section is shown in *Figure 5*. The depth section before and after pie-slice filtering is shown in *Figures 6* and *7*, respectively. Although the section clearly reveals the position of the NW-ward rising tectonic planes, the seismic events of opposite dip are almost completely suppressed. In the definition of the final model, both versions of the depth section (with and without pie-slice filtering) have been utilized.

The model is shown in *Figure 8*. The eroded Miocene surface was not too difficult to identify, as the reflection-free zone shows good agreement with the subsurface position of the Miocene formation known from boreholes. The fault structure was determined mainly on the basis of the layered nature of the upper part of the coal formation. The layered structure is an alteration of sandstone (subordinately: marl) and the coal seams. Acoustic velocities in sandstone increase with depth to a maximum value of 4500 m/s. On the other hand, velocities through coal layers barely change. In places where a trachydolerite intrusion has penetrated the coal, contact metamorphism induced a coking effect. At such sites velocities in the coal seam decrease (to 2000–2400 m/s), while the trachydolerite itself shows high velocities (5000–5800 m/s). Studies on core samples and acoustic logs prove the presence of both faults and overthrusts where the acoustic velocity abruptly drops (to 2000–2200 m/s). The overthrust planes crossing the coal-bearing formation seem to screen the deeper lying layers, as indicated by the deterioration of reflection quality; for example, note that the Triassic erosional surface interpreted at 200 m depth on the left side of Figure 7 and hit at about 800 m depth in the V–24 borehole is practically untraceable on the seismic data SE-ward from the overthrust plane subcropping at 2000 m horizontally.

The seismic character of the left side of Figure 7 is completely dissimilar

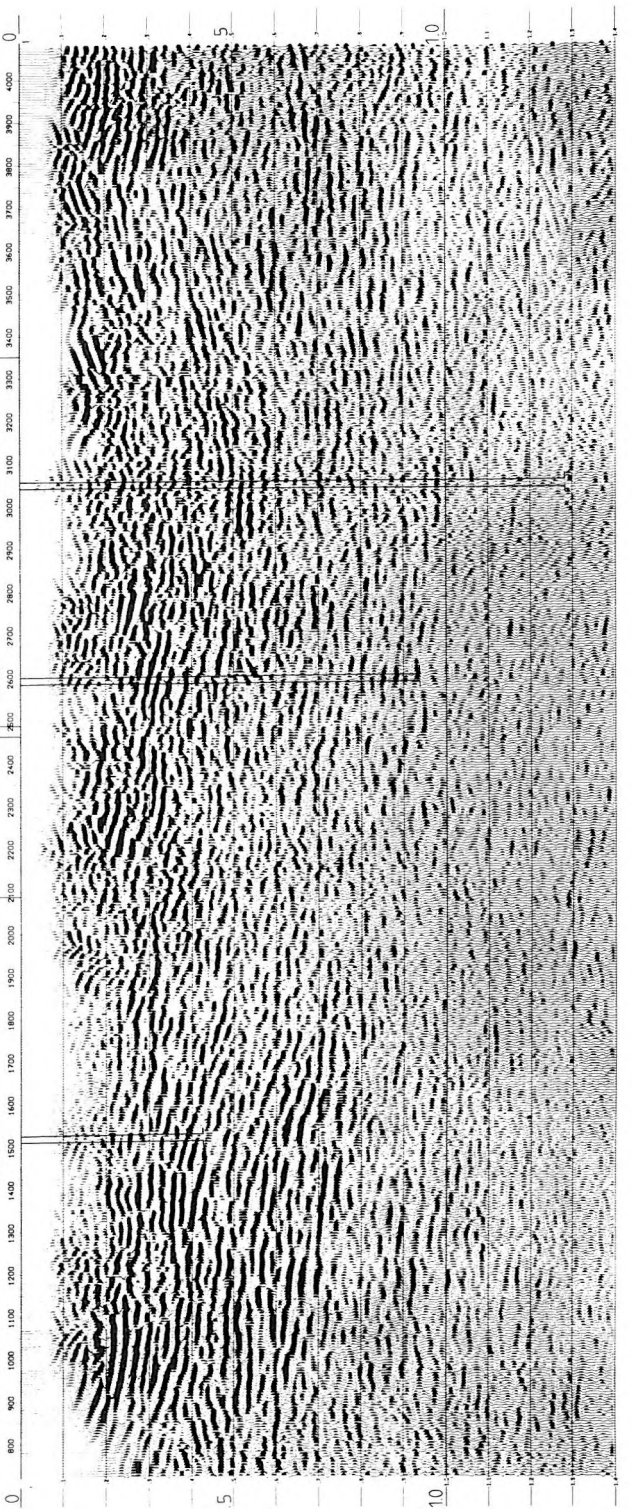

Fig. 4. Migrated time section

4. ábra. Migrált időszelvény

Рис. 4. Мигрированный временной разрез

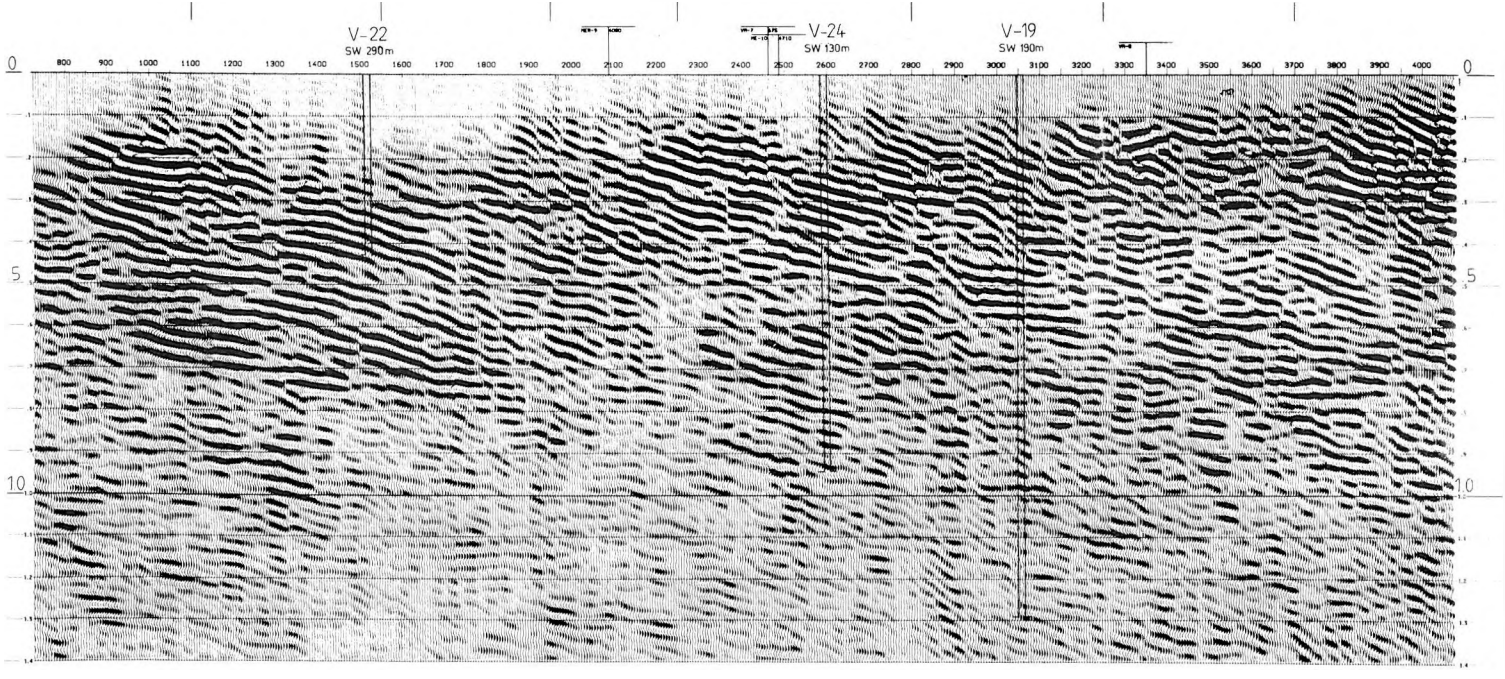

Fig. 5. Migrated time section with pie-slice filtering

5. ábra. Migrált időszelvény sebességszűréssel

Рис. 5. Мигрированный временной разрез с скоростной фильтрацией

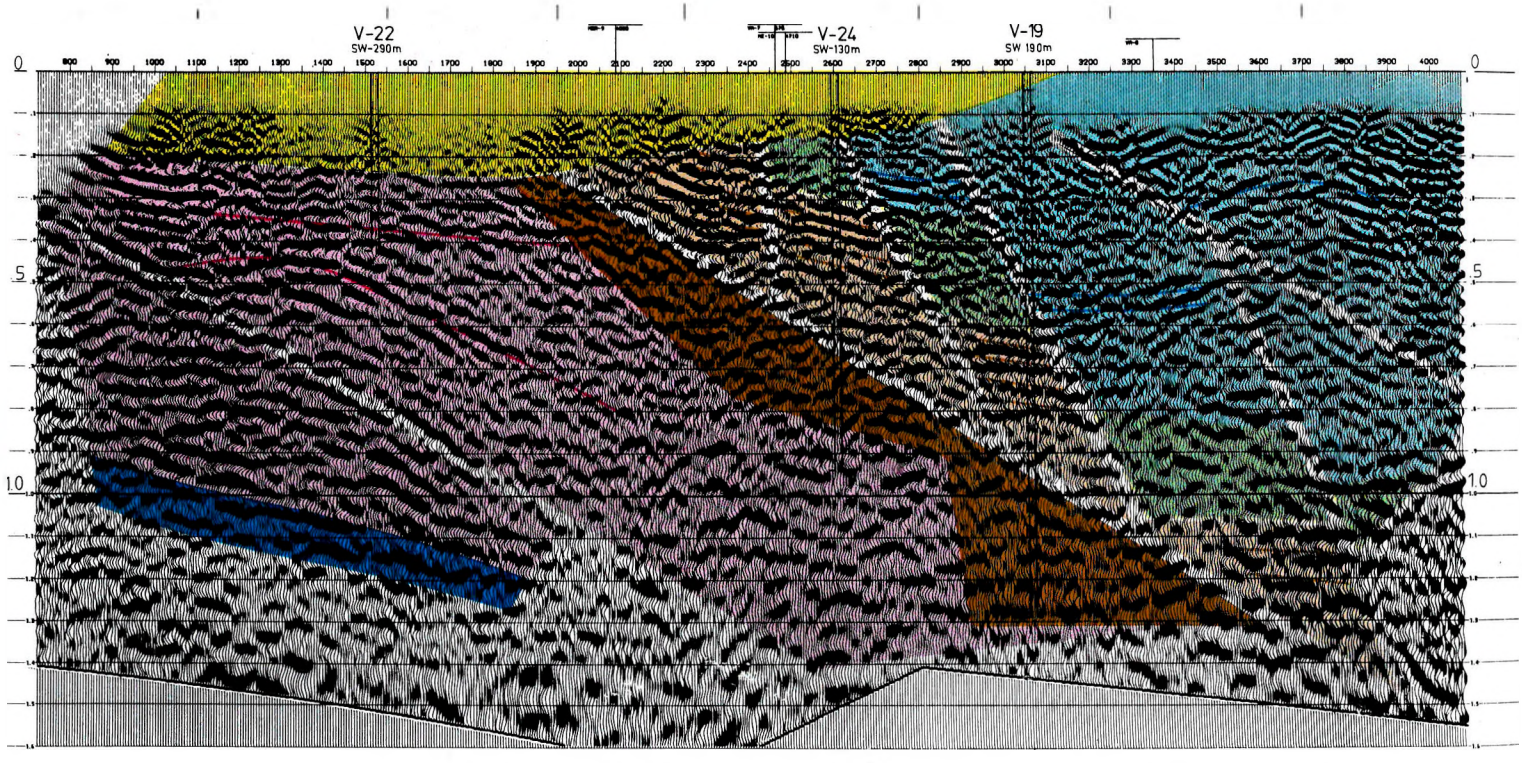

Fig. 6. Migrated depth section
Early Paleozoic: dark blue; Triassic: purple; Jurassic: Hettangian coal-bearing formation — brown, Sinemurian — green, Pliensbachian — light blue; Miocene: orange

6. ábra. Migrált mélységszelvény
Ópaleozoikum: sötétkék; triász: lila; jura: hettangi széntelepes összlet — barna, szinemuri — zöld, pliensbachi — világoskék; miocén: narancssárga

Рис. 6. Мигрированный глубинный разрез
Древний палеозой: темно-синний цвет, триас: лиловый, юра: угленосная толща геттанга — коричневый, синемурский — зеленый, плинсбахский — светлосинний; миоцен: оранжевый

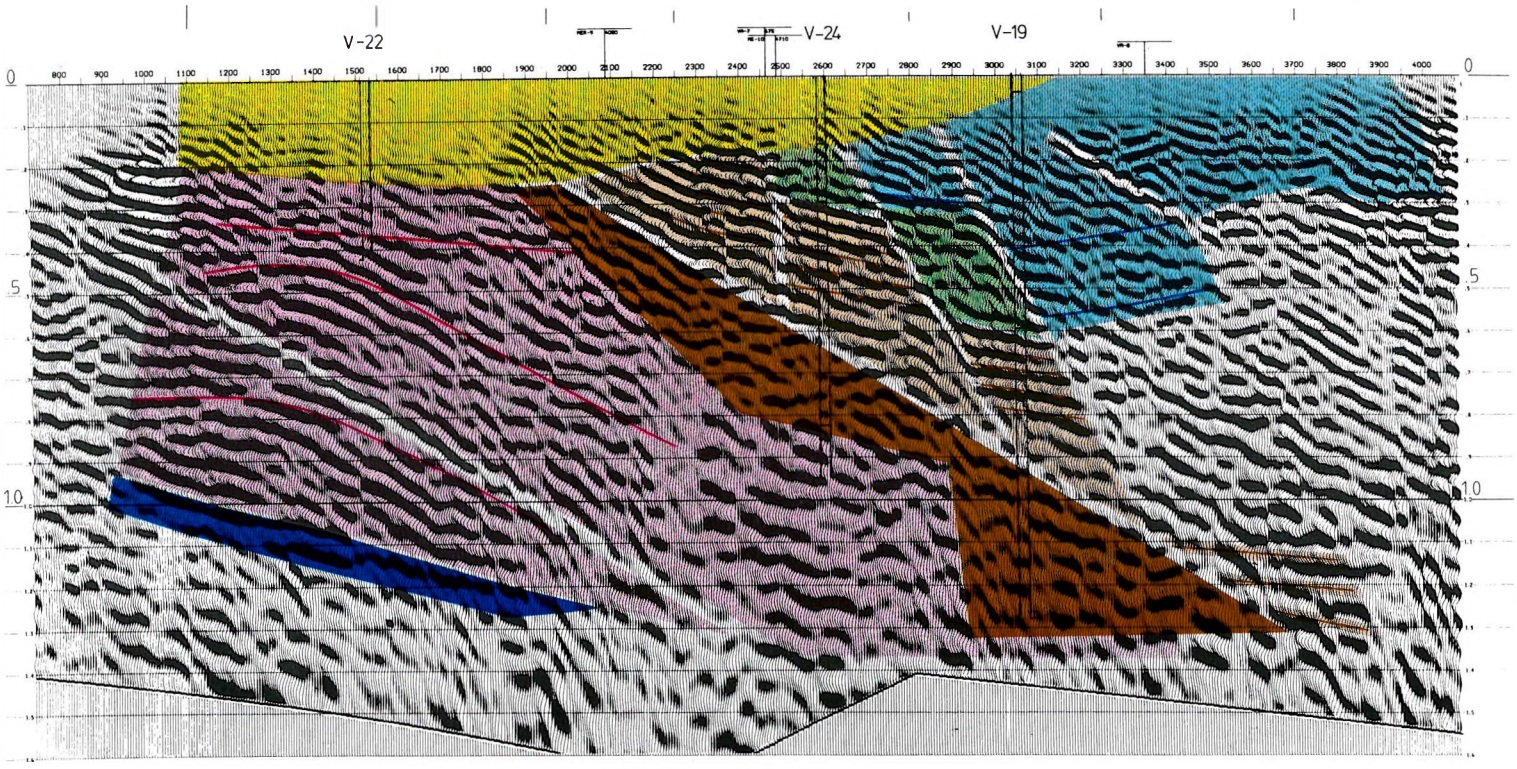

Fig. 7. Migrated depth section with pie-slice filtering
Early Paleozoic: dark blue; Triassic: purple; Jurassic: Hettangian coal-bearing formation — brown, Sinemurian — green, Pliensbachian — light blue; Miocene: orange

7. ábra. Migrált mélységszelvény sebességszűréssel
Ópaleozoikum: sötétkék; triász: lila; jura: hettangi széntelepes összlet — barna, szinemuri — zöld, pliensbachi — világoskék; miocén: narancssárga

Рис. 7. Мигрированный глубинный разрез с скоростной фильтрацией
Древний палеозой: темно-синий цвет, триас: лиловый, юра: угленосная толща геттанга — коричневый, синемурский — зеленый, плинсбахский — светлосиний; миоцен: оранжевый

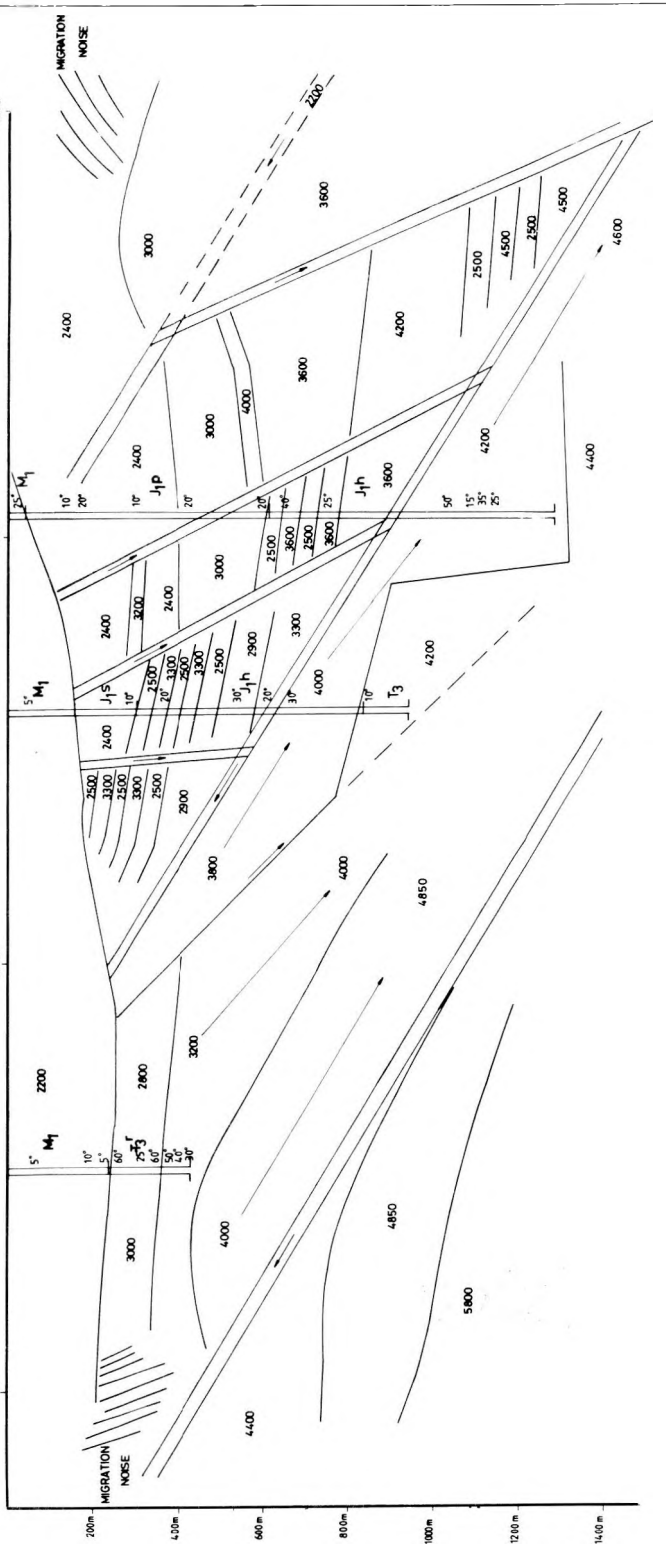

Fig. 8. Geologic model with borehole data and seismic velocities (in m/s) determined from seismic and acoustic data

8. ábra. A földtani modell a fúrási adatokkal és a szeizmikus- és akusztikus szelvényből megállapított terjedési sebességértékekkel (m/s)

Рис. 8. Геологическая модель с данными бурсния и значениями скорости распространения, определенными по сейсмическому разрезу и акустическому каротажу (м/с)

to the pattern after the appearance of the coal-bearing formation. Here, the presence of Middle and Lower Triassic strata can be assumed, the unconformably appearing deepest reflector of great interval velocity very likely corresponds to the surface of the early Paleozoic. If the modeling results show a fair agreement with the original seismic section, i.e. confirm the validity of the interpretation, all reflection profiles measured on the area will be reprocessed as this experimental one.

4. Calculation of the seismic response of the model

In the AIMS modeling package the interfaces between each layer must first be digitized in terms of horizontal distance and depth, and the physical properties of the rocks (i.e. rock velocity and density) must be defined for each layer. *Figure 9* shows a computer plot of the digitized model referenced to depth. Each layer boundary is defined to be a horizon and numbered. Next, normal-incidence ray tracing is performed. A ray perpendicular to each horizon is traced upward, refracting through horizons above until it emerges at a surface point. Those rays which emerge at a user-specified surface interval (analogous to a Common Depth Point interval) are saved and their two-way travel times and amplitude characteristics are calculated. Diffracted rays were not included in the model at this point.

Figure 10 shows all the rays emerging on the surface at 100-meter intervals. The raypath-sort phase of the modeling package will collect all the rays emerging at a common surface point. In order to demonstrate this as well as the effect of complex geology on the seismic response, *Figure 11* shows those rays emerging at surface position 3100. The seismic trace recorded at this position will be composed of reflected energy from layers 6, 7, 8, 14, 18, 19, 20, 21, 22, 37, and 9. Their horizontal positions at depth range from approximately 2700 to 3200 meters. Hence the time image is horizontally distorted.

Figure 12 is a plot of travel times of the rays from Figure 10 beneath their surface emergence point. Chevrons are plotted at the positions of the rays and indicate either negative (<) or positive (>) polarity of the reflection coefficients. Note that horizon 27 in time is mapped under position 2600 to 3000 meters, whereas its true lateral extent is from 2450 to 2800 meters (see bold lines on Figs. 10 and 12). The greater the dip of a reflecting interface, the greater will be its spatial distortion.

The spike-generation phase creates traces composed of spikes having the appropriate amplitude positioned at the two-way travel time of each ray. The amplitude is the reflection coefficient of the originating interface modified by transmission and spreading losses through the medium. These spike traces are then convolved with a user-defined wavelet (such as a Ricker, Klauder, or bandpass wavelet), the result being the two-dimensional seismic response of the model. In order to simulate the appearance of real seismic data, random noise can be added to the model (see Figure 15) at any time after spike trace gener-

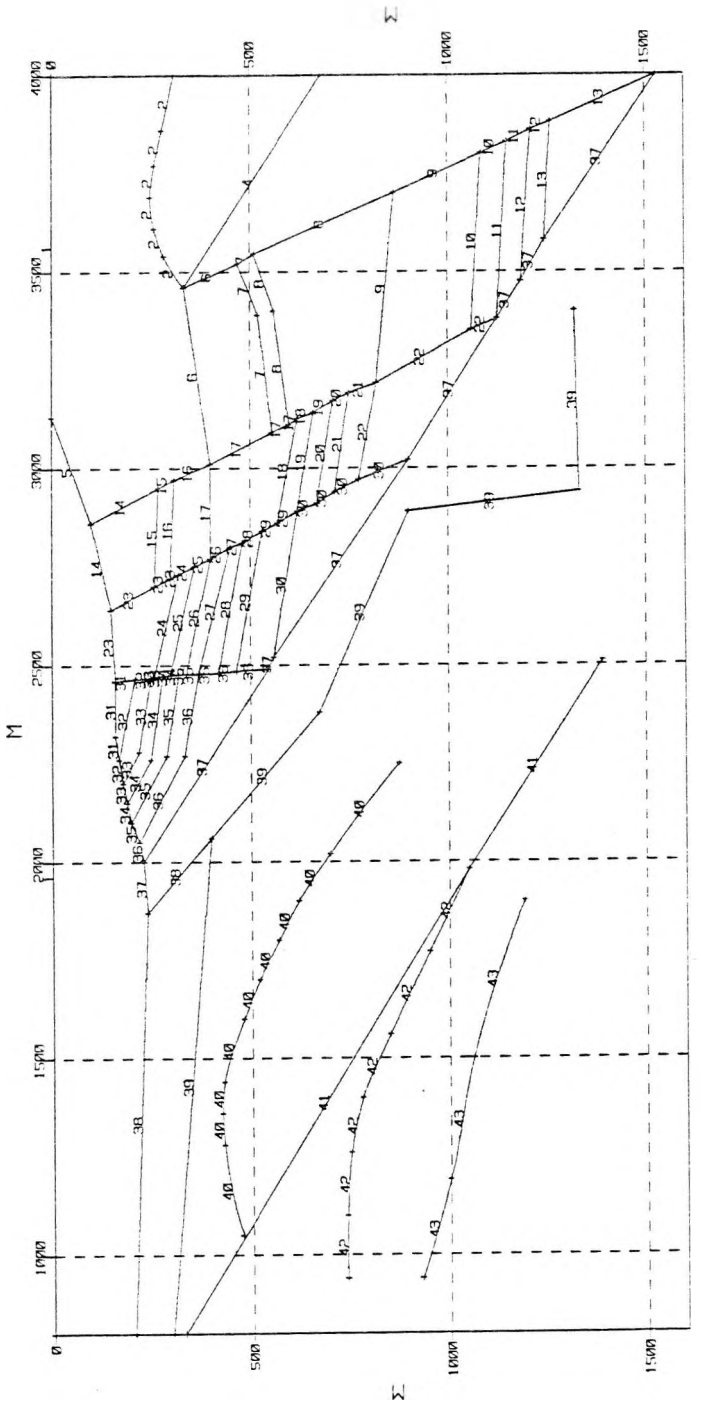

Fig. 9. Digitized model

9. ábra. A digitalizált modell

Рис. 9. Модель, преобразованная в цифровой кол

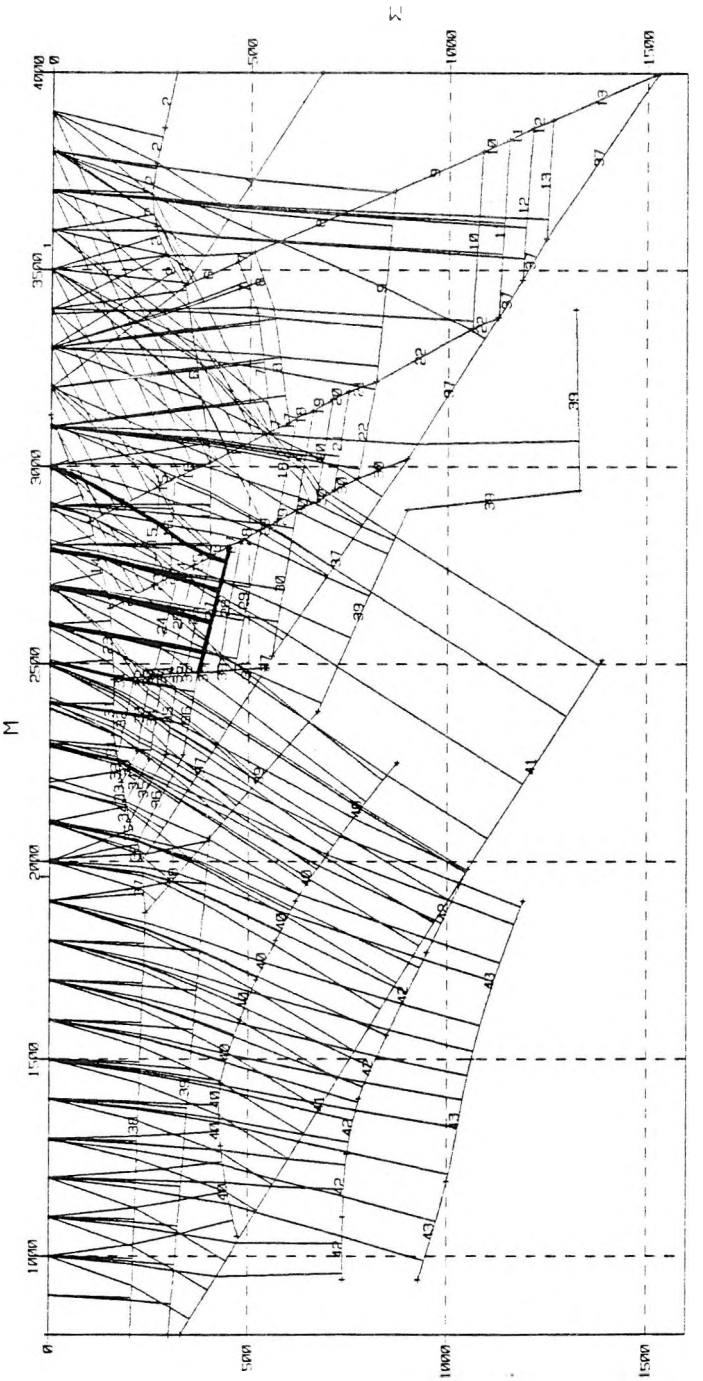

Fig. 10. Rays traced at 100 m surface intervals

10. ábra. A felszínre 100 m-ként bocsátott sugarak

Рис. 10. Лучи, приходящие к дневной поверхности через 100 м

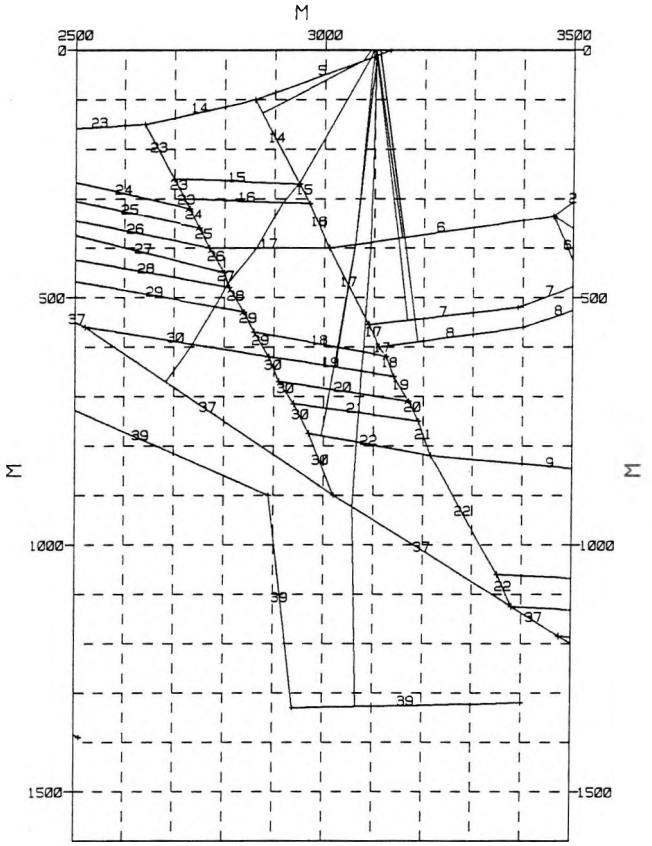

Fig. 11. Rays emerging at surface position 3100

11. ábra. A 3100 felszíni ponthoz érkező sugarak

Рис. 11. Лучи, приходящие к точке 3100 на дневной поверхности

ation, as well as gain function application or any other processing technique desirable.

Figure 13 is the seismic response of a 20 Hz Ricker wavelet convolved with spike traces at a 10-meter surface interval. The effects of transmission losses and spherical spreading on the reflection amplitude have been ignored; thus Figure 13 is the true amplitude response and can be considered to approximate an unmigrated, stacked section without diffractions.

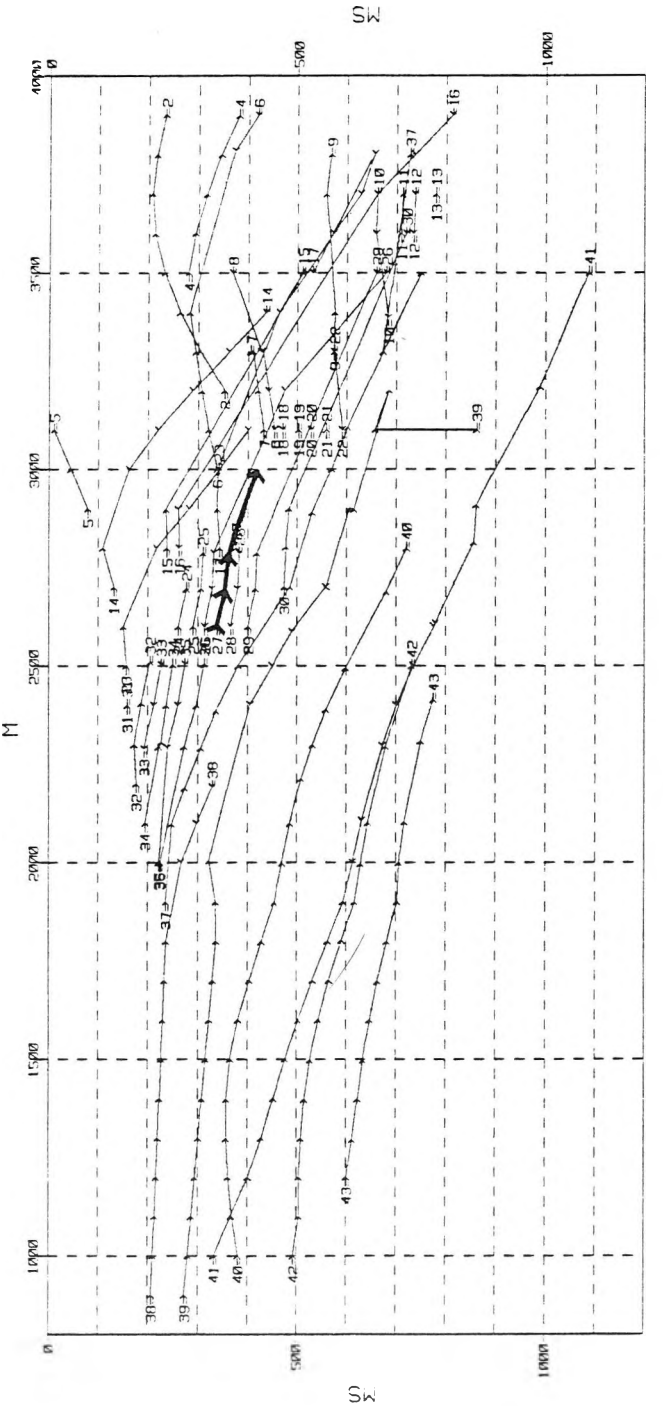

Fig. 12. Travel times of rays from Fig. 10

12. ábra. A 10. ábra sugaraihoz tartozó terjedési idők

Рис. 12. Времена распространения, относящиеся к лучам на рис. 10

5. Discussion and interpretation

Comparing Figure 13 to Figure 5 (the migrated time section with pie-slice filter) and to Figure 3 (the time section after refined processing) reveals areas of similarity and dissimilarity. In the horizontal range of 800 to 2,000 meters, the modeled response and the real data generally match. This is the area of the simplest geological conditions along the line. The layered, dipping, and faulted events between 2,100 m and 3,300 m horizontally, and 200 to 700 msec also show a good match. However, there are dissimilarities which cause some question as to the validity of the model.

One problem concerns the shallowest horizon, which outcrops at the surface position 3,100 and represents the erosional surface truncating the faulted, dipping coal beds. This shows a distinct reflection in the model but does not appear in the real data. Similarly, the fault plane interpreted as horizon No. 37 appears as a dipping reflector on the model but not on the data. Finally, horizon No. 39 was interpreted from borehole data to be a discontinuity in velocity and input to the model as such. It also appears as a dipping reflector on the model but cannot be found on the real data.

The discontinuous and segmented appearance of the reflection events shown in Figure 13 might be caused by the discontinuous normal gradient of the subsurface model, such as the fault boundaries. In this case, the normal-incident ray theory would not provide adequate seismic response because the reflection comes from an area, not simply from a single point source as assumed in ray-tracing. In an attempt to resolve some of these problems, we decided to calculate the wave-equation solution to the seismic response. The main difference between the wave-equation and ray-trace solution is that all diffracted energy is included in the wave-equation solution. The wave-equation solution to the model is shown in *Fig. 14*. The erosional surface mentioned earlier as well as the fault plane defined as horizon No 37 are both still present. However, the match between this solution and the original data is now much better, particularly in the area of the segmented reflecting events between 2,000 m and 3,500 m horizontally and 200 and 500 msec. Also, the strong reflector between 3,500 and 4,000 m horizontally, and 600 to 800 msec has lost its segmented appearance. This improvement is evident in other areas of the model also. *Figure 15* is the wave-equation response with random noise added in an attempt to match more closely the appearance of the original data.

6. Conclusions

The fact that erosional surfaces and fault planes appear as reflections in the model but do not appear in the original data is caused by a limitation in the modeling. The model requires that each change in physical property (e.g. velocity and density) be defined as a distinct layer boundary (called a horizon). Velocity transition zones, like those which sometimes appear in a highly faulted

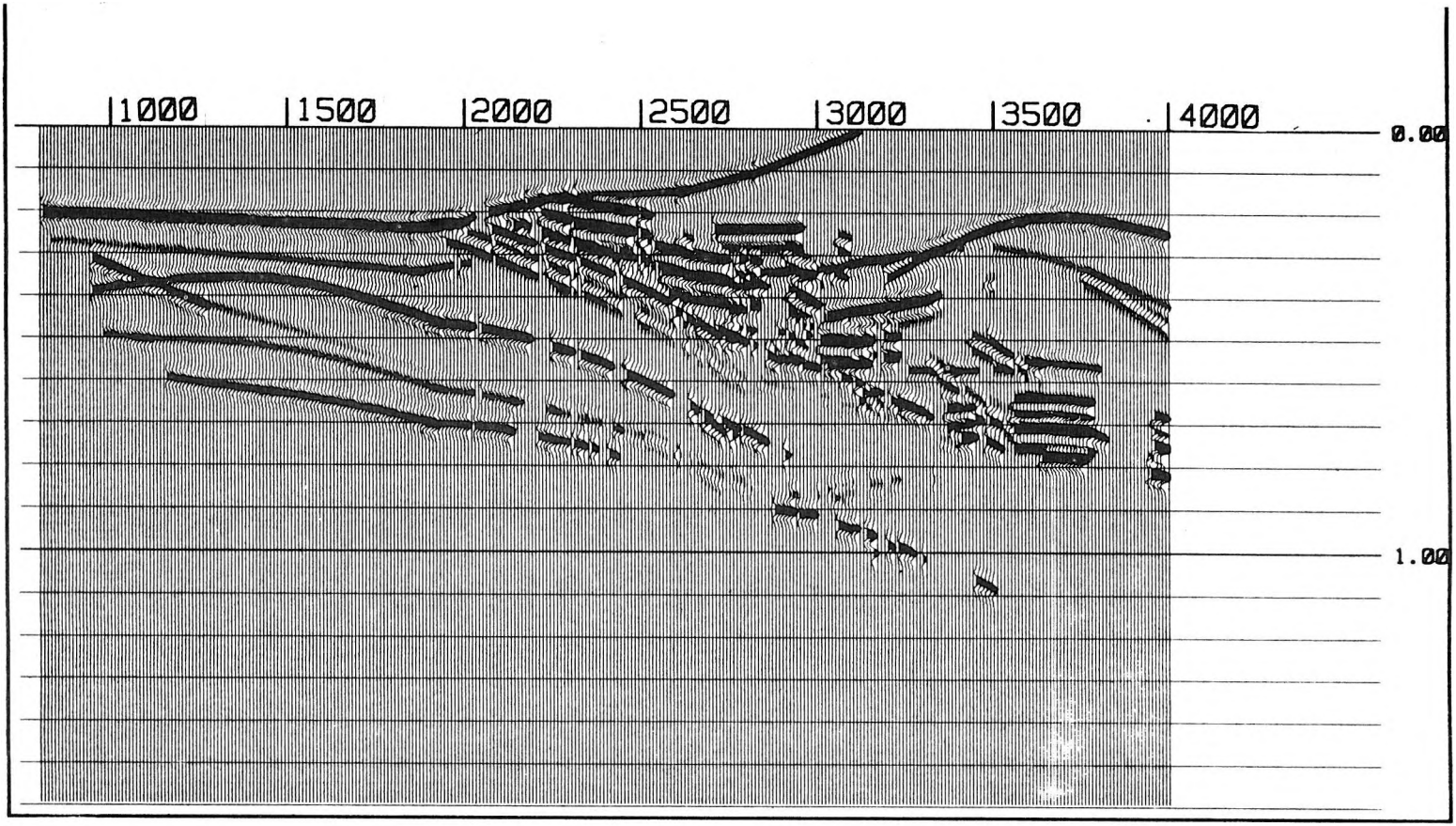

Fig. 13. Ray-trace response using 20 Hz Ricker wavelet

13. ábra. Sugárútvezetéssel, és 20 Hz-es Ricker wavelettel számított szintetikus szelvény

Рис. 13. Синтетический разрез, вычисленный по методу проведения по траектории и использованием импульса Риккера частотой 20 Гц

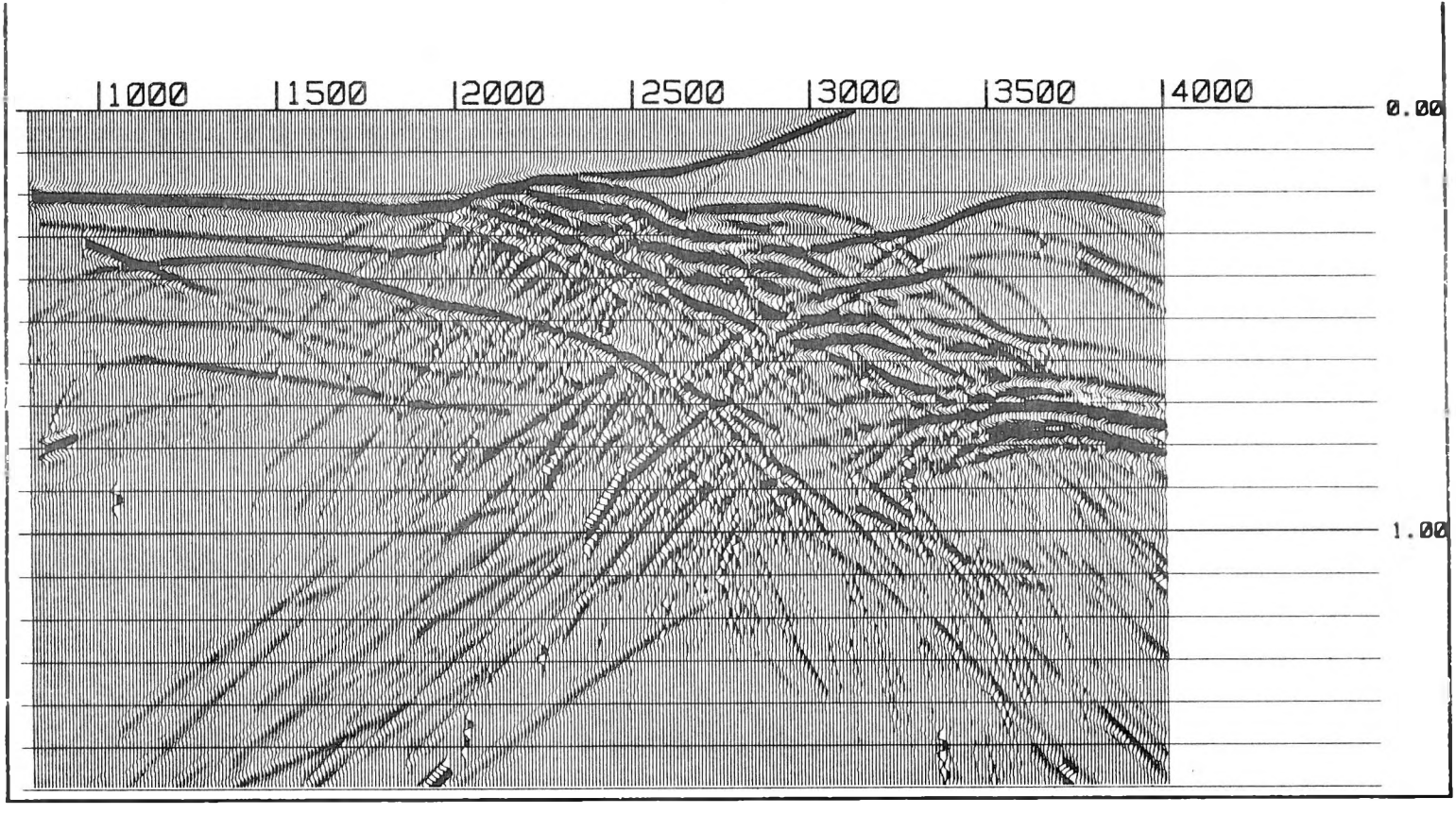

Fig. 14. Wave-equation response using 20 Hz Ricker wavelet

14. ábra. Hullámegyenlettel, és 20 Hz-es Ricker wavelettel számított szintetikus szelvény

Рис. 14. Синтетический разрез, вычисленный по волновому уравнению с использованием импульса Риккера частотой 20 Гц

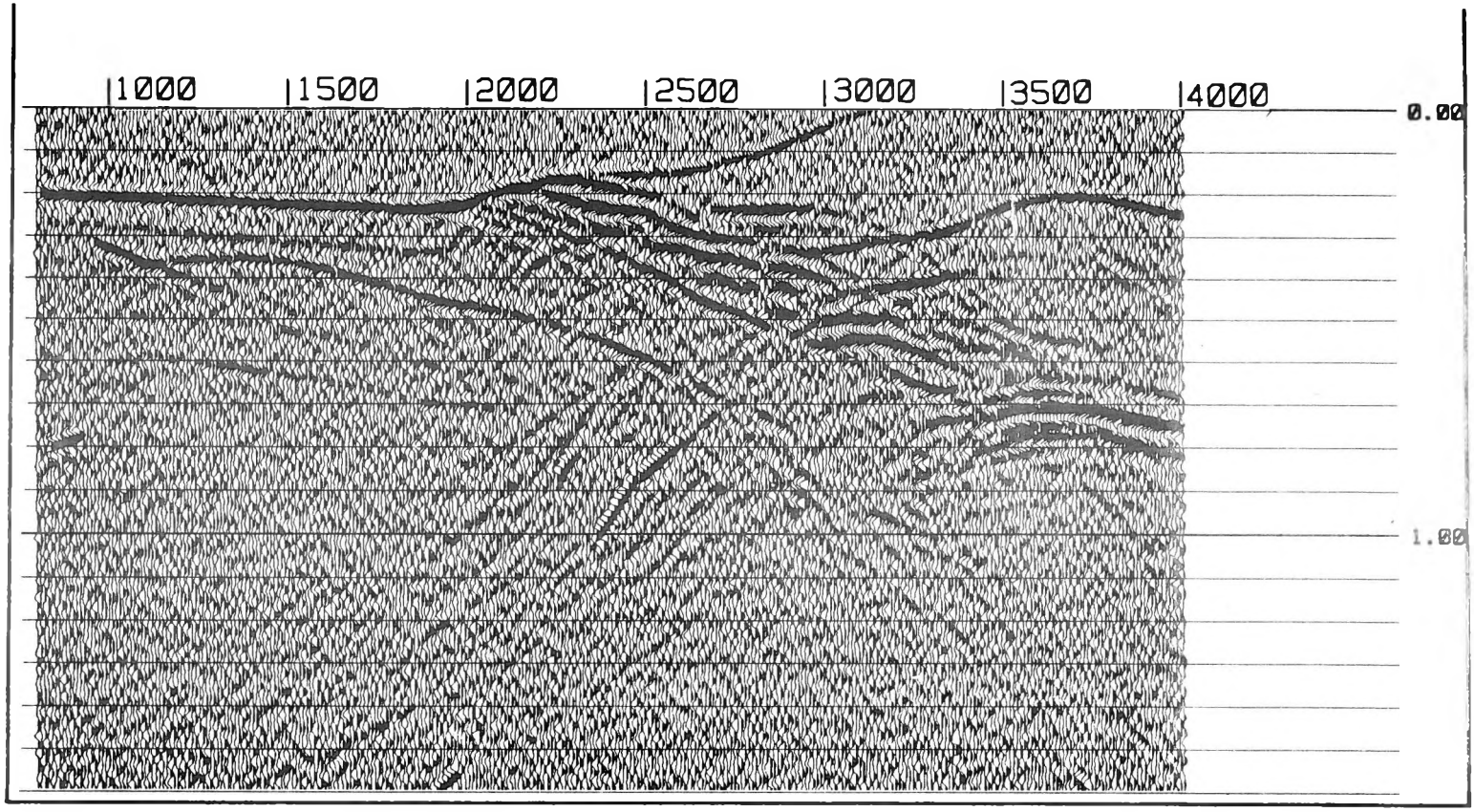

Fig. 15. Wave-equation response using 20 Hz Ricker wavelet with noise added

15. ábra. Hullámegyenlettel, 20 Hz-es Ricker wavelettel és zaj hozzáadásával számított szintetikus szelvény

Рис. 15. Синтетический разрез, вычисленный по волновому уравнению с использованием импульса Риккера частотой 20 Гц и добавлением шума

area, are extremely difficult to simulate in a model. Erosional surfaces, although having a distinct velocity discontinuity, are usually rough, highly irregular surfaces which occasionally give rise to no-reflection zones, because of their energy scattering properties. This type of surface is also difficult to model.

The model and geological knowledge showed excellent correlation in the coal-bearing area which has normal faults, as well as in the area to the northwest in which the rock units are not as deformed. The wave-equation solution shows that much of the energy dipping from right to left on the processed time section (Fig. 3) are diffractions. This confirms the validity of the migrated time section (Fig. 4) and gives credibility to the decision to use pie-slice filtering to aid in structural interpretation. Therefore, we conclude that the model is a reasonable geologic interpetation of the seismic cross section.

The geology of the study area is extremely complex, whereby a combination of reverse and normal faults truncate continuous layers. To be successful, the CDP method needs strata of reasonably continuous lateral extent and any fault intersecting the layer can violate this requirement. *Figure 16* shows the result of ray tracing a CDP gather (i.e. an assamblage of traces belonging to the same Common Depth Point) centered at surface position 2,700. To give it more clarity, only rays of horizons 16, 24, 27, 30 and 39 were traced. The complexity of this CDP gather is immediately obvious. Although the strata dip but slightly, the refraction of the rays through the fault planes cause a large scattering in the reflection points. This could give rise to errors in stacking velocity analysis, and can be compounded when migrating the data and converting to depth. *Figure 17* shows the synthetic CDP gather calculated from the raypaths shown in Figure 16. The travel times for horizon 39 are nearly equal for all source–receiver offsets and would, therefore, need an unreasonably high velocity in order to properly stack this reflection. This could be another reason why this fault plane does not appear on the real data. We see from this example that we are approaching the limits of the conventional CDP method. We therefore suggest that if further seismic reflection work is to be done in this area, great care be taken in the selection of recording and processing parameters.

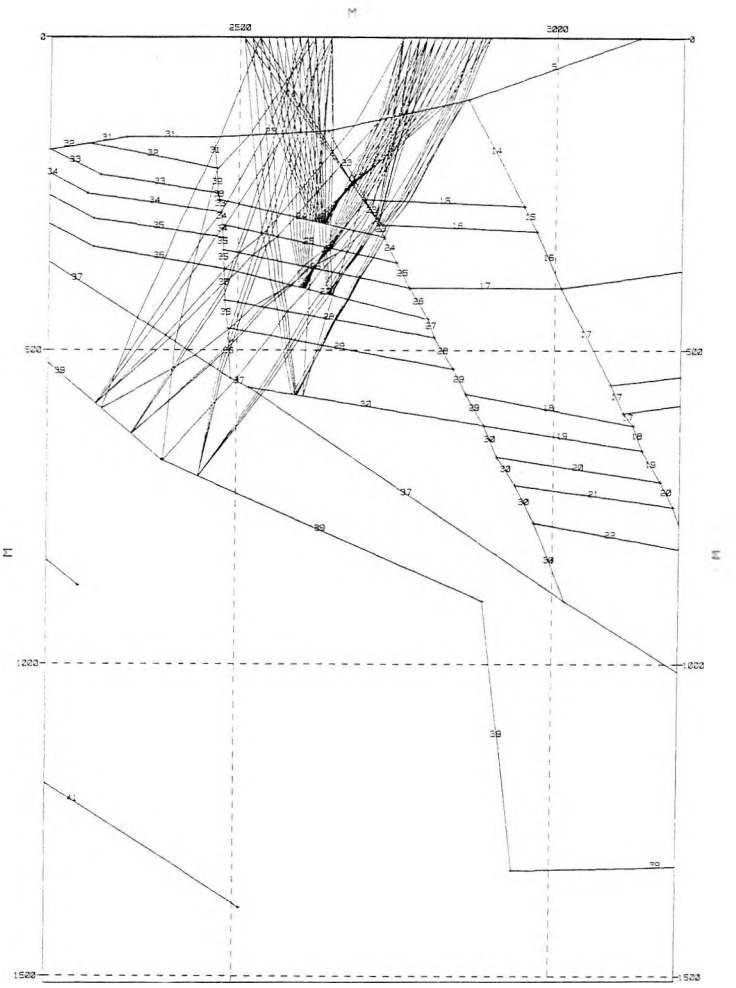

Fig. 16. Rays traced from CDP gather centered around surface position 2700, from layers 16, 24, 27, 30 and 39

16. ábra. A 2700 szelvénykaró környékéhez tartozó sugarak a 16, 24, 27, 30 és 39 sz. rétegről

Рис. 16. Лучи, относящиеся к окружности пикета № 2700 с пластов 16, 24, 27, 30 и 39

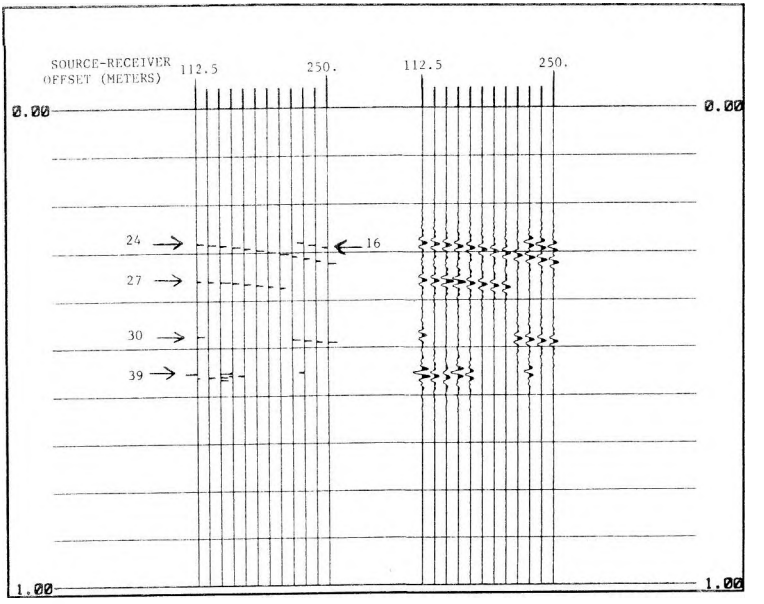

Fig. 17. Synthetic CDP gather from rays shown in Figure 16. Left: Spikes at the appropriate travel times. Right: Spikes convolved with 20–80 Hz bandpass wavelet

17. ábra. A 16. ábra sugarainak megfelelő szintetikus csatornagyűjtés. Baloldalt csúcsok, jobboldalt a csúcsok 20–80 Hz sávszűrés után

Рис. 17. Сбор синтетических каналов, соответствующих лучам на рис. 16. Налево — пики, направо — пики после полосовой фильтрации 20–80 Гц

APPENDIX

For the experimental seismic profile the field geometry was chosen as follows: an unusually short geophone-base distance (12.5 m instead of 25 m) and the minimal possible offset of 112.5 m that can be used in the presence of the vibrator-generated noise on the rocky ground (the exploration depth range was 1,500 m). The vertical resolving power was increased by the wide band of the input sweep (20–80 Hz). Although the coverage had originally been planned as twelve-fold, this could not be uniformly achieved along the whole profile because of the rough terrain. The low-velocity-layer also shows rapid changes: its average velocity is 600–1,000 m/s, its thickness is varying between 7–65 m. The layer below the low-velocity-layer is still variable, with a boundary velocity of 1,000–2,400 m/s. As referred to the 170 m datum plane (a.s.l.) static corrections range between 8–70 ms.

Steps of the refined processing of the VA-4/7 line:

1. Demultiplexing of the field material into 4-byte floating-point SDS–3 trace sequential format.
2. True amplitude recovery (RAMP) and VIBRODECON on the primary records with subsequent bandpass filtering (20–70 Hz) and normalization (NORM) based on total record length.
3. Rough stack after EDIT and STAT and normal moveout (KIN) with *a priori* velocity information.
4. Automatic improvement of the static corrections.
5. Velocity determinations after the automatic statics, by means of velocity scanning. Improved stack using updated velocity functions.
6. Zero-phase deconvolution on the refined stacked section with subsequent filtering (in 20–40 Hz, 30–60 Hz and 20–60 Hz bands).
7. Wave-equation migration, followed by the same filtering as in 6.
8. Pie-slice filter applied to the migrated time section (7 channels, 20–40 Hz frequency band, 1,000 m/s velocity cut-off).
9. Depth transformation with the determined velocity functions.

REFERENCES

GeoQuest 1983: AIMS Users Reference Manual

May B. T., Covey J. D. 1983: Structural inversion of salt dome flanks. Geophysics **38**, 8, pp. 1039–1050

Timár Z. 1984: The role of the SDS-3 program package in ELGI's seismic processing. Annual Report of the Eötvös Loránd Geophysical Institute of Hungary for 1983 pp. 139–142

SZEIZMIKUS MODELLEZÉS BONYOLULT TEKTONIKAI VISZONYOK KÖZÖTT

John J. MILLER, Myung W. LEE, KILÉNYI Éva, PETROVICS Ilona, BRAUN László és KORVIN Gábor

A mecseki fekete kőszén kutatását az ELGI 1955 óta szeizmikus refrakciós módszerrel, majd 1977 óta szeizmikus reflexiós módszerrel végzi. A terület bonyolult tektonikája, a rövid távon követhető határfelületek, amelyeket közel függőleges vetők és feltolódási síkok szabdalnak igen megnehezítik a szeizmikus anyag feldolgozását és értelmezését.

Az ELGI és a USGS együttműködése 1982-ben kezdődött a kétdimenziós modellezés használatára a Mecsekben. Az első modell nem eredményezett megfelelő egyezést a valódi szelvénnyel, ezért az anyagot újra feldolgoztuk és értelmeztük. A második modellezés során mind sugárút-vezetéses, mind hullámegyenletes modellezést alkalmaztunk a feladat megoldására. Ezúttal már lényegesen jobb egyezést kaptunk, de még mindig maradtak ellentmondások.

A tanulmány bemutatja, hogyan lehet a modellezést hasznosítani a feldolgozás és értelmezés elősegítésére, iteratív úton. Ugyanakkor rámutatunk a modellezés és a közös mélységpontos szeizmikus eljárás korlátaira az adott földtani viszonyok között.

СЕЙСМИЧЕСКОЕ МОДЕЛИРОВАНИЕ ПРИ СЛОЖНЫХ ТЕКТОНИЧЕСКИХ УСЛОВИЯХ

Джон Дж. МИЛЛЕР, Мюнг В. ЛИ, Эва КИЛЕНИ, Илона ПЕТРОВИЧ, Ласло БРАУН и Габор КОРВИН

Разведка месторождения черного угля в горах Мечек проводится институтом ЭЛГИ с 1955 г. с помощью сейсмического метода преломленных волн, а с 1977 г. — метода отраженных волн. Сложное тектоническое строение района, короткие расстояния прослеживания разделов, пересекаемых почти вертикальными сбросами и надвигами, весьма затрудняют обработку и интерпретацию материалов сейсморазведки.

Сотрудничество между ЭГЛИ и Геологической службой США началось в 1982 г. по применению двухмерного моделирования в горах Мечек. Первая модель не дала соответствующего совпадения с истинным разрезом, поэтому материал был заново обработан и подвергнут новой интерпретации. В процессе второго моделирования были использованы способ проведения по траектории, а также способ волнового уравнения для решения задачи. При этом было получено значительно лучшее совпадение, но все-таки остались некоторые противоречия.

В работе показано, как можно использовать моделирование для продвижения обработки и интерпретации путем повторения. В то же время отмечены ограничения моделирования и сейсморазведочного метода О.Г.Т. при данной геологической обстановке.

GEOPHYSICAL TRANSACTIONS 1985
Vol. 31. No. 1–3 pp. 257–268

HIGH RESOLUTION INTERVAL VELOCITIES

István KÉSMÁRKY*

The principal limit of the resolution of physical methods in the presence of random components (i.e. noise) is well known in statistical theory. However, there has been an increasing demand for a higher resolution of the physical parameters for exploration purposes. Therefore, an important research aim is to achieve a reasonable compromise between the two controversial requirements.

As demonstrated in this paper, the estimated interval velocities become very unrealiable and highly correlated if resolution is increased. To find a compromise, the reliability of interval velocity estimates must be increased to an acceptable level while ensuring that the estimates stay close to physical reality. This process should result, more or less, in smoothing the original rough estimates.

This paper consists of three parts. In the first part, the statistical description of interval velocity estimation errors is outlined. In the second part, the possibility of decreasing estimation errors is discussed by taking into consideration the highly correlated nature of interval velocity estimates via the computation of statistical residuals. In the third part a few synthetic examples of the application of the method is shown.

Keywords: interval velocity, Dix-formula, statistical estimation

1. Statistical behaviour of the interval velocity estimates

First let us look at the statistical description of the estimated interval velocity errors, the mean, the standard deviation, and covariance between various layers. Suppose that seismic measurements are made above a half space containing horizontal homogeneous layers. The spread parameters can be chosen arbitrarily. As a result of standard velocity analyses, we may have a great number of arrival time and stacking velocity pairs (t_0, v_s) corresponding to primary reflections spaced arbitrarily close to one another. All these hyperbolic parameters are supposed to contain statistical errors.The independence of the errors corresponding to each horizon is also assumed to be present. This is a realistic approach after a successful automated static correction.

The standard deviation and covariance of reflection hyperbola parameters, t_0 and v_s, can practically be deduced on the basis of the standard deviation, σ_t, of the random time shifts after the automatic static correction (see *APPENDIX A*). Thus, in the case of a known standard deviation, σ_t, the mean, standard deviation and covariance of hyperbola parameters, t_0 and v_s, can directly be estimated. These parameters can be regarded as secondary measurement data of known statistical behaviour.

* Geophysical Exploration Company, POB 213, Budapest, H–1391, Hungary
Manuscript received: 9 April, 1985

Now, the estimation of interval velocities by the well known Dix formula can be discussed. The formula is expressed by the error terms of each quantity:

$$(V_i + \Delta V_i) = \sqrt{\frac{(v_{s_i} + \Delta v_{s_i})^2 (t_{0_i} + \Delta t_{0_i}) - (v_{s_{i-1}} + \Delta v_{s_{i-1}})^2 (t_{0_{i-1}} + \Delta t_{0_{i-1}})}{(t_{0_i} + \Delta t_{0_i}) - (t_{0_{i-1}} + \Delta t_{0_{i-1}})}} \qquad (1)$$

where: V_i is the interval velocity of the i-th layer

ΔV_i is the error term of V_i

v_{s_n} and t_{0_n} is the stacking velocity and the zero offset arrival time of the n-th reflection, respectively.

The mean, standard deviation and covariance of interval velocity error term, ΔV_i, can be expressed after expanding the expression into Taylor series, retaining the linear terms and computing the expected values (see *APPENDIX B*).

In essence, it may be said that the interval velocity estimates are unbiased but, may have very large standard deviations in the case of small layer thicknesses or high noise level. The considerably large negative correlation between interval velocity estimates of the adjacent layers is of further complication.

For example a stacking velocity error of a certain reflection affects two (the upper and lower) interval velocity estimates in the opposite sense.

For a quick impression, an example of the standardized form of covariance matrix $\mathbf{C}$ of ΔV_i is:

$$\begin{bmatrix} 1.00 & -0.47 & 0.00 & . & . & 0.00 \\ -0.47 & 1.00 & -0.61 & & & 0.00 \\ 0.00 & -0.61 & 1.00 & & . & 0.00 \\ . & . & . & . & . & \\ . & & & . & . & . \\ 0.00 & 0.00 & 0.00 & & . & 1.00 \end{bmatrix}$$

It shows that, the covariance can be characterized by a tridiagonal matrix. Because of the large negative correlation, the interval velocity estimates show non-minimum standard deviations. Evaluating these statistical parameters, the interval velocity estimates can also be regarded as secondary (or tertiary) measured data at a later stage.

2. Correction of correlation terms

A tridiagonal matrix, whose off diagonals contain negative elements, describes an alternating, oscillatory stochastic process. It is also known that actual interval velocities vary systematically as sediment compaction varies therefore, interval velocities of different layers are not quite independent.

The residual computation method, well known from statistics, offers means to remove the correlation terms. The principle of the method is that terms predicted from all other estimation errors ΔV_k $(k \neq i)$ are subtracted from each

estimation error ΔV_i. The prediction can be carried out on the basis of a linear regression model, similar to the predictive deconvolution.

Let us introduce the variable ξ_i which is the difference of the interval velocity estimate, V_i, computed by Dix's formula, and an ideal estimate, v_i, to be determined later:

$$\xi_i = V_i - v_i \quad (= \Delta V_i). \tag{2}$$

(The statistical behaviour of ξ_i is the same as that of ΔV_i described in *APPENDIX B*.)

The residual η_i can be expressed by the inverse matrix **D** of the covariance matrix **C** (see *APPENDIX C*):

$$\eta_i = \frac{1}{D_{ii}} \sum_{k=1}^{M} \xi_k D_{ki} \tag{3}$$

where, D_{ki} and D_{ii} are elements of matrix **D** ($= \mathbf{C}^{-1}$) and M is the number of sedimentary layers. The values η_i are free from the correlation effect. The covariance of the residual has the following form (see *APPENDIX C*):

$$E\{\eta_i \eta_j\} = D_{ij} \cdot \det(\mathbf{D})/(D_{ii} D_{jj}) \tag{4}$$

This expression depends on the covariance matrix, **C** (and v_i) only. Equation (4) serves as the theoretical lower limit of the correlation between residuals, η_i and η_j. To achieve an estimate of minimum standard deviation, the sum square of the actual residuals $N = \sum_{i=1}^{M} \hat{\eta}_i$ must be minimized or decreased to the theoretical minimum formulated by eq. (4), where $\hat{}$ denotes the actual value during the iteration. Substituting ξ_i into the expression of η_i and norm N, a simple equation can be deduced, by equating the partial v_i derivates to zero:

$$\frac{\partial N}{\partial v_i} = \sum_j B_{ij} v_j - \sum_j B_{ij} V_j = 0$$

where,

$$B_{ij} = \sum_k D_{ki} D_{kj} / D_{kk}^2. \tag{5}$$

Trivial solution: $v_i = V_i$

Practical solution: $\sum_i^M (\hat{\eta}_i^2 / E\{\eta_i \eta_i\}) = M$

In spite of the meaningless trivial solution, the gradient vector can easily be used to decrease norm N step by step, starting from an arbitrary smooth velocity function $v_i^{(0)}$.

At the n-th step, N can be computed from $\hat{\xi}_k$ and **D**. The direction of the steepest descent of N can also be found varying the components $v_i^{(n)}$. Thus, $v_i^{(n+1)}$ ($i = 1, 2, \ldots, M$) can simply be reached by a displacement of a certain length, within the direction mentioned above.

To start the iteration, a reasonable choice for a smooth velocity function

is a simple stepwise function, which exactly obeys the local compaction trend and best fits to the interval velocities computed by the Dix formula.

To find a reasonable solution, a technique can be applied that is similar to the white noise addition method. All elements of covariance matrix **C** outside the main diagonal are multiplied by a constant α, with values between zero and one.

The case $\alpha = 0$ is equivalent to the application of the Dix formula without modification. If α is equal to 1, the result generally is a strongly smoothed stepwise function. An intermediate solution can be achieved by using α between 0 and 1.

3. Examples

A model example containing a velocity anomaly is shown in the next figures.*

Standard deviation, σ_t, of the random time shifts with which the original arrival time data were corrupted is 2 ms. (The source offset is 120 m, the geophone interval is 120 m and the coverage is 12 fold.) The solid line always shows the assumed noise-free model. The white lines (in the center of the grey zones) show the estimated velocities computed from noisy synthetic data. The grey areas show the standard deviations of the estimates. *Fig. 1* is the case of Dix's formula ($\alpha = 0$). The interpretation and decision on the existence of one (or more) low velocity anomaly are no easy tasks due to the large standard deviations.

Let us regard now the practical use of the resultant interval velocity estimate against the parameter α in the case of the given model *(Fig. 2)*. In the case of low noise level** the improvement is not significant, but in the case of high noise or small layer-thickness the improvement is considerably better expressed by the r.m.s. difference between the original noise-free interval velocities and estimates computed from synthetized noisy (t_0, v_s) pairs. The ideal solutions are represented by the absolute minima of the curves. The range of the curves (the relative improvement) is certainly greater in the latter case. In most cases, the value $\alpha = 0.9$ results in nearly optimum fit.

In the case of $\alpha = 1$ the result is always an extremely smooth (biased) stepwise velocity function. These solutions are very similar to one another, even when the noise levels are quite different. This is the reason why the curves converge in the case of $\alpha = 1$.

* The situation represented by this model is similar to that of the interval velocity problem of marine gas hydrates where the aim is to estimate the interval velocity of the free gas bearing layer under the gas hydrate layer.

** Decreasing the noise level ($\sigma_t = 0.5$ ms instead of $\sigma_t = 2$ ms) is equivalent to increasing the spread length or the coverage, according to *APPENDIX A*.

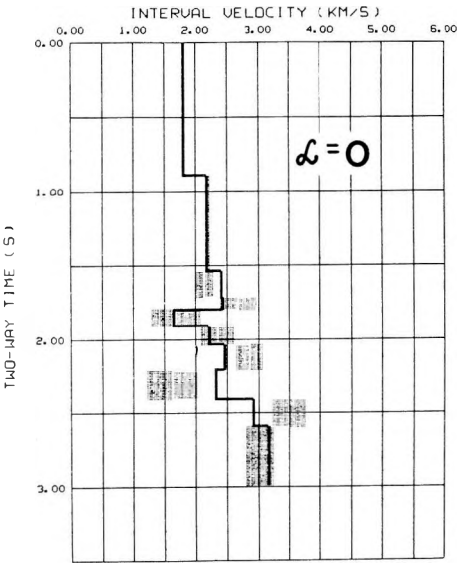

Fig. 1. Velocity function, computed by Dix's formula, for a model containing a velocity anomaly

1. ábra. Dix-formulával számított sebességeloszlás sebesség-anomáliát tartalmazó modellre

Рис. 1. Вычисленное по формуле Дикса распределение скоростей для модели, включающей в себя аномалию скорости

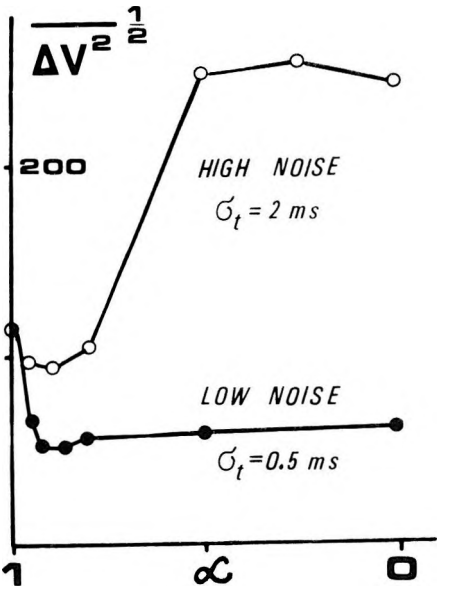

Fig. 2. Estimated interval velocity versus α

2. ábra. Becsült intervallumsebesség-értékek az α paraméter függvényében

Рис. 2. Оцениваемые значения интервальных скоростей в зависимости от параметра α

Figures 3. and *4.* show the results of the algorithm in the case of $\alpha = 0.9$ and $\alpha = 1.0$. The bulk of the large alternating errors was removed on the former and the anomaly is better recognizable. The latter result is rather smooth. The place of the anomaly is visible but its amplitude is rather small. Therefore, choosing $\alpha = 0.9$ is a compromise between an unbiased but inefficient estimate and an efficient but biased estimate. The estimate is biased because short interval velocity anomalies appear as gradual changes.

For example, if the noise level is high, the outstanding feature of short interval velocity anomalies may be completely smoothed out. This draws the attention of the interpreter, that the given quality of the available seismic data is not sufficient for certain conclusions.

It is worth noting that the whole process is in close analogy with the standard predictive deconvolution. In the predictive deconvolution process there is an oscillatory shotpoint wavelet to be removed from the trace. The autocorrelation function (acf) of the wavelet can be estimated from the trace itself. The inverse operator is computed from this acf.

In the interval velocity estimation, there is also an oscillatory term to be removed. The acf of this term and the prediction operator can be computed theoretically. The smooth function, v_i, to be determined should be that, from which the result of Dix's formula can be predicted with a given (minimum) variance.

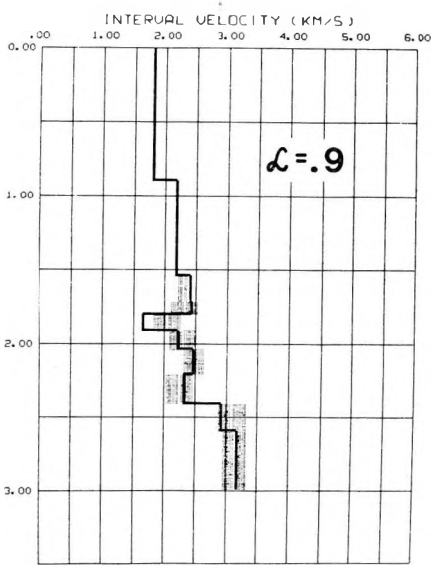

Fig. 3. Velocity function using the algorithm proposed ($\alpha = 0.9$)

3. ábra. Sebességeloszlás a javasolt algoritmus alkalmazásával, $\alpha = 0{,}9$ esetén

Рис. 3. Распределение скоростей при применении предлагаемого алгоритма, в случае $\alpha = 0{,}9$

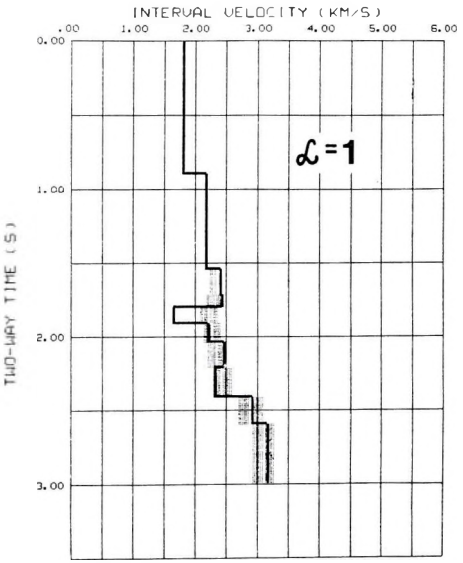

Fig. 4. Velocity function using the algorithm proposed ($\alpha = 1.0$)

4. ábra. Sebességeloszlás a javasolt algoritmus alkalmazásával, $\alpha = 1{,}0$ esetén

Рис. 4. Распределение скоростей при применении предлагаемого алгоритма, в случае $\alpha = 1{,}0$

4. Conclusions

- In the estimation of interval velocities no local maxima of the velocity spectrum have to be rejected in order to get small enough deviations. Such type of information loss can be avoided. Due to this feature, the method can comfortably be used for interpretation of automatically picked peaks on velocity spectra.
- The method retains the simple physical model during the interpretation. Some smoothing methods result in smooth curves or splines instead of such simple stepwise interval velocity functions.
- The method automatically assures that resolution increases, if the measured data are more reliable.
- The method is a useful tool to find efficient estimates in the case of highly correlated data.
- The display of standard deviations of the estimated physical parameters (interval velocities and depths) are especially useful for quick visual reckoning of the reliability of the interpretation.

APPENDIX A

Statistical description of the estimated reflection hyperbola parameters t_0 and v_s

A simple model of a reflection hyperbola located on a set of traces has the following form:

$$f_{ki}(A, v_s, t_0) = A\varphi\left(t_i - \sqrt{t_0^2 - \frac{x_k^2}{v_s^2}}\right) \tag{A.1}$$

where f_{ki} is a discrete element of a trace of a CMP (Common Mid Point) set,
k is the "offset" index (k runs from 1 to the actual coverage number),
i is the "time" index
A is the amplitude factor of the wavelet
$\varphi(\tau)$ is the known wave shape
t_i is the time variable
x_k is the offset variable
t_0 is the zero offset arrival time
v_s is the stacking velocity.

In the case of a regular spread, x_k can be expressed in the following simple form:

$$x_k = \Phi + (k-1)G \tag{A.2}$$

where, Φ is the actual spread offset and G is the geophone spacing within the given type of CMP set. So, the statistical model of the correspondent traces y_{ki} can be written:

$$y_{ki} = f_{ki} + n_{ki} \tag{A.3}$$

where, n_{ki} is the correlated random noise component of zero mean and standard deviation, σ.

The statistical interpretation theory gives means to the optimal estimation of parameters, t_0 and v_s, in the presence of noise. As a by-product, the standard deviations and covariances also can be estimated [HOLTZMAN 1971, SALÁT et al. 1982].

The effectiveness of the (pure quantitative) interpretation can be characterized by the information matrix **I**, which is the inverse of the covariance matrix of the estimated parameters in the above case.

The general element of the information matrix is:

$$I_{lm} = \sum_k \sum_i \sum_{i'} R_{ii'}^{-1} \frac{\partial f_{ki}(\bar{p})}{\partial p_l} \frac{\partial f_{ki'}(\bar{p})}{\partial p_m} \tag{A.4}$$

where, $R_{ii'}$ is the covariance matrix of the noise component, $\bar{p} = \{p_1, p_2, \ldots, p_n\}$ is the vector of unknown parameters.

Substituting (A.1) into (A.4), and applying indirect partial derivatives

$$\frac{\partial}{\partial v} = \frac{\partial}{\partial t_k}\frac{\partial t_k}{\partial v}, \qquad \text{where} \qquad t_k = \sqrt{t_0^2 + \frac{x_k^2}{v_s^2}} \tag{A.5}$$

and, using the spectral representation of quadratic forms, we get:

$$\begin{aligned} I_{vv} &= \frac{A^2}{\sigma^2} W \frac{1}{v_s^6} \sum_k \frac{x_k^4}{t_k^2} \\ I_{tt} &= \frac{A^2}{\sigma^2} W t_0^2 \sum_k \frac{1}{t_k^2} \\ I_{vt} &= -\frac{A^2}{\sigma^2} W \frac{t_0}{v_s^3} \sum_k \frac{x_k^2}{t_k^2} \end{aligned} \tag{A.6}$$

$$\text{where,} \quad W = \frac{1}{2\pi} \int_{-\omega_0}^{\omega_0} \frac{\omega^2 |\Phi(\omega)|^2}{r(\omega)} \mathrm{d}\omega \tag{A.7}$$

$\omega_0 = \pi/\Delta t$, Δt is the time spacing, $\Phi(\omega)$ and $r(\omega)$ are the Fourier transforms of the normalized autocorrelation functions of the wavelet φ, and the noise, respectively.

Inverting the 2×2 information matrix we obtain the covariance matrix of the estimated parameters:

$$\begin{aligned} D^2(v_s) &= \frac{\sigma^2}{A^2 W} v_s^6 \sum_k \frac{1}{t_k^2} / D \\ D^2(t_0) &= \frac{\sigma^2}{A^2 W} \sum_k \frac{x_k^4}{t_k^2} / (t_0^2 D) \\ E(v_s t_0) &= \frac{\sigma^2}{A^2 W} v_s^3 \sum_k \frac{x_k^2}{t_k^2} / (t_0 D) \end{aligned} \tag{A.8}$$

$$\text{where,} \quad D = \sum_k \frac{x_k^4}{t_k^2} \cdot \sum_k \frac{1}{t_k^2} - \left(\sum_k \frac{x_k^2}{t_k^2} \right)^2$$

Fortunately, very similar expressions can be derived from the case when a hyperbola is fitted by the least squares method to the arrival times corrupted by random time shifts of standard deviation σ_t [AL-CHALABI 1974, KÉSMÁRKY 1976, MARSCHALL 1978].

The only difference is that the factors $\sigma^2/(A^2 W)$ and t_k in eqs. (A.8) are replaced by σ_t^2 and t_0, respectively. Thus

$$\frac{\sigma^2}{A^2 W} \approx \sigma_t^2. \tag{A.9}$$

σ_t can easily be estimated at the final step of the automated static correction. This latter approach is much more simple for practical use.

APPENDIX B

Statistical description of the estimated interval velocities, V_i

Expressing the error term, ΔV_i from eq. (1), expanding it into Taylor series according to Δv_{s_i}, $\Delta v_{s_{i-1}}$, Δt_{0_i} and $\Delta t_{0_{i-1}}$, neglecting higher than first-order terms, we obtain (omitting the subscripts s and 0):

$$\Delta V_i = \frac{1}{V_i(t_i - t_{i-1})}\left\{v_i t_i \Delta v_i - v_{i-1} t_{i-1} \Delta v_{i-1} + \frac{v_i^2 - v_{i-1}^2}{2t_i}\left[t_i \Delta t_{i-1} - t_{i-1}\Delta t_i\right]\right\}$$

The expected values of significance are as follows (assuming "non static type" random time shifts):

$$\begin{aligned}
E(\Delta V_i \Delta V_j) = \frac{1}{V_i V_j T_i T_j}\Bigg[& + v_i v_j t_i t_j E(\Delta v_i \Delta v_j) - v_i v_{j-1} t_i t_{j-1} E(\Delta v_i \Delta v_{j-1}) + \\
& + \frac{v_j^2 - v_{j-1}^2}{2T_j}\left[v_i t_i t_j E(\Delta v_i \Delta t_{j-1}) - v_i t_i t_{j-1} E(\Delta v_i \Delta t_j)\right] - \\
& - v_{i-1} v_j t_{i-1} t_j E(\Delta v_{i-1} \Delta v_j) + v_{i-1} v_{j-1} t_{i-1} t_{j-1} E(\Delta v_{i-1} \Delta v_{j-1}) - \\
& - \frac{v_j^2 - v_{j-1}^2}{2T_j}\left[v_{i-1} t_{i-1} t_j E(\Delta v_{i-1} \Delta t_{j-1}) - v_{i-1} t_{i-1} t_{j-1} E(\Delta v_{i-1} \Delta t_j)\right] + \\
& + \frac{v_i^2 - v_{i-1}^2}{2T_i}\Bigg\{v_j t_j t_i E(\Delta v_j \Delta t_{i-1}) - v_{j-1} t_{j-1} t_i E(\Delta v_{j-1} \Delta t_{i-1}) + \\
& + \frac{v_j^2 - v_{j-1}^2}{2T_j}\left[t_i t_j E(\Delta t_{i-1} \Delta t_{j-1}) - t_i t_{j-1} E(\Delta t_{i-1} \Delta t_j)\right]\Bigg\} - \\
& - \frac{v_i^2 - v_{i-1}^2}{2T_i}\Bigg\{\left[v_j t_j t_{i-1} E(\Delta v_j \Delta t_i) - v_{j-1} t_{j-1} t_{i-1} E(\Delta v_{j-1} \Delta t_i) + \right. \\
& \left. + \frac{v_j^2 - v_{j-1}^2}{2T_j}\left[t_{i-1} t_j E(\Delta t_i \Delta t_{j-1}) - t_{i-1} t_{j-1} E(\Delta t_i \Delta t_j)\right]\right\}\Bigg]
\end{aligned}$$

where $T_i = t_i - t_{i-1}$

APPENDIX C

Linear prediction of correlated random variables

Let us determine the coefficients a_{1i} which satisfy the following condition [VINCZE 1968]:

$$E\{(\xi_1 - a_{12}\xi_2 - \cdots - a_{1M}\xi_M)^2\} = \min. \qquad \text{(C.1)}$$

Equating the partial a_{1i} derivates with zero, we get:

$$C_{i2}a_{12} + C_{i3}a_{13} + \cdots + C_{iM}a_{1M} = C_{i1}; \quad (i = 1, 2, \ldots, M) \tag{C.2}$$

where, $C_{ij} = E\{\xi_i \xi_j\}$.

Rearranging of eq. (C.2) yields (completing the system (C.2) with its first row):

$$\boldsymbol{C}\begin{bmatrix} 1 \\ -a_{12} \\ -a_{13} \\ \vdots \\ -a_{1M} \end{bmatrix} = \begin{bmatrix} S \\ 0 \\ 0 \\ \vdots \\ 0 \end{bmatrix} \tag{C.3}$$

where S is a constant. Eq. (C.3) is the same as the system used at the design of prediction error (optimum spike deconvolution) operators, although, matrix **C** does not exhibit the so-called Toeplitz symmetry.

The solution can simply be written as:

$$a_{1j} = -\frac{D_{1j}}{D_{11}} \tag{C.4}$$

The general solution has the form:

$$a_{ij} = -\frac{D_{ij}}{D_{ii}} \tag{C.5}$$

where D_{ij} is the ij-th element of matrix **D** ($=\mathbf{C}^{-1}$).

Now, the residual η_i can simply be expressed:

$$\eta_i = \xi_i - \sum_{j \neq i}^{M} a_{ij}\xi_j = \sum_{j=1}^{M} \frac{D_{ij}}{D_{ii}} \xi_j \tag{C.6}$$

The covariance of η_i can be written in the same way:

$$\begin{aligned} E\{\eta_i \eta_j\} &= E\left(\frac{1}{D_{ii}} \sum_k D_{ik}\xi_k \cdot \frac{1}{D_{jj}} \sum_l D_{jl}\xi_l\right) = \\ &= \frac{1}{D_{ii}D_{jj}} \sum_k \sum_l D_{ik}D_{jl}C_{kl} = \\ &= \frac{1}{D_{ii}D_{jj}} D_{ij} \cdot \det(\boldsymbol{D}) \end{aligned} \tag{C.7}$$

because of $\sum_l D_{jl}C_{kl} = \delta_{jk} \det(\boldsymbol{D})$

Acknowledgements

Data for this research was provided by the U.S. Geological Survey, under its agreement with the Hungarian Central Office of Geology. The assistance and review of this manuscript by Dr. John Grow, John J. Miller and Dr. Myung W. Lee is appreciated.

REFERENCES

AL-CHALABI M. 1974: An analysis of stacking, RMS, average and interval velocities over a horizontally layered ground. Geoph. Prospecting, **22**, 3, pp. 458–475

HOLTZMAN F. M. 1971: Statistical models of interpretation (in Russian). Nauka, Moscow, 327 p.

KÉSMÁRKY I. 1976: Investigations of seismic spread systems with regard to the quality of velocity estimation. Proceedings, 20th Geophysical Symposium, Budapest–Szentendre, 15–19. 9. 1975, OMKDK–TECHNOINFORM, Budapest, pp. 274–293

MARSCHALL R. 1978: Ermittlung des Seismischen Signals Näherungsweise Berechnung des Impedanzlogs. Univ. Kiel, seminar manuscript, pp. 13–17

SALÁT P., TARCSAY GY., CSEREPES L., VERMES M., DRAHOS D. 1982: Information-statistical methods of geophysical interpretation (in Hungarian). Tankönyvkiadó, Budapest, 302 p.

VINCZE I. 1968: Mathematical Statistics with industrial applications (in Hungarian). Műszaki Könyvkiadó, Budapest, 352 p.

NAGYFELBONTÁSÚ SEBESSÉGFÜGGVÉNY-BECSLÉS

KÉSMÁRKY István

A szeizmikus sztratigráfiai kutatás fontos célja, hogy az intervallumsebességeket minél pontosabban, minél nagyobb felbontással lehessen becsülni. Az intervallumsebességeket a Dix-formulával becsüljük. A formula alkalmazásánál problémát okoz, hogy minél vékonyabbak a figyelembe vett rétegek, a becsült paraméterek szórása és korreláltsága annál nagyobb. Egy lehetséges megoldás, hogy csupán egy bizonyos korlátnál nagyobb rétegvastagságokat veszünk figyelembe.

A szomszédos rétegek becsült intervallumsebességei közti nagy negatív korreláció figyelembevételével az ilyen információveszteségeket csökkenteni lehet. Az eljárás kisebb szórású és kevésbé oszcilláló sebességfüggvény-becsléseket eredményez, egyezésben a megfigyelhető kompakciós trendekkel. A kapott függvények a paraméterek szórásaival együtt ábrázolhatók, tömör formában. Az eljárás jól szemlélteti az anomális sebességű vékony rétegek detektálásának elvi korlátait.

ОЦЕНКА УРАВНЕНИЯ СКОРОСТИ С ВЫСОКОЙ РАЗРЕШАЮЩЕЙ СПОСОБНОСТЬЮ

Иштван КЕШМАРКИ

Для сейсмических стратиграфических исследований очень важно как можно с большой точностью и с высокой разрешающей способностью оценить скорость исследуемого интервала. Интервальные скорости оцениваются с помощью формулы Дикса. При применении этой формулы, возникает проблема, суть которой заключается в том, что чем тоньше исследуемые слои, тем с меньшей точностью можно определить оцениваемые параметры, тем больше их корреляция. Для разрешения этой проблемы, можно выбирать для изучения такие слои, мощность которых больше некоторой предельной мощности.

Используя значительную отрицательную корреляцию оцениваемых интервальных скоростей соседних слоев, можно уменьшить такого рода потери информации. В результате, при использовании этого метода, получаем такие оценки уравнения скорости, которые имеют больший разброс и колебания, по отношению к наблюдаемым компакционным трендам. Получаемые уравнения вместе с разбросом параметров можно изобразить в компактной форме. При применении этого метода хорошо прослеживаются теоретические границы детектирования тонких слоёв с аномальной скоростью.

GEOPHYSICAL TRANSACTIONS 1985
Vol. 31. No. 1–3 pp. 269–293

MEASUREMENT AND PROCESSING OF SHORT-OFFSET VERTICAL SEISMIC PROFILE DATA

Myung W. LEE*, John J. MILLER* and Gábor GÖNCZ**

During the past years, the Geophysical Exploration Company (GKV) developed a method of recording Vertical Seismic Profiles using small explosive charges in a shothole by loading the hole through a Y-shaped tube. This method allowed re-using of the shothole many times and ensured the waveshape of the downgoing pulse to be similar from shot to shot.

Two VSP data sets were processed by the U.S. Geological Survey (USGS) into kinematically interpretable sections. The processing algorithms were adapted to the hardware of the GKV.

This paper presents the results of VSPs recorded in Hungary and processed by GKV using this adapted software. The results are promising and further development of this field technique warranted.

Keywords: short-offset VSP, wave shaping, signal consistency, repetitive explosive source

1. Introduction

Within the last few years, the Geophysical Exploration Company of Hungary (GKV) has developed a successful vertical seismic profile (VSP) field procedure based on an explosive energy source. This procedure has become a standard method in GKV's seismic activity. However, GKV did not have sufficient capability to process VSP data. Concurrently, the U.S. Geological Survey (USGS) had considerable success in VSP data processing for similar field configurations [LEE and BALCH 1983], but lacked success with explosive energy sources. Therefore, these mutual interests resulted in a cooperative program in the field of vertical seismic profiling, whereby a few short-offset VSP measurements obtained by the GKV were analyzed and processed by the USGS. The primary aim of this processing was to obtain VSP sections that were easy to interpret kinematically. This paper outlines the VSP field procedure, data processing, and results of three examples of the VSP measurements: the wells of Szeghalom–15, Kismarja–30 and Endrőd-É–5 (for location see *Fig. 1*).

* United States Geological Survey, Denver Federal Center, Box 25045, Denver, Colorado 80225
** Geophysical Exploration Company (GKV), POB 213, Budapest, H–1391, Hungary
Manuscript received: 16 April, 1985

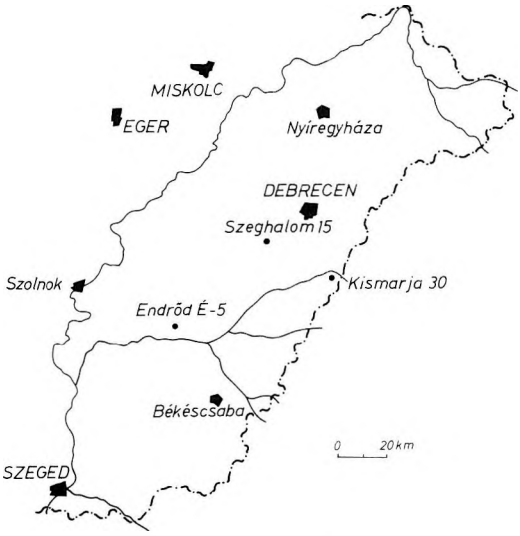

Fig. 1. Location map of the wells where VSP measurements were made

1. ábra. A cikkben szereplő VSP mérések helye a térképen

Рис. 1. Участки, где проводились наблюдения ВСП, и которые упомянуты в данной статье

2. The field procedure

The principle of VSP measurement is quite simple. The wavefield generated by a surface or near-surface energy source close to a wellhead is recorded by a downhole geophone which is clamped to the borehole wall. The geophone in the well detects the first arrival and the various downgoing and upgoing primary and multiple waves reflected in a layered earth. The wavefield is recorded in sequence at a given interval over the depth range to be investigated. *Figure 2* shows an idealized version of this configuration and the data set to be expected from such a configuration.

For the data sets presented in this paper, the measurements were carried out in cased, cemented wells using Geospace® WLS–1100-type downhole geophones and a DFS–IV® recorder. The wavefield was generated by explosive charges, and 6 to 7 channels were recorded per shot.

The shot and receiver-pattern geometry is illustrated in *Figure 3*. The upper part of the figure is a plan view and shows the shot holes; the lower part is a cross-sectional display showing the well and the geophones. The actual values of the various distances, shown in Figure 3, vary depending on the field circumstances. The shotpoint-to-well distance (that is, the offset L) should be as small as possible; in practice, it is 50–60 meters. The distance l is about 10 meters. The

® The use of trade names does not represent endorsement by the U.S. Geological Survey or the Geophysical Exploration Company of Hungary.

shot depth h is fixed by on-site test measurements in which a series of shots are recorded by the downhole geophone at a fixed depth and the shot generated from different depths. The shot depth generating the most concentrated first arrival is selected. The shot holes are drilled and prepared in advance.

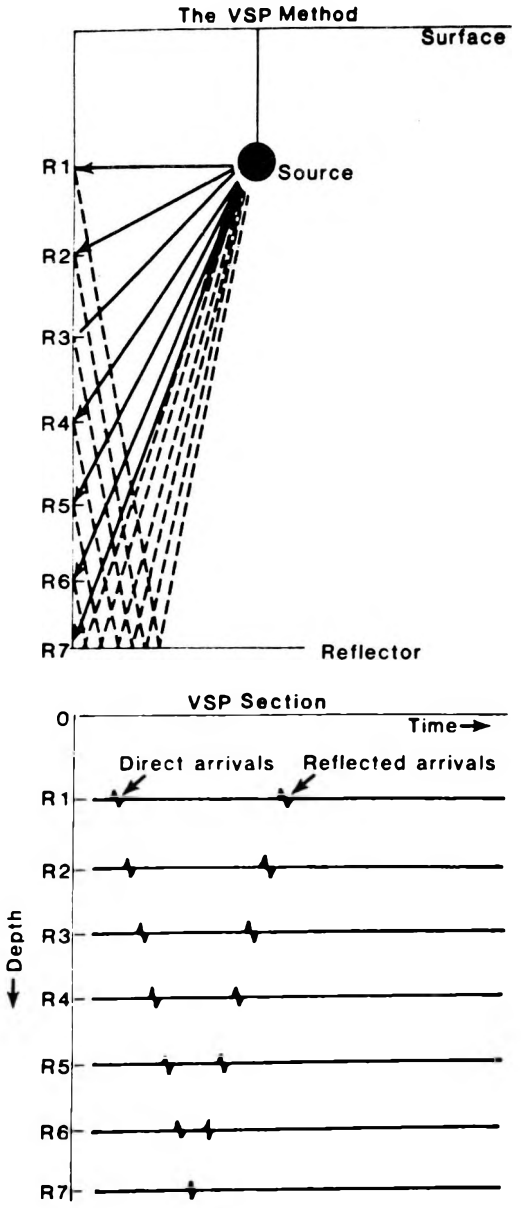

Fig. 2. Idealized VSP configuration [after Balch et al. 1982]
Top: Typical VSP field configuration
Bottom: Idealized data set from the top configuration

2. ábra. Idealizált VSP mérési elrendezés [Balch et al. 1982 nyomán]
Fenn: Tipikus VSP mérési elrendezés
Lenn: Idealizált mérési adatok

Рис. 2. Схема идеализированных измерений ВСП [по Balch et al. 1982]
Вверху: Расположение типичных измерений ВСП
Внизу: Данные идеализированных измерений

In order to obtain consistent wavelets from the different shots, small charges are used to maintain the condition of the shot hole for as long as possible. Usually explosive charges of 0.1 to 0.25 kg are used.

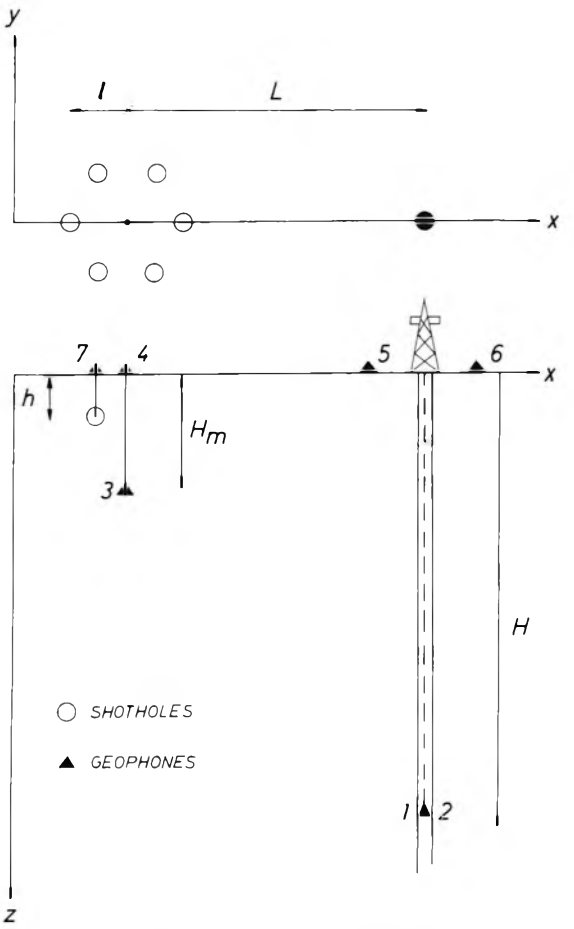

Fig. 3. The field geometry employed by GKV
Top: Plan view showing shot holes and borehole
Bottom: Cross-sectional view showing downhole geophone, shot hole, and monitor geophone locations

3. ábra. A GKV terepi mérési elrendezése
Fenn: Felülnézet, mely mutatja a mélyfúrást és a robbantólyukakat
Lenn: Keresztmetszet a geofonok elhelyezkedésével (kör: robbantópont, háromszög: geofon)

Рис. 3. Схема полевых измерений в ГКВ
Вверху: Полевая схема в плане, на которой показаны скважины глубокого бурения и взрывные скважины
Внизу: Размещение приёмников в разрезе

The charges are loaded through a Y-shaped junction of the drilling tube which is lifted a few meters before shooting to avoid damaging the tube. After shooting, the hole is flushed. The number of shots that can be made in a single shot hole is determined by how long the generated wavelet shapes remain similar, or until the charges can no longer be loaded safely. It has been our experience that 50 to 60 shots can be fired in one hole with a frequency of 1 shot every 3 minutes.

The geophone pattern is also shown in Figure 3. The downhole geophone is lowered to the depth H, and locked to the wall by a mechanical arm, controlled at the surface, providing a good coupling to the side of the borehole. The geophone detects the vertical component of the wavefield and records it on channels 1 and 2 with a 2 msec sampling rate. A near-field geophone is placed under the weathered zone at depth H_m (about 50–60 m) in a hole drilled in the center location of the shotholes. This geophone is recorded on channel 3. Other control geophones are planted on the surface. The one placed at the top of the near-field geophone hole is recorded on channel 4. The uphole geophone is recorded on channel 7. Two more geophones are located close to the wellhead and are recorded on channels 5 and 6.

To avoid distortion of the total wavefield, filters are not used, with the exception of a notch filter if necessary. The preamplifiers are set carefully and the sources of surface noise are eliminated or attenuated as much as possible. We have found this field procedure to be quite productive and it allows considerable energy in a broad frequency band to be generated and transmitted deep into the earth.

3. Processing

The processing philosophy and some algorithms were furnished by the USGS. These algorithms were adapted to GKV's computer system and were used to process the data presented in this paper. Traces from the downhole, uphole, and near-field geophones were used in the processing. The main purpose of the processing was to obtain easy-to-interpret kinematics on VSP sections. It was not our intention to study wavelet attenuation or variation of signal shape. Our main interest was in analyzing direct arrivals and upgoing primary reflections which can be used to support structural interpretation of the surface-recorded seismic data.

Trace selection, editing

The raw field records are displayed in large-scale format after demultiplexing. The objectives of this display are to edit unusable traces, choose between repeated shots, check polarity, etc. In addition, the approximate arrival times of the downgoing direct waves are measured. These approximate arrival times

are used later in automatic determination of the first arrival times. In this phase of the processing, the raw data are edited for the purpose of further processing.

Time corrections

The aim of static corrections of surface reflection seismic data is to compensate for the kinematic effects of the variation of shot depth and surface elevation. In short-offset VSP measurements, such effects are usually not significant. The positions of the downhole geophone are assumed to be correct; thus, geophone point corrections are not performed. Another source of the static time shifts is the variation of the shot depth, even though efforts to avoid this are made in the field.

To compensate for this effect, the downhole geophone traces are shifted with the average of the uphole times. Static time shifts could be introduced from shot to shot by the time difference between the zero time of the trace and the actual explosion time of the charge. The existence of this error can be seen from the records acquired from the same shothole and the same depth. In these records, the uphole times are different and the times of the first arrivals on the near-field traces are also different; these two differences are correlated. Therefore, a well geophone is corrected with the time difference between the time of the actual near trace and the average arrival time of the near traces.

Because the actual offset is not zero, a dynamic time shift is also present. On short-offset VSPs, this can be significant on shallow depth traces. Presently, this is corrected by approximation and for direct arrivals only. After time-shift corrections, the arrival time of the downgoing direct wave is known as a function of depth. From these arrival times, the average velocity function can be computed and an interval velocity model may also be constructed using statistical estimation techniques. One of the objectives of the short-offset VSP is to obtain the average velocity function in finely spaced intervals, and this function can be a valuable tool in the processing and interpretation of surface seismic measurements close to the well.

Wavelet shaping

The interpretive value of VSP data would be greatly increased if every shot emitted the same type of wavelet, whereby the wavelet variations recorded could be attributed to geologic conditions. However, the energy sources create variable wavelets, even when appropriate field procedures are carried out carefully. When shot holes are changed, this wavelet variation is especially striking. Numerical wavelet shaping, therefore, is required in order to convert variable wavelets to a standard waveshape. In this study, the near-field traces for wavelet shaping were used. One of the near-field wavelets is considered to be the standard, reference wavelet.

For each near-field trace, a deterministic shaping filter was designed using the selected reference wavelet as the desired output. These filters were applied to the appropriate downhole traces and produced rather similar wavelets on different traces.

The effectiveness of the shaping filters is shown in *Figures 4, 5, 6* and *7*. Figures 4 and 5 show VSP data from the Szeghalom–15 well; Figures 6 and 7 show data from the Kismarja–30 well. Figures 4 and 6 display the data before shaping; Figures 5 and 7 show the results after shaping. The effectiveness of shaping depends greatly on the assumption that the near-field wavelets recorded are similar to the source-generated wavelets at the wellphone.

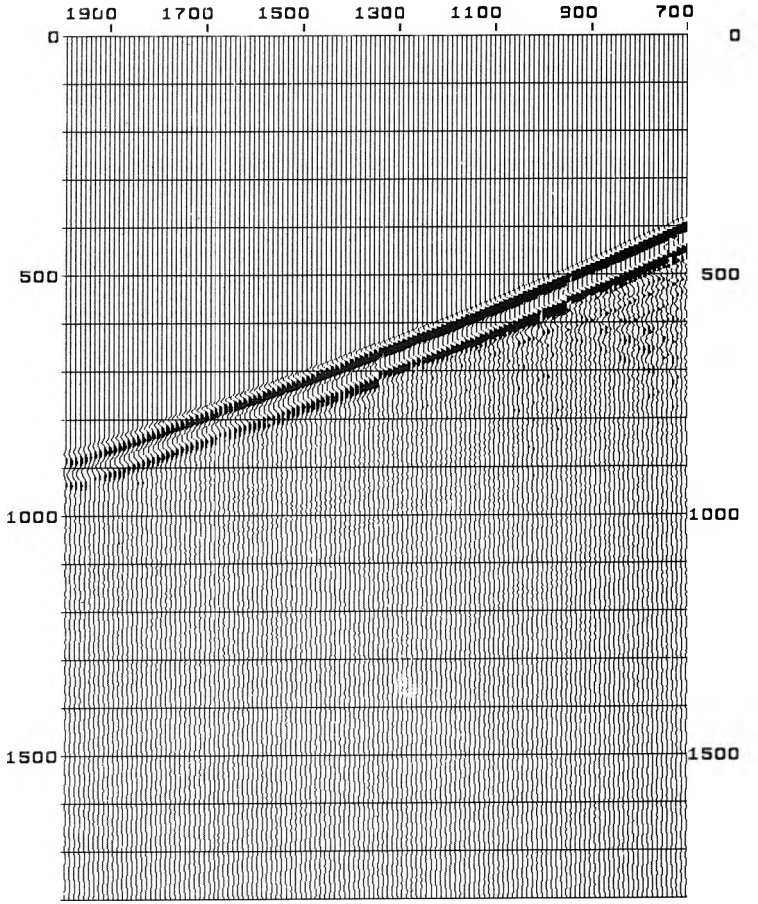

Fig. 4. Raw VSP data from Szeghalom–15 showing variation in signal shape

4. ábra. A Szeghalom–15 nyers VSP szelvénye

Рис. 4. Необработанный профиль ВСП Szeghalom–15

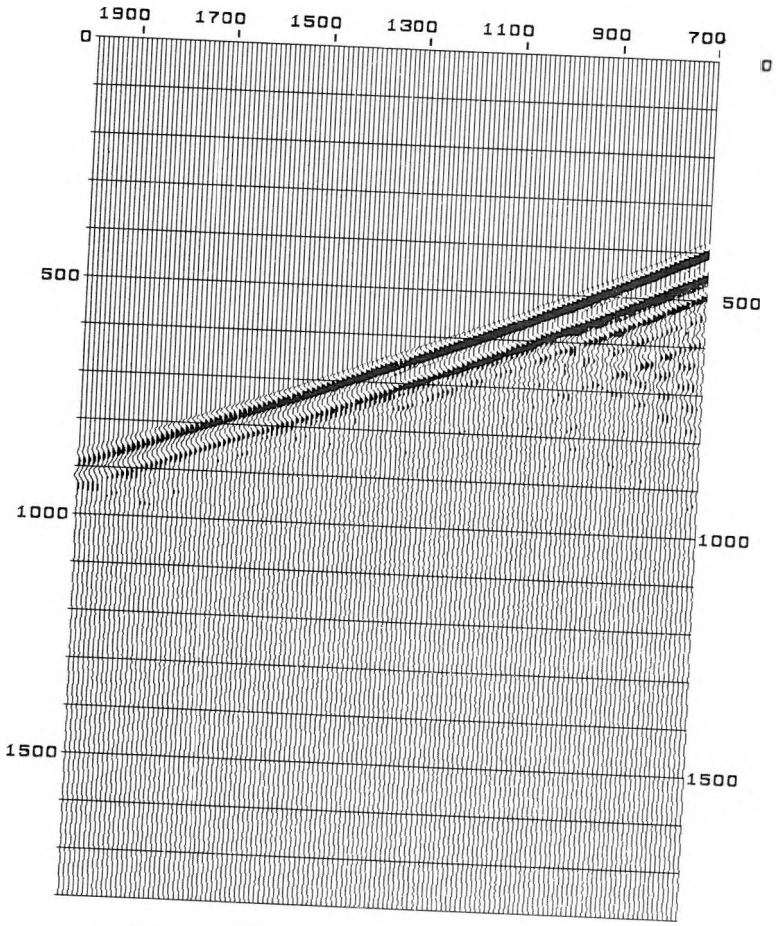

Fig. 5. Data from Figure 4 after wavelet shaping

5. ábra. A 4. ábra szelvénye jelalakszűrés után

Рис. 5. Профиль, изображенный на рис. 4, после корректирующей фильтрации

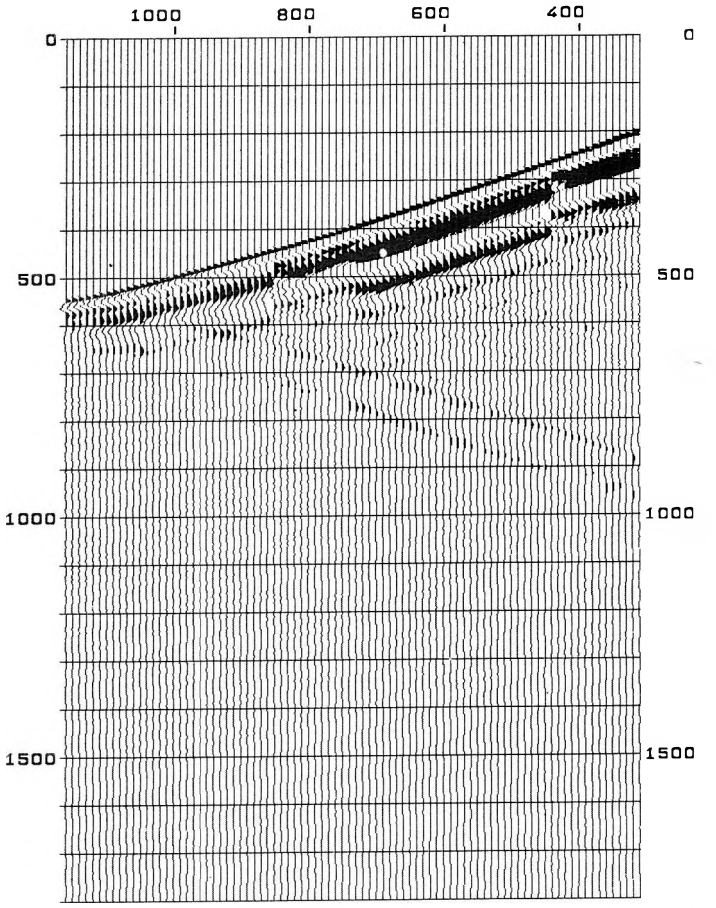

Fig. 6. Raw VSP data from Kismarja–30 showing variation in signal shape

6. ábra. A Kismarja–30 nyers VSP szelvénye

Рис. 6. Необработанный профиль ВСП Kismarja–30

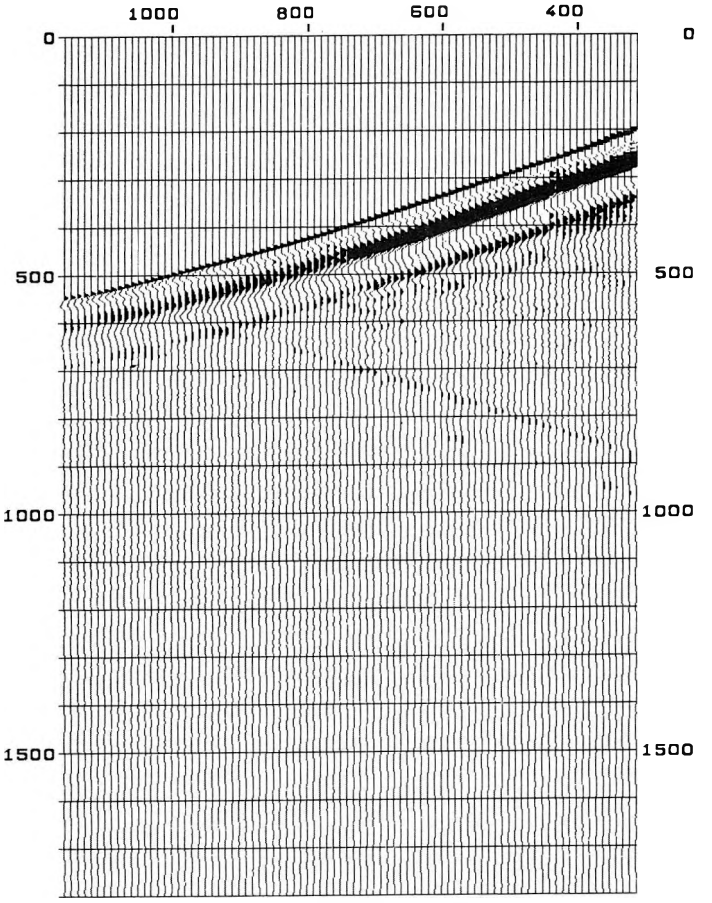

Fig. 7. Data from Figure 6 after wavelet shaping

7. ábra. A 6. ábrán látható szelvény jelalakszűrés után

Рис. 7. Профиль, показанный на рис. 6, после корректирующей фильтрации

Amplitude processing

The amplitudes of the signals of a raw VSP section vary as a function of time and depth also. The geometrical spreading of seismic energy is the dominant physical process that causes reduced amplitudes. It is desirable to reconstruct this energy spreading. A gain function, balancing the downgoing direct wave, is computed in an experimental way. For the Szeghalom–15 well, $G = T/250)^2$, where G is the gain function and T represents the one-way travel time. Further physical processes which affect the amplitude of the propagating seismic wavelet are not compensated for in our existing program package.

Velocity filtering

The well geophone detects both the downgoing and the upgoing wavefields, therefore, the VSP section is an interference of many different primary and multiple reflections. Both the downgoing and upgoing wavefields contain information, but it is desirable to separate these two types of waves. The basic tool to remove unwanted energy modes with different apparent velocities is the velocity filter.

The tube wave, shear waves, and converted waves also can be attenuated in this way; hence, the velocity filter may improve the signal-to-noise ratio too. The velocity filter used operates in the frequency–wavenumber (F–K) domain. The downgoing and upgoing events are separated by passing the appropriate quarter of the F–K plane, and applying a bandpass filter with an 80-Hz cut-off frequency simultaneously. There is a significant dynamic difference between the separated downgoing and upgoing wavefields. In the downgoing wavefield, the strongest event is the direct wave with downgoing multiples of lesser energy. The weaker upgoing wavefield consists of primary and multiple reflections. Therefore, the downgoing direct wave was attenuated by 10 dB, after which the two wavefields were combined to produce a well-balanced section. This VSP section was corrected for two-way travel time, which aligns the upgoing events.

The VSP data from the Kismarja–30 well, processed in this manner, can be seen in *Figure 8*. The upgoing wavefield of this section corrected to two-way time, can be seen in *Figure 9*, and the downgoing waves corrected to zero time are shown in *Figure 10*. Different types of waves can be seen clearly, for example, a downgoing direct wave, a strong upgoing reflected wave at 1,150 m, and their first surface multiples. A few weak reflections can be observed on the upper part of the upgoing wavefield. Similar VSP data from the Szeghalom–15 well are shown in *Figures 11*, *12* and *13*, respectively.

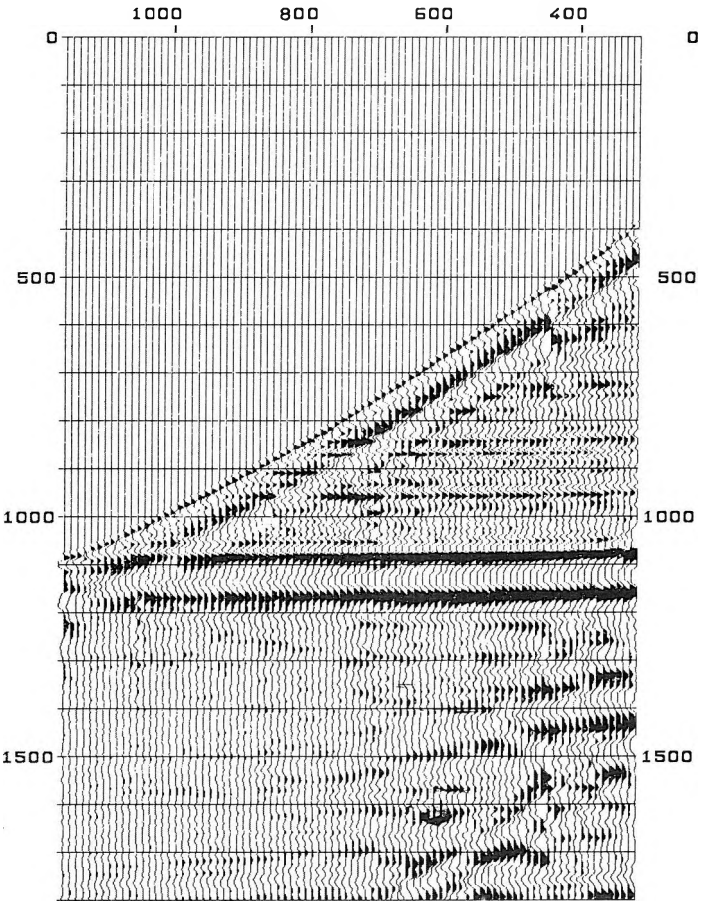

Fig. 8. VSP data obtained in the Kismarja–30 well after velocity filtering, attenuation of downgoing wavefield by 10 dB, and merging upgoing and downgoing wavefields. Data have been shifted to align upgoing events

8. ábra. A Kismarja–30 VSP szelvénye sebességszűrés és a lefelé haladó hullámtér 10 dB-lel való csillapítása, majd a le- és felfelé haladó hullámok összeadása után. A lefelé haladó hullámokat statikus tolással fázisba hoztuk

Рис. 8. Фильтрация по скорости профиля Kismarja–30 и перемещающееся вниз волновое поле с 10 д-м затуханием, затем вниз и вверх перемещающиеся поля после сложения со статическим сдвигом по фазе

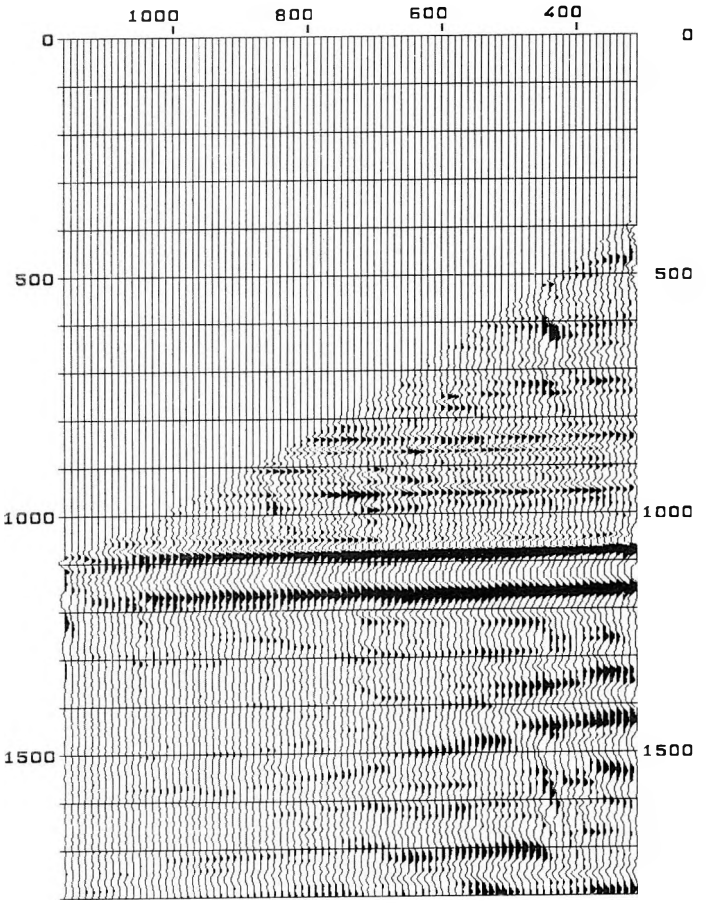

Fig. 9. The upgoing part of wavefield from Figure 8

9. ábra. A felfelé haladó hullámok a 8. ábrából

Рис. 9. Перемещающиеся вверх волны, изображенные на рис. 8

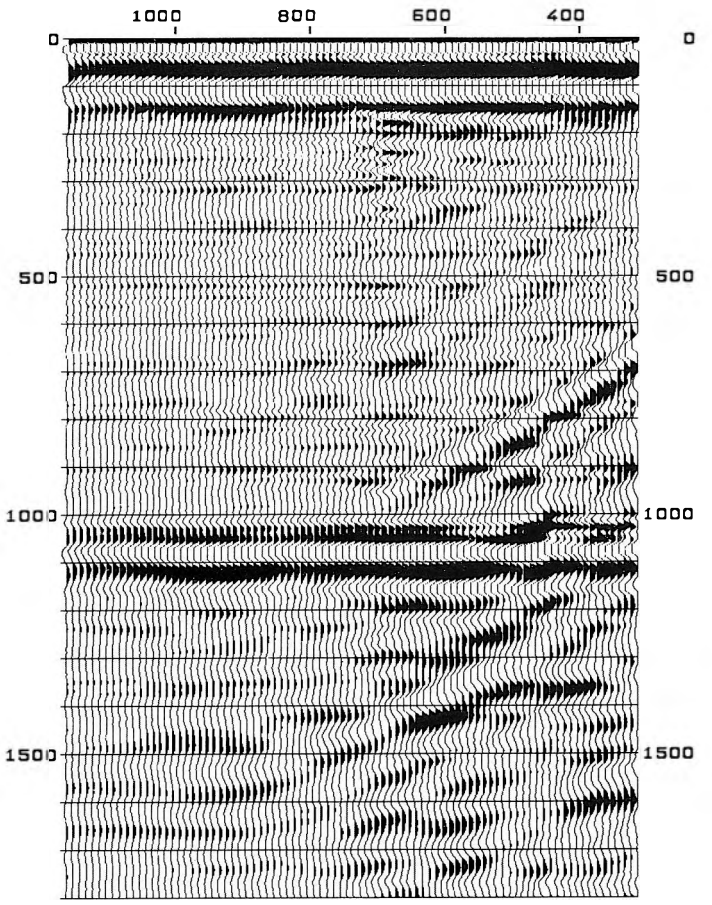

Fig. 10. The aligned, downgoing part of the wavefield from Figure 8

10. ábra. A fázisba hozott lefelé haladó hullámok a 8. ábrából

Рис. 10. Сдвинутые по фазе, перемещающиеся вниз волны, изображенные на рис. 8

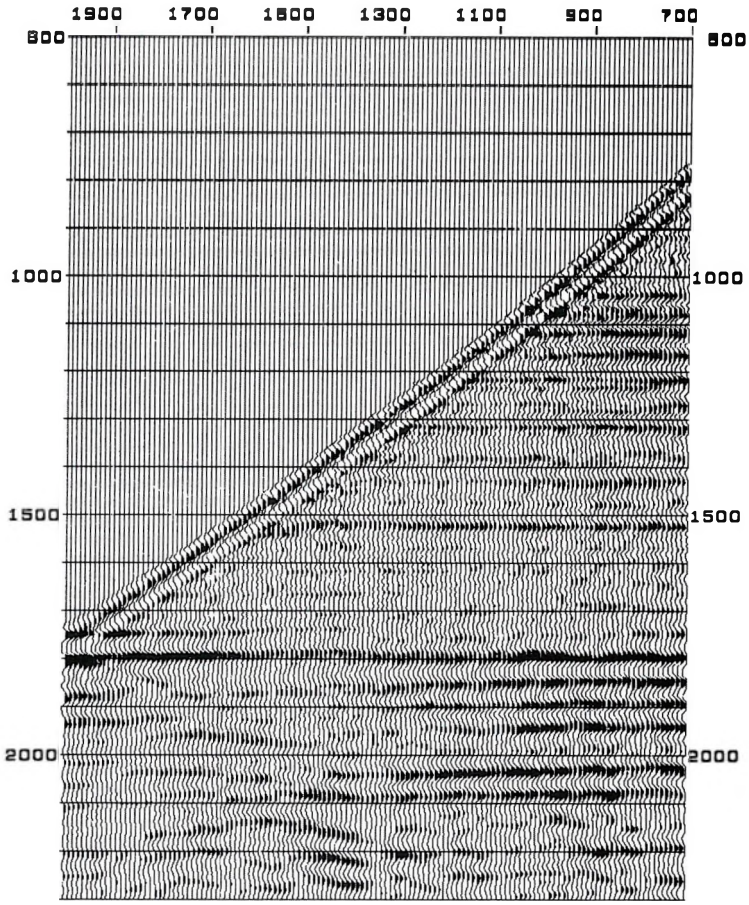

Fig. 11. VSP data from the Szeghalom–15 well processed as in Figure 8

11. ábra. Szeghalom–15 VSP szelvénye a 8. ábrához hasonlóan feldolgozva

Рис. 11. Обработка профиля ВСП Szeghalom–15, аналогичному рис. 8

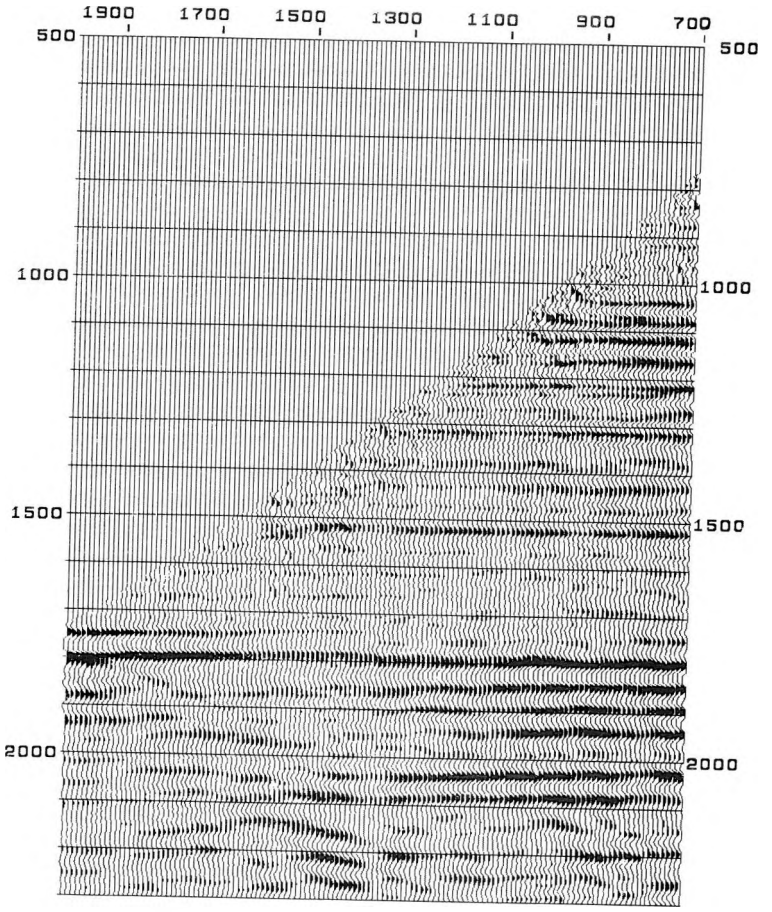

Fig. 12. The upgoing part of the wavefield from Figure 11

12. ábra. A felfelé haladó hullámok a 11. ábrából

Рис. 12. Перемещающиеся вверх волны, изображенные на рис. 11

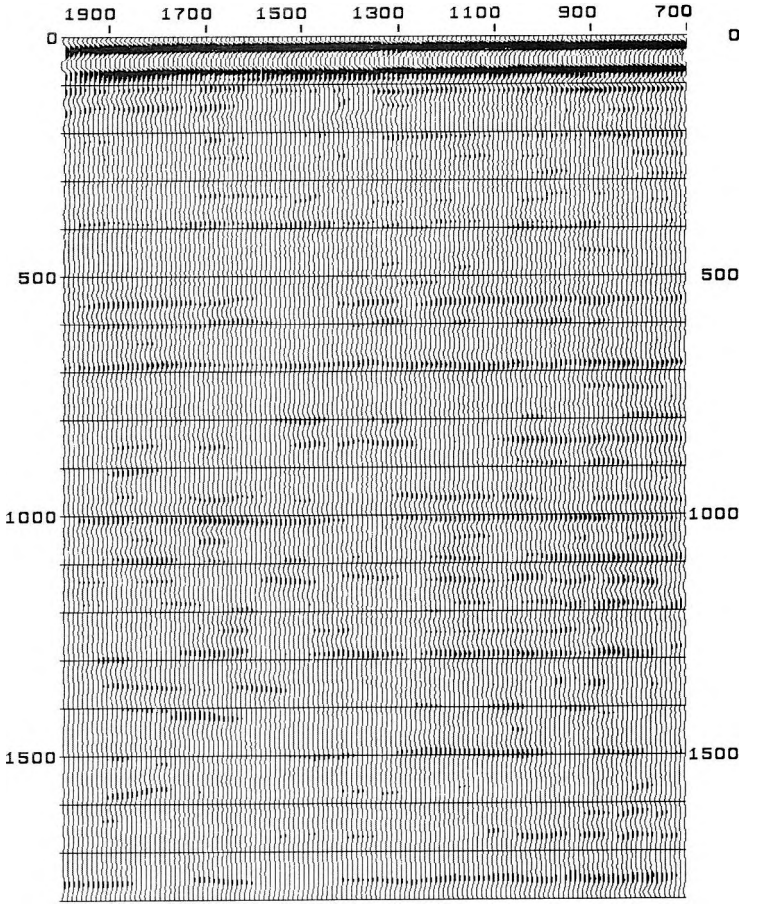

Fig. 13. The downgoing part of the wavefield from Figure 11

13. ábra. A lefelé haladó hullámok a 11. ábrából

Рис. 13. Перемещающиеся вниз волны, изображенные на рис. 11

Deconvolution based on the downgoing wave

The previous illustrations show that, the downgoing direct wave separated by a velocity filter is neither a spike nor a well-defined wavelet; it is a complicated wave train. This long wave train is reflected from the boundaries producing multiples and making the interpretation a complicated task. Therefore, it is desirable to apply spiking deconvolution to contract signals. The deconvolution operator is designed from a time window containing the downgoing direct wave. The advantage of using the direct wave to design deconvolution operators is that the signal strength is greater than that of the usual wavefield used to calculate deconvolution filters. The deconvolution increases the resolution of the VSP wavefield as can be seen in *Figures 14* and *15*, which are the deconvolution of Figures 8 and 11, respectively. *Figures 16* and *17* are the deconvolved, upgoing wavefields from Figures 9 and 12, respectively.

Cumulative vertical stacking

A simple and effective procedure that emphasizes upgoing reflections is the vertical summation of VSP traces which have, in phase, upgoing reflections along equal time lines. This procedure positions the traces at their proper two-way surface arrival times. The cumulative stacking of the deconvolved, upgoing wavefield at Kismarja–30 is shown in *Figure 18*. The good resolution of the reflections and the improved signal-to-noise ratio is apparent in this section. *Figure 19* shows the top few traces of the cumulative stacking of the upgoing wavefield at Endrőd-É–5 displayed next to the conventional surface data recorded near this well. The good correlation between the two data sets gives a high degree of confidence in reflector identification on the surface data.

4. Conclusion

VSP field procedure, employed by GKV, using explosive energy sources proved to be adequate, but should be improved to produce better quality data. The processing of the VSP data, based on the techniques and algorithms obtained from the USGS, is promising but should be further developed in order to better interpret the dynamics of the wavefield.

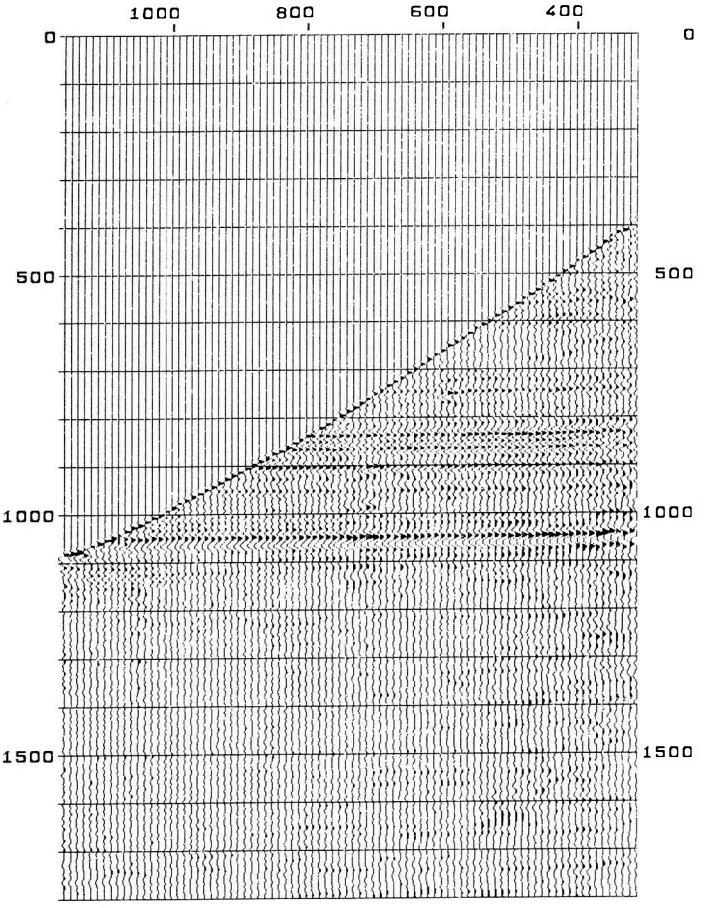

Fig. 14. VSP data from the Kismarja–30 well after deconvolution

14. ábra. A Kismarja–30 VSP szelvénye dekonvolúció után

Рис. 14. Профиль ВСП Kismarja–30 после деконволюции

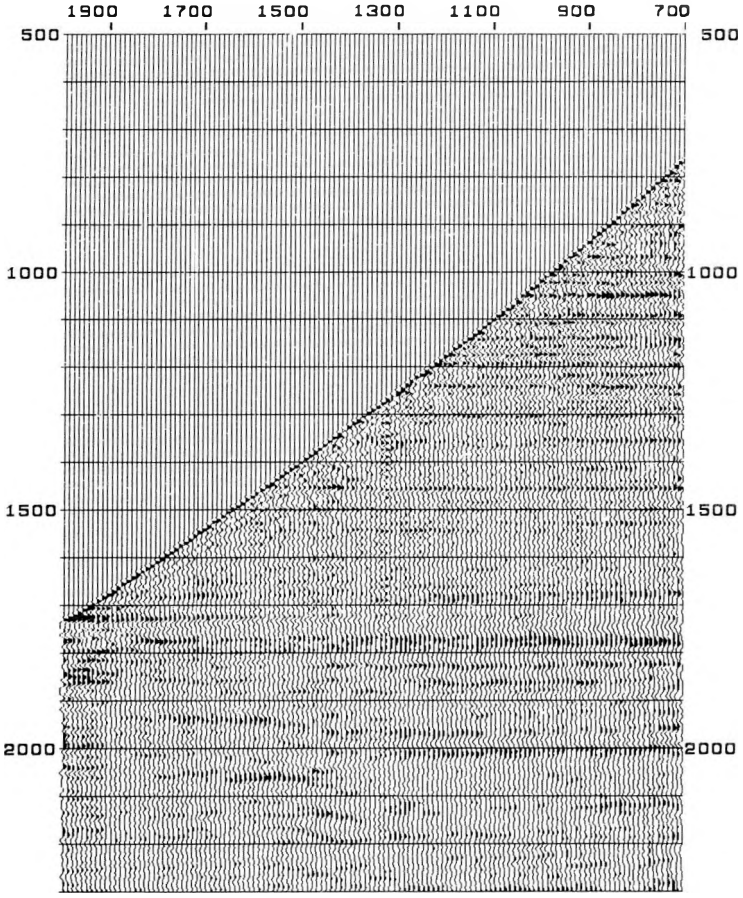

Fig. 15. VSP data from the Szeghalom–15 well after deconvolution

15. ábra. A Szeghalom–15 VSP szelvénye dekonvolúció után

Рис. 15. Профиль ВСП Szeghalom–15 после деконволюции

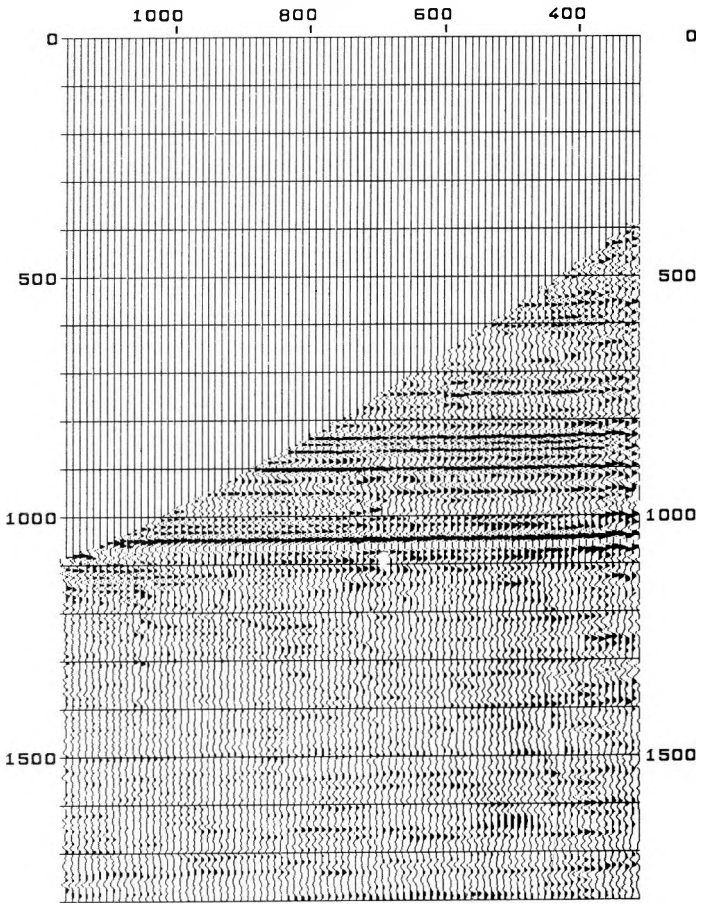

Fig. 16. Deconvolved, upgoing wavefield from Figure 14

16. ábra. Dekonvolvált felfelé haladó hullámtér a 14. ábrából

Рис. 16. Деконволюрованное, перемещающееся вверх волновое поле, изображенное на рис. 14

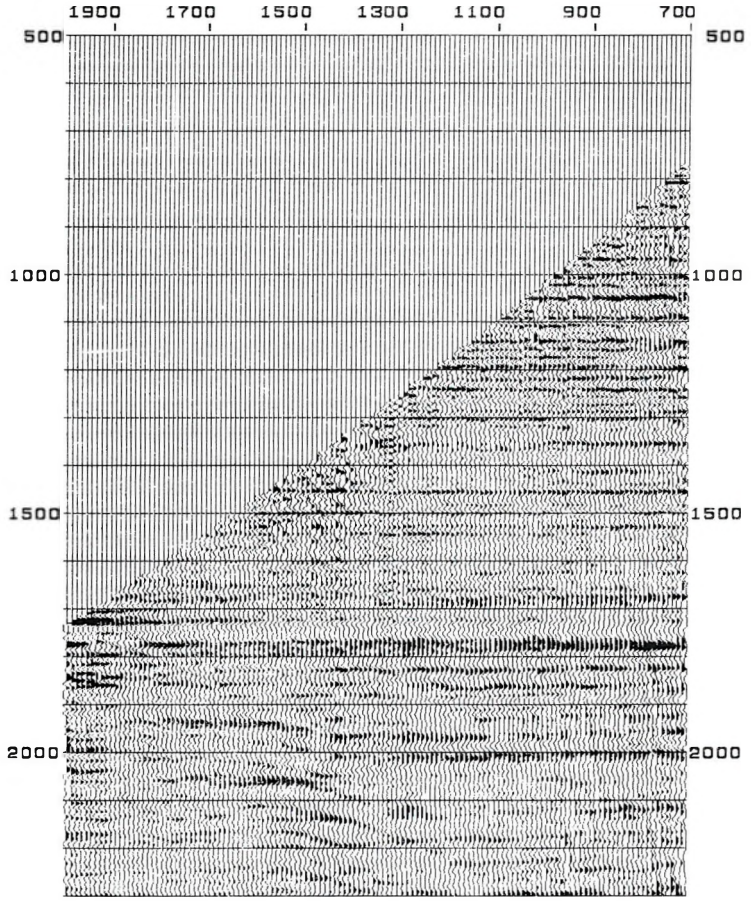

Fig. 17. Deconvolved, upgoing wavefield from Figure 15

17. ábra. Dekonvolvált felfelé haladó hullámtér a 15. ábrából

Рис. 17. Деконволюрованное, перемещающееся вверх волновое поле, изображенное на рис. 15

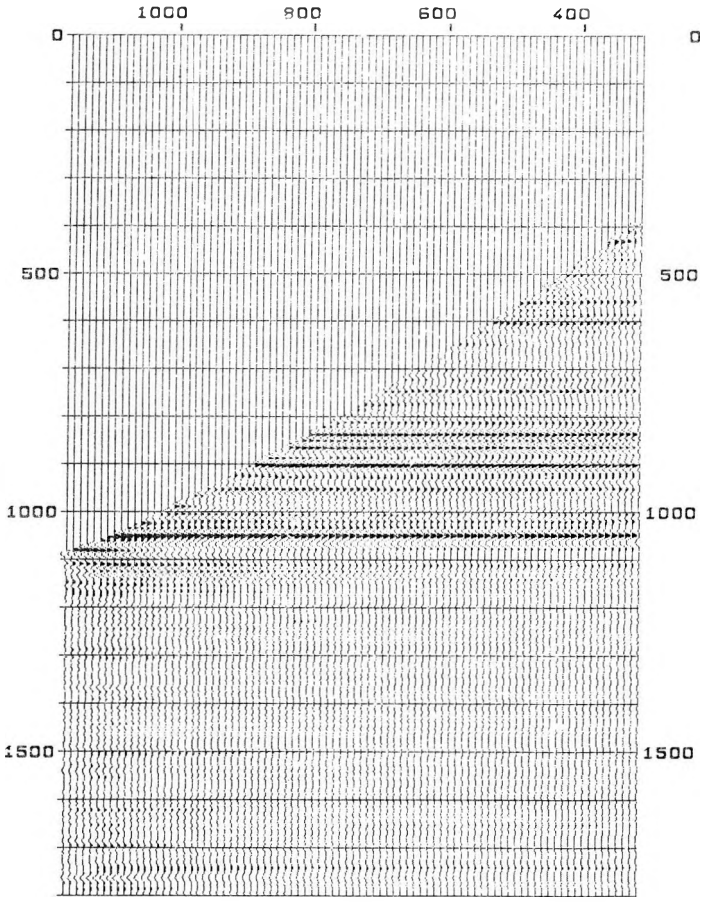

Fig. 18. Cumulatively summed version of Figure 16

18. ábra. A 16. ábrán látható szelvény kummulatív összegzés után

Рис. 18. Профиль, показанный на рис. 16, после куммулятивного суммирования

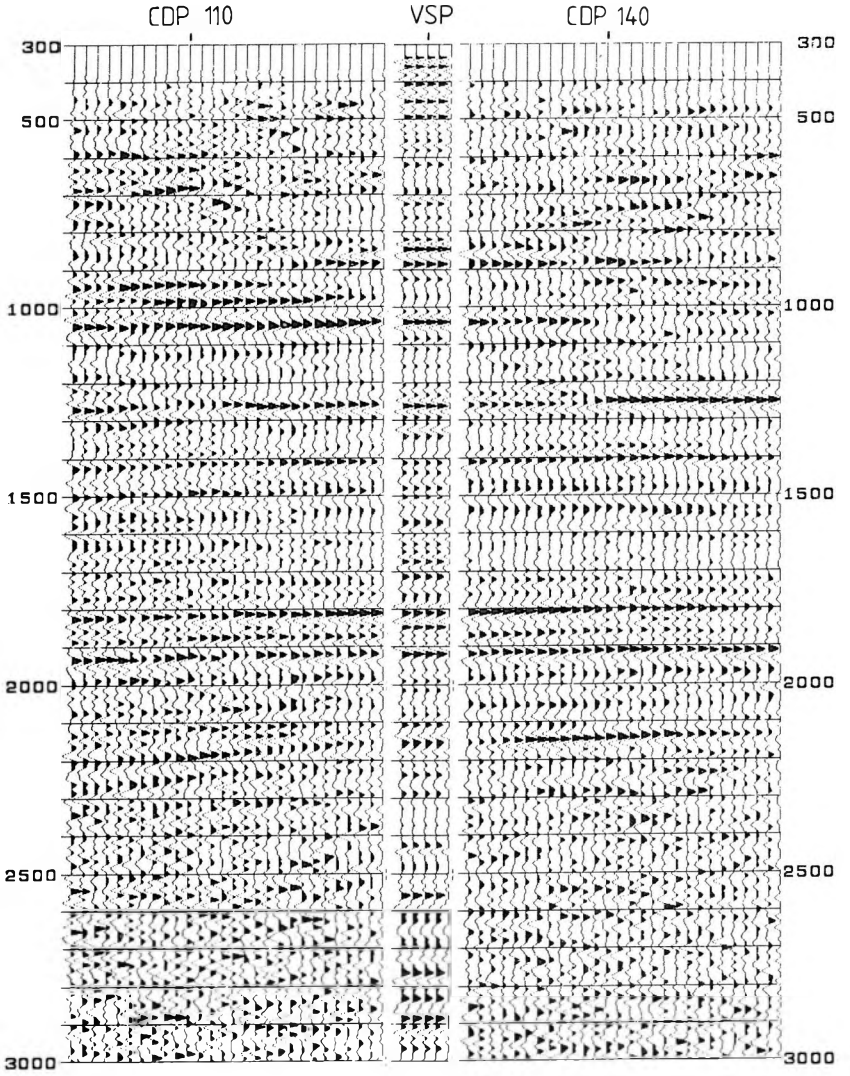

Fig. 19. Correlation between cumulatively summed VSP data and conventional surface reflection data near the Endrőd-É–5 well

19. ábra. Kummulatívan összegzett VSP reflexiós csatornák illesztése az Endrőd-É–5 fúrás közelében felszíni reflexiós időszelvényhez

Рис. 19. Соединение каналов отраженных волн куммулятивно просуммированного ВСП вблизи скважины Endrőd-É–5, к поверхностному временному разрезу отраженных волн

REFERENCES

BALCH A. H., LEE M. W., MILLER J. J. and Ryder R. T. 1982: The use of vertical seismic profiles in seismic investigations of the earth. Geophysics, **47**, 6, pp. 906–918

LEE M. W., BALCH A. H. 1983: Computer processing of vertical seismic profile data. Geophysics, **48**, 3, pp. 272–287

LYUKKÖZELI VSP MÉRÉSEK ÉS FELDOLGOZÁSUK

Myung W. LEE, John J. MILLER és GÖNCZ Gábor

Az elmúlt években a GKV kifejlesztett egy hatásos módszert kis töltetek alkalmazására, melyeket egy Y alakú cső segítségével juttatnak le a robbantólyukba. A módszer lehetővé teszi, hogy egy robbantólyukat sokszor felhasználjunk, miközben a lefelé haladó jelalak alig változik.

1983 elején a GKV két VSP mérési anyagát a USGS által kifejlesztett programrendszerrel feldolgoztuk Denverben, és kinematikailag jól kiértékelhető szelvényeket kaptunk. A feldolgozó algoritmusokat a GKV beépítette a saját feldolgozó rendszerébe.

A dolgozatban Magyarországon mért VSP adatokat mutatunk be, melyeket az adaptált programrendszerrel dolgoztunk fel. Az eredmények biztatóak, és a terepi mérési módszer sikeresnek bizonyult.

ТЕХНИКА ИЗМЕРЕНИЙ И СПОСОБЫ ОБРАБОТКИ ДАННЫХ ВСП ПРИ МИНИМАЛЬНОМ РАССТОЯНИИ МЕЖДУ ПУНКТОМ ВЗРЫВА И СКВАЖИНОЙ

Мюнг В. ЛИ, Джон Дж. МИЛЛЕР и Габор ГЁНЦ

В прошлых годах в Предприямии Геофизического Исследования ГТНГП (GKV) был развит один эффективный способ, заключающийся в применении небольших по массе зарядов, которым заполняют скважины при помощи У-образной трубы. Этот метод способствует тому, что можно использовать одну взрывную скважину неоднократно, в то время как перемещающаяся вниз форма сигнала едва изменяется. Ранее взрывной метод не был достаточно разработан, хотя и была потребность и в анализировании этого метода, и в соответствующих способах его обработки.

В начале 1983 г. два материала по ВСП были отвезены в USGS. Для их интерпретации была использована техника обработки, которая была разработана в USGS, используя которую мы могли бы получить кинематически хорошо понимаемые профили. Алгоритмы обработки были приспособлены к собственным способам обработки в GKV.

В данном отчете представлены результаты измерений ВСП в Венгрии, которые обрабатывались нами на собственном аглоритмическом программном обеспечении. Результаты обработки получились обнадеживающими, кроме того способ измерений хорошо себя зарекомендовал.

GEOPHYSICAL TRANSACTIONS 1985
Vol. 31. No. 1–3. pp. 295–310

TRANSIENT ELECTROMAGNETIC SOUNDINGS—DEVELOPMENT OF INTERPRETATION METHODS AND APPLICATION TO BAUXITE EXPLORATION

Kristóf KAKAS*, Frank C. FRISCHKNECHT**, József ÚJSZÁSZI*, Walter L. ANDERSON** and Ernő PRÁCSER*

Under a cooperative program between the U.S. Geological Survey and the Eötvös Loránd Geophysical Institute, central loop and single loop time-domain electromagnetic (TDEM) soundings were made at a number of localities in Hungary. The primary objective was to test the usefulness of the method in exploration for bauxite. The results of the soundings were interpreted by use of a nonlinear least-squares computer algorithm which fits the data with one-dimensional models. Interpretation of the data was generally complicated by the fact that most of the soundings were distorted due to lateral changes in the conductance of the overburden or other causes. Direct evidence of known bauxite deposits was not found. However, the results indicate that TDEM soundings can provide structural information useful to locating bauxite deposits indirectly. In two areas, evidence of a deep conductor beneath a bauxite deposit was found. The central loop or single loop techniques were found to be rather slow for routine exploration where a dense set of soundings is needed, therefore, in the future, fixed source or large loop configuration will be tested in bauxite exploration.

There are two serious problems in interpretation of TDEM sounding curves by computer inversion; the required computer time is excessive for inversion of all the data acquired in a routine survey and satisfactory results cannot be obtained when the sounding curves are highly distorted by lateral changes in resistivity. Anomalous zones can readily be identified by plotting the data in the form of pseudosections with time along the vertical axis. To produce quantitative information on the variation of resistivity with depth or the depth to interfaces between layers, methods termed TSH and TRH are being developed. The TSH method is based on an approximation for the response of a thin conductive sheet in a resistive half space and it yields apparent conductance versus apparent depth curves. The TRH method is based on the rate of diffusion downward of the eddy currents in a half-space and it produces a resistivity versus depth curve.

Keywords: transient electromagnetic sounding, bauxite prospecting, Marquardt inversion, time-domain electromagnetics

1. Introduction

Many of the principles of transient electromagnetic depth sounding have been understood for more than 30 years. Until the past several years, transient or time-domain electromagnetic (TDEM) soundings were generally made with heavy equipment and large offsets between source and receiver to sound to depths of up to several kilometers. In the last few years, highly portable

* Eötvös Loránd Geophysical Institute of Hungary, POB 35, Budapest, H-1440
** U. S. Geological Survey, Denver Federal Center, P.O. Box 25046, MS 964, Denver, Colorado 80225
Manuscript received: 3 January, 1985

equipment, which was developed primarily for exploration for conductive mineral deposits, has been employed for sounding to shallower depths using short times and short offsets between the source and receiver. Time-domain methods have a number of advantages over other geoelectrical sounding methods. Generally, TDEM soundings are more sensitive to the presence of conductive layers than other geoelectrical measurements. Most TDEM techniques are relatively insensitive to topography and high precision in surveying is not required. Measurements made with short offset configurations are not as likely to be distorted by lateral variations in resistivity as measurements made with long offset configurations, and it is much easier to make high-resolution TDEM measurements than frequency-domain measurements using short offsets.

The development and application of TDEM methods for high-resolution sounding to depths of 0.5–1.0 km is of great interest to the Eötvös Loránd Geophysical Institute (ELGI) and the U.S. Geological Survey (USGS). Cooperative studies between these two organizations have included an evaluation of short offset TDEM methods in sounding and as applied to bauxite exploration in Hungary, the development of mathematical tools for computer inversion of data taken about large loops, and the development of rapid techniques for interpreting TDEM soundings.

2. Field studies

During November 1982, experimental TDEM measurements were made jointly by USGS and ELGI personnel at a number of locations in Hungary. The objectives were to test the usefulness of the method in bauxite exploration and in shallow sounding for other purposes. The basic equipment was a Mark II SIROTEM® desinged by CSIRO [Buselli–O'Neill 1977]. An auxiliary high power switcher developed by the USGS was used for some of the work. Most measurements were made using the central loop configuration in which a small vertical-axis, multi-turn loop is placed at the center of a much larger square transmitter loop. By means of an electronic switch at the input of the receiver the SIROTEM instrument can also be used with a single loop for both transmitting and receiving; a few such measurements were made. Transmitting loops with sides having dimensions at 50, 100, 200, and 400 meters were used. The system transmits a train of bipolar nearly-square pulses with an off-power interval between pulses. Measurements can be made at up to 32 times (channels) after the end of the current pulse. Results from a minimum of 512 and a maximum of 4096 pulses can be stacked. Typically the results from two or more individual runs, using 2048 stacks were averaged. The number of channels of useful information depended on the signal-to-noise ratio which, in turn, depended on the resistivity of the earth, the transmitter current, and cultural background noise, which in Hungary, was generally noise from 50 Hz mains. Av-

® Use of trade names does not constitute endorsement either by ELGI or USGS

eraged values of the transient voltage were transformed to apparent resistivity using microcomputer programs developed by RAAB and FRISCHKNECHT [1983]. Apparent resistivity, as defined in their algorithm, is the resistivity of the homogeneous earth which would produce a response equal to the observed response. Apparent resistivity data were inverted using nonlinear least-squares programs developed by ANDERSON [1982/a, 1982/b], which fit data to one-dimensional models.

In Hungary, bauxite deposits typically occur in structural depressions or in sinkholes on the surface of high-resistivity Triassic carbonate rocks [BÁRDOSSY 1982, 1984]. The bauxite is covered by Quaternary and Tertiary deposits of sand, clay, marl, and sometimes limestone of high resistivity. The other materials generally have resistivities ranging from about 5 to 100 Ωm. The resistivity of bauxite is generally similar or a little higher than that of the overburden, excluding the limestone. Thus, the bauxite does not constitute a good target for direct detection by electrical methods. However, it is often possible to detect depressions on the surface of the Triassic carbonates. Ideally one could detect such depressions using a series of central or single loop soundings. Apparent resistivity curves calculated for a hypothetical 3-layer model in which the thickness of the bauxite layer is varied are shown in *Figure 1*. The curves do not exhibit a pronounced feature characteristic of the bauxite layer, nevertheless, it should be possible to resolve these various cases in the

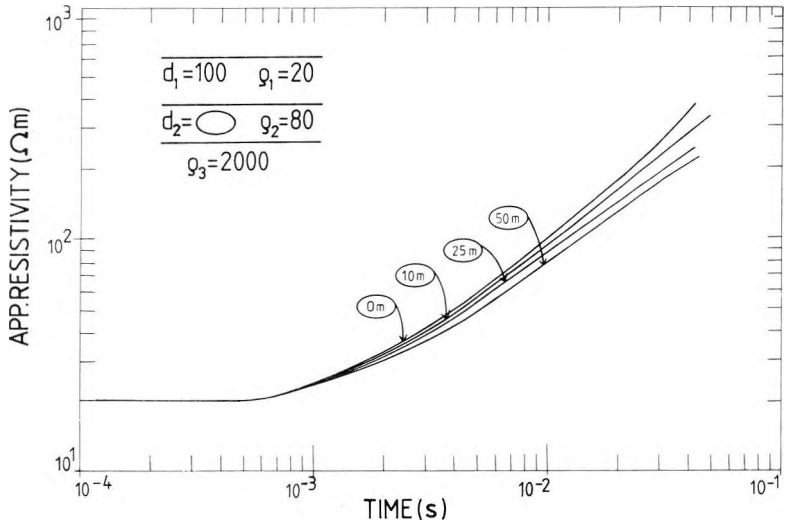

Fig. 1. Theoretical curves for a model containing a bauxite layer

1. ábra. Elméleti tranziens szondázási görbék bauxitréteget tartalmazó modell felett

Рис. 1. Теоретические кривые зондирования МПП над моделью, содержащей бокситовый слой

field. Of course, the effect of an actual bauxite deposit would be somewhat smaller than indicated in Figure 1 because such a deposit has finite lateral dimension usually on the order of 50–200 m.

Measurements were made at one site where the earth was known to be rather uniformly conductive to a depth of several hundred meters, and at five sites where bauxite deposits exist. Single- and central-loop measurements were made between the Gerecse and Buda hills, SE of Zsámbék, where it is known from resistivity soundings that there is a thick section having a rather uniform resistivity. A good fit to the observed data was obtained with the model indicated in *Figure 2*. Parameters for the conductive layers are generally well resolved. Parameters for the thin upper layer and the depth to the resistive basement are not well resolved. The indicated depth in Figure 2 is less than the actual depth of about 550 meters. However, another, somewhat poorer fit to the data was obtained with a model in which the depth to basement is 600 meters. It is interesting to note that in this example, where a conductive overburden overlies a resistive basement, the effective depth of investigation was on the order of the loop dimensions (400 meters) using a current of about 2 amperes.

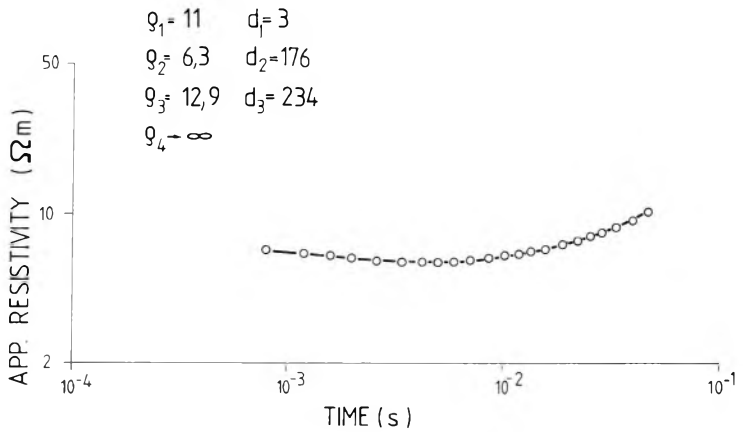

Fig. 2. Sounding curve and interpretation for nearly homogeneous half-space

2. ábra. Szondázási görbe és kiértékelése közel homogén féltér felett

Рис. 2. Кривая зондирования и ее интерпретация над полупространством, близком гомогенному

For the opposite case of an insulating layer over a conductive basement, the depth of investigation under the same conditions can be 3 or 4 times the loop dimension.

Results obtained from the SE Gerecse coal basin, NW of Zsámbék, are shown in *Figure 3*. Most of the parameters are fairly well resolved, although for the second layer the resistivity and thickness are not well resolved but its conductance. The resistivity of the basement is not well resolved and the depth to resistive basement is less than that given by a nearby borehole (380 m). The

calculated TDEM apparent resistivity curve fails to rise as sharply as the observed curve at late times. It was not possible to find a layered earth model which would produce a suitable fit to this part of the observed curve; in fact, the results in Figure 3 were obtained by neglecting the last four points on the curve in the inversion process. Failure to find a 1-dimensional model which will

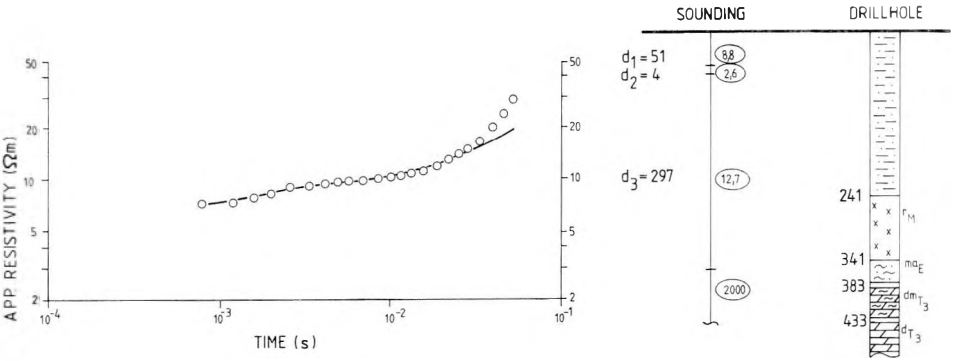

Fig. 3. Sounding curve and interpretation for the locality in the SE Gerecse coal basin
^{r}M = Miocene rhyolite tuff; ^{ma}E = Eocene marl with coal seams; $^{dm}T_3$ = Upper Triassic dolomitic marl; $^{d}T_3$ = Upper Triassic dolomite

3. ábra. Szondázási görbe és kiértékelésének összehasonlítása fúrási rétegsorral (Gerecse DK-i előtere)

Рис. 3. Кривая зондирования и сопоставление ее с интерпретации с результатами бурения (ЮВ предгорье гор Гереше)

^{r}M = риолитовый туф миоценового возраста; ^{ma}E = эоценовый мергель с углеродными слоями; $^{dm}T_3$ = верхне-триасовый доломитовый мергель; $^{d}T_3$ = верхне-триасовый доломит

fit the data indicates that the sounding curve is distorted by lateral variations in resistivity. In this case, abrupt thinning of the conductive layer in the vicinity of the sounding is the most likely cause of distortion and may account for the difference between the depths from the borehole and the sounding.

Three sounding curves obtained near Csabpuszta, the models obtained by computer inversion, and results from boreholes are shown in *Figure 4*. All three curves were fitted to a 5-layer model, although the presence of this many layers in not very obvious in sounding S–1. Good fits were found for *S*–1 and *S*–2. A layered earth model having a resistivity curve duplicating all of the details of *S*–3 was not found, indicating that *S*–3 is badly distorted by lateral variations in resistivity. This is not surprising considering the large differences observed between the three soundings. The values for the third and fifth layers, which have high resistivities, are not well resolved. The top of the third resistive layer coincides approximately with the top of middle Eocene sediments intersected by the boreholes. The top of the fourth conductive layer coincides rather closely

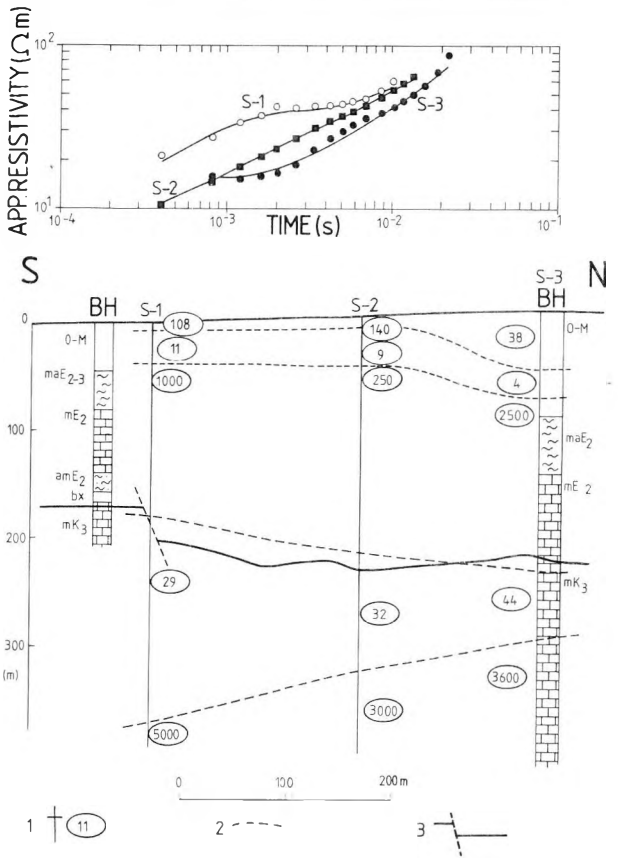

Fig. 4. Results of soundings for a locality near Csabpuszta 1 — layer resistivities and 2 — interface based on TDEM interpretation; 3 — surface of the Cretaceous limestone from drillholes, seismic measurements and multifrequency EM soundings; O – M = Oligocene – Miocene; $^{ma}E_2$ = Middle Eocene marl; $^{m}E_2$ = Middle Eocene limestone; $^{am}E_2$ = Middle Eocene argillaceous marl; bx = bauxite; $^{m}K_3$ = Upper Cretaceous limestone

4. ábra. A szondázások eredménye Csabpuszta környékén
1 — rétegellenállás és 2 — réteghatár a tranziens szondázások alapján; 3 — a felsőkréta mészkő (Ugodi Mészkő Formáció) felszíne fúrások, szeizmikus reflexiós és multifrekvenciás elektromágneses mérések alapján

Рис. 4. Результаты зондирования в окресности Чабпуста
1 — сопротивление слоя и 2 — граница между слоями по данным МПП, 3 — поверхность известняков верхнемелового возраста (угодская свита известняков) по данным бурений, МОВ и частотного электромагнитного зондирования

O–M = олигоцен–миоцен; $^{ma}E_2$ = среднеэоценовый мергель; $^{m}E_2$ = среднеэоценовый известняк; $^{am}E_2$ = среднеэоценовый аргиллитовый мергель; bx = боксит
$^{m}K_3$ = верхнемеловый известняк

Рис. 5. Результаты МПП на месторождении бокситов Баконьослоп
a) Кривые зондирования МПП и их приближение трехслойной (сплошная линия) и четырехслойной (пунктирная линия) моделями
b) Геологический разрез с результатами зондирований МПП
1 — трехслойным, 2 — четырехслойным приближением
c) Остаточные величины кривой затухания в зависимости от времени (порядкого номера канала)
d) Кажущееся удельное сопротивление в зависимости от времени (порядкого номера канала)

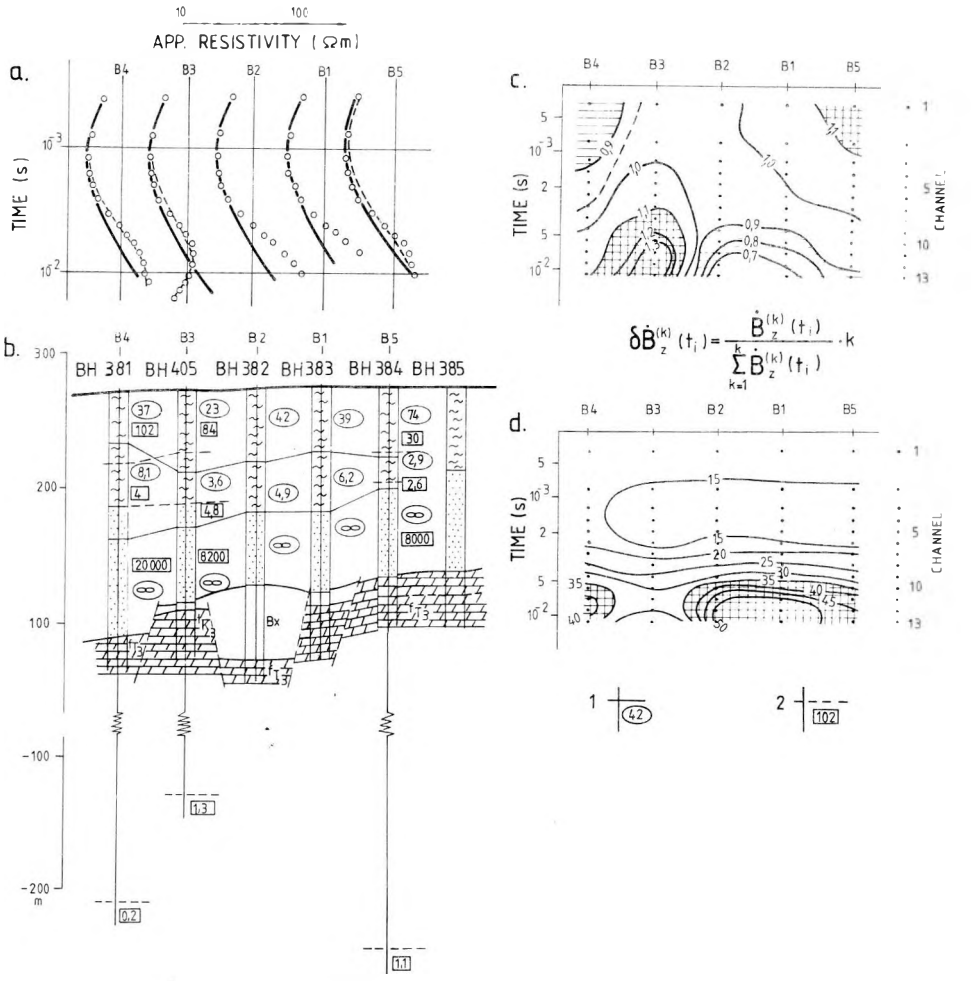

Fig. 5. Results of TDEM soundings from the Bakonyoszlop bauxite-prospecting area
a) TDEM sounding curves with 3-layer (solid line) and 4-layer (dashed line) model curves
b) Geologic section based on drillholes and electrical section interpreted from TDEM soundings
1 — result of 3-layer inversion; 2 — result of 4-layer inversion
c) Pseudosection of the residual decay curve as a function of the measurement time (channel number)
d) Pseudosection of the apparent resistivity as a function of the measurement time (channel number)

5. ábra. Tranziens eredmények, bakonyoszlopi bauxitelőfordulás
a) Tranziens szondázási görbék háromréteges (folytonos vonal) és négyréteges (szaggatott vonal) modellillesztéssel
b) Földtani szelvény a tranziens szondázások eredményeivel
1 — a háromréteges; 2 — a négyréteges közelítésből
c) Lecsengési görbe maradékértékei az idő (csatornaszám) függvényében
d) Látszólagos fajlagos ellenállás az idő (csatornaszám) függvényében

with the top of the Cretaceous sediments as found in the boreholes and by other geophysical measurements [KAKAS 1983]. The fifth layer appears to dip to the north in disconformity with the other layers. We might expect this layer to represent the Triassic carbonate basement but the interpreted depth for resistive basement at S–3 is too shallow according to the borehole. Nonetheless, resistive layers could be present in the Cretaceous section of this sequence.

Results of five soundings, made over a bauxite deposit in the Bakonyoszlop region are shown in *Figure 5*. The initial parts of all five soundings are very similar. The late time parts of soundings *B*1 and *B*2 rise too steeply to be fit with a layered earth model. Sounding *B*3 was fitted using a 4-layer model with a very conductive fourth layer and *B*4 and *B*5 were fitted approximately to a similar model. Since, with the possible exception of *B*3, the latter part of all of the soundings appears to be distorted, they were all fitted using 3-layer models and using only the first 6–8 points on the sounding curves. The results of this procedure are indicated by the solid lines and resistivity values shown on the cross section. The results obtained by fitting *B*3, *B*4, and *B*5 to 4-layer models are shown by dashed lines. Although the thicknesses and resistivities of the upper two layers are somewhat different for the two models, the conductances of the second layer are nearly the same suggesting that fitting only the first part of the sounding curves is a valid procedure. Values for the conductance of the second layer, as determined from the TDEM measurements, are a little higher than those obtained from interpretation of unpublished resistivity soundings made along the same profile. In a general way the 3 layers determined by TDEM measurements coincide with the lithology obtained from the borehole measurements. The conductive layers tend to correspond with sandstone and clay and the resistive layers with limestone and marl.

Data collected along a profile may be presented in a number of ways which emphasize qualitatively changes in the electrical section, such as those caused by faults or pinch-outs. To prepare the pseudosection shown in Figure 5/c, the difference between each decay curve and the average of all five curves were calculated, and the results were plotted and contoured with station position along the horizontal axis and time along the vertical axis. Since penetration depth increases with time, this pseudosection bears some resemblance to a true section. The principal anomaly coincides approximately with the known bauxite body. However, this simple procedure does not provide quantitative depth information and, with little doubt, the anomaly shown in Figure 5 is due to a conductive zone below the deposit rather than the bauxite deposit.

Similar pseudosections can be prepared by plotting and contouring apparent resistivity values as in Figure 5/d. In this pseudosection, a depression in the contours appears approximately beneath the bauxite deposit. Again let us emphasize that it is not the effect of the small bauxite deposit which is seen here, but rather a zone of low resistivity in the basement which has not been detected by other methods.

There is no independent evidence at this site to confirm the presence of a deep conductor as indicated by *B*3 or to suggest the cause of such a conductor.

Most likely, the conductive zone is a two- or three-dimensional feature rather than a layer and it may be displaced laterally from the profile. It is known from other localities in Hungary that fracture zones in dolomite, which are filled with water and sometimes clay, constitute conductors in the resistive basement. In fact, it has been suggested that structural depressions which may contain bauxite may sometimes be associated with such conductive zones in the basement.

The results for two soundings made near Bicske are shown in *Figure 6*. The soundings are very dissimilar, C–1 indicating the presence of 4 layers and C–2 indicating 3 layers. The conductances of the upper layer, as found from the two soundings, are quite similar and agree well with results of Slingram profiling.

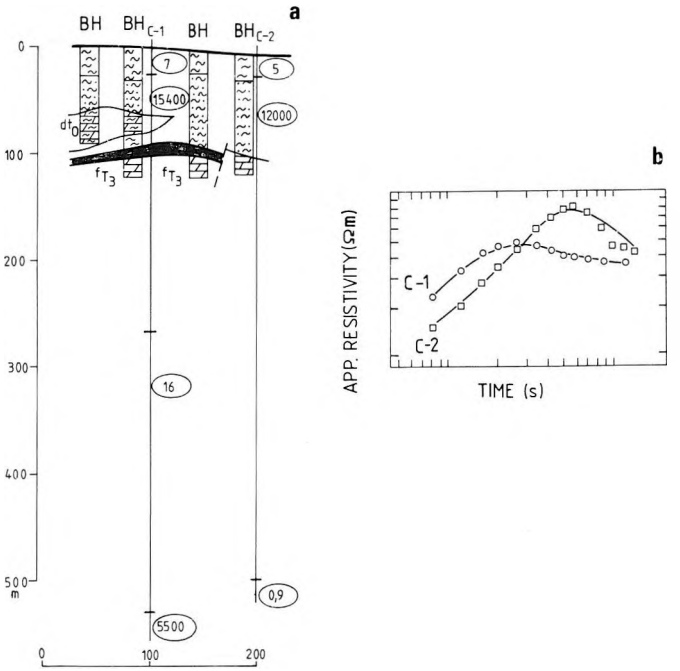

Fig. 6. Results of soundings from a locality near Bicske
a) Geological and electrical section
^{dt}O = Oligocene dolomite debris; $^{f}T_3$ = Upper Triassic Hauptdolomit
b) Sounding curves with the best-fit inversions

6. ábra. A szondázások eredményei Bicske környékén
a) Földtani–geoelektromos szelvény
b) Szondázási görbék a legjobban illeszkedő megoldásokkal

Рис. 6. Результаты зондирований в окресности Бичке
а) Геолого-геоэлектрический разрез
^{dt}O = доломитовые обломки олигоценового возраста; $^{f}T_3$ = верхнетриасовый основной доломит
b) Кривые зондирования и теоретические кривые, совместимые лучшим образом

The resistivities of the second layer are unrealistically high and are a result of fitting distorted curves. Other than the first layer, the models differ markedly from each other and do not correspond to known geologic features. Several attempts were made to fit the observed data with a model in which the upper layer was fixed to the depth to the Oligocene dolomite debris ($C-1$) or the depth to the Triassic basement ($C-2$); however satisfactory fits could not be obtained using these constraints. The resistivity for the deep conductor, as indicated by $C-2$, is unreasonably low. Likely, $C-2$ is badly distorted or contains some erroneous data points. However, the fact that $C-1$ indicates the presence of a conductive layer in the basement lends some support to the possibility of the existence of a conductor of unknown configuration in the basement.

The results given above indicate that the central-loop or single-loop TDEM methods can be used for sounding in the bauxite producing regions of western Hungary. However, the electrical sections there, which basically consist of conductive layers over a resistive basement, are not as easily resolved as in the opposite case when resistive rocks overlie conductive layers. Many of the sounding curves obtained are distorted; one of the primary causes is probably sharp lateral changes in the conductance of the conductive sediments. Previous experience with this method indicates that sounding curves taken near fairly pronounced lateral changes in resistivity can be fitted well to one-dimensional models even though the soundings are distorted [FRISCHKNECHT–RAAB 1984]. Thus, it is apparent that, lateral changes in resistivity in the localities studied in Hungary are very severe.

3. Fixed-source TDEM measurements

The central-loop and single-loop techniques are examples of moving-source methods in which the source is moved for each new station. Moving-source methods are very suitable for reconnaissance work where measurements are made at widely separated sites. They also have some advantages in that the geometrical relationship between source and receiver is constant. However, when a high density of stations along a profile is needed, the single- and central-loop techniques are very slow. Much higher rates of production can be achieved if the source loop is left in a fixed position for a series of measurements and the only receiver is moved for each new station. Besides being faster, fixed-source techniques offer an advantage over central- or single-loop techniques in that the horizontal component, as well as the vertical component of the field can be measured. While galvanic or "current gathering" effects are suppressed in the central or single loop techniques, they are enhanced at large source–receiver separations. The absence of galvanic effects simplifies interpretation but galvanic currents often identify the location of weak conductors that do not carry significant vortex currents due to direct induction. This phenomenon may be useful in bauxite exploration. Probably, the chief disad-

vantage of the fixed-source method for bauxite exploration is the changing geometry between source and receiver.

The USGS and ELGI have been working on interpretation techniques in anticipation of making TDEM soundings using the fixed-source method. ANDERSON [1984] has developed a very efficient computer program, using lagged convolution for computation of the horizontal and vertical frequency-domain fields inside and outside a large loop on a horizontally layered earth. A time-domain version of the same program is being evaluated. Following the general approach used by RAAB and FRISCHKNECHT [1983], Prácser has developed suitable expressions for calculation of apparent resistivity when a large loop is used. It appears that development of an inversion program for fixed-source soundings will not be a major task.

4. Development of other interpretation methods

Development of alternatives to interpretation by computer inversion is a major concern. In some areas, TDEM sounding curves can be interpreted easily but finding good fits to the data from the Csabpuszta, Bakonyoszlop and Bicske sites using four- and five-layer models required computation of many forward models for guidance, and many inversion runs using different starting parameters and constraints. The effort both in terms of personnel time and computer time was far too great to be practical in routine exploration. Furthermore, to achieve good results with the inversion technique used here, the sounding curves must not be seriously distorted by the presence of sharp lateral changes in the electrical section. Therefore, interpretative techniques which do not require large computer resources and which are stable and yield useful results when applied to distorted sounding curves are needed.

Pseudosections are useful in qualitative interpretation but they do not provide estimates of the depth to anomalous zones. A rapid means of making approximate depth estimates is needed for efficient conduct of field surveys as well as to provide final results when curve matching using one-dimensional models fails. What is needed is a simple and direct transform between time and depth; equivalent transforms exist for other methods such as magnetotellurics. The following two methods represent attempts to devise such transforms for time domain methods.

If a highly resistive half-space contains a thin, conductive layer, the transient response depends on an elementary algebraic expression [WAIT 1956]. For the case when the depth to that layer is of the order of the loop dimensions or greater WAIT's expression may be simplified to obtain a procedure for approximate inversion of sounding data. From the transient response we compute, at each time instant, the "apparent depth of investigation" and the total conductance of the section. The results of applying this procedure to a theoretical curve are plotted as a function of time *(Figure 7/a)*. In this diagram the effect of the conductive layer at 300 m is observed as a sharp feature at about 800 microsecs.

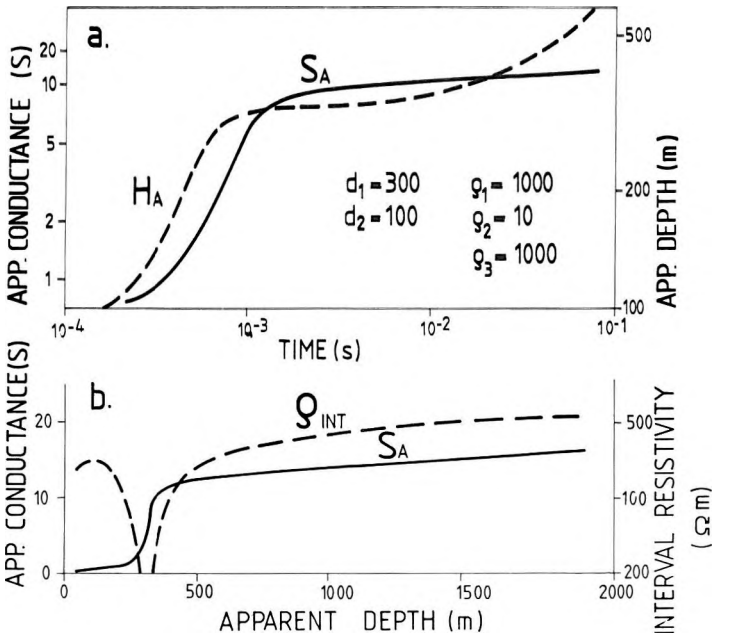

Fig. 7. Application of the TSH method for a theoretical model
a) Apparent conductance versus time and apparent depth versus time curves
b) Apparent conductance and interval resistivity versus apparent depth curves

7. ábra. A TSH kiértékelés vizsgálata elméleti görbéken
a) Látszólagos vezetőképesség–idő és látszólagos mélység–idő görbe
b) Látszólagos vezetőképesség- és intervallum-ellenállás–látszólagos mélység görbe

Рис. 7. Анализ интерпретации "TSH" на теоретических кривых
a) Кривые кажущейся проводимости–времени и кажущейся глубины–времени
b) Кривые кажущейся проводимости–кажущейся глубины и интервального сопротивления–кажущейся глубины

We can produce a more descriptive and clear display if we plot the total conductance as a function of the apparent depth *(Figure 7/b)*. From this plot the layers can be identified and the depths of the layer boundaries can be estimated. We have plotted also what we term the "interval-resistivity curve"; it is computed from differences in the apparent conductances and depth. This plot is also useful in preliminary interpretation. This method might be called the TSH method because we established a transformation between the time, T, and depth, H, using the conductance, S.

The second method is based on the velocity with which transient eddy currents move downward and outward from the transmitter loop in a homogeneous half-space [NABIGHIAN 1979]. The effective depth of the currents, or "smoke ring", is a function of time and half-space resistivity. For the central-loop configuration a short formula can be used to transform the apparent resistivity versus time function to apparent resistivity versus apparent depth

function. We can call this technique a TRH method because it is a transformation between the time, T, and depth, H, using the resistivity, R. We are testing this technique on theoretical and field results. In this simplest form it seems to work well for a conductive layer over an insulator, but not for the opposite case. Work is continuing to try to find a suitable modification which will make the technique more useful. The TSH and TRH methods require little computer time and can also be applied to distorted sounding curves, but improvements must be made before these techniques will be useful in routine work.

Efficient application of TDEM soundings in a large exploration program requires an integrated program of data acquisition and interpretation. A block diagram illustrating proposed relationships between data acquisition, rapid methods of interpretation, and interpretation based on curve fitting is shown in *Figure 8*.

5. Conclusions

Direct evidence of the bauxite deposits at two of the locations (Bakonyoszlop and Bicske) where transient field measurements were made cannot be discerned from the data. This is not surprising considering the size and resistivity of the deposits and the complexity of the electrical section of these sites. It appears that such deposits can be detected only indirectly by mapping their structural settings. The central-loop time-domain method can provide needed structural information in areas where lateral changes in resistivity are gradual, but sounding curves which are badly distorted by sharp lateral changes in resistivity cannot be fully interpreted using existing techniques. If the central-loop configuration is applied in areas similar to the sites at Csabpuszta and Bicske, we recommend using a station spacing of one-half or possibly one-quarter of the side of the loop to help cope with lateral variations. We also recommend making measurements at earlier times to define better the near-surface part of the electrical section. To increase productivity, we suggest use of large-loop TDEM techniques.

Existing inversion or curve fitting techniques using one-dimensional models are too slow and too sensitive to distortions in the data to be adequate for routine interpretation of data, such as would be acquired in bauxite exploration. Some success was achieved in developing more rapid and robust methods of interpretation but substantial improvements must be made before these methods will be useful in routine interpretation.

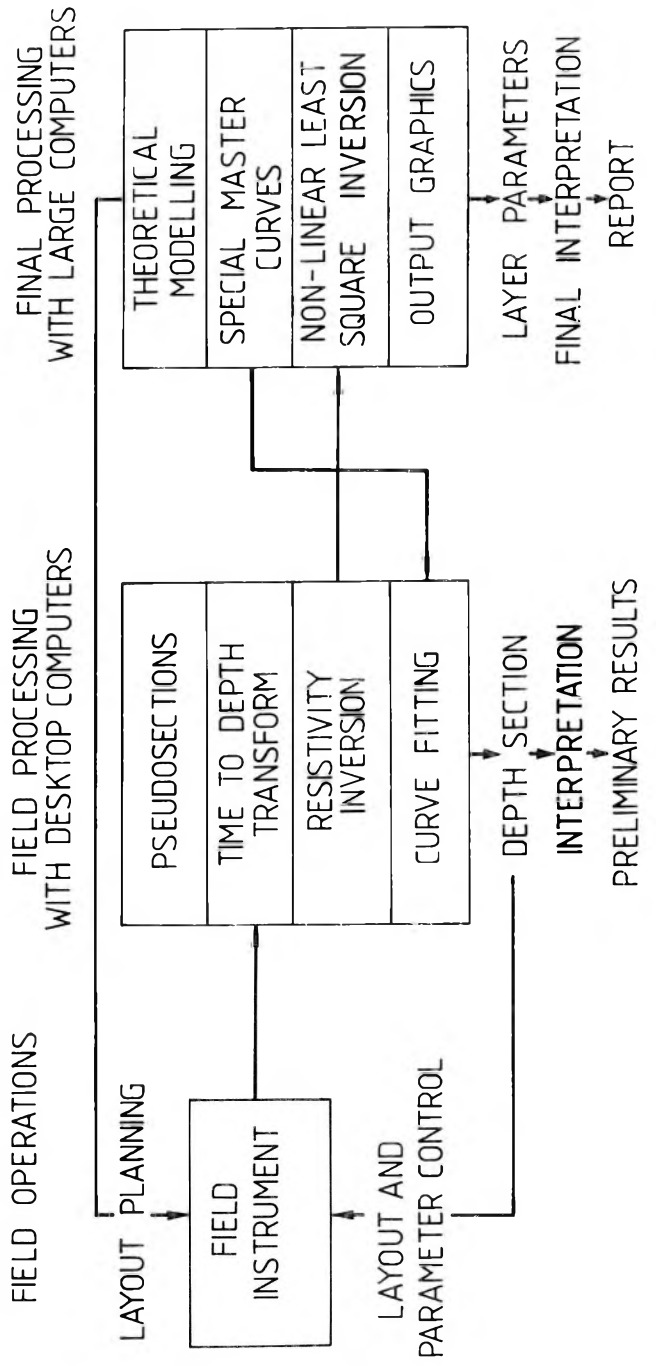

Fig. 8. Block diagram for acquisition and interpretation procedure of TDEM data

8. ábra. A tranziens mérések adatgyűjtési és kiértékelési rendszerének vázlata

Рис. 8. Блок схема системы сбора данных и интерпретации МПП

REFERENCES

ANDERSON W. L. 1982/a: Nonlinear least-squares inversion of transient soundings for a coincident loop system (Program NLSTCO). U.S. Geological Survey Open-file report 87–1064, 34 p.

ANDERSON W. L. 1982/b: Nonlinear least-squares inversion of transient soundings for a central induction loop system (Program NLSTCI). U.S. Geological Survey Open-file report 82–1129, 34 p.

ANDERSON W. L. 1984: Fast evaluation of H_r and H_z field soundings near a rectangular loop source on a layered earth (Program HRZRECT). U.S. Geological Survey Open-file report 82–1129, 34 p.

BÁRDOSSY GY. 1982: "Karst bauxites": Elsevier, 441 p.

BÁRDOSSY GY. 1984: European bauxite deposits: Proceedings of the 1984 Bauxite Symposium, Los Angeles, California, February 27 – March 1, 1984, Society Mining Engineers, pp. 412–435

BUSELLI G., O'NEILL B. 1977: SIROTEM: A new portable instrument for multichannel transient electromagnetic measurements. Australian Society of Exploration Geophysics, **8,** 3, pp. 82–87

FRISCHKNECHT F. C., RAAB P. V. 1984: Time-domain electromagnetic soundings at the Nevada Test Site, Nevada. Geophysics, **49,** 7, pp. 981–992

KAKAS K. 1983: Electromagnetic measurements for bauxite deposited on Upper Cretaceous carbonate rocks (in Hungarian). ELGI 1982. évi jel. (Annual Report) pp. 26–27

NABIGHIAN M. N. 1979: Quasi-static transient response of a conducting halfspace – An approximate representation. Geophysics, **44,** 10, pp. 1700–1705

RAAB P. V., FRISCHKNECHT F. C. 1983: Desktop computer processing of coincident and central loop time-domain electromagnetic data. U.S. Geological Survey Open-file report 83–240, 43 p.

WAIT J. R. 1956: Shielding of a transient electromagnetic dipole field by a conductive sheet. Canadian Journal of Geophysics, **34,** pp. 890–893

A TRANZIENS ELEKTROMÁGNESES SZONDÁZÁSOK KIÉRTÉKELÉSI MÓDSZEREINEK FEJLESZTÉSE ÉS A SZONDÁZÁSOK ALKALMAZÁSA A BAUXITKUTATÁSBAN

KAKAS Kristóf, Frank C. FRISCHKNECHT, UJSZÁSZI József, Walter L. ANDERSON és PRÁCSER Ernő

Az USGS és az ELGI együttműködésének keretében kísérleti tranziens szondázásokat végeztünk több bauxittároló szerkezet felett a Dunántúli-középhegységben. A szondázásokat egydimenziós Marquardt-inverzióval értékeltük ki. A kiértékelést megnehezítette, hogy a szondázások nagy része (főleg a fedőellenállás inhomogenitása miatt) torzult volt. Bár a bauxittelepeket közvetlenül nem lehetett kimutatni, az eredmények azt mutatják, hogy a tranziens szondázásokból kapott szerkezeti kép a bauxittestek indirekt detektálására alkalmas. Két bauxitelőforduláson a bauxittest alatt jólvezető mélyzóna volt kimutatható. Nagy területek hálózatos felmérésére akár a középponti vevőtekercses, akár az egyhurkos elrendezés alkalmazása lassú, ezért gazdaságtalan; erre a TURAM (nagykeretes) elrendezést tervezzük használni.

A számítógépes inverziós kiértékelésnek komoly hátránya egyrészt, hogy sok számítógépidőt igényel, másrészt, hogy torz görbék kiértékelésére nem alkalmas. Kvalitatív kiértékeléshez (anomális zónák kijelöléséhez) az adatokat pszeudoszelvények formájában, az idő függvényében ábrázolhatjuk. Az ellenállás–mélység függvény, vagy a határfelületek mélységének kvantitatív meghatározásához a TSH és a TRH eljárást kívánjuk alkalmazni. A TSH eljárás a nagyellenállású féltérben települő vékony vezető réteg feltételezésén alapul, és vezetőképesség–mélység függvényt eredményez. A TRH eljárás a szondázási görbe mélységtranszformációját végzi el, az örvényáramok maximumának mélység–idő összefüggése alapján.

РАЗВИТИЕ СПОСОБОВ ИНТЕРПРЕТАЦИИ ДАННЫХ ЭЛЕКТРОМАГНИТНЫХ ЗОНДИРОВАНИЙ ПО МЕТОДУ ПЕРЕХОДНЫХ ПРОЦЕССОВ И ПРИМЕНЕНИЕ ЗОНДИРОВАНИЙ ДЛЯ РАЗВЕДКИ БОКСИТОВ

Криштоф КАКАШ, Френк Ц. ФРИШКНЕХТ, Йожеф УЙСАСИ, Вальтер Л. АНДЕРСОН и Эрнё ПРАЧЕР

В рамках сотрудничества между Геологической службой США и ЭЛГИ были проведены экспериментальные зондирования по методу переходных процессов под некоторыми бокситоносными структурами в районе Задунайского среднегорья. Зондирования были обработаны одномерной инверсией Маркарта. Интерпретация данных была затруднена искажением большой части кривых (главным образом из-за неоднородности сопротивлений в покрове). Хотя нельзя было прямо выявить бокситовые залежи, результаты указывают на то, что полученная в результате зондирования по методу переходных процессов структурная картина позволяет выделять бокситовые тела косвенным путем. На двух месторождениях боксита в подошве бокситового тела была выделена хорошо проводящая глубинная зона.

Для съемки обширных районов по сети применение установок как со средней приемной катушкой, так и с одной петлой оказывается медленным, и поэтому неэкономичным способом; для такой цели предусматривается применине установки ТУРАМ (с большой рамой).

Серьезным недостатком инверсионной интерпретации на ЭВМ является высокая потребность в машинном времени, с одной стороны, и негодность ее для интерпретации искаженных кривых с другой. Для качественной интерпретации (выделения аномальных зон) данные могут изображаться в виде псевдо-разрезов в зависимости от времени. Для определений зависимости сопротивления от глубины, или для количественного определения глубины залегания разрезов в настоящее время разрабатываются способы TSH и TRH.

Способ TSH основан на предположении наличия тонкого проводящего слоя в высокоомном полупространстве и в результате дает функцию зависимости проводимости от глубины. Способ TRH выполняет преобразование кривой зондирования по глубине на основании зависимости глубины максимума вихревых токов от времени.

GEOPHYSICAL TRANSACTIONS 1985.
Vol. 31. No. 1-3. pp. 311-330

COMPARISON OF INTERPRETATION METHODS FOR TIME DOMAIN SPECTRAL INDUCED POLARIZATION DATA

László VERŐ*, Bruce D. SMITH**, Walter L. ANDERSON**
and József CSÖRGEI*

Two approaches to the interpretation of time-domain induced polarization (TDIP) are: the use of an exponentiai power series model and the use of generalized complex impedance (resistivity) or the Cole–Cole model. The exponential model is demonstrated to fit observed decay curves well and produces parameters describing changes in curve shape. Parametric changes can, in some cases, be correlated with changes in rock type or mineral texture, but they lack clear physical significance.

The Cole–Cole model can be used to fit decay curves with the same accuracy as the exponential model. Advantages in its use to interpret time-domain induced polarization are; 1. putting time- and frequency-domain measurements on a common basis, 2. the model can be related conceptually to certain polarization mechanisms, 3. it can predict the variation in decay curve shape caused by finite pulse times of different lengths, 4. the model provides a stable numerical approximation to electromagnetic coupling. In addition simultaneous inversion of decay curves with different short pulse times can be used to obtain information available from long pulse times.

Keywords: induced polarization, time domain, Cole–Cole model, interpretation, inversion

1. Introduction

Time domain (TD) and frequency domain (FD) measurement of induced polarization (IP) processes has had a long history of successful applications to metallic mineral exploration [SUMNER 1976]. More recently IP methods have been used in exploration for non-metallic minerals (hydrocarbons, coal), geothermal resources and increasingly for ground water resources [WASHBURNE 1982]. Expanded applications of the IP method to define more subtle anomalies, require advanced interpretation methods. To a certain extent this has been accomplished for FDIP [PELTON et al. 1978, 1983, 1984]. However, similar advances have not been made in TDIP. This paper briefly reviews some of the existing methods to interpret TDIP data, and introduces a new method of interpretation that bridges the gap between TD and FD induced polarization applications.

* Eötvös Loránd Geophysical Institute of Hungary, POB 35, Budapest, H-1440
** U.S. Geological Survey, Denver Federal Center, P.O.Box 25046, MS 964, Denver, Colorado 80225
Manuscript received: 14 January, 1985

2. Basic principles

A brief review of the IP method is warranted because of the geologic orientation of other papers in this volume. Excellent more technical summaries are given by SUMNER (1976), and WASHBURNE (1982). In field IP surveys, current is injected into the earth through current electrodes and a resulting voltage (V_P) is measured across potential electrodes (*Figure 1/a*). For TD surveys, the current is turned on for a length of time (termed pulse or on-time) then turned off (termed off-time). The transmitted waveform is then repeated with current flow in the opposite direction. The pair of positive and negative on-off waveforms constitutes a cycle. If the target in Figure 1/a is polarizable, then the voltage at the potential electrodes may have a form such as shown in *Figure 1/b*. The polarization of the target creates a transient decay voltage and corresponding charging response as observed in the received waveform. The cycle of transmitted pulses is repeated with successive measurements of the received waveform averaged until the desired signal-to-noise ratio is obtained (if possible).

In TD measurements the most commonly measured parameter is the chargeability m, which is defined as the ratio of the received voltage just after the turn-off (V_s, *Figure 1/c*) to the voltage (V_p) just before turn-off [SEIGEL 1959, DOLAN 1967, MCLAUGHLIN 1967]:

$$m = V_s/V_p. \tag{1}$$

However, because most transmitters are less than ideal and because there are electronic limitations in receivers, only the apparent value of m is measured:

$$m' = V'_s/V'_p. \tag{2}$$

This parameter neglects the shape of the decay curve, which contains information about the polarization process [WAIT 1959, BERTIN–LOEB 1976, ERKEL et al. 1979, and HALVERSON et al. 1979]. Clearly, the shape of the decay curve must be described by sampling the transient voltage at several time points along the decay curve. Previous work on the analysis of decay curves has demonstrated that variations in its shape can in some cases be attributed to differences in rock types [PELTON et al. 1978]. However, the approach to curve shape analysis and its interpretation is far from uniform or standard [WAIT 1959, KOMAROV et al. 1979, ERKEL et al. 1979, JOHNSON 1984].

In contrast, analysis of multifrequency IP data (analogous to measurements of many points along the TD decay waveform) has become much more standardized through the use of the Cole–Cole model of IP processes [PELTON et al. 1978, 1983, 1984]. We will discuss this model in a subsequent section. The applications of this method to TD data, or more specifically, spectral TDIP data, has been debated in several papers. For example, TOMBS [1981] suggests that IP instruments with short pulse times cannot be used to discriminate rock types by curve shape analysis. Recently, SOININEN [1984] has claimed that TD curve shape characteristics are not interpretable in terms of frequency domain

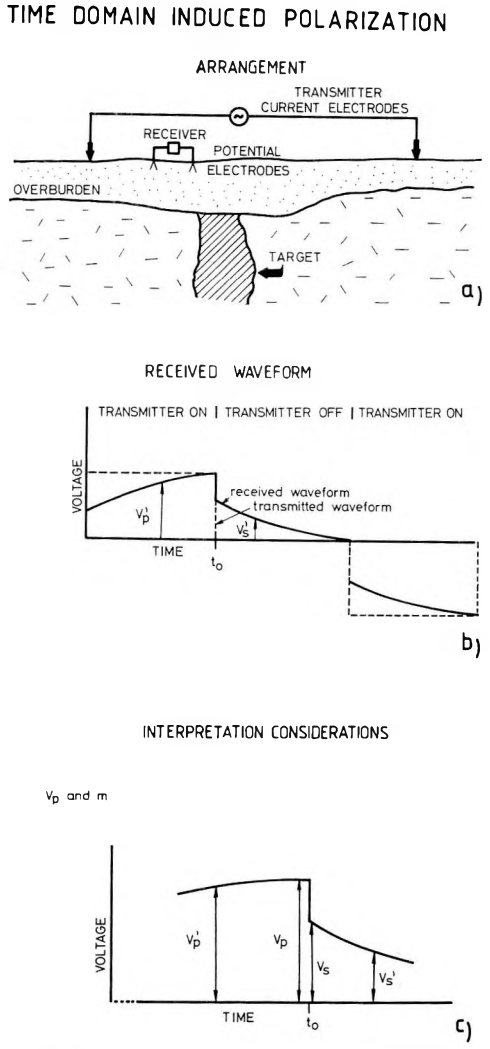

Fig. 1. Principles of time domain induced polarization: *a)* example of arrangement of transmitter (current) and receiver (voltage) electrodes, *b)* conceptual shape of the received waveform, *c)* measured voltages (V_P' and V_S') and theoretical values (V_P, V_S)

1. ábra. Az időtartománybeli gerjesztett polarizáció alapelvei: *a)* példa az adó (áram) és vevő (feszültség) elektródák elrendezésére, *b)* a mért jel elvi alakja, *c)* a mért feszültségek (V_P' és V_S') és az elméleti értékek (V_P, V_S)

Рис. 1. Основные принципы вызванной поляризации во временной области: *a)* пример расположения задающих (токовых) и приемных (потенциальных) электродов; *b)* принципиальная форма измеренного сигнала; *c)* измеренные напряжения (V_P' и V_S') и их теоретические значения (V_P и V_S)

models. However, JOHNSON [1984] has demonstrated compatibility between TD and FD curve shape analysis. The following discussion will hopefully lead to a unification of TD and FD intepretation.

A final interpretation issue concerns inversion, the process of determining parameters of a model from the measurement data. A basic consideration in the inversion of IP data is to define an appropriate model to describe the measurement data. Once the model is defined, then the inversion technique must be chosen. Two methods of data inversion are by curve matching using an album of forward model curves, or by using a computer to find model parameters that best fit the measurement data in a least-squares sense. Curve matching methods have been used or proposed by TOMBS [1981] and JAIN [1981]. We favor the least-squares computer inversion methods using a linearized form of the forward model. PELTON et al. [1983, 1984] have described in detail some of the fundamentals of this type of inversion method for FD data.

3. Exponential model

Derivation and application of the exponential model for the interpretation of time domain IP data has been described in detail by ERKEL et al. [1979] and CSÖRGEI et al. [1983]. The following discussion summarizes this work in order to demonstrate its application to TDIP data analysis.

The general form of the exponential equation is

$$V_t = W_o + \sum_{i=1}^{N} W_i e^{(-t/\tau_i)} \tag{3}$$

where

V_t = decay voltage at time t (volts)
t = time after turn off (milliseconds)
N = number of exponential terms
W_i = amplitude of ith term (volts)
τ_i = time constant of ith term (milliseconds)
W_o = constant value (volts)

Though this equation is not particularly justified by induced polarization theory, it may fit the observed decay waveform quite well. The amplitude terms can be directly related to the chargeability since they describe the instantaneous drop in voltage at the turn-off time ($t=0$ in Figure 1/b). This equation can be used to fit observed decay curves by the inversion methods mentioned previously. Experience with fitting several thousand decay curves has demonstrated that for normal decay curves the data can be easily fitted within a predicted observation error. Consequently equation (3) is an adequate mathematical (as opposed to physical) representation of the TDIP decay waveform.

One major consideration in the implementation of equation (3) is the number of components required to obtain a good data fit. *Figure 2* shows the effect of using 3, 4 and 6 components of the series to fit a TDIP decay waveform.

The computer program, written for a Hewlett Packard 9845® desktop computer, automatically increases the number of components, until the least-square error reaches either an asymptotic value or reaches the estimated data error. Generally at least four components or nine parameters are required.

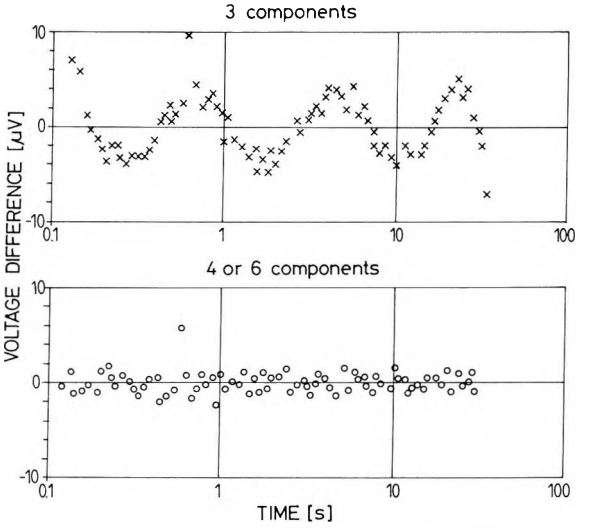

Fig. 2. Difference between observed and computed voltages using 3, 4 or 6 exponential components

2. ábra. A 3, illetve 4 vagy 6 exponenciális összetevő alapján számított és a mért feszültségek közti különbségek

Рис. 2. Расхождение измеренных и расчетных напряжений на основе 3-х, 4-х и 6-и экспоненциальных членов

Interpretation of resulting values of the time constants presents another problem since the mathematical model does not have any physical meaning in terms of induced polarization processes. To some extent the laboratory IP response of samples from a given geologic setting can be used to establish trends associated with certain types of mineralization, alteration, or mineralogy. *Figure 3* shows typical results from laboratory measurements of different types of sulfide-bearing rocks. This figure demonstrates that each type, depending on the nature of the sulfide distribution, is associated with a different set of amplitude values (W_i/W_1).

One limitation of the exponential model is that the distribution of amplitude values may change as a function of the pulse duration. The general trend of the distribution of W_i/W_1 is preserved for long pulse times (Figure 3/b). However, there are distinct differences at different pulse times even though the

® Use of trade names does not constitute endorsement either by the Eötvös Loránd Geophysical Institute, or the U.S. Geological Survey

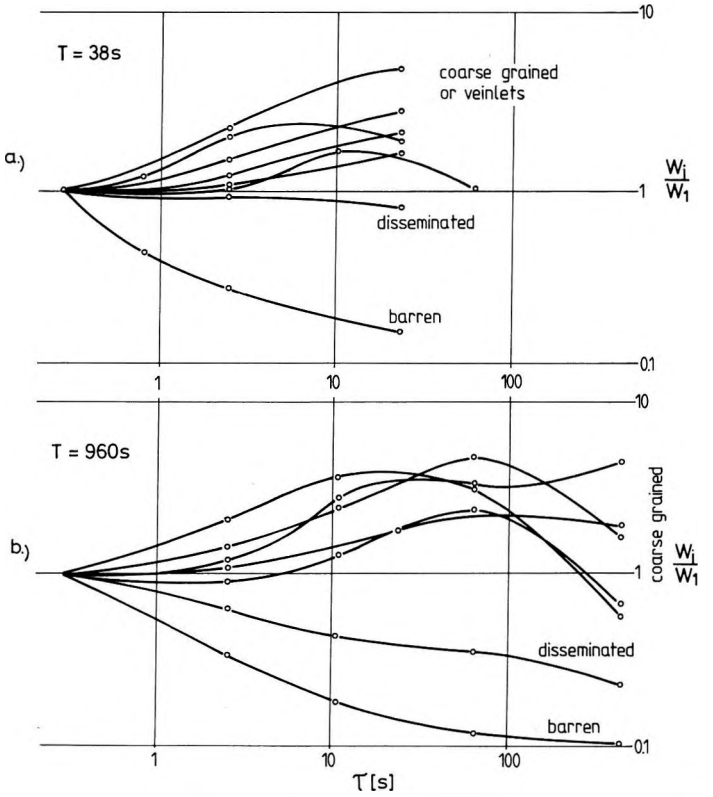

Fig. 3. Normalized amplitude (W_i/W_1) plotted as a function of time constant (τ_i) for different textures of sulfide-bearing rocks: *a)* charging time of 38 seconds, *b)* charging time of 960 seconds

3. ábra. A τ_i időállandó függvényében ábrázolt normált amplitúdó (W_i/W_1) különböző szulfid tartalmú kőzetekre *a)* a gerjesztési idő 38 másodperc, *b)* a gerjesztési idő 960 másodperc

Рис. 3. Зависимость нормированной амплитуды (W_i/W_1) от постоянной времени τ_i для горных пород с разными содержаниями сульфидов. Время возбуждения: *a)* 38 сек; *b)* 960 сек

physical polarization process presumably remains the same. This point will be discussed in the subsequent section on the interpretation of field measurements.

General conclusions from use of the exponential model are:

1. It can be used to fit adequately observed decay curves within the tolerance of measurement errors.

2. The inversion of the model is computationally efficient and can be implemented on a desktop computer system for routine interpretations.

3. The model cannot account for changes in the shape of the decay curve as a function of different pulse durations.

4. Changes in the decay waveform can be correlated with mineralization type, based upon laboratory sample measurements of different types of sulfide mineral distribution within the rock (massive, disseminated and barren).

4. Cole–Cole model

Development of the fundamental equation describing IP behavior in the FD using the Cole–Cole model is given by PELTON et al. [1978, 1983, 1984]. This model is an attempt to bridge the gap between electrochemical models with rather complex equations [e.g., WONG 1979, OLHOEFT 1982] and the more qualitative methods such as the previously described exponential series model. Polarization of a medium reflects its capability to store and release electrical energy. The mechanisms which create the polarization process are varied and complex. However, one easily understood mechanism is interface polarization, shown graphically in *Figure 4/a*. Current can pass directly through the media via the unblocked pore path. In the partially blocked pore path, the conductive (metallic) particle impedes the flow of current which creates a net electrical charge at the interface between the particle and electrolyte. When the current source is turned off, the net charge around the particle discharges. The charge and discharge is termed a polarization process.

The Cole–Cole model can be used in a qualitative way to describe this

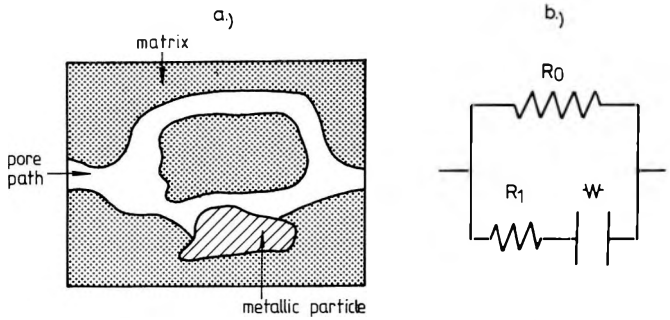

Fig. 4. Principles of Cole–Cole model applied to induced polarization: *a)* conceptual model of the induced polarization process, and *b)* an electrical circuit which describes the electrical behavior

4. ábra. A gerjesztett polarizációban alkalmazott Cole–Cole modell: *a)* a gerjesztett polarizációs folyamat elvi modellje, *b)* az elektromos viselkedést megadó helyettesítő áramkör

Рис. 4. Модель Кол–Кол, использованная в методе вызванной поляризации: *а)* принципиальная модель процесса вызванной поляризации; *b)* эквивалентная схема, описывающая электрическое поведение

polarization process. The electrical circuit shown in *Figure 4/b* is an analog to the schematic polarization process shown in Figure 4/a. Resistance of the open pore path is given by the resistance R_0 while the blocked pore path is represented by a series combination of a resistor and a complex impedance element (like a capacitor) termed the Warburg impedance. The Cole–Cole model expresses the variation in complex resistivity or impedance as a function of frequency:

$$Z(\omega) = R_0 \left\{ 1 - m \left[1 - \frac{1}{1 + (i\omega\tau)^c} \right] \right\}. \tag{4}$$

Each of the parameters of the model, above, can be expressed in terms of the electrical circuit as shown in Figure 4/b and are defined as follows

R_0 = dc resistivity (Ωm)
m = chargeability (volts per volt)
τ = the time constant (seconds)
c = frequency dependence (dimensionless)
ω = angular frequency (radians per second)
i = $\sqrt{-1}$

The time constant given in the Cole–Cole model is not the same as time constants in the exponential model (equation 3). When $m = 1.0$, the Cole–Cole model becomes approximately an exponential with time constant τ, but there is no strict mathematical relation between the two models. What is important here, to recognize that the Cole–Cole model can be related to a physical polarization mechanism, such as shown in Figure 4/a. Other polarization mechanisms, that can be related to the Cole–Cole model, include double layer interface polarization [KLEIN et al. 1984], packing of conductive spheres with a resistive coating [WAIT 1959], and some electrochemical processes [WONG 1979].

The electrical nature of the earth or even a rock sample is clearly more complex than a simple electrical circuit (Figure 4). A much more realistic model is a collection or distribution of electrical circuits. Both theory and controlled experimentation *(Figure 5/a)* have shown that the grain size of polarizable particles can be directly related to the time constant (τ in equation 4). This observation leads to a basis on which rock types can be discriminated through use of the Cole–Cole model. A classical example is discrimination of graphites and sulfides which have different effective grain sizes leading to markedly different time constants *(Figure 5/b)* [PELTON et al. 1978, SMITH et al. 1983]. Another example is discrimination of economic and non-economic sulfides in some porphyry copper deposits because of a difference in the texture of the sulfide minerals [OSTRANDER–ZONGE 1978].

The Cole–Cole model has been used to interpret many different types of FDIP data. From the previous discussion advantages of using the Cole–Cole model are:

1) It can be related to certain polarization mechanisms.

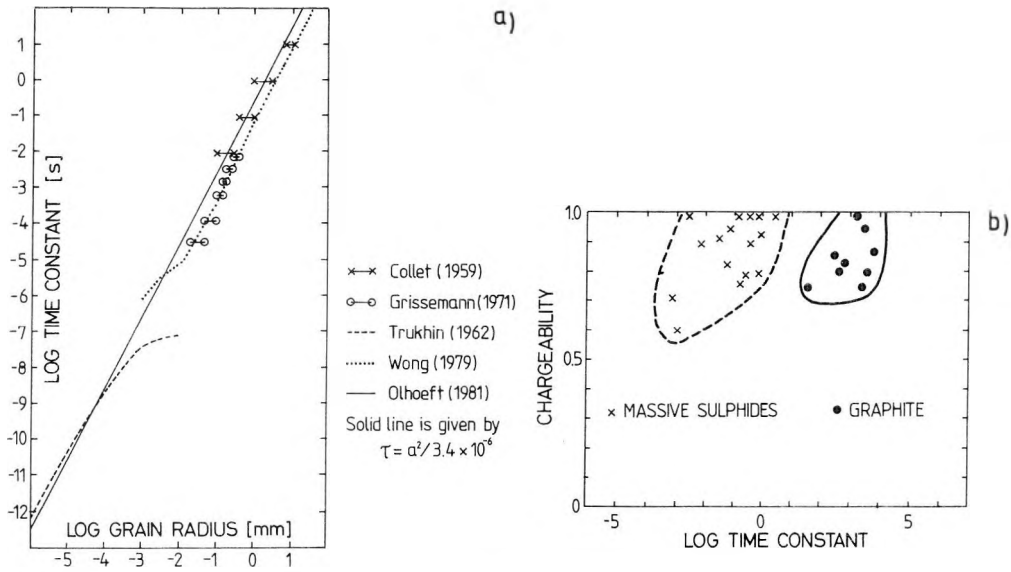

Fig. 5. Time constant variations: *a)* versus grain size, and *b)* versus chargeability for graphites and massive sulfides

5. ábra. Az időállandó kapcsolata *a)* a szemcseméretel, és *b)* a gerjeszthetőséggel, grafit és massziv szulfidok esetében

Рис. 5. Связь постоянной времени *a)* с диаметром зерен и *b)* с возбуждаемостью для графитов и массивных сульфидов

2) Variations of the model parameters can be related to textural variations leading to possible rock type discrimination.

3) The model has a minimum number of parameters to describe most FDIP data, and

4) The variations in pulse shape for different pulse times can be predicted.

A closed form of equation (4) does not exist for the time domain. This has lead to some problems in adapting its use to TDIP investigations. In solving the forward problem we wanted to duplicate as closely as possible the actual waveform used in field measurements. The particular method presented here is described in detail by ANDERSON and SMITH [1984] and only summarized below. The step function response (e.g. infinitely long pulse time) is computed using a convolution approach described by GUPTASARMA [1982]. Under certain circumstances the convolution method does not provide numerically accurate answers. In this case (automatically detected by the program) an integral equation [LEE 1981] is numerically solved to yield greater accuracy. Numerical solution of the integral equation, though, is too slow for routine use.

Having found the solution of equation (4) in time domain for an infinitely long pulse (step function) the next step is to compute the response for a series of finite positive and negative pulses (Figure 1/b). The response is computed by summation of the step function response over appropriate time intervals deter-

mined by selected positive and negative on-off times [WAIT 1982]. The resulting program can be used to compute voltages at specified times on the decay waveform for any on-time *(TP1)*, off-time *(TP2)* or number of cycles *(NP)*. Summation over a number of cycles is analogous to the stacking procedure in field measurements.

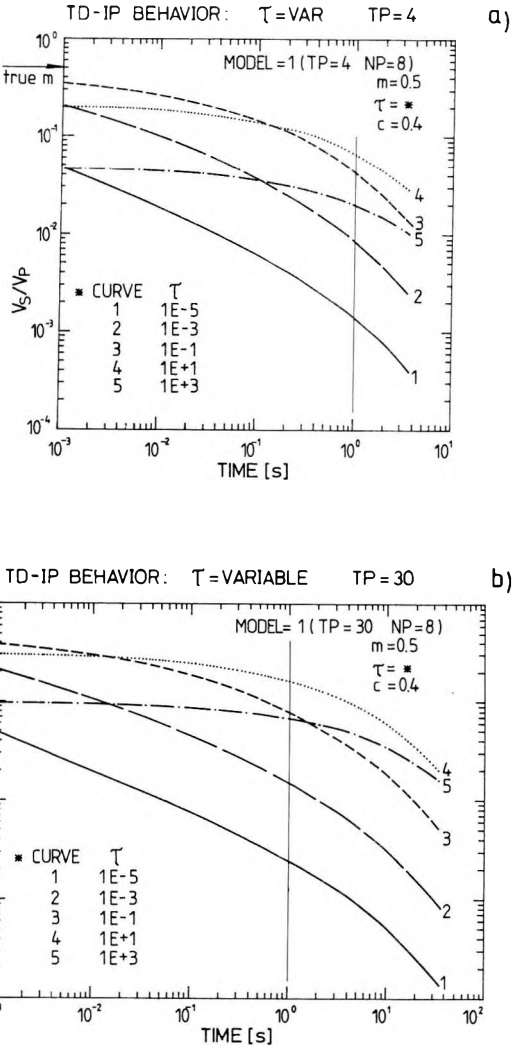

Fig. 6. Forward Cole–Cole model solutions for variable time constants: *a)* 4 second pulse time, *b)* 30 second pulse time

6. ábra. A Cole–Cole modell alapján, különböző időállandókra számolt lecsengési görbék: *a)* a gerjesztési idő 4 másodperc, *b)* a gerjesztési idő 30 másodperc

Рис. 6. Кривые затухания, рассчитанные на основе модели Кол–Кол для разных постоянных времени. Длительность возбуждения: *a)* 4 сек; *b)* 30 сек

One of the applications of the forward problem is to examine characteristics of the TDIP response as determined by the Cole–Cole model. *Figure 6* illustrates a set of curves generated for two different pulse times with the time constant variable. The other parameters of the model have been held to constant values ($R_0 = 1$, $m = .5$ and $c = .4$). A few interesting observations can be made from these curves.

The theoretical value of m, the chargeability, for all of the curves is .5. This represents the value of voltage at the instant of voltage turn-off. In practice the finite pulse m is measured at some time after turn-off which is seldom less than 1 millisecond, the earliest time in Figure 6. Even though more than eight decades of values for the time constant have been used the estimated value of m at 1 millisecond will always be less than the true value, for both long and short time constant polarization processes. In the case of short time constants, most of the decay occurs before measurements begin, leading to an underestimate of m. The measured values of the long time constant curves for 4 and 30 s pulses show that the longer pulse time yields an asymptotic voltage value that is closer to the true value of m, but is still a considerable underestimate. The case where the time constant is longer than the pulse time (curves 4 and 5 in Figure 6/a and curve 5 in Figure 6/b) presents a different problem in estimating the true chargeability. The voltage value for this curve at 1 millisecond is an asymptotic value which is practically the same as would be observed at the shut-off time. However, the observed value of m will never be the same as the theoretical value because of the difference in the IP process time constant and the pulse duration. Only in the limiting case of an infinitely long pulse would the true value of m be observed.

This discrepancy between the true and observed value of m for long time constant processes is the reason that Tombs [1981] concluded that only long charging times could be used to discriminate between long and short time constant IP processes. However, a complete analysis of curve shapes, partially indicated in Figure 6, can provide the missing information. This point is discussed in more detail in the following section, but obviously use of the Cole–Cole model in inversion of field TDIP allows the true value of m to be estimated.

Effects of varying the other Cole–Cole model parameters can be studied in a similar way as was done for the time constant given above. The general conclusion from the above discussion is that the forward problem computations are an effective way to evaluate the behavior of time domain induced polarization.

5. Applications

In the following discussion we compare applications of the exponential model (equation 1) and the Cole–Cole model (equation 4) to interpretation of spectral time-domain IP data. An example of data from a well-digitized decay wave form is shown in *Figure 7*. The computed curve (solid line in Figure 7) is the same for both the Cole–Cole (C–C) and the exponential model parameters

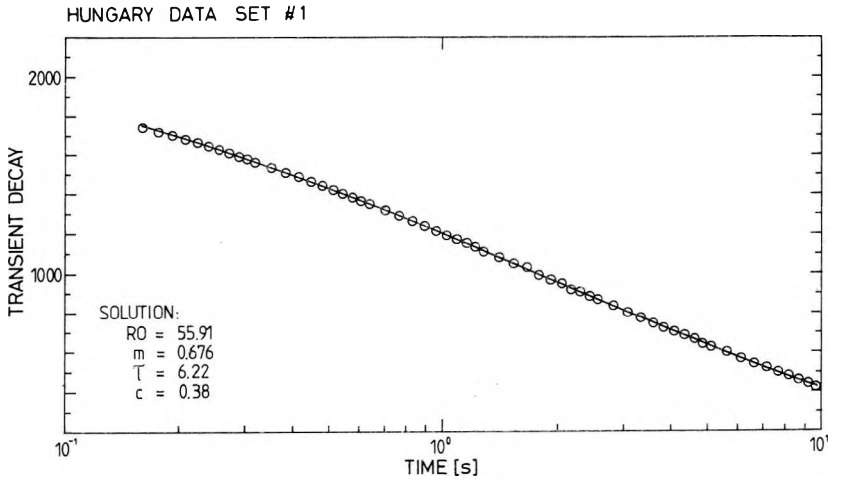

Fig. 7. Decay curve showing observed values (circles) and computed least-squares fit (solid line) using Cole–Cole model

7. ábra. Mért lecsengési görbe (körök) és a hozzá a legkisebb négyzetek elve alapján illesztett Cole–Cole modell (folytonos vonal)

Рис. 7. Измеренная кривая затухания (кружки) и модель Кол–Кол, согласованная по принципу наименьших квадратов (сплошная линия)

given in *Table I.* Seven parameters were required for the exponential model whereas only four are needed for the C–C model. In general we have found that the C–C model is a simpler parameterization of most decay curves because less parameters are required for a good fit to the data.

As discussed previously there is no simple relationship between parameters of the two models. However, we have found empirically that, generally the *average* time constant of the exponential model is most closely related to the C–C model time constant for decay curves free of problems discussed below.

Exponential	
Amplitudes (μV)	Time constants (s)
W_0 48	
W_1 840	τ_1 11.9
W_2 648	τ_2 1.64
W_3 456	τ_3 0.31
$m' = 0.165$	Average $\tau = 4.6$
Cole–Cole	
R_0 55.9 Ωm	τ 6.2 s
m 0.676	c 0.38

Table I. Comparison of exponential and Cole–Cole parameters

I. táblázat. Az exponenciális és Cole–Cole paraméterek összehasonlítása

Табл. I. Сравнение параметров экспоненциальной модели и модели Кол–Кол

Consequently, presentation of interpretations using the exponential model might best use the average time constant value as indicated in Table I.

Three types of problems can be encountered in interpretation:

1) Discrepancies between the true and observed value of chargeability,

2) Effects of electromagnetic coupling, and

3) Determination of model parameters for long time constant decays using short or finite pulses.

The problem of discrepancies between observed and true values of chargeability, illustrated schematically in Figure 1/c, has been discussed previously. The second problem is illustrated in *Figure 8*.

As shown in Table I the value of chargeability (m') estimated from the exponential model is about a factor of four smaller than the true value (m) predicted by the C–C model. The forward problem solutions shown in Figure 6/b demonstrate why there is a discrepancy between values of m' and m. The charging time for field measurements shown in Figure 7 is 32 seconds and the C–C model parameters are intermediate between curves 3 and 4 of Figure 6/b. Considering that the first voltage sampling time for this example is 160

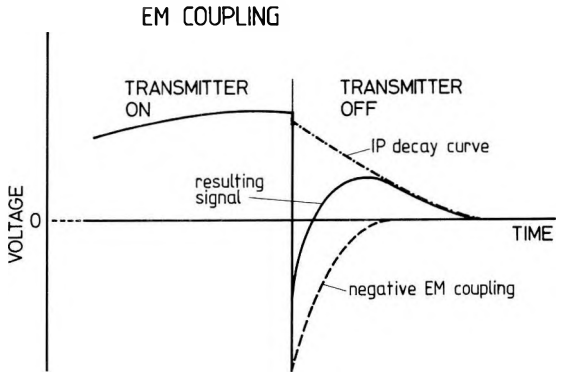

Fig. 8. Electromagnetic coupling can produce strong negative response near beginning of decay

8. ábra. Az elektromágneses csatolás nagy negatív feszültségeket okozhat a lecsengés kezdeti szakaszában

Рис. 8. В начальной стадии затухания электромагнитная связь может вызвать большие отрицательные напряжения.

milliseconds (.160 seconds), the general difference between m' and m is compatible with the forward solutions.

The problem of electromagnetic (EM) coupling (Figure 8) is a complicated question that has been widely debated [e.g. PELTON et al. 1978, and WYNN–ZONGE 1975]. Without going into details, EM coupling is caused by electromagnetic wave propagation produced when either initiating or terminating galvanic current flow into the ground. The switching of galvanic currents in turn causes inductive currents to flow within confined conductors. In addition, some EM

coupling is due to currents induced between the wires connecting the transmitter and receiver electrodes (Figure 1/a). Cases where the EM coupling acts to oppose the polarization process is termed negative EM coupling. This negative EM coupling is schematically shown in Figure 8 where the transient decay curve has a negative component, causing its amplitude to increase and then decrease as a function of time. The general effect of EM coupling is to obscure the polarization process. Hence, a major interpretational problem is to identify the EM and IP components in order to separate them.

The exponential model has been applied to the data shown in *Figure 9* which have a strong negative coupling component. As described by CSÖRGEI et al. [1983], inversion of data with negative EM coupling is numerically very unstable using the exponential model. In the case of these data, the time constant of the first term had to be held to a fixed value in order to obtain realistic model parameters. The exponential model parameters *(Table II)*, consist of two exponential terms. The first term can be interpreted to be associated with the negative coupling (note negative amplitude) and the second term with the IP effect. However, data interpretation along the complete profile demonstrates that the second exponential term is also influenced by EM coupling [CSÖRGEI et al. 1983]. Thus the exponential model does not lead to a clear separation of EM and IP effects.

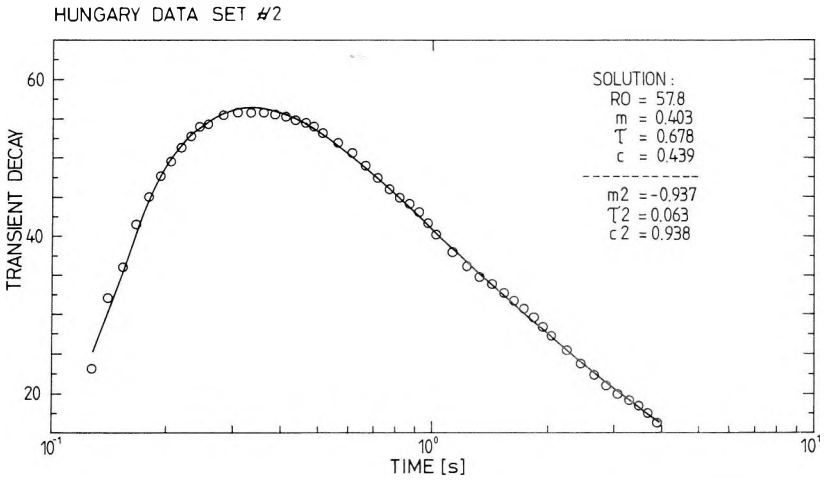

Fig. 9. Decay curve with negative electromagnetic coupling at beginning of decay (observations are circles and least-squares theoretical solution is solid line)

9. ábra. Lecsengési görbe negatív elektromágneses csatolással a lecsengés kezdeti szakaszában (a mért értékeket a körök jelentik, a legkisebb négyzeteken alapuló elméleti megoldás a folytonos vonal)

Рис. 9. Кривая затухания с отрицательной электромагнитной связью в начальной стадии затухания (кружки — измеренные значения; сплошная линия — теоретическое решение на основе наименьших квадратов)

Exponential			
Amplitudes (μV)			Time constants (s)
W_0	29		
W_1	−294	EM	τ_1 0.06
W_2	56	IP	τ_2 1.43
$m' = -0.18$			$m'_2 = 0.035$
		Cole–Cole	
EM m_1	−0.94	IP	m_2 0.403
τ_1	0.063		τ_2 0.068
c_1	0.94		c_2 0.439

Table II. Comparison of exponential and Cole–Cole parameters for decay curves with EM coupling

II. táblázat. Az exponenciális és Cole–Cole paraméterek összehasonlítása EM csatolást is tartalmazó lecsengési görbére

Табл. II. Сравнение параметров экспоненциальной модели и модели Кол–Кол для кривой затухания, включающая в себя и ЭМ связь

The C–C model parameters, given in Table II, show that two models, i.e. sum of two terms (equation 4), must be used. As discussed by PELTON et al. [1978], the EM coupling effects can be represented by the C–C model. However, there is only an empirical basis for its application in this case. In practice, the C–C model was found to be numerically much more stable than use of the exponential model in data inversion. The component with negative chargeability (Table II) is the presumed negative coupling. Analysis of other examples along the same profile as examined by CSÖRGEI et al. [1983] generally indicates that the spatial variation of the presumed IP parameters is less influenced by the strong EM coupling than the corresponding variation using the exponential model.

Comparison of parameters determined for each type of model (Table II) demonstrates the following. The C–C model parameters for the EM coupling are typical of values observed in frequency-domain measurements. Interestingly, the exponential and the C–C model yield the same general value of the time constant for EM coupling. This is due to the fact that the m_2 and c_2 parameters yield very nearly an exponential decay waveform when they have near-unity values (PELTON et al. 1983, 1984). However, there is not as good an agreement between the two IP time constants, because the intermediate value of m does not approximate an exponential decay. Addition of another exponential term might improve agreement between averaged τ values, as in the case of the first data set analysis. Again there is a difference between the predicted m values (voltage at time = 0).

Conclusions from the brief analysis of negative EM coupling are:

1) The C–C model yields numerically more stable and realistic results for strong EM coupling problems,

2) Time constants for both models are similar for the EM coupling,

3) The C–C model provides better estimate of the IP process in the presence of EM coupling, and

4) Neither model has a theoretical basis for approximating EM coupling.

The final interpretational problem to be discussed is the interpretation of long time constant IP processes with short pulse times. This problem was discussed previously in terms of forward model computations, where it was shown that the exponential model cannot predict variations in decay curve shapes due to different pulse times.

When short pulse times are used with long time constant processes, the interpreted time constant is always much shorter than the true time constant. The traditional solution to this problem has been to use long pulse times (HALVERSON et al. 1979). However, a new alternate approach is possible through use of the Cole–Cole model.

The variation in decay curve shape for an IP process with a 1,000 second time constant is shown in *Figure 10* for different pulse times. Differences in curve shapes as a function of different pulse times indicate that a long time constant polarization process is present. If the time constant is much shorter than the pulse time, then there would be no difference in the curve shape for different pulse times.

An alternate method to using a long pulse time, proposed here, is to use two or more short pulse times. Differences in the resulting decay curve shape can be interpreted with the C–C model by simultaneous inversion of the different decay curve shapes. This interpretational method has obvious practical advantages. For the example, shown in Figure 10, a pulse length of 600 seconds

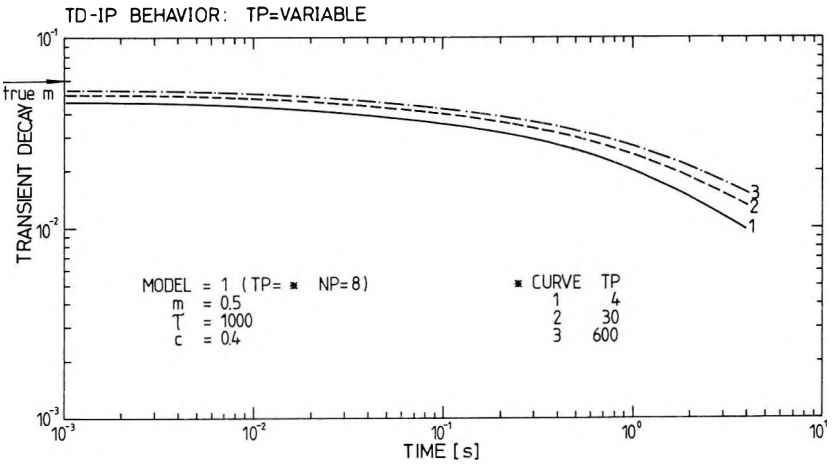

Fig. 10. Forward model results for a Cole–Cole model having a long time constant for different pulse times (*TP*)

10. ábra. Hosszú időállandójú Cole–Cole modellre vonatkozó elméleti lecsengési görbék különböző gerjesztési idők (*TP*) esetén

Рис. 10. Теоретические кривые затухания для модели Кол–Кол с большой постоянной времени в случае разных времен возбуждения (*TP*)

is needed to determine accurately the 1,000 second time constant. For one complete cycle of positive and negative pulses 40 minutes would be required. Of course, even more time would be needed for signal stacking of repeated cycles.

A practical application of this interpretation method is shown by data in *Figure 11*. The example is taken from TDIP measurements made over a zone of carbonaceous rocks which have a long time constant based on laboratory and field FDIP measurements. TDIP measurements were made with both two- and four-second pulses, which had one set of common time points along the decay curve. Interpretation of the data from a single pulse yielded an estimated time constant of the order of 20 seconds. This is markedly shorter than the minimum time constant of 500 seconds determined by an FDIP measurement using the same electrodes. The data shown in Figure 11 are somewhat noisy but the difference in waveforms clearly indicates that a long time constant process is present. A simultaneous inversion of both sets of data yields a time constant of 900 seconds. This is much more compatible with FDIP results. Thus, use of two short time pulses in simultaneous inversion can provide information equivalent to a single long pulse.

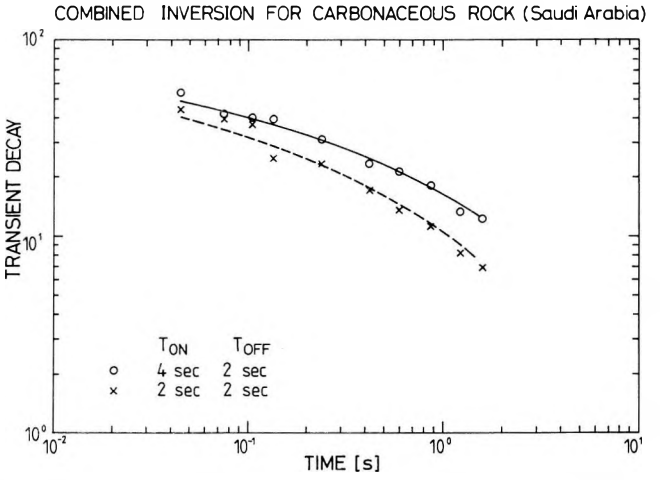

Fig. 11. Simultaneous inversion of time-domain induced polarization measurements (circles and x's) over a carbonaceous rock unit with a long time constant

11. ábra. Hosszú időállandóval jellemezhető szén tartalmú kőzeteken végzett időtartománybeli gerjesztett polarizációs mérések (körök és x-ek) egyidejű inverziója

Рис. 11. Одновременная инверсия измерений вызванной поляризации во временной области с разными временами возбуждения (кружки и х-ы) над углистыми горными породами, характеризующимися большим постоянным времени

6. Conclusions

The application of the Cole–Cole (C–C) model in a generalized inversion of time-domain IP data is a new approach to interpretation. This model has certain advantages and disadvantages over the use of an exponential series model. A major advantage of using the C–C model is that time- and frequency-domain interpretations can be put on a common basis. The exponential model is a purely mathematical representation in contrast to the C–C model, which is, at least conceptually, based upon certain polarization mechanisms. The computations for a completely generalized time domain C–C model, however, are at least an order of magnitude more complex (slower) than for the exponential model.

Both C–C and exponential models can be used to characterize TDIP decay curves to an arbitrary degree of accuracy. The parameters of either model can be correlated with variations in decay curve shape that, in some cases, indicate specific rock types or mineral textures. However, exponential model parameters cannot be related easily to existing studies done in the frequency domain. In addition, different exponential parameters are required to fit curves measured with different pulse times. The C–C model application does not have either limitation.

Electromagnetic coupling effects can be approximated numerically by either model. Neither model is related by theory to EM coupling. The Cole–Cole model does offer numerically stable solutions that have a clear separation of EM and IP effects in many cases.

Simultaneous inversion of different short pulse time decay curves with the Cole–Cole model allows long time constant IP processes to be identified. This application is not possible with the exponential model.

Acknowledgments

The research described in this report was made possible by the efforts of Paul Teleki (U.S. Geological Survey), Oszkár Ádám (Central Office of Geology, Hungary) and Pál Müller (Eötvös Loránd Geophysical Institute of Hungary). The late András Erkel (ELGI) gave many practical insights to development and application of time domain IP measurements which have been critical to the success of the cooperative program.

REFERENCES

Anderson W. L., Smith B. D. 1984: Nonlinear least-squares inversion of transient induced polarization data (Program NLSTIP). USGS Open-File Report 82–86, 65 p.

Bertin J., Loeb J. 1976: Experimental and theoretical aspects of induced polarization. Geoexploration Monograph Series 1, No. 7, Berlin, Gebrüder Borntraeger, **1**, 250 p.

Csörgei J., Erkel A., Verő L. 1983: Time domain IP equipment and method for source discrimination. Geophysical Transactions, **29,** 4, pp. 345–361

Dolan W. M. 1967: Considerations concerning measurement standards and design of pulsed IP equipment, Part 1. in Proceedings of the symposium on induced electrical polarization, Berkeley, University of California, pp. 2–16

Erkel A., Simon P., Verő L. 1979: Measurement and interpretation of the dynamic characteristics of induced polarization decay curves. Geophysical Transactions, **25,** pp. 61–72

Grissemann C. 1971: Examination of the frequency dependent conductivity of ore-containing rock on artificial models. Scientific Report No. 2, Electronics Laboratory, Univ. of Innsbruck, Austria, 12 p.

Guptasarma D. 1982: Computation of the time-domain response of a polarizable ground. Geophysics, **47,** 11, pp. 1574–1576

Halverson M. O., Zinn W. A., McAlister E. O., Ellis R., Yates W. C. 1979: Some results of a series of geologically controlled field tests of broadband spectral induced polarization. Paper presented at the 49th Annual International SEG Meeting, Nov. 4–8, New Orleans, 51 p. [abs: Geophysics, 1980, **45,** 4, p. 579]

Jain S. C. 1981: Master curves for derivation of Cole–Cole parameters from multichannel time domain data. Report No. IND/74/012–20, NARJ Hyderabad, India

Johnson J. M. 1984: Spectral IP parameters as determined through time domain measurements. Geophysics **49,** 11, pp. 1979–1992

Klein J. D., Biegler T., Horne M. D. 1984: Mineral interfacial processes in the method of induced polarization. Geophysics, **49,** 7, pp. 1105–1114

Komarov V. A., Mikhailov G. N., Khloponina L. S., Ioffe L. M., Smirnov A. A. 1979: Methodological guide for geoelectric system SVP74. (in Russian), Lenuprizdat, Leningrad, pp. 32–33

Lee T. 1981: Short Note—The Cole–Cole model in time domain induced polarization. Geophysics, **46,** 6, pp. 932–933

McLaughlin G. H. 1967: Considerations concerning measurement standards and desing of pulsed IP equipment: induced polarization receiver. Part 2. in Proceedings of the symposium on induced electrical polarization, Berkeley, University of California, pp. 17–31

Olhoeft G. R. 1982: Electrical properties of rocks and minerals. Short course notes, Golden, Colorado, 150 p.

Ostrander A. G., Zonge K. L. 1978: Complex resistivity measurements of sulfide-bearing synthetic rocks. Presented at the 48th Annual International SEG Meeting, San Francisco, Nov. 1, 37 p. [abs: Geophysics, 1979, **44,** 3, p. 409]

Pelton W. H., Ward S. H., Hallof P. G., Sill W. R., Nelson P. H. 1978: Mineral discrimination and removal of inductive coupling with multifrequency IP. Geophysics, **34,** 3, pp. 588–609

Pelton W. H., Sill W. R., Smith B. D. 1983: Interpretation of complex resistivity and dielectric data, Part I. Geophysical Transactions, **29,** 4, pp. 297–330

Pelton W. H., Sill W. R., Smith B. D. 1984: Interpretation of complex resistivity and dielectric data, Part II. Geophysical Transactions, **30,** 1, pp. 11–45

Seigel H. O. 1959: Mathematical formulation of type curves for IP. Geophysics, **24,** 3, pp. 547–565

Smith B. D., Tippens C. L., Flanigan V. J., Sadek H. 1983: Preliminary results of spectral induced polarization measurements, Wadi Bidah District, Kingdom of Saudi Arabia, Open-File Report USGS-OF-03-70, 23 p.

Soininen H. 1984: Short Note—Inapplicability of pulse train time-domain measurements to spectral induced polarization. Geophysics, **49,** 6, pp. 826–827

Sumner J. S. 1976: Principles of induced polarization for geophysical exploration. Amsterdam, Elsevier, 277 p.

Tombs J. M. C. 1981: The feasibility of making spectral IP measurements in the time domain. Geoexploration, **19,** pp. 91–102

Wait J. R. 1959: A phenomenological theory of overvoltage for metallic particles, in J. R. Wait, ed., New York, Pergamon, pp. 22–28

Wait J. 1982: Geo-Electromagnetism. Academic Press, New York, N.Y., 168 p.

WASHBURNE J. C. 1982: Parameterization of spectral induced polarization data and laboratory and in situ spectral induced polarization measurements. West Shasta copper-zinc district, Shasta, Calif.: MS Thesis T-2591 (unpublished), Colorado School of Mines, 268 p.

WONG J. 1979: An electrochemical model of induced polarization phenomenon in disseminated sulfide ores. Geophysics, **44,** 7, pp. 1245–1265

WYNN J. C., ZONGE K. L. 1975: EM coupling, its intrinsic value, its removal, and the cultural coupling problem. Geophysics, **40,** 5, pp. 831–850

IDŐTARTOMÁNYBELI SPEKTRÁLIS GERJESZTETT POLARIZÁCIÓS ADATOK ÉRTELMEZÉSI MÓDSZEREINEK ÖSSZEHASONLÍTÁSA

VERŐ László, Bruce D. SMITH, Walter L. ANDERSON és CSÖRGEI József

Az időtartománybeli gerjesztett polarizációs mérések értelmezésének két útja lehet: az exponenciális hatványsor modell, illetve az általánosított komplex impedancia (ellenállás) vagy Cole–Cole modell segítségével. Bebizonyosodott, hogy az exponenciális modell jól illeszthető a mért lecsengési görbékhez és így olyan paramétereket kapunk, amelyek leírják a görbealak változásait. A paraméterek változásait ugyan néha kapcsolatba lehet hozni a közettípus, vagy ércesedési szövet változásaival, de lényegében nincs világos fizikai jelentésük.

A Cole–Cole modellel ugyanolyan pontosan lehet a lecsengési görbéket közelíteni, mint az exponenciális modellel. Az időtartománybeli gerjesztett polarizációs mérések értelmezésében való használata a következő előnyökkel jár: 1) Az idő- és frekvencia-tartománybeli méréseket közös alapra helyezi. 2) A modell elvileg kapcsolatba hozható bizonyos polarizációs mechanizmusokkal. 3) Megadja a különböző, véges hosszúságú gerjesztő impulzusok hatására bekövetkező változásokat a lecsengési görbe alakjában. 4) A modell az elektromágneses csatolásra is stabil numerikus közelítést ad.

Ezen felül különböző rövid idejű gerjesztő impulzusokhoz tartozó lecsengési görbék egyidejű inverziója arra is felhasználható, hogy olyan információt kapjunk, amely egyébként csak hosszú gerjesztési időkkel kapható meg.

СРАВНЕНИЕ МЕТОДОВ ИНТЕРПРЕТАЦИИ ДАННЫХ СПЕКТРАЛЬНОЙ ВЫЗВАННОЙ ПОЛЯРИЗАЦИИ ВО ВРЕМЕННОЙ ОБЛАСТИ

Ласло ВЕРЁ, Брус Д. СМИС, Вальтер Л. АНДЕРСОН и Йожеф ЧЁРГЕИ

Измерения методом вызванной поляризации во временной области интерпретируются двумя способами: по модели суммы экспоненциальных членов; при помощи обобщенного комплексного сопротивления или модели Кол–Кол. Доказано, что экспоненциальной моделью хорошо описываются измеренные кривые затухания, и так получаются параметры, хорошо описывающие изменения формы кривой. Изменения параметров иногда связываются с изменениями типа горных пород или текстуры оруденения, но они по сути дела не имеют ясного физического значения.

При помощи модели Кол–Кол кривые затухания аппроксимируются с такой же точностью, как и при помощи экспоненциальной. Использование модели Кол–Кол в интерпретации измерений вызванной поляризации во временной области имеет следующие преимущества: 1) Дается общая основа для измерений во временной и частотной областях. 2) Данная модель в принципе может быть связана с определенными механизмами поляризации. 3) Она описывает изменения формы кривой спада, вызываемые разными импульсами возбуждения конечной длительности. 4) Модель дает устойчивое численное приближение также и электромагнитной связи.

Кроме того, одновременная инверсия кривых спада от разных коротких импульсов возбуждения позволяет получить информацию, которая в иных условиях доступна лишь при использовании длительных возбуждающих импульсов.

GEOPHYSICAL TRANSACTIONS
Vol. 31. No. 1–3. pp. 331–335

APPLICATION OF THE GEOLOGIC RETRIEVAL AND SYNOPSIS (GRASP) PROGRAM AT THE EÖTVÖS LORÁND GEOPHYSICAL INSTITUTE OF HUNGARY

Roger W. BOWEN*, Ferenc CSERCSIK** and László ZILAHI-SEBESS**

The GRASP system was implemented and applied to various data management tasks at the Eötvös Loránd Geophysical Institute (ELGI) including a mineral resources data base, and a computer based catalogue of ELGI's library.

In addition to the large-sclae GRASP system a scaled-down version named MICRO-GRASP, written in BASIC, has also been implemented. Further development for geological applications pose some special problems, in particular, how to establish logical connections between different GRASP data bases. A solution, based on a new version of GASP is proposed.

Keywords: GRASP, mineral resources, DBMS, data retrieval, information system

1. Introduction

The GRASP (Geologic Retrieval and Synopsis Program [BOWEN–BOTBOL 1975], developed by the U.S. Geological Survey) was installed on the RYAD–35 computer of the Eötvös Loránd Geophysical Institute (ELGI) in 1981. On account of limitations of the hardware–software environment, the original implementation had no conversational capabilities. In 1982 the system was converted to run in a conversational mode.

Our experiences with GRASP have been very favorable. In the following sections we review these experiences to show some of the uses to which GRASP has been applied at ELGI.

2. Catalogue of mineral resources

At present, the computerized recording of the mineral resources of Hungary is produced in batch mode in ELGI's computer center. The required reports of typical data are collected once a year. Summaries are created giving the status as of the January 1, the yearly changes in mineral resources, and the causes of the changes. Data entered for processing is based on information obtained from three types of questionnaires [SOMOS 1982]:

* U.S. Geological Survey, 920 National Center, Reston, Virginia 22092
** Eötvös Loránd Geophysical Institute of Hungary POB 35, Budapest, H–1440
Manuscript received (revised form): 1 August, 1985

— data of the mining district (41 different data fields)
— data of the block group (21 different data fields), and
— data of the block (71 different data fields).

From these records, reports are produced for all geographic blocks, mining districts and companies according to both *in situ* and *industrially economical* mineral resources. Further reports are produced on the changes based on different geological categories and on the various utilizations of raw materials. Without striving for completeness, let us only mention a few of them: different reports are computed on the economical-, reserve-, and non-economical mineral resource data sets for all categories [PRUZSINA 1976]. A tabulation of changes is prepared showing the sets from the beginning of the year to the end, the type of changes according to their origin (e.g. geological–geophysical research, mining, research for mineral objects, modification of the economic environment, change of expense limits, etc.). Special uses can be made of the specific qualitative means, the geographical distribution of the economical minerals, and for other reasons.

This recording method (i.e. processing once a year) cannot answer questions which arise during the course of a year. Therefore, the application of GRASP becomes particularly useful, as our experience has shown for data from several mining districts. Data sets, derived from the computed mineral resources, are checked and processed by the software-interface program CONVERT. Once the data base has been generated by CONVERT, various queries can be quickly answered by GRASP. These queries are answered by using the 'CONDITIONS', 'LOGIC' and 'SEARCH' commands in GRASP. A type code defines the type attribute of the data collection (e.g. mining district, block group, or block). Note that different data structures mean different GRASP data bases. Special codes are used to differentiate those mining districts, which are under exploration, from those which are producing. 'FUNCTION' command is used for statistical analysis of numeric data fields. Also, one can separate records on the basis of quantitative parameters which fall between given limits. Importantly, the user does not need to predefine his queries.

The capability to update the GRASP data bases, according to the current changes, permits new geological data to be quickly integrated into the data bases. These data bases can subsequently be used as input to the next yearly computation. Since informational reports on the mineral resources are produced at different levels, correspondingly different levels of GRASP data bases can be generated. Individual levels can be defined by the application area, and by the purpose of use. These include:

— Raw data (original measurements)
— Mining district data
— Summaries.

3. Library information system

The computer-based catalogue of ELGI's Geophysical Library provided another opportunity to apply GRASP. Its form is based on standard bibliographic information supplemented with relevant references. The record structure is as follows:

ITEM/SOURCE/TITLE/AUTHORS/FIRM/JOURNAL/VOL/NO/PAGE/YEAR/DESCR/REF

SOURCE — The library where the publication is available
DESCR — Descriptors (keywords)
REF — References

The data in the REF field are values of ITEM which correspond to other records in the same data base. Incompletely described data are flagged. For instance, if the library, where a certain publication is available to users, is unknown, "R" is entered in the SOURCE field. In such a case, of course, other fields will also be left incomplete until the required information is obtained.

Let us show by an example, how to make a separation by means of references. Suppose that we would like to collect the publications which refer to the works on seismic refraction written by Oliver J. and/or Ewing M.

First, search criteria are established by the 'CONDITIONS' command:

ENTER COMMAND: 'CONDITIONS' (or 'COND') — the apostrophe indicates the user's input

A. 'AUTHORS CS OLIVER J.' (CS means "contains substring")
B. 'AUTHORS CS EWING M.'
C. 'DESCR CS SEISMIC REFRACTION'
D. <cr> — (empty line to terminate the current GRASP function).

In the second step the conditions are combined by means of the 'LOGIC' command:

ENTER COMMAND: 'LOGIC' (or 'LOGI')
ENTER LOGIC: '(A + B)*C' (or'(A. OR. B). AND.C')

The next step is the separation:

ENTER COMMAND: 'SEARCH' (or 'SEAR')
INPUT FILE: 'PUBL' — (Logical name of data base)
OUTPUT FILE: OUT1 — (Logical name of the output file, arbitrarily defined by user)

The 'LIST' command is then used to generate a listing of item numbers in OUT1 file. Thus, GRASP has provided the item numbers of those papers by Oliver J. and/or Ewing M. whose subjects is the seismic refraction technique. Let us suppose, for example, that these numbers are: 1015,226,4832,12. The following step is the actual search for the publications which refer to these items:

ENTER COMMAND: 'COND'

A. 'REF CS ,1015,' (item numbers are embedded in commas to provide a unique value)
B. 'REF CS ,226,'
C. 'REF CS ,4832,'

D. 'REF CS ,12,'
ENTER COMMAND: 'LOGIC'
ENTER LOGIC: 'A + B + C + D'
ENTRE COMMAND: 'SEARCH'
INPUT FILE: 'PUBL'
OUTPUT FILE: 'OUT2' — (for storing the selected records)
After the search command has terminated, the OUT2 file contains the information on the publications which refer to the seismic refraction works of Oliver J. and/or Ewing M., completing the retrieval by references.

This method has certain limitations:

— The number of conditions are limited by the number of letters in the English alphabet.
— The reading and manual entry of all generated item numbers, that a user has to perform, is time-consuming and mistake-prone.

These limitations can be overcome by adding a new GRASP command which allows selection based on matching values from a separate file of keys instead of selection based on the 'COND' and 'LOGIC' commands. A temporary file containing the item numbers (i.e. the keys) would be created using the 'LIST' command. This temporary file is used by the new command to complete the selection. This command can be implemented similar to the 'LINK' command, which is a feature of GRASP on USGS computers. Collaboration on the implementation of this command on ELGI's computer is currently under progress.

4. Further development

In addition to the large-scale GRASP system there is a smaller version named MICRO-GRASP which is written in the BASIC language. The characteristics of MICRO-GRASP and the expanding use of personal computers stimulate further development in the real-time updating of records and a possibility to employ floppy drives.

Geologic applications pose a further problem: namely, how can a logical connection be established between different GRASP data bases without the need of storing all original and secondary data together? In other words, how can inevitable redundancies, storage, and access-time problems be eliminated. GRASP has a very favorable feature which suggests the solution: it can access up to 10 data bases during a single execution. However, they cannot be accessed simultaneously. The LINK command will provide a partial solution by means of pseudo simultaneity, which must be extended to effective simultaneity in order to connect/combine data bases with different structures. There are many suggestions, both in literature and in practice, but original criteria of GRASP, namely portability and data/machine independence should be preserved. Certainly, these require further consultations and should be a joint venture of the interested specialists.

REFERENCES

BOWEN R. W., BOTBOL J. M. 1975: The geologic retrieval and synopsis program (GRASP). Geological Survey Professional Paper 966, U.S. Dept. Int. Washington

SOMOS L. 1982: Computer data base of hard mineral resources of Hungary (in Hungarian). MÁFI Report, Budapest

PRUZSINA J. 1976: Computer processing in the mineral recources management (in Hungarian with English abstract). MÁFI Évi Jel. az 1974. évről pp. 507–517

A GRASP ADATBÁZIS KEZELŐ PROGRAMRENDSZER ALKALMAZÁSA AZ ELGI-BEN

Roger W. BOWEN, CSERCSIK Ferenc és ZILAHI-SEBESS László

A cikk bemutatja a GRASP rendszer néhány alkalmazását az ELGI-ben, és az azokkal szerzett tapasztalatokat. Ezek a területek:

— ásványvagyon adatbázis,

— az ELGI szakkönyvtárának számítógépes információs rendszere,

A nagygépes GRASP verzió mellett a BASIC nyelven írt MICRO-GRASP programot is használjuk. A geológiai alkalmazások fölvetnek néhány további problémát, mint pl.: hogyan lehet különböző GRASP adatbázisok között logikai kapcsolatot létesíteni. A cikk a GRASP új verziója alapján megoldást is javasol a kérdésre.

ПРИМЕНЕНИЕ СИСТЕМЫ ПРОГРАММ УПРАВЛЕНИЯ БАЗОЙ ДАННЫХ В ВЕНГЕРСКОМ ГЕОФИЗИЧЕСКОМ ИНСТИТУТЕ им. Л. ЭТВЕША

Роджер В. БОЕН, Ференц ЧЕРЧИК, Ласло ЗИЛАХИ-ШЕБЕШ

В статье демонстрируются некоторые применения системы GRASP в ЭЛГИ, и полученные опыты. Области применения:

— база данных минеральных ресурсов,

— компьютеризованный каталог геофизической библиотеки ЭЛГИ,

Рядом с версией GRASP-а на мощной ЭВМ, также применяется программа MICRO-GRASP, записанная на языке BASIC. Применением управления базой данных в области геологии возникают новые проблемы, например, каким образом создать логическую связь между разными базами данных GRASP-а. На основе новой версии GRASP-а статья предлагает решение вопроса.

Acknowledgements

Editors of this volume wish to express their appreciation for the support given, since 1979, to the cooperative research program by Drs. John Reinemund and Dallas Peck of the U.S. Geological Survey, Drs. József Fülöp and Viktor Dank of the Hungarian Central Office of Geology, (Központi Földtani Hivatal) and Tamás Körner and György Nádor of the International Cultural Institute of Hungary (Nemzetközi Kultúrális Intézet). For continued support of the scientific projects, thanks are due to Dr. Pál Müller of the Eötvös Loránd Geophysical Institute of Hungary (Eötvös Loránd Geofizikai Intézet), Károly Molnár and Béla Rádler of the Geophysical Exploration Company of Hungary (Geofizikai Kutató Vállalat), Dr. Géza Hámor of the Hungarian Geological Survey (Magyar Állami Földtani Intézet), and Dr. Sándor Doleschall of the Hungarian Hydrocarbon Institute (Szénhidrogénipari Kutató–Fejlesztő Intézet).

The Conference on "Results of the Cooperative Research in Geosciences between the Central Office of Geology of Hungary (KFH) and the United States Geological Survey," held in Budapest, October 1–3, 1984, was made possible, in part, by the International Cultural Institute. The support of Honorable Nicolas M. Salgo, Ambassador of the United States is also appreciated.

For providing the facilities and for publishing the proceedings of this conference, special thanks are expressed, respectively, to the Eötvös Loránd Geophysical Institute and the National Oil and Gas Trust of Hungary.